TECHNISCHE UNIVERSITÄT MÜNCHEN
TUM School of Engineering and Design

Dissertation

On the Decomposition of Periodic Signals into its Fundamental Parameters

Markus Landerer

TECHNISCHE UNIVERSITÄT MÜNCHEN

TUM School of Engineering and Design

On the Decomposition of Periodic Signals into its Fundamental Parameters

Markus Landerer

Vollständiger Abdruck der von der TUM School of Engineering and Design der Technischen Universität München zur Erlangung eines

Doktors der Ingenieurwissenschaften (Dr.-Ing.)

genehmigten Dissertation.

Vorsitz:		Prof. Dr. Marcelo Lobo Heldwein
Prüfende der Dissertation:	1.	Prof. Dr.-Ing. Christoph M. Hackl
	2.	Prof. Dr. Thomas Hamacher
	3.	Prof. Marta Molinas

Die Dissertation wurde am 19.09.2023 bei der Technischen Universität München eingereicht und durch die TUM School of Engineering and Design am 17.04.2024 angenommen.

Ich,

Markus Landerer

erkläre an Eides statt, dass ich die bei der promotionsführenden Einrichtung

TUM School of Engineering and Design

der TUM zur Promotionsprüfung vorgelegte Arbeit mit dem Titel:

On the Decomposition of Periodic Signals into its Fundamental Parameters

unter der Anleitung und Betreuung durch:

Prof. Dr.-Ing. habil. Christoph M. Hackl

ohne sonstige Hilfe erstellt und bei der Abfassung nur die gemäß § 7 Abs. 6 und 7 angegebenen Hilfsmittel benutzt habe.

[x] Ich habe keine Organisation eingeschaltet, die gegen Entgelt Betreuer*innen für die Anfertigung von Dissertationen sucht, oder die mir obliegenden Pflichten hinsichtlich der Prüfungsleistungen für mich ganz oder teilweise erledigt.

[x] Ich habe die Dissertation in dieser oder ähnlicher Form in keinem anderen Prüfungsverfahren als Prüfungsleistung vorgelegt.

[ ] Teile der Dissertation wurden in ___ veröffentlicht.

[x] Ich habe den angestrebten Doktorgrad noch nicht erworben und bin nicht in einem früheren Promotionsverfahren für den angestrebten Doktorgrad endgültig gescheitert.

[ ] Ich habe bereits am ___ bei der promotionsführenden Einrichtung ___ der Hochschule ___ unter Vorlage einer Dissertation mit dem Thema ___ die Zulassung zur Promotion beantragt mit dem Ergebnis: ___.

[ ] Ich habe keine Kenntnis über ein strafrechtliches Ermittlungsverfahren in Bezug auf wissenschaftsbezogene Straftaten gegen mich oder eine rechtskräftige strafrechtliche Verurteilung mit Wissenschaftsbezug.

Die öffentlich zugängliche Promotionsordnung sowie die Richtlinien zur Sicherung guter wissenschaftlicher Praxis und für den Umgang mit wissenschaftlichem Fehlverhalten der TUM sind mir bekannt, insbesondere habe ich die Bedeutung von § 27 PromO (Nichtigkeit der Promotion) und § 28 PromO (Entzug des Doktorgrades) zur Kenntnis genommen. Ich bin mir der Konsequenzen einer falschen Eidesstattlichen Erklärung bewusst.

Mit der Aufnahme meiner personenbezogenen Daten in die Alumni-Datei bei der TUM bin ich

[x] einverstanden [ ] nicht einverstanden.

München, July 3, 2024 ???

Ort, Datum Unterschrift

This document is typeset with LaTeX/TeX.

Contents

List of Figures

List of Tables

Nomenclature

$\mathbb{N} \subset \mathbb{Q} \subset \mathbb{R} \subset \mathbb{C}$: .... Set of natural, rational, real and complex numbers
$s \in \mathbb{C}$: .... Scalar
$\mathbb{C}_{\mathrm{NHP}} := \{\alpha \in \mathbb{C} \mid \Re(\alpha) < 0\}$: .... Set of complex numbers with negative real part
$\mathbb{N}^r \subset \mathbb{Q}^r \subset \mathbb{R}^r \subset \mathbb{C}^r, r \in \mathbb{N}$: .... Set of natural, rational, real and complex vectors
$\boldsymbol{v} \in \mathbb{C}^r$: .... Column vector
$\boldsymbol{i}_{i,r} \in \mathbb{R}^r$: .... i-th unit vector
$\|\boldsymbol{v}\| \in \mathbb{R}$ .... Euclidean norm of $\boldsymbol{v}$
$\mathbb{N}^{r\times c} \subset \mathbb{Q}^{r\times c} \subset \mathbb{R}^{r\times c} \subset \mathbb{C}^{r\times c}, r, c \in \mathbb{N}$: .... Set of natural, rational, real and complex matrices
$\boldsymbol{M} \in \mathbb{C}^{r\times c}$: .... Matrix with r rows and c columns
$\boldsymbol{M}^\top \in \mathbb{C}^{c\times r}, \boldsymbol{v}^\top \in \mathbb{C}^r$: .... Conjugate transposed matrix and vector
$\boldsymbol{0}_r \in \mathbb{R}^r, \boldsymbol{0}_{r\times c} \in \mathbb{R}^{r\times c}$: .... Zero column vector and matrix
$\boldsymbol{I}_r \in \mathbb{R}^{r\times r}$: .... Identity matrix
$\boldsymbol{M} > 0, \boldsymbol{M} \in \mathbb{C}^{r\times r}$: .... Short notation for: $\forall\, \boldsymbol{x} \in \mathbb{C}^r \setminus \{\boldsymbol{0}_r\} : \boldsymbol{x}^\top \boldsymbol{M}\boldsymbol{x} > 0$
$\operatorname{diag}(s_1, \ldots, s_n) \in \mathbb{C}^{n\times n}$: .... Diagonal matrix with entries $s_1, \ldots, s_n$
$\operatorname{blkdiag}(\boldsymbol{M}_1, \ldots, \boldsymbol{M}_n) \in \mathbb{C}^{\sum_{i=1}^n r_i \times \sum_{i=1}^n c_i}$: .... Block diagonal matrix with entries $\boldsymbol{M}_1, \ldots, \boldsymbol{M}_n$
$\sum_{j_1<j_i=1\backslash k}^n$: .... Abbreviation for $\sum_{j_1=1, j_1\neq k}^n \sum_{j_2=j_1+1, j_1\neq k}^n \cdots \sum_{j_i=j_{i-1}+1, j_1\neq k}^n$
$\prod_{j_1<j_i=1\backslash k}^n$: .... Abbreviation for $\prod_{j_1=1, j_1\neq k}^n \prod_{j_2=j_1+1, j_1\neq k}^n \cdots \prod_{j_i=j_{i-1}+1, j_1\neq k}^n$
$\sum_{j_1<j_0=1}^n$: .... Special case of $\sum_{j_1<j_i=1}^n$. It is defined $\sum_{j_1<j_0=1}^n = 1$
$\sum_{k\in j\backslash i}, \prod_{k\in j\backslash i}$: .... Abbreviation for $\sum_{\substack{k\in\{j_1,\ldots,j_n\}\\ k\notin\{i_1,\ldots,i_m\}}}, \prod_{\substack{k\in\{j_1,\ldots,j_n\}\\ k\notin\{i_1,\ldots,i_m\}}}$
$v, \widehat{v}$: .... Value and its estimate
$v, \underline{v}$: .... Value and its transformed representation
$\mathcal{U}(f)$: .... Physical unit of f
$\mathcal{L}^\infty(\mathbb{A}; \mathbb{B})$: .... Space of essentially bounded functions mapping from $\mathbb{A}$ to $\mathbb{B}$
$\mathcal{C}(\mathbb{A}; \mathbb{B})$: .... Space of continuous functions mapping from $\mathbb{A}$ to $\mathbb{B}$

Abstract

This thesis deals with the decomposition of periodic signals into their fundamental parameters. Based on the well known *Frequency Adaptive Observer* (FAO) that consists of *Second Order Generalized Integrator* (SOGI) and *Frequency Locked Loop* (FLL), three different systems (esFAO, mFAO, tFAO) based on the concept of observers are developed. Hereby, each observer has unique characteristics. All observers are designed to estimate amplitudes and phase angles of a predefined number of harmonic components out of the periodic signal as well as its fundamental angular frequency. All observers are further developed such that they imply the estimation of offset. The prescription of settling time and the possibility to estimate the angular frequencies of a given number of harmonic components with largest amplitude are named as special characteristics of some of the observers. Then, the basis for another system (eFAO) which is not completed yet, is acquired. The developed observers are evaluated using error metrics and compared to each other. Finally, they are investigated experimentally, also in comparison to well known methods from literature.

Kurzzusammenfassung

Diese Dissertation befasst sich mit der Dekomposition periodischer Signale in deren fundamentale Parameter. Ausgehend von der bereits bekannten Methode des *Frequency Adaptive Observer* (FAO), welcher sich aus *Second Order Generalized Integrator* (SOGI) und *Frequency Locked Loop* (FLL) zusammensetzt, werden drei verschiedene Systeme (esFAO, mFAO, tFAO), welche auf dem Konzept eines Beobachters beruhen, entwickelt. Jeder Beobachter weist hierbei seine eigenen Charakteristika auf. Allen Beobachter gemein sind die Funktionalitäten, Amplituden und Phasen einer vordefinierten Anzahl an harmonischen Komponenten aus dem periodischen Signal zu schätzen sowie dessen Fundamentalfrequenz. Alle Beobachter sind dahingehend weiterentwickelt, dass sie auch die Schätzung eines Gleichanteils miteinbeziehen. Als spezielle Eigenschaften von einigen der entwickelten Beobachter sind die Einstellung einer gewünschten Einschwingzeit und die Möglichkeit, die Frequenzen einer vorgegebenen Anzahl an harmonischen Komponenten mit größter Amplitude gesondert zu schätzen, genannt. Anschließend wird die Grundlage für ein weiteres, noch nicht fertig gestelltes System (eFAO) erarbeitet. Die entwickelten Beobachter werden mit Hilfe von Fehlermetriken bewertet und miteinander verglichen. Abschließend werden diese experimentell untersucht, auch im Vergleich zu bekannten Methoden aus der Literatur.

Chapter 1

Introduction

This thesis deals with the online decomposition of unknown periodic signals into its amplitudes, phase angles and angular frequencies. But, at first, the relevance of this issue is motivated in Section 1.1. Afterwards, a detailed overview of existing methods is presented in Section 1.2 from which the remaining field of research is deduced and gaps are filled. A summary of the decomposition methods proposed in this thesis as well as a description of the structure of this thesis is given in Section 1.3.

1.1 Motivation

Periodic signals are present everywhere in the surrounding world. For example, acoustic or optic signals, population developments, and electric, mechanic, biologic or climatic processes can be modeled by periodic functions. Hereby, any periodic function is uniquely defined by amplitude, phase angle, offset, and angular frequency. In the following, some of these examples are described in more detail where periodic functions must be analyzed.

Acoustic signals, used e.g. for conversation or music, are characterized by loudness (amplitude) and pitch (frequency), where the phase angle is not relevant in this context [1]. Especially for speech recognition, the typically distorted signals must be decomposed into their fundamental parameters amplitude and frequency. Thus, characteristic patterns can be recognized that relate to syllables [2].

Another example are optical signals. These play an important role when taking into account fiberglass technology. It can be used for information transfer where a large amount of data is coded onto a wide frequency range that promotes fast communication [3]. Afterwards, the transmitted information must be decoded again, which means that the incoming signals frequencies and amplitudes are analyzed. Other applications may be found in optical sensors.

As a last field of application, examples in electrical energy systems (e.g. power grid, inverters, electrical machines) are considered. The first thing to mention is that, in accordance to the norm 'IEC TS 62749:2020 RLV', certain restrictions to the voltage are formulated. E.g., the allowed range for the fundamental frequency in Europe is defined as $50\,\mathrm{Hz} \pm 0.2\,\mathrm{Hz}$. Considering three-phase-four-wire transmission lines, the fourth (neutral) line also has limitations to the current flowing through it. Moreover, to keep the overall grid balanced, which is also described in this norm, the well-known Fortescue transformation [4] must be applied to the three-phase signals. However, this transformation needs pure sinusoids, i.e. the three (or four) phase voltages and currents must be decomposed in real-time. Transformers are other applications in electrical networks. For example, an impedance spectroscopy of transformer insulations can be used to identify the transformer's state of health, where especially the low-frequency range is of interest [5, 6]. It also is worth noting that the proper functionality of grid converters, that are used

to couple sustainable energy systems, such as solar or wind power plants, mainly depends on the voltage quality on the grid side. Voltage abnormalities such as frequency drifts, offset or voltage sags might cause detoriated converter performance [7]. A reason for poor voltage quality may be found in the decentralized power generation by sustainable energy systems. Because these significantly depend on natural chaotic events (clouds, lulls, etc.), the overall grid inertia diminishes due to the fluctuating and non-controllable generation and consumption that leads to frequency deviations. Concluding, all these examples show that online decomposition and monitoring of the grid voltages and currents is necessary to identify and counteract possible faults. This ensures stability and quality of frequency and voltages and thus prevents blackouts. Another very important aspect is that, in addition to economic damage caused by powerless or destroyed equipment, faults can also pose a danger to humans.
As motivated, a lot of fields of application exist in which periodic functions must be decomposed into their amplitudes, frequencies, phase angles, and offset. Hence, the aim is to develop an intelligent method of how to extract these in real-time.

1.2 State-of-the-art estimation and detection methods

To begin with, throughout this thesis two kinds of principles for acquiring values using dynamical systems are used. The first one is *detection* and means the calculation of values using the results of the dynamic system and its input (i.e. with feedthrough). The second one is *estimation* and means the calculation of values using only the results of the dynamical system (i.e. without feedthrough).
The most popular solution for the problem of signal decomposition is the *Discrete Fourier Transformation* (DFT), which is often used in signal processing. Related to the DFT is the *Fast Fourier Transformation*, which is an efficient implementation of the DFT [8]. It requires a time frame that is divided (discretized) into smaller time frames of equal length. Based on the large time frame, it can detect all amplitudes, phase angles, and frequencies comprised in the signal to be decomposed. The detectable frequencies (and related amplitudes and phases) are limited to a lower and upper boundary. The lower boundary is defined by the length of the large frame and the upper by the length of the small one. Moreover, inside this frequency band, only discrete frequencies can be detected that also arise via discretization.
In recent years considerable progress was achieved in the field of signal decomposition by developing a new method known as *Direct-Second Order Generalized Integrator-Frequency Locked Loop* (DC-SOGI-FLL). It also will be used in this thesis. The basic component of this method is a SOGI whose task is to estimate amplitudes and phase angles of all harmonics. A DC component is included to estimate offset. To cover angular frequency estimation as well, a FLL is attached; it should be noted that other frequency estimation methods like the *Phase Locked Loop* (PLL) [9–14] exists, which are not addressed in this thesis.
Many applications for the SOGI with or without angular frequency adaption by a PLL or FLL already exist. For example, it is used in Static Compensators or Distributed Static Compensators [12, 15–23], in Shunt Active Power Filters [9, 24–33], in synchronization techniques for grids or other applications [13, 34–96]. It is also used often for filtering issues [97–139]. Besides filtering, the filters' task is the provision of orthogonal signal components [140–149] that are needed for the Fortescue transformation [4] to calculate symmetrical components [150–180], for PLLs [45, 181–243] or FLLs [244–277], for explicit fundamental or harmonic extraction [278–309] or for other applications like electrical generators, transformers, inverters, converters, electrical vehicles or PV systems to name a few [310–460].
In the following, the progress in research until now is reviewed for each component of the DC-SOGI-FLL.

In [461], a system is described that is capable of estimating the fundamental parameters (amplitude, phase and frequency) of a randomly distorted signal with offset. This system is not based on the SOGI-method, but on Moving Average Filters. However, it is not designed for estimation of harmonics or offset. Another system, called the PI-SOGI, is based on the SOGI system combined with a PI controller for calculating the derivative of the input signal where cascading n PI-SOGIs results in the n-th derivative [462]. A system for extracting the fundamental component based on Zero Crossing Detection is shown in [463]. A different system for filtering out the fundamental amplitude is considered in [464]; it is denoted as the Multi Harmonic Decoupling Cell. Also, it permits the estimation of harmonics. Sliding mode observers for parameter estimations are studied in [465]. The authors of [466] report a quadrature signal generation method based on Derivative Elements. A Second Order Generalized Differentiator to suppress offset is published in [467]. In [468], a Frequency Fixed SOGI (FFSOGI) is proposed where the resulting outputs from the SOGI are incorrect, if the actual frequency is not equal to the fixed one. To solve this issue, the outputs are corrected by a frequency estimated by a PLL which permits a faster performance. However, from Figure 3 in this article, it can be seen that the proposed FFSOGI contains an algebraic loop. This method is extended by an adaptive tuning for the SOGI in [469]. Another method to achieve a faster performance is proposed in [470]. In view of adaptive tuning, [471] introduces a wavelet transformation. It is used for online parameter tuning to satisfy desired filtering characteristics of the SOGI. The authors of [472, 473] introduce a system of dual SOGIs (two parallel SOGIs, called DSOGI) with joint frequency adaption, one for each of the α and β components resulting from the Clarke-transformation where the γ component is neglected. Its purpose is to calculate the positive and/or negative sequence of a possibly unbalanced three-phase signal. Clearly, no information on the zero sequence can be acquired with this approach[1]. In view of the same aim, [474] report a system called Reduced Order Generalized Integrator (ROGI), that directly feeds both signals from the transformation (α and β) to one SOGI structure. It is designed to halve the computational burden with respect to the DSOGI. An alternative to the basic SOGI is illustrated in [475]. It is called Enhanced Adaptive Filter and is designed to provide estimates of the input and the respective quadrature signal[2]. In view of harmonic and offset filtering, [476] compares two prefilter techniques for the SOGI-FLL. The first technique (SOGI-FLL with prefilter) is described in [477] and the second (SOGI-FLL with in-loop filter with feedback) is found in [478–480]. In [481], a different comparison is done which includes a Third Order Generalized Integrator (TOGI). It is an extension of the SOGI to filter offset [482–484]. Offset filtering is also an aim in [485] wherein the authors attached an All Pass Filter after the SOGI structure. A Zero-tracking SOGI-FLL (ZT-SOGI-FLL) is proposed in [228]. It is designed to have better dynamic and stability characteristics than the conventional SOGI-FLL. In [486], the authors claim to propose a Novel Second Order Generalized Integrator (NSOGI) for offset filtering; however, the NSOGI is doubted to be novel. Instead, the authors just use a different gain selection and arrangement that can be transferred to the normal SOGI (with a preceding gain). Lowpass SOGIs (LSOGI) and Highpass SOGIs (HSOGI) are benchmarked to the standard SOGI in [487] to determine their advantages. The difference between LSOGI, HSOGI and standard SOGI is found in the output signal acquisition. In [488] another method on how to acquire the quadrature signal (called the Second Order Adaptive Filter (SOAF)) is shown. It is compared to the SOGI method and the SOGI is better than the SOAF in all investigated characteristics (e.g. Band width, settling time, total harmonic distortion of the fundamental component). A review and Linear Time Periodic Modeling of some types of SOGI-FLL is presented in [489].

[1] According to the Fortescue transformation, a negative sequence consisting of zero signals for all times does *not* imply a balanced three-phase signal.

[2] The quadrature signal has 90 degrees phase angle delay with respect to the input signal.

Until now, almost all citations dealt with single SOGIs which solely allow the extraction of one component of the input signal. A parallelization of SOGIs for extraction of multiple harmonics can be found in [490–493]. A modified parallelized SOGI system, called the Multi-Magnitude Integrator-Orthogonal Signal Generator (MMI-QSG) is found in [494]. Therein, the authors claim that the Magnitude Integrator-Orthogonal Signal Generator approach has better dynamic response than the SOGI that is verified in a single experiment. The DSOGI (see above) is parallelized in [495]. A comparison of parallel SOGIs to a DFT, FFT and others is published in [496]. The authors of [497] provide a stability proof of the generic parallelization and show the allowed tuning range for the gains. However, it is based on an assumption: all gains are assumed to be positive where the case of (at least one) negative gain(s) is not considered.
So far, nearly all of the cited papers do not consider the estimation or detection of offset in the input signal, although some were designed to filter it (e.g. TOGI). For explicit detection, in [498–500] an easy way on how to obtain offset from the SOGI outputs is shown. Offset estimation is shown in [501] where also a damped SOGI is proposed. Another method on how to obtain an estimate for offsets is shown in [502]. The SOGI capable of estimating offset, called the DC-SOGI, is also used for the DSOGI [7, 503, 504]. The LSOGI and HSOGI are extended to the Extended State HSOGI (ESHSOGI) and the Extended State LSOGI (ESLSOGI) in [505] to additionally estimate offset. A good overview of existing methods for offset detection, filtering or estimation can be found in [506, 507]. Besides the already mentioned DC-SOGI and SOGI with prefilter, these papers additionally cover a SOGI with delayed signal cancellation, a SOGI with complex coefficient filter and a notch filter[3]. The authors of [508] describe a globally stable PLL with offset filtering capability. Another SOGI-PLL with offset filtering capability is proposed in [509]. In [510], the authors claim to introduce an improved SOGI-FLL that is designed for special focus on any offset in the input signal. However, since the authors failed to setup appropriate equations, one must rely on Figure 1 within this paper for implementation. However, from this figure it can be concluded that the implementation shown must be wrong, since the frequency integrator is always multiplied by zero and, hence, outputs a constant frequency. A parallelization of the DC-SOGI structure is described in [511] that is based on a Kalman Filter which is almost similar to a DC-SOGI. The only difference to the common SOGI is an additional tuning parameter. Although they briefly mention that a general parallelization is possible, neither is it mathematically shown nor is it explicitly validated. The basic concept for such a SOGI with additional tuning is also shown in [512] but this is put into perspective as they set the additional tuning factor as a function of the others. It also comes with an offset estimator. Alternative approaches for offset estimation are shown in [513]. These use a parallelization of extended SOGIs, called Accurate Magnitude Integrators (AMI) (with three integrators per AMI) and an offset estimator block. In [514], a parallelization of order three is shown where each harmonic estimation block consists of a SOGI with in-loop filter (as above) and an offset estimator (i.e. five integrators per block).
For now, only the amplitude, phase angle and offset was considered although frequency estimation was also part of some of the papers. Hereby, the fundamental frequency was usually adapted by a FLL or PLL. Hence, in the following, the focus is placed on publications explicitly dealing with frequency estimation. A common way for frequency estimation is found in the FLL with the SOGI or DC-SOGI as a basis that often comes with a Gain Normalization as described in [515]. It is compared to other frequency adaptive systems related to the FLL in [516–519]. Another comparison of different FLLs is shown in [520]. The authors concludes that, by proper gain selection, the investigated FLLs are equivalent. Anonther FLL is found in [521] wherein the classic FLL is extended by additional signal modifications. The authors of [522] show a tuning

[3] A rather unusual name for the SOGI is "Adaptive Notch Filter" (ANF); since this term is also used in other contexts, this thesis sticks to the widely used expression "SOGI".

for the FLL based on fuzzy logic. Another adaptive tuning variant, called Auto Adjustable Gain, is shown in [523]. An additional method for enhancing the FLL performance is found in [524] that includes a saturation and anti-wind up. The authors of [525] present a FLL that is tuned adaptively by characteristics of the SOGI. In [526], a FLL for estimating the fundamental angular frequency even under heavily distorted signal conditions is proposed. In [527], a slightly modified SOGI-FLL with an additional SOGI as prefilter is proposed. It is designed for robust behavior when being fed with signals characterized by offset, harmonics or phase angle jumps. The authors of [528] introduce a SOGI with shifted frequency, i.e. the estimated reference frequency is artificially shifted by an enforced constant (initial) frequency in the SOGI. The frequency integrator then estimates the gap between the constant frequency and the actual one. However, functionality cannot be guaranteed in the proposed setting since any constant frequency set too high will prohibit the frequency estimation to converge. In [529], a study on three-phase FLLs is carried out. The authors of [530] analyze a FLL based on high-order Complex Band Pass Filters. In [531, 532], a Linear Time Periodic modeling of a SOGI with FLL is performed to get insight into the stability region and robustness of the FLL. The same task is done for a DC-SOGI with FLL in [533] and for parallelized SOGIs with FLL in [534]. A method on how to obtain the fundamental frequency as the differential of the estimated angle of a frequency fixed SOGI is explained in [535]. A FLL for the TOGI is developed in [536] that shows better filtering and dynamical characteristics. Other single phase frequency estimators can be found in [537–544] which are based on Cascaded Delayed Signal Cancellation, alternative orthogonal signal generators with adaptive frequency estimators, Discrete Fourier Transformations, Recursive Discrete Fourier Transformations, Inverse Recursive Discrete Fourier Transformations, Modulating Functions Frequency Estimators, Particle Swarm Optimization or Teager Energy Operator.

In terms of stability, no signal decomposition system has yet been properly studied (the only exception is [497]). Stability is considered in [545] for parallelized TOGIs and in [546] for a SOGI-FLL with active noise cancellation. The authors of [547, 548] show a globally stable single-phase parameter detection system. In [549], it is extended to three-phase systems. In the last three approaches, no signal with offset was considered, which is the case in [550]. However, these methods still require knowledge on the harmonic orders, i.e. they only are able to estimate the fundamental frequency.

This issue is addressed in the following literature. The first publication to note is [551]; it is based on coordinate transformations. It estimates all parameters (amplitudes, phase angles and frequencies of all harmonics) and is denoted as the Full Parameter Identification (FPI). However, the estimation is performed in transformed coordinates, which does not permit a calculation of back-transformed estimates. In fact, it cannot be solved analytically for a system order greater than four. In [552], frequency estimates based on the algebraic derivative method in the frequency domain are obtained. Back to the parallelized SOGI, a globally stable frequency adaption for each SOGI-block based on the averaging approach is reported in [553]. However, it does not consider signals comprising offset. The authors of [554] show a method for estimating squared harmonic frequencies that requires a very long estimation time, up to half a minute. A method for estimating the frequency out of a TOGI is shown in [555]. This is extended for parallelized TOGIs in [556] which permits estimating multiple frequencies. However, no generic tuning rule or stability is shown; additionally, convergence seems to be highly dependent on tuning and initial values (briefly investigated in Section 4 of this thesis).

To fully review the progress in the recent years, some discretization methods for SOGIs and/or FLLs are considered in [557–569].

1.3 Proposed methods and structure of this thesis

From the review made in Section 1.2, to the best knowledge of the author, no generic system capable of estimating offset, amplitudes, phase angles and frequencies of a prescribed number of harmonics with an acceptable performance is known. Thus, the aim of this thesis is to develop such a system (called observer, cf. Definition 2.1). It should be

- capable of estimating amplitude, phase angle, angular frequency, and offset;
- generically extendable to n amplitudes, phase angles and angular frequencies (where n is a natural number);
- robust to parameter variations – that is, the performance of the system is normed to amplitude and angular frequency of the signal to be decomposed; and
- exponentially stable.

In order to create an understanding of the development, this thesis proposes methods that improve performance and/or capability step by step compared to the most common state-of-the-art methods known from the literature. To give an introductory overview, all proposed methods are listed in the following:

- The **enhanced standard Frequency Adaptive Observer with High Pass Filter** (**esFAO**) is a very simple parameter detection method with only moderate improvements in performance and capability. It is able to estimate a predefined number of amplitudes and phase angles with prescribed harmonic orders, offset, and the fundamental angular frequency. The stability range of the system is bounded. Parts of it were already published in [570].
- The **modified Frequency Adaptive Observer** (**mFAO**) is constructed to significantly accelerate the performance when frequency adaption is neglected; in fact, it theoretically allows for an infinitely fast settling time. It is capable of estimating a predefined number of amplitudes and phase angles with prescribed harmonic orders. If frequency adaption is included, then it is capable of estimating the fundamental angular frequency but at cost of deceleration. The stability range of this system is bounded. Parts of this method were published in [571]. Based thereon the **modified Frequency Adaptive Observer with offset** (**mFAO$_\circ$**) is constructed to expand the capability of the mFAO for estimation of offset. Parts of it were already published in [572].
- The **transformed Frequency Adaptive Observer** (**tFAO**) is based on the work in [548] and designed for estimating multiple amplitudes, phase angles, and angular frequencies without knowing their harmonic orders. It is based on a coordinate transformation. The systems stability range is theoretically unbounded, i.e. global. An extension of this system, the **transformed Frequency Adaptive Observer with offset** (**tFAO$_\circ$**), is developed to estimate offset. Both methods are back-transformed into original (α, β) coordinates.
- Ideas for the **exponential Frequency Adaptive Observer** (**eFAO**) and the **exponential Frequency Adaptive Observer with offset** (**eFAO$_\circ$**) are shown, but they are not finished yet. The aim of these observers is to estimate a given number of amplitudes, phase angles, angular frequencies without knowledge on their harmonic orders and offset (in case of eFAO$_\circ$) within a prescribed time frame. The stability range will be bounded.

To conclude this section, the thesis' structure is shown in the following. Starting with Section 2, the most important mathematical definitions and relations used throughout this thesis are shown. Section 3 contains the theoretical part dealing with the derivation of the proposed methods. All methods are verified by simulative and experimental setups and compared to each other and selected literature in Section 4. Finally, Section 5 completes this thesis with a summary and also shows remaining problems.

Chapter 2

Mathematical preliminaries

In this chapter, the most important definitions, mathematical facts, observations and claims used throughout this thesis are collected. Where possible, the proofs are omitted and can be found in the respective references.

Definition 2.1 (Observer)**.** *Let $t_0 \in \mathbb{R}$. Consider a system of $n \in \mathbb{N}$ autonomous differential equations and output y*

$$\forall\, t \geq t_0\colon \quad \left.\begin{aligned} \tfrac{\mathrm{d}}{\mathrm{d}t}\boldsymbol{x}(t) &= \boldsymbol{f}(\boldsymbol{x}(t)) \in \mathbb{R}^n, \quad \boldsymbol{x}(t_0) = \boldsymbol{x}_0 \\ y(t) &= g(\boldsymbol{x}(t)) \in \mathbb{R} \end{aligned}\right\} \tag{2.1}$$

with some vector valued function $\boldsymbol{f}$ and scalar function g. Hereby, only the output y is measurable. Then, another system

$$\begin{aligned} \tfrac{\mathrm{d}}{\mathrm{d}t}\widehat{\boldsymbol{x}}(t) &= \boldsymbol{h}(\widehat{\boldsymbol{x}}(t), y(t)), \quad \widehat{\boldsymbol{x}}(t_0) = \widehat{\boldsymbol{x}}_0 \\ \widehat{y}(t) &= g(\widehat{\boldsymbol{x}}(t)) \end{aligned}$$

is called observer, *if it satisfies*

$$\lim_{t\to\infty} \boldsymbol{x}(t) - \widehat{\boldsymbol{x}}(t) \to \mathbf{0}_n.$$

Fact 2.2 (Observability of autonomous systems)**.** *[573] Consider the autonomous system (2.1). This system is observable, if and only if the equation*

$$\boldsymbol{y}(\boldsymbol{x}(t)) := \begin{pmatrix} y(t) & \tfrac{\mathrm{d}}{\mathrm{d}t}y(t) & \cdots & \tfrac{\mathrm{d}^{n-1}}{\mathrm{d}t^{n-1}}y(t) \end{pmatrix}^\top \tag{2.2}$$

is uniquely solvable for $\boldsymbol{x}$. If system (2.1) is linear in $\boldsymbol{x}$, then the well known requirement for observability [574, Sec. 2.3.1] is obtained.

Note 2.3. *If (2.1) is observable, then an observer for (2.1) exists.*

Fact 2.4 (Trigonometric identities)**.** *[575, p. 124f] Let $x_1, x_2, \ldots, x_n, a_1, a_2, \ldots, a_n \in \mathbb{R}$. Then, the following holds:*

$$\left.\begin{aligned} \sin(x_1 \pm x_2) &= \sin(x_1)\cos(x_2) \pm \cos(x_1)\sin(x_2)\,, \\ \cos(x_1 \pm x_2) &= \cos(x_1)\cos(x_2) \mp \sin(x_1)\sin(x_2)\,, \end{aligned}\right\} \tag{2.3}$$

$$\left.\begin{aligned} \sin\left(\operatorname{arctan2}\left(\tfrac{x_2}{x_1}\right)\right) &= \tfrac{x_2}{\sqrt{x_1^2+x_2^2}}, \\ \cos\left(\operatorname{arctan2}\left(\tfrac{x_2}{x_1}\right)\right) &= \tfrac{x_1}{\sqrt{x_1^2+x_2^2}}, \end{aligned}\right\} \tag{2.4}$$

$$\sum_{i=1}^{n} a_i \cos(x_i) = \sqrt{\sum_{i=1}^{n}\sum_{i=1}^{n} a_i a_j \cdot \cos(x_i - x_j)}\cos\left(x_1 + \operatorname{arctan2}\left(\frac{\sum_{i=1}^{n} a_i \sin(x_i - x_1)}{\sum_{i=1}^{n} a_i \cos(x_i - x_1)}\right)\right), \tag{2.5}$$

$$\operatorname{arctan2}\left(\tfrac{x_2x_3 \pm x_1x_4}{x_1x_3 \mp x_2x_4}\right) = \operatorname{arctan2}\left(\tfrac{x_2}{x_1}\right) \pm \operatorname{arctan2}\left(\tfrac{x_4}{x_3}\right). \tag{2.6}$$

Hereby, the arctan2*-function is defined as*

$$\operatorname{arctan2}\left(\tfrac{y}{x}\right) := \begin{cases} \arctan\left(\frac{y}{x}\right), & x > 0 \\ \arctan\left(\frac{y}{x}\right) + \pi, & x < 0 \wedge y > 0 \\ \pi, & x < 0 \wedge y = 0 \\ \arctan\left(\frac{y}{x}\right) - \pi, & x < 0 \wedge y < 0 \\ \frac{\pi}{2}, & x = 0 \wedge y > 0 \\ -\frac{\pi}{2}, & x = 0 \wedge y < 0 \\ 0, & x = y = 0. \end{cases} \tag{2.7}$$

Fact 2.5 (Hurwitz matrix characteristic)**.** *[576, Fact 11.17.6] Let $\boldsymbol{A} \in \mathbb{R}^{n\times n}$ and let $\chi_{\boldsymbol{A}}(s) := \det(s\boldsymbol{I}_n - \boldsymbol{A})$ be decomposed into $\chi_{\boldsymbol{A}}(s) = \chi^e_{\boldsymbol{A}}(s) + \chi^o_{\boldsymbol{A}}(s)$ with only even and odd powers, respectively. Then, $\boldsymbol{A}$ is a Hurwitz matrix if and only if the following three conditions hold:*

(i) all coefficients of $\chi_{\boldsymbol{A}}(s)$ are positive,

(ii) for all $s^e \in \left\{s \in \mathbb{C} \,\middle|\, \chi^e_{\boldsymbol{A}}(s) = 0\right\}$ and for all $s^o \in \left\{s \in \mathbb{C} \,\middle|\, \chi^o_{\boldsymbol{A}}(s) = 0\right\}$, the condition $\Re\left(s^e\right) = \Re\left(s^o\right) = 0$ holds and

(iii) the roots are interlaced on the imaginary axis, i.e. for any two consecutive roots of the even (or odd) polynomial, there exists exactly one root of the odd (or even) polynomial in between.

Observation 2.6 (Solution of a specific definite integral)**.** *Let $\omega, \omega_1, \omega_2 \in \mathbb{R} \setminus \{0\}$, $\phi_1, \phi_2 \in \mathbb{R}$ and $t \in \mathbb{R}$. Then, the following holds:*

$$\begin{aligned} &\int_t^{t+\frac{2\pi}{\omega}} \cos(\omega_1\tau + \phi_1)\cos(\omega_2\tau + \phi_2)\,\mathrm{d}\tau \\ &= \begin{cases} \frac{\sin\left(\phi_1+\phi_2+(\omega_1+\omega_2)t+\frac{2(\omega_1+\omega_2)\pi}{\omega}\right) - \sin\left(\phi_1+\phi_2+(\omega_1+\omega_2)t\right)}{2(\omega_1+\omega_2)}, & \omega_1 \neq \omega_2 \wedge \omega = \omega_1 - \omega_2 \\ \frac{\pi}{\omega}\cos(\phi_1 - \phi_2), & \omega = \omega_1 = \omega_2 \end{cases} \end{aligned} \tag{2.8}$$

Proof. Observe that

$$\begin{aligned} &\int_t^{t+\frac{2\pi}{\omega}} \cos(\omega_1\tau + \phi_1)\cos(\omega_2\tau + \phi_2)\,\mathrm{d}\tau \\ \overset{(2.3)}{=} &\int_t^{t+\frac{2\pi}{\omega}} \cos(\omega_1\tau)\cos(\omega_2\tau)\cos(\phi_1)\cos(\phi_2) - \cos(\omega_1\tau)\sin(\omega_2\tau)\cos(\phi_1)\sin(\phi_2)\,\mathrm{d}\tau \\ &- \int_t^{t+\frac{2\pi}{\omega}} \sin(\omega_1\tau)\cos(\omega_2\tau)\sin(\phi_1)\cos(\phi_2) + \sin(\omega_1\tau)\sin(\omega_2\tau)\sin(\phi_1)\sin(\phi_2)\,\mathrm{d}\tau \end{aligned}$$

$$
\begin{aligned}
&\overset{[575,\text{ p. }165]}{=} \cos(\phi_1)\cos(\phi_2)\left[\frac{\sin\left((\omega_1-\omega_2)\left(t+\frac{2\pi}{\omega}\right)\right)}{2(\omega_1-\omega_2)}+\frac{\sin\left((\omega_1+\omega_2)\left(t+\frac{2\pi}{\omega}\right)\right)}{2(\omega_1+\omega_2)}\right]\\
&\quad-\cos(\phi_1)\sin(\phi_2)\left[\frac{\cos\left((\omega_1-\omega_2)\left(t+\frac{2\pi}{\omega}\right)\right)}{2(\omega_1-\omega_2)}-\frac{\cos\left((\omega_1+\omega_2)\left(t+\frac{2\pi}{\omega}\right)\right)}{2(\omega_1+\omega_2)}\right]\\
&\quad-\cos(\phi_1)\cos(\phi_2)\left[\frac{\sin\left((\omega_1-\omega_2)t\right)}{2(\omega_1-\omega_2)}+\frac{\sin\left((\omega_1+\omega_2)t\right)}{2(\omega_1+\omega_2)}\right]\\
&\quad+\cos(\phi_1)\sin(\phi_2)\left[\frac{\cos\left((\omega_1-\omega_2)t\right)}{2(\omega_1-\omega_2)}-\frac{\cos\left((\omega_1+\omega_2)t\right)}{2(\omega_1+\omega_2)}\right]\\
&\quad+\sin(\phi_1)\cos(\phi_2)\left[\frac{\cos\left((\omega_1-\omega_2)\left(t+\frac{2\pi}{\omega}\right)\right)}{2(\omega_1-\omega_2)}+\frac{\cos\left((\omega_1+\omega_2)\left(t+\frac{2\pi}{\omega}\right)\right)}{2(\omega_1+\omega_2)}\right]\\
&\quad+\sin(\phi_1)\sin(\phi_2)\left[\frac{\sin\left((\omega_1-\omega_2)\left(t+\frac{2\pi}{\omega}\right)\right)}{2(\omega_1-\omega_2)}-\frac{\sin\left((\omega_1+\omega_2)\left(t+\frac{2\pi}{\omega}\right)\right)}{2(\omega_1+\omega_2)}\right]\\
&\quad-\sin(\phi_1)\cos(\phi_2)\left[\frac{\cos\left((\omega_1-\omega_2)t\right)}{2(\omega_1-\omega_2)}+\frac{\cos\left((\omega_1+\omega_2)t\right)}{2(\omega_1+\omega_2)}\right]\\
&\quad-\sin(\phi_1)\sin(\phi_2)\left[\frac{\sin\left((\omega_1-\omega_2)t\right)}{2(\omega_1-\omega_2)}-\frac{\sin\left((\omega_1+\omega_2)t\right)}{2(\omega_1+\omega_2)}\right]\\
&\overset{(2.3)}{=} -\cos(\phi_1)\frac{\sin\left(\phi_2-(\omega_1-\omega_2)\left(t+\frac{2\pi}{\omega}\right)\right)}{2(\omega_1-\omega_2)}+\cos(\phi_1)\frac{\sin\left(\phi_2+(\omega_1+\omega_2)\left(t+\frac{2\pi}{\omega}\right)\right)}{2(\omega_1+\omega_2)}\\
&\quad+\cos(\phi_1)\frac{\sin\left(\phi_2-(\omega_1-\omega_2)t\right)}{2(\omega_1-\omega_2)}-\cos(\phi_1)\frac{\sin\left(\phi_2+(\omega_1+\omega_2)t\right)}{2(\omega_1+\omega_2)}\\
&\quad+\sin(\phi_1)\frac{\cos\left(\phi_2-(\omega_1-\omega_2)\left(t+\frac{2\pi}{\omega}\right)\right)}{2(\omega_1-\omega_2)}+\sin(\phi_1)\frac{\cos\left(\phi_2+(\omega_1+\omega_2)\left(t+\frac{2\pi}{\omega}\right)\right)}{2(\omega_1+\omega_2)}\\
&\quad-\sin(\phi_1)\frac{\cos\left(\phi_2-(\omega_1-\omega_2)t\right)}{2(\omega_1-\omega_2)}-\sin(\phi_1)\frac{\cos\left(\phi_2+(\omega_1+\omega_2)t\right)}{2(\omega_1+\omega_2)}\\
&\overset{(2.3)}{=} \frac{\sin\left(\phi_1-\phi_2+(\omega_1-\omega_2)\left(t+\frac{2\pi}{\omega}\right)\right)}{2(\omega_1-\omega_2)}-\frac{\sin\left(\phi_1-\phi_2+(\omega_1-\omega_2)t\right)}{2(\omega_1-\omega_2)}\\
&\quad+\frac{\sin\left(\phi_1+\phi_2+(\omega_1+\omega_2)\left(t+\frac{2\pi}{\omega}\right)\right)}{2(\omega_1+\omega_2)}-\frac{\sin\left(\phi_1+\phi_2+(\omega_1+\omega_2)t\right)}{2(\omega_1+\omega_2)}.
\end{aligned}
\tag{2.9}
$$

Setting $\omega = \omega_1 - \omega_2$ simplifies (2.9) to

$$
\int_t^{t+\frac{2\pi}{\omega_1-\omega_2}} \cos(\omega_1\tau+\phi_1)\cos(\omega_2\tau+\phi_2)\,\mathrm{d}\tau = \frac{\sin\left(\phi_1+\phi_2+(\omega_1+\omega_2)\left(t+\frac{2\pi}{\omega}\right)\right)-\sin\left(\phi_1+\phi_2+(\omega_1+\omega_2)t\right)}{2(\omega_1+\omega_2)} \tag{2.10}
$$

what shows the first part of assertion (2.8).
Setting $\omega_1 = \omega_2$ instead, (2.9) can be simplified to

$$
\lim_{\omega_2\to\omega_1} \int_t^{t+\frac{2\pi}{\omega}} \cos(\omega_1\tau+\phi_1)\cos(\omega_2\tau+\phi_2)\,\mathrm{d}\tau
$$

$$
\begin{aligned}
&\overset{(2.9)}{=} && \lim_{\omega_2\to\omega_1} \frac{\sin\Big(\phi_1-\phi_2+(\omega_1-\omega_2)\big(t+\frac{2\pi}{\omega}\big)\Big)-\sin\big(\phi_1-\phi_2+(\omega_1-\omega_2)t\big)}{2(\omega_1-\omega_2)} \\
& && +\frac{\sin\Big(\phi_1+\phi_2+(\omega_1+\omega_2)\big(t+\frac{2\pi}{\omega}\big)\Big)-\sin\big(\phi_1+\phi_2+(\omega_1+\omega_2)t\big)}{2(\omega_1+\omega_2)} \\
&\overset{[575,\text{ p. }130]}{=} && \lim_{\omega_2\to\omega_1} \frac{\big(t+\frac{2\pi}{\omega}\big)\cos\Big(\phi_1-\phi_2+(\omega_1-\omega_2)\big(t+\frac{2\pi}{\omega}\big)\Big)-t\cos\big(\phi_1-\phi_2+(\omega_1-\omega_2)t\big)}{2} \\
& && +\frac{\sin\Big(\phi_1+\phi_2+2\omega_1\big(t+\frac{2\pi}{\omega}\big)\Big)-\sin\big(\phi_1+\phi_2+2\omega_1 t\big)}{4\omega_1} \\
&= && \tfrac{\pi}{\omega}\cos(\phi_1-\phi_2)+\frac{\sin\Big(\phi_1+\phi_2+2\omega_1\big(t+\frac{2\pi}{\omega}\big)\Big)-\sin\big(\phi_1+\phi_2+2\omega_1 t\big)}{4\omega_1}. \qquad (2.11)
\end{aligned}
$$

With the choice $\omega = \omega_1 = \omega_2$, (2.11) can be simplified to

$$
\int_t^{t+\frac{2\pi}{\omega}} \cos(\omega\tau+\phi_1)\cos(\omega\tau+\phi_2)\,\mathrm{d}\tau = \tfrac{\pi}{\omega}\cos(\phi_1-\phi_2). \qquad (2.12)
$$

This completes the proof. □

Claim 2.7. *Define the physical unit function $\mathcal{U}$ that returns the physical unit* U *of an expression e, i.e. $\mathcal{U}(e) = \mathrm{U}$. Further consider a exponentially stable dynamical system*

$$
\forall\, t \geq t_0 \in \mathbb{R}\colon \quad \tfrac{\mathrm{d}}{\mathrm{d}t}\widehat{\boldsymbol{x}} = \boldsymbol{f}(\widehat{\boldsymbol{x}}, \boldsymbol{x}, \boldsymbol{L}), \qquad \widehat{\boldsymbol{x}}(t_0) = \widehat{\boldsymbol{x}}_0 \qquad (2.13)
$$

with estimates $\widehat{\boldsymbol{x}} = (\widehat{x}_1, \ldots, \widehat{x}_n)^\top \in \mathbb{R}^n$ of generating states $\boldsymbol{x} \in \mathbb{R}^n$ and system gain $\boldsymbol{L} \in \mathbb{R}^{n\times n}$, $n \in \mathbb{N}$. The generating states model a sinusoidal signal characterized by angular frequencies $\boldsymbol{\omega}$, amplitudes $\boldsymbol{a}$ and (unitless) phase angles $\boldsymbol{\varphi}$.
It is claimed that the settling time t_{set} of (2.13) is (approximately) proportional to some linear map in $\boldsymbol{\omega}$ and independent of $\boldsymbol{a}$, if and only if $\boldsymbol{L}$ is chosen as $\boldsymbol{L} \neq \boldsymbol{L}(\boldsymbol{x})$ such that for every $i \in \{1, \ldots, n\}$ it holds that

$$
\mathcal{U}\big(f_i(\widehat{\boldsymbol{x}}, \boldsymbol{x}, \boldsymbol{L})\big) = \mathcal{U}(x_i)\mathcal{U}(\omega).
$$

Fact 2.8 (Lyapunov identity). *[577, Corollary 3.3.47] Let $\boldsymbol{A} \in \mathbb{R}^{n\times n}$ be Hurwitz. Then, for any given $0 < \boldsymbol{Q} = \boldsymbol{Q}^\top \in \mathbb{R}^{n\times n}$ there exists a $0 < \boldsymbol{P} = \boldsymbol{P}^\top \in \mathbb{R}^{n\times n}$ such that*

$$
\boldsymbol{A}^\top\boldsymbol{P} + \boldsymbol{P}\boldsymbol{A} = -\boldsymbol{Q}. \qquad (2.14)
$$

Fact 2.9 (Scalar inequalities). *Let $a, b \in \mathbb{R}$ and let $m \in \mathbb{R}_{>0}$. Then, the following is true:*

$$
2ab = \tfrac{a^2}{m} + mb^2 - \left(\tfrac{a}{\sqrt{m}} - \sqrt{m}b\right)^2 \leq \tfrac{a^2}{m} + mb^2. \qquad (2.15)
$$

Further, let $\boldsymbol{a} \in \mathbb{R}^n$ and $\boldsymbol{A} = \boldsymbol{A}^\top \in \mathbb{R}^{n\times n}$ where $\lambda_{\min}(\boldsymbol{A}), \lambda_{\max}(\boldsymbol{A}) \in \mathbb{R}$[1] denote the minimal and maximal eigenvalues of $\boldsymbol{A}$. Then, the following holds:

$$
\lambda_{\min}(\boldsymbol{A})\,\|\boldsymbol{a}\|^2 \leq \boldsymbol{a}^\top\boldsymbol{A}\boldsymbol{a} \leq \lambda_{\max}(\boldsymbol{A})\,\|\boldsymbol{a}\|^2. \qquad (2.16)
$$

[1] The eigenvalues of a hermitian matrix are always real [575, p. 112].

Fact 2.10 (Bellman-Gronwall-Lemma (differential form)). *[578] For $t_0 < t_1 \in \mathbb{R}$, let $f(\cdot), g(\cdot) \in \mathcal{C}([t_0, t_1); \mathbb{R})$ and let $h(\cdot) \in \mathcal{C}^1([t_0, t_1); \mathbb{R})$. Then, if*

$$\forall\, t \in [t_0, t_1): \quad \tfrac{\mathrm{d}}{\mathrm{d}t} h(t) \leq g(t) + f(t)h(t)$$

is satisfied, the following holds:

$$\forall\, t \in [t_0, t_1): \quad h(t) \leq h(t_0)\mathrm{e}^{\int_{t_0}^{t} f(\tau)\mathrm{d}\tau} + \int_{t_0}^{t} g(\tau)\mathrm{e}^{\int_{\tau}^{t} f(\iota)\mathrm{d}\iota}\mathrm{d}\tau. \tag{2.17}$$

Observation 2.11 (Summation I). *Let $\kappa_1, \kappa_2, \ldots, \kappa_n \in \mathbb{C}$. Further let $\mathbb{K} := \{k_1, \ldots, k_l\} \subseteq \{1, \ldots, n\} \subseteq \mathbb{N}$, $l := |\mathbb{K}|$ and $j \in \mathbb{N}$. Then, the following holds:*

$$\prod_{\substack{i=1 \\ i \notin \mathbb{K}}}^{n} (\kappa_j - \kappa_i) = \kappa_j^{n-l} - \kappa_j^{n-l-1} \sum_{\substack{i=1 \\ i \notin \mathbb{K}}}^{n} \kappa_i + \cdots + (-1)^{n-l+1} \kappa_j \sum_{\substack{i=1 \\ i \notin \mathbb{K}}}^{n} \prod_{\substack{h=1 \\ h \notin i, \mathbb{K}}}^{n} \kappa_h + (-1)^{n-l} \prod_{\substack{i=1 \\ i \notin \mathbb{K}}}^{n} \kappa_i. \tag{2.18}$$

Proof. The proof is conducted via mathematical induction.
Initial case. For $n = 1$ and $\mathbb{K} = \varnothing$ it follows

$$\prod_{\substack{i=1 \\ i \notin \varnothing}}^{1} (\kappa_j - \kappa_i) = \kappa_j - \kappa_1 \quad \text{and} \quad \kappa_j^{1-0} + (-1)^{1-0} \prod_{\substack{i=1 \\ i \notin \varnothing}}^{1} \kappa_j = \kappa_j - \kappa_1.$$

Induction step. Observe that the following holds

$$\begin{aligned}
&\prod_{\substack{i=1 \\ i \notin \mathbb{K}}}^{n+1} (\kappa_j - \kappa_i) = (\kappa_j - \kappa_{n+1}) \prod_{\substack{i=1 \\ i \notin \mathbb{K}}}^{n} (\kappa_j - \kappa_i) \\
\overset{(2.18)}{=}\; & (\kappa_j - \kappa_{n+1}) \left(\kappa_j^{n-l} - \kappa_j^{n-l-1} \sum_{\substack{i=1 \\ i \notin \mathbb{K}}}^{n} \kappa_i + \cdots + (-1)^{n-l+1} \kappa_j \sum_{\substack{i=1 \\ i \notin \mathbb{K}}}^{n} \prod_{\substack{h=1 \\ h \notin i, \mathbb{K}}}^{n} \kappa_h + (-1)^{n-l} \prod_{\substack{i=1 \\ i \notin \mathbb{K}}}^{n} \kappa_i \right) \\
=\; & \kappa_j^{n-l+1} - \kappa_j^{n-l} \sum_{\substack{i=1 \\ i \notin \mathbb{K}}}^{n} \kappa_i + \cdots + (-1)^{n-l} \kappa_j \prod_{\substack{i=1 \\ i \notin \mathbb{K}}}^{n} \kappa_i \\
& - \kappa_j^{n-l} \kappa_{n+1} - \cdots - (-1)^{n-l+1} \kappa_j \kappa_{n+1} \sum_{\substack{i=1 \\ i \notin \mathbb{K}}}^{n} \prod_{\substack{h=1 \\ h \notin i, \mathbb{K}}}^{n} \kappa_h - (-1)^{n-l} \kappa_{n+1} \prod_{\substack{i=1 \\ i \notin \mathbb{K}}}^{n} \kappa_i \\
=\; & \kappa_j^{(n+1)-l} - \kappa_j^{(n+1)-l-1} \sum_{\substack{i=1 \\ i \notin \mathbb{K}}}^{n+1} \kappa_i + \cdots + (-1)^{(n+1)-l+1} \kappa_j \sum_{\substack{i=1 \\ i \notin \mathbb{K}}}^{n+1} \prod_{\substack{h=1 \\ h \notin i, \mathbb{K}}}^{n+1} \kappa_h + (-1)^{(n+1)-l} \prod_{\substack{i=1 \\ i \notin \mathbb{K}}}^{n+1} \kappa_i.
\end{aligned}$$

This completes the proof. □

Note 2.12. *Let $\kappa_1, \kappa_2, \ldots, \kappa_n \in \mathbb{C}$. Further let $\mathbb{K} := \{k_1, \ldots, k_l\} \subseteq \{1, \ldots, n\} \subseteq \mathbb{N}$, $l := |\mathbb{K}|$ and $j \in \mathbb{N}$. In view of the definition in the Nomenclature, the following holds:*

$$\sum_{i=1}^{n-l+1} (-\kappa_j)^{i-1} \sum_{h_1 < h_{n-l+1-i} = 1 \setminus \mathbb{K}}^{n} \prod_{k \in h} \kappa_k \overset{(2.18)}{=} \prod_{\substack{i=1 \\ i \notin \mathbb{K}}}^{n} (\kappa_i - \kappa_j). \tag{2.19}$$

Observation 2.13 (Summation II). *Let $n \in \mathbb{N}$, $\kappa_1, \ldots, \kappa_n, \upsilon_1, \ldots, \upsilon_n \in \mathbb{C}$ and $c, r \in \{1, \ldots, n\}$. Then, the following holds:*

$$\sum_{i=1}^{n} \sum_{j_1 < j_{n-i} = 1 \setminus r}^{n} \prod_{k \in j} \kappa_k^2 \sum_{l \in j} \frac{\upsilon_l}{\kappa_l} (-\kappa_c^2)^{i-1} = \sum_{\substack{j=1 \\ j \neq r}}^{n} \kappa_j \upsilon_j \prod_{\substack{k=1 \\ k \neq r,j}}^{n} \left(\kappa_k^2 - \kappa_c^2\right). \tag{2.20}$$

Proof. The proof is conducted via mathematical induction.
Firstly, note that the following is true:

$$\sum_{i=1}^{n} \sum_{j_1 < j_{n-i} = 1 \setminus r}^{n} \prod_{k \in j} \kappa_k^2 \sum_{l \in j} \frac{\upsilon_l}{\kappa_l} (-\kappa_c^2)^{i-1} = \sum_{i=1}^{n} \sum_{j_1 < j_{n-i} = 1 \setminus r}^{n} \sum_{l \in j} \kappa_l \upsilon_l \prod_{k \in j \setminus l} \kappa_k^2 (-\kappa_c^2)^{i-1}.$$

Initial case. For $n = 1$ it follows

$$\sum_{i=1}^{1} \sum_{j_1 < j_{1-i} = 1 \setminus 1}^{1} \sum_{l \in j} \kappa_l \upsilon_l \prod_{k \in j \setminus l} \kappa_k^2 (-\kappa_1^2)^{i-1} = 0 \quad \text{and} \quad \sum_{\substack{j=1 \\ j \neq 1}}^{1} \kappa_j \upsilon_j \prod_{\substack{k=1 \\ k \neq 1,j}}^{1} \left(\kappa_k^2 - \kappa_1^2\right) = 0.$$

Induction step. Observe that the following holds

$$\begin{aligned}
& \sum_{i=1}^{n+1} \sum_{j_1 < j_{n+1-i} = 1 \setminus r}^{n+1} \sum_{l \in j} \kappa_l \upsilon_l \prod_{k \in j \setminus l} \kappa_k^2 (-\kappa_c^2)^{i-1} \\
= \quad & \sum_{i=1}^{n} \sum_{j_1 < j_{n+1-i} = 1 \setminus r}^{n+1} \sum_{l \in j} \kappa_l \upsilon_l \prod_{k \in j \setminus l} \kappa_k^2 (-\kappa_c^2)^{i-1} + \underbrace{\sum_{j_1 < j_0 = 1 \setminus r}^{n+1} \sum_{l \in j} \kappa_l \upsilon_l \prod_{k \in j \setminus l} \kappa_k^2 (-\kappa_c^2)^{n}}_{=0} \\
= \quad & \sum_{i=1}^{n} \sum_{j_1 < j_{n+1-i} = 1 \setminus r}^{n} \sum_{l \in j} \kappa_l \upsilon_l \prod_{k \in j \setminus l} \kappa_k^2 (-\kappa_c^2)^{i-1} \\
& + \kappa_{n+1}^2 \sum_{i=1}^{n} \sum_{j_1 < j_{n-i} = 1 \setminus r}^{n} \sum_{l \in j} \kappa_l \upsilon_l \prod_{k \in j \setminus l} \kappa_k^2 (-\kappa_c^2)^{i-1} \\
& + \kappa_{n+1} \upsilon_{n+1} \sum_{i=1}^{n} \sum_{j_1 < j_{n-i} = 1 \setminus r}^{n} \prod_{k \in j} \kappa_k^2 (-\kappa_c^2)^{i-1} \\
\overset{(2.19),\,(2.20)}{=} \quad & -\kappa_c^2 \sum_{i=2}^{n} \sum_{j_1 < j_{n+1-i} = 1 \setminus r}^{n} \sum_{l \in j} \kappa_l \upsilon_l \prod_{k \in j \setminus l} \kappa_k^2 (-\kappa_c^2)^{i-2} + \underbrace{\sum_{j_1 < j_n = 1 \setminus r}^{n} \sum_{l \in j} \kappa_l \upsilon_l \prod_{k \in j \setminus l} \kappa_k^2}_{=0} \\
& + \kappa_{n+1}^2 \sum_{\substack{j=1 \\ j \neq r}}^{n} \kappa_j \upsilon_j \prod_{\substack{k=1 \\ k \neq r,j}}^{n} \left(\kappa_k^2 - \kappa_c^2\right) + \kappa_{n+1} \upsilon_{n+1} \prod_{\substack{k=1 \\ k \neq r}}^{n} \left(\kappa_k^2 - \kappa_c^2\right) \\
= \quad & -\kappa_c^2 \sum_{i=1}^{n-1} \sum_{j_1 < j_{n-i} = 1 \setminus r}^{n} \sum_{l \in j} \kappa_l \upsilon_l \prod_{k \in j \setminus l} \kappa_k^2 (-\kappa_c^2)^{i-1} - \kappa_c^2 \underbrace{\sum_{j_1 < j_0 = 1 \setminus r}^{n} \sum_{l \in j} \kappa_l \upsilon_l \prod_{k \in j \setminus l} \kappa_k^2 (-\kappa_c^2)^{n-1}}_{=0}
\end{aligned}$$

$$
\begin{aligned}
&\quad +\kappa_{n+1}^2 \sum_{\substack{j=1\\ j\neq r}}^{n} \kappa_j \upsilon_j \prod_{\substack{k=1\\ k\neq r,j}}^{n} \left(\kappa_k^2 - \kappa_c^2\right) + \kappa_{n+1}\upsilon_{n+1} \prod_{\substack{k=1\\ k\neq r}}^{n} \left(\kappa_k^2 - \kappa_c^2\right)\\
&= -\kappa_c^2 \sum_{i=1}^{n} \sum_{j_1<j_{n-i}=1\setminus r}^{n} \sum_{l\in j} \kappa_l \upsilon_l \prod_{k\in j\setminus l} \kappa_k^2 (-\kappa_c^2)^{i-1}\\
&\quad +\kappa_{n+1}^2 \sum_{\substack{j=1\\ j\neq r}}^{n} \kappa_j \upsilon_j \prod_{\substack{k=1\\ k\neq r,j}}^{n} \left(\kappa_k^2 - \kappa_c^2\right) + \kappa_{n+1}\upsilon_{n+1} \prod_{\substack{k=1\\ k\neq r}}^{n} \left(\kappa_k^2 - \kappa_c^2\right)\\
&\overset{(2.20)}{=} -\kappa_c^2 \sum_{\substack{j=1\\ j\neq r}}^{n} \kappa_j \upsilon_j \prod_{\substack{k=1\\ k\neq r,j}}^{n} \left(\kappa_k^2 - \kappa_c^2\right) + \kappa_{n+1}^2 \sum_{\substack{j=1\\ j\neq r}}^{n} \kappa_j \upsilon_j \prod_{\substack{k=1\\ k\neq r,j}}^{n} \left(\kappa_k^2 - \kappa_c^2\right) + \kappa_{n+1}\upsilon_{n+1} \prod_{\substack{k=1\\ k\neq r}}^{n} \left(\kappa_k^2 - \kappa_c^2\right)\\
&= \sum_{\substack{j=1\\ j\neq r}}^{n} \kappa_j \upsilon_j \prod_{\substack{k=1\\ k\neq r,j}}^{n+1} \left(\kappa_k^2 - \kappa_c^2\right) + \kappa_{n+1}\upsilon_{n+1} \prod_{\substack{k=1\\ k\neq r,n+1}}^{n+1} \left(\kappa_k^2 - \kappa_c^2\right) = \sum_{\substack{j=1\\ j\neq r}}^{n+1} \kappa_j \upsilon_j \prod_{\substack{k=1\\ k\neq r,j}}^{n+1} \left(\kappa_k^2 - \kappa_c^2\right).
\end{aligned}
$$

This completes the proof. □

Claim 2.14. *Let $n \in \mathbb{N}$ and $\kappa_1, \ldots, \kappa_n \in \mathbb{C}$. Then, the following is claimed:*

$$
\sum_{i=1}^{n} (-1)^{i+n} \prod_{\substack{k=1\\ k\neq i}}^{n} \kappa_k \prod_{k_1<k_2=1\setminus i}^{n} \left(\kappa_{k_1} - \kappa_{k_2}\right) = \prod_{k_1<k_2=1}^{n} \left(\kappa_{k_1} - \kappa_{k_2}\right). \tag{2.21}
$$

Observation 2.15 (Summation III). *Let $n \in \mathbb{N}$, $\kappa_1, \ldots, \kappa_n \in \mathbb{C}$ and $c \in \{1, \ldots, n\}$. Then, the following holds:*

$$
\sum_{\substack{i=1\\ i\neq c}}^{n} \left(\frac{1}{\kappa_i - \kappa_c} - \frac{\kappa_c \prod\limits_{\substack{k=1\\ k\neq c,i}}^{n} (\kappa_c - \kappa_k)}{\kappa_i \prod\limits_{\substack{k=1\\ k\neq i}}^{n} (\kappa_i - \kappa_k)} \right) - \frac{1}{\kappa_c} = -\frac{\prod\limits_{\substack{k=1\\ k\neq c}}^{n} (\kappa_k - \kappa_c)}{\prod\limits_{k=1}^{n} \kappa_k}. \tag{2.22}
$$

Proof. The proof is conducted via mathematical induction.
Initial case. For $n = 1$ it follows

$$
\sum_{\substack{i=1\\ i\neq 1}}^{1} \left(\frac{1}{\kappa_i - \kappa_1} - \frac{\kappa_1 \prod\limits_{\substack{k=1\\ k\neq 1,i}}^{1} (\kappa_1 - \kappa_k)}{\kappa_i \prod\limits_{\substack{k=1\\ k\neq i}}^{1} (\kappa_i - \kappa_k)} \right) - \frac{1}{\kappa_1} = -\frac{1}{\kappa_1} \quad \text{and} \quad -\frac{\prod\limits_{\substack{k=1\\ k\neq 1}}^{n} (\kappa_k - \kappa_1)}{\prod\limits_{k=1}^{n} \kappa_k} = -\frac{1}{\kappa_1}.
$$

Induction step. Observe that the following holds

$$
\begin{aligned}
&\sum_{\substack{i=1\\ i\neq c}}^{n+1} \left(\frac{1}{\kappa_i - \kappa_c} - \frac{\kappa_c \prod\limits_{\substack{k=1\\ k\neq c,i}}^{n+1} (\kappa_c - \kappa_k)}{\kappa_i \prod\limits_{\substack{k=1\\ k\neq i}}^{n+1} (\kappa_i - \kappa_k)} \right) - \frac{1}{\kappa_c}\\
&= \sum_{\substack{i=1\\ i\neq c}}^{n} \left(\frac{1}{\kappa_i - \kappa_c} - \frac{\kappa_c - \kappa_{n+1}}{\kappa_i - \kappa_{n+1}} \frac{\kappa_c \prod\limits_{\substack{k=1\\ k\neq c,i}}^{n} (\kappa_c - \kappa_k)}{\kappa_i \prod\limits_{\substack{k=1\\ k\neq i}}^{n} (\kappa_i - \kappa_k)} \right) - \frac{1}{\kappa_c} + \frac{1}{\kappa_{n+1} - \kappa_c} - \frac{\kappa_c \prod\limits_{\substack{k=1\\ k\neq c}}^{n} (\kappa_c - \kappa_k)}{\kappa_{n+1} \prod\limits_{k=1}^{n} (\kappa_{n+1} - \kappa_k)}
\end{aligned}
$$

$$= \sum_{\substack{i=1\\i\neq c}}^{n}\left(\frac{1}{\kappa_i-\kappa_c} - \frac{\kappa_c\prod\limits_{\substack{k=1\\k\neq c,i}}^{n}(\kappa_c-\kappa_k)}{\kappa_i\prod\limits_{\substack{k=1\\k\neq i}}^{n}(\kappa_i-\kappa_k)}\right) - \frac{1}{\kappa_c} - \sum_{\substack{i=1\\i\neq c}}^{n}\frac{\kappa_c\prod\limits_{\substack{k=1\\k\neq c}}^{n}(\kappa_c-\kappa_k)}{\kappa_i\prod\limits_{\substack{k=1\\k\neq i}}^{n+1}(\kappa_i-\kappa_k)} + \frac{1}{\kappa_{n+1}-\kappa_c} - \frac{\kappa_c\prod\limits_{\substack{k=1\\k\neq c}}^{n}(\kappa_c-\kappa_k)}{\kappa_{n+1}\prod\limits_{k=1}^{n}(\kappa_{n+1}-\kappa_k)}$$

$$\overset{(2.22)}{=} -\frac{\prod\limits_{\substack{k=1\\k\neq c}}^{n}(\kappa_k-\kappa_c)}{\prod\limits_{k=1}^{n}\kappa_k} - \sum_{i=1}^{n+1}\frac{\kappa_c\prod\limits_{\substack{k=1\\k\neq c}}^{n}(\kappa_c-\kappa_k)}{\kappa_i\prod\limits_{\substack{k=1\\k\neq i}}^{n+1}(\kappa_i-\kappa_k)}$$

$$= -\frac{\prod\limits_{\substack{k=1\\k\neq c}}^{n}(\kappa_k-\kappa_c)}{\prod\limits_{k=1}^{n}\kappa_k} - \frac{\kappa_c\prod\limits_{\substack{k=1\\k\neq c}}^{n}(\kappa_k-\kappa_c)\sum\limits_{i=1}^{n+1}(-1)^{i+n}\prod\limits_{\substack{k=1\\k\neq i}}^{n+1}\kappa_k\prod\limits_{k_1<k_2=1\setminus i}^{n+1}\left(\kappa_{k_1}-\kappa_{k_2}\right)}{\prod\limits_{k=1}^{n+1}\kappa_k\prod\limits_{k_1<k_2=1}^{n+1}\left(\kappa_{k_1}-\kappa_{k_2}\right)}$$

$$\overset{(2.21)}{=} -\frac{\kappa_{n+1}\prod\limits_{\substack{k=1\\k\neq c}}^{n}(\kappa_k-\kappa_c)}{\prod\limits_{k=1}^{n+1}\kappa_k} + \frac{\kappa_c\prod\limits_{\substack{k=1\\k\neq c}}^{n}(\kappa_k-\kappa_c)\prod\limits_{k_1<k_2=1}^{n+1}\left(\kappa_{k_1}-\kappa_{k_2}\right)}{\prod\limits_{k=1}^{n+1}\kappa_k\prod\limits_{k_1<k_2=1}^{n+1}\left(\kappa_{k_1}-\kappa_{k_2}\right)} = \frac{(-\kappa_{n+1}+\kappa_c)\prod\limits_{\substack{k=1\\k\neq c}}^{n}(\kappa_k-\kappa_c)}{\prod\limits_{k=1}^{n+1}\kappa_k} = -\frac{\prod\limits_{\substack{k=1\\k\neq c}}^{n+1}(\kappa_k-\kappa_c)}{\prod\limits_{k=1}^{n+1}\kappa_k}.$$

This completes the proof. □

Fact 2.16 (Strictly positive realness). *[579, p. 127, Theorem 3.5.1] Let $\mathcal{G}(s)$ be a rational transfer function with relative degree $|rd\,(\mathcal{G}(s))| \leq 1$*[2] *taking on real values for real s and not being identically zero for all s. Then, the transfer function $\mathcal{G}(s)$ is* strictly positive real *if and only if the following conditions are satisfied:*

(i) $\mathcal{G}(s)$ *is analytic in* $\Re(s) \geq 0$,

(ii) $\forall\,\omega \in \mathbb{R}\colon \Re(\mathcal{G}(\jmath\omega)) > 0$ *and*

$$(iii)\quad \begin{cases} \lim\limits_{|\omega|\to\infty} \omega^2\Re(\mathcal{G}(\jmath\omega)) > 0, & rd\,(\mathcal{G}(s)) = 1 \text{ or} \\ \lim\limits_{|\omega|\to\infty} \frac{\Re(\mathcal{G}(\jmath\omega))}{\jmath\omega} > 0, & rd\,(\mathcal{G}(s)) = -1. \end{cases}$$

Fact 2.17 (Meyer-Kalman-Yakubovich-Lemma). *[579, p. 129f, Lemma 3.5.4] Let $n \in \mathbb{N}$, $\boldsymbol{A} \in \mathbb{R}^{n\times n}$ be Hurwitz, $\boldsymbol{b}, \boldsymbol{c} \in \mathbb{R}^n$ and $d \in \mathbb{R}$ and let $\mathcal{G}(s) := d + \boldsymbol{c}^\top(s\boldsymbol{I} - \boldsymbol{A})^{-1}\boldsymbol{b}$ be strictly positive real. Then, for any given $0 < \boldsymbol{Q} = \boldsymbol{Q}^\top \in \mathbb{R}^{n\times n}$, there exists $0 < q \in \mathbb{R}$, $\boldsymbol{q} \in \mathbb{R}^n$ and $0 < \boldsymbol{P} = \boldsymbol{P}^\top \in \mathbb{R}^{n\times n}$ such that*

$$\boldsymbol{A}^\top\boldsymbol{P} + \boldsymbol{P}\boldsymbol{A} = -\boldsymbol{q}\boldsymbol{q}^\top - q\boldsymbol{Q} \quad \text{and} \quad \boldsymbol{P}\boldsymbol{b} - \boldsymbol{c} = \pm\boldsymbol{q}\sqrt{2d}. \tag{2.23}$$

Fact 2.18 (Invariance principle of LaSalle). *[580] Let $\boldsymbol{\alpha}_0 = \boldsymbol{0}_n, n \in \mathbb{N}$ be an equilibrium of $\frac{\mathrm{d}}{\mathrm{d}t}\boldsymbol{\alpha} = f(\boldsymbol{\alpha})$ (i.e. $f(\boldsymbol{\alpha}_0) = \boldsymbol{0}_n$) and let, for $\beta \in \mathbb{R}_{>0}$ and $\gamma \in \mathbb{R}_{<0}$, $V\colon \mathbb{R}^n \mapsto [0,\beta]$ be positive definite and let $\frac{\mathrm{d}}{\mathrm{d}t}V\colon \mathbb{R}^n \mapsto [0,\gamma]$ be negative semi-definite. Then, $\boldsymbol{\alpha}_0$ is locally asymptotic stable if the largest positive invariant subset $\mathbb{M}$ of $\mathbb{S} := \left\{\boldsymbol{\alpha} \in \mathbb{R}^n \middle|\, \frac{\mathrm{d}}{\mathrm{d}t}V(\boldsymbol{\alpha}) = 0\right\}$ is $\mathbb{M} = \{\boldsymbol{0}_n\}$. Moreover, if $V(\boldsymbol{\alpha})$ is unbounded, i.e. $\beta \to \infty$, $\boldsymbol{\alpha}_0$ is globally asymptotic stable.*

[2] A function $f(x)$ is called *rational*, if it can be written as a fraction of two polynomial functions: $f(x) = \frac{n(x)}{d(x)}$. Its relative degree is defined as the difference between the degrees of the denominator and nominator polynomial, i.e. $\mathrm{rd}\,(f) := \deg(d) - \deg(n)$.

Observation 2.19 (Time derivative of matrix exponential with time dependent matrix)**.** *Let $n \in \mathbb{N}$ and let $\boldsymbol{A} \in \mathbb{R}^{n\times n}$ be time dependent and invertible. If a decomposition*

$$\boldsymbol{A}(t) = \boldsymbol{V}\boldsymbol{D}(t)\boldsymbol{V}^{-1}, \tag{2.24}$$

exists with $\boldsymbol{V}$ being constant and $\boldsymbol{D}$ being in diagonal (or Jordan normal) form, the following holds true:

$$\tfrac{\mathrm{d}}{\mathrm{d}t}\mathrm{e}^{\boldsymbol{A}(t)t} = \mathrm{e}^{\boldsymbol{A}(t)t}\big(\boldsymbol{A}(t) + t\tfrac{\mathrm{d}}{\mathrm{d}t}\boldsymbol{A}(t)\big). \tag{2.25}$$

Proof. First of all, the argument t is dropped. Observe that

$$\begin{aligned}
\tfrac{\mathrm{d}}{\mathrm{d}t}\mathrm{e}^{\boldsymbol{A}t} &= \tfrac{\mathrm{d}}{\mathrm{d}t}\sum_{k=0}^{\infty}\tfrac{\boldsymbol{A}^k t^k}{k!} = \sum_{k=1}^{\infty}\tfrac{\boldsymbol{A}^k t^{k-1}}{(k-1)!} + \tfrac{\frac{\mathrm{d}}{\mathrm{d}t}\boldsymbol{A}t}{1!} + \tfrac{(\frac{\mathrm{d}}{\mathrm{d}t}\boldsymbol{A}\boldsymbol{A}+\boldsymbol{A}\frac{\mathrm{d}}{\mathrm{d}t}\boldsymbol{A})t^2}{2!}\\
&+ \tfrac{(\frac{\mathrm{d}}{\mathrm{d}t}\boldsymbol{A}\boldsymbol{A}^2+\boldsymbol{A}\frac{\mathrm{d}}{\mathrm{d}t}\boldsymbol{A}\boldsymbol{A}+\boldsymbol{A}^2\frac{\mathrm{d}}{\mathrm{d}t}\boldsymbol{A})t^3}{3!} + \tfrac{(\frac{\mathrm{d}}{\mathrm{d}t}\boldsymbol{A}\boldsymbol{A}^3+\boldsymbol{A}\frac{\mathrm{d}}{\mathrm{d}t}\boldsymbol{A}\boldsymbol{A}^2+\boldsymbol{A}^2\frac{\mathrm{d}}{\mathrm{d}t}\boldsymbol{A}\boldsymbol{A}+\boldsymbol{A}^3\frac{\mathrm{d}}{\mathrm{d}t}\boldsymbol{A})t^4}{4!} + \cdots\\
&= \mathrm{e}^{\boldsymbol{A}t}\boldsymbol{A} + \big(\tfrac{\boldsymbol{I}_n t}{1!} + \tfrac{\boldsymbol{A}t^2}{2!} + \tfrac{\boldsymbol{A}^2t^3}{3!} + \tfrac{\boldsymbol{A}^3t^4}{4!} + \cdots\big)\tfrac{\mathrm{d}}{\mathrm{d}t}\boldsymbol{A}\\
&+ \big(\tfrac{\boldsymbol{I}_n t^2}{2!} + \tfrac{\boldsymbol{A}t^3}{3!} + \tfrac{\boldsymbol{A}^2t^4}{4!} + \cdots\big)\tfrac{\mathrm{d}}{\mathrm{d}t}\boldsymbol{A}\boldsymbol{A} + \big(\tfrac{\boldsymbol{I}_n t^3}{3!} + \tfrac{\boldsymbol{A}t^4}{4!} + \cdots\big)\tfrac{\mathrm{d}}{\mathrm{d}t}\boldsymbol{A}\boldsymbol{A}^2 + \cdots\\
&= \mathrm{e}^{\boldsymbol{A}t}\boldsymbol{A} + \big(\boldsymbol{I}_n + \tfrac{\boldsymbol{A}t}{1!} + \tfrac{\boldsymbol{A}^2t^2}{2!} + \tfrac{\boldsymbol{A}^3t^3}{3!} + \tfrac{\boldsymbol{A}^4t^4}{4!} + \cdots - \boldsymbol{I}_n\big)\boldsymbol{A}^{-1}\tfrac{\mathrm{d}}{\mathrm{d}t}\boldsymbol{A}\\
&+ \big(\boldsymbol{I}_n + \tfrac{\boldsymbol{A}t}{1!} + \tfrac{\boldsymbol{A}^2t^2}{2!} + \tfrac{\boldsymbol{A}^3t^3}{3!} + \tfrac{\boldsymbol{A}^4t^4}{4!} + \cdots - \boldsymbol{I}_n - \tfrac{\boldsymbol{A}t}{1!}\big)\boldsymbol{A}^{-2}\tfrac{\mathrm{d}}{\mathrm{d}t}\boldsymbol{A}\boldsymbol{A}\\
&+ \big(\boldsymbol{I}_n + \tfrac{\boldsymbol{A}t}{1!} + \tfrac{\boldsymbol{A}^2t^2}{2!} + \tfrac{\boldsymbol{A}^3t^3}{3!} + \tfrac{\boldsymbol{A}^4t^4}{4!} + \cdots - \boldsymbol{I}_n - \tfrac{\boldsymbol{A}t}{1!} - \tfrac{\boldsymbol{A}^2t^2}{2!}\big)\boldsymbol{A}^{-3}\tfrac{\mathrm{d}}{\mathrm{d}t}\boldsymbol{A}\boldsymbol{A}^2 + \cdots\\
&= \mathrm{e}^{\boldsymbol{A}t}\boldsymbol{A} + \big(\mathrm{e}^{\boldsymbol{A}t} - \boldsymbol{I}_n\big)\boldsymbol{A}^{-1}\tfrac{\mathrm{d}}{\mathrm{d}t}\boldsymbol{A} + \big(\mathrm{e}^{\boldsymbol{A}t} - \boldsymbol{I}_n - \tfrac{\boldsymbol{A}t}{1!}\big)\boldsymbol{A}^{-2}\tfrac{\mathrm{d}}{\mathrm{d}t}\boldsymbol{A}\boldsymbol{A}\\
&+ \big(\mathrm{e}^{\boldsymbol{A}t} - \boldsymbol{I}_n - \tfrac{\boldsymbol{A}t}{1!} - \tfrac{\boldsymbol{A}^2t^2}{2!}\big)\boldsymbol{A}^{-3}\tfrac{\mathrm{d}}{\mathrm{d}t}\boldsymbol{A}\boldsymbol{A}^2 + \cdots\\
&= \mathrm{e}^{\boldsymbol{A}t}\boldsymbol{A} + \big(\mathrm{e}^{\boldsymbol{A}t} - \boldsymbol{I}_n\big)\boldsymbol{A}^{-1}\big(\tfrac{\mathrm{d}}{\mathrm{d}t}\boldsymbol{A} + \boldsymbol{A}^{-1}\tfrac{\mathrm{d}}{\mathrm{d}t}\boldsymbol{A}\boldsymbol{A} + \boldsymbol{A}^{-2}\tfrac{\mathrm{d}}{\mathrm{d}t}\boldsymbol{A}\boldsymbol{A}^2 + \cdots\big)\\
&- \boldsymbol{A}^{-1}\Big(\big(\tfrac{\mathrm{d}}{\mathrm{d}t}\boldsymbol{A} + \boldsymbol{A}^{-1}\tfrac{\mathrm{d}}{\mathrm{d}t}\boldsymbol{A}\boldsymbol{A} + \cdots\big)\tfrac{\boldsymbol{A}t}{1!} + \big(\tfrac{\mathrm{d}}{\mathrm{d}t}\boldsymbol{A} + \cdots\big)\tfrac{\boldsymbol{A}^2t^2}{2!} + \cdots\Big)\\
&= \mathrm{e}^{\boldsymbol{A}t}\boldsymbol{A} + \mathrm{e}^{\boldsymbol{A}t}\boldsymbol{A}^{-1}\sum_{k=0}^{\infty}\boldsymbol{A}^{-k}\tfrac{\mathrm{d}}{\mathrm{d}t}\boldsymbol{A}\boldsymbol{A}^k - \boldsymbol{A}^{-1}\sum_{k=0}^{\infty}\boldsymbol{A}^{-k}\tfrac{\mathrm{d}}{\mathrm{d}t}\boldsymbol{A}\boldsymbol{A}^k\mathrm{e}^{\boldsymbol{A}t}\\
&+ \lim_{r\to\infty}\boldsymbol{A}^{-1}\Big(\boldsymbol{A}^{-r}\tfrac{\mathrm{d}}{\mathrm{d}t}\boldsymbol{A}\boldsymbol{A}^r\tfrac{\boldsymbol{A}t}{1!} + \big(\boldsymbol{A}^{-r+1}\tfrac{\mathrm{d}}{\mathrm{d}t}\boldsymbol{A}\boldsymbol{A}^{r-1} + \boldsymbol{A}^{-r}\tfrac{\mathrm{d}}{\mathrm{d}t}\boldsymbol{A}\boldsymbol{A}^r\big)\tfrac{\boldsymbol{A}^2t^2}{2!} + \cdots\Big)\\
&= \mathrm{e}^{\boldsymbol{A}t}\boldsymbol{A} + \boldsymbol{A}^{-1}\sum_{k=0}^{\infty}\boldsymbol{A}^{-k}\big(\mathrm{e}^{\boldsymbol{A}t}\tfrac{\mathrm{d}}{\mathrm{d}t}\boldsymbol{A} - \tfrac{\mathrm{d}}{\mathrm{d}t}\boldsymbol{A}\mathrm{e}^{\boldsymbol{A}t}\big)\boldsymbol{A}^k\\
&+ \lim_{r\to\infty}\boldsymbol{A}^{-r-1}\sum_{k=0}^{\infty}\tfrac{\boldsymbol{A}^kt^k}{(k+1)!}\sum_{l=0}^{k}\boldsymbol{A}^l\tfrac{\mathrm{d}}{\mathrm{d}t}\boldsymbol{A}\boldsymbol{A}^{-l}\boldsymbol{A}^{r+1}t\\
&\overset{(2.24)}{=} \mathrm{e}^{\boldsymbol{A}t}\boldsymbol{A} + \boldsymbol{A}^{-1}\sum_{k=0}^{\infty}\boldsymbol{A}^{-k}\boldsymbol{V}\big(\mathrm{e}^{\boldsymbol{D}t}\tfrac{\mathrm{d}}{\mathrm{d}t}\boldsymbol{D} - \tfrac{\mathrm{d}}{\mathrm{d}t}\boldsymbol{D}\mathrm{e}^{\boldsymbol{D}t}\big)\boldsymbol{V}^{-1}\boldsymbol{A}^k\\
&+ \boldsymbol{V}\lim_{r\to\infty}\sum_{k=0}^{\infty}\boldsymbol{D}^{-r-1}\tfrac{\boldsymbol{D}^kt^k}{(k+1)!}\sum_{l=0}^{k}\boldsymbol{D}^l\tfrac{\mathrm{d}}{\mathrm{d}t}\boldsymbol{D}\boldsymbol{D}^{-l}\boldsymbol{D}^{r+1}\boldsymbol{V}^{-1}t\\
&= \mathrm{e}^{\boldsymbol{A}t}\boldsymbol{A} + \boldsymbol{V}\sum_{k=0}^{\infty}\tfrac{\boldsymbol{D}^kt^k}{(k+1)!}\sum_{l=0}^{k}\tfrac{\mathrm{d}}{\mathrm{d}t}\boldsymbol{D}\boldsymbol{V}^{-1}t\\
&\overset{(2.24)}{=} \mathrm{e}^{\boldsymbol{A}t}\boldsymbol{A} + t\mathrm{e}^{\boldsymbol{A}t}\tfrac{\mathrm{d}}{\mathrm{d}t}\boldsymbol{A}
\end{aligned}$$

where in the last steps, commutativity of

(i) two matrices in diagonal and/or Jordan normal form and

(ii) any (quadratic) matrix or its inverse and respective matrix exponential

was used. This completes the proof. $\square$

Definition 2.20 (Performance measures)**.** *Define, for all* $t \in \mathbb{T} := \{\tau | \, t_0 \leq \tau \leq t_\infty\} \subset \mathbb{R}$, *the scalar error function* $e \colon \mathbb{T} \to \mathbb{R}$. *Then, the error metrics* Integral of Absolute Error *(IAE) and* Integral of Time-weighted Absolute Error *(ITAE) are defined as*

$$\forall\, t \in \mathbb{T}\colon \quad \begin{aligned} &\mathcal{M}_{\mathrm{IAE}} \colon \mathbb{T} \to \mathbb{R}_{\geq 0}, \qquad && t \mapsto \mathcal{M}_{\mathrm{IAE}}(t) := \int_{t_0}^{t} |e(\tau)| \, \mathrm{d}\tau \\ &\mathcal{M}_{\mathrm{ITAE}} \colon \mathbb{T} \to \mathbb{R}_{\geq 0}, \qquad && t \mapsto \mathcal{M}_{\mathrm{ITAE}}(t) := \int_{t_0}^{t} \tau \, |e(\tau)| \, \mathrm{d}\tau. \end{aligned} \tag{2.26}$$

Chapter 3

Signal decomposition

This chapter describes the proposed methods for decomposing a signal into its fundamental parameters. It is divided into six sections:

Section 3.1 introduces the generation of arbitrary signals;

Section 3.2 shows the *enhanced standard Frequency Adaptive Observer with High Pass Filter* (esFAO);

Section 3.3 shows the *modified Frequency Adaptive Observer* (mFAO) and the *modified Frequency Adaptive Observer with offset* (mFAO$_\circ$);

Section 3.4 shows the *transformation-based Frequency Adaptive Observer* in transformed coordinates (tFAO) and the *transformation-based Frequency Adaptive Observer with offset* in transformed coordinates (tFAO$_\circ$);

Section 3.5 shows the *transformation-based Frequency Adaptive Observer* in α, β coordinates (tFAO) and the *transformation-based Frequency Adaptive Observer with offset* in α, β coordinates (tFAO$_\circ$); and

Section 3.6 illustrates an idea for the *exponential Frequency Adaptive Observer* (eFAO) and the *exponential Frequency Adaptive Observer with offset* (eFAO$_\circ$).

Each section is subdivided into different sections. These are briefly summarized at the beginning of the respective section. All *Frequency Adaptive Observer*s (FAO) are a combination of parallelized *Second Order Generalized Integrator*s (SOGI) for estimation of amplitudes ($\widehat{a}$) and phase angles ($\widehat{\phi}$) and a *Frequency Locked Loop* (FLL) for angular frequency estimation ($\widehat{\omega}$). A general FAO is pictured in Figure 3.1.

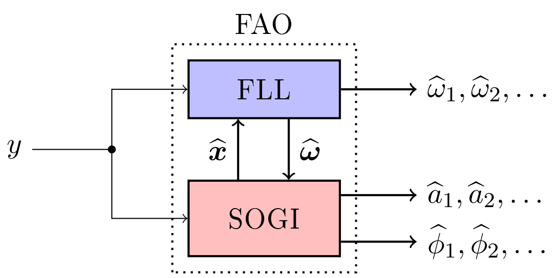

Figure 3.1: *Frequency Adaptive Observer consisting of parallelized Second Order Generalized Integrators and a Frequency Locked Loop.*

These FAOs are designed for single-phase applications. Simulative results are shown throughout this chapter to illustrate characteristics of the proposed FAOs. At the end of each section, test signals (defined in Section 3.1) are evaluated by the respective system to show its benefits. Experimental validations are presented in Chapter 4. Additionally, mathematical proofs are shown along with the derivations.

3.1 The internal model principle: Generation of periodic signals

To start with, any periodic signal can be represented by

$$\forall\, t_0 \geq 0: \quad y(t) = a_0(t) + \sum_{j=1}^{n_\infty} a_j(t) \cos(\phi_j(t))$$

with offset $a_0(t)$, amplitude $a_j(t)$ and phase angle $\phi_j(t)$ of the j-th component. The order of the j-th component is denoted as ν_j, and all ν_j are collected in $\mathbb{H}_\infty$. It is denoted as the set of harmonic orders. It contains positive and possibly unbounded rational numbers, is sorted and possibly unlimited, i.e.

$$\mathbb{H}_\infty := \{\nu_1, \nu_2, \nu_3, \dots, \nu_\infty\} \subseteq \mathbb{Q}_{>0}, \quad 1 \in \mathbb{H}_\infty, \quad \max(\mathbb{H}_\infty) \to \infty \quad \text{and} \quad |\mathbb{H}_\infty| =: n_\infty \to \infty. \tag{3.1}$$

The component relating to the harmonic order 1 is said to be the fundamental component and all other components are said to be harmonic components. Note that also harmonic numbers lesser than one are permitted. Further, the phase angle of each harmonic component is given by

$$\phi_j(t) = \int_{t_0}^{t} \omega_j(\tau)\mathrm{d}\tau + \phi_{j,0}$$

with the angular frequency $\omega_j(t)$ and initial phase angle $\phi_{j,0}$ of the j-th component. All variables (offset, amplitudes, and angular frequencies) are allowed to be time-varying. However, they are assumed to be constant on certain time intervals:

Assumption 3.1.1. *Defining the total time interval*

$$\mathbb{T} := [t_0, t_1, t_2, \dots, t_\infty) \subseteq \mathbb{R}_{\geq 0}, \qquad t_\infty \to \infty$$

what is divided into subintervals

$$\mathbb{T}_i := [t_i, t_{i+1}) \qquad \textit{such that} \qquad \mathbb{T} = \mathbb{T}_0 \cup \mathbb{T}_1 \cup \mathbb{T}_2 \cup \cdots.$$

In each $\mathbb{T}_i$, all *parameters (offset, amplitudes, and angular frequencies) are constant. Consequently, the input signal on each time interval can be written as*

$$\forall\, \mathbb{T}_i \subset \mathbb{T}, \forall\, t \in \mathbb{T}_i: \quad y(t) = a_0 + \sum_{j=1}^{n_\infty} a_j \cos(\phi_j(t)) = a_0 + \overbrace{\sum_{j=1}^{n_\infty} \underbrace{a_j \cos(\omega_j(t - t_i) + \phi_{j,t_i})}_{=: y_j(t)}}^{=: y_\sim(t)}. \tag{3.2}$$

Note that for readability, the rest of the chapter refers to any time interval $\mathbb{T}_i \subset \mathbb{T}$ what therefore is not explicitly mentioned anymore. Now, any sinusoidal signal can be generated by a harmonic oscillator given in its state-space representation by

$$\left.\begin{array}{rrcl} \forall\, t \in \mathbb{T}_i\colon & \frac{\mathrm{d}}{\mathrm{d}t} \overbrace{\begin{pmatrix} x_j^\alpha(t) \\ x_j^\beta(t) \end{pmatrix}}^{=:\, \boldsymbol{x}_j(t) \,\in\, \mathbb{R}^2} & = & \omega_j \overbrace{\begin{bmatrix} 0 & -1 \\ 1 & 0 \end{bmatrix}}^{=:\, \widetilde{\boldsymbol{J}} \,\in\, \mathbb{R}^{2\times 2}} \boldsymbol{x}_j(t), \quad \boldsymbol{x}_j(t_i) = \boldsymbol{x}_{j,t_i}, \\ & y_j(t) & = & \underbrace{\begin{pmatrix} 1 & 0 \end{pmatrix}}_{=:\, \widetilde{\boldsymbol{c}}^\top \,\in\, \mathbb{R}^2} \boldsymbol{x}_j(t). \end{array}\right\} \tag{3.3}$$

Consequently, the generation of n_∞ harmonics is represented by

$$\left.\begin{array}{rrcl} \forall\, t \in \mathbb{T}_i\colon & \frac{\mathrm{d}}{\mathrm{d}t} \overbrace{\begin{pmatrix} \boldsymbol{x}_1(t) \\ \boldsymbol{x}_2(t) \\ \vdots \\ \boldsymbol{x}_{n_\infty}(t) \end{pmatrix}}^{=:\, \boldsymbol{x}(t) \,\in\, \mathbb{R}^{2n_\infty}} & = & \overbrace{\begin{bmatrix} \omega_1 \widetilde{\boldsymbol{J}} & \boldsymbol{0}_{2\times 2} & \cdots & \boldsymbol{0}_{2\times 2} \\ \boldsymbol{0}_{2\times 2} & \omega_2 \widetilde{\boldsymbol{J}} & \cdots & \boldsymbol{0}_{2\times 2} \\ \vdots & \vdots & \ddots & \vdots \\ \boldsymbol{0}_{2\times 2} & \boldsymbol{0}_{2\times 2} & \cdots & \omega_{n_\infty} \widetilde{\boldsymbol{J}} \end{bmatrix}}^{=:\, \boldsymbol{J}(\boldsymbol{\omega}) \,\in\, \mathbb{R}^{2n_\infty \times 2n_\infty}} \boldsymbol{x}(t), \quad \boldsymbol{x}(t_i) = \boldsymbol{x}_{t_i} \\ & y_\sim(t) & = & \underbrace{\begin{pmatrix} \widetilde{\boldsymbol{c}}^\top & \cdots & \widetilde{\boldsymbol{c}}^\top \end{pmatrix}}_{=:\, \boldsymbol{c}^\top \,\in\, \mathbb{R}^{2n_\infty}} \boldsymbol{x}(t). \end{array}\right\} \tag{3.4}$$

Hereby, all angular frequencies are collected in the vector

$$\boldsymbol{\omega} := \left(\omega_1, \ldots, \omega_{n_\infty}\right)^\top \in \mathbb{R}^n.$$

Each angular frequency can be written in dependency on the fundamental one by

$$\forall\, j \in \{1, \ldots, n_\infty\}: \quad \omega_j = \nu_j \omega_1 \tag{3.5}$$

what permits a decomposition of $\boldsymbol{J}$ into

$$\boldsymbol{J}(\boldsymbol{\omega}) \overset{(3.4)}{=} \omega_1 \underbrace{\begin{bmatrix} \widetilde{\boldsymbol{J}} & \boldsymbol{0}_{2\times 2} & \cdots & \boldsymbol{0}_{2\times 2} \\ \boldsymbol{0}_{2\times 2} & \nu_2 \widetilde{\boldsymbol{J}} & \cdots & \boldsymbol{0}_{2\times 2} \\ \vdots & \vdots & \ddots & \vdots \\ \boldsymbol{0}_{2\times 2} & \boldsymbol{0}_{2\times 2} & \cdots & \nu_\infty \widetilde{\boldsymbol{J}} \end{bmatrix}}_{=:\, \boldsymbol{N} \,\in\, \mathbb{R}^{(2n_\infty)\times(2n_\infty)}}. \tag{3.6}$$

Second, any constant (e.g. offset) can be modeled by

$$\left.\begin{array}{rrcl} \forall\, t \in \mathbb{T}_i\colon & \frac{\mathrm{d}}{\mathrm{d}t} x_0(t) & = & 0 \cdot x_0(t), \quad x_0(t_i) = x_{0,t_i}, \\ & y_=(t) & = & 1 \cdot x_0(t) \end{array}\right\} \tag{3.7}$$

what, combined with (3.4), leads to the overall generation system

$$\left.\begin{array}{rrcl} \forall\, t \in \mathbb{T}_i\colon & \frac{\mathrm{d}}{\mathrm{d}t} \overbrace{\begin{pmatrix} x_0(t) \\ \boldsymbol{x}(t) \end{pmatrix}}^{=:\, \boldsymbol{x}_\circ(t) \,\in\, \mathbb{R}^{2n_\infty+1}} & = & \overbrace{\begin{bmatrix} 0 & \boldsymbol{0}_{2n_\infty}^\top \\ \boldsymbol{0}_{2n_\infty} & \boldsymbol{J}(\boldsymbol{\omega}) \end{bmatrix}}^{=:\, \boldsymbol{J}_\circ(\boldsymbol{\omega}) \,\in\, \mathbb{R}^{(2n_\infty+1)\times(2n_\infty+1)}} \boldsymbol{x}_\circ(t), \quad \boldsymbol{x}_\circ(t_i) = \boldsymbol{x}_{\circ,t_i} \\ & y(t) & = & \underbrace{\begin{pmatrix} 1 & \boldsymbol{c}^\top \end{pmatrix}}_{=:\, \boldsymbol{c}_\circ^\top \,\in\, \mathbb{R}^{2n_\infty+1}} \boldsymbol{x}_\circ(t) = y_=(t) + y_\sim(t). \end{array}\right\} \tag{3.8}$$

Again, pulling out the fundamental angular frequency from the system matrix yields

$$\boldsymbol{J}_\circ(\boldsymbol{\omega}) \overset{(3.8)}{=} \omega_1 \underbrace{\begin{bmatrix} 0 & \mathbf{0}_{2n_\infty}^\top \\ \mathbf{0}_{2n_\infty} & \boldsymbol{N} \end{bmatrix}}_{=: \boldsymbol{N}_\circ \in \mathbb{R}^{2n_\infty+1\times 2n_\infty+1}} . \tag{3.9}$$

(3.2) and (3.8) are related by

$$\forall\, t \in \mathbb{T}_i\colon\; a_0(t) = x_0(t),\; a_j(t) = \sqrt{(x_j^\alpha)^2(t) + (x_j^\beta)^2(t)} \quad \text{and} \quad \phi_j(t) = \operatorname{arctan2}\left(\frac{x_j^\beta(t)}{x_j^\alpha(t)}\right). \tag{3.10}$$

For both equations (3.4) and (3.8), the time derivative of $\boldsymbol{\omega}$ is given as

$$\forall\, j \in \{1, \dots, n_\infty\}: \quad \tfrac{\mathrm{d}}{\mathrm{d}t}\boldsymbol{\omega} = \mathbf{0}_{n_\infty} \quad \overset{(3.5)}{\Longrightarrow} \quad \tfrac{\mathrm{d}}{\mathrm{d}t}\nu_j = 0. \tag{3.11}$$

The test signals for evaluating the proposed methods mentioned in the introduction are defined as

$$\left.\begin{aligned} y_{\text{test},N}(t) &:= 50\,\mathrm{V}\cos\big(2\pi 50 t + \tfrac{\pi}{3}\big) + 10\,\mathrm{V}\cos\big(2\cdot 2\pi 50 t - \tfrac{\pi}{3}\big) \\ y_{\text{test},N_\circ}(t) &:= -20\,\mathrm{V} + 50\,\mathrm{V}\cos\big(2\pi 50 t + \tfrac{\pi}{3}\big) + 10\,\mathrm{V}\cos\big(2\cdot 2\pi 50 t - \tfrac{\pi}{3}\big) \\ y_{\text{test},Q}(t) &:= 50\,\mathrm{V}\cos\big(2\pi 50 t + \tfrac{\pi}{3}\big) + 10\,\mathrm{V}\cos\big(1.5\cdot 2\pi 50 t - \tfrac{\pi}{3}\big) \\ y_{\text{test},Q_\circ}(t) &:= -20\,\mathrm{V} + 50\,\mathrm{V}\cos\big(2\pi 50 t + \tfrac{\pi}{3}\big) + 10\,\mathrm{V}\cos\big(1.5\cdot 2\pi 50 t - \tfrac{\pi}{3}\big)\,. \end{aligned}\right\} \tag{3.12}$$

In Figure 3.2[1], their amplitudes and frequencies are plotted.
Note that, for readability, the argument t is always dropped in the following.

3.2 The enhanced standard Frequency Adaptive Observer

This section reintroduces the *standard Second Order Generalized Integrator* (sSOGI) and *standard Frequency Locked Loop* (sFLL). In this thesis, the combination of both is called the *standard Frequency Adaptive Observer* (sFAO)[2]. The goal of this section is to enhance the sSOGI in terms of estimation speed and offset detection[3]. The resulting system is called the *enhanced standard Frequency Adaptive Observer* (esFAO); parts of it were published by the author in [570].
This section is subdivided as follows:

Section 3.2.1 introduces the SOGI principle and the sSOGI,

Section 3.2.2 describes the parallelization of sSOGIs,

Section 3.2.3 discusses the feedback gains of the parallelized sSOGIs,

Section 3.2.4 explains the enhancement of the parallelized sSOGIs with respect to estimation speed (esSOGI),

Section 3.2.5 expands the parallelized esSOGIs to detect offset,

Section 3.2.6 introduces the FLL principle and the sFLL,

Section 3.2.7 discusses the tuning of the FLL and expands it in view of stability (esFLL) and

[1] Simulation parameters: $T_s = 100\,\mu\mathrm{s}$, Solver: ode4.
[2] In common literature (e.g. [522]), it is called SOGI-FLL instead.
[3] Recall that in this thesis, detection means calculation with feedthrough and estimation means calculation without feedthrough.

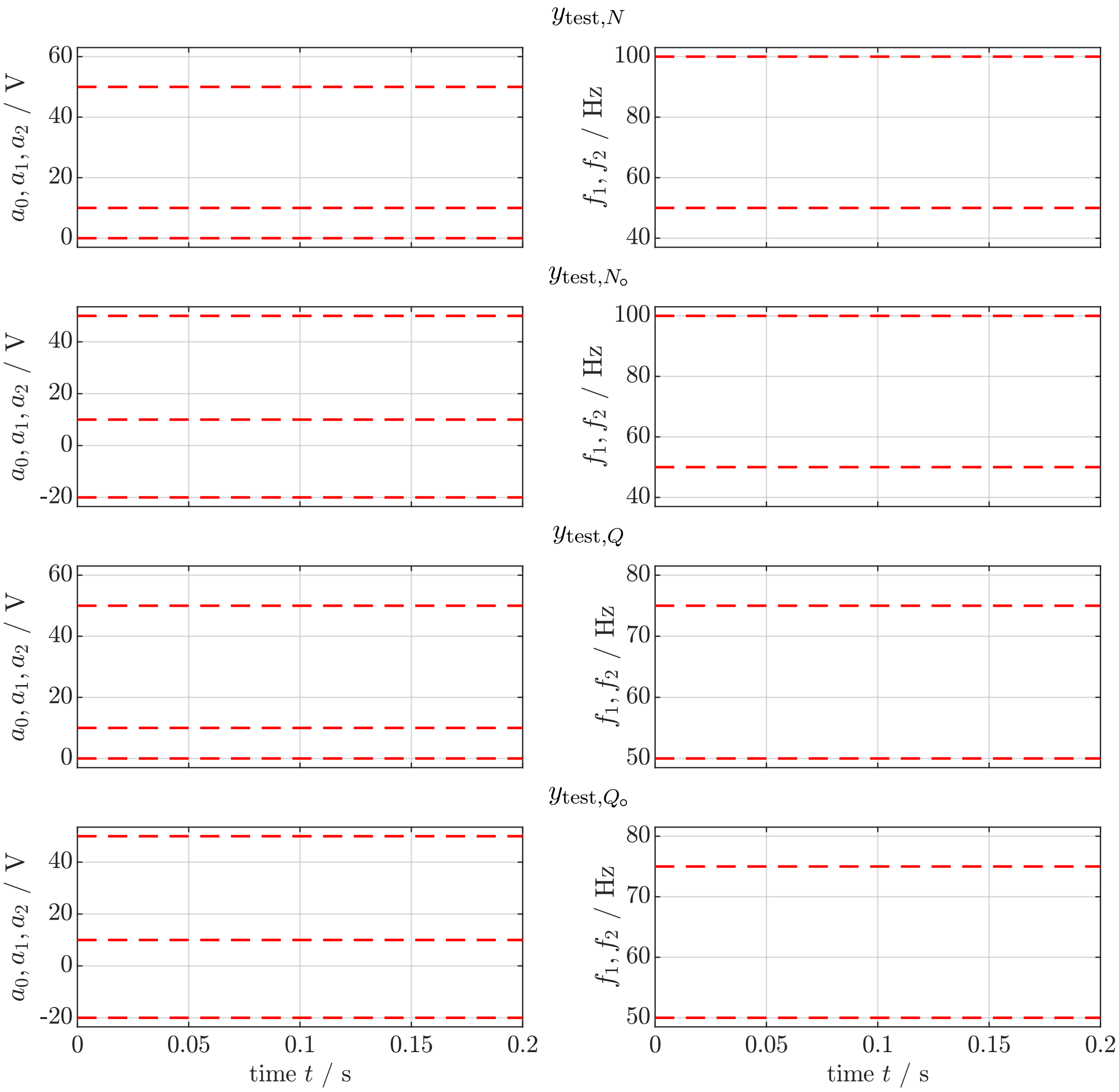

Figure 3.2: *Offset, amplitudes and frequencies of the test signals (- - -).*

Section 3.2.8 summarizes and proves the stability of the overall system (esFAO).

3.2.1 The principle idea of a SOGI

First of all, a short recapitulation of the SOGI principle is given [515]. Since a SOGI's purpose is to reduplicate sinusoidal signals, it is based on a harmonic oscillator. The sinusoid's angular frequency $\widehat{\omega}$ is defined by the total oscillation gain Ω, which represents the gain to a signal in a single circulation (see blue arrow in Figure 3.3). The angular frequency then is given by

$$\widehat{\omega} = \sqrt{-\Omega} > 0.$$

Note that, although the angular frequency $\widehat{\omega}$ is assumed to be positive, also negative frequencies are allowed in a mathematical sense. This is not the case in physical systems where the angular frequency is positive per definition. A block diagram of a harmonic oscillator consists of two integrators with initial values $\widehat{x}^{\alpha}_{t_0}$ and $\widehat{x}^{\beta}_{t_0}$ connected to a circle as shown in Figure 3.3 where two commonly used models of such harmonic oscillators are shown.

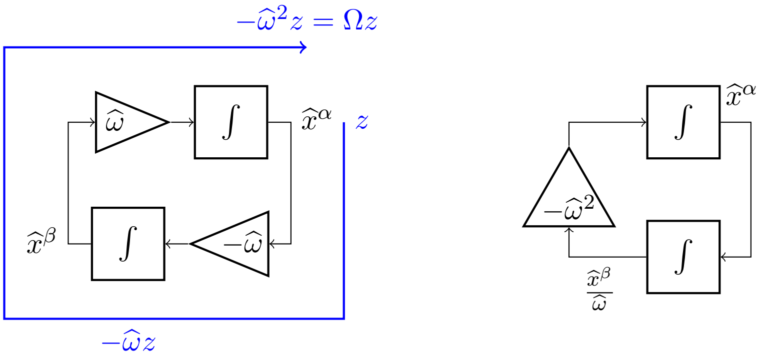

Figure 3.3: *Two different types of harmonic oscillators.*

So far, a harmonic oscillator outputs a signal with fixed angular frequency $\widehat{\omega} = \sqrt{-\Omega}$. The amplitude $\widehat{a}$ of the output signal is defined by the integrator's initial values $\widehat{x}^{\alpha}_{t_0}, \widehat{x}^{\beta}_{t_0}$ and the ratio of the frequency gains between the integrators in the harmonic oscillator. If the ratio is equal to one which is the most common case, the amplitude is given as $\widehat{a} = \sqrt{(\widehat{x}^{\alpha}_{t_0})^2 + (\widehat{x}^{\beta}_{t_0})^2}$. Recall that the purpose of a SOGI is to reduplicate a given signal with unknown amplitude[4]. To cover this issue, the harmonic oscillator must be extended such that it is fed by the difference between reference signal y and estimated signal $\widehat{y} = \widehat{x}^{\alpha}$. This difference is further referred to as the signal estimation error

$$e_y := y - \widehat{y}. \tag{3.13}$$

To have some influence options on the performance of the resulting system, the signal estimation error e_y is multiplied by some gain l^{α}. The resulting system is called *Adaptive Notch Filter* (ANF) or *standard Second Order Generalized Integrator* (sSOGI), indicated by the subscript "s". Two common structures of such sSOGIs (or ANFs) are shown in Figure 3.4.

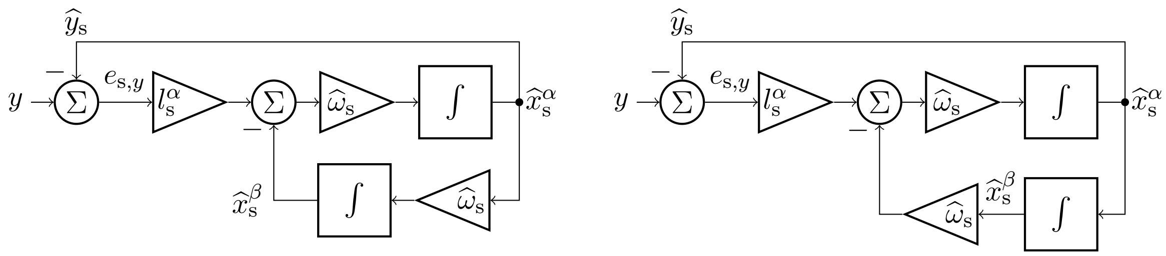

Figure 3.4: *Two different types of sSOGIs (or ANFs).*

The estimate $\widehat{y}_{\mathrm{s}}$ of the input is given by the state $\widehat{x}^{\alpha}_{\mathrm{s}}$ and is called "direct signal". It has the same amplitude and phase angle as the input signal, if the resonance angular frequency $\widehat{\omega}_{\mathrm{s}}$ matches the signal's actual angular frequency ω. As a consequence, the signal estimation error $e_{\mathrm{s},y}$ will tend to zero and the harmonic oscillator keeps oscillating without external input. From Figure 3.4 it can be seen that an additional signal, $\widehat{x}^{\beta}_{\mathrm{s}}$, is available; this signal is called "quadrature signal". Considering the left block diagram, $\widehat{x}^{\beta}_{\mathrm{s}}$ has the same amplitude and a phase angle shifted by $\frac{\pi}{2}$ with respect to the input signal y, if the harmonic oscillator's angular frequency $\widehat{\omega}_{\mathrm{s}}$ is identical to the signal's angular frequency ω. In case of the right block diagram, the only difference is that the amplitude of $\widehat{x}^{\beta}_{\mathrm{s}}$ is damped by ω. The gain l^{α}_{s} remains unspecified for now; from now

[4] The angular frequency is unknown as well. This is considered in Section 3.2.6.

on, only the left type of sSOGI from Figure 3.4 is considered.
As mentioned above, the signal estimation error $e_{\mathrm{s},y}$ will tend to zero if the signal's angular frequency ω and the harmonic oscillator's angular frequency $\widehat{\omega}_\mathrm{s}$ are identical. Otherwise, although the harmonic oscillator produces signals with angular frequency $\widehat{\omega}_\mathrm{s}$ (instead of ω), the signal estimation error $e_{\mathrm{s},y}$ superposes the harmonic oscillator's signals such that all signals ($e_{\mathrm{s},y}$, $\widehat{x}_\mathrm{s}^\alpha$, $\widehat{x}_\mathrm{s}^\beta$) oscillate with the angular frequency ω of the input signal y. In other words, exemplarily for the estimated direct signal $\widehat{x}_\mathrm{s}^\alpha$, in quasi-steady state it holds that

$$\widehat{x}_\mathrm{s}^\alpha = a(\widehat{\omega}_\mathrm{s}, \omega, t)\cos(\widehat{\omega}_\mathrm{s} t + \phi(\widehat{\omega}_\mathrm{s}, \omega, t)) = A(\widehat{\omega}_\mathrm{s}, \omega)\cos(\omega t + \Phi(\widehat{\omega}_\mathrm{s}, \omega)) .$$

In either case, the amplitudes and phase angles of the estimated signals $\widehat{x}_\mathrm{s}^\alpha$ and $\widehat{x}_\mathrm{s}^\beta$ and the signal estimation error $e_{\mathrm{s},y}$ with respect to the input signal are obtained by calculating amplitude and phase responses. These responses describe the distortion of an input signal

$$\forall\, t \in \mathbb{T}_i\colon \quad y = a\cos(\phi) ,$$

to a signal $\mathrm{x} = aA_\mathrm{x}(\omega)\cos(\phi + \Phi_\mathrm{x}(\omega))$ where $\mathrm{x} \in \left\{\widehat{x}_\mathrm{s}^\alpha, \widehat{x}_\mathrm{s}^\beta, e_{\mathrm{s},y}\right\}$. A_x is called the amplitude response and Φ_x the phase response. These are calculated by using the transfer function

$$\mathcal{X}(s) := \tfrac{\mathrm{x}(s)}{y(s)} \quad \Rightarrow \quad \mathcal{X}(\jmath\omega) = \Re(\mathcal{X}(\jmath\omega)) + \jmath\Im(\mathcal{X}(\jmath\omega))$$

as

$$A_\mathrm{x}(\omega) = \sqrt{\Re(\mathcal{X}(\jmath\omega))^2 + \Im(\mathcal{X}(\jmath\omega))^2} \qquad \text{and} \qquad \Phi_\mathrm{x}(\omega) = \operatorname{arctan2}\!\left(\tfrac{\Im(\mathcal{X}(\jmath\omega))}{\Re(\mathcal{X}(\jmath\omega))}\right) . \tag{3.14}$$

However, a transfer function must not contain time-dependent parameters. Consequently, for the sSOGI, the harmonic oscillator's angular frequency must be assumed as constant. Then, the sSOGI's transfer functions are given by

$$\mathcal{X}_\mathrm{s}^\alpha(s) := \tfrac{\widehat{x}_\mathrm{s}^\alpha(s)}{y(s)} = \tfrac{\widehat{\omega}_\mathrm{s} l_\mathrm{s}^\alpha s}{s^2 + \widehat{\omega}_\mathrm{s} l_\mathrm{s}^\alpha s + \widehat{\omega}_\mathrm{s}^2},\ \mathcal{X}_\mathrm{s}^\beta(s) := \tfrac{\widehat{x}^\beta(s)}{y(s)} = \tfrac{\widehat{\omega}_\mathrm{s}^2 l_\mathrm{s}^\alpha}{s^2 + \widehat{\omega}_\mathrm{s} l_\mathrm{s}^\alpha s + \widehat{\omega}_\mathrm{s}^2},\ \mathcal{E}_{\mathrm{s},y}(s) := \tfrac{e_y(s)}{y(s)} = \tfrac{s^2 + \widehat{\omega}_\mathrm{s}^2}{s^2 + \widehat{\omega}_\mathrm{s} l_\mathrm{s}^\alpha s + \widehat{\omega}_\mathrm{s}^2};$$

details on their derivation are shown in Appendix A. The respective amplitude and phase responses, also shown in Appendix A, are obtained as

$$\begin{array}{rrcl rcl}
 & A_{\mathcal{X}_\mathrm{s}^\alpha}(\omega) & = & \frac{\omega\widehat{\omega}_\mathrm{s} l_\mathrm{s}^\alpha}{\sqrt{(\widehat{\omega}_\mathrm{s}^2 - \omega^2)^2 + \omega^2\widehat{\omega}_\mathrm{s}^2 (l_\mathrm{s}^\alpha)^2}}, & \Phi_{\mathcal{X}_\mathrm{s}^\alpha}(\omega) & = & \operatorname{arctan2}\!\left(\frac{\widehat{\omega}_\mathrm{s}^2 - \omega^2}{\omega\widehat{\omega}_\mathrm{s} l_\mathrm{s}^\alpha}\right), \\
 & A_{\mathcal{X}_\mathrm{s}^\beta}(\omega) & = & \frac{\widehat{\omega}_\mathrm{s}^2 l_\mathrm{s}^\alpha}{\sqrt{(\widehat{\omega}_\mathrm{s}^2 - \omega^2)^2 + \omega^2\widehat{\omega}_\mathrm{s}^2 (l_\mathrm{s}^\alpha)^2}}, & \Phi_{\mathcal{X}_\mathrm{s}^\beta}(\omega) & = & \operatorname{arctan2}\!\left(\frac{-\omega\widehat{\omega}_\mathrm{s} l_\mathrm{s}^\alpha}{\widehat{\omega}_\mathrm{s}^2 - \omega^2}\right), \\
\text{and} & A_{\mathcal{E}_{\mathrm{s},y}}(\omega) & = & \frac{\widehat{\omega}_\mathrm{s}^2 - \omega^2}{\sqrt{(\widehat{\omega}_\mathrm{s}^2 - \omega^2)^2 + \omega^2\widehat{\omega}_\mathrm{s}^2 (l_\mathrm{s}^\alpha)^2}}, & \Phi_{\mathcal{E}_{\mathrm{s},y}}(\omega) & = & \operatorname{arctan2}\!\left(\frac{-\omega\widehat{\omega}_\mathrm{s} l_\mathrm{s}^\alpha}{\widehat{\omega}_\mathrm{s}^2 - \omega^2}\right).
\end{array} \tag{3.15}$$

Note that the amplitude and phase responses show the system's reaction to an input signal when the system is in quasi-steady state. Moreover, the system only tends to quasi-steady state if it is stable, which can be influenced by the feedback gain l_s^α. To show the allowed tuning range of l_s^α, a brief stability analysis is conducted. The differential equations describing the left sSOGI shown in Figure 3.4 are obtained as

$$\forall\, t \in \mathbb{T}_i\colon \quad \left.\begin{array}{rcl}
\frac{\mathrm{d}}{\mathrm{d}t}\begin{pmatrix}\widehat{x}_\mathrm{s}^\alpha \\ \widehat{x}_\mathrm{s}^\beta\end{pmatrix} & = & \widehat{\omega}_\mathrm{s}\begin{bmatrix}-l_\mathrm{s}^\alpha & -1 \\ 1 & 0\end{bmatrix}\begin{pmatrix}\widehat{x}_\mathrm{s}^\alpha \\ \widehat{x}_\mathrm{s}^\beta\end{pmatrix} + \widehat{\omega}_\mathrm{s}\begin{pmatrix}l_\mathrm{s}^\alpha \\ 0\end{pmatrix} y, \quad \begin{pmatrix}\widehat{x}_\mathrm{s}^\alpha(t_i) \\ \widehat{x}_\mathrm{s}^\beta(t_i)\end{pmatrix} = \begin{pmatrix}\widehat{x}_{\mathrm{s},t_i}^\alpha \\ \widehat{x}_{\mathrm{s},t_i}^\beta\end{pmatrix} \\
\widehat{y}_\mathrm{s} & = & \begin{pmatrix}1 & 0\end{pmatrix}\begin{pmatrix}\widehat{x}_\mathrm{s}^\alpha \\ \widehat{x}_\mathrm{s}^\beta\end{pmatrix} .
\end{array}\right\} \tag{3.16}$$

This system is stable if all eigenvalues of the system matrix are in the negative complex half plane. The eigenvalues are given by

$$\begin{aligned} &\det\left(\begin{bmatrix} s & 0 \\ 0 & s \end{bmatrix} - \widehat{\omega}_\mathrm{s}\begin{bmatrix} -l_\mathrm{s}^\alpha & -1 \\ 1 & 0 \end{bmatrix}\right) = s\left(s + \widehat{\omega}_\mathrm{s} l_\mathrm{s}^\alpha\right) + \widehat{\omega}_\mathrm{s}^2 = 0 \\ \implies \quad & s \in \left\{-\widehat{\omega}_\mathrm{s}\left(\frac{l_\mathrm{s}^\alpha}{2} \pm \sqrt{\frac{(l_\mathrm{s}^\alpha)^2}{4} - 1}\right)\right\}. \end{aligned} \tag{3.17}$$

Hence, if and only if the gain l_s^α is chosen positive, the system is stable and the signal estimation error $e_{\mathrm{s},y}$ decreases exponentially. In this case, the system matrix is called a *Hurwitz matrix*. Hereby, the choice $l_\mathrm{s}^\alpha = 2$ minimizes the maximal eigenvalue leading to a faster settling time. Figure 3.5 shows the influence of l_s^α on the sSOGI's estimation performance[5].

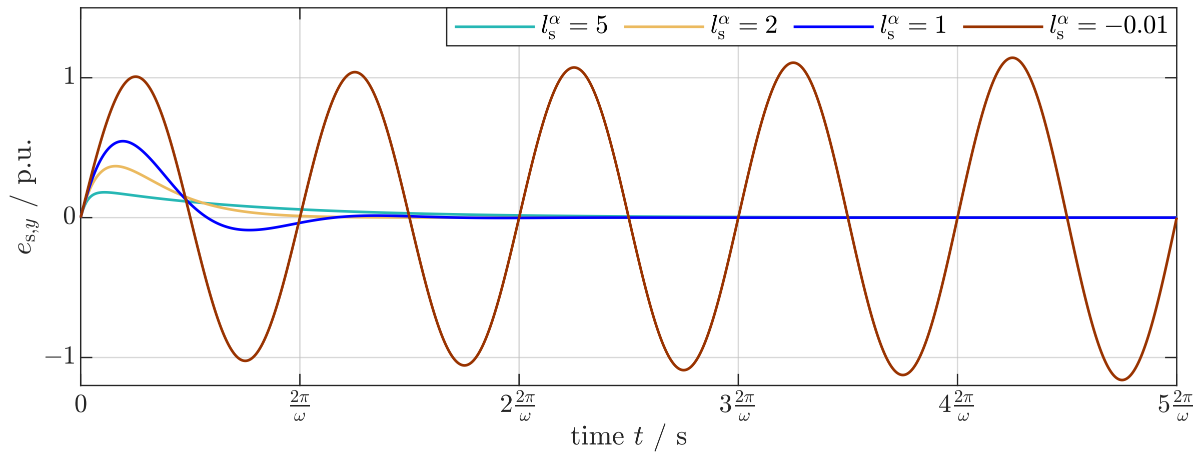

Figure 3.5: *Influence of the gain l_s^α on the estimation performance of the sSOGI.*

As predicted, for $l_\mathrm{s}^\alpha < 0$, the system becomes unstable which can be seen in the rising signal estimation error amplitude. For $l_\mathrm{s}^\alpha = 2$, the fastest decrease is achieved. For the other choices of l_s^α, the system is still stable but decreasing more slowly. This can also be seen in the *Integral of Time-weighted Absolute Error* (ITAE) (see Definition 2.20) penalizing slow decrease (whereas the *Integral of Absolute Error* (IAE) penalizes high overshooting). These measures are shown for the used gains in Table 3.1.

l_s^α	5	**2**	1	−0.1
$\mathcal{M}_\mathrm{IAE}$ / Vs	**0.31784**	0.31830	0.44231	6.89359
$\mathcal{M}_\mathrm{ITAE}$ / Vs^2	0.00501	**0.00203**	0.00312	0.35366

Table 3.1: *IAE and ITAE for the different choices of l_s^α.*

Coming back to the oscillation characteristic of a sSOGI, a decomposition of the system matrix reveals

$$\widehat{\omega}_\mathrm{s}\begin{bmatrix} -l_\mathrm{s}^\alpha & -1 \\ 1 & 0 \end{bmatrix} = \widehat{\omega}_\mathrm{s}\underbrace{\begin{bmatrix} 0 & -1 \\ 1 & 0 \end{bmatrix}}_{\overset{(3.3)}{=}\widetilde{\boldsymbol{J}}} - \widehat{\omega}_\mathrm{s}\begin{pmatrix} l_\mathrm{s}^\alpha \\ 0 \end{pmatrix}\underbrace{\begin{pmatrix} 1 & 0 \end{pmatrix}}_{\overset{(3.3)}{=}\widetilde{\boldsymbol{c}}^\top}.$$

[5] Simulation parameters: $T_s = 1\,\mu\mathrm{s}$, $y = 100\sin(2\pi 50t)$, Solver: ode4. All initial values are 0.

Note that the term including $\widetilde{\boldsymbol{J}}$ represents the harmonic oscillator and the remaining term represents the feedback.

3.2.2 Parallelization of sSOGIs

Until now, the basic SOGI principle as well as its system characteristics were described. However, such a system is only capable of estimating a single component. The next step is the estimation of multiple components. Therefore, a parallelization of sSOGIs is a very intuitive approach. More precisely, harmonic oscillators with different resonance angular frequencies $\widehat{\omega}_{\mathrm{s},j} := \mu_j \widehat{\omega}_{\mathrm{s},1}$ are parallelized. It must be highlighted that only prescribed orders μ_j collected in the finite set $\mathbb{H}_n$ can be used. Clearly, only if $\mathbb{H}_n = \mathbb{H}_\infty$, the input signal y can be reconstructed perfectly. However, this is very unlikely since $\mathbb{H}_\infty$ possibly is unbounded and, moreover, unknown in general. The prescribed, sorted set of harmonic orders is defined as

$$\mathbb{H}_n := \{\mu_1, \dots, \mu_n\} \subset \mathbb{Q}_{>0}, \quad 1 \in \mathbb{H}_n, \quad \max(\mathbb{H}_n) < \infty, \qquad |\mathbb{H}_n| =: n < \infty. \tag{3.18}$$

n is called the *system order*. The assumed set $\mathbb{H}_n$ and the actual set $\mathbb{H}_\infty$ have at least one element in common, i.e. it holds that

$$1 \in (\mathbb{H}_n \cap \mathbb{H}_\infty) \quad \text{and} \quad |\mathbb{H}_n \cap \mathbb{H}_\infty| \geq 1.$$

Each harmonic oscillator is fed by the signal estimation error $e_{\mathrm{s},y}$. This error is the difference of the input y and the sum $\widehat{y}_{\mathrm{s}} = \sum_{j=1}^{n} \widehat{x}_{\mathrm{s},j}^{\alpha}$ of the direct signal outputs from each SOGI. Hence, a straightforward mathematical description results in the parallelized sSOGIs

$$\forall\, t \in \mathbb{T}_i: \quad \tfrac{\mathrm{d}}{\mathrm{d}t}\widehat{\boldsymbol{x}}_{\mathrm{s}} = \widehat{\omega}_{\mathrm{s},1} \underbrace{\left(\boldsymbol{N} - \boldsymbol{l}_{\mathrm{s}}\boldsymbol{c}^\top\right)}_{=:\, \boldsymbol{A}_{\mathrm{s}} \in \mathbb{R}^{2n\times 2n}} \widehat{\boldsymbol{x}}_{\mathrm{s}} + \widehat{\omega}_{\mathrm{s},1}\boldsymbol{l}_{\mathrm{s}} y, \quad \widehat{\boldsymbol{x}}_{\mathrm{s}}(t_i) = \widehat{\boldsymbol{x}}_{\mathrm{s},t_i}, \quad \widehat{y}_{\mathrm{s}} = \boldsymbol{c}^\top \widehat{\boldsymbol{x}}_{\mathrm{s}} \tag{3.19}$$

with $\boldsymbol{c}$ as introduced in (3.4), $\boldsymbol{N}$ as in (3.6), $\widehat{\boldsymbol{x}}_{\mathrm{s}} := \left(\widehat{x}_{\mathrm{s},1}^{\alpha}, \widehat{x}_{\mathrm{s},1}^{\beta}, \cdots, \widehat{x}_{\mathrm{s},n}^{\alpha}, \widehat{x}_{\mathrm{s},n}^{\beta}\right) \in \mathbb{R}^{2n}$ and $\boldsymbol{l}_{\mathrm{s}} := \left(l_{\mathrm{s},1}^{\alpha}, 0, \cdots, l_{\mathrm{s},n}^{\alpha}, 0\right) \in \mathbb{R}^{2n}$. To visualize (3.19), Figure 3.6 shows the corresponding block diagram and a corresponding detailed single sSOGI for the j-th component.

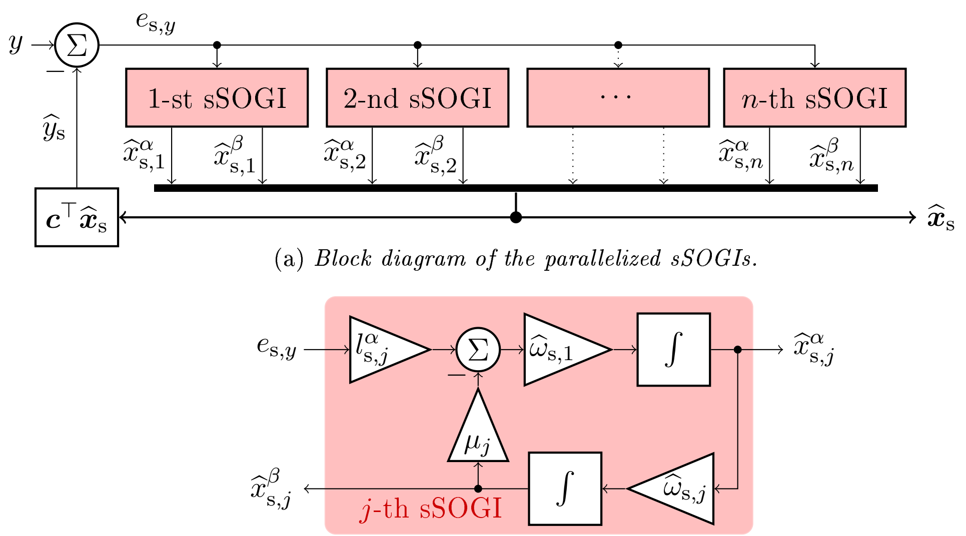

(a) *Block diagram of the parallelized sSOGIs.*

(b) *Construction of the j-th sSOGI.*

Figure 3.6: *(a): The parallelized structure of sSOGIs and (b): the j-th sSOGI for estimating amplitude and phase of the j-th component.*

To understand the functionality of this system, the system's transfer functions are given by (see Appendix A)

$$
\begin{aligned}
\mathcal{X}^{\alpha}_{\mathrm{s},i}(s) &:= \frac{\widehat{x}^{\alpha}_{\mathrm{s},i}(s)}{y(s)} = \frac{s\widehat{\omega}_{\mathrm{s},1} l^{\alpha}_{\mathrm{s},i} \prod\limits_{\substack{k=1\\k\neq i}}^{n} \left(s^2+\widehat{\omega}^2_{\mathrm{s},k}\right)}{\prod\limits_{k=1}^{n}\left(s^2+\widehat{\omega}^2_{\mathrm{s},k}\right)+\sum\limits_{j=1}^{n} s\widehat{\omega}_{\mathrm{s},1} l^{\alpha}_{\mathrm{s},j} \prod\limits_{\substack{k=1\\k\neq j}}^{n}\left(s^2+\widehat{\omega}^2_{\mathrm{s},k}\right)}, \\
\mathcal{X}^{\beta}_{\mathrm{s},i}(s) &:= \frac{\widehat{x}^{\beta}_{\mathrm{s},i}(s)}{y(s)} = \frac{\widehat{\omega}_{\mathrm{s},1}\widehat{\omega}_{\mathrm{s},i} l^{\alpha}_{\mathrm{s},i} \prod\limits_{\substack{k=1\\k\neq i}}^{n} \left(s^2+\widehat{\omega}^2_{\mathrm{s},k}\right)}{\prod\limits_{k=1}^{n}\left(s^2+\widehat{\omega}^2_{\mathrm{s},k}\right)+\sum\limits_{j=1}^{n} s\widehat{\omega}_{\mathrm{s},1} l^{\alpha}_{\mathrm{s},j} \prod\limits_{\substack{k=1\\k\neq j}}^{n}\left(s^2+\widehat{\omega}^2_{\mathrm{s},k}\right)}, \\
\mathcal{E}_{\mathrm{s},y}(s) &:= \frac{e_{\mathrm{s},y}(s)}{y(s)} = \frac{\prod\limits_{k=1}^{n} \left(s^2+\widehat{\omega}^2_{\mathrm{s},k}\right)}{\prod\limits_{k=1}^{n}\left(s^2+\widehat{\omega}^2_{\mathrm{s},k}\right)+\sum\limits_{j=1}^{n} s\widehat{\omega}_{\mathrm{s},1} l^{\alpha}_{\mathrm{s},j} \prod\limits_{\substack{k=1\\k\neq j}}^{n}\left(s^2+\widehat{\omega}^2_{\mathrm{s},k}\right)}.
\end{aligned}
\tag{3.20}
$$

By defining the abbreviations

$$
\rho_{\mathrm{s}}(\omega) := \prod_{k=1}^{n}\left(\widehat{\omega}^2_{\mathrm{s},k}-\omega^2\right) \quad \text{and} \quad \upsilon_{\mathrm{s}}(\omega) := \sum_{j=1}^{n} \omega\widehat{\omega}_{\mathrm{s},1} l^{\alpha}_{\mathrm{s},j} \prod_{\substack{k=1\\k\neq j}}^{n}\left(\widehat{\omega}^2_{\mathrm{s},k}-\omega^2\right),
$$

the respective amplitude and phase responses are calculated depending on the input angular frequency ω with the formulas given in Appendix (A) as follows

$$
\begin{aligned}
A_{\mathcal{X}^{\alpha}_{\mathrm{s},i}}(\omega_j) &= \frac{\omega_j\widehat{\omega}_{\mathrm{s},1} l^{\alpha}_{\mathrm{s},i} \prod\limits_{\substack{k=1\\k\neq i}}^{n}\left(\widehat{\omega}^2_{\mathrm{s},k}-\omega_j^2\right)}{\sqrt{\rho^2_{\mathrm{s}}(\omega_j)+\upsilon^2_{\mathrm{s}}(\omega_j)}}, \quad \Phi_{\mathcal{X}^{\alpha}_{\mathrm{s},i}}(\omega_j) = \operatorname{arctan2}\left(\frac{\rho_{\mathrm{s}}(\omega_j)}{\upsilon_{\mathrm{s}}(\omega_j)}\right), \\
A_{\mathcal{X}^{\beta}_{\mathrm{s},i}}(\omega_j) &= \frac{\widehat{\omega}_{\mathrm{s},1}\widehat{\omega}_{\mathrm{s},i} l^{\alpha}_{\mathrm{s},i} \prod\limits_{\substack{k=1\\k\neq i}}^{n}\left(\widehat{\omega}^2_{\mathrm{s},k}-\omega_j^2\right)}{\sqrt{\rho^2_{\mathrm{s}}(\omega_j)+\upsilon^2_{\mathrm{s}}(\omega_j)}}, \quad \Phi_{\mathcal{X}^{\beta}_{\mathrm{s},i}}(\omega_j) = \operatorname{arctan2}\left(\frac{-\upsilon_{\mathrm{s}}(\omega_j)}{\rho_{\mathrm{s}}(\omega_j)}\right), \\
A_{\mathcal{E}_{\mathrm{s},y}}(\omega_j) &= \frac{\prod\limits_{k=1}^{n}\left(\widehat{\omega}^2_{\mathrm{s},k}-\omega_j^2\right)}{\sqrt{\rho^2_{\mathrm{s}}(\omega_j)+\upsilon^2_{\mathrm{s}}(\omega_j)}}, \quad \Phi_{\mathcal{E}_{\mathrm{s},y}}(\omega_j) = \operatorname{arctan2}\left(\frac{-\upsilon_{\mathrm{s}}(\omega_j)}{\rho_{\mathrm{s}}(\omega_j)}\right).
\end{aligned}
\tag{3.21}
$$

They give information on how an input component y_j (see (3.2)) with angular frequency ω_j is represented in the signal estimation error $e_{\mathrm{s},y}$, direct $\widehat{x}^{\alpha}_{\mathrm{s},i}$ or quadrature $\widehat{x}^{\beta}_{\mathrm{s},i}$ signals. More precisely, the amplitude response indicates the amplification of y_j to the investigated signals and the phase response indicates the phase angle lag. Since the actual input signal usually is a superposition of various components with different frequencies ω_j, for every component, the amplitude and phase responses (3.21) must be calculated for each angular frequency ω_j and then superposed again. From (3.21) one can deduce that the i-th sSOGI outputs the i-th harmonic component y_i (and its quadrature component) of the input signal. Other input components y_j are canceled, if their angular frequency is comprised in the parallelized sSOGIs, or filtered (with respective damping and phase angle delay), if not.
With the obtained direct $\widehat{x}^{\alpha}_{\mathrm{s},i}$ and quadrature $\widehat{x}^{\beta}_{\mathrm{s},i}$ signals for each component, its amplitude and phase angle can be calculated as follows:

$$
\forall t \in \mathbb{T}\colon \quad \widehat{a}_{\mathrm{s},i} = \sqrt{(\widehat{x}^{\alpha}_{\mathrm{s},i})^2+(\widehat{x}^{\beta}_{\mathrm{s},i})^2} \qquad \text{and} \qquad \widehat{\phi}_{\mathrm{s},i} = \operatorname{arctan2}\left(\frac{\widehat{x}^{\beta}_{\mathrm{s},i}}{\widehat{x}^{\alpha}_{\mathrm{s},i}}\right). \tag{3.22}
$$

3.2.3 Stability of the parallelized sSOGIs

In Section 3.2.1, the relation between feedback gain l_{s}^{α} and stability for a single sSOGI was investigated. In this section, this relation is investigated for the parallelized sSOGIs; it is stated in the following theorem.

Theorem 3.2.1 (Hurwitz system matrix)**.** *Let $\mathbb{H}_n$ as in (3.18) and $\boldsymbol{A}_{\mathrm{s}}$ as in (3.19). Then, if and only if for all $i \in \{1, \ldots, n\}$ it holds that $l_{\mathrm{s},i}^{\alpha} > 0$, the system matrix $\boldsymbol{A}_{\mathrm{s}}$ is a Hurwitz matrix, i.e.*

$$\forall\, i \in \{1, \ldots, n\} : l_{\mathrm{s},i}^{\alpha} > 0 \quad \Rightarrow \quad \left\{ s \in \mathbb{C} \,\middle|\, \chi_{\boldsymbol{A}_{\mathrm{s}}}(s) := \det(s\boldsymbol{I}_{2n} - \boldsymbol{A}_{\mathrm{s}}) = 0 \right\} \subset \mathbb{C}_{NHP}.$$

Proof. First note that the characteristic polynomial of $\widehat{\omega}_{\mathrm{s},1}\boldsymbol{A}_{\mathrm{s}}$ in (3.19) is given by the denominator of (3.20). It is reduced to the characteristic polynomial of the system matrix $\boldsymbol{A}_{\mathrm{s}}$ by normalization with respect to the angular frequency $\widehat{\omega}_{\mathrm{s},1}$, i.e.

$$\begin{aligned} \chi_{\widehat{\omega}_{\mathrm{s},1}\boldsymbol{A}_{\mathrm{s}}}(s) &= \det(s\boldsymbol{I}_{2n} - \widehat{\omega}_1 \boldsymbol{A}_{\mathrm{s}}) \overset{\widehat{s} := \frac{s}{\widehat{\omega}_{\mathrm{s},1}}}{=} \det(\widehat{\omega}_{\mathrm{s},1}\widehat{s}\boldsymbol{I}_{2n} - \widehat{\omega}_1 \boldsymbol{A}_{\mathrm{s}}) \\ &= \widehat{\omega}_{\mathrm{s},1}^{2n}\det(\widehat{s}\boldsymbol{I}_{2n} - \boldsymbol{A}_{\mathrm{s}}) =: \widehat{\omega}_{\mathrm{s},1}^{2n}\chi_{\boldsymbol{A}_{\mathrm{s}}}(\widehat{s}) \end{aligned} \tag{3.23}$$

$$\begin{aligned} \Rightarrow\ \chi_{\boldsymbol{A}_{\mathrm{s}}}(\widehat{s}) &\overset{(3.20)}{=} \frac{1}{\widehat{\omega}_{\mathrm{s},1}^{2n}} \left[\prod_{k=1}^{n} \left(\widehat{\omega}_{\mathrm{s},1}^2 \widehat{s}^2 + \widehat{\omega}_{\mathrm{s},k}^2\right) + \sum_{j=1}^{n} \widehat{\omega}_{\mathrm{s},1}^2 \widehat{s} l_{\mathrm{s},j}^{\alpha} \prod_{\substack{k=1\\k\neq j}}^{n} \left(\widehat{\omega}_{\mathrm{s},1}^2 \widehat{s}^2 + \widehat{\omega}_{\mathrm{s},k}^2\right) \right] \\ &\overset{(3.5)}{=} \prod_{k=1}^{n} \left(\widehat{s}^2 + \mu_k^2\right) + \sum_{j=1}^{n} \widehat{s} l_{\mathrm{s},j}^{\alpha} \prod_{\substack{k=1\\k\neq j}}^{n} \left(\widehat{s}^2 + \mu_k^2\right). \end{aligned} \tag{3.24}$$

Now, by splitting (3.24) into $\chi_{\boldsymbol{A}_{\mathrm{s}}}(\widehat{s}) = \chi_{\boldsymbol{A}_{\mathrm{s}}}^{e}(\widehat{s}) + \chi_{\boldsymbol{A}_{\mathrm{s}}}^{o}(\widehat{s})$ where $\chi_{\boldsymbol{A}_{\mathrm{s}}}^{e}(\widehat{s})$ and $\chi_{\boldsymbol{A}_{\mathrm{s}}}^{o}(\widehat{s})$ have even and odd orders, resp., Fact 2.5 can be used to investigate the Hurwitz property.
Therefore, all three conditions listed in Fact 2.5 are shown: It is easy to see that if for all $i \in \{1, \ldots, n\}$, $l_{\mathrm{s},i}^{\alpha} > 0$ is satisfied, the coefficients are products and sums of positive constants. Hence, all coefficients of the characteristic polynomial $\chi_{\boldsymbol{A}_{\mathrm{s}}}(\widehat{s})$ are positive, which shows that condition (i) is satisfied.
Next conditions (ii) and (iii) are shown. Note that the roots of the even polynomial $\chi_{\boldsymbol{A}_{\mathrm{s}}}^{e}(\widehat{s})$ are given by

$$\forall\, i \in \{1, \ldots, n\} :\ (\widehat{s}_i^{e})_{1,2} = \pm \jmath \mu_i \quad \Longrightarrow \quad \Re((\widehat{s}_i^{e})_{1,2}) = 0,$$

Except $\widehat{s}_0^{o} = 0$ (clearly, with $\Re(\widehat{s}_0^{o}) = 0$), all other roots of the odd polynomial $\chi_{\boldsymbol{A}_{\mathrm{s}}}^{o}(\widehat{s})$ cannot be computed analytically but can be assessed using the intermediate value theorem. Therefore, consider two consecutive positive imaginary roots $\widehat{s}_i^{e}$ and $\widehat{s}_j^{e}$ of the even polynomial $\chi_{\boldsymbol{A}_{\mathrm{s}}}^{e}(\widehat{s})$, $i, j \in \{1, \ldots, h, i, j, k, \ldots, n\}$. Inserting these roots into the odd polynomial $\chi_{\boldsymbol{A}_{\mathrm{s}}}^{o}(\widehat{s})$ yields

$$\begin{aligned} \chi_{\boldsymbol{A}_{\mathrm{s}}}^{o}(\widehat{s}_i^{e}) &= \jmath \mu_i l_{\mathrm{s},i}^{\alpha} \underbrace{(1-\mu_i^2)\ldots(\mu_h^2-\mu_i^2)}_{=:H_i} \left(\mu_j^2 - \mu_i^2\right) \underbrace{(\mu_k^2-\mu_i^2)\ldots(\mu_n^2-\mu_i^2)}_{=:K_i}, \\ \chi_{\boldsymbol{A}_{\mathrm{s}}}^{o}(\widehat{s}_j^{e}) &= \jmath \mu_j l_{\mathrm{s},j}^{\alpha} \underbrace{(1-\mu_j^2)\ldots(\mu_h^2-\mu_j^2)}_{=:H_j} \left(\mu_i^2 - \mu_j^2\right) \underbrace{(\mu_k^2-\mu_j^2)\ldots(\mu_n^2-\mu_j^2)}_{=:K_j}. \end{aligned} \tag{3.25}$$

Now, according to the intermediate value theorem, a continuous function f has at least one root in the open interval (a, b) if $f(a)$ and $f(b)$ have opposite signs [575, p. 132]. Since the terms H_i, H_j, K_i and K_j contain an equal amount of positive and negative factors and $\mathbb{H}_n \subset \mathbb{Q}_{>0}$, if and only if $\operatorname{sign}(l^{\alpha}_{\mathrm{s},i}) = \operatorname{sign}(l^{\alpha}_{\mathrm{s},j})$ it follows $\operatorname{sign}(\chi^{o}_{\boldsymbol{A}_\mathrm{s}}(\widehat{s}^{e}_{i})) = -\operatorname{sign}(\chi^{o}_{\boldsymbol{A}_\mathrm{s}}(\widehat{s}^{e}_{j}))$. In this case, it follows from the intermediate value theorem that there exists $\widehat{s}^{o} \in \left(\widehat{s}^{e}_{i}, \widehat{s}^{e}_{j}\right)$ such that $\chi^{o}_{\boldsymbol{A}_\mathrm{s}}(\widehat{s}^{o}) = 0$. Hence, $\Re(\widehat{s}^{o}) = 0$ and $\Im(\widehat{s}^{e}_{i}) < \Im(\widehat{s}^{o}) < \Im(\widehat{s}^{e}_{j})$. If two consecutive negative roots or two roots with opposing signs are used instead, the result is identical. Next, according to the fundamental theorem of algebra, a polynomial of m-th order has exactly m roots on $\mathbb{C}$ [575, p. 63]. Since $\deg(\chi^{o}_{\boldsymbol{A}_\mathrm{s}}(\widehat{s})) = 2n-1$ and $\deg(\chi^{e}_{\boldsymbol{A}_\mathrm{s}}(\widehat{s})) = 2n$, for each two consecutive roots of $\chi^{e}_{\boldsymbol{A}_\mathrm{s}}(\widehat{s}) = 0$ there exists exactly one root of $\chi^{o}_{\boldsymbol{A}_\mathrm{s}}(\widehat{s}) = 0$ in between. Thus, conditions (ii) and (iii) are fulfilled. Hence, the matrix $\boldsymbol{A}_\mathrm{s}$ is a Hurwitz matrix. This completes the proof. □

3.2.4 Design of the gain vector: the parallelized esSOGIs

So far, the system is well understood, except for the choice of the gain vector $\boldsymbol{l}_\mathrm{s}$. In literature, common choices are $\boldsymbol{l}_\mathrm{s} = \sqrt{2}\boldsymbol{c}$ [492] and $\boldsymbol{l}_\mathrm{s} = \boldsymbol{c}$ [497]. These usually are chosen such that a certain filtering characteristic is obtained (cf. (3.21)). However, these choices usually result in very slow system dynamics and shall therefore be improved here. The goal of this section is to provide a general method for optimizing the tuning of parallelized sSOGIs in terms of speed of the estimation. An important fact in this context is that the estimation speed of linear systems is determined by its largest eigenvalue. This eigenvalue is referred to as the dominant eigenvalue in the following. Hence, a vector

$$\boldsymbol{l}_\mathrm{es} := \begin{pmatrix} l^{\alpha}_{\mathrm{es},1} & 0 & l^{\alpha}_{\mathrm{es},2} & 0 & \cdots & l^{\alpha}_{\mathrm{es},n} & 0 \end{pmatrix}^{\top} \tag{3.26}$$

(where the subscript “es” means “enhanced standard”) minimizing the dominant eigenvalue of $\boldsymbol{A}_\mathrm{es} := \boldsymbol{N} - \boldsymbol{l}_\mathrm{es}\boldsymbol{c}^{\top}$ must be found. More mathematically speaking, the task is to minimize the following function

$$\lambda_{\max}(\boldsymbol{A}_\mathrm{es}(\boldsymbol{l}_\mathrm{es})) := \min_{\boldsymbol{l}_\mathrm{es}\in\mathbb{R}^{2n}} \left\{ \max_{\Re(\lambda)} \{ \lambda \in \mathbb{C} |\, \det(\lambda \boldsymbol{I}_{2n} - \boldsymbol{A}_\mathrm{es}(\boldsymbol{l}_\mathrm{es})) = 0 \} \right\} \tag{3.27}$$

where λ denotes an eigenvalue. Usually, the eigenvalues can be calculated from the characteristic polynomial $\chi_{\boldsymbol{A}_\mathrm{s}}$ in (3.24). Since this polynomial of degree $2n$ is not factorisable and solutions for random polynomials only can be determined analytically for $0 \leq n \leq 4$ [581], a general and direct correlation between gains and eigenvalues cannot be deduced. Thus, it must be solved numerically by the gradient method [575]. This method takes advantage of characteristics of the matrix $\boldsymbol{A}_\mathrm{es}$: (i) a set of eigenvalues correlates uniquely to a feedback vector $\boldsymbol{l}_\mathrm{es}$ and (ii) for any two vectors $\boldsymbol{l}_{\mathrm{es},1}$, $\boldsymbol{l}_{\mathrm{es},2}$ for which it holds that $\boldsymbol{l}_{\mathrm{es},1} \approx \boldsymbol{l}_{\mathrm{es},2}$, the same holds true for the corresponding eigenvalues. Hence, an algorithm (implemented as MATLAB-code) is developed, beginning with an initial gain vector `lvec_init` and searching the direction minimizing the dominant eigenvalue by the trial and error method. Hereby, the calculation of the eigenvalues is done numerically by the `eig`-function. In the case that in one step multiple equivalent directions are found, the algorithm chooses the last option. The algorithm terminates, if the minimal dominant eigenvalue is found, i.e. if there does not exist any direction resulting in a more minimal dominant eigenvalue *and* if this eigenvalue has negative real part. The respective MATLAB-code is shown in Appendix B.

The enhanced system, referred to as the *enhanced standard SOGI* (esSOGI), is given in its state space representation by

$$\forall\, t \in \mathbb{T}_i: \quad \begin{aligned} \tfrac{\mathrm{d}}{\mathrm{d}t}\widehat{\boldsymbol{x}}_\mathrm{es} &= \widehat{\omega}_{\mathrm{es},1}\boldsymbol{A}_\mathrm{es}\widehat{\boldsymbol{x}}_\mathrm{es} + \widehat{\omega}_{\mathrm{es},1}\boldsymbol{l}_\mathrm{es} y, \quad \widehat{\boldsymbol{x}}_\mathrm{es}(t_i) = \widehat{\boldsymbol{x}}_{\mathrm{es},t_i} \\ \widehat{y}_\mathrm{es} &= \boldsymbol{c}^{\top}\widehat{\boldsymbol{x}}_\mathrm{es}. \end{aligned} \tag{3.28}$$

To validate the parallelized SOGIs graphically, an exemplary simulation is shown in Figure 3.7[6].

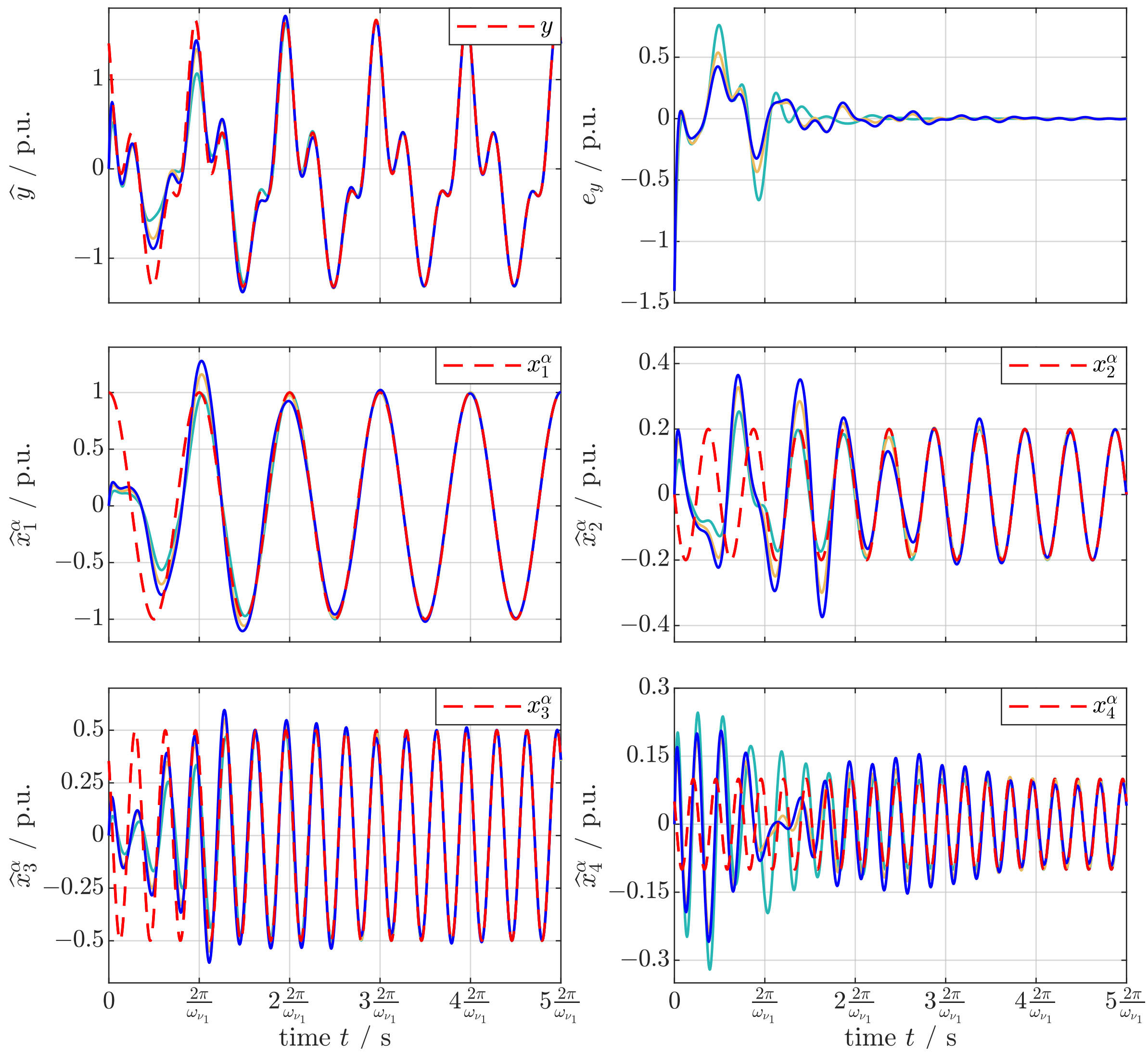

Figure 3.7: *Comparison between parallelized esSOGIs with tuning $\boldsymbol{l}_{\mathrm{es}}$ according to (3.27) (—), parallelized ANFs with tuning $\boldsymbol{l}_{\mathrm{s}} = \boldsymbol{c}$ (—) and parallelized sSOGIs with tuning $\boldsymbol{l}_{\mathrm{s}} = \sqrt{2}\boldsymbol{c}$ (—). Shown are the input y and its decomposition into the direct signals x_1^α – x_4^α, their estimates $\widehat{y}$, $\widehat{x}_1^\alpha$ – $\widehat{x}_4^\alpha$ and the signal estimation error e_y.*

As can be seen in Figure 3.7, the parallelized esSOGIs accurately detects all signal components. Although it is faster than parallelized ANFs and parallelized sSOGIs, it takes about three fundamental periods for the system to settle down. In comparison to Figure 3.5 where only a fundamental system was used, the system with order $n = 4$ is slower. Thus, the question of dependency between the system order n and the dominant eigenvalue $\lambda_{\max}(\boldsymbol{A}_{\mathrm{es}})$ arises. It is answered in Figure 3.8. Hereby, the set $\mathbb{H}_n$ is assumed to be $\mathbb{H}_n = \{1, 2, \ldots, n\} \subset \mathbb{N}$. In Figure 3.8, also the choices from literature, i.e. $\boldsymbol{l}_{\mathrm{s}} \in \{\sqrt{2}\boldsymbol{c}, \boldsymbol{c}\}$ corresponding to parallelized sSOGI and parallelized ANFs, respectively, are shown.

[6] Simulation parameters: $T_s = 1\,\mu\mathrm{s}$, $y = 100\cos(2\pi 50t) + 20\cos(4\pi 50t + \frac{\pi}{2}) + 50\cos(6\pi 50t + \frac{\pi}{4}) + 10\cos(8\pi 50t + \frac{\pi}{3})$, Solver: ode4. All initial values are 0.

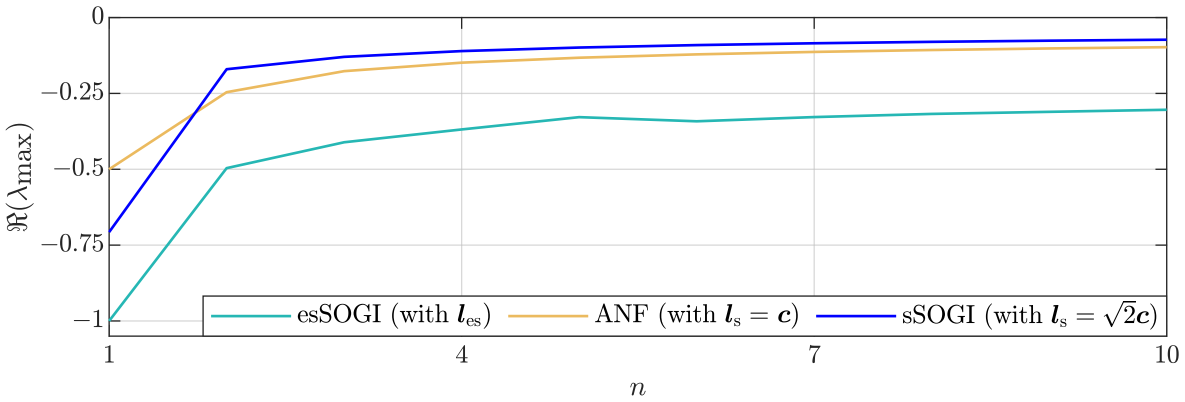

Figure 3.8: *The real part of the dominant eigenvalue $\Re(\lambda_{max})$ of $\boldsymbol{A}_{\mathrm{s}}$ and $\boldsymbol{A}_{\mathrm{es}}$ versus the system order n for different choices of $\boldsymbol{l}_{\mathrm{s}}$ and $\boldsymbol{l}_{\mathrm{es}}$.*

Clearly, for higher system orders, the dominant eigenvalue is getting larger which results in a slower overall system response.

3.2.5 HPF and APC

For now, the system is not capable of detecting offset. On the contrary, the presence of offset in the input signal y will lead to a malfunctioning system as can be seen from the amplitude and phase responses (3.21) (by inserting $\omega_j = 0\,\frac{\mathrm{rad}}{\mathrm{s}}$). Although in the direct signals $\widehat{x}^{\alpha}_{\mathrm{s},i}$ any offset is filtered out completely (and therefore in the estimate of the input $\widehat{y}$ as well), it is still present in the quadrature signals. In view of post processing applications such as the Fortescue transformation [4], it could deteriorate their performance. Hence, an intuitive solution is given by filtering any offset from the input signal, which can be done by a *High Pass Filter* (HPF). Such a HPF has the state space representation

$$\forall t \in \mathbb{T}_i: \quad \left.\begin{array}{rcl} \frac{\mathrm{d}}{\mathrm{d}t} x_{\mathrm{hpf}} & = & -\omega_{\mathrm{hpf}} x_{\mathrm{hpf}} + \omega_{\mathrm{hpf}} y, \quad x_{\mathrm{hpf}}(t_i) = x_{\mathrm{hpf},t_i} \\ y_{\mathrm{hpf}} & = & -x_{\mathrm{hpf}} + y, \end{array}\right\} \tag{3.29}$$

with a constant and positive cut-off angular frequency ω_{hpf}. The filter's transfer function is given by

$$\mathcal{Y}_{\mathrm{hpf}}(s) := \frac{y_{\mathrm{hpf}}(s)}{y(s)} = \frac{s}{s+\omega_{\mathrm{hpf}}}. \tag{3.30}$$

Its amplitude and phase response follow as

$$A_{\mathcal{X}_{\mathrm{hpf}}}(\omega) = \frac{\omega}{\sqrt{\omega_{\mathrm{hpf}}^2+\omega^2}} \quad \text{and} \quad \Phi(\omega)_{\mathcal{X}_{\mathrm{hpf}}} = \operatorname{arctan2}\left(\frac{\omega_{\mathrm{hpf}}}{\omega}\right). \tag{3.31}$$

A High Pass Filter is drawn in Figure 3.9.

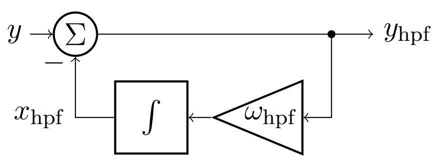

Figure 3.9: *A HPF.*

By feeding the HPF's output signal y_{hpf} to the parallelized esSOGIs, this signal comes without offset, at least in quasi-steady state. On the other hand, each harmonic component is damped and shifted according to (3.31). Consequently, the parallelized esSOGIs estimate these distorted signals, which must be reconstructed again. This can be done in quasi-steady state by an *Amplitude Phase Correction* (APC), which is stated in the following proposition.

Proposition 3.2.2 (Amplitude Phase Correction for HPF). *Let $t \in \mathbb{T}$, $\omega_{\mathrm{hpf}}, \omega > 0$, $a, \phi \in \mathbb{R}$, and let $y := a\cos(\omega t + \phi)$ and $y_{\mathrm{hpf}} := aA_{\mathcal{X}_{\mathrm{hpf}}}(\omega)\cos(\omega t + \phi + \Phi_{\mathcal{X}_{\mathrm{hpf}}}(\omega))$ be the in- and output of a High Pass Filter in quasi-steady state. Further, let q and q_{hpf} be signals having identical amplitude and a phase lag of $-\frac{\pi}{2}$ with respect to y and y_{hpf}, respectively. Then, there exists a correction (transformation) matrix*

$$\boldsymbol{C}_{\mathrm{hpf}} := \begin{bmatrix} 1 & \frac{\omega_{\mathrm{hpf}}}{\omega} \\ -\frac{\omega_{\mathrm{hpf}}}{\omega} & 1 \end{bmatrix} \in \mathbb{R}^{2\times 2} \tag{3.32}$$

such that the amplitude- and phase-corrected signals $\widetilde{y}_{\mathrm{hpf}}$ and $\widetilde{q}_{\mathrm{hpf}}$ have identical phase and amplitude as the input signals, i.e. $y = \widetilde{y}_{\mathrm{hpf}}$ and $q = \widetilde{q}_{\mathrm{hpf}}$ for all $t \in \mathbb{T}$.

Proof. Define

$$\begin{pmatrix} \widetilde{y}_{\mathrm{hpf}} \\ \widetilde{q}_{\mathrm{hpf}} \end{pmatrix} := \boldsymbol{C}_{\mathrm{hpf}} \begin{pmatrix} y_{\mathrm{hpf}} \\ q_{\mathrm{hpf}} \end{pmatrix}, \qquad \boldsymbol{C}_{\mathrm{hpf}} := \begin{bmatrix} c_{\mathrm{hpf},1} & -c_{\mathrm{hpf},2} \\ c_{\mathrm{hpf},2} & c_{\mathrm{hpf},1} \end{bmatrix} \tag{3.33}$$

and observe that

$$\begin{pmatrix} \widetilde{y}_{\mathrm{hpf}} \\ \widetilde{q}_{\mathrm{hpf}} \end{pmatrix} = \begin{bmatrix} c_{\mathrm{hpf},1} & -c_{\mathrm{hpf},2} \\ c_{\mathrm{hpf},2} & c_{\mathrm{hpf},1} \end{bmatrix} \begin{pmatrix} y_{\mathrm{hpf}} \\ q_{\mathrm{hpf}} \end{pmatrix} = \underbrace{\begin{bmatrix} y_{\mathrm{hpf}} & -q_{\mathrm{hpf}} \\ q_{\mathrm{hpf}} & y_{\mathrm{hpf}} \end{bmatrix}}_{=:\boldsymbol{S}_{\mathrm{hpf}}} \begin{pmatrix} c_{\mathrm{hpf},1} \\ c_{\mathrm{hpf},2} \end{pmatrix}. \tag{3.34}$$

Note that, for all $(y_{\mathrm{hpf}}, q_{\mathrm{hpf}}) \in \mathbb{R}^2 \setminus \{\mathbf{0}_2\}$, the matrix $\boldsymbol{S}_{\mathrm{hpf}}$ is invertible:

$$\begin{aligned} \boldsymbol{S}_{\mathrm{hpf}}^{-1} &= \tfrac{1}{(y_{\mathrm{hpf}})^2 + (q_{\mathrm{hpf}})^2} \begin{bmatrix} y_{\mathrm{hpf}} & q_{\mathrm{hpf}} \\ -q_{\mathrm{hpf}} & y_{\mathrm{hpf}} \end{bmatrix} \\ &\overset{\text{def.}}{=} \tfrac{1}{aA_{\mathcal{X}_{\mathrm{hpf}}}(\omega)} \begin{bmatrix} \cos\big(\omega t + \phi + \Phi_{\mathcal{X}_{\mathrm{hpf}}}(\omega)\big) & \sin\big(\omega t + \phi + \Phi_{\mathcal{X}_{\mathrm{hpf}}}(\omega)\big) \\ -\sin\big(\omega t + \phi + \Phi_{\mathcal{X}_{\mathrm{hpf}}}(\omega)\big) & \cos\big(\omega t + \phi + \Phi_{\mathcal{X}_{\mathrm{hpf}}}(\omega)\big) \end{bmatrix}. \end{aligned} \tag{3.35}$$

Therefore, equation (3.34) has a unique solution for $c_{\mathrm{hpf},1}$ and $c_{\mathrm{hpf},2}$. More precisely, by invoking (2.3), one obtains

$$\begin{pmatrix} c_{\mathrm{hpf},1} \\ c_{\mathrm{hpf},2} \end{pmatrix} = \boldsymbol{S}_{\mathrm{hpf}}^{-1} \begin{pmatrix} \widetilde{y}_{\mathrm{hpf}} \\ \widetilde{q}_{\mathrm{hpf}} \end{pmatrix} \overset{!}{=} \boldsymbol{S}_{\mathrm{hpf}}^{-1} \begin{pmatrix} y \\ q \end{pmatrix} \overset{(3.35)}{=} \tfrac{1}{A_{\mathcal{X}_{\mathrm{hpf}}}(\omega)} \begin{pmatrix} \cos\big(\Phi_{\mathcal{X}_{\mathrm{hpf}}}(\omega)\big) \\ -\sin\big(\Phi_{\mathcal{X}_{\mathrm{hpf}}}(\omega)\big) \end{pmatrix} \overset{(3.31)}{=} \begin{pmatrix} 1 \\ -\frac{\omega_{\mathrm{hpf}}}{\omega} \end{pmatrix}. \tag{3.36}$$

Inserting (3.36) into (3.33) yields the matrix in (3.32). This completes the proof. □

In conclusion, by using an HPF as a prefilter to the parallelized esSOGIs, the amplitude and phase distortions resulting from the HPF can be corrected by the APC. Since every harmonic component with angular frequency ω_i is damped and shifted uniquely, for every estimated harmonic component, an APC with angular frequency ω_i (i.e. $\boldsymbol{C}_{\mathrm{hpf},\omega_i}$) is required such that

$$\forall t \in \mathbb{T}, \forall i \in \{1, \dots, n\}: \quad \begin{pmatrix} \widetilde{x}_{y,i} \\ \widetilde{x}_{q,i} \end{pmatrix} := \boldsymbol{C}_{\mathrm{hpf},i} \begin{pmatrix} \widehat{x}^{\alpha}_{\mathrm{es},i} \\ \widehat{x}^{\beta}_{\mathrm{es},i} \end{pmatrix}. \tag{3.37}$$

This also allows the detection of an offset present in the input signal y, but due to the HPF-APC structure, not in the corrected output signals. These signals are merged in the vector

$\widetilde{\boldsymbol{x}} := (\widetilde{x}_{y,1}, \widetilde{x}_{q,1}, \ldots, \widetilde{x}_{y,n}, \widetilde{x}_{q,n})^\top$. Thus, a subtraction of input and estimated output yields the detected offset

$$\forall t \in \mathbb{T}: \quad \widetilde{x}_0 = y - \boldsymbol{c}^\top \widetilde{\boldsymbol{x}}. \tag{3.38}$$

Remark 3.2.3. *Besides the possibility to detect offset, an HPF-APC can also be used to suppress low-order harmonics without the typical amplitude and phase distortions in quasi-steady state.*

Remark 3.2.4. *Considering a Low Pass Filter (LPF) that can be used solely for pre-filtering of high-order harmonics, the derivation of the corresponding matrices $\boldsymbol{C}_{\mathrm{lpf},i}$ is similar as for the matrices $\boldsymbol{C}_{\mathrm{hpf},i}$ and results in*

$$\boldsymbol{C}_{\mathrm{lpf},i} := \begin{bmatrix} 1 & -\frac{\omega_i}{\omega_{\mathrm{hpf}}} \\ \frac{\omega_i}{\omega_{\mathrm{hpf}}} & 1 \end{bmatrix}. \tag{3.39}$$

Its derivation is shown in Appendix C.

Remark 3.2.5. *In the matrices $\boldsymbol{C}_{\mathrm{hpf},i}$ and $\boldsymbol{C}_{\mathrm{lpf},i}$, the actual angular frequencies ω_i, if unknown, must be replaced by the estimated angular frequencies $\widehat{\omega}_{\mathrm{es},i}$.*

3.2.6 The principle idea of an FLL

This section addresses angular frequency estimation. Therefore, at first, the principle idea of a *Frequency Locked Loop* (FLL) is reviewed. It is based on quasi-steady state observations. For these observations, the solutions of the signal estimation error and states of (3.28) in quasi-steady state are required. More precisely, the impact of every harmonic component comprised in the input y to the signal estimation error $e_{\mathrm{es},y}$ and the states $\widehat{x}^\alpha_{\mathrm{es},i}$ and $\widehat{x}^\beta_{\mathrm{es},i}$ is given by

$$\left.\begin{aligned} \widehat{x}^\alpha_{\mathrm{es},i} &= \sum_{j=1}^{n_\infty} a_j A_{\mathcal{X}^\alpha_{\mathrm{es},i}}(\omega_j) \cos\Big(\omega_j t + \phi_j + \Phi_{\mathcal{X}^\alpha_{\mathrm{es},i}}(\omega_j)\Big) =: \sum_{j=1}^{n_\infty} \widehat{x}^\alpha_{\mathrm{es},i,j}, \\ \widehat{x}^\beta_{\mathrm{es},i} &= \sum_{j=1}^{n_\infty} a_j A_{\mathcal{X}^\beta_{\mathrm{es},i}}(\omega_j) \cos\Big(\omega_j t + \phi_j + \Phi_{\mathcal{X}^\beta_{\mathrm{es},i}}(\omega_j)\Big) =: \sum_{j=1}^{n_\infty} \widehat{x}^\beta_{\mathrm{es},i,j}, \\ \text{and} \quad e_{\mathrm{es},y} &= \sum_{j=1}^{n_\infty} a_j A_{\mathcal{E}_{\mathrm{es},y}}(\omega_j) \cos\big(\omega_j t + \phi_j + \Phi_{\mathcal{E}_{\mathrm{es},y}}(\omega_j)\big) =: \sum_{j=1}^{n_\infty} e_{\mathrm{es},y,j}. \end{aligned}\right\} \tag{3.40}$$

The amplitude and phase responses with subscript "es" result from (3.21) by replacing all $l^\alpha_{\mathrm{s},i}$ by $l^\alpha_{\mathrm{es},i}$. The principle idea for a FLL is stated in the following proposition.

Proposition 3.2.6 (Sign-correct adaption for the enhanced standard Frequency Locked Loop over one period)**.** *Let $i \in \{1, \ldots, n\}$, $\omega_i > 0$ and $T_i := \frac{2\pi}{\omega_i}$ and $\nu_i = \mu_i$. Consider system (3.28) with $\widehat{\omega}_{\mathrm{es},i} > 0$ and $\widehat{\boldsymbol{x}}_{\mathrm{es},i,i} := (\widehat{x}^\alpha_{\mathrm{es},i,i}, \widehat{x}^\beta_{\mathrm{es},i,i})^\top$ and the integral*

$$\forall i \in \{1, \ldots, n\}: \quad \int_t^{t+T_i} e_{\mathrm{es},y,i}(\tau) \boldsymbol{\sigma}^\top_{\mathrm{es},i} \widehat{\boldsymbol{x}}_{\mathrm{es},i,i}(\tau) d\tau. \tag{3.41}$$

Therein, $e_{\mathrm{es},y,i}$ is the component of the signal estimation error with angular frequency ω_i and $\widehat{x}^\alpha_{\mathrm{es},i,i}, \widehat{x}^\beta_{\mathrm{es},i,i}$ are components of the i-th states with angular frequency ω_i. All signals are assumed to be in quasi-steady state. Then, the following holds

$$\forall i \in \{1, \ldots, n\}\ \forall \boldsymbol{\sigma}_{\mathrm{es},i} \in \left\{ \begin{pmatrix} \kappa_1 \\ \kappa_2 \end{pmatrix} \in \mathbb{R}^2 \middle| \kappa_2 l^\alpha_{\mathrm{es},i} < 0 \right\}:$$

$$\int_{t}^{t+T_i} e_{\mathrm{es},y,i}\boldsymbol{\sigma}_{\mathrm{es},i}^\top \widehat{\boldsymbol{x}}_{\mathrm{es},i,i}\, d\tau \begin{cases} \geq 0, & \widehat{\omega}_{\mathrm{es},1} < \omega_1 \\ = 0, & \widehat{\omega}_{\mathrm{es},1} = \omega_1 \\ \leq 0, & \widehat{\omega}_{\mathrm{es},1} > \omega_1. \end{cases} \tag{3.42}$$

Moreover, if for any $\kappa \in \mathbb{R}_{<0}$ $\boldsymbol{\sigma}_{\mathrm{es},\nu} = (0,\, \kappa)^\top$ *is chosen, then the phase angles of* $e_{\mathrm{es},y,i}$ *and* $\boldsymbol{\sigma}_{\mathrm{es},i}^\top \widehat{\boldsymbol{x}}_{\mathrm{es},i,i}$ *are identical.*

Proof. Define for all $i \in \{1, \ldots, n\}$ $\boldsymbol{\sigma}_{\mathrm{es},i} := (\sigma_{\mathrm{es},i}^\alpha,\, \sigma_{\mathrm{es},i}^\beta)^\top \in \mathbb{R}^2$ and observe that

$$\begin{aligned}\boldsymbol{\sigma}_{\mathrm{es},i}^\top \widehat{\boldsymbol{x}}_{\mathrm{es},i,i} \overset{(3.40)}{=} {} & \sigma_{\mathrm{es},i}^\alpha a_i A_{\mathcal{X}_{\mathrm{es},i}^\alpha}(\omega_i) \cos\Big(\omega_i t + \phi_i + \Phi_{\mathcal{X}_{\mathrm{es},i}^\alpha}(\omega_i)\Big) \\ & + \sigma_{\mathrm{es},i}^\beta a_i A_{\mathcal{X}_{\mathrm{es},i}^\beta}(\omega_i) \cos\Big(\omega_i t + \phi_i + \Phi_{\mathcal{X}_{\mathrm{es},i}^\beta}(\omega_i)\Big).\end{aligned} \tag{3.43}$$

Invoking (2.5) it follows

$$\begin{aligned}\boldsymbol{\sigma}_{\mathrm{es},i}^\top \widehat{\boldsymbol{x}}_{\mathrm{es},i,i} \overset{(3.43)}{=} {} & \Big[\big(\sigma_{\mathrm{es},i}^\alpha a_i A_{\mathcal{X}_{\mathrm{es},i}^\alpha}(\omega_i)\big)^2 + \big(\sigma_{\mathrm{es},i}^\beta a_i A_{\mathcal{X}_{\mathrm{es},i}^\beta}(\omega_i)\big)^2 \\ & + 2\sigma_{\mathrm{es},i}^\alpha \sigma_{\mathrm{es},i}^\beta a_i^2 A_{\mathcal{X}_{\mathrm{es},i}^\alpha}(\omega_i) A_{\mathcal{X}_{\mathrm{es},i}^\beta}(\omega_i) \cos\Big(\Phi_{\mathcal{X}_{\mathrm{es},i}^\beta}(\omega_i) - \Phi_{\mathcal{X}_{\mathrm{es},i}^\alpha}(\omega_i)\Big)\Big]^{\frac{1}{2}} \\ & \cdot \cos\left(\omega_i t + \phi_i + \Phi_{\mathcal{X}_{\mathrm{es},i}^\beta}(\omega_i)\right. \\ & \left. + \operatorname{arctan2}\left(\frac{\sigma_{\mathrm{es},i}^\alpha A_{\mathcal{X}_{\mathrm{es},i}^\alpha}(\omega_i) \sin\Big(\Phi_{\mathcal{X}_{\mathrm{es},i}^\alpha}(\omega_i) - \Phi_{\mathcal{X}_{\mathrm{es},i}^\beta}(\omega_i)\Big)}{\sigma_{\mathrm{es},i}^\beta A_{\mathcal{X}_{\mathrm{es},i}^\beta}(\omega_i) + \sigma_{\mathrm{es},i}^\alpha A_{\mathcal{X}_{\mathrm{es},i}^\alpha}(\omega_i) \cos\Big(\Phi_{\mathcal{X}_{\mathrm{es},i}^\alpha}(\omega_i) - \Phi_{\mathcal{X}_{\mathrm{es},i}^\beta}(\omega_i)\Big)}\right)\right) \\ \overset{(3.21)}{=} {} & \left[(\sigma_{\mathrm{es},i}^\alpha)^2 a_i^2 \frac{\omega_i^2 \widehat{\omega}_{\mathrm{es},1}^2 (l_{\mathrm{es},i}^\alpha)^2 \prod_{\substack{k=1 \\ k\neq i}}^{n} \big(\widehat{\omega}_{\mathrm{es},k}^2 - \omega_i^2\big)^2}{\rho_{\mathrm{es}}^2(\omega_i) + \upsilon_{\mathrm{es}}^2(\omega_i)} + (\sigma_{\mathrm{es},i}^\beta)^2 a_i^2 \frac{\widehat{\omega}_{\mathrm{es},1}^2 \widehat{\omega}_{\mathrm{es},i}^2 (l_{\mathrm{es},i}^\alpha)^2 \prod_{\substack{k=1 \\ k\neq i}}^{n} \big(\widehat{\omega}_{\mathrm{es},k}^2 - \omega_i^2\big)^2}{\rho_{\mathrm{es}}^2(\omega_i) + \upsilon_{\mathrm{es}}^2(\omega_i)}\right. \\ & \left. + 2\sigma_{\mathrm{es},i}^\alpha \sigma_{\mathrm{es},i}^\beta a_i^2 \frac{\omega_i \widehat{\omega}_{\mathrm{es},1}^2 \widehat{\omega}_{\mathrm{es},i} (l_{\mathrm{es},i}^\alpha)^2 \prod_{\substack{k=1 \\ k\neq i}}^{n} \big(\widehat{\omega}_{\mathrm{es},k}^2 - \omega_i^2\big)^2}{\rho_{\mathrm{es}}^2(\omega_i) + \upsilon_{\mathrm{es}}^2(\omega_i)} \cos\Big(\Phi_{\mathcal{X}_{\mathrm{es},i}^\beta}(\omega_i) - \Phi_{\mathcal{X}_{\mathrm{es},i}^\alpha}(\omega_i)\Big)\right]^{\frac{1}{2}} \\ & \cdot \cos\left(\omega_i t + \phi_i + \Phi_{\mathcal{X}_{\mathrm{es},i}^\beta}(\omega_i)\right. \\ & \left. + \operatorname{arctan2}\left(\frac{\sigma_{\mathrm{es},i}^\alpha \omega_i \sin\left(\Phi_{\mathcal{X}_{\mathrm{es},i}^\alpha}(\omega_i) - \Phi_{\mathcal{X}_{\mathrm{es},i}^\beta}(\omega_i)\right)}{\sigma_{\mathrm{es},i}^\beta \widehat{\omega}_{\mathrm{es},i} + \sigma_{\mathrm{es},i}^\alpha \omega_i \cos\left(\Phi_{\mathcal{X}_{\mathrm{es},i}^\alpha}(\omega_i) - \Phi_{\mathcal{X}_{\mathrm{es},i}^\beta}(\omega_i)\right)}\right)\right) \\ \overset{(3.21)}{=} {} & \frac{a_i l_{\mathrm{es},i}^\alpha \widehat{\omega}_{\mathrm{es},1} \prod_{\substack{k=1 \\ k\neq i}}^{n} \big(\widehat{\omega}_{\mathrm{es},k}^2 - \omega_i^2\big)}{\sqrt{\rho_{\mathrm{es}}^2(\omega_i) + \upsilon_{\mathrm{es}}^2(\omega_i)}} \Big[(\sigma_{\mathrm{es},i}^\alpha)^2 \omega_i^2 + (\sigma_{\mathrm{es},i}^\beta)^2 \widehat{\omega}_{\mathrm{es},i}^2 \\ & + 2\sigma_{\mathrm{es},i}^\alpha \sigma_{\mathrm{es},i}^\beta \omega_i \widehat{\omega}_{\mathrm{es},i} \cos\Big(\operatorname{arctan2}\Big(\tfrac{-\upsilon_{\mathrm{es}}(\omega_i)}{\rho_{\mathrm{es}}(\omega_i)}\Big) - \operatorname{arctan2}\Big(\tfrac{\rho_{\mathrm{es}}(\omega_i)}{\upsilon_{\mathrm{es}}(\omega_i)}\Big)\Big)\Big]\end{aligned}$$

$$
\begin{aligned}
&\cdot \cos\Bigg(\omega_i t + \phi_i + \operatorname{arctan2}\left(\frac{-\upsilon_{\mathrm{es}}(\omega_i)}{\rho_{\mathrm{es}}(\omega_i)}\right) \\
&+ \operatorname{arctan2}\left(\frac{\sigma^{\alpha}_{\mathrm{es},i}\omega_i \sin\left(\operatorname{arctan2}\left(\frac{\rho_{\mathrm{es}}(\omega_i)}{\upsilon_{\mathrm{es}}(\omega_i)}\right) - \operatorname{arctan2}\left(\frac{-\upsilon_{\mathrm{es}}(\omega_i)}{\rho_{\mathrm{es}}(\omega_i)}\right)\right)}{\sigma^{\beta}_{\mathrm{es},i}\widehat{\omega}_{\mathrm{es},i} + \sigma^{\alpha}_{\mathrm{es},i}\omega_i \cos\left(\operatorname{arctan2}\left(\frac{\rho_{\mathrm{es}}(\omega_i)}{\upsilon_{\mathrm{es}}(\omega_i)}\right) - \operatorname{arctan2}\left(\frac{-\upsilon_{\mathrm{es}}(\omega_i)}{\rho_{\mathrm{es}}(\omega_i)}\right)\right)}\right)\Bigg) \\
\overset{(2.6)}{=}\ & \frac{a_i l^{\alpha}_{\mathrm{es},i}\widehat{\omega}_{\mathrm{es},1} \prod_{\substack{k=1\\k\neq i}}^{n} \left(\widehat{\omega}^2_{\mathrm{es},k} - \omega_i^2\right)}{\sqrt{\rho^2_{\mathrm{es}}(\omega_i) + \upsilon^2_{\mathrm{es}}(\omega_i)}} \Big[(\sigma^{\alpha}_{\mathrm{es},i})^2\omega_i^2 + (\sigma^{\beta}_{\mathrm{es},i})^2\widehat{\omega}^2_{\mathrm{es},i} \\
&+ 2\sigma^{\alpha}_{\mathrm{es},i}\sigma^{\beta}_{\mathrm{es},i}\omega_i\widehat{\omega}_{\mathrm{es},i}\cos\left(\operatorname{arctan2}\left(\frac{-\upsilon^2_{\mathrm{es}}(\omega_i) - \rho^2_{\mathrm{es}}(\omega_i)}{0}\right)\right)\Big]^{\frac{1}{2}} \\
&\cdot \cos\Bigg(\omega_i t + \phi_i + \operatorname{arctan2}\left(\frac{-\upsilon_{\mathrm{es}}(\omega_i)}{\rho_{\mathrm{es}}(\omega_i)}\right) \\
&+ \operatorname{arctan2}\left(\frac{\sigma^{\alpha}_{\mathrm{es},i}\omega_i \sin\left(\operatorname{arctan2}\left(\frac{\rho^2_{\mathrm{es}}(\omega_i) + \upsilon^2_{\mathrm{es}}(\omega_i)}{0}\right)\right)}{\sigma^{\beta}_{\mathrm{es},i}\widehat{\omega}_{\mathrm{es},i} + \sigma^{\alpha}_{\mathrm{es},i}\omega_i \cos\left(\operatorname{arctan2}\left(\frac{\rho^2_{\mathrm{es}}(\omega_i) + \upsilon^2_{\mathrm{es}}(\omega_i)}{0}\right)\right)}\right)\Bigg) \\
\overset{(2.7)}{=}\ & \frac{a_i l^{\alpha}_{\mathrm{es},i}\widehat{\omega}_{\mathrm{es},1} \prod_{\substack{k=1\\k\neq i}}^{n} \left(\widehat{\omega}^2_{\mathrm{es},k} - \omega_i^2\right)\sqrt{(\sigma^{\alpha}_{\mathrm{es},i})^2\omega_i^2 + (\sigma^{\beta}_{\mathrm{es},i})^2\widehat{\omega}^2_{\mathrm{es},i}}}{\sqrt{\rho^2_{\mathrm{es}}(\omega_i) + \upsilon^2_{\mathrm{es}}(\omega_i)}} \\
&\cdot \cos\left(\omega_i t + \phi_i + \operatorname{arctan2}\left(\frac{-\upsilon_{\mathrm{es}}(\omega_i)}{\rho_{\mathrm{es}}(\omega_i)}\right) + \operatorname{arctan2}\left(\frac{\sigma^{\alpha}_{\mathrm{es},i}\omega_i}{\sigma^{\beta}_{\mathrm{es},i}\widehat{\omega}_{\mathrm{es},i}}\right)\right) \\
\overset{(2.6)}{=}\ & \frac{a_i l^{\alpha}_{\mathrm{es},i}\widehat{\omega}_{\mathrm{es},1} \prod_{\substack{k=1\\k\neq i}}^{n} \left(\widehat{\omega}^2_{\mathrm{es},k} - \omega_i^2\right)\sqrt{(\sigma^{\alpha}_{\mathrm{es},i})^2\omega_i^2 + (\sigma^{\beta}_{\mathrm{es},i})^2\widehat{\omega}^2_{\mathrm{es},i}}}{\sqrt{\rho^2_{\mathrm{es}}(\omega_i) + \upsilon^2_{\mathrm{es}}(\omega_i)}} \\
&\cdot \cos\left(\omega_i t + \phi_i + \operatorname{arctan2}\left(\frac{\sigma^{\alpha}_{\mathrm{es},i}\omega_i\rho_{\mathrm{es}}(\omega_i) - \sigma^{\beta}_{\mathrm{es},i}\widehat{\omega}_{\mathrm{es},i}\upsilon_{\mathrm{es}}(\omega_i)}{\sigma^{\alpha}_{\mathrm{es},i}\omega_i\upsilon_{\mathrm{es}}(\omega_i) + \sigma^{\beta}_{\mathrm{es},i}\widehat{\omega}_{\mathrm{es},i}\rho_{\mathrm{es}}(\omega_i)}\right)\right).
\end{aligned}
\tag{3.44}
$$

Now, multiplying $\boldsymbol{\sigma}^{\top}_{\mathrm{es},i}\widehat{\boldsymbol{x}}_{\mathrm{es},i,i}$ and $e_{\mathrm{es},y,i}$ yields

$$
\begin{aligned}
e_{\mathrm{es},y,i}\boldsymbol{\sigma}^{\top}_{\mathrm{es},i}\widehat{\boldsymbol{x}}_{\mathrm{es},i,i} \overset{(3.40),(3.44)}{=}\ & a_i A_{\mathcal{E}_{\mathrm{es},y}}(\omega_i)\cos\left(\omega_i t + \phi_i + \Phi_{\mathcal{E}_{\mathrm{es},y}}(\omega_i)\right) \\
&\cdot \frac{a_i l^{\alpha}_{\mathrm{es},i}\widehat{\omega}_{\mathrm{es},1} \prod_{\substack{k=1\\k\neq i}}^{n} \left(\widehat{\omega}^2_{\mathrm{es},k} - \omega_i^2\right)\sqrt{(\sigma^{\alpha}_{\mathrm{es},i})^2\omega_i^2 + (\sigma^{\beta}_{\mathrm{es},i})^2\widehat{\omega}^2_{\mathrm{es},i}}}{\sqrt{\rho^2_{\mathrm{es}}(\omega_i) + \upsilon^2_{\mathrm{es}}(\omega_i)}} \\
&\cdot \cos\left(\omega_i t + \phi_i + \operatorname{arctan2}\left(\frac{\sigma^{\alpha}_{\mathrm{es},i}\omega_i\rho_{\mathrm{es}}(\omega_i) - \sigma^{\beta}_{\mathrm{es},i}\widehat{\omega}_{\mathrm{es},i}\upsilon_{\mathrm{es}}(\omega_i)}{\sigma^{\alpha}_{\mathrm{es},i}\omega_i\upsilon_{\mathrm{es}}(\omega_i) + \sigma^{\beta}_{\mathrm{es},i}\widehat{\omega}_{\mathrm{es},i}\rho_{\mathrm{es}}(\omega_i)}\right)\right) \\
\overset{(3.21)}{=}\ & \frac{a_i^2 l^{\alpha}_{\mathrm{es},i}\widehat{\omega}_{\mathrm{es},1}\left(\widehat{\omega}^2_{\mathrm{es},i} - \omega_i^2\right) \prod_{\substack{k=1\\k\neq i}}^{n} \left(\widehat{\omega}^2_{\mathrm{es},k} - \omega_i^2\right)^2 \sqrt{(\sigma^{\alpha}_{\mathrm{es},i})^2\omega_i^2 + (\sigma^{\beta}_{\mathrm{es},i})^2\widehat{\omega}^2_{\mathrm{es},i}}}{\rho^2_{\mathrm{es}}(\omega_i) + \upsilon^2_{\mathrm{es}}(\omega_i)} \\
&\cdot \cos\left(\omega_i t + \phi_i + \operatorname{arctan2}\left(\frac{-\upsilon_{\mathrm{es}}(\omega_i)}{\rho_{\mathrm{es}}(\omega_i)}\right)\right) \\
&\cdot \cos\left(\omega_i t + \phi_i + \operatorname{arctan2}\left(\frac{\sigma^{\alpha}_{\mathrm{es},i}\omega_i\rho_{\mathrm{es}}(\omega_i) - \sigma^{\beta}_{\mathrm{es},i}\widehat{\omega}_{\mathrm{es},i}\upsilon_{\mathrm{es}}(\omega_i)}{\sigma^{\alpha}_{\mathrm{es},i}\omega_i\upsilon_{\mathrm{es}}(\omega_i) + \sigma^{\beta}_{\mathrm{es},i}\widehat{\omega}_{\mathrm{es},i}\rho_{\mathrm{es}}(\omega_i)}\right)\right).
\end{aligned}
\tag{3.45}
$$

Solving the integral (3.41) over one period $T_i = \frac{2\pi}{\omega_i}$ yields

$$
\begin{aligned}
&\int_t^{t+\frac{2\pi}{\omega_i}} e_{\mathrm{es},y,i}\boldsymbol{\sigma}_{\mathrm{es},i}^\top \widehat{\boldsymbol{x}}_{\mathrm{es},i,i}\mathrm{d}\tau \\
&\overset{(3.45)}{=} \frac{a_i^2 l_{\mathrm{es},i}^\alpha \widehat{\omega}_{\mathrm{es},1}\left(\widehat{\omega}_{\mathrm{es},i}^2-\omega_i^2\right)\prod_{\substack{k=1\\k\neq i}}^n\left(\widehat{\omega}_{\mathrm{es},k}^2-\omega_i^2\right)^2\sqrt{(\sigma_{\mathrm{es},i}^\alpha)^2\omega_i^2+(\sigma_{\mathrm{es},i}^\beta)^2\widehat{\omega}_{\mathrm{es},i}^2}}{\rho_{\mathrm{es}}^2(\omega_i)+\upsilon_{\mathrm{es}}^2(\omega_i)} \\
&\quad\cdot \int_t^{t+\frac{2\pi}{\omega_i}} \cos\left(\omega_i\tau+\phi_i+\operatorname{arctan2}\left(\frac{-\upsilon_{\mathrm{es}}(\omega_i)}{\rho_{\mathrm{es}}(\omega_i)}\right)\right) \\
&\quad\cdot \cos\left(\omega_i\tau+\phi_i+\operatorname{arctan2}\left(\frac{\sigma_{\mathrm{es},i}^\alpha\omega_i\rho_{\mathrm{es}}(\omega_i)-\sigma_{\mathrm{es},i}^\beta\widehat{\omega}_{\mathrm{es},i}\upsilon_{\mathrm{es}}(\omega_i)}{\sigma_{\mathrm{es},i}^\alpha\omega_i\upsilon_{\mathrm{es}}(\omega_i)+\sigma_{\mathrm{es},i}^\beta\widehat{\omega}_{\mathrm{es},i}\rho_{\mathrm{es}}(\omega_i)}\right)\right)\mathrm{d}\tau \\
&\overset{(2.8)}{=} \frac{a_i^2 l_{\mathrm{es},i}^\alpha \widehat{\omega}_{\mathrm{es},1}\left(\widehat{\omega}_{\mathrm{es},i}^2-\omega_i^2\right)\prod_{\substack{k=1\\k\neq i}}^n\left(\widehat{\omega}_{\mathrm{es},k}^2-\omega_i^2\right)^2\sqrt{(\sigma_{\mathrm{es},i}^\alpha)^2\omega_i^2+(\sigma_{\mathrm{es},i}^\beta)^2\widehat{\omega}_{\mathrm{es},i}^2}}{\rho_{\mathrm{es}}^2(\omega_i)+\upsilon_{\mathrm{es}}^2(\omega_i)} \\
&\quad\cdot \frac{\pi}{\omega_i}\cos\left(\operatorname{arctan2}\left(\frac{\sigma_{\mathrm{es},i}^\alpha\omega_i\rho_{\mathrm{es}}(\omega_i)-\sigma_{\mathrm{es},i}^\beta\widehat{\omega}_{\mathrm{es},i}\upsilon_{\mathrm{es}}(\omega_i)}{\sigma_{\mathrm{es},i}^\alpha\omega_i\upsilon_{\mathrm{es}}(\omega_i)+\sigma_{\mathrm{es},i}^\beta\widehat{\omega}_{\mathrm{es},i}\rho_{\mathrm{es}}(\omega_i)}\right)-\operatorname{arctan2}\left(\frac{-\upsilon_{\mathrm{es}}(\omega_i)}{\rho_{\mathrm{es}}(\omega_i)}\right)\right) \\
&\overset{(2.6)}{=} \frac{a_i^2 l_{\mathrm{es},i}^\alpha \widehat{\omega}_{\mathrm{es},1}\left(\widehat{\omega}_{\mathrm{es},i}^2-\omega_i^2\right)\prod_{\substack{k=1\\k\neq i}}^n\left(\widehat{\omega}_{\mathrm{es},k}^2-\omega_i^2\right)^2\sqrt{(\sigma_{\mathrm{es},i}^\alpha)^2\omega_i^2+(\sigma_{\mathrm{es},i}^\beta)^2\widehat{\omega}_{\mathrm{es},i}^2}}{\rho_{\mathrm{es}}^2(\omega_i)+\upsilon_{\mathrm{es}}^2(\omega_i)} \\
&\quad\cdot \frac{\pi}{\omega_i}\cos\left(\operatorname{arctan2}\left(\frac{\sigma_{\mathrm{es},i}^\alpha\omega_i}{\sigma_{\mathrm{es},i}^\beta\widehat{\omega}_{\mathrm{es},i}}\right)\right) \overset{(2.4),(3.5)}{=} \frac{\pi a_i^2 l_{\mathrm{es},i}^\alpha\sigma_{\mathrm{es},i}^\beta\mu_i^2\widehat{\omega}_{\mathrm{es},1}^2\left(\widehat{\omega}_{\mathrm{es},1}^2-\omega_1^2\right)\prod_{\substack{k=1\\k\neq i}}^n\left(\widehat{\omega}_{\mathrm{es},k}^2-\omega_i^2\right)^2}{\omega_1\left(\rho_{\mathrm{es}}^2(\omega_i)+\upsilon_{\mathrm{es}}^2(\omega_i)\right)}. \qquad (3.46)
\end{aligned}
$$

Since $\omega_i > 0$, observe that only $\widehat{\omega}_{\mathrm{es},1}^2 - \omega_1^2$ can change its sign in (3.46). All other terms of the nominator and denominator, except for $l_{\mathrm{es},i}^\alpha\sigma_{\mathrm{es},i}^\beta$, are non-negative. Hence, for $\sigma_{\mathrm{es},i}^\beta l_{\mathrm{es},i}^\alpha < 0$ what, due to $l_{\mathrm{es},i} > 0$ (cf. Section 3.2.1) implies $\sigma_{\mathrm{es},\nu}^\beta < 0$, the following condition is satisfied

$$
\forall\,\boldsymbol{\sigma}_{\mathrm{es},i} \in \left\{\begin{pmatrix}\kappa_1\\\kappa_2\end{pmatrix}\in\mathbb{R}^2 \,\middle|\, \kappa_2 l_{\mathrm{es},i}^\alpha < 0\right\}: \qquad \int_t^{t+T_i} e_{\mathrm{es},y,i}\boldsymbol{\sigma}_{\mathrm{es},i}^\top\widehat{\boldsymbol{x}}_{\mathrm{es},i,i}\mathrm{d}\tau \begin{cases}\geq 0, & \widehat{\omega}_{\mathrm{es},1} < \omega_1\\ = 0, & \widehat{\omega}_{\mathrm{es},1} = \omega_1\\ \leq 0, & \widehat{\omega}_{\mathrm{es},1} > \omega_1.\end{cases}
$$

This proves assertion (3.42). Moreover, for all $\kappa < 0$ and if and only if $\boldsymbol{\sigma}_{\mathrm{es},i} = (0,\,\kappa)^\top$, the phase angle of $\boldsymbol{\sigma}_{\mathrm{es},i}^\top\widehat{\boldsymbol{x}}_{\mathrm{es},i,i}$ is given by

$$
\begin{aligned}
\Phi_{\boldsymbol{\sigma}_{\mathrm{es},i}^\top\widehat{\boldsymbol{x}}_{\mathrm{es},i,i}} &\overset{(3.44)}{=} \operatorname{arctan2}\left(\frac{\sigma_{\mathrm{es},i}^\alpha\omega_1\rho_{\mathrm{es}}(\omega_i)-\sigma_{\mathrm{es},i}^\beta\widehat{\omega}_{\mathrm{es},1}\upsilon_{\mathrm{es}}(\omega_i)}{\sigma_{\mathrm{es},i}^\alpha\omega_1\upsilon_{\mathrm{es}}(\omega_i)+\sigma_{\mathrm{es},i}^\beta\widehat{\omega}_{\mathrm{es},1}\rho_{\mathrm{es}}(\omega_i)}\right) \\
&\overset{\boldsymbol{\sigma}_{\mathrm{es},i}=(0,\kappa)^\top}{=} \operatorname{arctan2}\left(\frac{-\upsilon_{\mathrm{es}}(\omega_i)}{\rho_{\mathrm{es}}(\omega_i)}\right) \overset{(3.21)}{=} \Phi_{\mathcal{E}_{\mathrm{es},y}}(\omega_i).
\end{aligned}
$$

This completes the proof. □

Remark 3.2.7. *In Proposition 3.2.6, the expression* $\int_t^{t+T_i} e_{\mathrm{es},y,i}\boldsymbol{\sigma}_{\mathrm{es},i}^\top\widehat{\boldsymbol{x}}_{\mathrm{es},i,i}d\tau$ *was investigated. However, in view of implementation, only the expression* $\int_t^{t+T_i} e_{\mathrm{es},y}\boldsymbol{\sigma}_{\mathrm{es},i}^\top\widehat{\boldsymbol{x}}_{\mathrm{es},i}d\tau$ *can be evaluated. In the case of higher orders* $n \geq 2$*, or if* $\mathbb{H}_n \neq \mathbb{H}_\infty$*, this integral can be split up into terms* $\int_t^{t+T_i} e_{\mathrm{es},y,i}\boldsymbol{\sigma}_{\mathrm{es},i}^\top\widehat{\boldsymbol{x}}_{\mathrm{es},i,i}d\tau$ *with* $\nu_i = \mu_i$ *(which, according to Proposition 3.2.6, are helpful) and* *others, e.g.* $\int_t^{t+T_i} e_{\text{es},y,j}\boldsymbol{\sigma}_{\text{es},i}^\top \widehat{\boldsymbol{x}}_{\text{es},i,j}\, d\tau$*. The aim of this Remark is to cover these and to show their influence. For any* $T \in \mathbb{R}$*, they are given in general by*

$$\forall\, h,i,j \in \{1,\ldots,n\}: \qquad \int\limits_t^{t+T} e_{\text{es},y,h}\boldsymbol{\sigma}_{\text{es},i}^\top \widehat{\boldsymbol{x}}_{\text{es},i,j}\, d\tau.$$

Repeating the procedure described in the proof for Proposition 3.2.6 up to (3.45) and assuming $\omega_h > \omega_j$*, the integral expression with* $T = \frac{2\pi}{\omega_h-\omega_j}$ *follows as*

$$\begin{aligned}
&\int\limits_t^{t+\frac{2\pi}{\omega_h-\omega_j}} e_{\text{es},y,h}\boldsymbol{\sigma}_{\text{es},i}^\top \widehat{\boldsymbol{x}}_{\text{es},i,j}\, d\tau \\
&\overset{(3.45)}{=} \frac{a_h a_j l_{\text{es},i}^\alpha \widehat{\omega}_{\text{es},1} \prod\limits_{k=1}^{n}\left(\widehat{\omega}_{\text{es},k}^2-\omega_h^2\right)\prod\limits_{\substack{k=1\\k\neq i}}^{n}\left(\widehat{\omega}_{\text{es},k}^2-\omega_j^2\right)\sqrt{(\sigma_{\text{es},i}^\alpha)^2\omega_j^2+(\sigma_{\text{es},i}^\beta)^2\widehat{\omega}_{\text{es},j}^2}}{\sqrt{\rho_{\text{es}}^2(\omega_h)+\upsilon_{\text{es}}^2(\omega_h)}\sqrt{\rho_{\text{es}}^2(\omega_j)+\upsilon_{\text{es}}^2(\omega_j)}} \\
&\quad\cdot \int\limits_t^{t+\frac{2\pi}{\omega_h-\omega_j}} \cos\Bigg(\omega_h\tau+\phi_h+\operatorname{arctan2}\left(\frac{-\upsilon_{\text{es}}(\omega_h)}{\rho_{\text{es}}(\omega_h)}\right)\Bigg) \\
&\quad\cdot\cos\Bigg(\omega_j\tau+\phi_j+\operatorname{arctan2}\left(\frac{\sigma_{\text{es},i}^\alpha\omega_j\rho_{\text{es}}(\omega_j)-\sigma_{\text{es},i}^\beta\widehat{\omega}_{\text{es},j}\upsilon_{\text{es}}(\omega_j)}{\sigma_{\text{es},i}^\alpha\omega_j\upsilon_{\text{es}}(\omega_j)+\sigma_{\text{es},i}^\beta\widehat{\omega}_{\text{es},j}\rho_{\text{es}}(\omega_j)}\right)\Bigg)\, d\tau \\
&\overset{(2.8)}{=} \frac{a_h a_j l_{\text{es},i}^\alpha \widehat{\omega}_{\text{es},1} \prod\limits_{k=1}^{n}\left(\widehat{\omega}_{\text{es},k}^2-\omega_h^2\right)\prod\limits_{\substack{k=1\\k\neq i}}^{n}\left(\widehat{\omega}_{\text{es},k}^2-\omega_j^2\right)\sqrt{(\sigma_{\text{es},i}^\alpha)^2\omega_j^2+(\sigma_{\text{es},i}^\beta)^2\widehat{\omega}_{\text{es},j}^2}}{\sqrt{\rho_{\text{es}}^2(\omega_h)+\upsilon_{\text{es}}^2(\omega_h)}\sqrt{\rho_{\text{es}}^2(\omega_j)+\upsilon_{\text{es}}^2(\omega_j)}} \\
&\quad\cdot\Bigg(\frac{\sin\left(\phi_h+\phi_j+(\omega_h+\omega_j)\left(t+\frac{2\pi}{\omega_h-\omega_j}\right)+\operatorname{arctan2}\left(\frac{-\upsilon_{\text{es}}(\omega_h)}{\rho_{\text{es}}(\omega_h)}\right)+\operatorname{arctan2}\left(\frac{\sigma_{\text{es},i}^\alpha\omega_j\rho_{\text{es}}(\omega_j)-\sigma_{\text{es},i}^\beta\widehat{\omega}_{\text{es},j}\upsilon_{\text{es}}(\omega_j)}{\sigma_{\text{es},i}^\alpha\omega_j\upsilon_{\text{es}}(\omega_j)+\sigma_{\text{es},i}^\beta\widehat{\omega}_{\text{es},j}\rho_{\text{es}}(\omega_j)}\right)\right)}{2(\omega_h+\omega_j)} \\
&\quad-\frac{\sin\left(\phi_h+\phi_j+(\omega_h+\omega_j)t+\operatorname{arctan2}\left(\frac{-\upsilon_{\text{es}}(\omega_h)}{\rho_{\text{es}}(\omega_h)}\right)+\operatorname{arctan2}\left(\frac{\sigma_{\text{es},i}^\alpha\omega_j\rho_{\text{es}}(\omega_j)-\sigma_{\text{es},i}^\beta\widehat{\omega}_{\text{es},j}\upsilon_{\text{es}}(\omega_j)}{\sigma_{\text{es},i}^\alpha\omega_j\upsilon_{\text{es}}(\omega_j)+\sigma_{\text{es},i}^\beta\widehat{\omega}_{\text{es},j}\rho_{\text{es}}(\omega_j)}\right)\right)}{2(\omega_h+\omega_j)}\Bigg) \\
&\overset{(2.6)}{=} \frac{a_h a_j l_{\text{es},i}^\alpha \widehat{\omega}_{\text{es},1} \prod\limits_{k=1}^{n}\left(\widehat{\omega}_{\text{es},k}^2-\omega_h^2\right)\prod\limits_{\substack{k=1\\k\neq i}}^{n}\left(\widehat{\omega}_{\text{es},k}^2-\omega_j^2\right)\sqrt{(\sigma_{\text{es},i}^\alpha)^2\omega_j^2+(\sigma_{\text{es},i}^\beta)^2\widehat{\omega}_{\text{es},j}^2}}{\sqrt{\rho_{\text{es}}^2(\omega_h)+\upsilon_{\text{es}}^2(\omega_h)}\sqrt{\rho_{\text{es}}^2(\omega_j)+\upsilon_{\text{es}}^2(\omega_j)}} \\
&\quad\cdot\frac{\sin\left(\phi_h+\phi_j+(\omega_h+\omega_j)\left(t+\frac{2\pi}{\omega_h-\omega_j}\right)+\delta\right)-\sin\left(\phi_h+\phi_j+(\omega_h+\omega_j)t+\delta\right)}{2(\omega_h+\omega_j)} \\
&\overset{(2.3)}{=} \frac{a_h a_j l_{\text{es},i}^\alpha \widehat{\omega}_{\text{es},1} \prod\limits_{k=1}^{n}\left(\widehat{\omega}_{\text{es},k}^2-\omega_h^2\right)\prod\limits_{\substack{k=1\\k\neq i}}^{n}\left(\widehat{\omega}_{\text{es},k}^2-\omega_j^2\right)\sqrt{(\sigma_{\text{es},i}^\alpha)^2\omega_j^2+(\sigma_{\text{es},i}^\beta)^2\widehat{\omega}_{\text{es},j}^2}}{\sqrt{\rho_{\text{es}}^2(\omega_h)+\upsilon_{\text{es}}^2(\omega_h)}\sqrt{\rho_{\text{es}}^2(\omega_j)+\upsilon_{\text{es}}^2(\omega_j)}} \\
&\quad\cdot\Bigg(\frac{\sin\left(\phi_h+\phi_j+(\omega_h+\omega_j)\left(t+\frac{2\pi}{\omega_h-\omega_j}\right)\right)\cos(\delta)+\cos\left(\phi_h+\phi_j+(\omega_h+\omega_j)\left(t+\frac{2\pi}{\omega_h-\omega_j}\right)\right)\sin(\delta)}{2(\omega_h+\omega_j)} \\
&\quad-\frac{\sin\left(\phi_h+\phi_j+(\omega_h+\omega_j)t\right)\cos(\delta)+\cos\left(\phi_h+\phi_j+(\omega_h+\omega_j)t\right)\sin(\delta)}{2(\omega_h+\omega_j)}\Bigg)
\end{aligned}$$

$$\begin{aligned}
&\overset{(2.4)}{=} \frac{a_h a_j l^{\alpha}_{\mathrm{es},i} \widehat{\omega}_{\mathrm{es},1} \prod\limits_{k=1}^{n} \left(\widehat{\omega}^2_{\mathrm{es},k} - \omega_h^2\right) \prod\limits_{\substack{k=1\\k\neq i}}^{n} \left(\widehat{\omega}^2_{\mathrm{es},k} - \omega_j^2\right)}{(\rho^2_{\mathrm{es}}(\omega_h) + \upsilon^2_{\mathrm{es}}(\omega_h))(\rho^2_{\mathrm{es}}(\omega_j) + \upsilon^2_{\mathrm{es}}(\omega_j))} \\
&\quad \cdot \Bigg(\frac{\sigma^{\alpha}_{\mathrm{es},i} \omega_j (\rho_{\mathrm{es}}(\omega_h) \upsilon_{\mathrm{es}}(\omega_j) + \upsilon_{\mathrm{es}}(\omega_h) \rho_{\mathrm{es}}(\omega_j)) + \sigma^{\beta}_{\mathrm{es},i} \widehat{\omega}_{\mathrm{es},j} (\rho_{\mathrm{es}}(\omega_h) \rho_{\mathrm{es}}(\omega_j) - \upsilon_{\mathrm{es}}(\omega_h) \upsilon_{\mathrm{es}}(\omega_j))}{2(\omega_h + \omega_j)} \\
&\quad \cdot \left(\sin\!\left(\phi_h + \phi_j + (\omega_h + \omega_j) \left(t + \tfrac{2\pi}{\omega_h - \omega_j}\right)\right) - \sin\!\left(\phi_h + \phi_j + (\omega_h + \omega_j)\, t\right) \right) \\
&\quad + \frac{\sigma^{\alpha}_{\mathrm{es},i} \omega_j (\rho_{\mathrm{es}}(\omega_h) \rho_{\mathrm{es}}(\omega_j) - \upsilon_{\mathrm{es}}(\omega_h) \upsilon_{\mathrm{es}}(\omega_j)) - \sigma^{\beta}_{\mathrm{es},i} \widehat{\omega}_{\mathrm{es},j} (\rho_{\mathrm{es}}(\omega_h) \upsilon_{\mathrm{es}}(\omega_j) + \upsilon_{\mathrm{es}}(\omega_h) \rho_{\mathrm{es}}(\omega_j))}{2(\omega_h + \omega_j)} \\
&\quad \cdot \left(\cos\!\left(\phi_h + \phi_j + (\omega_h + \omega_j) \left(t + \tfrac{2\pi}{\omega_h - \omega_j}\right)\right) - \cos\!\left(\phi_h + \phi_j + (\omega_h + \omega_j)\, t\right) \right) \Bigg)
\end{aligned} \tag{3.47}$$

wherein

$$\delta = \operatorname{arctan2}\left(\frac{\sigma^{\alpha}_{\mathrm{es},i} \omega_j (\rho_{\mathrm{es}}(\omega_h) \rho_{\mathrm{es}}(\omega_j) - \upsilon_{\mathrm{es}}(\omega_h) \upsilon_{\mathrm{es}}(\omega_j)) - \sigma^{\beta}_{\mathrm{es},i} \widehat{\omega}_{\mathrm{es},j} (\rho_{\mathrm{es}}(\omega_h) \upsilon_{\mathrm{es}}(\omega_j) + \upsilon_{\mathrm{es}}(\omega_h) \rho_{\mathrm{es}}(\omega_j))}{\sigma^{\alpha}_{\mathrm{es},i} \omega_j (\rho_{\mathrm{es}}(\omega_h) \upsilon_{\mathrm{es}}(\omega_j) + \upsilon_{\mathrm{es}}(\omega_h) \rho_{\mathrm{es}}(\omega_j)) + \sigma^{\beta}_{\mathrm{es},i} \widehat{\omega}_{\mathrm{es},j} (\rho_{\mathrm{es}}(\omega_h) \rho_{\mathrm{es}}(\omega_j) - \upsilon_{\mathrm{es}}(\omega_h) \upsilon_{\mathrm{es}}(\omega_j))} \right).$$

From this expression, no tendency is recognizable. Assuming $\omega_h = \omega_j$ instead what implies $\phi_h = \phi_j$, $a_h = a_j$ and $\mu_i \neq \nu_j$, the result for $T = \frac{2\pi}{\omega_h}$ is obtained as

$$\begin{aligned}
&\int_t^{t+\frac{2\pi}{\omega_h}} e_{\mathrm{es},y,h} \boldsymbol{\sigma}^{\top}_{\mathrm{es},i} \widehat{\boldsymbol{x}}_{\mathrm{es},i,h}\, d\tau \\
&\overset{(3.45)}{=} \frac{a_h^2 l^{\alpha}_{\mathrm{es},i} \widehat{\omega}_{\mathrm{es},1} \left(\widehat{\omega}^2_{\mathrm{es},i} - \omega_h^2\right) \prod\limits_{\substack{k=1\\k\neq i}}^{n} \left(\widehat{\omega}^2_{\mathrm{es},k} - \omega_h^2\right)^2 \sqrt{(\sigma^{\alpha}_{\mathrm{es},i})^2 \omega_h^2 + (\sigma^{\beta}_{\mathrm{es},i})^2 \widehat{\omega}^2_{\mathrm{es},h}}}{\rho^2_{\mathrm{es}}(\omega_h) + \upsilon^2_{\mathrm{es}}(\omega_h)} \\
&\quad \cdot \int_t^{t+\frac{2\pi}{\omega_h}} \cos\!\left(\omega_h \tau + \phi_h + \operatorname{arctan2}\left(\frac{-\upsilon_{\mathrm{es}}(\omega_h)}{\rho_{\mathrm{es}}(\omega_h)}\right)\right) \\
&\quad \cdot \cos\!\left(\omega_h \tau + \phi_h + \operatorname{arctan2}\left(\frac{\sigma^{\alpha}_{\mathrm{es},i} \omega_h \rho_{\mathrm{es}}(\omega_h) - \sigma^{\beta}_{\mathrm{es},i} \widehat{\omega}_{\mathrm{es},h} \upsilon_{\mathrm{es}}(\omega_h)}{\sigma^{\alpha}_{\mathrm{es},i} \omega_h \upsilon_{\mathrm{es}}(\omega_h) + \sigma^{\beta}_{\mathrm{es},i} \widehat{\omega}_{\mathrm{es},h} \rho_{\mathrm{es}}(\omega_h)}\right)\right) d\tau \\
&\overset{(2.8)}{=} \frac{a_h^2 l^{\alpha}_{\mathrm{es},i} \widehat{\omega}_{\mathrm{es},1} \left(\widehat{\omega}^2_{\mathrm{es},i} - \omega_h^2\right) \prod\limits_{\substack{k=1\\k\neq i}}^{n} \left(\widehat{\omega}^2_{\mathrm{es},k} - \omega_h^2\right)^2 \sqrt{(\sigma^{\alpha}_{\mathrm{es},i})^2 \omega_h^2 + (\sigma^{\beta}_{\mathrm{es},i})^2 \widehat{\omega}^2_{\mathrm{es},h}}}{\rho^2_{\mathrm{es}}(\omega_h) + \upsilon^2_{\mathrm{es}}(\omega_h)} \\
&\quad \cdot \frac{\pi}{\omega_h} \cos\!\left(\operatorname{arctan2}\left(\frac{-\upsilon_{\mathrm{es}}(\omega_h)}{\rho_{\mathrm{es}}(\omega_h)}\right) - \operatorname{arctan2}\left(\frac{\sigma^{\alpha}_{\mathrm{es},i} \omega_h \rho_{\mathrm{es}}(\omega_h) - \sigma^{\beta}_{\mathrm{es},i} \widehat{\omega}_{\mathrm{es},h} \upsilon_{\mathrm{es}}(\omega_h)}{\sigma^{\alpha}_{\mathrm{es},i} \omega_h \upsilon_{\mathrm{es}}(\omega_h) + \sigma^{\beta}_{\mathrm{es},i} \widehat{\omega}_{\mathrm{es},h} \rho_{\mathrm{es}}(\omega_h)}\right)\right) \\
&\overset{(2.6)}{=} \frac{\pi a_h^2 l^{\alpha}_{\mathrm{es},i} \widehat{\omega}_{\mathrm{es},1} \left(\widehat{\omega}^2_{\mathrm{es},i} - \omega_h^2\right) \prod\limits_{\substack{k=1\\k\neq i}}^{n} \left(\widehat{\omega}^2_{\mathrm{es},k} - \omega_h^2\right)^2 \sqrt{(\sigma^{\alpha}_{\mathrm{es},i})^2 \omega_h^2 + (\sigma^{\beta}_{\mathrm{es},i})^2 \widehat{\omega}^2_{\mathrm{es},h}}}{\omega_h(\rho^2_{\mathrm{es}}(\omega_h) + \upsilon^2_{\mathrm{es}}(\omega_h))} \cos\!\left(\operatorname{arctan2}\left(\frac{-\sigma^{\alpha}_{\mathrm{es},i} \omega_h}{\sigma^{\beta}_{\mathrm{es},i} \widehat{\omega}_{\mathrm{es},h}}\right)\right) \\
&\overset{(2.4)}{=} \frac{\pi a_h^2 \sigma^{\beta}_{\mathrm{es},i} l^{\alpha}_{\mathrm{es},i} \widehat{\omega}_{\mathrm{es},1} \widehat{\omega}_{\mathrm{es},h} \left(\widehat{\omega}^2_{\mathrm{es},i} - \omega_h^2\right) \prod\limits_{\substack{k=1\\k\neq i}}^{n} \left(\widehat{\omega}^2_{\mathrm{es},k} - \omega_h^2\right)^2}{\omega_h(\rho^2_{\mathrm{es}}(\omega_h) + \upsilon^2_{\mathrm{es}}(\omega_h))}.
\end{aligned} \tag{3.48}$$

Since all factors are positive except for $\sigma^{\beta}_{\mathrm{es},i} l^{\alpha}_{\mathrm{es},i} < 0$ and

$$\widehat{\omega}^2_{\mathrm{es},i} - \omega_h^2 \overset{(3.5)}{=} \mu_i^2 \left(\widehat{\omega}^2_{\mathrm{es},1} - \frac{\nu_h^2}{\mu_i^2} \omega_1^2\right),$$

it follows

$$\forall\, \boldsymbol{\sigma}_{\mathrm{es},i} \in \left\{ \begin{pmatrix} \kappa_1 \\ \kappa_2 \end{pmatrix} \in \mathbb{R}^2 \middle| \kappa_2 l^{\alpha}_{\mathrm{es},i} < 0 \right\}: \quad \int\limits_{t}^{t+\frac{2\pi}{\omega_h}} e_{\mathrm{es},y,h} \boldsymbol{\sigma}^{\top}_{\mathrm{es},i} \widehat{\boldsymbol{x}}_{\mathrm{es},i,h}\, d\tau \begin{cases} \geq 0, & \widehat{\omega}_{\mathrm{es},1} < \frac{\nu_h}{\nu_i}\omega_1 \\ = 0, & \widehat{\omega}_{\mathrm{es},1} = \frac{\nu_h}{\nu_i}\omega_1 \\ \leq 0, & \widehat{\omega}_{\mathrm{es},1} > \frac{\nu_h}{\nu_i}\omega_1. \end{cases} \tag{3.49}$$

Note that this counteracts the desired goal.
In conclusion, although the statement of Proposition 3.2.6 suggests that for each i-th component to be estimated, a vector $\boldsymbol{\sigma}_{\mathrm{es},i}$ *should be multiplied by the respective states, this is counterproductive due to (3.49). To illustrate this, consider the following example. Assume that an input signal contains more than one harmonic component, e.g.*

$$\forall\, t \geq t_0\colon \quad y = a_1 \cos(\omega_1 t + \phi_1) + a_2 \cos(\omega_2 t + \phi_2)$$

where the fundamental amplitude a_1 *dominates* a_2*. This signal shall be estimated by parallelized esSOGIs. Assume that the parallelized esSOGIs have appropriate orders* $\mathbb{H}_n = \mathbb{H}_\infty = \{1, \nu\}$ *but are initialized with a wrong reference angular frequency* $\widehat{\omega}_{\mathrm{es},1} \neq \omega_1$*. Consequently, the signal estimation error* $e_{\mathrm{es},y}$ *as well as the parallelized esSOGIs states* $\widehat{x}^{\alpha}_{\mathrm{es},i}, \widehat{x}^{\beta}_{\mathrm{es},i}$ *contain all angular frequency components included in the input signal (in the quasi-stationary state). Now, if all parallelized esSOGI states are weighted by* $\boldsymbol{\sigma}_{\mathrm{es},i}$ *and multiplied by the signal estimation error, for the given example this would result in*

$$\begin{aligned} e_{\mathrm{es},y} \left(\boldsymbol{\sigma}^{\top}_{\mathrm{es},1} \widehat{\boldsymbol{x}}_{\mathrm{es},1} + \boldsymbol{\sigma}^{\top}_{\mathrm{es},2} \widehat{\boldsymbol{x}}_{\mathrm{es},2} \right) &\overset{(3.40)}{=} e_{\mathrm{es},y,1} \boldsymbol{\sigma}^{\top}_{\mathrm{es},1} \widehat{\boldsymbol{x}}_{\mathrm{es},1,1} + e_{\mathrm{es},y,1} \boldsymbol{\sigma}^{\top}_{\mathrm{es},1} \widehat{\boldsymbol{x}}_{\mathrm{es},1,2} + e_{\mathrm{es},y,1} \boldsymbol{\sigma}^{\top}_{\mathrm{es},2} \widehat{\boldsymbol{x}}_{\mathrm{es},2,1} \\ &+ e_{\mathrm{es},y,1} \boldsymbol{\sigma}^{\top}_{\mathrm{es},2} \widehat{\boldsymbol{x}}_{\mathrm{es},2,2} + e_{\mathrm{es},y,2} \boldsymbol{\sigma}^{\top}_{\mathrm{es},1} \widehat{\boldsymbol{x}}_{\mathrm{es},1,1} + e_{\mathrm{es},y,2} \boldsymbol{\sigma}^{\top}_{\mathrm{es},1} \widehat{\boldsymbol{x}}_{\mathrm{es},1,2} + e_{\mathrm{es},y,2} \boldsymbol{\sigma}^{\top}_{\mathrm{es},2} \widehat{\boldsymbol{x}}_{\mathrm{es},2,1} + e_{\mathrm{es},y,2} \boldsymbol{\sigma}^{\top}_{\mathrm{es},2} \widehat{\boldsymbol{x}}_{\mathrm{es},2,2}. \end{aligned}$$

As investigated above, only the terms $e_{\mathrm{es},y,1} \boldsymbol{\sigma}^{\top}_{\mathrm{es},1} \widehat{\boldsymbol{x}}_{\mathrm{es},1,1}$ *and* $e_{\mathrm{es},y,2} \boldsymbol{\sigma}^{\top}_{\mathrm{es},2} \widehat{\boldsymbol{x}}_{\mathrm{es},2,2}$ *help finding the correct estimate of the angular frequency (cf. (3.46)). Meanwhile, the terms* $e_{\mathrm{es},y,1} \boldsymbol{\sigma}^{\top}_{\mathrm{es},2} \widehat{\boldsymbol{x}}_{\mathrm{es},2,1}$ *and* $e_{\mathrm{es},y,\omega_2} \boldsymbol{\sigma}^{\top}_{\mathrm{es},1} \widehat{\boldsymbol{x}}_{\mathrm{es},1,2}$ *disturb the correct estimation (cf. (3.48)). For all other terms, their contribution is unclear (cf. (3.47)). Hence, the following sum dominates the angular frequency adaption*

$$\begin{aligned} e_{\mathrm{es},y,1} \boldsymbol{\sigma}^{\top}_{\mathrm{es},1} \widehat{\boldsymbol{x}}_{\mathrm{es},1,1} + e_{\mathrm{es},y,1} \boldsymbol{\sigma}^{\top}_{\mathrm{es},2} \widehat{\boldsymbol{x}}_{\mathrm{es},2,1} &\overset{(3.46),(3.48)}{=} \\ &\frac{\pi a_1^2 \widehat{\omega}^2_{\mathrm{es},1} \left(l^{\alpha}_{\mathrm{es},1} \sigma^{\beta}_{\mathrm{es},1} \nu^4 \left(\widehat{\omega}^2_{\mathrm{es},1} - \omega_1^2\right) \left(\widehat{\omega}^2_{\mathrm{es},1} - \frac{\omega_1^2}{\nu^2}\right)^2 + l^{\alpha}_{\mathrm{es},2} \sigma^{\beta}_{\mathrm{es},2} \nu^2 \left(\widehat{\omega}^2_{\mathrm{es},1} - \frac{\omega_1^2}{\nu^2}\right) \left(\widehat{\omega}^2_{\mathrm{es},1} - \omega_1^2\right)^2 \right)}{\omega_1 \left(\rho^2_{\mathrm{es}}(\omega_1) + \upsilon^2_{\mathrm{es}}(\omega_1)\right)}. \end{aligned}$$

It has three equilibria: (i) $\widehat{\omega}_{\mathrm{es},1} = \omega_1$*, (ii)* $\widehat{\omega}_{\mathrm{es},1} = \frac{\omega_1}{\nu}$ *and (iii)* $\widehat{\omega}_{\mathrm{es},1} = \sqrt{\frac{l^{\alpha}_{\mathrm{es},1} \sigma^{\beta}_{\mathrm{es},1} + l^{\alpha}_{\mathrm{es},2} \sigma^{\beta}_{\mathrm{es},2}}{l^{\alpha}_{\mathrm{es},1} \sigma^{\beta}_{\mathrm{es},1} \nu^2 + l^{\alpha}_{\mathrm{es},2} \sigma^{\beta}_{\mathrm{es},2}}}\,\omega_1$*. Therefore, considering all states* $\widehat{x}_{\mathrm{es},i}$ *weighted by* $\sigma_{\mathrm{es},i}$ *does not lead to a correct estimate of the angular frequency. In contrast, if the adaption considers only the fundamental components (with highest amplitude), the result for the angular frequency derivative would be*

$$e_{\mathrm{es},y} \boldsymbol{\sigma}^{\top}_{\mathrm{es},1} \widehat{\boldsymbol{x}}_{\mathrm{es},1} \overset{(3.40)}{=} e_{\mathrm{es},y,1} \boldsymbol{\sigma}^{\top}_{\mathrm{es},1} \widehat{\boldsymbol{x}}_{\mathrm{es},1,1} + e_{\mathrm{es},y,1} \boldsymbol{\sigma}^{\top}_{\mathrm{es},1} \widehat{\boldsymbol{x}}_{\mathrm{es},1,2} + e_{\mathrm{es},y,2} \boldsymbol{\sigma}^{\top}_{\mathrm{es},1} \widehat{\boldsymbol{x}}_{\mathrm{es},1,1} + e_{\mathrm{es},y,2} \boldsymbol{\sigma}^{\top}_{\mathrm{es},1} \widehat{\boldsymbol{x}}_{\mathrm{es},1,2}.$$

Although this expression still includes an disturbing term $e_{\mathrm{es},y,2} \boldsymbol{\sigma}^{\top}_{\mathrm{es},1} \widehat{\boldsymbol{x}}_{\mathrm{es},1,2}$*, its impact can be neglected when* a_2 *is assumed to be significantly smaller than* a_1*. Then, the fundamental term* $e_{\mathrm{es},y,1} \boldsymbol{\sigma}^{\top}_{\mathrm{es},1} \widehat{\boldsymbol{x}}_{\mathrm{es},1,1}$ *dominates and, hence, leads to a correct estimate of the angular frequency* $\widehat{\omega}_{\mathrm{es},1}$*.*

Thus, the following adaption law for the *enhanced standard Frequency Locked Loop* (esFLL) is proposed:

$$\forall t \in \mathbb{T}_i\colon \quad \tfrac{\mathrm{d}}{\mathrm{d}t}\widehat{\omega}_{\mathrm{es},1} = \gamma_{\mathrm{es}} e_{\mathrm{es},y} \boldsymbol{\sigma}_{\mathrm{es},1}^{\top} \widehat{\boldsymbol{x}}_{\mathrm{es},1}, \quad \widehat{\omega}_{\mathrm{es},1}(t_i) = \widehat{\omega}_{\mathrm{es},1,t_i} \tag{3.50}$$

with some angular frequency gain $\gamma_{\mathrm{es}} > 0$.

3.2.7 Gain normalization and output saturation for the esFLL

Now that the angular frequency adaption of the esFLL has been investigated, the *Gain Normalization* (GN) for the esFLL is introduced. Its purpose is to normalize the performance of angular frequency adaption with respect to the input signal. A common way to design a GN is to cancel the influence of the input signal's amplitude by the respective estimated amplitude as reported in [515]. Accordingly, the angular frequency adaption law is

$$\forall t \in \mathbb{T}_i\colon \quad \tfrac{\mathrm{d}}{\mathrm{d}t}\widehat{\omega}_{\mathrm{es},1} = \frac{\Gamma_{\mathrm{es}} \widehat{\omega}_{\mathrm{es},1} e_{\mathrm{es},y} \boldsymbol{\sigma}_{\mathrm{es},1}^{\top} \widehat{\boldsymbol{x}}_{\mathrm{es},1}}{\max(\|\widehat{\boldsymbol{x}}_{\mathrm{es},1}\|^2, \varepsilon_{\mathrm{es}})}, \quad \widehat{\omega}_{\mathrm{es},1}(t_i) = \widehat{\omega}_{\mathrm{es},1,t_i} \tag{3.51}$$

with some $\Gamma_{\mathrm{es}} > 0$ and $\varepsilon_{\mathrm{es}} > 0$. Hereby, the constant $\varepsilon_{\mathrm{es}}$ serves as a lower limit for the estimated amplitude to avoid division by zero. However, it is derived by using linearizations as reported in [516]. A variation of this GN-method is found in [476]:

$$\forall t \in \mathbb{T}_i\colon \quad \tfrac{\mathrm{d}}{\mathrm{d}t}\widehat{\omega}_{\mathrm{es},1} = \frac{\Gamma_{\mathrm{es}} e_{\mathrm{es},y} \boldsymbol{\sigma}_{\mathrm{es},1}^{\top} \widehat{\boldsymbol{x}}_{\mathrm{es},1}}{\max(\|\widehat{\boldsymbol{x}}_{\mathrm{es},1}\|^2, \varepsilon_{\mathrm{es}})}, \quad \widehat{\omega}_{\mathrm{es},1}(t_i) = \widehat{\omega}_{\mathrm{es},1,t_i}. \tag{3.52}$$

Both methods do not normalize the angular frequency adaption with respect to the input angular frequency. In fact, the settling time is non-linear dependent on the input angular frequency as will be shown later. To resolve this issue, a total normalization considering amplitude and angular frequency normalization is proposed. According to Claim 2.7 and assuming that y has the unit $\mathcal{U}(y) = \mathrm{U}$, it follows

$$\mathcal{U}(\gamma_{\mathrm{es}}) = \tfrac{1}{\mathrm{U}^2\mathrm{s}^2} \qquad \Longrightarrow \qquad \gamma_{\mathrm{es}} = \frac{\widehat{\omega}_{\mathrm{es},1}^2}{\max(\|\widehat{\boldsymbol{x}}_{\mathrm{es},1}\|^2, \varepsilon_{\mathrm{es}})}\Gamma_{\mathrm{es}}, \qquad \mathcal{U}(\Gamma_{\mathrm{es}}) = 1.$$

This results in the proposed angular frequency adaption law

$$\forall t \in \mathbb{T}_i\colon \quad \tfrac{\mathrm{d}}{\mathrm{d}t}\widehat{\omega}_{\mathrm{es},1} = \frac{\Gamma_{\mathrm{es}} \widehat{\omega}_{\mathrm{es},1}^2 e_{\mathrm{es},y} \boldsymbol{\sigma}_{\mathrm{es},1}^{\top} \widehat{\boldsymbol{x}}_{\mathrm{es},1}}{\max(\|\widehat{\boldsymbol{x}}_{\mathrm{es},1}\|^2, \varepsilon_{\mathrm{es}})}, \quad \widehat{\omega}_{\mathrm{es},1}(t_i) = \widehat{\omega}_{\mathrm{es},1,t_i}. \tag{3.53}$$

To show the effectiveness of the proposed GN, comparative simulations are made rating the performances of three overall systems (esSOGI and esFLL). Such an overall system is called *enhanced standard Frequency Adaptive Observer* (esFAO). Each of the three FAOs uses one of the mentioned GNs. In these simulations, the FAOs are fed by an input signal whose angular frequency is varied over a wide range. For each tested angular frequency, (i) the sampling and simulation time is adapted to the respective input angular frequency such that every test uses an equal amount of samples and (ii) the performances of the FAOs are analyzed in terms of the normlized settling time $t_{\mathrm{set,n}}$. The normalized settling time indicates how much oscillations of the input signal are needed for the estimated angular frequencies to reach and stay within the 1%-band around the reference angular frequency. More precisely, it is defined as

$$\forall t \geq \tfrac{2\pi}{\omega_1} t_{\mathrm{set,n}} \wedge \nexists t < \tfrac{2\pi}{\omega_1} t_{\mathrm{set,n}}\colon \quad 0.99\omega_1 \leq \widehat{\omega}_{\mathrm{es},1} \leq 1.01\omega_1. \tag{3.54}$$

Additionally, to incorporate dependencies from initializations, two different initial values for the estimated angular frequencies are used: $\widehat{\omega}_{\mathrm{es},1,t_i} \in \{0.5\omega_1, 1.5\omega_1\}$. Figure 3.10[7] illustrates the

[7] Simulations parameters: Number of Samples = 400000, $\omega_1 \in \left\{2\pi 10\,\frac{\mathrm{rad}}{\mathrm{s}}, 2\pi 15\,\frac{\mathrm{rad}}{\mathrm{s}}, \ldots, 2\pi 200\,\frac{\mathrm{rad}}{\mathrm{s}}\right\}$, $y = \cos(\omega_1 t)$, Solver: ode4. $\boldsymbol{l}_{\mathrm{es}} = (2,\, 0)^{\top}$, $\boldsymbol{\sigma}_{\mathrm{es},1} = (0,\, -2)^{\top}$, $\varepsilon_{\mathrm{es}} = 0.01$. All initial values (except for the angular

simulation results.

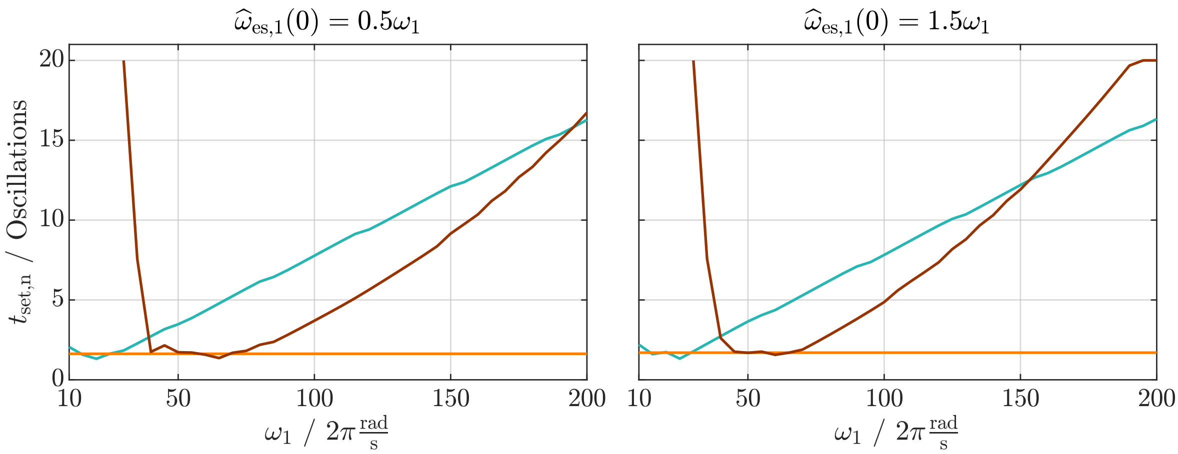

Figure 3.10: *Comparison of different Gain Normalizations in view of the normed settling time t_{set} that is plotted against the input angular frequency ω_1; (3.51): —, (3.52): —, (3.53): —.*

As can be seen from the left and right plot in Figure 3.10, for the known GN methods ((3.51): — and (3.52): —), the normalized settling times depend on the reference angular frequency. This does not hold true for the proposed GN method ((3.53): —) that is constant in the investigated angular frequency range. However, it also can be seen that the settling time is dependent on the chosen initial values for all investigated GN methods. For some frequencies (where $t_{\mathrm{set,n}} = 20$), (3.52) (—) is not able to estimate the correct angular frequency within the given time frame and for $\omega_1 \in \left\{2\pi 10\,\frac{\mathrm{rad}}{\mathrm{s}}, \dots 2\pi 25\,\frac{\mathrm{rad}}{\mathrm{s}}\right\}$, it even diverges.
Thus, (3.53) is the best choice for an adaption law for the angular frequency $\widehat{\omega}_{\mathrm{es},1}$. Nevertheless, it is based on quasi-steady state observations. The quasi-steady state only can be reached, if the linear system (3.28) is stable. This is the case, if the estimated angular frequency is positive[8]. Thus, it must be kept positive which is achieved by an *output saturation* (OS). In detail, the OS limits the estimated angular frequency to lower and upper bounds $0 < \underline{\omega}_{\mathrm{es},1} < \overline{\omega}_{\mathrm{es},1}$, resp. To distinguish between the estimated and the saturated angular frequency, the estimated one is referred to as $\widehat{\omega}_{\mathrm{es},1}$ and the saturated one as $\widehat{\omega}'_{\mathrm{es},1}$. The resulting angular frequency estimation is illustrated in Figure 3.11.

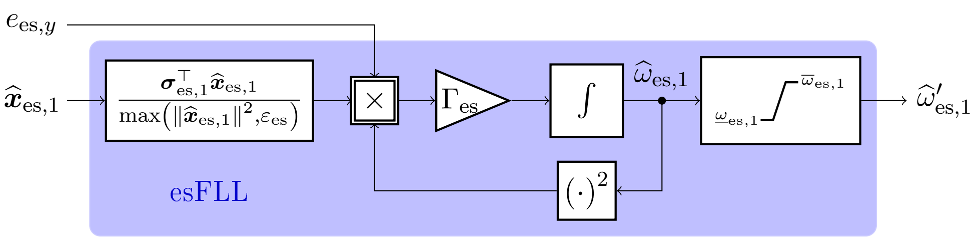

Figure 3.11: *Block diagram of the esFLL.*

3.2.8 Summary and stability proof of the esFAO

In this section, the overall system consisting of HPF, parallelized esSOGIs, esFLL and APC, called the *enhanced standard Frequency Adaptive Observer* (esFAO) is summarized. Its mathe-

frequency) are 0.

[8] All eigenvalues of $\boldsymbol{A}_{\mathrm{es}}$ are multiples of the estimated angular frequency.

matical representation is given by

$$
\forall t \in \mathbb{T}_i\colon \quad \left.\begin{array}{rcll}
\frac{\mathrm{d}}{\mathrm{d}t} x_{\mathrm{hpf}} & = & -\omega_{\mathrm{hpf}} x_{\mathrm{hpf}} + \omega_{\mathrm{hpf}} y, & x_{\mathrm{hpf}}(t_i) = x_{\mathrm{hpf},t_i}, \\
y_{\mathrm{hpf}} & = & -x_{\mathrm{hpf}} + y & \\
\frac{\mathrm{d}}{\mathrm{d}t} \widehat{\boldsymbol{x}}_{\mathrm{es}} & = & \widehat{\omega}_{\mathrm{es},1} \boldsymbol{A}_{\mathrm{es}} \widehat{\boldsymbol{x}}_{\mathrm{es}} + \widehat{\omega}_{\mathrm{es},1} \boldsymbol{l}_{\mathrm{es}} y_{\mathrm{hpf}}, & \widehat{\boldsymbol{x}}_{\mathrm{es}}(t_i) = \widehat{\boldsymbol{x}}_{\mathrm{es},t_i}, \\
\frac{\mathrm{d}}{\mathrm{d}t} \widehat{\omega}'_{\mathrm{es},1} & = & \frac{\Gamma_{\mathrm{es}} \widehat{\omega}'^{2}_{\mathrm{es},1} e_{\mathrm{es},y} \boldsymbol{\sigma}_{\mathrm{es},1}^{\top} \widehat{\boldsymbol{x}}_{\mathrm{es},1}}{\max(\|\widehat{\boldsymbol{x}}_{\mathrm{es},1}\|^2, \varepsilon_{\mathrm{es}})}, & \widehat{\omega}'_{\mathrm{es},1}(t_i) = \widehat{\omega}'_{\mathrm{es},1,t_i}, \\
\widehat{\omega}_{\mathrm{es},1} & = & \mathrm{sat}_{\underline{\omega}_{\mathrm{es},1}}^{\overline{\omega}_{\mathrm{es},1}}\left(\widehat{\omega}'_{\mathrm{es},1}\right), & \\
\widetilde{\boldsymbol{x}}_{\mathrm{es}} & = & \underset{1,\ldots,n}{\mathrm{blkdiag}}\left(\boldsymbol{C}_{\mathrm{hpf},i}\right) \widehat{\boldsymbol{x}}_{\mathrm{es}}, & \\
\widetilde{y}_{\mathrm{es}} & = & \boldsymbol{c}^{\top} \widetilde{\boldsymbol{x}}_{\mathrm{es}}, & \\
\widetilde{x}_{\mathrm{es},0} & = & y - \widetilde{y}_{\mathrm{es}}. &
\end{array}\right\} \tag{3.55}
$$

Its block diagram is illustrated in Figure 3.12.

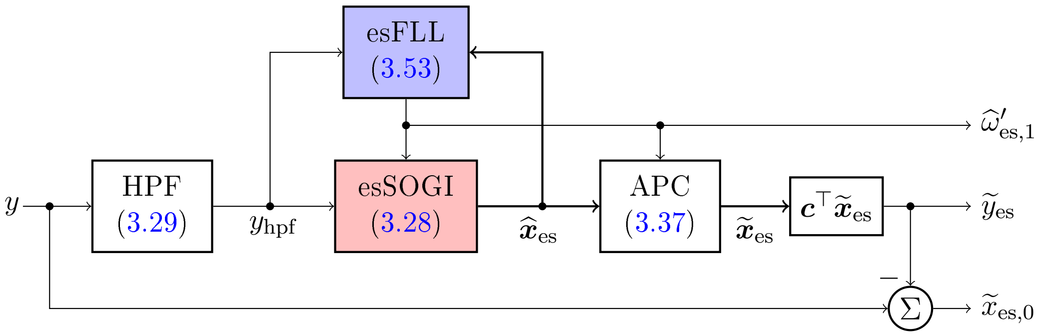

Figure 3.12: *Block diagram of the esFAO.*

To evaluate the esFAO's performance, the test signals introduced in (3.12) and shown in Figure 3.2 are processed by the esFAO. The results are shown in Figure 3.13[9].
Firstly note that, although one estimate for each of the angular frequencies comprised in the input signal is shown, the esFLL only estimates the fundamental one. The other results from this fundamental one by multiplication (and is not estimated). In the case of correctly assumed harmonic orders $\mathbb{H}_\infty = \mathbb{H}_n$, the esFAO settles down within 78.2 ms ($y_{\mathrm{test},N}$) and 86.2 ms ($y_{\mathrm{test},N_\circ}$) where (3.54) was evaluated in view of the estimated angular frequency $\widehat{\omega}'_{\mathrm{es},1}$. If the actual harmonic orders $\mathbb{H}_\infty$ do not match the assumed ones $\mathbb{H}_n$ ($y_{\mathrm{test},Q}, y_{\mathrm{test},Q_\circ}$), the esFAO fails to estimate all parameters satisfactory. However, it still is able to give a rough estimate of the fundamental angular frequency ω_1.
In the following, a stability proof is presented. Note that the HPF is stable for all $\omega_{\mathrm{hpf}} > 0$, which therefore is neglected in the proof.

Theorem 3.2.8 (Bounded-input bounded-state/bounded-output stability of the dynamics of the esFAO)**.** *Consider an essentially bounded input signal, i.e.* $y_{\mathrm{hpf}} \in \mathcal{L}^\infty(\mathbb{R}_{\geq 0}; \mathbb{R})$ *and assume that (i) the estimated fundamental angular frequency is continuous, bounded and uniformly bounded away from zero by* $\overline{\omega}_{\mathrm{es},1} \geq \widehat{\omega}'_{\mathrm{es},1} \geq \underline{\omega}_{\mathrm{es},1} > 0$*, i.e.* $\widehat{\omega}'_{\mathrm{es},1} \in \mathcal{L}^\infty\left(\mathbb{R}_{\geq 0}; \left[\underline{\omega}_{\mathrm{es},1}, \overline{\omega}_{\mathrm{es},1}\right]\right)$ *and (ii) the system matrix* $\boldsymbol{A}_{\mathrm{es}}$ *in (3.28) is a Hurwitz matrix. Then, the time-varying system (3.28) is bounded-input bounded-state/bounded-output stable, i.e.*

$$
\forall t \in \mathbb{T}_i\colon \quad \exists\, c_{\mathrm{es}}, \widetilde{c}_{\mathrm{es}} > 0\colon \qquad \|\widehat{\boldsymbol{x}}_{\mathrm{es}}\| \leq c_{\mathrm{es}} \quad \textit{and} \quad |\widehat{y}_{\mathrm{es}}| \leq \widetilde{c}_{\mathrm{es}}.
$$

[9] Simulation parameters (in addition to Footnote 1): $\mathbb{H}_n = \{1, 2\}$, $\omega_{\mathrm{hpf}} = 2\pi 500$, $\boldsymbol{l}_{\mathrm{es}} = (0.667,\ 0,\ 1.328,\ 0)^\top$, $\Gamma_{\mathrm{es}} = 0.375$, $\boldsymbol{\sigma}_{\mathrm{es},1} = (0,\ -0.667)^\top$, $\varepsilon_{\mathrm{es}} = 10^{-5}$, $\underline{\omega}_{\mathrm{es},1} = 2\pi 35$, $\overline{\omega}_{\mathrm{es},1} = 2\pi 65$.

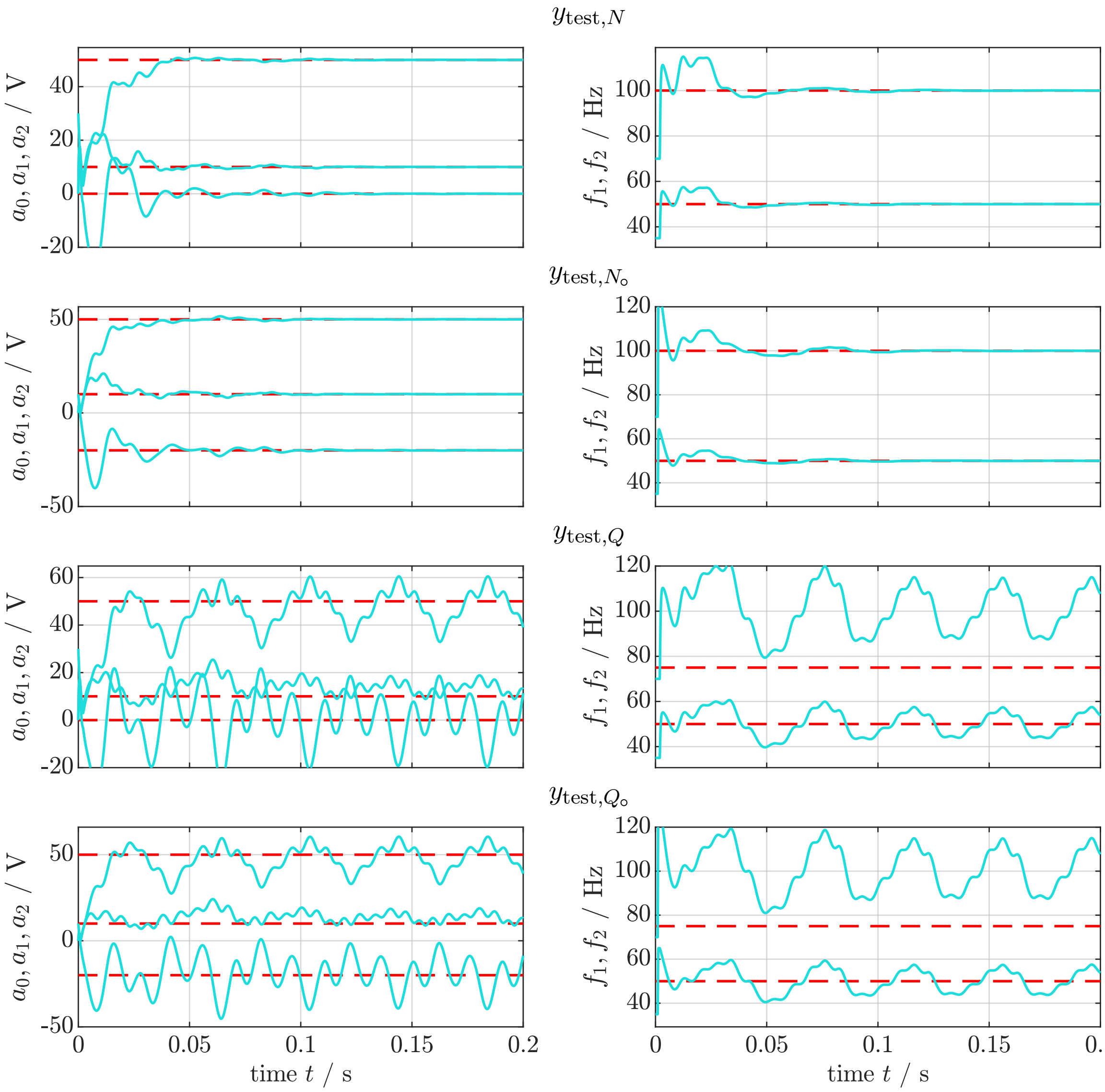

Figure 3.13: *Continuation of Figure 3.2. Offset, amplitudes and frequencies of the test signals estimated/detected by the esFAO (——).*

Proof. Since $\boldsymbol{A}_{\text{es}}$ is Hurwitz, Fact 2.8 holds, which implies the existence of symmetric matrix $0 < \boldsymbol{P}_{\text{es}} \in \mathbb{R}^{2n \times 2n}$. Next, consider the nonnegative Lyapunov-like function

$$V_{\text{es}} \colon \mathbb{R}^{2n} \to \mathbb{R}_{\geq 0}, \quad \widehat{\boldsymbol{x}}_{\text{es}} \mapsto V_{\text{es}}(\widehat{\boldsymbol{x}}_{\text{es}}) := \widehat{\boldsymbol{x}}_{\text{es}}^\top \boldsymbol{P}_{\text{es}} \widehat{\boldsymbol{x}}_{\text{es}}.$$

The right-hand side of (3.28) is locally Lipschitz continuous with bounded Lipschitz constant and bounded exogenous perturbation. Hence, the solution of (3.28) exists globally on $\mathbb{R}_{\geq 0}$ [577, Theorem 2.2.14 & Proposition 2.2.19] (but still might diverge as $t \to \infty$). The time derivative of V_{es} along the solution of (3.28) is, for all $t \geq t_i$, given and upper bounded by

$$\begin{aligned}
\tfrac{\mathrm{d}}{\mathrm{d}t} V_{\text{es}}(\widehat{\boldsymbol{x}}_{\text{es}}) &= \tfrac{\mathrm{d}}{\mathrm{d}t}\widehat{\boldsymbol{x}}_{\text{es}}^\top \boldsymbol{P}_{\text{es}} \widehat{\boldsymbol{x}}_{\text{es}} + \widehat{\boldsymbol{x}}_{\text{es}}^\top \boldsymbol{P}_{\text{es}} \tfrac{\mathrm{d}}{\mathrm{d}t}\widehat{\boldsymbol{x}}_{\text{es}} \\
&\overset{(3.19)}{=} \widehat{\omega}'_{\text{es},1}\left[\widehat{\boldsymbol{x}}_{\text{es}}^\top (\boldsymbol{A}_{\text{es}}^\top \boldsymbol{P}_{\text{es}} + \boldsymbol{P}_{\text{es}} \boldsymbol{A}_{\text{es}}) \widehat{\boldsymbol{x}}_{\text{es}} + 2 \widehat{\boldsymbol{x}}_{\text{es}}^\top \boldsymbol{P}_{\text{es}} \boldsymbol{l}_{\text{es}} y_{\text{hpf}}\right] \\
&\overset{(2.14)}{=} \widehat{\omega}'_{\text{es},1}\left[-\widehat{\boldsymbol{x}}_{\text{es}}^\top \boldsymbol{Q}_{\text{es}} \widehat{\boldsymbol{x}}_{\text{es}} + 2 \widehat{\boldsymbol{x}}_{\text{es}}^\top \boldsymbol{P}_{\text{es}} \boldsymbol{l}_{\text{es}} y_{\text{hpf}}\right]
\end{aligned}$$

$$
\begin{aligned}
&\overset{(2.16)}{\leq} && \widehat{\omega}'_{\mathrm{es},1}\Big[-\lambda_{\min}(\boldsymbol{Q}_{\mathrm{es}})\,\|\widehat{\boldsymbol{x}}_{\mathrm{es}}\|^2 + 2\,\underbrace{\|\widehat{\boldsymbol{x}}_{\mathrm{es}}\|}_{=:\,a}\,\underbrace{\|\boldsymbol{P}_{\mathrm{es}}\|\,\|\boldsymbol{l}_{\mathrm{es}}\|\,\|y_{\mathrm{hpf}}\|_{\infty}}_{=:\,b}\Big] \\
&\overset{(2.15)}{\leq} && \widehat{\omega}'_{\mathrm{es},1}\Big[-\underbrace{\big(\lambda_{\min}(\boldsymbol{Q}_{\mathrm{es}})-\tfrac{1}{m}\big)}_{\exists\, m\geq 1\,\text{s.t.}\,(\cdot)\geq \epsilon_{\mathrm{es},m}>0}\,\|\widehat{\boldsymbol{x}}_{\mathrm{es}}\|^2 + \underbrace{m\,\|\boldsymbol{P}_{\mathrm{es}}\|^2\,\|\boldsymbol{l}_{\mathrm{es}}\|^2\,\|y_{\mathrm{hpf}}\|^2_{\infty}}_{=:\,c_{\mathrm{es},m}<\infty}\Big] \\
&\overset{(2.16)}{\leq} && -\tfrac{\epsilon_{\mathrm{es},m}\underline{\omega}_{\mathrm{es},1}}{\lambda_{\max}(\boldsymbol{P}_{\mathrm{es}})}V_{\mathrm{es}}(\widehat{\boldsymbol{x}}_{\mathrm{es}}) + c_{\mathrm{es},m}\overline{\omega}_{\mathrm{es},1} \\
\overset{(2.17)}{\Longrightarrow}\; V_{\mathrm{es}}(\widehat{\boldsymbol{x}}_{\mathrm{es}}) &\leq && V_{\mathrm{es}}(\widehat{\boldsymbol{x}}_{\mathrm{es},t_i}) + 2c_{\mathrm{es},m}\overline{\omega}_{\mathrm{es},1}\tfrac{\lambda_{\max}(\boldsymbol{P}_{\mathrm{es}})}{\epsilon_{\mathrm{es},m}\underline{\omega}_{\mathrm{es},1}}.
\end{aligned}
\tag{3.56}
$$

Hence, in view of Fact 2.9 and (3.56), and with $\boldsymbol{c}$ as in (3.4), one can conclude that

$$
\forall\, t\in\mathbb{T}_i:\;\|\widehat{\boldsymbol{x}}_{\mathrm{es}}\| \leq \sqrt{\tfrac{1}{\lambda_{\min}(\boldsymbol{P}_{\mathrm{es}})}\left(V_{\mathrm{es}}(\widehat{\boldsymbol{x}}_{\mathrm{es},t_i}) + 2c_{\mathrm{es},m}\overline{\omega}_{\mathrm{es},1}\tfrac{\lambda_{\max}(\boldsymbol{P}_{\mathrm{es}})}{\epsilon_{\mathrm{es},m}\underline{\omega}_{\mathrm{es},1}}\right)} =: c_{\mathrm{es}} < \infty
$$

$$
\text{and}\quad |\widehat{y}_{\mathrm{es}}| \overset{(3.19)}{\leq} \|\boldsymbol{c}\|\,\|\widehat{\boldsymbol{x}}_{\mathrm{es}}\| \leq \|\boldsymbol{c}\|\,c_{\mathrm{es}} =: \widetilde{c}_{\mathrm{es}} < \infty.
$$

This completes the proof. □

Theorem 3.2.9 (Boundedness and exponential decrease of the signal estimation error of the esFAO)**.** *Let $\overline{\omega}_{\mathrm{es},1} \geq \widehat{\omega}'_{\mathrm{es},1} \geq \underline{\omega}_{\mathrm{es},1} > 0$ be bounded. Consider any continuous and bounded input signal, i.e. $y_{\mathrm{hpf}} \in \mathcal{C}(\mathbb{R}_{\geq 0};\mathbb{R}_{>0}) \cap \mathcal{L}^{\infty}(\mathbb{R}_{\geq 0};\mathbb{R})$ and assume that y_{hpf} is fed to the parallelized esSOGIs (3.19) with $\boldsymbol{A}_{\mathrm{es}}$ being a Hurwitz matrix. Then, the signal estimation error, defined by*

$$
\forall\, t\in\mathbb{T}_i:\quad \boldsymbol{e}_{\mathrm{es}} := \boldsymbol{x} - \widehat{\boldsymbol{x}}_{\mathrm{es}} \tag{3.57}
$$

with $\boldsymbol{x}$ as in (3.4) and $\widehat{\boldsymbol{x}}_{\mathrm{es}}$ as in (3.19), is bounded, i.e. there exists $c_{\mathrm{es},e} > 0$ such that $\|\boldsymbol{e}_{\mathrm{es}}\| \leq c_{\mathrm{es},e}$ for all $t \geq t_i$. Moreover, if $\omega_1 = \widehat{\omega}'_{\mathrm{es},1}$ and $\mathbb{H}_{\infty} = \mathbb{H}_n$ for all $t \geq t_i$, then the norm of the signal estimation error is exponentially decreasing, i.e. there exist constants $c_{\mathrm{es},V}, \mu_{\mathrm{es},V} > 0$ such that

$$
\forall\, t\in\mathbb{T}_i:\quad \|\boldsymbol{e}_{\mathrm{es}}\| \leq c_{\mathrm{es},V}\,\|\boldsymbol{e}_{\mathrm{es},t_i}\|\,\mathrm{e}^{-\mu_{\mathrm{es},V}\frac{t-t_i}{2}}.
$$

Proof. First, define the angular frequency error as

$$
e_{\mathrm{es},\omega} := \omega_1 - \widehat{\omega}'_{\mathrm{es},1} \tag{3.58}
$$

and the estimation error vector as

$$
\boldsymbol{e}_{\mathrm{es}} := \boldsymbol{x} - \widehat{\boldsymbol{x}}_{\mathrm{es}}. \tag{3.59}
$$

Next, evaluating the time derivative of the signal estimation error vector yields

$$
\begin{aligned}
\tfrac{\mathrm{d}}{\mathrm{d}t}\boldsymbol{e}_{\mathrm{es}} &\overset{(3.4),(3.19)}{=} \omega_1\boldsymbol{N}\boldsymbol{x} - \widehat{\omega}'_{\mathrm{es},1}\left(\boldsymbol{N} - \boldsymbol{l}_{\mathrm{es}}\boldsymbol{c}^{\top}\right)\widehat{\boldsymbol{x}}_{\mathrm{es}} - \widehat{\omega}'_{\mathrm{es},1}\boldsymbol{l}_{\mathrm{es}}y_{\mathrm{hpf}} \\
&\overset{(3.58),(3.59)}{=} e_{\mathrm{es},\omega}\boldsymbol{N}\boldsymbol{x} + \widehat{\omega}'_{\mathrm{es},1}\boldsymbol{N}\boldsymbol{e}_{\mathrm{es}} - \widehat{\omega}'_{\mathrm{es},1}\boldsymbol{l}_{\mathrm{es}}\boldsymbol{c}^{\top}\boldsymbol{e}_{\mathrm{es}} \\
&\overset{(3.19)}{=} e_{\mathrm{es},\omega}\boldsymbol{N}\boldsymbol{x} + \widehat{\omega}'_{\mathrm{es},1}\boldsymbol{A}_{\mathrm{es}}\boldsymbol{e}_{\mathrm{es}}.
\end{aligned}
\tag{3.60}
$$

Now, the time derivative of the Lyapunov-like function $V_{\mathrm{es}} = \boldsymbol{e}_{\mathrm{es}}^{\top}\boldsymbol{P}_{\mathrm{es}}\boldsymbol{e}_{\mathrm{es}}$ (with $\boldsymbol{P}_{\mathrm{es}}$ as introduced in Theorem 3.2.8) is given for all $t \geq t_i$, along the solution of (3.60), as follows

$$
\tfrac{\mathrm{d}}{\mathrm{d}t}V_{\mathrm{es}}(\boldsymbol{e}_{\mathrm{es}}) \;=\; \tfrac{\mathrm{d}}{\mathrm{d}t}\boldsymbol{e}_{\mathrm{es}}^{\top}\boldsymbol{P}_{\mathrm{es}}\boldsymbol{e}_{\mathrm{es}} + \boldsymbol{e}_{\mathrm{es}}^{\top}\boldsymbol{P}_{\mathrm{es}}\tfrac{\mathrm{d}}{\mathrm{d}t}\boldsymbol{e}_{\mathrm{es}}
$$

$$
\begin{aligned}
&\overset{(3.60)}{=} && \widehat{\omega}'_{\mathrm{es},1} \boldsymbol{e}_{\mathrm{es}}^\top \left(\boldsymbol{A}_{\mathrm{es}}^\top \boldsymbol{P}_{\mathrm{es}} + \boldsymbol{P}_{\mathrm{es}} \boldsymbol{A}_{\mathrm{es}} \right) \boldsymbol{e}_{\mathrm{es}} + 2 e_{\mathrm{es},\omega} \boldsymbol{e}_{\mathrm{es}}^\top \boldsymbol{P}_{\mathrm{es}} \boldsymbol{N} \boldsymbol{x} \\
&\overset{(2.14)}{=} && -\widehat{\omega}'_{\mathrm{es},1} \boldsymbol{e}_{\mathrm{es}}^\top \boldsymbol{Q}_{\mathrm{es}} \boldsymbol{e}_{\mathrm{es}} + 2 e_{\mathrm{es},\omega} \boldsymbol{e}_{\mathrm{es}}^\top \boldsymbol{P}_{\mathrm{es}} \boldsymbol{N} \boldsymbol{x} \\
&\overset{(2.16)}{\leq} && -\widehat{\omega}'_{\mathrm{es},1} \lambda_{\min}(\boldsymbol{Q}_{\mathrm{es}}) \left\| \boldsymbol{e}_{\mathrm{es}} \right\|^2 + 2 \underbrace{\sqrt{\widehat{\omega}'_{\mathrm{es},1}} \left\| \boldsymbol{e}_{\mathrm{es}} \right\|}_{=:\,a} \underbrace{\tfrac{\| e_{\mathrm{es},\omega} \|_\infty}{\sqrt{\widehat{\omega}'_{\mathrm{es},1}}} \left\| \boldsymbol{P}_{\mathrm{es}} \right\| \left\| \boldsymbol{N} \right\| \left\| \boldsymbol{x} \right\|_\infty}_{=:\,b} \\
&\overset{(2.15)}{\leq} && -\widehat{\omega}'_{\mathrm{es},1} \underbrace{\left(\lambda_{\min}(\boldsymbol{Q}_{\mathrm{es}}) - \tfrac{1}{m} \right)}_{\exists m \geq 1 \text{ s.t. } (\cdot) \geq \epsilon'_{\mathrm{es},m} > 0} \left\| \boldsymbol{e}_{\mathrm{es}} \right\|^2 + \tfrac{\| e_{\mathrm{es},\omega} \|_\infty^2}{\widehat{\omega}'_{\mathrm{es},1}} \underbrace{m \left\| \boldsymbol{P}_{\mathrm{es}} \right\|^2 \left\| \boldsymbol{N} \right\|^2 \left\| \boldsymbol{x} \right\|_\infty^2}_{=:\, c'_{\mathrm{es},m} < \infty} \\
&\overset{(2.16)}{\leq} && -\underbrace{\tfrac{\epsilon'_{\mathrm{es},m} \underline{\omega}_{\mathrm{es},1}}{\lambda_{\max}(\boldsymbol{P}_{\mathrm{es}})}}_{=:\, \mu_{\mathrm{es},V} > 0} V_{\mathrm{es}}(\boldsymbol{e}_{\mathrm{es}}) + \tfrac{\| e_{\mathrm{es},\omega} \|_\infty^2}{\underline{\omega}_{\mathrm{es},1}} c'_{\mathrm{es},m}
\end{aligned}
$$

$$
\overset{(2.17)}{\Longrightarrow} V_{\mathrm{es}}(\boldsymbol{e}_{\mathrm{es}}) \leq V_{\mathrm{es}}(\boldsymbol{e}_{\mathrm{es},t_i}) \mathrm{e}^{-\mu_{\mathrm{es},V}(t-t_i)} + \tfrac{\| e_{\mathrm{es},\omega} \|_\infty^2}{\underline{\omega}_{\mathrm{es},1}} c'_{\mathrm{es},m} \int_{t_i}^t \mathrm{e}^{-\mu_{\mathrm{es},V}(t-\tau)} \mathrm{d}\tau. \tag{3.61}
$$

Hence,

$$
\begin{aligned}
\forall t \in \mathbb{T}_i\colon \quad \left\| \boldsymbol{e}_{\mathrm{es}} \right\|^2 &\leq \tfrac{1}{\lambda_{\min}(\boldsymbol{P}_{\mathrm{es}})} \left[V_{\mathrm{es}}(\boldsymbol{e}_{\mathrm{es},t_i}) \mathrm{e}^{-\mu_{\mathrm{es},V}(t-t_i)} + \tfrac{\| e_{\mathrm{es},\omega} \|_\infty^2}{\underline{\omega}_{\mathrm{es},1}} c'_{\mathrm{es},m} \int_{t_i}^t \mathrm{e}^{-\mu_{\mathrm{es},V}(t-\tau)} \mathrm{d}\tau \right] \\
&\overset{(2.16)}{\leq} \underbrace{\tfrac{\lambda_{\max}(\boldsymbol{P}_{\mathrm{es}})}{\lambda_{\min}(\boldsymbol{P}_{\mathrm{es}})}}_{=:\, c_{\mathrm{es},V}^2 > 0} \left\| \boldsymbol{e}_{\mathrm{es},t_i} \right\|^2 \mathrm{e}^{-\mu_{\mathrm{es},V}(t-t_i)} + \tfrac{\| e_{\mathrm{es},\omega} \|_\infty^2 c'_{\mathrm{es},m}}{\underline{\omega}_{\mathrm{es},1} \lambda_{\min}(\boldsymbol{P}_{\mathrm{es}})} \int_{t_i}^t \mathrm{e}^{-\mu_{\mathrm{es},V}(t-\tau)} \mathrm{d}\tau := c_{\mathrm{es},e} < \infty,
\end{aligned} \tag{3.62}
$$

and clearly, for all $t \in \mathbb{T}_i$ where $e_{\mathrm{es},\omega} = 0$ and $\mathbb{H}_n = \mathbb{H}_\infty$, the estimation error decreases exponentially. This completes the proof. □

3.3 The modified Frequency Adaptive Observer and the modified Frequency Adaptive Observer with offset

In the previous section, we have seen that the parallelized esSOGIs are able to estimate the direct and quadrature signals generated by the internal model (3.4). The main disadvantage of the parallelized esSOGIs was found in a significant limitation of its estimation speed. To tackle this problem, this section discusses a more general type of SOGI that is based on a LUENBERGER-like observer. The basic idea in this context is to construct an observer for (3.4) (which was published by the author in [571]), called the *modified Second Order Generalized Integrator* (mSOGI). As the esSOGI, the mSOGI requires an estimate of the angular frequency. It is provided by the *modified Frequency Locked Loop* (mFLL). The overall system (mSOGI and mFLL) is called the *modified Frequency Adaptive Observer* (mFAO). Additionally, an extension for estimating offset is proposed where the respective observer is based on (3.8) (which was published by the author in [572]). The respective components *modified Second Order Generalized Integrator with offset* ($\mathrm{mSOGI}_\circ$) and *modified Frequency Locked Loop with offset* ($\mathrm{mFLL}_\circ$) construct the *modified Frequency Adaptive Observer with offset* ($\mathrm{mFAO}_\circ$).
This section is structured as follows:

Section 3.3.1 proves the observability of (3.4) and (3.8),

Section 3.3.2 constructs observers for (i) (3.4) (mSOGI) and (ii) (3.8) ($\mathrm{mSOGI}_\circ$),

Section 3.3.3 discusses the feedback gain selection for these observers, Section 3.3.4 describes the angular frequency estimation including advanced stabilization mechanisms, and

Section 3.3.5 summarizes and proves the stability of the overall systems.

3.3.1 Observability

As mentioned above, the goal of this section is to construct an observer based estimation system. Hereby, the systems to be observed are given in (3.4) and (3.8). Therefore, the first step is to check observability. This is stated in the following proposition.

Proposition 3.3.1 (Observability of generation systems (3.4) and (3.8))**.** *Let* $\boldsymbol{J}$, $\boldsymbol{J}_\circ$, $\boldsymbol{c}$, $\boldsymbol{c}_\circ$ *be as in* (3.4) *or* (3.8), *respectively. Then, if and only if* $\omega_1 \neq 0$ *and* $\mathbb{H}_\infty \subseteq \mathbb{R} \setminus \{0\}$ *where for all* $\nu_i, \nu_j \in \mathbb{H}_\infty$, $i \neq j$, *it holds that* $|\nu_i| \neq |\nu_j|$, *the systems* $(\boldsymbol{c}^\top, \boldsymbol{J})$ *and* $(\boldsymbol{c}_\circ^\top, \boldsymbol{J}_\circ)$ *are observable.*

Proof. Note that the following is true:

$$\forall\, l \in \mathbb{Z}: \quad \widetilde{\boldsymbol{J}}^l \overset{(3.3)}{=} \begin{cases} (-1)^{\frac{l-1}{2}} \widetilde{\boldsymbol{J}}, & l \text{ odd} \\ (-1)^{\frac{l}{2}} \boldsymbol{I}_2, & l \text{ even} \end{cases}. \tag{3.63}$$

Testing the pair $(\boldsymbol{c}^\top, \boldsymbol{J})$ for observability [574, Sec. 2.3.1] yields that

$$\begin{aligned}
\boldsymbol{O}(\boldsymbol{\omega}) \quad &:= \begin{bmatrix} \boldsymbol{c}^\top \\ \boldsymbol{c}^\top \boldsymbol{J}(\boldsymbol{\omega}) \\ \vdots \\ \boldsymbol{c}^\top \boldsymbol{J}^{2n_\infty - 2}(\boldsymbol{\omega}) \\ \boldsymbol{c}^\top \boldsymbol{J}^{2n_\infty - 1}(\boldsymbol{\omega}) \end{bmatrix} \overset{(3.6)}{=} \begin{bmatrix} \boldsymbol{c}^\top \\ \omega_1 \boldsymbol{c}^\top \boldsymbol{N} \\ \vdots \\ \omega_1^{2n_\infty - 2} \boldsymbol{c}^\top \boldsymbol{N}^{2n_\infty - 2} \\ \omega_1^{2n_\infty - 1} \boldsymbol{c}^\top \boldsymbol{N}^{2n_\infty - 1} \end{bmatrix} \\
&= \begin{bmatrix} \boldsymbol{c}^\top \\ \omega_1 \boldsymbol{c}^\top \operatorname*{blkdiag}_{1,\dots,n_\infty}\big(\nu_i \widetilde{\boldsymbol{J}}\big) \\ \vdots \\ \omega_1^{2n_\infty - 2} \boldsymbol{c}^\top \operatorname*{blkdiag}_{1,\dots,n_\infty}\big(\nu_i^{2n_\infty - 2} \widetilde{\boldsymbol{J}}^{2n_\infty - 2}\big) \\ \omega_1^{2n_\infty - 1} \boldsymbol{c}^\top \operatorname*{blkdiag}_{1,\dots,n_\infty}\big(\nu_i^{2n_\infty - 1} \widetilde{\boldsymbol{J}}^{2n_\infty - 1}\big) \end{bmatrix} \\
&\overset{(3.3),(3.4),(3.5),(3.63)}{=} \begin{bmatrix} 1 & 0 & \cdots & 1 & 0 \\ 0 & -\omega_1 & \cdots & 0 & -\omega_{n_\infty} \\ \vdots & \vdots & \ddots & \vdots & \vdots \\ \frac{(-\omega_1^2)^{n_\infty}}{-\omega_1^2} & 0 & \cdots & \frac{(-\omega_{n_\infty}^2)^{n_\infty}}{-\omega_{n_\infty}^2} & 0 \\ 0 & \frac{(-\omega_1^2)^{n_\infty}}{\omega_1} & \cdots & 0 & \frac{(-\omega_{n_\infty}^2)^{n_\infty}}{\omega_{n_\infty}} \end{bmatrix} \\
&=: \begin{bmatrix} \boldsymbol{O}_1(\omega_1) & \cdots & \boldsymbol{O}_{n_\infty}(\omega_{n_\infty}) \\ \vdots & \ddots & \vdots \\ \frac{(-\omega_1^2)^{n_\infty}}{-\omega_1^2} \boldsymbol{O}_1(\omega_1) & \cdots & \frac{(-\omega_{n_\infty}^2)^{n_\infty}}{-\omega_{n_\infty}^2} \boldsymbol{O}_{n_\infty}(\omega_{n_\infty}) \end{bmatrix}, \quad \boldsymbol{O}_i(\omega_i) := \begin{bmatrix} 1 & 0 \\ 0 & -\omega_i \end{bmatrix}.
\end{aligned} \tag{3.64}$$

The large matrix must have full rank, i.e. $\operatorname{rank}(\boldsymbol{O}) = 2n_\infty$. This is the case, if and only if the following conditions are satisfied: (i) $\omega_1 \neq 0$ and (ii) $\mathbb{H}_\infty \subseteq \mathbb{R} \setminus \{0\}$ where for all pairwise different elements $\nu_i, \nu_j \in \mathbb{H}_\infty$, it holds that that $|\nu_i| \neq |\nu_j|$. This proves the observability of the pair

$(\boldsymbol{c}^\top, \boldsymbol{J})$.
An observability test for the pair $(\boldsymbol{c}_\circ^\top, \boldsymbol{J}_\circ)$ shows

$$\boldsymbol{O}_\circ(\boldsymbol{\omega}) := \begin{bmatrix} \boldsymbol{c}_\circ^\top \\ \boldsymbol{c}_\circ^\top \boldsymbol{J}_\circ(\boldsymbol{\omega}) \\ \vdots \\ \boldsymbol{c}_\circ^\top \boldsymbol{J}_\circ^{2n_\infty}(\boldsymbol{\omega}) \end{bmatrix} \overset{(3.8)}{=} \begin{bmatrix} 1 & \boldsymbol{c}^\top \\ \boldsymbol{0}_{2n_\infty} & \begin{bmatrix} \boldsymbol{c}^\top \\ \vdots \\ \boldsymbol{c}^\top \boldsymbol{J}^{2n_\infty - 1}(\boldsymbol{\omega}) \end{bmatrix} \boldsymbol{J}(\boldsymbol{\omega}) \end{bmatrix} \overset{(3.64)}{=} \begin{bmatrix} 1 & \boldsymbol{c}^\top \\ \boldsymbol{0}_{2n_\infty} & \boldsymbol{O}\boldsymbol{J}(\boldsymbol{\omega}) \end{bmatrix}. \tag{3.65}$$

Note that $\boldsymbol{J}$ has full rank if $\boldsymbol{O}$ has full rank since $\omega_1 \neq 0$. Thus, $\boldsymbol{O}\boldsymbol{J}$ has full rank and therefore $\boldsymbol{O}_\circ$ has full rank which proves the observability of the pair $(\boldsymbol{c}_\circ^\top, \boldsymbol{J}_\circ)$. □

3.3.2 Observer construction: The parallelized mSOGIs and the parallelized mSOGIs with offset

With the knowledge of observability, LUENBERGER-like observers are constructed for the generating system (3.4) in Section 3.3.2.1 and for (3.8) in Section 3.3.2.2. As in Section 3.2.2, they use the set $\mathbb{H}_n$ instead of $\mathbb{H}_\infty$.

3.3.2.1 The parallelized mSOGIs

First thing to note is that the observer is not based on the matrix $\boldsymbol{J}$ as in (3.4) but the matrix $\boldsymbol{N}$ as in (3.6). According to Proposition (3.3.1), the pair $(\boldsymbol{c}^\top, \boldsymbol{N})$ is observable[10]. This observer is a parallelization of *modified Second Order Generalized Integrators* (mSOGI) and denoted by the subscript "m". It is constructed in a straight forward manner as follows [574, Sec. 2.3.1]

$$\left.\begin{aligned} \forall t \in \mathbb{T}_i\colon \qquad \tfrac{\mathrm{d}}{\mathrm{d}t}\widehat{\boldsymbol{x}}_\mathrm{m} &= \widehat{\omega}_{\mathrm{m},1} \overbrace{\left(\boldsymbol{N} - \boldsymbol{l}_\mathrm{m}\boldsymbol{c}^\top\right)}^{=:\,\boldsymbol{A}_\mathrm{m} \in \mathbb{R}^{2n\times 2n}} \widehat{\boldsymbol{x}}_\mathrm{m} + \widehat{\omega}_{\mathrm{m},1}\boldsymbol{l}_\mathrm{m} y, \quad \widehat{\boldsymbol{x}}_\mathrm{m}(t_i) = \widehat{\boldsymbol{x}}_{\mathrm{m},t_i} \\ \widehat{y}_\mathrm{m} &= \boldsymbol{c}^\top \widehat{\boldsymbol{x}}_\mathrm{m} \end{aligned}\right\} \tag{3.66}$$

wherein

$$\begin{aligned} \widehat{\boldsymbol{x}}_\mathrm{m} &:= (\widehat{x}_{\mathrm{m},1}^\alpha, \widehat{x}_{\mathrm{m},1}^\beta, \cdots, \widehat{x}_{\mathrm{m},n}^\alpha, \widehat{x}_{\mathrm{m},n}^\beta)^\top \in \mathbb{R}^{2n} && \text{(state vector)} \\ \text{and} \quad \boldsymbol{l}_\mathrm{m} &:= (l_{\mathrm{m},1}^\alpha, l_{\mathrm{m},1}^\beta, \cdots, l_{\mathrm{m},n}^\alpha, l_{\mathrm{m},n}^\beta)^\top \in \mathbb{R}^{2n} && \text{(gain vector).} \end{aligned}$$

A visualization of (3.66), especially in view of the additional gains $l_{\mathrm{m},\nu}^\beta$ with respect to (3.19) or (3.28), is given in Figure 3.14. The parallel structure is inherited by Figure 3.6 (a).

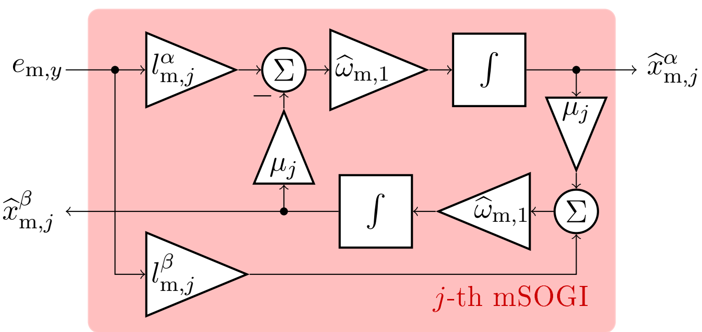

Figure 3.14: *The j-th mSOGI for amplitude and phase estimation of the j-th component.*

[10] If $\omega_1 = 1$, it holds that $\boldsymbol{J} = \boldsymbol{N}$

To complete the structural analysis, according to Appendix A the system's amplitude and phase responses follow with

$$\begin{aligned} \rho_{\mathrm{m}}(\omega) &:= \prod_{k=1}^{n}\left(\widehat{\omega}_{\mathrm{m},k}^2-\omega^2\right)-\sum_{j=1}^{n}\widehat{\omega}_{\mathrm{m},1}\widehat{\omega}_{\mathrm{m},j}l_{\mathrm{m},j}^{\beta}\prod_{\substack{k=1\\k\neq j}}^{n}\left(\widehat{\omega}_{\mathrm{m},k}^2-\omega^2\right) \\ \text{and}\quad \upsilon_{\mathrm{m}}(\omega) &:= \sum_{j=1}^{n}\omega\widehat{\omega}_{\mathrm{m},1}l_{\mathrm{m},j}^{\alpha}\prod_{\substack{k=1\\k\neq j}}^{n}\left(\widehat{\omega}_{\mathrm{m},k}^2-\omega^2\right), \end{aligned} \tag{3.67}$$

as

$$\begin{aligned} A_{\mathcal{X}_{\mathrm{m},i}^{\alpha}}(\omega_j) &= \frac{\widehat{\omega}_{\mathrm{m},1}\prod_{\substack{k=1\\k\neq i}}^{n}\left(\widehat{\omega}_{\mathrm{m},k}^2-\omega_j^2\right)\sqrt{\omega_j^2(l_{\mathrm{m},i}^{\alpha})^2+\widehat{\omega}_{\mathrm{m},i}^2(l_{\mathrm{m},i}^{\beta})^2}}{\sqrt{\rho_{\mathrm{m}}^2(\omega_j)+\upsilon_{\mathrm{m}}^2(\omega_j)}} \\ \Phi_{\mathcal{X}_{\mathrm{m},i}^{\alpha}}(\omega_j) &= \operatorname{arctan2}\left(\frac{\rho_{\mathrm{m}}(\omega_j)\omega_j l_{\mathrm{m},i}^{\alpha}+\upsilon_{\mathrm{m}}(\omega_j)\widehat{\omega}_{\mathrm{m},i}l_{\mathrm{m},i}^{\beta}}{\upsilon_{\mathrm{m}}(\omega_j)\omega_j l_{\mathrm{m},i}^{\alpha}-\rho_{\mathrm{m}}(\omega_j)\widehat{\omega}_{\mathrm{m},i}l_{\mathrm{m},i}^{\beta}}\right) \\ A_{\mathcal{X}_{\mathrm{m},i}^{\beta}}(\omega_j) &= \frac{\widehat{\omega}_{\mathrm{m},1}\prod_{\substack{k=1\\k\neq i}}^{n}\left(\widehat{\omega}_{\mathrm{m},k}^2-\omega_j^2\right)\sqrt{\widehat{\omega}_{\mathrm{m},i}^2(l_{\mathrm{m},i}^{\alpha})^2+\omega_j^2(l_{\mathrm{m},i}^{\beta})^2}}{\sqrt{\rho_{\mathrm{m}}^2(\omega_j)+\upsilon_{\mathrm{m}}^2(\omega_j)}} \\ \Phi_{\mathcal{X}_{\mathrm{m},i}^{\beta}}(\omega_j) &= \operatorname{arctan2}\left(\frac{-\upsilon_{\mathrm{m}}(\omega_j)\widehat{\omega}_{\mathrm{m},i}l_{\mathrm{m},i}^{\alpha}+\rho_{\mathrm{m}}(\omega_j)\omega_j l_{\mathrm{m},i}^{\beta}}{\rho_{\mathrm{m}}(\omega_j)\widehat{\omega}_{\mathrm{m},i}l_{\mathrm{m},i}^{\alpha}+\upsilon_{\mathrm{m}}(\omega_j)\omega_j l_{\mathrm{m},i}^{\beta}}\right) \\ A_{\mathcal{E}_{\mathrm{m},y}}(\omega_j) &= \frac{\prod_{k=1}^{n}\left(\widehat{\omega}_{\mathrm{m},k}^2-\omega_j^2\right)}{\sqrt{\rho_{\mathrm{m}}^2(\omega_j)+\upsilon_{\mathrm{m}}^2(\omega_j)}} \quad\text{and}\quad \Phi_{\mathcal{E}_{\mathrm{m},y}}(\omega_j)=\operatorname{arctan2}\left(\frac{-\upsilon_{\mathrm{m}}(\omega_j)}{\rho_{\mathrm{m}}(\omega_j)}\right). \end{aligned} \tag{3.68}$$

Remark 3.3.2. *System (3.66) is a generalization of systems (3.19) or (3.28), respectively; by a proper choice of the gain vector $\boldsymbol{l}_{\mathrm{m}}$ where all $l_{\mathrm{m},i}^{\beta}=0, i\in\{1,\ldots,n\}$, the parallelized mSOGIs become the parallized (enhanced) standard SOGIs.*

3.3.2.2 The parallelized mSOGIs with offset

The construction of the observer for (3.8) can be done similarly to equation (3.66). The observer is based on $\boldsymbol{N}_{\circ}$ as in (3.9):

$$\left.\begin{aligned} \forall\, t\in\mathbb{T}_i:\qquad \tfrac{\mathrm{d}}{\mathrm{d}t}\widehat{\boldsymbol{x}}_{\mathrm{m}_\circ} &= \widehat{\omega}_{\mathrm{m}_\circ,1}\overbrace{\left(\boldsymbol{N}_{\circ}-\boldsymbol{l}_{\mathrm{m}_\circ}\boldsymbol{c}_{\circ}^{\top}\right)}^{=:\,\boldsymbol{A}_{\mathrm{m}_\circ}\in\mathbb{R}^{2n+1\times 2n+1}}\widehat{\boldsymbol{x}}_{\mathrm{m}_\circ}+\widehat{\omega}_{\mathrm{m}_\circ,1}\boldsymbol{l}_{\mathrm{m}_\circ}y,\quad \widehat{\boldsymbol{x}}_{\mathrm{m}_\circ}(t_i)=\widehat{\boldsymbol{x}}_{\mathrm{m}_\circ,t_i} \\ \widehat{y}_{\mathrm{m}_\circ} &= \boldsymbol{c}_{\circ}^{\top}\widehat{\boldsymbol{x}}_{\mathrm{m}_\circ} \end{aligned}\right\} \tag{3.69}$$

wherein

$$\begin{aligned} \widehat{\boldsymbol{x}}_{\mathrm{m}_\circ} &:= (\widehat{x}_{\mathrm{m}_\circ,0},\,\widehat{x}_{\mathrm{m}_\circ,1}^{\alpha},\,\widehat{x}_{\mathrm{m}_\circ,1}^{\beta},\,\cdots,\,\widehat{x}_{\mathrm{m}_\circ,n}^{\alpha},\,\widehat{x}_{\mathrm{m}_\circ,n}^{\beta})^{\top}\in\mathbb{R}^{2n+1} \qquad \text{(state vector)} \\ \text{and}\quad \boldsymbol{l}_{\mathrm{m}_\circ} &:= (l_{\mathrm{m}_\circ,0},\,l_{\mathrm{m}_\circ,1}^{\alpha},\,l_{\mathrm{m}_\circ,1}^{\beta},\,\cdots,\,l_{\mathrm{m}_\circ,n}^{\alpha},\,l_{\mathrm{m}_\circ,n}^{\beta})^{\top}\mathbb{R}^{2n+1} \qquad \text{(gain vector)}. \end{aligned}$$

The observer, called the parallelized *modified Second Order Generalized Integrator with offset* (mSOGI$_\circ$) and denoted by the subscript "m$_\circ$", is illustrated in accordance to (3.69) in Figure 3.15. Therein, the structure of a single modified Second Order Generalized Integrator with offset is identical to the one shown in Figure 3.14.

With

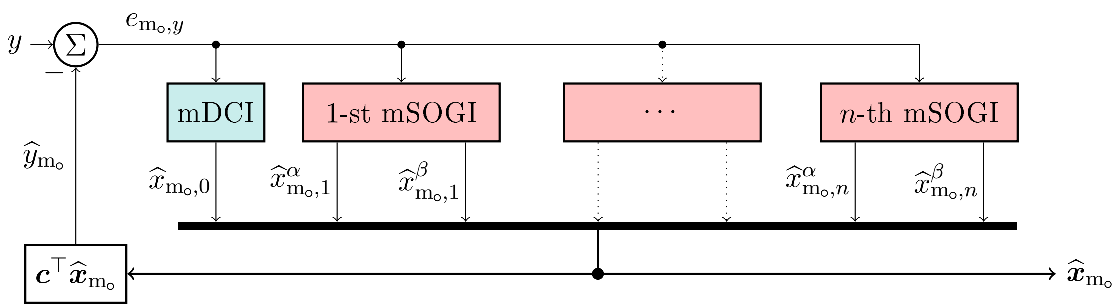

(a) *Block diagram of the parallelized mSOGI$_\circ$.*

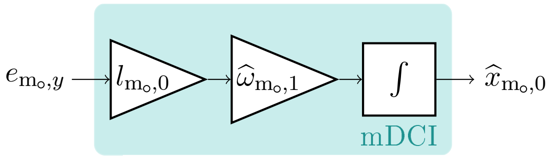

(b) *Construction of the mDCI.*

Figure 3.15: *(a): The parallelized structure of the mSOGI$_\circ$ and (b): Offset estimator. The j-th mSOGI is depicted in Figure 3.14.*

$$
\begin{aligned}
\rho_{\mathrm{m}_\circ}(\omega) \quad &:= \quad \omega\prod_{k=1}^{n}\left(\widehat{\omega}^2_{\mathrm{m}_\circ,k}-\omega^2\right) - \omega\widehat{\omega}_{\mathrm{m}_\circ,1}\sum_{j=1}^{n}\widehat{\omega}_{\mathrm{m}_\circ,j} l^\beta_{\mathrm{m}_\circ,j}\prod_{k=1,\,k\neq j}^{n}\left(\widehat{\omega}^2_{\mathrm{m}_\circ,k}-\omega^2\right) \\
\text{and}\quad \upsilon_{\mathrm{m}_\circ}(\omega) \quad &:= \quad \omega^2\widehat{\omega}_{\mathrm{m}_\circ,1}\sum_{j=1}^{n} l^\alpha_{\mathrm{m}_\circ,j}\prod_{k=1,\,k\neq j}^{n}\left(\widehat{\omega}^2_{\mathrm{m}_\circ,k}-\omega^2\right) - \widehat{\omega}_{\mathrm{m}_\circ,\nu_1} l_{\mathrm{m}_\circ,0}\prod_{k=1}^{n}\left(\widehat{\omega}^2_{\mathrm{m}_\circ,k}-\omega^2\right),
\end{aligned}
\tag{3.70}
$$

the amplitude and phase responses of this system follow according to Appendix A as

$$
\begin{aligned}
A_{\mathcal{X}_{\mathrm{m}_\circ,0}}(\omega_j) &= \frac{\widehat{\omega}_{\mathrm{m}_\circ,1} l_{\mathrm{m}_\circ,0}\prod_{k=1}^{n}\left(\widehat{\omega}^2_{\mathrm{m}_\circ,k}-\omega_j^2\right)}{\sqrt{\rho^2_{\mathrm{m}_\circ}(\omega_j)+\upsilon^2_{\mathrm{m}_\circ}(\omega_j)}}, \quad \Phi_{\mathcal{X}_{\mathrm{m}_\circ,0}}(\omega_j) = \operatorname{arctan2}\left(\frac{-\rho_{\mathrm{m}_\circ}(\omega_j)}{-\upsilon_{\mathrm{m}_\circ}(\omega_j)}\right), \\
A_{\mathcal{X}^\alpha_{\mathrm{m}_\circ,i}}(\omega_j) &= \frac{\omega_j\widehat{\omega}_{\mathrm{m}_\circ,1}\prod_{\substack{k=1\\k\neq i}}^{n}\left(\widehat{\omega}^2_{\mathrm{m}_\circ,k}-\omega_j^2\right)\sqrt{\omega_j^2(l^\alpha_{\mathrm{m}_\circ,i})^2+\widehat{\omega}^2_{\mathrm{m}_\circ,i}(l^\beta_{\mathrm{m}_\circ,i})^2}}{\sqrt{\rho^2_{\mathrm{m}_\circ}(\omega_j)+\upsilon^2_{\mathrm{m}_\circ}(\omega_j)}}, \\
\Phi_{\mathcal{X}^\alpha_{\mathrm{m}_\circ,i}}(\omega_j) &= \operatorname{arctan2}\left(\frac{\rho_{\mathrm{m}_\circ}(\omega_j)\omega_j l^\alpha_{\mathrm{m}_\circ,i}+\upsilon_{\mathrm{m}_\circ}(\omega_j)\widehat{\omega}_{\mathrm{m}_\circ,i} l^\beta_{\mathrm{m}_\circ,i}}{\upsilon_{\mathrm{m}_\circ}(\omega_j)\omega_j l^\alpha_{\mathrm{m}_\circ,i}-\rho_{\mathrm{m}_\circ}(\omega_j)\widehat{\omega}_{\mathrm{m}_\circ,i} l^\beta_{\mathrm{m}_\circ,i}}\right), \\
A_{\mathcal{X}^\beta_{\mathrm{m}_\circ,i}}(\omega_j) &= \frac{\omega_j\widehat{\omega}_{\mathrm{m}_\circ,1}\prod_{\substack{k=1\\k\neq i}}^{n}\left(\widehat{\omega}^2_{\mathrm{m}_\circ,k}-\omega_j^2\right)\sqrt{\widehat{\omega}^2_{\mathrm{m}_\circ,i}(l^\alpha_{\mathrm{m}_\circ,i})^2+\omega_j^2(l^\beta_{\mathrm{m}_\circ,i})^2}}{\sqrt{\rho^2_{\mathrm{m}_\circ}(\omega_j)+\upsilon^2_{\mathrm{m}_\circ}(\omega_j)}}, \\
\Phi_{\mathcal{X}^\beta_{\mathrm{m}_\circ,i}}(\omega_j) &= \operatorname{arctan2}\left(\frac{-\upsilon_{\mathrm{m}_\circ}(\omega_j)\widehat{\omega}_{\mathrm{m}_\circ,i} l^\alpha_{\mathrm{m}_\circ,i}+\rho_{\mathrm{m}_\circ}(\omega_j)\omega_j l^\beta_{\mathrm{m}_\circ,i}}{\rho_{\mathrm{m}_\circ}(\omega_j)\widehat{\omega}_{\mathrm{m}_\circ,i} l^\alpha_{\mathrm{m}_\circ,i}+\upsilon_{\mathrm{m}_\circ}(\omega_j)\omega_j l^\beta_{\mathrm{m}_\circ,i}}\right), \\
A_{\mathcal{E}_{\mathrm{m}_\circ,y}}(\omega_j) &= \frac{\omega_j\prod_{k=1}^{n}\left(\widehat{\omega}^2_{\mathrm{m}_\circ,k}-\omega_j^2\right)}{\sqrt{\rho^2_{\mathrm{m}_\circ}(\omega_j)+\upsilon^2_{\mathrm{m}_\circ}(\omega_j)}} \quad \text{and} \quad \Phi_{\mathcal{E}_{\mathrm{m}_\circ,y}}(\omega_j) = \operatorname{arctan2}\left(\frac{-\upsilon_{\mathrm{m}_\circ}(\omega_j)}{\rho_{\mathrm{m}_\circ}(\omega_j)}\right).
\end{aligned}
\tag{3.71}
$$

3.3.3 Pole placement for the parallelized mSOGIs and the parallelized mSOGIs with offset

Unlike the parallelized (e)sSOGIs from Section 3.2, the parallelized mSOGIs and parallelized mSOGI$_\circ$s have exactly as many gains as states. This allows to choose all eigenvalues of the system matrices $\boldsymbol{A}_{\mathrm{m}}$ and $\boldsymbol{A}_{\mathrm{m}_\circ}$, respectively. The results of the so called *pole placement* are appropriate feedback gain vectors $\boldsymbol{l}_{\mathrm{m}}$ and $\boldsymbol{l}_{\mathrm{m}_\circ}$, respectively. The calculation of the gain vectors $\boldsymbol{l}_{\mathrm{m}}$ and $\boldsymbol{l}_{\mathrm{m}_\circ}$ is shown in the following, where at first, a preliminary observation must be made: Consider the matrix

$$\left.\begin{aligned} \boldsymbol{\Lambda}_{\mathrm{m}}^{-1} &:= \begin{bmatrix} \boldsymbol{\Lambda}_{\mathrm{m},1}^{-1} & \boldsymbol{\Lambda}_{\mathrm{m},2}^{-1} & \cdots & \boldsymbol{\Lambda}_{\mathrm{m},n}^{-1} \\ \sum\limits_{\substack{j=1\\ j\neq 1}}^{n} \mu_j^2 \boldsymbol{\Lambda}_{\mathrm{m},1}^{-1} & \sum\limits_{\substack{j=1\\ j\neq 2}}^{n} \mu_j^2 \boldsymbol{\Lambda}_{\mathrm{m},2}^{-1} & \cdots & \sum\limits_{\substack{j=1\\ j\neq n}}^{n} \mu_j^2 \boldsymbol{\Lambda}_{\mathrm{m},n}^{-1} \\ \vdots & \vdots & \ddots & \vdots \\ \prod\limits_{\substack{j=1\\ j\neq 1}}^{n} \mu_j^2 \boldsymbol{\Lambda}_{\mathrm{m},1}^{-1} & \prod\limits_{\substack{j=1\\ j\neq 2}}^{n} \mu_j^2 \boldsymbol{\Lambda}_{\mathrm{m},2}^{-1} & \cdots & \prod\limits_{\substack{j=1\\ j\neq n}}^{n} \mu_j^2 \boldsymbol{\Lambda}_{\mathrm{m},n}^{-1} \end{bmatrix}, \\ \text{where} \quad \forall\, i \in \{1,\ldots,n\}\,,\ \mu_i \in \mathbb{H}_n:& \quad \boldsymbol{\Lambda}_{\mathrm{m},i}^{-1} := \begin{bmatrix} 1 & 0 \\ 0 & -\mu_i \end{bmatrix}. \end{aligned}\right\} \tag{3.72}$$

Its inverse is given by

$$\boldsymbol{\Lambda}_{\mathrm{m}} = \begin{bmatrix} \frac{\mu_1^{2(n-1)}}{\prod\limits_{\substack{j=1\\ j\neq 1}}^{n}(\mu_1^2-\mu_j^2)} \boldsymbol{\Lambda}_{\mathrm{m},1} & -\frac{\mu_1^{2(n-2)}}{\prod\limits_{\substack{j=1\\ j\neq 1}}^{n}(\mu_1^2-\mu_j^2)} \boldsymbol{\Lambda}_{\mathrm{m},1} & \cdots & \frac{(-1)^{n+1}}{\prod\limits_{\substack{j=1\\ j\neq 1}}^{n}(\mu_1^2-\mu_j^2)} \boldsymbol{\Lambda}_{\mathrm{m},1} \\ \frac{\mu_2^{2(n-1)}}{\prod\limits_{\substack{j=1\\ j\neq 2}}^{n}(\mu_2^2-\mu_j^2)} \boldsymbol{\Lambda}_{\mathrm{m},2} & -\frac{\mu_2^{2(n-2)}}{\prod\limits_{\substack{j=1\\ j\neq 2}}^{n}(\mu_2^2-\mu_j^2)} \boldsymbol{\Lambda}_{\mathrm{m},2} & \cdots & \frac{(-1)^{n+1}}{\prod\limits_{\substack{j=1\\ j\neq 2}}^{n}(\mu_2^2-\mu_j^2)} \boldsymbol{\Lambda}_{\mathrm{m},2} \\ \vdots & \vdots & \ddots & \vdots \\ \frac{\mu_n^{2(n-1)}}{\prod\limits_{\substack{j=1\\ j\neq n}}^{n}(\mu_n^2-\mu_j^2)} \boldsymbol{\Lambda}_{\mathrm{m},n} & -\frac{\mu_n^{2(n-2)}}{\prod\limits_{\substack{j=1\\ j\neq n}}^{n}(\mu_n^2-\mu_j^2)} \boldsymbol{\Lambda}_{\mathrm{m},n} & \cdots & \frac{(-1)^{n+1}}{\prod\limits_{\substack{j=1\\ j\neq n}}^{n}(\mu_n^2-\mu_j^2)} \boldsymbol{\Lambda}_{\mathrm{m},n} \end{bmatrix}, \tag{3.73}$$

since the product of the r-th row of $\boldsymbol{\Lambda}_{\mathrm{m}}$ and the c-th column of $\boldsymbol{\Lambda}_{\mathrm{m}}^{-1}$ yields

$$\begin{aligned} &\frac{\mu_r^{2(n-1)}}{\prod\limits_{\substack{j=1\\ j\neq r}}^{n}(\mu_r^2-\mu_j^2)} \boldsymbol{\Lambda}_{\mathrm{m},r}\boldsymbol{\Lambda}_{\mathrm{m},c}^{-1} - \frac{\mu_r^{2(n-2)}}{\prod\limits_{\substack{j=1\\ j\neq r}}^{n}(\mu_r^2-\mu_j^2)} \boldsymbol{\Lambda}_{\mathrm{m},r} \sum_{\substack{j=1\\ j\neq c}}^{n} \mu_j^2 \boldsymbol{\Lambda}_{\mathrm{m},c}^{-1} + \cdots + \frac{(-1)^{n+1}}{\prod\limits_{\substack{j=1\\ j\neq r}}^{n}(\mu_r^2-\mu_j^2)} \boldsymbol{\Lambda}_{\mathrm{m},r} \prod_{\substack{j=1\\ j\neq c}}^{n} \mu_j^2 \boldsymbol{\Lambda}_{\mathrm{m},c}^{-1} \\ &= \left(\mu_r^{2(n-1)} - \mu_r^{2(n-2)} \sum_{\substack{j=1\\ j\neq c}}^{n} \mu_j^2 + \cdots + (-1)^{n+1} \prod_{\substack{j=1\\ j\neq c}}^{n} \mu_j^2 \right) \frac{\boldsymbol{\Lambda}_{\mathrm{m},r}\boldsymbol{\Lambda}_{\mathrm{m},c}^{-1}}{\prod\limits_{\substack{j=1\\ j\neq r}}^{n}(\mu_r^2-\mu_j^2)} \\ &\overset{(2.18)}{=} \prod_{\substack{j=1\\ j\neq c}}^{n} \left(\mu_r^2 - \mu_j^2\right) \frac{\boldsymbol{\Lambda}_{\mathrm{m},r}\boldsymbol{\Lambda}_{\mathrm{m},c}^{-1}}{\prod\limits_{\substack{j=1\\ j\neq r}}^{n}(\mu_r^2-\mu_j^2)} = \begin{cases} \boldsymbol{0}_{2\times 2}, & c \neq r \\ \boldsymbol{I}_2, & c = r. \end{cases} \end{aligned}$$

Now, the statements can be formulated.

Proposition 3.3.3 (Pole placement for the parallelized mSOGIs and the parallelized mSOGI$_\circ$s)**.** *Let* $\mathrm{x} \in \{\mathrm{m}, \mathrm{m}_\circ\}$ *and let* $v = 2n$ *if* $\mathrm{x} = \mathrm{m}$ *or* $v = 2n+1$ *if* $\mathrm{x} = \mathrm{m}_\circ$*. Let* $\boldsymbol{N}_{\mathrm{x}}$[11] *as in* (3.6) *or* (3.9) *and* $\boldsymbol{c}_{\mathrm{x}}$ *as in* (3.4) *or* (3.8)*, respectively. Let* $\mathbb{H}_n$ *be given as in* (3.18) *and let* $\boldsymbol{\Lambda}_{\mathrm{m}}$ *be as in* (3.73)*.*

[11] The subscript "x" is also inherited by the generation parameters and variables; the model specific subscript "m" is neglected in this case.

Further let

$$\boldsymbol{\Lambda}_{\mathrm{m}_\circ}^{-1} = \begin{bmatrix} \boldsymbol{c}'_{\mu_\circ} & \boldsymbol{\Lambda}_{\mathrm{m}}^{-1} \\ \prod_{j=1}^{n} \mu_j^2 & \boldsymbol{0}_{2n}^\top \end{bmatrix} \quad \Rightarrow \quad \boldsymbol{\Lambda}_{\mathrm{m}_\circ} = \begin{bmatrix} \boldsymbol{0}_{2n}^\top & \frac{1}{\prod_{j=1}^{n} \mu_j^2} \\ \boldsymbol{\Lambda}_{\mathrm{m}} & -\frac{1}{\prod_{j=1}^{n} \mu_j^2} \boldsymbol{\Lambda}_{\mathrm{m}} \boldsymbol{c}'_{\mu_\circ} \end{bmatrix} \tag{3.74}$$

$$\textit{where} \quad \boldsymbol{c}'_{\mu_\circ} := \begin{pmatrix} 1 & 0 & \sum_{j=1}^{n} \mu_j^2 & 0 & \cdots & \sum_{j=1}^{n} \prod_{k=1,\, k\neq j}^{n} \mu_k^2 & 0 \end{pmatrix}^\top . \tag{3.75}$$

Consider the matrix $\boldsymbol{A}_{\mathrm{m}} := \boldsymbol{N} - \boldsymbol{l}_{\mathrm{m}} \boldsymbol{c}^\top$ *or* $\boldsymbol{A}_{\mathrm{m}_\circ} := \boldsymbol{N}_\circ - \boldsymbol{l}_{\mathrm{m}_\circ} \boldsymbol{c}_\circ^\top$*, resp., with characteristic polynomial* $\chi_{\boldsymbol{A}_{\mathrm{x}}}(s) := \frac{\chi_{\widehat{\omega}_{\mathrm{x},1}\boldsymbol{A}_{\mathrm{x}}}(\widehat{\omega}_{\mathrm{x},1} s)}{\widehat{\omega}_{\mathrm{x},1}^{2n}}$*. Let*

$$\boldsymbol{c}_{\mu,\mathrm{x}} := \begin{cases} \begin{pmatrix} 0 & \sum_{j=1}^{n} \mu_j^2 & \cdots & 0 & \prod_{j=1}^{n} \mu_j^2 \end{pmatrix}^\top, & \mathrm{x} = \mathrm{m} \\ \begin{pmatrix} 0 & \sum_{j=1}^{n} \mu_j^2 & \cdots & 0 & \prod_{j=1}^{n} \mu_j^2 & 0 \end{pmatrix}^\top, & \mathrm{x} = \mathrm{m}_\circ. \end{cases} \tag{3.76}$$

Let, for all $i \in \{1, \ldots, v\}$*,* $\lambda_{\mathrm{x},i} \in \mathbb{C}$ *be the prescribed roots of the desired characteristic polynomial*

$$\chi_{\boldsymbol{A}_{\mathrm{x}},\mathrm{des}}(s) := \prod_{i=1}^{v} (s - \lambda_{\mathrm{x},i}) . \tag{3.77}$$

The coefficients of $\chi_{\boldsymbol{A}_{\mathrm{x}},\mathrm{des}}$ *are collected in*

$$\boldsymbol{\lambda}_{\mathrm{x}} := \begin{pmatrix} -\sum_{j=1}^{v} \lambda_{\mathrm{x},j} & \sum_{j=1}^{v} \lambda_{\mathrm{x},j} \sum_{k=j+1}^{v} \lambda_{\mathrm{x},k} & \cdots & (-1)^v \prod_{j=1}^{v} \lambda_{\mathrm{x},j} \end{pmatrix}^\top .$$

If and only if the feedback gain vector $\boldsymbol{l}_{\mathrm{x}}$ *is chosen as*

$$\boldsymbol{l}_{\mathrm{x}} = \boldsymbol{\Lambda}_{\mathrm{x}} (\boldsymbol{\lambda}_{\mathrm{x}} - \boldsymbol{c}_{\mu,\mathrm{x}}) , \tag{3.78}$$

then the desired characteristic polynomial $\chi_{\boldsymbol{A}_{\mathrm{x}},\mathrm{des}}(s)$ *and the actual characteristic polynomial* $\chi_{\boldsymbol{A}_{\mathrm{x}}}(s)$ *have identical coefficients and, hence,* $\boldsymbol{A}_{\mathrm{x}}$ *is a matrix with eigenvalues* $\lambda_{\mathrm{x},i}$*.*

Proof. Recall that the characteristic polynomial $\chi_{\boldsymbol{A}_{\mathrm{x}}}$ can be deduced as follows

$$\chi_{\widehat{\omega}_{\mathrm{x},1}\boldsymbol{A}_{\mathrm{x}}}(\widehat{\omega}_{\mathrm{x},1} s) := \det(s\widehat{\omega}_{\mathrm{x},1}\boldsymbol{I}_v - \widehat{\omega}_{\mathrm{x},1}\boldsymbol{A}_{\mathrm{x}}) = \widehat{\omega}_{\mathrm{x},1}^v \det(s\boldsymbol{I}_v - \boldsymbol{A}_{\mathrm{x}}) =: \widehat{\omega}_{\mathrm{x},1}^v \chi_{\boldsymbol{A}_{\mathrm{x}}}(s) \tag{3.79}$$

$$\Rightarrow \chi_{\boldsymbol{A}_{\mathrm{x}}}(s) \overset{(A.9),\,(A.18)}{=} \begin{cases} \prod_{k=1}^{n} (s^2 + \mu_k^2) + \sum_{j=1}^{n} \big(s l_{\mathrm{m},j}^{\alpha} - \mu_j l_{\mathrm{m},j}^{\beta}\big) \prod_{k=1,\, k\neq j}^{n} (s^2 + \mu_k^2), & \mathrm{x} = \mathrm{m} \\ (s + l_{\mathrm{m}_\circ,0}) \prod_{k=1}^{n} (s^2 + \mu_k^2) + s \sum_{j=1}^{n} \big(s l_{\mathrm{m}_\circ,j}^{\alpha} - \mu_j l_{\mathrm{m}_\circ,j}^{\beta}\big) \prod_{k=1,\, k\neq j}^{n} (s^2 + \mu_k^2), & \mathrm{x} = \mathrm{m}_\circ. \end{cases}$$

Collect the coefficients of $\chi_{\boldsymbol{A}_{\mathrm{x}}}(s)$ in the following coefficient vector

$$\boldsymbol{c}_{\boldsymbol{A}_{\mathrm{x}}} := \boldsymbol{c}_{\mu,\mathrm{x}} + \underbrace{\begin{cases} \begin{pmatrix} \sum_{j=1}^{n} l_{\mathrm{m},i}^{\alpha} & -\sum_{j=1}^{n} \mu_j l_{\mathrm{m},j}^{\beta} & \cdots & \sum_{j=1}^{n} l_{\mathrm{m},j}^{\alpha} \prod_{\substack{k=1 \\ k\neq j}}^{n} \mu_k^2 & -\sum_{j=1}^{n} \mu_j l_{\mathrm{m},j}^{\beta} \prod_{\substack{k=1 \\ k\neq j}}^{n} \mu_k^2 \end{pmatrix}, & \mathrm{x} = \mathrm{m} \\ \begin{pmatrix} l_{\mathrm{m}_\circ,0} + \sum_{j=1}^{n} l_{\mathrm{m}_\circ,i}^{\alpha} & -\sum_{j=1}^{n} \mu_j l_{\mathrm{m}_\circ,j}^{\beta} & \cdots & -\sum_{j=1}^{n} \mu_j l_{\mathrm{m}_\circ,j}^{\beta} \prod_{\substack{k=1 \\ k\neq j}}^{n} \mu_k^2 & l_{\mathrm{m}_\circ,0} \prod_{j=1}^{n} \mu_j^2 \end{pmatrix}, & \mathrm{x} = \mathrm{m}_\circ \end{cases}}_{=:\widetilde{\boldsymbol{\lambda}}_{\mathrm{x}}} \tag{3.80}$$

and observe

$$\widetilde{\boldsymbol{\lambda}}_{\mathrm{x}} = \boldsymbol{\Lambda}_{\mathrm{x}}^{-1} \boldsymbol{l}_{\mathrm{x}}. \tag{3.81}$$

The desired polynomial in (3.77) should have the same coefficients, merged in the coefficient vector $\boldsymbol{\lambda}_{\mathrm{x}}$. A comparison of $\boldsymbol{c}_{\boldsymbol{A}_{\mathrm{x}}}$ and $\boldsymbol{\lambda}_{\mathrm{x}}$ yields

$$\boldsymbol{\lambda}_{\mathrm{x}} \overset{!}{=} \boldsymbol{c}_{\boldsymbol{A}_{\mathrm{x}}} \overset{(3.80)}{=} \boldsymbol{c}_{\mu,\mathrm{x}} + \widetilde{\boldsymbol{\lambda}}_{\mathrm{x}} \overset{(3.81)}{=} \boldsymbol{c}_{\mu,\mathrm{x}} + \boldsymbol{\Lambda}_{\mathrm{x}}^{-1} \boldsymbol{l}_{\mathrm{x}} \tag{3.82}$$

with $\boldsymbol{\Lambda}_{\mathrm{x}}^{-1}$ as in (3.72) or (3.74), respectively. Solving for $\boldsymbol{l}_{\mathrm{x}}$ proves the assertion

$$\Longrightarrow \quad \boldsymbol{l}_{\mathrm{x}} = \boldsymbol{\Lambda}_{\mathrm{x}} \left(\boldsymbol{\lambda}_{\mathrm{x}} - \boldsymbol{c}_{\mu,\mathrm{x}} \right). \tag{3.83}$$

□

Remark 3.3.4. *Let* $\mathrm{x} \in \{\mathrm{m}, \mathrm{m}_\circ\}$ *and let* $v = 2n$ *if* $\mathrm{x} = \mathrm{m}$ *or* $v = 2n+1$ *if* $\mathrm{x} = \mathrm{m}_\circ$. *For all eigenvalues* $\lambda_{\mathrm{x},i} \in \mathbb{C}_{NHP}$, $i \in \{1, \dots, v\}$, *the matrix* $\boldsymbol{A}_{\mathrm{x}}$ *is a Hurwitz matrix.*

Remark 3.3.5. MATLAB *provides the* `place` *command for pole placement. However, this command does not allow choosing eigenvalues with a multiplicity greater than* $\mathrm{rank}(\boldsymbol{c}) = \mathrm{rank}(\boldsymbol{c}_\circ) = 1$ *(i.e. every eigenvalue must be unique). If this is desired, the manual pole placement* (3.78) *must be implemented.*

Remark 3.3.6. *As already noted in Section 3.2.4, the dominant eigenvalue defines the settling time of the system. This also is shown in Figure 3.16*[12] *visualizing the influence of this eigenvalue to a single mSOGI. For a comparison, its eigenvalues are chosen as* $(\lambda_{\mathrm{m},1}, \lambda_{\mathrm{m},2}) \in \{(-1,-1), (-2,-2), (-3,-3)\}$.

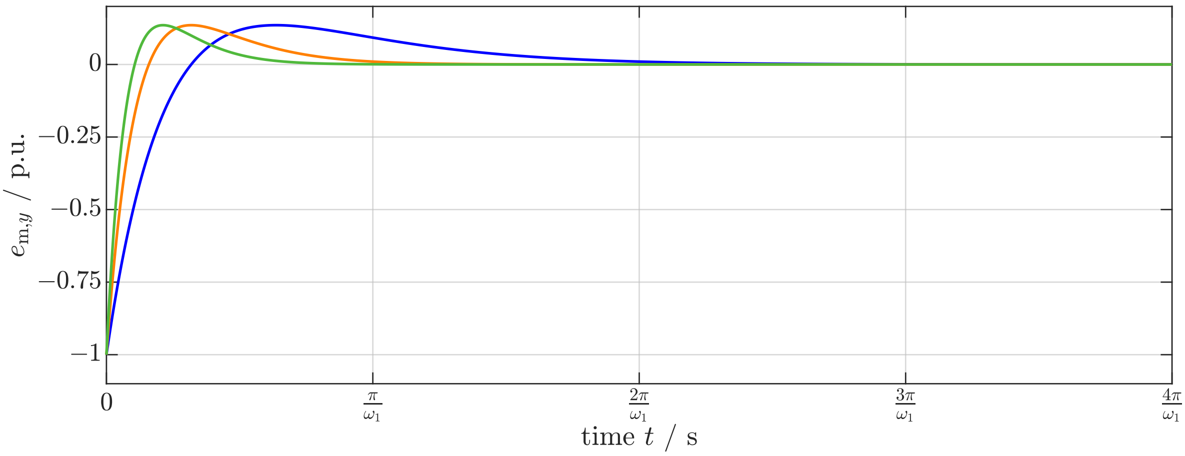

Figure 3.16: *Influence of the dominant eigenvalue: Convergence of the signal estimation error for* $\lambda_{\max} \in \{-1(\text{—}), -2(\text{—})\ \&\ -3(\text{—})\}$.

Apparently, the choice of $\lambda_{\max} = -3$ *leads to the fastest decrease; the normalized settling time (similar to that defined in* (3.54)*) is obtained as* $t_{\mathrm{set,n}} = 0.333$. *For* $\lambda_{\max} = -2$ *and* $\lambda_{\max} = -1$, *it is* $t_{\mathrm{set,n}} = 0.499$ *and* $t_{\mathrm{set,n}} = 0.997$, *resp.*

3.3.4 The mFLL and the mFLL with offset

With the linear observers described, now the angular frequency adaption is put into focus. As in Section 3.2.6, it is based on quasi-steady state observations. Due to the changes in the observer

[12]Simulation parameters: $T_s = 1\,\mu\mathrm{s}$, $y = \cos(2\pi 50 t)$, Solver: ode4. All initial values are 0.

gains $\boldsymbol{l}_{\mathrm{m}}$ and $\boldsymbol{l}_{\mathrm{m}_\circ}$ with respect to the former gains $\boldsymbol{l}_{\mathrm{s}}$ and $\boldsymbol{l}_{\mathrm{es}}$, it is to be expected that the angular frequency adaption law must be adjusted accordingly. Hence, the aim of this section is to investigate the necessary adjustments. These firstly are observed in a general manner. Afterwards, sub-structured into the Sections 3.3.4.1 for the mFLL and 3.3.4.2 for the mFLL$_\circ$, the respective angular frequency adaption laws are formulated.

Proposition 3.3.7 (Sign-correct adaption over one period for the mFLL and the mFLL$_\circ$)**.** *Let be* $\mathrm{x} \in \{\mathrm{m}, \mathrm{m}_\circ\}$*. Let* $i \in \{1, \ldots, n\}$, $\omega_i > 0$, $T_i := \frac{2\pi}{\omega_i}$ *and* $\nu_i = \mu_i$*. Consider system* (3.66) *or* (3.69)*, respectively, with* $\widehat{\omega}_{\mathrm{x},i} > 0$*. Let the system's signals be given in quasi-steady state by*

$$\left.\begin{array}{rcl} \widehat{x}^{\alpha}_{\mathrm{x},i} & = & \sum\limits_{j=1}^{n_\infty} a_j A_{\mathcal{X}^{\alpha}_{\mathrm{x},i}}(\omega_j) \cos\Big(\omega_j t + \phi_j + \Phi_{\mathcal{X}^{\alpha}_{\mathrm{x},i}}(\omega_j)\Big) =: \sum\limits_{j=1}^{n_\infty} \widehat{x}^{\alpha}_{\mathrm{x},i,j}, \\ \widehat{x}^{\beta}_{\mathrm{x},i} & = & \sum\limits_{j=1}^{n_\infty} a_j A_{\mathcal{X}^{\beta}_{\mathrm{x},i}}(\omega_j) \cos\Big(\omega_j t + \phi_j + \Phi_{\mathcal{X}^{\beta}_{\mathrm{x},i}}(\omega_j)\Big) =: \sum\limits_{j=1}^{n_\infty} \widehat{x}^{\beta}_{\mathrm{m},i,j} \\ \textit{and} \quad e_{\mathrm{x},y} & = & \sum\limits_{j=1}^{n_\infty} a_j A_{\mathcal{E}_{\mathrm{x},y}}(\omega_j) \cos\big(\omega_j t + \phi_j + \Phi_{\mathcal{E}_{\mathrm{x},y}}(\omega_j)\big) =: \sum\limits_{j=1}^{n_\infty} e_{\mathrm{x},y,j} \end{array}\right\} \tag{3.84}$$

and let be $\widehat{\boldsymbol{x}}_{\mathrm{x},i,i} := (\widehat{x}^{\alpha}_{\mathrm{x},i,i}, \widehat{x}^{\beta}_{\mathrm{x},i,i})^\top$*. Consider the integral*

$$\forall\, i \in \{1, \ldots, n\}: \qquad \int\limits_{t}^{t+T_i} e_{\mathrm{x},y,i} \boldsymbol{\sigma}^\top_{\mathrm{x},i} \widehat{\boldsymbol{x}}_{\mathrm{x},i,i}\, d\tau. \tag{3.85}$$

Then, the following holds

$$\forall\, i \in \{1, \ldots, n\}\ \forall\, \boldsymbol{\sigma}_{\mathrm{x},i} \in \left\{ \begin{pmatrix} \kappa_1 \\ \kappa_2 \end{pmatrix} \in \mathbb{R}^2 \,\middle|\, \kappa_2 l^{\alpha}_{\mathrm{x},i} - \kappa_1 l^{\beta}_{\mathrm{x},i} < 0 \right\}:$$

$$\int\limits_{t}^{t+T_i} e_{\mathrm{x},y,i} \boldsymbol{\sigma}^\top_{\mathrm{x},i} \widehat{\boldsymbol{x}}_{\mathrm{x},i,i}\, d\tau \begin{cases} \geq 0, & \widehat{\omega}_{\mathrm{x},i} < \omega_i \\ = 0, & \widehat{\omega}_{\mathrm{x},i} = \omega_i \\ \leq 0, & \widehat{\omega}_{\mathrm{x},i} > \omega_i. \end{cases} \tag{3.86}$$

Moreover, if $\boldsymbol{\sigma}_{\mathrm{x},i} = \kappa \widetilde{\boldsymbol{J}} \boldsymbol{l}_{\mathrm{x}} = \kappa(-l^{\beta}_{\mathrm{x},\nu}, l^{\alpha}_{\mathrm{x},\nu})^\top$ *is chosen where* $\kappa \in \mathbb{R}_{<0}$*, then the phase angles of* $e_{\mathrm{x},y,\omega_i}$ *and* $\boldsymbol{\sigma}^\top_{\mathrm{x},i} \widehat{\boldsymbol{x}}_{\mathrm{x},i,i}$ *are identical.*

Proof. Defining for all $i \in \{1, \ldots, n\}$ $\boldsymbol{\sigma}^\top_{\mathrm{x},i} := (\sigma^{\alpha}_{\mathrm{x},i}, \sigma^{\beta}_{\mathrm{x},i})^\top \in \mathbb{R}^2$ and repeating the procedure as in the proof of Proposition 3.2.6 yields

$$\int\limits_{t}^{t+\frac{2\pi}{\omega_i}} e_{\mathrm{x},y,i} \boldsymbol{\sigma}^\top_{\mathrm{x},i} \widehat{\boldsymbol{x}}_{\mathrm{x},i,i} \mathrm{d}\tau = \frac{\pi a_i^2 \left(\sigma^{\beta}_{\mathrm{x},i} l^{\alpha}_{\mathrm{x},i} - \sigma^{\alpha}_{\mathrm{x},i} l^{\beta}_{\mathrm{x},i}\right) \nu_i^2 \widehat{\omega}^2_{\mathrm{x},1} \left(\widehat{\omega}^2_{\mathrm{x},1} - \omega_1^2\right) \prod\limits_{\substack{k=1 \\ k \neq i}}^{n} \left(\widehat{\omega}^2_{\mathrm{x},i} - \omega_i^2\right)^2}{\omega_1 (\rho^2_{\mathrm{x}}(\omega_i) + \upsilon^2_{\mathrm{x}}(\omega_i))}. \tag{3.87}$$

Since $\omega_i > 0$, only $\widehat{\omega}^2_{\mathrm{x},1} - \omega_1^2$ can change its sign in (3.87). Thus, if and only if $\sigma^{\beta}_{\mathrm{x},i} l^{\alpha}_{\mathrm{x},i} - \sigma^{\alpha}_{\mathrm{x},i} l^{\beta}_{\mathrm{x},i} < 0$, it holds that

$$\forall\, \boldsymbol{\sigma}_{\mathrm{x},i} \in \left\{ \begin{pmatrix} \kappa_1 \\ \kappa_2 \end{pmatrix} \in \mathbb{R}^2 \,\middle|\, \kappa_2 l^{\alpha}_{\mathrm{x},\nu} - \kappa_1 l^{\beta}_{\mathrm{x},\nu} < 0 \right\}: \quad \int\limits_{t}^{t+T_i} e_{\mathrm{x},y,i} \boldsymbol{\sigma}^\top_{\mathrm{x},\nu} \widehat{\boldsymbol{x}}_{\mathrm{x},i,i} \mathrm{d}\tau \begin{cases} \geq 0, & \widehat{\omega}_{\mathrm{x},1} < \omega_1 \\ = 0, & \widehat{\omega}_{\mathrm{x},1} = \omega_1 \\ \leq 0, & \widehat{\omega}_{\mathrm{x},1} > \omega_1, \end{cases}$$

which proves assertion (3.86). Next, for all $\kappa < 0$ and if and only if $\boldsymbol{\sigma}_{\mathrm{x},i} = \kappa(-l^{\beta}_{\mathrm{x},\nu}, l^{\alpha}_{\mathrm{x},\nu})^\top$, the phase angle of $\boldsymbol{\sigma}_{\mathrm{x},i}^{\top}\widehat{\boldsymbol{x}}_{\mathrm{x},i,i}$ is identical to the phase angle of $e_{\mathrm{x},y,i}$ since

$$\Phi_{\boldsymbol{\sigma}_{\mathrm{x},i}^{\top}\widehat{\boldsymbol{x}}_{\mathrm{x},i,i}} = \operatorname{arctan2}\left(\frac{\sigma_{\mathrm{x},i}^{\beta}\left(l_{\mathrm{x},i}^{\alpha}\widehat{\omega}_{\mathrm{x},1}\upsilon_{\mathrm{x}}(\omega_i)-l_{\mathrm{x},i}^{\beta}\omega_1\rho_{\mathrm{x}}(\omega_i)\right)-\sigma_{\mathrm{x},i}^{\alpha}\left(l_{\mathrm{x},i}^{\alpha}\omega_1\rho_{\mathrm{x}}(\omega_i)+l_{\mathrm{x},i}^{\beta}\widehat{\omega}_{\mathrm{x},1}\upsilon_{\mathrm{x}}(\omega_i)\right)}{-\sigma_{\mathrm{x},i}^{\beta}\left(l_{\mathrm{x},i}^{\alpha}\widehat{\omega}_{\mathrm{x},1}\rho_{\mathrm{x}}(\omega_i)+l_{\mathrm{x},i}^{\beta}\omega_1\upsilon_{\mathrm{x}}(\omega_i)\right)-\sigma_{\mathrm{x},i}^{\alpha}\left(l_{\mathrm{x},i}^{\alpha}\omega_1\upsilon_{\mathrm{x}}(\omega_i)-l_{\mathrm{x},i}^{\beta}\widehat{\omega}_{\mathrm{x},1}\rho_{\mathrm{x}}(\omega_i)\right)}\right)$$
$$\overset{\boldsymbol{\sigma}_{\mathrm{x},i}=\kappa(-l_{\mathrm{x},i}^{\beta},l_{\mathrm{x},i}^{\alpha})^{\top}}{=} \operatorname{arctan2}\left(\frac{-\upsilon_{\mathrm{x}}(\omega_i)}{\rho_{\mathrm{x}}(\omega_i)}\right) \overset{(3.68),(3.71)}{=} \Phi_{\mathcal{E}_{\mathrm{x},y}}(\omega_i)$$

which completes the proof. □

Remark 3.3.8. *As stated in Remark 3.2.7, it is advisable to use only the fundamental components for angular frequency adaption for the same reasons mentioned therein.*

3.3.4.1 The mFLL

According to Proposition 3.3.7 and Remark 3.3.8, the adaption law for the angular frequency, called the *modified Frequency Locked Loop* (mFLL), is chosen with $\gamma_{\mathrm{m}} > 0$ as follows

$$\forall t \in \mathbb{T}_i: \quad \tfrac{\mathrm{d}}{\mathrm{d}t}\widehat{\omega}_{\mathrm{m},1} = \gamma_{\mathrm{m}} e_{\mathrm{m},y}\boldsymbol{\sigma}_{\mathrm{m},1}^{\top}\widehat{\boldsymbol{x}}_{\mathrm{m},1}, \quad \widehat{\omega}_{\mathrm{m},1}(t_i) = \widehat{\omega}_{\mathrm{m},1,t_i} \tag{3.88}$$

Remark 3.3.9. *Recall that in Remark 3.3.2, it is stated that the parallelized mSOGIs are generalized parallelized (e)sSOGIs. The same holds true for* (3.88) *with respect to* (3.50).

In the following, a *Gain Normalization* (GN), a *sign-correct Anti Windup decision function* (AW), a *Rate Limitation* (RL) and a *Low Pass Filter* (LPF) are applied to the mFLL to improve its stability and performance. Since the parallelized mSOGIs as well as the mFLL are generalizations of the parallelized (e)sSOGIs & (e)sFLL, the GN is identical to the one as described in Section 3.2.7. The AW is designed to ensure stability of the parallelized mSOGIs and mFLL[13]. A RL is applied to smooth the adaption. Additionally, the mFLL input signals $e_{\mathrm{m},y}$ and $\widehat{\boldsymbol{x}}_{\mathrm{m},1}$ are low-pass filtered to damp higher harmonics. This is necessary, especially in view of the amplitude and phase responses of the parallelized mSOGIs (3.68). A comparison of those to the responses of the parallelized esSOGIs (3.21) is illustrated in Figure 3.17[14].

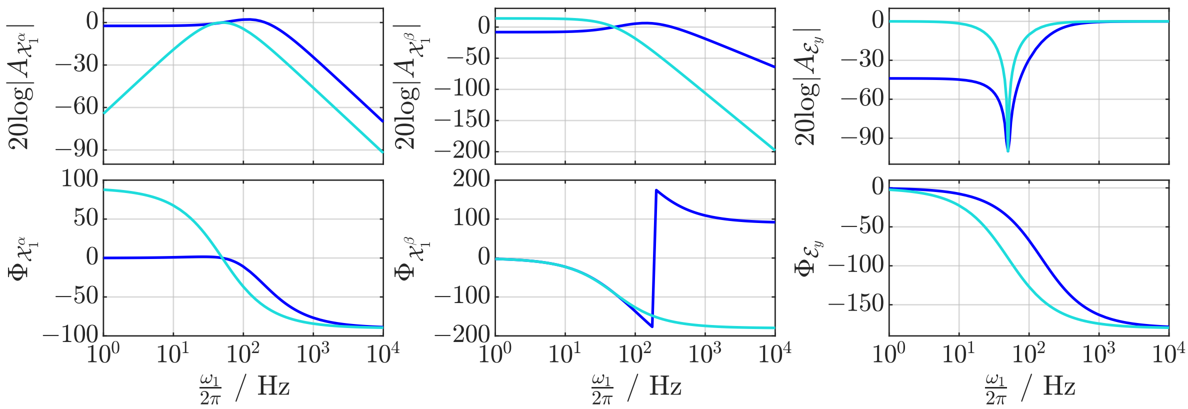

Figure 3.17: *The amplitude and phase response of the signals $\widehat{x}_{\mathrm{m},1}^{\alpha}$, $\widehat{x}_{\mathrm{m},1}^{\beta}$ and $e_{\mathrm{m},y}$ (—) and $\widehat{x}_{\mathrm{es},1}^{\alpha}$, $\widehat{x}_{\mathrm{es},1}^{\beta}$ and $e_{\mathrm{es},y}$ (—) for $\mathbb{H}_n = \mathbb{H}_\infty = \{1\}$.*

[13]For the parallelized (e)sFLLs, the Output Saturation only guarantees stability of the parallelized (e)sSOGIs but not of the (e)sFLL.

[14]Simulation parameters: $\frac{\omega_1}{2\pi} \in \{1, 1.25, \ldots, 10, 12.5, \ldots, 100, 125, \ldots, 1000, 1250, \ldots, 10000\}$, $\widehat{\omega}_{\mathrm{es},1} = \widehat{\omega}_{\mathrm{m},1} = 2\pi 50$, $\boldsymbol{l}_{\mathrm{es}} = (2,0)^{\top}$, $\boldsymbol{l}_{\mathrm{m}} = (6,-8)^{\top}$.

In view of the amplitude responses depicted in the top row of Figure 3.17, it gets clear that the mSOGI (—) is much more noise sensitive for higher (angular) frequencies than the esSOGI (—). More precisely, in comparison to the fundamental direct signal $\widehat{x}^{\alpha}_{\mathrm{es},1}$ (left column), $\widehat{x}^{\alpha}_{\mathrm{m},1}$ has a higher amplification of all angular frequency components (in the observed range). Especially in a small range ($50\,\mathrm{Hz} = \frac{\widehat{\omega}_1}{2\pi} < \frac{\omega_1}{2\pi} < 200\,\mathrm{Hz}$) above the angular frequency $\widehat{\omega}_1$ of the SOGIs, the respective angular frequency components are not damped but amplified. For the quadrature signals $\widehat{x}^{\beta}_{\mathrm{es},1}$ and $\widehat{x}^{\beta}_{\mathrm{m},1}$ (middle column), in the range ($1\,\mathrm{Hz} < \frac{\omega_1}{2\pi} < \frac{\widehat{\omega}_1}{2\pi} = 50\,\mathrm{Hz}$), the mSOGI has better (noise) attenuation than the esSOGI. Again, for certain angular frequencies ($50\,\mathrm{Hz} = \frac{\widehat{\omega}_1}{2\pi} < \frac{\omega_1}{2\pi} < 325\,\mathrm{Hz}$) above the SOGIs' angular frequency $\widehat{\omega}_1$, the mSOGI amplifies the respective components overproportionally. For all angular frequency components larger than the angular frequency $\widehat{\omega}_1$, the esSOGI attenuates these frequencies better than the mSOGI. However, the signal estimation error of the mSOGI (right column) has better noise attenuation for all angular frequency components. For higher frequencies ($1\,\mathrm{kHz} \geq \frac{\widehat{\omega}_1}{2\pi}$), the amplification of these angular frequency components is approximately the same for esSOGI and mSOGI.
Hence, the signals $\widehat{\boldsymbol{x}}_{\mathrm{m},1}$ must be filtered by a *Low Pass Filter* (LPF) (see Figure 3.18).

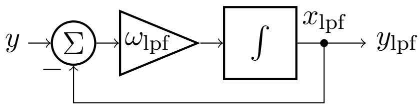

Figure 3.18: *A LPF.*

To maintain the relation of the amplitude and phase responses between the signal estimation error $e_{\mathrm{m},y}$ and the states $\widehat{\boldsymbol{x}}_{\mathrm{m},1}$, the signal estimation error $e_{\mathrm{m},y}$ must be filtered as well. With $\omega_{\mathrm{m,lpf}}$ being the cut-off angular frequency of the LPF, the LPF's state space representation is given by

$$\forall t \in \mathbb{T}_i\colon \quad \frac{\mathrm{d}}{\mathrm{d}t} \underbrace{\begin{pmatrix} e_{\mathrm{m,lpf},y} \\ \widehat{\boldsymbol{x}}_{\mathrm{m,lpf},1} \end{pmatrix}}_{=:\widehat{\boldsymbol{x}}_{\mathrm{m,lpf}} \in \mathbb{R}^3} = -\omega_{\mathrm{m,lpf}} \widehat{\boldsymbol{x}}_{\mathrm{m,lpf}} + \omega_{\mathrm{m,lpf}} \begin{pmatrix} e_{\mathrm{m},y} \\ \widehat{\boldsymbol{x}}_{\mathrm{m},1} \end{pmatrix}, \quad \widehat{\boldsymbol{x}}_{\mathrm{m,lpf}}(t_i) = \widehat{\boldsymbol{x}}_{\mathrm{m,lpf},t_i}. \tag{3.89}$$

Next, the AW decision function is defined as

$$\mathrm{aw}^{\overline{\omega}_{\mathrm{m}}}_{\underline{\omega}_{\mathrm{m}}}(\delta_1, \delta_2) = \begin{cases} 0, & \delta_1 \geq \overline{\omega}_{\mathrm{m}} \ \wedge\ \delta_2 > 0 \\ 0, & \delta_1 \leq \underline{\omega}_{\mathrm{m}} \ \wedge\ \delta_2 < 0 \\ 1, & \text{else.} \end{cases}$$

Therein, $\underline{\omega}_{\mathrm{m}}, \overline{\omega}_{\mathrm{m}} > 0$ are the lower and upper limits of the AW decision function. The last modification to the basic angular frequency adaption law (3.88) is the RL which is a saturation of $\frac{\mathrm{d}}{\mathrm{d}t}\widehat{\omega}_{\mathrm{m},1}$ with lower and upper limits $\underline{z}_{\mathrm{m}}, \overline{z}_{\mathrm{m}}$, i.e.

$$\mathrm{sat}^{\overline{z}_{\mathrm{m}}}_{\underline{z}_{\mathrm{m}}}(\delta) = \begin{cases} \overline{z}_{\mathrm{m}}, & \delta > \overline{z}_{\mathrm{m}} \\ \delta, & \underline{z}_{\mathrm{m}} \leq \delta \leq \overline{z}_{\mathrm{m}} \\ \underline{z}_{\mathrm{m}}, & \underline{z}_{\mathrm{m}} < \delta. \end{cases}$$

Thus, the modified angular frequency adaption law is given by

$$\forall t \in \mathbb{T}_i\colon \quad \frac{\mathrm{d}}{\mathrm{d}t}\widehat{\omega}_{\mathrm{m},1} = \underbrace{\mathrm{sat}^{\overline{z}_{\mathrm{m}}}_{\underline{z}_{\mathrm{m}}}\left(\frac{\Gamma_{\mathrm{m}} \widehat{\omega}^2_{\mathrm{m},1} e_{\mathrm{m,lpf},y} \boldsymbol{\sigma}^\top_{\mathrm{m},1} \widehat{\boldsymbol{x}}_{\mathrm{m,lpf},1}}{\max\left(\left\|\widehat{\boldsymbol{x}}_{\mathrm{m,lpf},1}\right\|^2, \varepsilon_{\mathrm{m}}\right)}\right)}_{=:z_{\mathrm{m}}} \mathrm{aw}^{\overline{\omega}_{\mathrm{m}}}_{\underline{\omega}_{\mathrm{m}}}(\widehat{\omega}_{\mathrm{m},1}, z_{\mathrm{m}}) \tag{3.90}$$

wherein $\widehat{\omega}_{\mathrm{m},1}(t_i) = \widehat{\omega}_{\mathrm{m},1,t_i}$ and $\Gamma_{\mathrm{m}} > 0$. To justify these modifications, Figure 3.19[15] shows the influence of each part step by step.

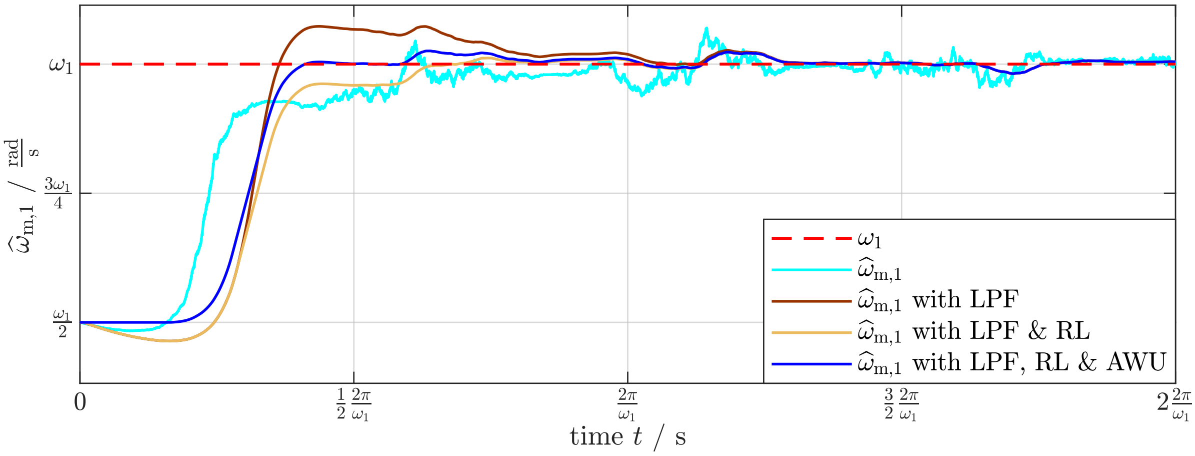

Figure 3.19: *The impact of single modifications to the frequency adaption.*

The angular frequency estimation without modifications (—) is very noisy. Applying an LPF (—) results in a much smoother curve, but also comes with overshooting. The RL (—) removes this overshoot, which, on the other hand, results in a slower performance. Finally, the AWU (—) speeds up the performance again.
The resulting block diagram of the mFLL is illustrated in Figure 3.20.

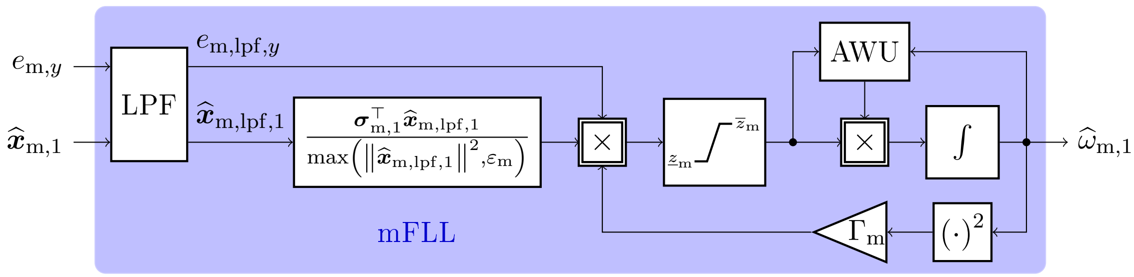

Figure 3.20: *The mFLL.*

3.3.4.2 The mFLL with offset

The design of the *modified Frequency Locked Loop with offset* (mFLL$_\circ$) is similar to the design of the mFLL described in Section 3.3.4.1. Hence, the LPF is described as follows

$$\forall t \in \mathbb{T}_i: \quad \frac{\mathrm{d}}{\mathrm{d}t} \underbrace{\begin{pmatrix} e_{\mathrm{m}_\circ,\mathrm{lpf},y} \\ \widehat{\boldsymbol{x}}_{\mathrm{m}_\circ,\mathrm{lpf},1} \end{pmatrix}}_{=: \widehat{\boldsymbol{x}}_{\mathrm{m}_\circ,\mathrm{lpf}} \in \mathbb{R}^3} = -\omega_{\mathrm{m}_\circ,\mathrm{lpf}} \widehat{\boldsymbol{x}}_{\mathrm{m}_\circ,\mathrm{lpf}} + \omega_{\mathrm{m}_\circ,\mathrm{lpf}} \begin{pmatrix} e_{\mathrm{m}_\circ,y} \\ \widehat{\boldsymbol{x}}_{\mathrm{m}_\circ,1} \end{pmatrix}, \quad \widehat{\boldsymbol{x}}_{\mathrm{m}_\circ,\mathrm{lpf}}(t_i) = \widehat{\boldsymbol{x}}_{\mathrm{m}_\circ,\mathrm{lpf},t_i} \tag{3.91}$$

[15]Simulation parameters: $T_s = 1\,\mu\mathrm{s}$, $y = \cos(2\pi 50 t) + n$ with noise function n, Noise power= 10^{-6}, Noise seed= 23341, $\boldsymbol{l}_{\mathrm{m}} = (6, -8)^\top$, $\boldsymbol{\sigma}_{\mathrm{m},1} = (-8, -6)^\top$, $\Gamma_{\mathrm{m}} = 0.37$, $\omega_{\mathrm{m,lpf}} = 2\pi 100$, $\underline{z}_{\mathrm{m}} = -2\pi 1000$, $\overline{z}_{\mathrm{m}} = 2\pi 1000$, $\underline{\omega}_{\mathrm{m}} = 2\pi 40$, $\overline{\omega}_{\mathrm{m}} = 2\pi 60$, Solver: ode4. All initial values are 0 except for $\widehat{\omega}_{\mathrm{m},1}(0) = 2\pi 25$.

and the angular frequency adaption law is given by

$$\forall t \in \mathbb{T}_i: \quad \tfrac{\mathrm{d}}{\mathrm{d}t}\widehat{\omega}_{\mathrm{m}_\circ,1} = \underbrace{\mathrm{sat}_{\underline{z}_{\mathrm{m}_\circ}}^{\overline{z}_{\mathrm{m}_\circ}}\left(\frac{\Gamma_{\mathrm{m}_\circ}\widehat{\omega}^2_{\mathrm{m}_\circ,1} e_{\mathrm{m}_\circ,\mathrm{lpf},y}\boldsymbol{\sigma}^\top_{\mathrm{m}_\circ,1}\widehat{\boldsymbol{x}}_{\mathrm{m}_\circ,\mathrm{lpf},1}}{\max\left(\left\|\widehat{\boldsymbol{x}}_{\mathrm{m}_\circ,\mathrm{lpf},1}\right\|^2, \varepsilon_{\mathrm{m}_\circ}\right)}\right)}_{=:\, z_{\mathrm{m}_\circ}} \mathrm{aw}_{\underline{\omega}_{\mathrm{m}_\circ}}^{\overline{\omega}_{\mathrm{m}_\circ}}\left(\widehat{\omega}_{\mathrm{m}_\circ,1}, z_{\mathrm{m}_\circ}\right) \tag{3.92}$$

with $\widehat{\omega}_{\mathrm{m}_\circ,1}(t_i) = \widehat{\omega}_{\mathrm{m}_\circ,1,t_i}$ and $\Gamma_{\mathrm{m}_\circ} > 0$. The block diagram of the mFLL$_\circ$ is identical to the one of the mFLL (with m$_\circ$ instead of m). It is depicted in Figure 3.20.

Remark 3.3.10. *Instead of using a Low Pass Filter inside the mFLL or mFLL$_\circ$, the LPF can be placed before the mFAO or mFAO$_\circ$ to filter the input signal instead. Consequently, only one filter is needed leading to amplitude and phase deviations of the observer input signal. As noted in Remark 3.2.4, this requires post processing APCs (cf. (3.39)).*

Remark 3.3.11. *Let* $\mathrm{x} \in \{\mathrm{m}, \mathrm{m}_\circ\}$. *For all* $\boldsymbol{\sigma}_{\mathrm{x},1}$ *that are element of the set described in (3.86), the adaption speed depends on the phase angle difference between* $\boldsymbol{\sigma}^\top_{\mathrm{x},1}\widehat{\boldsymbol{x}}_{\mathrm{x},1,1}$ *and* $e_{\mathrm{x},y,1}$. *The speed is maximized for identical phase angles, (i.e.* $\Phi_{\boldsymbol{\sigma}^\top_{\mathrm{x},1}\widehat{\boldsymbol{x}}_{\mathrm{x},1,1}} = \Phi_{\mathcal{E}_{\mathrm{x},y}}(\omega_1)$*) due to (2.8). This results in the specific choice*

$$\boldsymbol{\sigma}_{\mathrm{x},1} = -\widetilde{\boldsymbol{J}}\left(l^\alpha_{\mathrm{x},1}\; l^\beta_{\mathrm{x},1}\right)^\top. \tag{3.93}$$

3.3.5 Summary and stability proof of the mFAO and the mFAO with offset

This section completes the investigations on the parallelized mSOGIs with the mFLL, called the *modified Frequency Adaptive Observer* (mFAO) and the parallelized mSOGI$_\circ$s with the mFLL$_\circ$, called the *modified Frequency Adaptive Observer with offset* (mFAO$_\circ$). In Sections 3.3.5.1 and 3.3.5.2, a complete mathematical and graphical representation for the mFAO and the mFAO$_\circ$, respectively, is shown. These are evaluated using the test signals introduced in (3.12) and shown in Figure 3.2. Afterwards, both systems are proven in view of stability.

3.3.5.1 Summary of the mFAO

The mFAO is mathematically described as follows

$$\forall t \in \mathbb{T}_i: \quad \left.\begin{aligned} \tfrac{\mathrm{d}}{\mathrm{d}t}\widehat{\boldsymbol{x}}_{\mathrm{m}} &= \widehat{\omega}_{\mathrm{m},1}\boldsymbol{A}_{\mathrm{m}}\widehat{\boldsymbol{x}}_{\mathrm{m}} + \widehat{\omega}_{\mathrm{m},1}\boldsymbol{l}_{\mathrm{m}} y, && \widehat{\boldsymbol{x}}_{\mathrm{m}}(t_i) = \widehat{\boldsymbol{x}}_{\mathrm{m},t_i}, \\ \tfrac{\mathrm{d}}{\mathrm{d}t}\widehat{\boldsymbol{x}}_{\mathrm{m,lpf}} &= -\omega_{\mathrm{m,lpf}}\widehat{\boldsymbol{x}}_{\mathrm{m,lpf}} + \omega_{\mathrm{m,lpf}}\begin{pmatrix} e_{\mathrm{m},y} \\ \widehat{\boldsymbol{x}}_{\mathrm{m},1}\end{pmatrix}, && \widehat{\boldsymbol{x}}_{\mathrm{m,lpf}}(t_i) = \widehat{\boldsymbol{x}}_{\mathrm{m,lpf},t_i} \\ z_{\mathrm{m}} &= \frac{\Gamma_{\mathrm{m}}\widehat{\omega}^2_{\mathrm{m},1} e_{\mathrm{m,lpf},y}\boldsymbol{\sigma}^\top_{\mathrm{m},1}\widehat{\boldsymbol{x}}_{\mathrm{m,lpf},1}}{\max\left(\left\|\widehat{\boldsymbol{x}}_{\mathrm{m,lpf},1}\right\|^2, \varepsilon_{\mathrm{m}}\right)} && \\ \tfrac{\mathrm{d}}{\mathrm{d}t}\widehat{\omega}_{\mathrm{m},1} &= \mathrm{sat}_{\underline{z}_{\mathrm{m}}}^{\overline{z}_{\mathrm{m}}}(z_{\mathrm{m}})\, \mathrm{aw}_{\underline{\omega}_{\mathrm{m}}}^{\overline{\omega}_{\mathrm{m}}}(\widehat{\omega}_{\mathrm{m},1}, z_{\mathrm{m}}), && \widehat{\omega}_{\mathrm{m},1}(t_i) = \widehat{\omega}_{\mathrm{m},1,t_i} \\ \widehat{y}_{\mathrm{m}} &= \boldsymbol{c}^\top\widehat{\boldsymbol{x}}_{\mathrm{m}}. && \end{aligned}\right\} \tag{3.94}$$

Its block diagram is shown in Figure 3.21.

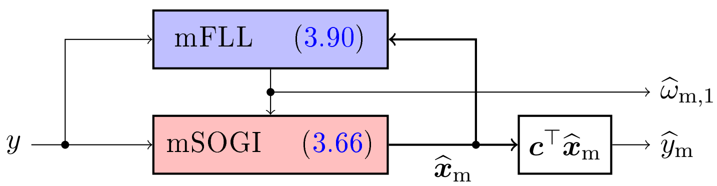

Figure 3.21: *Block diagram of the mFAO.*

Figure 3.22[16] shows the evaluation of the mFAO where the test signals from (3.12) are used.

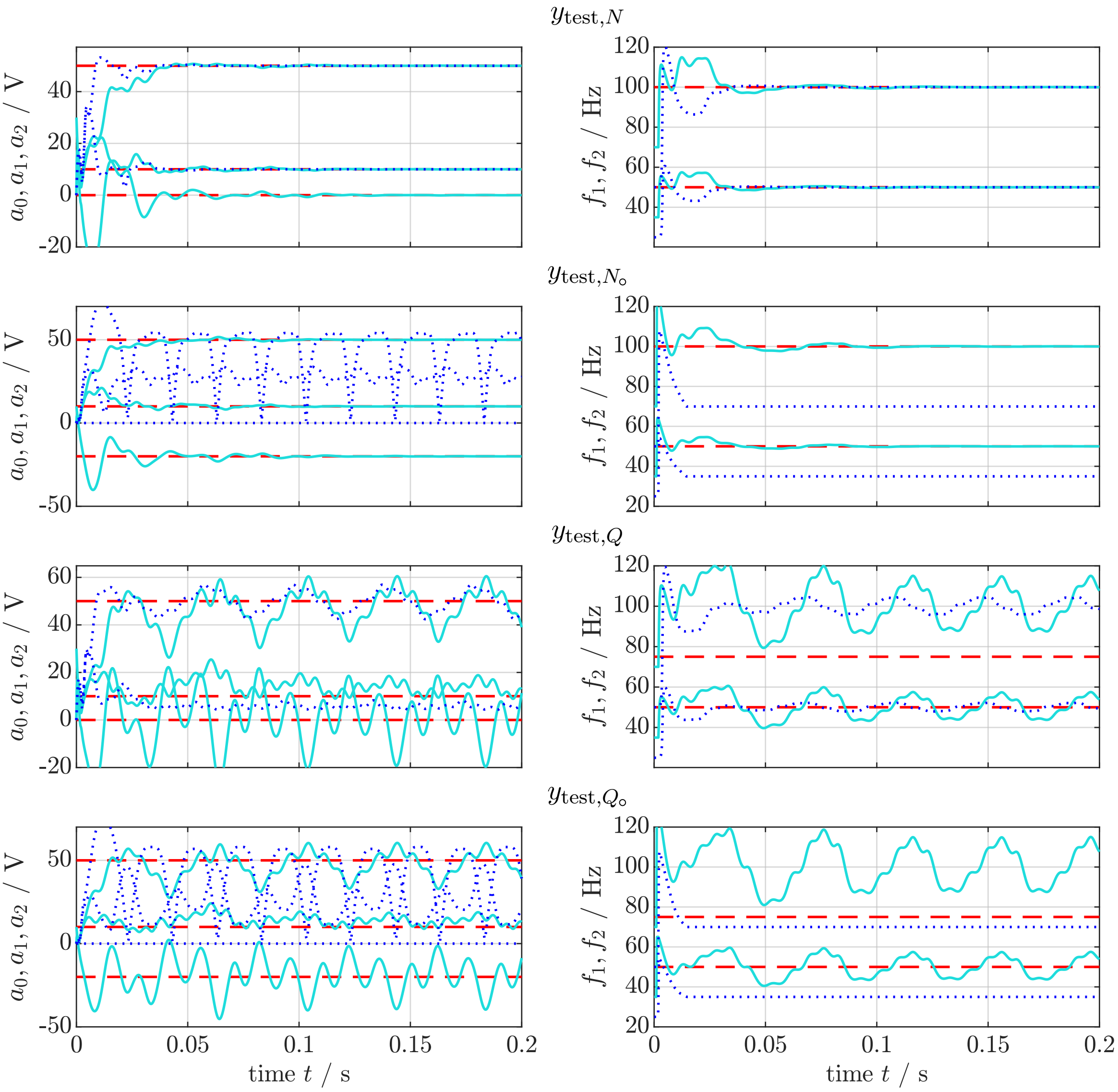

Figure 3.22: *Continuation of Figure 3.13. Offset, amplitudes and frequencies of the test signals estimated by the mFAO (·····).*

Note that, although one estimate for each frequency is shown, the mFLL only estimates the fundamental one. The other results from this fundamental one by multiplication (and is not estimated). Since the mFAO cannot estimste offset, no estimate for this value is plotted. If the harmonic orders are assumed correctly, i.e. $\mathbb{H}_\infty = \mathbb{H}_n$, and no offset is present in the input y ($y_{\text{test},N}$) the mFAO settles in 33.3 ms which was evaluated for the angular frequency by using (3.54). Hence, it is an improvement to the esFAO. However, when offset is included in the input y ($y_{\text{test},N_\circ}$), the mFAO cannot estimate the amplitudes and frequencies anymore. In fact, frequency estimation fails completely and is only held stable by the anti windup. If $\mathbb{H}_\infty$ is not equal to $\mathbb{H}_n$ ($y_{\text{test},Q}, y_{\text{test},Q_\circ}$), the mFAO fails to estimate the parameters. But, if no offset is present, it at

[16]Simulation parameters (in addition to Footnote 9): $\mathbb{H}_n = \{1, 2\}$, $\boldsymbol{l}_\text{m} = (7.5, -0.9375, -1.5, -6.28125)^\top$, $\omega_{\text{m,lpf}} = 2\pi 100$, $\Gamma_\text{m} = 0.2756$, $\boldsymbol{\sigma}_{\text{m},1} = (-0.9375, -7.5)^\top$, $\varepsilon_\text{m} = 10^{-5}$, $\underline{z}_\text{m} = -2\pi 10^5$, $\overline{z}_\text{m} = 2\pi 10^5$, $\underline{\omega}_\text{m} = 2\pi 35$, $\overline{\omega}_\text{m} = 2\pi 65$.

least gives a rough estimate of the fundamental angular frequency ω_1.

3.3.5.2 Summary of the mFAO with offset

The mathematical description for the mFAO$_\circ$ follows as

$$\forall t \in \mathbb{T}_i\colon \quad \left.\begin{aligned} \tfrac{\mathrm{d}}{\mathrm{d}t}\widehat{\boldsymbol{x}}_{\mathrm{m}_\circ} &= \widehat{\omega}_{\mathrm{m}_\circ,1}\boldsymbol{A}_{\mathrm{m}_\circ}\widehat{\boldsymbol{x}}_{\mathrm{m}_\circ} + \widehat{\omega}_{\mathrm{m}_\circ,1}\boldsymbol{l}_{\mathrm{m}_\circ}y, && \widehat{\boldsymbol{x}}_{\mathrm{m}_\circ}(t_i) = \widehat{\boldsymbol{x}}_{\mathrm{m}_\circ,t_i}, \\ \tfrac{\mathrm{d}}{\mathrm{d}t}\widehat{\boldsymbol{x}}_{\mathrm{m}_\circ,\mathrm{lpf}} &= -\omega_{\mathrm{m}_\circ,\mathrm{lpf}}\widehat{\boldsymbol{x}}_{\mathrm{m}_\circ,\mathrm{lpf}} + \omega_{\mathrm{m}_\circ,\mathrm{lpf}}\begin{pmatrix} e_{\mathrm{m}_\circ,y} \\ \widehat{\boldsymbol{x}}_{\mathrm{m}_\circ,1}\end{pmatrix}, && \widehat{\boldsymbol{x}}_{\mathrm{m}_\circ,\mathrm{lpf}}(t_i) = \widehat{\boldsymbol{x}}_{\mathrm{m}_\circ,\mathrm{lpf},t_i} \\ z_{\mathrm{m}_\circ} &= \frac{\Gamma_{\mathrm{m}_\circ}\widehat{\omega}^2_{\mathrm{m}_\circ,1}e_{\mathrm{m}_\circ,\mathrm{lpf},y}\boldsymbol{\sigma}^\top_{\mathrm{m}_\circ,1}\widehat{\boldsymbol{x}}_{\mathrm{m}_\circ,\mathrm{lpf},1}}{\max\left(\left\|\widehat{\boldsymbol{x}}_{\mathrm{m}_\circ,\mathrm{lpf},1}\right\|^2, \varepsilon_{\mathrm{m}_\circ}\right)} \\ \tfrac{\mathrm{d}}{\mathrm{d}t}\widehat{\omega}_{\mathrm{m}_\circ,1} &= \mathrm{sat}^{\overline{z}_{\mathrm{m}_\circ}}_{\underline{z}_{\mathrm{m}_\circ}}(z_{\mathrm{m}_\circ})\,\mathrm{aw}^{\overline{\omega}_{\mathrm{m}_\circ}}_{\underline{\omega}_{\mathrm{m}_\circ}}(\widehat{\omega}_{\mathrm{m}_\circ,1}, z_{\mathrm{m}_\circ}), && \widehat{\omega}_{\mathrm{m}_\circ,1}(t_i) = \widehat{\omega}_{\mathrm{m}_\circ,1,t_i} \\ \widehat{y}_{\mathrm{m}_\circ} &= \boldsymbol{c}_\circ^\top\widehat{\boldsymbol{x}}_{\mathrm{m}_\circ} \end{aligned}\right\} \tag{3.95}$$

and the block diagram in Figure 3.23.

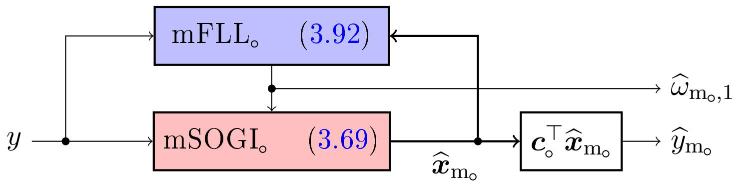

Figure 3.23: *Block diagram of the mFAO$_\circ$.*

In Figure 3.24[17], the evaluation of the mFAO$_\circ$ is plotted where the test signals from (3.12) are used.
Note that, although one estimate for each frequency is shown, the mFLL$_\circ$ only estimates the fundamental component. The other results from this fundamental one by multiplication (and is not estimated). In case of correctly assumed harmonic orders $\mathbb{H}_\infty = \mathbb{H}_n$ ($y_{\mathrm{test},N}, y_{\mathrm{test},N_\circ}$) the mFAO$_\circ$ correctly estimates the amplitudes a_i and the fundamental angular frequency ω_1. Compared to the mFAO, the normed settling time (obtained by evaluating the angular frequency using (3.54)) is larger for the mFAO$_\circ$, which is 60.2 ms ($y_{\mathrm{test},N}$) and 48.1 ms ($y_{\mathrm{test},N_\circ}$). Nevertheless, it still outruns the esFAO. On the other hand, when actual harmonic orders $\mathbb{H}_\infty$ are not equal to the assumed ones $\mathbb{H}_n$ ($y_{\mathrm{test},Q}, y_{\mathrm{test},Q_\circ}$), the mFAO$_\circ$ cannot estimate the parameters anymore and the estimation fails. However, the fundamental angular frequency ω_1 can still be roughly estimated.

Theorem 3.3.12 (Bounded-input bounded-state/bounded-output stability of the dynamics of the mFAO and mFAO$_\circ$)**.** *Let be* $\mathrm{x} \in \{\mathrm{m}, \mathrm{m}_\circ\}$. *Consider an essentially bounded input signal, i.e.* $y \in \mathcal{L}^\infty(\mathbb{R}_{\geq 0}; \mathbb{R})$ *and assume that (i) the estimated fundamental angular frequency is continuous, bounded and uniformly bounded away from zero by* $\epsilon_{\omega,\mathrm{x}} > 0$*, i.e.* $\widehat{\omega}_{\mathrm{x},1} \in \mathcal{L}^\infty(\mathbb{R}_{\geq 0}; \mathbb{R}_{>0})$*, and (ii) the system matrix* $\boldsymbol{A}_\mathrm{x}$ *in* (3.66) *or* (3.69)*, respectively, is a Hurwitz matrix. Then, the time-varying system* (3.66) *or* (3.69)*, respectively, is bounded-input bounded-state/bounded-output stable, i.e.*

$$\forall t \in \mathbb{T}_i\colon \quad \exists\, c_\mathrm{x}, \widetilde{c}_\mathrm{x} > 0\colon \quad \|\widehat{\boldsymbol{x}}_\mathrm{x}\| \leq c_\mathrm{x} \quad \textit{and} \quad |\widehat{y}_\mathrm{x}| \leq \widetilde{c}_\mathrm{x}.$$

Proof. Let t_ω be the rise time to the limits of the AW decision function of the mFLL or the mFLL$_\circ$, respectively. Since $\widehat{\omega}_{\mathrm{x},1}$ is bounded where, for all $t \geq t_0$ it holds that $\widehat{\omega}_{\mathrm{x},1} > 0$ and,

[17] Simulation parameters (in addition to Footnote 16): $\mathbb{H}_n = \{1, 2\}$, $\boldsymbol{l}_{\mathrm{m}_\circ} = (7.6171875, 6.09375, -12.1875, -6.2109375, -5.15625)^\top$, $\omega_{\mathrm{m}_\circ,\mathrm{lpf}} = 2\pi 100$, $\Gamma_{\mathrm{m}_\circ} = 0.33$, $\boldsymbol{\sigma}_{\mathrm{m}_\circ,1} = (-12.1875, -6.09375)^\top$, $\varepsilon_{\mathrm{m}_\circ} = 10^{-5}$, $\underline{z}_{\mathrm{m}_\circ} = -2\pi 10^5$, $\overline{z}_{\mathrm{m}_\circ} = 2\pi 10^5$, $\underline{\omega}_{\mathrm{m}_\circ} = 2\pi 35$, $\overline{\omega}_{\mathrm{m}_\circ} = 2\pi 65$.

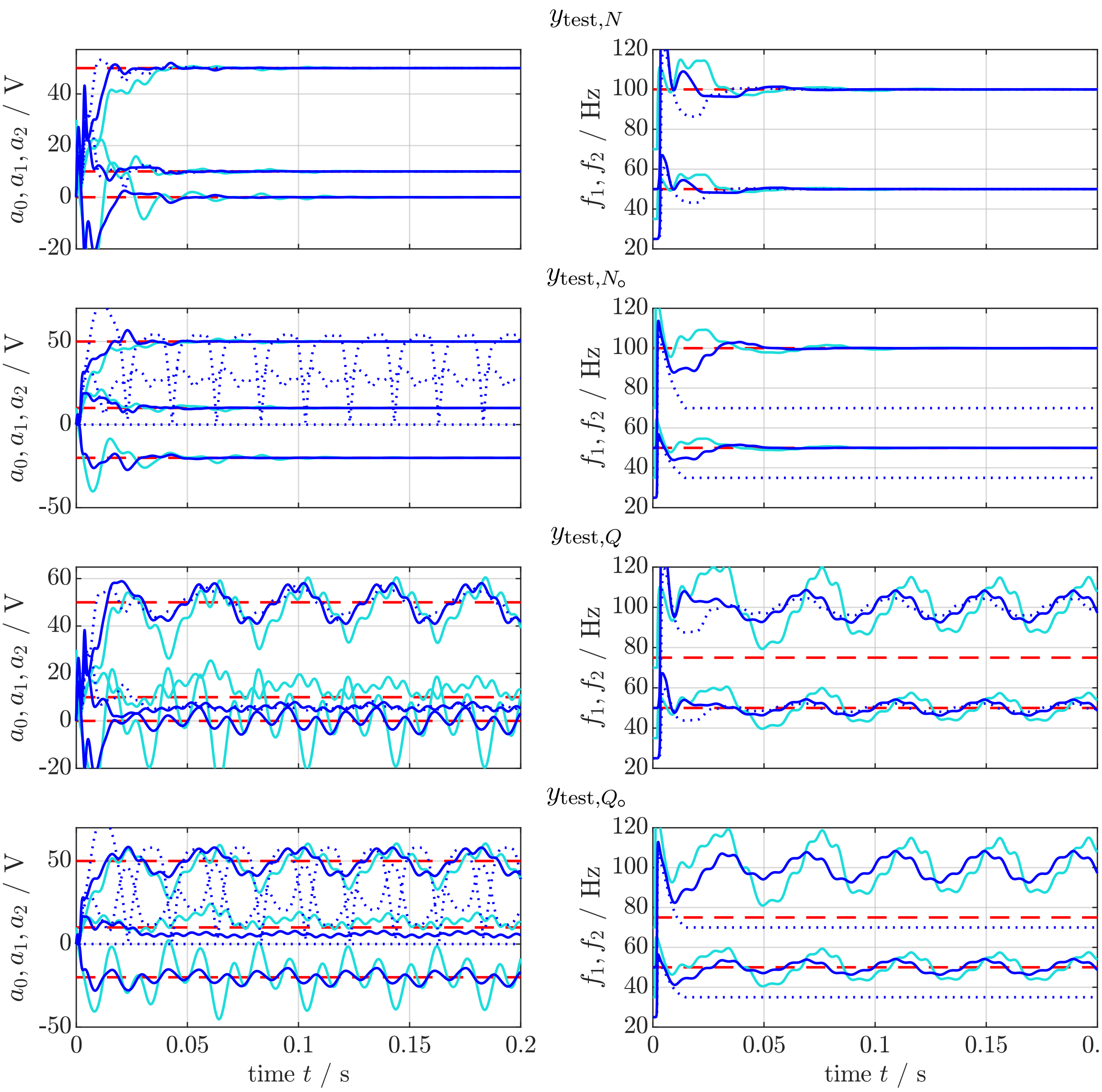

Figure 3.24: *Continuation of Figure 3.22. Offset, amplitudes and frequencies of the test signals estimated by the mFAO$_\circ$ (——).*

moreover, for all $t \geq t_\omega$ it holds that $\overline{\omega}_\text{x} \geq \widehat{\omega}_{\text{x},1} \geq \underline{\omega}_\text{x}$, the idea described in the proof of Theorem 3.2.8 can be repeated. This completes the proof. □

Theorem 3.3.13 (Boundedness and exponential decrease of the signal estimation error of the mFAO and mFAO$_\circ$)**.** *Let be* $\text{x} \in \{\text{m}, \text{m}_\circ\}$*. Let, for all* $t \geq t_0$*,* $\widehat{\omega}_{\text{x},1} > \epsilon_{\omega,\text{x}}$ *be bounded. Consider any continuous and bounded input signal, i.e.* $y \in \mathcal{C}(\mathbb{R}_{\geq 0}; \mathbb{R}_{>0}) \cap \mathcal{L}^\infty(\mathbb{R}_{\geq 0}; \mathbb{R})$ *and assume that* y *is fed to the parallelized mSOGIs (3.66) or the parallelized mSOGI$_\circ$s (3.69), respectively, with* $\boldsymbol{A}_\text{x}$ *being a Hurwitz matrix. Then, the estimation error, defined by*

$$\forall t \in \mathbb{T}_i: \quad \boldsymbol{e}_\text{x} := \boldsymbol{x}_\text{x} - \widehat{\boldsymbol{x}}_\text{x}, \quad \boldsymbol{e}_{\text{x},t_i} = \boldsymbol{x}_{\text{x},t_i} - \widehat{\boldsymbol{x}}_{\text{x},t_i} \tag{3.96}$$

with $\boldsymbol{x}_\text{x}$ *as in (3.4) or (3.8) and* $\widehat{\boldsymbol{x}}_\text{x}$ *as in (3.66) or (3.69), respectively, is bounded, i.e. there exists* $c_{\text{x},e} > 0$ *such that* $\|\boldsymbol{e}_\text{x}\| \leq c_{\text{x},e}$ *for all* $t \geq t_i$*. Moreover, if* $\omega_1 = \widehat{\omega}_{\text{x},1}$*,* $\mathbb{H}_\infty = \mathbb{H}_n$ *and* $a_0 = 0$ *if* $\text{x} = \text{m}$ *for all* $t \in \mathbb{T}_i$*, then the norm of the estimation error decreases exponentially, i.e. there* *exist constants* $c_{\mathrm{x},V}, \mu_{\mathrm{x},V} > 0$ *such that*

$$\forall\, t \in \mathbb{T}_i: \quad \|\boldsymbol{e}_{\mathrm{x}}\| \leq c_{\mathrm{x},V} \|\boldsymbol{e}_{\mathrm{x},t_i}\| \,\mathrm{e}^{-\mu_{\mathrm{x},V}(t-t_i)}.$$

Proof. The proof is identical to the proof of Theorem 3.2.9. □

3.4 The transformation-based Frequency Adaptive Observer in transformed frame and the transformation-based Frequency Adaptive Observer with offset in transformed frame

In Section 3.3, observers were constructed with the purpose of observing the generating systems (3.4) and (3.8). However, for proper functionality, the harmonic numbers collected in $\mathbb{H}_n$ had to be (at least roughly) known. Hence, the following section addresses this problem where the basic idea, that already was published in [548], is to transform the generation system into *Controllable Canonical Form* (CCF). This section's structure is as follows:

Section 3.4.1 describes the transformation of the generation systems (3.4) and (3.8) to CCF,

Section 3.4.2 briefly restates observability,

Section 3.4.3 constructs observers for the transformed systems,

Section 3.4.4 discusses the gain selection for both systems and

Section 3.4.5 proves stability for both methods where, as an outcome, the angular frequency adaption laws can be formulated.

3.4.1 Transformation to Controllable Canonical Form

First of all, the transformation into *Controllable Canonical Form* (CCF) is described. To this end, at first the transformation of (3.4) is explained and, based thereon, (3.8) is transformed afterwards.

3.4.1.1 Transformation of the generation system without offset to Controllable Canonical Form

The basic idea for the transformation to CCF was already reported in [548], which defined the transformation of system (3.4) to CCF as

$$\underline{\boldsymbol{x}} := \boldsymbol{T}(\boldsymbol{\omega})\boldsymbol{x}. \tag{3.97}$$

where here and in the following, all symbols marked by an underline (i.e. "_") represent an expression in transformed coordinates. The transformation matrix $\boldsymbol{T}$ and its inverse matrix are given by

$$\boldsymbol{T}(\boldsymbol{\omega}) := \begin{bmatrix} \boldsymbol{T}_1(\boldsymbol{\omega}) & \cdots & \boldsymbol{T}_{n_\infty}(\boldsymbol{\omega}) \\ \vdots & \ddots & \vdots \\ (-\omega_1^2)^{n_\infty-1}\boldsymbol{T}_1(\boldsymbol{\omega}) & \cdots & (-\omega_{n_\infty}^2)^{n_\infty-1}\boldsymbol{T}_{n_\infty}(\boldsymbol{\omega}) \end{bmatrix} \in \mathbb{R}^{2n_\infty \times 2n_\infty}, \tag{3.98}$$

$$\boldsymbol{T}^{-1}(\boldsymbol{\omega}) = \begin{bmatrix} \frac{(-1)^{n_\infty+1}\prod\limits_{\substack{j=1\\j\neq 1}}^{n_\infty}\omega_j^2}{\prod\limits_{\substack{j=1\\j\neq 1}}^{n_\infty}\left(\omega_1^2-\omega_j^2\right)}\boldsymbol{T}_1^{-1}(\boldsymbol{\omega}) & \cdots & \frac{(-1)^{n_\infty+1}}{\prod\limits_{\substack{j=1\\j\neq 1}}^{n_\infty}\left(\omega_1^2-\omega_j^2\right)}\boldsymbol{T}_1^{-1}(\boldsymbol{\omega}) \\ \vdots & \ddots & \vdots \\ \frac{(-1)^{n_\infty+1}\prod\limits_{\substack{j=1\\j\neq n_\infty}}^{n_\infty}\omega_j^2}{\prod\limits_{\substack{j=1\\j\neq n_\infty}}^{n_\infty}\left(\omega_{n_\infty}^2-\omega_j^2\right)}\boldsymbol{T}_{n_\infty}^{-1}(\boldsymbol{\omega}) & \cdots & \frac{(-1)^{n_\infty+1}}{\prod\limits_{\substack{j=1\\j\neq n_\infty}}^{n_\infty}\left(\omega_{n_\infty}^2-\omega_j^2\right)}\boldsymbol{T}_{n_\infty}^{-1}(\boldsymbol{\omega}) \end{bmatrix} \tag{3.99}$$

since the product of the r-th row of $\boldsymbol{T}^{-1}$ and the c-th row of $\boldsymbol{T}$ yields

$$\begin{aligned} &\frac{(-1)^{n_\infty+1}\prod\limits_{\substack{j=1\\j\neq r}}^{n_\infty}\omega_j^2}{\prod\limits_{\substack{j=1\\j\neq r}}^{n_\infty}\left(\omega_r^2-\omega_j^2\right)}\boldsymbol{T}_r^{-1}(\boldsymbol{\omega})\boldsymbol{T}_c(\boldsymbol{\omega}) + \cdots - \frac{(-1)^{n_\infty+1}}{\prod\limits_{\substack{j=1\\j\neq r}}^{n_\infty}\left(\omega_r^2-\omega_j^2\right)}\boldsymbol{T}_r^{-1}(\boldsymbol{\omega})\frac{(-\omega_c^2)^{n_\infty}}{\omega_c^2}\boldsymbol{T}_c(\boldsymbol{\omega}) \\ &\quad = \left((-1)^{n_\infty+1}\prod_{\substack{j=1\\j\neq r}}^{n_\infty}\omega_j^2 + \cdots - \omega_c^{2n_\infty-4}\sum_{\substack{j=1\\j\neq r}}^{n_\infty}\omega_j^2 + \omega_c^{2n_\infty-2}\right)\frac{\boldsymbol{T}_r^{-1}(\boldsymbol{\omega})\boldsymbol{T}_c(\boldsymbol{\omega})}{\prod\limits_{\substack{j=1\\j\neq r}}^{n_\infty}\left(\omega_r^2-\omega_j^2\right)} \\ &\quad \overset{(2.18)}{=} \prod_{\substack{j=1\\j\neq r}}^{n_\infty}\left(\omega_c^2-\omega_j^2\right)\frac{\boldsymbol{T}_r^{-1}(\boldsymbol{\omega})\boldsymbol{T}_c(\boldsymbol{\omega})}{\prod\limits_{\substack{j=1\\j\neq r}}^{n_\infty}\left(\omega_r^2-\omega_j^2\right)} = \begin{cases}\boldsymbol{0}_{2\times 2}, & c\neq r\\ \boldsymbol{I}_2, & c = r.\end{cases} \end{aligned}$$

In $\boldsymbol{T}$, each sub matrix $\boldsymbol{T}_i$ is defined as

$$\forall\, i\in\{1,\ldots,n_\infty\}: \quad \boldsymbol{T}_i(\boldsymbol{\omega}) := \frac{\sum\limits_{j=1}^{n_\infty}(-1)^j\omega_i^{2j-2}\begin{bmatrix}-\underline{c}_{\mathrm{t},j}^{\alpha}(\boldsymbol{\omega}) & -\omega_i\underline{c}_{\mathrm{t},j}^{\beta}(\boldsymbol{\omega})\\ -\omega_i^2\underline{c}_{\mathrm{t},j}^{\beta}(\boldsymbol{\omega}) & \omega_i\underline{c}_{\mathrm{t},j}^{\alpha}(\boldsymbol{\omega})\end{bmatrix}}{\left(\sum\limits_{j=1}^{n_\infty}(-1)^j\omega_i^{2j-2}\underline{c}_{\mathrm{t},j}^{\alpha}(\boldsymbol{\omega})\right)^2 + \left(\sum\limits_{j=1}^{n_\infty}(-1)^j\omega_i^{2j-1}\underline{c}_{\mathrm{t},j}^{\beta}(\boldsymbol{\omega})\right)^2}. \tag{3.100}$$

The transformation parameters $\underline{c}_{\mathrm{t},i}^{\alpha}$ and $\underline{c}_{\mathrm{t},i}^{\beta}$, $i\in\{1,\ldots,n_\infty\}$ are constant. Hence, since the frequencies ω_i are assumed to be constant, the time derivative of (3.97) results in

$$\forall\, t\in\mathbb{T}_i: \quad \left.\begin{aligned} \tfrac{\mathrm{d}}{\mathrm{d}t}\underline{\boldsymbol{x}} &= \boldsymbol{T}(\boldsymbol{\omega})\boldsymbol{J}(\boldsymbol{\omega})\boldsymbol{x} = \overbrace{\boldsymbol{T}(\boldsymbol{\omega})\boldsymbol{J}(\boldsymbol{\omega})\boldsymbol{T}^{-1}(\boldsymbol{\omega})}^{=:\,\underline{\boldsymbol{J}}(\boldsymbol{\omega})}\underline{\boldsymbol{x}}, \quad \underline{\boldsymbol{x}}(t_i) = \underline{\boldsymbol{x}}_{t_i} = \boldsymbol{T}(\boldsymbol{\omega})\boldsymbol{x}_{t_i}\\ y &= \boldsymbol{c}^\top\boldsymbol{x} = \underbrace{\boldsymbol{c}^\top\boldsymbol{T}^{-1}(\boldsymbol{\omega})}_{=:\,\underline{\boldsymbol{c}}_{\mathrm{t}}^\top(\boldsymbol{\omega})}\underline{\boldsymbol{x}}. \end{aligned}\right\} \tag{3.101}$$

The resulting matrix $\underline{\boldsymbol{J}}$ is in CCF, i.e.

$$\underline{\boldsymbol{J}}(\boldsymbol{\omega}) = \begin{bmatrix} 0 & 1 & \cdots & 0 & 0\\ 0 & 0 & \cdots & 0 & 0\\ \vdots & \vdots & \ddots & \vdots & \vdots\\ 0 & 0 & \cdots & 0 & 1\\ -\prod\limits_{j=1}^{n_\infty}\omega_j^2 & 0 & \cdots & -\sum\limits_{j=1}^{n_\infty}\omega_j^2 & 0 \end{bmatrix} =: \begin{bmatrix} 0 & 1 & \cdots & 0 & 0\\ 0 & 0 & \cdots & 0 & 0\\ \vdots & \vdots & \ddots & \vdots & \vdots\\ 0 & 0 & \cdots & 0 & 1\\ -\underline{\theta}_{n_\infty} & 0 & \cdots & -\underline{\theta}_1 & 0 \end{bmatrix} =: \underline{\boldsymbol{J}}(\underline{\boldsymbol{\theta}}). \tag{3.102}$$

Due to the specific choice of $\boldsymbol{T}_i$, the output vector $\underline{\boldsymbol{c}}_{\mathrm{t}}$ collects the transformation parameters

$$\underline{\boldsymbol{c}}_{\mathrm{t}}(\boldsymbol{\omega}) = \begin{pmatrix} \underline{c}^{\alpha}_{\mathrm{t},1}(\boldsymbol{\omega}) & \underline{c}^{\beta}_{\mathrm{t},1}(\boldsymbol{\omega}) & \underline{c}^{\alpha}_{\mathrm{t},2}(\boldsymbol{\omega}) & \underline{c}^{\beta}_{\mathrm{t},2}(\boldsymbol{\omega}) & \cdots & \underline{c}^{\alpha}_{\mathrm{t},n_\infty}(\boldsymbol{\omega}) & \underline{c}^{\beta}_{\mathrm{t},n_\infty}(\boldsymbol{\omega}) \end{pmatrix}^{\top}. \tag{3.103}$$

The transformed angular frequencies

$$\left.\begin{aligned} \underline{\theta}_1 &= \sum_{j=1}^{n_\infty} \omega_j^2 \\ \underline{\theta}_i &= \sum_{j_1<j_i=1}^{n_\infty} \prod_{k\in j} \omega_k^2 \\ \underline{\theta}_{n_\infty} &= \prod_{j=1}^{n_\infty} \omega_j^2 \end{aligned}\right\} \tag{3.104}$$

are collected in the transformed angular frequency vector

$$\underline{\boldsymbol{\theta}} := \begin{pmatrix} \underline{\theta}_1 & \underline{\theta}_2 & \cdots & \underline{\theta}_{n_\infty} \end{pmatrix}^{\top} \in \mathbb{R}^{n_\infty}. \tag{3.105}$$

They refer to the matrix $\underline{\boldsymbol{J}}$ via

$$\underline{\boldsymbol{J}}(\underline{\boldsymbol{\theta}}) = \begin{bmatrix} 0 & 1 & \cdots & 0 & 0 \\ \vdots & \vdots & \ddots & \vdots & \vdots \\ 0 & 0 & \cdots & 0 & 1 \\ 0 & 0 & \cdots & 0 & 0 \end{bmatrix} - \underbrace{\begin{pmatrix} 0 \\ \vdots \\ 0 \\ 1 \end{pmatrix}}_{=:\,\underline{\boldsymbol{b}}\in\mathbb{R}^{2n_\infty}} \underline{\boldsymbol{\theta}}^{\top} \underbrace{\begin{bmatrix} 0 & 0 & 0 & 0 & \cdots & 1 & 0 \\ \vdots & \vdots & \vdots & \vdots & \iddots & \vdots & \vdots \\ 0 & 0 & 1 & 0 & \cdots & 0 & 0 \\ 1 & 0 & 0 & 0 & \cdots & 0 & 0 \end{bmatrix}}_{=:\,\underline{\boldsymbol{\Sigma}}\in\mathbb{R}^{n_\infty\times 2n_\infty}}. \tag{3.106}$$

This completes the description of the transformation of (3.4) to CCF.

3.4.1.2 Transformation of the generation system with offset to Controllable Canonical Form

Similar to (3.97), the transformation for (3.8) is defined as

$$\underline{\boldsymbol{x}}_{\circ} := \boldsymbol{T}_{\circ}(\boldsymbol{\omega})\boldsymbol{x}_{\circ}. \tag{3.107}$$

The transformation matrix $\boldsymbol{T}_{\circ}$ uses a matrix $\overline{\boldsymbol{T}}$ based on $\boldsymbol{T}$ from (3.98) and is given by

$$\boldsymbol{T}_{\circ}(\boldsymbol{\omega}) := \begin{bmatrix} t_{\mathrm{s}}(\boldsymbol{\omega}) & \boldsymbol{t}_{\mathrm{r}}^{\top}(\boldsymbol{\omega}) \\ \boldsymbol{t}_{\mathrm{c}}(\boldsymbol{\omega}) & \overline{\boldsymbol{T}}(\boldsymbol{\omega}) \end{bmatrix} \in \mathbb{R}^{(2n_\infty+1)\times(2n_\infty+1)} \tag{3.108}$$

whereas its inverse is obtained as

$$\boldsymbol{T}_{\circ}^{-1}(\boldsymbol{\omega}) = \begin{bmatrix} \frac{1+\boldsymbol{t}_{\mathrm{r}}^{\top}(\boldsymbol{\omega})\left(t_{\mathrm{s}}(\boldsymbol{\omega})\overline{\boldsymbol{T}}(\boldsymbol{\omega})-\boldsymbol{t}_{\mathrm{c}}(\boldsymbol{\omega})\boldsymbol{t}_{\mathrm{r}}^{\top}(\boldsymbol{\omega})\right)^{-1}\boldsymbol{t}_{\mathrm{c}}(\boldsymbol{\omega})}{t_{\mathrm{s}}(\boldsymbol{\omega})} & -\frac{\boldsymbol{t}_{\mathrm{r}}^{\top}(\boldsymbol{\omega})}{t_{\mathrm{s}}(\boldsymbol{\omega})}\left(\overline{\boldsymbol{T}}(\boldsymbol{\omega}) - \frac{\boldsymbol{t}_{\mathrm{c}}(\boldsymbol{\omega})\boldsymbol{t}_{\mathrm{r}}^{\top}(\boldsymbol{\omega})}{t_{\mathrm{s}}(\boldsymbol{\omega})}\right)^{-1} \\ -\frac{1}{t_{\mathrm{s}}(\boldsymbol{\omega})}\left(\overline{\boldsymbol{T}}(\boldsymbol{\omega}) - \frac{\boldsymbol{t}_{\mathrm{c}}(\boldsymbol{\omega})\boldsymbol{t}_{\mathrm{r}}^{\top}(\boldsymbol{\omega})}{t_{\mathrm{s}}(\boldsymbol{\omega})}\right)^{-1}\boldsymbol{t}_{\mathrm{c}}(\boldsymbol{\omega}) & \left(\overline{\boldsymbol{T}}(\boldsymbol{\omega}) - \frac{\boldsymbol{t}_{\mathrm{c}}(\boldsymbol{\omega})\boldsymbol{t}_{\mathrm{r}}^{\top}(\boldsymbol{\omega})}{t_{\mathrm{s}}(\boldsymbol{\omega})}\right)^{-1} \end{bmatrix}. \tag{3.109}$$

Taking the time derivative of (3.107) yields

$$\tfrac{\mathrm{d}}{\mathrm{d}t}\underline{\boldsymbol{x}}_{\circ} = \boldsymbol{T}_{\circ}(\boldsymbol{\omega})\boldsymbol{J}_{\circ}(\boldsymbol{\omega})\boldsymbol{x}_{\circ} = \underbrace{\boldsymbol{T}_{\circ}(\boldsymbol{\omega})\boldsymbol{J}_{\circ}(\boldsymbol{\omega})\boldsymbol{T}_{\circ}^{-1}(\boldsymbol{\omega})}_{=:\,\underline{\boldsymbol{J}}_{\circ}(\boldsymbol{\omega})}\underline{\boldsymbol{x}}_{\circ}$$

$$\overset{(3.8),\,(3.108),\,(3.109)}{=} \begin{bmatrix} -\frac{\boldsymbol{t}_\mathrm{r}^\top(\boldsymbol{\omega})\boldsymbol{J}(\boldsymbol{\omega})}{t_\mathrm{s}(\boldsymbol{\omega})}\left(\overline{\boldsymbol{T}}(\boldsymbol{\omega}) - \frac{\boldsymbol{t}_\mathrm{c}(\boldsymbol{\omega})\boldsymbol{t}_\mathrm{r}^\top(\boldsymbol{\omega})}{t_\mathrm{s}(\boldsymbol{\omega})}\right)^{-1}\boldsymbol{t}_\mathrm{c}(\boldsymbol{\omega}) & \boldsymbol{t}_\mathrm{r}^\top(\boldsymbol{\omega})\boldsymbol{J}(\boldsymbol{\omega})\left(\overline{\boldsymbol{T}}(\boldsymbol{\omega}) - \frac{\boldsymbol{t}_\mathrm{c}(\boldsymbol{\omega})\boldsymbol{t}_\mathrm{r}^\top(\boldsymbol{\omega})}{t_\mathrm{s}(\boldsymbol{\omega})}\right)^{-1} \\ -\frac{\overline{\boldsymbol{T}}(\boldsymbol{\omega})\boldsymbol{J}(\boldsymbol{\omega})}{t_\mathrm{s}(\boldsymbol{\omega})}\left(\overline{\boldsymbol{T}}(\boldsymbol{\omega}) - \frac{\boldsymbol{t}_\mathrm{c}(\boldsymbol{\omega})\boldsymbol{t}_\mathrm{r}^\top(\boldsymbol{\omega})}{t_\mathrm{s}(\boldsymbol{\omega})}\right)^{-1}\boldsymbol{t}_\mathrm{c}(\boldsymbol{\omega}) & \overline{\boldsymbol{T}}(\boldsymbol{\omega})\boldsymbol{J}(\boldsymbol{\omega})\left(\overline{\boldsymbol{T}}(\boldsymbol{\omega}) - \frac{\boldsymbol{t}_\mathrm{c}(\boldsymbol{\omega})\boldsymbol{t}_\mathrm{r}^\top(\boldsymbol{\omega})}{t_\mathrm{s}(\boldsymbol{\omega})}\right)^{-1} \end{bmatrix} \underline{\boldsymbol{x}}_\circ. \tag{3.110}$$

To obtain $\underline{\boldsymbol{J}}_\circ$ in CCF,

$$\boldsymbol{t}_\mathrm{c}(\boldsymbol{\omega}) = \boldsymbol{0}_{2n_\infty} \quad \text{and} \quad \boldsymbol{t}_\mathrm{r}(\boldsymbol{\omega}) = -\boldsymbol{J}^{-1}(\boldsymbol{\omega})\overline{\boldsymbol{T}}^\top(\boldsymbol{\omega})\boldsymbol{i}_{1,2n_\infty}$$

must hold. Moreover, the south-eastern sub matrix $\overline{\boldsymbol{T}}\boldsymbol{J}\overline{\boldsymbol{T}}^{-1}$ must be in CCF as well. However, this is already the case if $\overline{\boldsymbol{T}}$ is chosen similar to $\boldsymbol{T}$ as in (3.98) but with

$$\forall i \in \{1,\dots,n_\infty\}: \quad \overline{\boldsymbol{T}}_{\circ,i}(\boldsymbol{\omega}) = \frac{-\begin{bmatrix} 0 & \frac{\underline{c}_{\mathrm{t}_\circ,0}(\boldsymbol{\omega})}{\omega_i} \\ \underline{c}_{\mathrm{t}_\circ,0}(\boldsymbol{\omega}) & 0\end{bmatrix} + \sum_{j=1}^{n_\infty}(-1)^j\omega_i^{2j-2}\begin{bmatrix} -\underline{c}^\alpha_{\mathrm{t}_\circ,j}(\boldsymbol{\omega}) & -\omega_i\underline{c}^\beta_{\mathrm{t}_\circ,j}(\boldsymbol{\omega}) \\ -\omega_i^2\underline{c}^\beta_{\mathrm{t}_\circ,j}(\boldsymbol{\omega}) & \omega_i\underline{c}^\alpha_{\mathrm{t}_\circ,j}(\boldsymbol{\omega})\end{bmatrix}}{\left(\sum_{j=1}^{n_\infty}(-1)^j\omega_i^{2j-2}\underline{c}^\alpha_{\mathrm{t}_\circ,j}(\boldsymbol{\omega})\right)^2 + \left(\frac{\underline{c}_{\mathrm{t}_\circ,0}(\boldsymbol{\omega})}{\omega_i} + \sum_{j=1}^{n_\infty}(-1)^j\omega_i^{2j-1}\underline{c}^\beta_{\mathrm{t}_\circ,j}(\boldsymbol{\omega})\right)^2} \tag{3.111}$$

instead of $\boldsymbol{T}_i$. This choice, together with

$$t_\mathrm{s}(\boldsymbol{\omega}) = \frac{1}{\underline{c}_{\mathrm{t}_\circ,0}(\boldsymbol{\omega})}$$

leads to a similar structure of $\underline{\boldsymbol{c}}_{\mathrm{t}_\circ}$ like $\underline{\boldsymbol{c}}_\mathrm{t}$ as in (3.103). Hence, the resulting system in CCF is given by

$$\left.\begin{aligned} \forall t \in \mathbb{T}_i: \quad \tfrac{\mathrm{d}}{\mathrm{d}t}\underline{\boldsymbol{x}}_\circ &= \underline{\boldsymbol{J}}_\circ(\boldsymbol{\omega})\underline{\boldsymbol{x}}_\circ, \quad \underline{\boldsymbol{x}}_\circ(t_i) = \underline{\boldsymbol{x}}_{\circ,t_i} = \boldsymbol{T}_\circ(\boldsymbol{\omega})\boldsymbol{x}_{\circ,t_i} \\ y &= \boldsymbol{c}_\circ^\top\boldsymbol{x}_\circ = \underbrace{\boldsymbol{c}_\circ^\top\boldsymbol{T}_\circ^{-1}(\boldsymbol{\omega})}_{=:\,\underline{\boldsymbol{c}}_{\mathrm{t}_\circ}^\top(\boldsymbol{\omega})}\underline{\boldsymbol{x}}_\circ \end{aligned}\right\} \tag{3.112}$$

where

$$\left.\begin{aligned} \underline{\boldsymbol{J}}_\circ(\underline{\boldsymbol{\theta}}) &= \begin{bmatrix} 0 & 1 & 0 & 0 & 0 & \cdots & 0 & 0 \\ 0 & 0 & 1 & 0 & 0 & \cdots & 0 & 0 \\ \vdots & \vdots & \vdots & \vdots & \vdots & \ddots & \vdots & \vdots \\ 0 & 0 & 0 & 0 & 0 & \cdots & 0 & 1 \\ 0 & -\underline{\theta}_{n_\infty} & 0 & -\underline{\theta}_{n_\infty-1} & 0 & \cdots & -\underline{\theta}_1 & 0 \end{bmatrix} \quad \text{and} \\ \underline{\boldsymbol{c}}_{\mathrm{t}_\circ}(\boldsymbol{\omega}) &= \begin{pmatrix} \underline{c}_{\mathrm{t}_\circ,0}(\boldsymbol{\omega}) & \underline{c}^\alpha_{\mathrm{t}_\circ,1}(\boldsymbol{\omega}) & \underline{c}^\beta_{\mathrm{t}_\circ,1}(\boldsymbol{\omega}) & \cdots & \underline{c}^\alpha_{\mathrm{t}_\circ,n_\infty}(\boldsymbol{\omega}) & \underline{c}^\beta_{\mathrm{t}_\circ,n_\infty}(\boldsymbol{\omega}) \end{pmatrix}^\top. \end{aligned}\right\} \tag{3.113}$$

The frequencies are collected in the transformed angular frequency vector $\underline{\boldsymbol{\theta}}$ as in (3.105). Thus, the matrix $\underline{\boldsymbol{J}}_\circ$ can be decomposed into

$$\underline{\boldsymbol{J}}_\circ(\underline{\boldsymbol{\theta}}) = \begin{bmatrix} 0 & 1 & \cdots & 0 & 0 \\ \vdots & \vdots & \ddots & \vdots & \vdots \\ 0 & 0 & \cdots & 0 & 1 \\ 0 & 0 & \cdots & 0 & 0 \end{bmatrix} - \underbrace{\begin{pmatrix} 0 \\ \boldsymbol{b} \end{pmatrix}}_{=:\,\underline{\boldsymbol{b}}_\circ \in \mathbb{R}^{2n_\infty+1}} \underline{\boldsymbol{\theta}}^\top \underbrace{\begin{bmatrix} \boldsymbol{0}_n & \underline{\boldsymbol{\Sigma}} \end{bmatrix}}_{=:\,\underline{\boldsymbol{\Sigma}}_\circ \in \mathbb{R}^{n_\infty \times (2n_\infty+1)}}. \tag{3.114}$$

This completes the description of the transformation of (3.8) into CCF.

3.4.2 Observability

Before the observer construction can be done, at first, the observability must be clarified again since this characteristic might change with state dependent similarity transformations.

Proposition 3.4.1 (Observability of transformed generation systems (3.101) and (3.112)). *Let $\underline{\boldsymbol{J}}_{\mathrm{x}}$, $\underline{\boldsymbol{c}}_{\mathrm{x}}$ be as in (3.101) or (3.112), resp., and $\boldsymbol{T}_{\mathrm{x}}$ as in (3.98) or (3.108), resp. Further, let $v = 2n_\infty - 1$ if no offset is considered and $v = 2n_\infty$ otherwise. Then, if and only if $\omega_1 \neq 0$, $\mathbb{H}_\infty \subseteq \mathbb{R}\setminus\{0\}$ where for all $\nu_i, \nu_j \in \mathbb{H}_\infty$, $i \neq j$, it holds that $|\nu_i| \neq |\nu_j|$ and $\det(\boldsymbol{T}_{\mathrm{x}}) \neq 0$, the systems $(\underline{\boldsymbol{c}}_{\mathrm{t}}^\top, \underline{\boldsymbol{J}})$ and $(\underline{\boldsymbol{c}}_{\mathrm{t}_\circ}^\top, \underline{\boldsymbol{J}}_\circ)$ are observable.*

Proof. According to [574, Sec. 2.3.1], investigate

$$\underline{\boldsymbol{O}}_{\mathrm{x}}(\boldsymbol{\omega}) := \begin{bmatrix} \underline{\boldsymbol{c}}_{\mathrm{x}}^\top(\underline{\boldsymbol{\theta}}) \\ \vdots \\ \underline{\boldsymbol{c}}_{\mathrm{x}}^\top(\underline{\boldsymbol{\theta}})\underline{\boldsymbol{J}}_{\mathrm{x}}^{v}(\underline{\boldsymbol{\theta}}) \end{bmatrix} \overset{(3.101)}{=} \begin{bmatrix} \boldsymbol{c}_{\mathrm{x}}^\top \boldsymbol{T}_{\mathrm{x}}^{-1}(\boldsymbol{\omega}) \\ \vdots \\ \boldsymbol{c}_{\mathrm{x}}^\top \boldsymbol{J}_{\mathrm{x}}^{v}(\boldsymbol{\omega})\boldsymbol{T}_{\mathrm{x}}^{-1}(\boldsymbol{\omega}) \end{bmatrix} \overset{(3.64)}{=} \boldsymbol{O}_{\mathrm{x}}(\boldsymbol{\omega})\boldsymbol{T}_{\mathrm{x}}^{-1}(\boldsymbol{\omega}) \tag{3.115}$$

which must have full rank. This holds if (i) $\boldsymbol{O}_{\mathrm{x}}$ has full rank (which was stated in Proposition 3.3.1) and if (ii) the transformation matrix $\boldsymbol{T}_{\mathrm{x}}$ is invertible. Hence, this shows the observability of the pairs $(\underline{\boldsymbol{c}}_{\mathrm{t}}^\top, \underline{\boldsymbol{J}})$ and $(\underline{\boldsymbol{c}}_{\mathrm{t}_\circ}^\top, \underline{\boldsymbol{J}}_\circ)$ and completes the proof. □

3.4.3 Observer construction: The parallelized tSOGIs in transformed frame and the parallelized tSOGIs with offset in transformed frame

The next step, similar to Section 3.3.2, is the construction of a LUENBERGER-based observer. However, as in Sections 3.2.2 and 3.3.2, not the whole systems (3.101) and (3.112) with $\mathbb{H}_\infty$ can be observed. Instead, a reduced subsystem must be used. But, unlike the (e)sFAO, the mFAO, and the mFAO$_\circ$, the reduced set of harmonic numbers is not fixed to some selected values, but is estimated by the frequency adaptive observer and denoted as $\widehat{\mathbb{H}}_n$. However, its cardinality must be set before observer construction and is denoted by $n := |\widehat{\mathbb{H}}_n|$. This cardinality is identical to the system order. In the following, the observer for system (3.101) is constructed in Section 3.4.3.1 and the observer for (3.112) in Section 3.4.3.2.

3.4.3.1 The parallelized tSOGIs in transformed frame

A direct construction of the observer yields, where the subscript "t" means "transformation-based",

$$\forall t \in \mathbb{T}_i\colon \quad \left.\begin{aligned} \tfrac{\mathrm{d}}{\mathrm{d}t}\widehat{\underline{\boldsymbol{x}}}_{\mathrm{t}} &= \overbrace{\left(\underline{\boldsymbol{J}}(\widehat{\underline{\boldsymbol{\theta}}}_{\mathrm{t}}) - \underline{\boldsymbol{l}}_{\mathrm{t}}(\underline{\boldsymbol{\theta}})\underline{\boldsymbol{c}}_{\mathrm{t}}^\top(\underline{\boldsymbol{\theta}})\right)}^{=:\widetilde{\underline{\boldsymbol{A}}}_{\mathrm{t}}(\underline{\boldsymbol{\theta}},\widehat{\underline{\boldsymbol{\theta}}}_{\mathrm{t}})\in\mathbb{R}^{2n\times 2n}}\widehat{\underline{\boldsymbol{x}}}_{\mathrm{t}} + \underline{\boldsymbol{l}}_{\mathrm{t}}(\underline{\boldsymbol{\theta}})y, \quad \widehat{\underline{\boldsymbol{x}}}_{\mathrm{t}}(t_i) = \widehat{\underline{\boldsymbol{x}}}_{\mathrm{t},t_i} \\ \widehat{\underline{y}}_{\mathrm{t}} &= \underline{\boldsymbol{c}}_{\mathrm{t}}^\top(\underline{\boldsymbol{\theta}})\widehat{\underline{\boldsymbol{x}}}_{\mathrm{t}} \end{aligned}\right\} \tag{3.116}$$

with the state vector $\widehat{\underline{\boldsymbol{x}}}_{\mathrm{t}} := (\widehat{\underline{x}}_{\mathrm{t},1}^{\alpha}, \widehat{\underline{x}}_{\mathrm{t},1}^{\beta}, \cdots, \widehat{\underline{x}}_{\mathrm{t},n}^{\alpha}, \widehat{\underline{x}}_{\mathrm{t},n}^{\beta})^\top$. Since this system already contains the maximal amount of degrees of freedom (collected in $\underline{\boldsymbol{c}}_{\mathrm{t}}$), the observer gain is not required to allow for any further ones and thus can be selected to define system characteristics. As will be discussed in Sections 3.4.4 and 3.4.5, it is advantageous to choose $\underline{\boldsymbol{l}}_{\mathrm{t}}$ as proposed in [548]:

$$\underline{\boldsymbol{l}}_{\mathrm{t}}(\underline{\boldsymbol{\theta}}) := \begin{pmatrix} 0 & 0 & \cdots & 0 & 0 & \frac{1}{\underline{c}_{\mathrm{t},n}^{\beta}(\underline{\boldsymbol{\theta}})} & 1 \end{pmatrix}^\top \in \mathbb{R}^{2n}. \tag{3.117}$$

The block diagram of the so-called parallelized *transformation-based Second Order Generalized Integrators* (tSOGI) in transformed frame is illustrated in Figure 3.25[18].

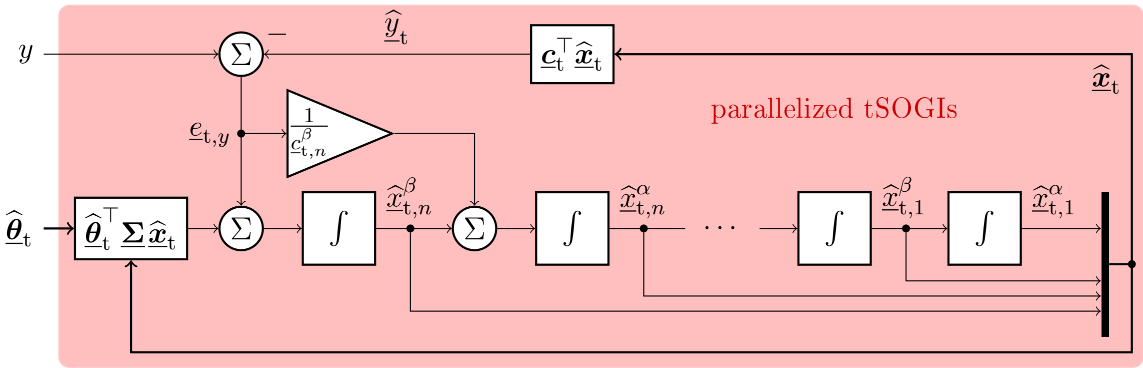

Figure 3.25: *Block diagram of the parallelized tSOGIs in transformed frame.*

3.4.3.2 The parallelized tSOGIs with offset in transformed frame

For the parallelized *transformation-based Second Order Generalized Integrators with offset* (tSOGI$_\circ$) in transformed frame, the observer equations are obtained as follows

$$\left.\begin{aligned}\forall t\in\mathbb{T}_i:\qquad \tfrac{\mathrm{d}}{\mathrm{d}t}\widehat{\underline{\boldsymbol{x}}}_{\mathrm{t}_\circ} &= \overbrace{\Big(\underline{\boldsymbol{J}}_{\circ}(\widehat{\underline{\boldsymbol{\theta}}}_{\mathrm{t}_\circ})-\underline{\boldsymbol{l}}_{\mathrm{t}_\circ}(\underline{\boldsymbol{\theta}})\underline{\boldsymbol{c}}_{\mathrm{t}_\circ}^{\top}(\underline{\boldsymbol{\theta}})\Big)}^{=:\,\widetilde{\underline{\boldsymbol{A}}}_{\mathrm{t}_\circ}(\underline{\boldsymbol{\theta}},\widehat{\underline{\boldsymbol{\theta}}}_{\mathrm{t}_\circ})\,\in\,\mathbb{R}^{2n+1\times 2n+1}}\widehat{\underline{\boldsymbol{x}}}_{\mathrm{t}_\circ}+\underline{\boldsymbol{l}}_{\mathrm{t}_\circ}(\underline{\boldsymbol{\theta}})y,\quad \widehat{\underline{\boldsymbol{x}}}_{\mathrm{t}_\circ}(t_i)=\widehat{\underline{\boldsymbol{x}}}_{\mathrm{t}_\circ,t_i}\\ \widehat{\underline{y}}_{\mathrm{t}_\circ} &= \underline{\boldsymbol{c}}_{\mathrm{t}_\circ}^{\top}(\underline{\boldsymbol{\theta}})\widehat{\underline{\boldsymbol{x}}}_{\mathrm{t}_\circ}\end{aligned}\right\}\tag{3.118}$$

with

$$\begin{aligned}\widehat{\underline{\boldsymbol{x}}}_{\mathrm{t}_\circ} &:= \left(\widehat{\underline{x}}_{\mathrm{t}_\circ,0},\,\widehat{\underline{x}}^{\alpha}_{\mathrm{t}_\circ,1},\,\widehat{\underline{x}}^{\beta}_{\mathrm{t}_\circ,1},\,\cdots,\,\widehat{\underline{x}}^{\alpha}_{\mathrm{t}_\circ,n},\,\widehat{\underline{x}}^{\beta}_{\mathrm{t}_\circ,n}\right)^{\top}\in\mathbb{R}^{2n+1}\\ \text{and}\quad \underline{\boldsymbol{l}}_{\mathrm{t}_\circ}(\underline{\boldsymbol{\theta}}) &:= \Big(0,\,0,\,\cdots,\,0,\,0,\,\tfrac{1}{\underline{c}^{\beta}_{\mathrm{t}_\circ,n}(\underline{\boldsymbol{\theta}})},\,1\Big)^{\top}\in\mathbb{R}^{2n+1}.\end{aligned}\tag{3.119}$$

The block diagram for the parallelized tSOGI$_\circ$s in transformed frame is similar to that in Figure 3.25.

3.4.4 Pole placement for the parallelized tSOGIs in transformed frame and the parallelized tSOGIs with offset in transformed frame

With the observer equations known, the gains $\underline{c}^{\alpha}_{\mathrm{t},i}$ and $\underline{c}^{\beta}_{\mathrm{t},i}$ as well as $\underline{c}_{\mathrm{t}_\circ,0}$, $\underline{c}^{\alpha}_{\mathrm{t}_\circ,i}$ and $\underline{c}^{\beta}_{\mathrm{t}_\circ,i}$, $i\in\{1,\ldots,n\}$ must be selected for the sake of the matrices $\widetilde{\underline{\boldsymbol{A}}}_{\mathrm{t}}$ and $\widetilde{\underline{\boldsymbol{A}}}_{\mathrm{t}_\circ}$ being Hurwitz matrices. Therefore, pole placement is used which requires the system matrices' characteristic polynomials. Note that if a matrix is in CCF, the characteristic polynomial can be obtained directly from the system matrix' last row [582, Sec. 6.1.2]. By an appropriate choice of the observer gain vectors $\underline{\boldsymbol{l}}_{\mathrm{t}}$ and $\underline{\boldsymbol{l}}_{\mathrm{t}_\circ}$, this structure can be achieved. In fact, that is why the observer gain vectors $\underline{\boldsymbol{l}}_{\mathrm{t}}$ and $\underline{\boldsymbol{l}}_{\mathrm{t}_\circ}$ were designed as in Section 3.4.3. For example, the system matrix for the tSOGI in transformed

[18] Although the parallelized tSOGIs in the transformed frame do not have a parallel structure as shown, for example, by the parallelized mSOGIs in Figure 3.14, they are called such for consistency. Their transfer functions and the respective amplitude and phase responses are neglected since they are not needed.

frame is given by

$$\underline{\widetilde{\boldsymbol{A}}}_{\mathrm{t}}(\underline{\boldsymbol{\theta}}, \underline{\widehat{\boldsymbol{\theta}}}_{\mathrm{t}}) = \begin{bmatrix} 0 & 1 & \cdots & 0 & 0 \\ 0 & 0 & \cdots & 0 & 0 \\ \vdots & \vdots & \ddots & \vdots & \vdots \\ 0 & 0 & \cdots & 1 & 0 \\ -\frac{\underline{c}^{\alpha}_{\mathrm{t},1}(\underline{\boldsymbol{\theta}})}{\underline{c}^{\beta}_{\mathrm{t},n}(\underline{\boldsymbol{\theta}})} & -\frac{\underline{c}^{\beta}_{\mathrm{t},1}(\underline{\boldsymbol{\theta}})}{\underline{c}^{\beta}_{\mathrm{t},n}(\underline{\boldsymbol{\theta}})} & \cdots & -\frac{\underline{c}^{\alpha}_{\mathrm{t},n}(\underline{\boldsymbol{\theta}})}{\underline{c}^{\beta}_{\mathrm{t},n}(\underline{\boldsymbol{\theta}})} & 0 \\ -\underline{\widehat{\theta}}_{\mathrm{t},n} - \underline{c}^{\alpha}_{\mathrm{t},1}(\underline{\boldsymbol{\theta}}) & -\underline{c}^{\beta}_{\mathrm{t},1}(\underline{\boldsymbol{\theta}}) & \cdots & -\underline{\widehat{\theta}}_{\mathrm{t},1} - \underline{c}^{\alpha}_{\mathrm{t},n}(\underline{\boldsymbol{\theta}}) & -\underline{c}^{\beta}_{\mathrm{t},n}(\underline{\boldsymbol{\theta}}) \end{bmatrix}$$

whose north-western sub matrix is again in CCF. According to [582, Sec. 6.1], its characteristic polynomial and the one for $\underline{\widetilde{\boldsymbol{A}}}_{\mathrm{t}_\circ}$ can be collected as

$$\left.\begin{aligned} \chi_{\underline{\widetilde{\boldsymbol{A}}}_{\mathrm{t}}}(s,\underline{\boldsymbol{\theta}}) &= \left(s + \underline{c}^{\beta}_{\mathrm{t},n}(\underline{\boldsymbol{\theta}})\right) \overbrace{\left(\frac{\underline{c}^{\alpha}_{\mathrm{t},1}(\underline{\boldsymbol{\theta}})}{\underline{c}^{\beta}_{\mathrm{t},n}(\underline{\boldsymbol{\theta}})} + \frac{\underline{c}^{\beta}_{\mathrm{t},1}(\underline{\boldsymbol{\theta}})}{\underline{c}^{\beta}_{\mathrm{t},n}(\underline{\boldsymbol{\theta}})} s + \cdots + \frac{\underline{c}^{\alpha}_{\mathrm{t},n}(\underline{\boldsymbol{\theta}})}{\underline{c}^{\beta}_{\mathrm{t},n}(\underline{\boldsymbol{\theta}})} s^{2n-2} + s^{2n-1}\right)}^{=:\chi_{\underline{\widetilde{\boldsymbol{A}}}_{\mathrm{t}},\mathrm{red}}(s,\underline{\boldsymbol{\theta}})} \\ \chi_{\underline{\widetilde{\boldsymbol{A}}}_{\mathrm{t}_\circ}}(s,\underline{\boldsymbol{\theta}}) &= \left(s + \underline{c}^{\beta}_{\mathrm{t}_\circ,n}(\underline{\boldsymbol{\theta}})\right) \underbrace{\left(\frac{\underline{c}_{\mathrm{t}_\circ,0}(\underline{\boldsymbol{\theta}})}{\underline{c}^{\beta}_{\mathrm{t}_\circ,n}(\underline{\boldsymbol{\theta}})} + \frac{\underline{c}^{\alpha}_{\mathrm{t}_\circ,1}(\underline{\boldsymbol{\theta}})}{\underline{c}^{\beta}_{\mathrm{t}_\circ,n}(\underline{\boldsymbol{\theta}})} s + \cdots + \frac{\underline{c}^{\alpha}_{\mathrm{t}_\circ,n}(\underline{\boldsymbol{\theta}})}{\underline{c}^{\beta}_{\mathrm{t}_\circ,n}(\underline{\boldsymbol{\theta}})} s^{2n-1} + s^{2n}\right)}_{=:\chi_{\underline{\widetilde{\boldsymbol{A}}}_{\mathrm{t}_\circ},\mathrm{red}}(s,\underline{\boldsymbol{\theta}})} . \end{aligned}\right\} \tag{3.120}$$

Note that these are independent of the estimated transformed angular frequencies $\underline{\widehat{\theta}}_{\mathrm{t},i}$ and $\underline{\widehat{\theta}}_{\mathrm{t}_\circ,i}$, respectively.

Proposition 3.4.2 (Pole placement for the parallelized tSOGIs in transformed frame and the parallelized tSOGI$_\circ$s in transformed frame)**.** *Let* $\mathrm{x} \in \{\mathrm{t}, \mathrm{t}_\circ\}$ *and let* $v = 2n-1$ *if* $\mathrm{x} = \mathrm{t}$ *or* $v = 2n$ *if* $\mathrm{x} = \mathrm{t}_\circ$*, respectively. Let* $\underline{\boldsymbol{J}}$ *be as in* (3.116) *or* $\underline{\boldsymbol{J}}_\circ$ *as in* (3.118) *(summarized as* $\underline{\boldsymbol{J}}_{\mathrm{x}}$*), respectively, and* $\underline{\boldsymbol{l}}_{\mathrm{x}}$ *as in* (3.117) *or* (3.119)*, respectively. Let*

$$\underline{\boldsymbol{\Lambda}}_{\mathrm{x}} := \begin{bmatrix} 0 & 0 & \cdots & 1 \\ \vdots & \vdots & \iddots & \vdots \\ 0 & 1 & \cdots & 0 \\ 1 & 0 & \cdots & 0 \end{bmatrix} = \underline{\boldsymbol{\Lambda}}_{\mathrm{x}}^\top = \underline{\boldsymbol{\Lambda}}_{\mathrm{x}}^{-1} \in \mathbb{R}^{v\times v}. \tag{3.121}$$

Further let $\underline{\lambda}_{\mathrm{x},i} \in \mathbb{C}$, $i \in \{1,\ldots,v+1\}$ *be the desired eigenvalues of* $\underline{\widetilde{\boldsymbol{A}}}_{\mathrm{x}} := \underline{\boldsymbol{J}}_{\mathrm{x}} - \underline{\boldsymbol{l}}_{\mathrm{x}}\underline{\boldsymbol{c}}_{\mathrm{x}}^\top$*. Let*

$$\underline{\boldsymbol{\lambda}}_{\mathrm{x,red}}(\underline{\boldsymbol{\theta}}) := \left(-\sum_{i=1}^{v} \underline{\lambda}_{\mathrm{x},i}(\underline{\boldsymbol{\theta}}) \quad \sum_{i=1}^{v} \underline{\lambda}_{\mathrm{x},i}(\underline{\boldsymbol{\theta}}) \sum_{j=i+1}^{v} \underline{\lambda}_{\mathrm{x},j}(\underline{\boldsymbol{\theta}}) \quad \cdots \quad (-1)^v \prod_{i=1}^{v} \underline{\lambda}_{\mathrm{x},i}(\underline{\boldsymbol{\theta}})\right)^\top$$

be the vector containing the coefficients of the reduced desired characteristic polynomial

$$\chi_{\underline{\widetilde{\boldsymbol{A}}}_{\mathrm{x}},\mathrm{red,des}}(s,\underline{\boldsymbol{\theta}}) := \prod_{i=1}^{v} \left(s - \underline{\lambda}_{\mathrm{x},i}(\underline{\boldsymbol{\theta}})\right).$$

If and only if the output vector $\underline{\boldsymbol{c}}_{\mathrm{x}}$ *is chosen as follows*

$$\underline{\boldsymbol{c}}_{\mathrm{x}}(\underline{\boldsymbol{\theta}}) = -\begin{bmatrix} \underline{\boldsymbol{\Lambda}}_{\mathrm{x}} & \boldsymbol{0}_v \\ \boldsymbol{0}_v^\top & 1 \end{bmatrix} \begin{pmatrix} \underline{\lambda}_{\mathrm{x},v+1}(\underline{\boldsymbol{\theta}})\underline{\boldsymbol{\lambda}}_{\mathrm{x,red}}(\underline{\boldsymbol{\theta}}) \\ \underline{\lambda}_{\mathrm{x},v+1}(\underline{\boldsymbol{\theta}}) \end{pmatrix}, \tag{3.122}$$

then the desired characteristic polynomial

$$\chi_{\underline{\widetilde{\boldsymbol{A}}}_{\mathrm{x}},\mathrm{des}}(s,\underline{\boldsymbol{\theta}}) := \big(s - \underline{\lambda}_{\mathrm{x},v+1}(\underline{\boldsymbol{\theta}})\big)\,\chi_{\underline{\widetilde{\boldsymbol{A}}}_{\mathrm{x}},\mathrm{red,des}}(s,\underline{\boldsymbol{\theta}})$$

and the actual characteristic polynomial given in (3.120) *have identical coefficients and, hence,* $\underline{\widetilde{\boldsymbol{A}}}_{\mathrm{x}}$ *is a matrix with eigenvalues* $\underline{\lambda}_{\mathrm{x},i}$.

Proof. Define the reduced output vector as follows

$$\underline{\boldsymbol{c}}_{\mathrm{x,red}}(\underline{\boldsymbol{\theta}}) := \begin{cases} \begin{pmatrix} \underline{c}^{\alpha}_{\mathrm{t},1}(\underline{\boldsymbol{\theta}}) & \underline{c}^{\beta}_{\mathrm{t},1}(\underline{\boldsymbol{\theta}}) & \dots & \underline{c}^{\alpha}_{\mathrm{t},n}(\underline{\boldsymbol{\theta}}) \end{pmatrix}^{\top} \in \mathbb{R}^{v}, & \mathrm{x} = \mathrm{t} \\ \begin{pmatrix} \underline{c}_{\mathrm{t}_\circ,0}(\underline{\boldsymbol{\theta}}) & \underline{c}^{\alpha}_{\mathrm{t}_\circ,1}(\underline{\boldsymbol{\theta}}) & \underline{c}^{\beta}_{\mathrm{t}_\circ,1}(\underline{\boldsymbol{\theta}}) & \dots & \underline{c}^{\alpha}_{\mathrm{t}_\circ,n}(\underline{\boldsymbol{\theta}}) \end{pmatrix}^{\top} \in \mathbb{R}^{v}, & \mathrm{x} = \mathrm{t}_\circ \end{cases}$$

and collect the coefficients of the reduced characteristic polynomial $\chi_{\underline{\widetilde{\boldsymbol{A}}}_{\mathrm{x}},\mathrm{red}}$ in (3.120) in

$$\boldsymbol{c}_{\underline{\widetilde{\boldsymbol{A}}}_{\mathrm{x}},\mathrm{red}}(\underline{\boldsymbol{\theta}}) := \begin{cases} \begin{pmatrix} \frac{\underline{c}^{\alpha}_{\mathrm{t},n}(\underline{\boldsymbol{\theta}})}{\underline{c}^{\beta}_{\mathrm{t},n}(\underline{\boldsymbol{\theta}})} & \dots & \frac{\underline{c}^{\beta}_{\mathrm{t},1}(\underline{\boldsymbol{\theta}})}{\underline{c}^{\beta}_{\mathrm{t},n}(\underline{\boldsymbol{\theta}})} & \frac{\underline{c}^{\alpha}_{\mathrm{t},1}(\underline{\boldsymbol{\theta}})}{\underline{c}^{\beta}_{\mathrm{t},n}(\underline{\boldsymbol{\theta}})} \end{pmatrix}^{\top} \in \mathbb{R}^{v}, & \mathrm{x} = \mathrm{t} \\ \begin{pmatrix} \frac{\underline{c}^{\alpha}_{\mathrm{t},n}(\underline{\boldsymbol{\theta}})}{\underline{c}^{\beta}_{\mathrm{t},n}(\underline{\boldsymbol{\theta}})} & \dots & \frac{\underline{c}^{\beta}_{\mathrm{t},1}(\underline{\boldsymbol{\theta}})}{\underline{c}^{\beta}_{\mathrm{t},n}(\underline{\boldsymbol{\theta}})} & \frac{\underline{c}^{\alpha}_{\mathrm{t},1}(\underline{\boldsymbol{\theta}})}{\underline{c}^{\beta}_{\mathrm{t},n}(\underline{\boldsymbol{\theta}})} & \frac{\underline{c}_{\mathrm{t},0}(\underline{\boldsymbol{\theta}})}{\underline{c}^{\beta}_{\mathrm{t},n}(\underline{\boldsymbol{\theta}})} \end{pmatrix}^{\top} \in \mathbb{R}^{v}, & \mathrm{x} = \mathrm{t}_\circ. \end{cases} \tag{3.123}$$

Observe that the relation between $\underline{\boldsymbol{c}}_{\mathrm{x,red}}$ and $\boldsymbol{c}_{\underline{\widetilde{\boldsymbol{A}}}_{\mathrm{x}},\mathrm{red}}$ is given by

$$\boldsymbol{c}_{\underline{\widetilde{\boldsymbol{A}}}_{\mathrm{x}},\mathrm{red}}(\underline{\boldsymbol{\theta}}) = \frac{1}{\underline{c}^{\beta}_{\mathrm{x},n}(\underline{\boldsymbol{\theta}})}\boldsymbol{\Lambda}_{\mathrm{x}}\underline{\boldsymbol{c}}_{\mathrm{x,red}}(\underline{\boldsymbol{\theta}}). \tag{3.124}$$

In view of the characteristic polynomial $\chi_{\underline{\widetilde{\boldsymbol{A}}}_{\mathrm{x}}}$ as given in (3.120), one eigenvalue can be assigned directly as

$$\underline{c}^{\beta}_{\mathrm{x},n}(\underline{\boldsymbol{\theta}}) = -\underline{\lambda}_{\mathrm{x},v+1}(\underline{\boldsymbol{\theta}}). \tag{3.125}$$

The other elements of $\underline{\boldsymbol{c}}_{\mathrm{x}}$, collected in $\underline{\boldsymbol{c}}_{\mathrm{x,red}}$, follow by a comparison of $\underline{\boldsymbol{\lambda}}_{\mathrm{x,red}}$ and $\boldsymbol{c}_{\underline{\widetilde{\boldsymbol{A}}}_{\mathrm{x}},\mathrm{red}}$ as

$$\begin{aligned} \underline{\boldsymbol{\lambda}}_{\mathrm{x,red}}(\underline{\boldsymbol{\theta}}) \overset{!}{=} \boldsymbol{c}_{\underline{\widetilde{\boldsymbol{A}}}_{\mathrm{x}},\mathrm{red}}(\underline{\boldsymbol{\theta}}) &\overset{(3.124)}{=} \frac{1}{\underline{c}^{\beta}_{\mathrm{x},n}(\underline{\boldsymbol{\theta}})}\boldsymbol{\Lambda}_{\mathrm{x}}\underline{\boldsymbol{c}}_{\mathrm{x,red}}(\underline{\boldsymbol{\theta}}) \\ \implies \quad \underline{\boldsymbol{c}}_{\mathrm{x,red}}(\underline{\boldsymbol{\theta}}) &\overset{(3.121)}{=} \underline{c}^{\beta}_{\mathrm{x},n}(\underline{\boldsymbol{\theta}})\boldsymbol{\Lambda}_{\mathrm{x}}\underline{\boldsymbol{\lambda}}_{\mathrm{x,red}}(\underline{\boldsymbol{\theta}}) \overset{(3.125)}{=} -\underline{\lambda}_{\mathrm{x},v+1}(\underline{\boldsymbol{\theta}})\boldsymbol{\Lambda}_{\mathrm{x}}\underline{\boldsymbol{\lambda}}_{\mathrm{x,red}}(\underline{\boldsymbol{\theta}}). \end{aligned} \tag{3.126}$$

Hence, the total output vector is given by

$$\underline{\boldsymbol{c}}_{\mathrm{x}}(\underline{\boldsymbol{\theta}}) = \begin{pmatrix} \underline{\boldsymbol{c}}_{\mathrm{x,red}}(\underline{\boldsymbol{\theta}}) \\ \underline{c}^{\beta}_{\mathrm{x},n}(\underline{\boldsymbol{\theta}}) \end{pmatrix} \overset{(3.125),(3.126)}{=} \begin{pmatrix} -\underline{\lambda}_{\mathrm{x},v+1}(\underline{\boldsymbol{\theta}})\boldsymbol{\Lambda}_{\mathrm{x}}\underline{\boldsymbol{\lambda}}_{\mathrm{x,red}}(\underline{\boldsymbol{\theta}}) \\ -\underline{\lambda}_{\mathrm{x},v+1}(\underline{\boldsymbol{\theta}}) \end{pmatrix} = -\begin{bmatrix} \boldsymbol{\Lambda}_{\mathrm{x}} & \boldsymbol{0}_v \\ \boldsymbol{0}_v^{\top} & 1 \end{bmatrix} \begin{pmatrix} \underline{\lambda}_{\mathrm{x},v+1}(\underline{\boldsymbol{\theta}})\underline{\boldsymbol{\lambda}}_{\mathrm{x,red}}(\underline{\boldsymbol{\theta}}) \\ \underline{\lambda}_{\mathrm{x},v+1}(\underline{\boldsymbol{\theta}}) \end{pmatrix}.$$

This completes the proof. □

Remark 3.4.3. *Let* $\mathrm{x} \in \{\mathrm{t}, \mathrm{t}_\circ\}$. *For all eigenvalues* $\underline{\lambda}_{\mathrm{x},i} \in \mathbb{C}_{NHP}$, $i \in \{1, \dots, v\}$, *the matrix* $\underline{\widetilde{\boldsymbol{A}}}_{\mathrm{x}}$ *is a Hurwitz matrix. Moreover, note that if for any set it holds that* $p := \big|\{\underline{\lambda}_{\mathrm{x},1}, \dots, \underline{\lambda}_{\mathrm{x},v}\}\big| > 1$ *(p different eigenvalues), the resulting matrix* $\underline{\widetilde{\boldsymbol{A}}}_{\mathrm{x}}$ *is not unique. Instead, there exist p matrices* $\underline{\widetilde{\boldsymbol{A}}}_{\mathrm{x}}$ *with eigenvalues* $\underline{\lambda}_{\mathrm{x},i}$ *dependent on the choice for* $\underline{c}^{\beta}_{\mathrm{x},n}$ *which is illustrated in the following example.*
Consider $\mathrm{x} = \mathrm{t}_\circ$, $n = 1$ *and choose the eigenvalues as* $\underline{\lambda}_{\mathrm{t}_\circ,1} = -a$, $\underline{\lambda}_{\mathrm{t}_\circ,2} = -b + \jmath c$ *and* $\underline{\lambda}_{\mathrm{t}_\circ,3} = -b - \jmath c$ *where* $a, b \in \mathbb{R}_{>0}$ *and* $c \in \mathbb{R} \setminus \{0\}$. *Further consider* $\underline{\widehat{\theta}}_{\mathrm{t}_\circ,1} \in \mathbb{R}$. *The possible output vectors*

$\underline{\boldsymbol{c}}_{\mathrm{t}_\circ}$ *follow as*

$$\underline{\boldsymbol{c}}_{\mathrm{t}} \in \left\{ \begin{pmatrix} a(b^2+c^2) \\ 2ab \\ a \end{pmatrix}, \begin{pmatrix} a(b^2+c^2) \\ ab+b^2+c^2-\jmath ac \\ b-\jmath c \end{pmatrix}, \begin{pmatrix} a(b^2+c^2) \\ ab+b^2+c^2+\jmath ac \\ b+\jmath c \end{pmatrix} \right\}.$$

Those lead to system matrices

$$\widetilde{\underline{\boldsymbol{A}}}_{\mathrm{t}_\circ} \in \left\{ \begin{bmatrix} 0 & 1 & 0 \\ -\frac{a(b^2+c^2)}{a} & -\frac{2ab}{a} & 0 \\ -a(b^2+c^2) & -\widehat{\underline{\theta}}_{\mathrm{t}_\circ,1} - 2ab & -a \end{bmatrix}, \begin{bmatrix} 0 & 1 & 0 \\ -\frac{a(b^2+c^2)}{b-\jmath c} & -\frac{ab+b^2+c^2-\jmath ac}{b-\jmath c} & 0 \\ -a(b^2+c^2) & -\widehat{\underline{\theta}}_{\mathrm{t}_\circ,1} - ab - b^2 - c^2 + \jmath ac & -b+\jmath c \end{bmatrix}, \begin{bmatrix} 0 & 1 & 0 \\ -\frac{a(b^2+c^2)}{b+\jmath c} & -\frac{ab+b^2+c^2+\jmath ac}{b+\jmath c} & 0 \\ -a(b^2+c^2) & -\widehat{\underline{\theta}}_{\mathrm{t}_\circ,1} - ab - b^2 - c^2 - \jmath ac & -b-\jmath c \end{bmatrix} \right\}.$$

3.4.5 Stability proof and summary of the tFAO in transformed frame and the tFAO with offset in transformed frame

Although angular frequency adaption was not considered yet for the tSOGI in transformed frame as well as the tSOGI$_\circ$ in transformed frame, stability proofs for these systems are carried out. However, from these proofs, angular frequency adaption laws can be deduced. Therefore, summaries of the overall systems are given at the end of the section. In these summaries, evaluations of the respective systems using the test signals defined in (3.12) are not feasible, since this would imply a comparison of signals in α, β and transformed coordinates. But before the proofs can be formulated, some preliminary observations are required.
For the following observations, let be $\mathrm{x} \in \{\mathrm{t}, \mathrm{t}_\circ\}$ and $v = 2n-1$ if $\mathrm{x} = \mathrm{t}$ or $v = 2n$ if $\mathrm{x} = \mathrm{t}_\circ$. Define the transformed angular frequency error matrix as

$$\underline{\boldsymbol{E}}_{\mathrm{x},\omega}(\underline{\boldsymbol{\theta}}, \widehat{\underline{\boldsymbol{\theta}}}_{\mathrm{x}}) := \underline{\boldsymbol{J}}_{\mathrm{x}}(\underline{\boldsymbol{\theta}}) - \underline{\boldsymbol{J}}_{\mathrm{x}}(\widehat{\underline{\boldsymbol{\theta}}}_{\mathrm{x}}). \tag{3.127}$$

Note that it only consists of the transformed angular frequency errors defined by and collected in

$$\underline{\boldsymbol{e}}_{\mathrm{x},\omega} := \underline{\boldsymbol{\theta}} - \widehat{\underline{\boldsymbol{\theta}}}_{\mathrm{x}}, \tag{3.128}$$

i.e. $\underline{\boldsymbol{E}}_{\mathrm{x},\omega}$ can be rewritten as

$$\underline{\boldsymbol{E}}_{\mathrm{x},\omega}(\underline{\boldsymbol{\theta}}, \widehat{\underline{\boldsymbol{\theta}}}_{\mathrm{x}}) = -\underline{\boldsymbol{b}}_{\mathrm{x}} \underline{\boldsymbol{e}}_{\mathrm{x},\omega}^\top \boldsymbol{\Sigma}_{\mathrm{x}} \tag{3.129}$$

according to (3.106) or (3.114), respectively. Next, introduce the signal estimation error as

$$\underline{\boldsymbol{e}}_{\mathrm{x}} := \underline{\boldsymbol{x}}_{\mathrm{x}} - \widehat{\underline{\boldsymbol{x}}}_{\mathrm{x}}. \tag{3.130}$$

Its state space representation is given by

$$\begin{aligned} \forall t \in \mathbb{T}_i: \quad \tfrac{\mathrm{d}}{\mathrm{d}t}\underline{\boldsymbol{e}}_{\mathrm{x}} &\overset{(3.101),(3.116)}{=} \underline{\boldsymbol{J}}_{\mathrm{x}}(\underline{\boldsymbol{\theta}})\underline{\boldsymbol{x}}_{\mathrm{x}} - \left(\underline{\boldsymbol{J}}_{\mathrm{x}}(\widehat{\underline{\boldsymbol{\theta}}}_{\mathrm{x}}) - \underline{\boldsymbol{l}}_{\mathrm{x}}(\underline{\boldsymbol{\theta}})\underline{\boldsymbol{c}}_{\mathrm{x}}^\top(\underline{\boldsymbol{\theta}})\right)\widehat{\underline{\boldsymbol{x}}}_{\mathrm{x}} - \underline{\boldsymbol{l}}_{\mathrm{x}}(\underline{\boldsymbol{\theta}})\underline{\boldsymbol{c}}_{\mathrm{x}}^\top(\underline{\boldsymbol{\theta}})\underline{\boldsymbol{x}}_{\mathrm{x}} \\ &\overset{(3.127),(3.130)}{=} \underline{\boldsymbol{J}}_{\mathrm{x}}(\underline{\boldsymbol{\theta}})\underline{\boldsymbol{e}}_{\mathrm{x}} - \underline{\boldsymbol{l}}_{\mathrm{x}}(\underline{\boldsymbol{\theta}})\underline{\boldsymbol{c}}_{\mathrm{x}}^\top(\underline{\boldsymbol{\theta}})\underline{\boldsymbol{e}}_{\mathrm{x}} + \underline{\boldsymbol{E}}_{\mathrm{x},\omega}(\underline{\boldsymbol{\theta}}, \widehat{\underline{\boldsymbol{\theta}}}_{\mathrm{x}})\widehat{\underline{\boldsymbol{x}}}_{\mathrm{x}} \end{aligned}$$

$$\begin{aligned} & \overset{(3.106),(3.116)}{=} && \underline{\boldsymbol{A}}_{\mathrm{x}}(\underline{\boldsymbol{\theta}})\underline{\boldsymbol{e}}_{\mathrm{x}} - \underline{\boldsymbol{b}}_{\mathrm{x}}\underline{\boldsymbol{e}}_{\mathrm{x},\omega}^{\top}\underline{\boldsymbol{\Sigma}}_{\mathrm{x}}\underline{\widehat{\boldsymbol{x}}}_{\mathrm{x}}, \quad \underline{\boldsymbol{e}}_{\mathrm{x}}(t_i) = \underline{\boldsymbol{e}}_{\mathrm{x},t_i} && (3.131)\\ \underline{e}_{\mathrm{x},y} & = && \underline{\boldsymbol{c}}_{\mathrm{x}}^{\top}(\underline{\boldsymbol{\theta}})\underline{\boldsymbol{e}}_{\mathrm{x}} = y - \underline{\widehat{y}}_{\mathrm{x}}. && (3.132)\end{aligned}$$

Therein, the matrix

$$\underline{\boldsymbol{A}}_{\mathrm{x}}(\underline{\boldsymbol{\theta}}) := \underline{\boldsymbol{J}}_{\mathrm{x}}(\underline{\boldsymbol{\theta}}) - \underline{\boldsymbol{l}}_{\mathrm{x}}(\underline{\boldsymbol{\theta}})\underline{\boldsymbol{c}}_{\mathrm{x}}^{\top}(\underline{\boldsymbol{\theta}}) \tag{3.133}$$

denotes the nominal system matrix. It is $\underline{\widetilde{\boldsymbol{A}}}_{\mathrm{x}}$ as introduced in (3.116) and (3.118), resp., where for $i \in \{1, \ldots, n\}$ the estimated transformed angular frequencies $\underline{\widehat{\theta}}_{\mathrm{x},i}$ are replaced by the actual frequencies $\underline{\theta}_i$. For example, $\underline{\boldsymbol{A}}_{\mathrm{t}}$ is given by

$$\underline{\boldsymbol{A}}_{\mathrm{t}}(\underline{\boldsymbol{\theta}}) = \begin{bmatrix} 0 & 1 & \cdots & 0 & 0\\ \vdots & \vdots & \ddots & \vdots & \vdots\\ 0 & 0 & \cdots & 1 & 0\\ -\frac{\underline{c}_{\mathrm{t},1}^{\alpha}(\underline{\boldsymbol{\theta}})}{\underline{c}_{\mathrm{t},n}^{\beta}(\underline{\boldsymbol{\theta}})} & -\frac{\underline{c}_{\mathrm{t},1}^{\beta}(\underline{\boldsymbol{\theta}})}{\underline{c}_{\mathrm{t},n}^{\beta}(\underline{\boldsymbol{\theta}})} & \cdots & -\frac{\underline{c}_{\mathrm{t},n}^{\alpha}(\underline{\boldsymbol{\theta}})}{\underline{c}_{\mathrm{t},n}^{\beta}(\underline{\boldsymbol{\theta}})} & 0\\ -\underline{\theta}_n - \underline{c}_{\mathrm{t},1}^{\alpha}(\underline{\boldsymbol{\theta}}) & -\underline{c}_{\mathrm{t},1}^{\beta}(\underline{\boldsymbol{\theta}}) & \cdots & -\underline{\theta}_1 - \underline{c}_{\mathrm{t},n}^{\alpha}(\underline{\boldsymbol{\theta}}) & -\underline{c}_{\mathrm{t},n}^{\beta}(\underline{\boldsymbol{\theta}}) \end{bmatrix}.$$

In view of Fact 2.16, Equation (3.131) can be made *strictly positive real*. This is shown in the following.
Rewrite the matrix $\underline{\boldsymbol{A}}_{\mathrm{x}}$ in (3.133) as $\underline{\boldsymbol{A}}_{\mathrm{x}} =: \left[\begin{smallmatrix} \boldsymbol{C} & \boldsymbol{0}_v \\ \boldsymbol{v}^{\top} & -\underline{c}_{\mathrm{x},n}^{\beta}\end{smallmatrix}\right]$. The error transfer function with input

$$\underline{z}_{\mathrm{x}} := -\underline{\boldsymbol{e}}_{\mathrm{x},\omega}^{\top}\underline{\boldsymbol{\Sigma}}_{\mathrm{x}}\underline{\widehat{\boldsymbol{x}}}_{\mathrm{x}}$$

is defined by

$$\begin{aligned} \mathcal{E}_{\mathrm{t},y}(s,\underline{\boldsymbol{\theta}}) & := && \frac{\underline{e}_{\mathrm{t},y}(s)}{\underline{z}_{\mathrm{t}}(s)} = \underline{\boldsymbol{c}}_{\mathrm{t}}^{\top}(\underline{\boldsymbol{\theta}})\left(s\boldsymbol{I}_{2n} - \underline{\boldsymbol{A}}_{\mathrm{t}}(\underline{\boldsymbol{\theta}})\right)^{-1}\underline{\boldsymbol{b}}\\ & \overset{(3.103),(3.106)}{=} && \begin{pmatrix} \underline{c}_{\mathrm{t},1}^{\alpha}(\underline{\boldsymbol{\theta}}) & \cdots & \underline{c}_{\mathrm{t},n}^{\beta}(\underline{\boldsymbol{\theta}})\end{pmatrix} \begin{bmatrix} (s\boldsymbol{I}_{2n-1} - \boldsymbol{C}(\underline{\boldsymbol{\theta}}))^{-1} & \boldsymbol{0}_{2n}\\ \frac{\boldsymbol{v}^{\top}(\underline{\boldsymbol{\theta}})(s\boldsymbol{I}_{2n-1}-\boldsymbol{C}(\underline{\boldsymbol{\theta}}))^{-1}}{s+\underline{c}_{\mathrm{t},n}^{\beta}(\underline{\boldsymbol{\theta}})} & \frac{1}{s+\underline{c}_{\mathrm{t},n}^{\beta}(\underline{\boldsymbol{\theta}})}\end{bmatrix}\begin{pmatrix}0\\ \vdots\\ 0\\ 1\end{pmatrix}\\ & = && \frac{\underline{c}_{\mathrm{t},n}^{\beta}(\underline{\boldsymbol{\theta}})}{s+\underline{c}_{\mathrm{t},n}^{\beta}(\underline{\boldsymbol{\theta}})} \qquad (3.134)\end{aligned}$$

if $\mathrm{x} = \mathrm{t}$ or

$$\mathcal{E}_{\mathrm{t_o},y}(s,\underline{\boldsymbol{\theta}}) := \frac{\underline{e}_{\mathrm{t_o},y}(s)}{\underline{z}_{\mathrm{t_o}}(s)} = \frac{\underline{c}_{\mathrm{t_o},n}^{\beta}(\underline{\boldsymbol{\theta}})}{s+\underline{c}_{\mathrm{t_o},n}^{\beta}(\underline{\boldsymbol{\theta}})} \tag{3.135}$$

if $\mathrm{x} = \mathrm{t_o}$. It shall be tested for strict positive realness. It must fulfill the assertions of Fact 2.16: If and only if $\underline{c}_{\mathrm{x},n}^{\beta} \in \mathbb{R}\setminus\{0\}$, $\mathcal{E}_{\mathrm{x},y}$ is a rational function with relative degree $\mathrm{rd}\left(\mathcal{E}_{\mathrm{x},y}\right) = 1$, $\mathcal{E}_{\mathrm{x},y}$ takes only real values for real s, and $\mathcal{E}_{\mathrm{x},y}$ is not identically zero for all s. Thus, checking the conditions for strict positive realness of Fact 2.16 shows that $\mathcal{E}_{\mathrm{x},y}$ is strictly positive real.

Remark 3.4.4. *The requirement $\underline{c}_{\mathrm{x},n}^{\beta} \in \mathbb{R}\setminus\{0\}$ influences the allowed range and assignment of the eigenvalues for pole placement described in Proposition 3.4.2, if the tSOGI in transformed frame is considered. Considering the tSOGI$_\mathrm{o}$ in transformed frame instead, this requirement does not influence the allowed range, since one eigenvalue must be real anyway (assuming a real-valued implementation). On the other hand, one of the real eigenvalues must be assigned to $\underline{c}_{\mathrm{t_o},n}^{\beta}$, see Remark 3.4.3.*

Next, the strict positive realness of (3.131) allows to invoke the Meyer-Kalman-Yakubovich-

Lemma 2.17

$$\underline{\boldsymbol{A}}_{\mathrm{x}}^{\top}(\boldsymbol{\theta})\underline{\boldsymbol{P}}_{\mathrm{x}}(\boldsymbol{\theta})+\underline{\boldsymbol{P}}_{\mathrm{x}}(\boldsymbol{\theta})\underline{\boldsymbol{A}}_{\mathrm{x}}(\boldsymbol{\theta}) = \underbrace{-\underline{\widetilde{\boldsymbol{q}}}_{\mathrm{x}}(\boldsymbol{\theta})\underline{\widetilde{\boldsymbol{q}}}_{\mathrm{x}}^{\top}(\boldsymbol{\theta}) - \underline{\widetilde{q}}_{\mathrm{x}}(\boldsymbol{\theta})\underline{\widetilde{\boldsymbol{Q}}}_{\mathrm{x}}(\boldsymbol{\theta})}_{=:-\underline{\boldsymbol{Q}}_{\mathrm{x}}(\boldsymbol{\theta})} \quad \text{and} \quad \underline{\boldsymbol{c}}_{\mathrm{x}}(\boldsymbol{\theta}) = \underline{\boldsymbol{P}}_{\mathrm{x}}(\boldsymbol{\theta})\underline{\boldsymbol{b}}_{\mathrm{x}} \tag{3.136}$$

where $\underline{\widetilde{\boldsymbol{Q}}}_{\mathrm{x}} = \underline{\widetilde{\boldsymbol{Q}}}_{\mathrm{x}}^{\top} > 0$ can be chosen arbitrarily. Note that the usual statement "for any given $\underline{\boldsymbol{Q}}_{\mathrm{x}} = \underline{\boldsymbol{Q}}_{\mathrm{x}}^{\top} > 0$" does *not* hold anymore if additionally $\underline{\boldsymbol{P}}_{\mathrm{x}}\underline{\boldsymbol{b}}_{\mathrm{x}} = \underline{\boldsymbol{c}}_{\mathrm{x}}$ must be fulfilled. More precisely, $\underline{\boldsymbol{Q}}_{\mathrm{x}}$ is restricted to a bounded set as shown in the following example.

Example 3.4.5. *Let* $\underline{\boldsymbol{J}} = \begin{bmatrix} 0 & 1 \\ -\underline{\theta} & 0 \end{bmatrix}$, $\underline{\boldsymbol{c}}_{\mathrm{t}} = \begin{pmatrix} \underline{c}_{\mathrm{t}}^{\alpha} \\ \underline{c}_{\mathrm{t}}^{\beta} \end{pmatrix}$, $\underline{\boldsymbol{l}}_{\mathrm{t}} = \begin{pmatrix} \frac{1}{\underline{c}_{\mathrm{t}}^{\beta}} \\ 1 \end{pmatrix}$, $\underline{\boldsymbol{b}} = \begin{pmatrix} 0 \\ 1 \end{pmatrix}$, *let* $\underline{\boldsymbol{A}}_{\mathrm{t}} = \underline{\boldsymbol{J}} - \underline{\boldsymbol{l}}_{\mathrm{t}}\underline{\boldsymbol{c}}_{\mathrm{t}}^{\top}$ *be Hurwitz and let* $\mathcal{E}_{\mathrm{t},y} = \underline{\boldsymbol{c}}_{\mathrm{t}}^{\top}\left(s\boldsymbol{I}_2 - \underline{\boldsymbol{A}}_{\mathrm{t}}\right)^{-1}\underline{\boldsymbol{b}}$ *be strictly positive real. Then,* $\underline{\boldsymbol{P}}_{\mathrm{t}}$ *can be determined as follows*

$$\underline{\boldsymbol{P}}_{\mathrm{t}} \overset{(3.136)}{=} \begin{bmatrix} p & \underline{c}_{\mathrm{t}}^{\alpha} \\ \underline{c}_{\mathrm{t}}^{\alpha} & \underline{c}_{\mathrm{t}}^{\beta} \end{bmatrix}, \quad p \in \mathbb{R}$$

which leads to a restricted set for $\underline{\boldsymbol{Q}}_{\mathrm{t}}$ *given by*

$$\underline{\boldsymbol{Q}}_{\mathrm{t}} \in \left\{ \boldsymbol{Q} \in \mathbb{R}^{2\times 2} \,\middle|\, \exists p \in \mathbb{R} : \boldsymbol{Q} = \begin{bmatrix} 2\frac{\underline{c}_{\mathrm{t}}^{\alpha}}{\underline{c}_{\mathrm{t}}^{\beta}}p + 2\underline{\theta}\underline{c}_{\mathrm{t}}^{\alpha} + 2(\underline{c}_{\mathrm{t}}^{\alpha})^2 & \frac{(\underline{c}_{\mathrm{t}}^{\alpha})^2}{\underline{c}_{\mathrm{t}}^{\beta}} + \underline{\theta}\underline{c}_{\mathrm{t}}^{\beta} + 2\underline{c}_{\mathrm{t}}^{\alpha}\underline{c}_{\mathrm{t}}^{\beta} \\ \frac{(\underline{c}_{\mathrm{t}}^{\alpha})^2}{\underline{c}_{\mathrm{t}}^{\beta}} + \underline{\theta}\underline{c}_{\mathrm{t}}^{\beta} + 2\underline{c}_{\mathrm{t}}^{\alpha}\underline{c}_{\mathrm{t}}^{\beta} & 2(\underline{c}_{\mathrm{t}}^{\beta})^2 \end{bmatrix} > 0 \right\}.$$

The eigenvalues of $\underline{\boldsymbol{Q}}_{\mathrm{t}}$*, needed for the estimation bounds in stability proofs (see e.g.* (3.56) *or* (3.61)*), are given by*

$$\begin{aligned} \lambda(\underline{\boldsymbol{Q}}_{\mathrm{t}}) = {} & \frac{\underline{c}_{\mathrm{t}}^{\alpha}}{\underline{c}_{\mathrm{t}}^{\beta}}p + \underline{\theta}\underline{c}_{\mathrm{t}}^{\alpha} + (\underline{c}_{\mathrm{t}}^{\alpha})^2 + (\underline{c}_{\mathrm{t}}^{\beta})^2 \\ & \pm \sqrt{\left(\frac{\underline{c}_{\mathrm{t}}^{\alpha}}{\underline{c}_{\mathrm{t}}^{\beta}}p + \underline{\theta}\underline{c}_{\mathrm{t}}^{\alpha} + (\underline{c}_{\mathrm{t}}^{\alpha})^2 - (\underline{c}_{\mathrm{t}}^{\beta})^2\right)^2 + \left(\frac{(\underline{c}_{\mathrm{t}}^{\alpha})^2}{\underline{c}_{\mathrm{t}}^{\beta}} + \underline{\theta}\underline{c}_{\mathrm{t}}^{\beta} + 2\underline{c}_{\mathrm{t}}^{\alpha}\underline{c}_{\mathrm{t}}^{\beta}\right)^2}. \end{aligned}$$

For the positive definiteness of $\underline{\boldsymbol{Q}}_{\mathrm{t}}$*, they are required to be positive. This implies*

$$p > \frac{\underline{c}_{\mathrm{t}}^{\beta}}{\underline{c}_{\mathrm{t}}^{\alpha}}\left(\left(\frac{(\underline{c}_{\mathrm{t}}^{\alpha})^2}{2(\underline{c}_{\mathrm{t}}^{\beta})^2} + \frac{\underline{\theta}}{2} + \underline{c}_{\mathrm{t}}^{\alpha}\right)^2 - \underline{\theta}\underline{c}_{\mathrm{t}}^{\alpha} - (\underline{c}_{\mathrm{t}}^{\alpha})^2\right)$$

which gives a lower bound for p*. Clearly, there does not exist an upper bound for* p*, but in view of*

$$\lim_{p\to\infty} \lambda_{\min}(\underline{\boldsymbol{Q}}_{\mathrm{t}}) \to 2(\underline{c}_{\mathrm{t}}^{\beta})^2$$

and since the eigenvalues are continuous functions of p *it is obvious that there exists a maximal* $\lambda_{\min}(\underline{\boldsymbol{Q}}_{\mathrm{t}})$*. Hence,* $\underline{\boldsymbol{Q}}_{\mathrm{t}}$ *cannot be chosen arbitrarily.*

This leads to the following assumption.

Assumption 3.4.6. *Let* $\mathrm{x} \in \{\mathrm{t}, \mathrm{t}_{\circ}\}$*. Let* $\underline{\boldsymbol{J}}_{\mathrm{x}}, \underline{\boldsymbol{b}}_{\mathrm{x}}$ *be as in* (3.106) *or* (3.114)*, respectively,* $\underline{\boldsymbol{c}}_{\mathrm{x}}$ *as in* (3.103) *or* (3.113)*, respectively and* $\underline{\boldsymbol{l}}_{\mathrm{x}}$ *as in* (3.117) *or* (3.119)*. Let* $\underline{\boldsymbol{A}}_{\mathrm{x}}$ *as in* (3.133) *be a Hurwitz matrix, let* $\mathcal{E}_{\mathrm{x},y}$ *be strictly positive real and let the norm of the transformed angular frequency error vector be bounded by* $\left\|\underline{\boldsymbol{e}}_{\mathrm{x},\omega}\right\| \le \underline{c}_{\mathrm{x},e,\omega} < \infty$*. Although the minimal eigenvalue of* $\underline{\boldsymbol{Q}}_{\mathrm{x}}$ *fulfilling* (3.136) *is limited to an upper bound as shown in Example 3.4.5, assume that it still satisfies the following inequality:*

$$\exists\, m \ge 1: \quad \lambda_{\min}(\underline{\boldsymbol{Q}}_{\mathrm{x}}(\boldsymbol{\theta})) - \tfrac{1}{m} - 2\underline{c}_{\mathrm{x},e,\omega}\left\|\underline{\boldsymbol{c}}_{\mathrm{x}}(\boldsymbol{\theta})\right\|\left\|\underline{\boldsymbol{\Sigma}}_{\mathrm{x}}\right\| \ge \underline{\epsilon}_{\mathrm{x},m} > 0. \tag{3.137}$$

Now, the stability proof can be formulated.

Theorem 3.4.7 (Bounded-input bounded-state/bounded-output stability of the dynamics of the tFAO and tFAO$_\circ$ in transformed frame)**.** *Let* $\mathrm{x} \in \{\mathrm{t}, \mathrm{t}_\circ\}$ *and* $v = 2n$ *if* $\mathrm{x} = \mathrm{t}$ *or* $v = 2n+1$ *if* $\mathrm{x} = \mathrm{t}_\circ$*. Consider an essentially bounded input signal, i.e.* $y \in \mathcal{L}^\infty(\mathbb{R}_{\geq 0}; \mathbb{R})$ *and assume that (i) the matrix* $\underline{\boldsymbol{A}}_\mathrm{x}$ *as in* (3.133) *is a Hurwitz matrix, (ii)* $\underline{c}^{\beta}_{\mathrm{x},n}$ *is a real scalar and (iii) angular frequency adaption is globally asymptotic stable such that* $\left\|\underline{\boldsymbol{e}}_{\mathrm{x},\omega}\right\| \leq \underline{c}_{\mathrm{x},e,\omega} < \infty$*. Then, the time-varying systems* (3.116) *and* (3.118) *are bounded-input bounded-state/bounded-output stable, i.e.*

$$\forall\, t \in \mathbb{T}_i\colon \quad \exists\, \underline{c}_\mathrm{x}, \widetilde{\underline{c}}_\mathrm{x} > 0\colon \quad \|\widehat{\underline{\boldsymbol{x}}}_\mathrm{x}\| \leq \underline{c}_\mathrm{x} \quad \textit{and} \quad \left|\widehat{\underline{y}}_\mathrm{x}\right| \leq \widetilde{\underline{c}}_\mathrm{x}.$$

Proof. Firstly, since $\underline{\boldsymbol{A}}_\mathrm{x}$ is a Hurwitz matrix and $\underline{c}^{\beta}_{\mathrm{x},n} \in \mathbb{R}$, equation (3.136) holds. Secondly, introduce the non-negative Lyapunov-like function

$$\underline{V}_{\mathrm{x},x}\colon \mathbb{R}^v \to \mathbb{R}_{\geq 0},\ \widehat{\underline{\boldsymbol{x}}}_\mathrm{x} \mapsto \underline{V}_{\mathrm{x},x}(\widehat{\underline{\boldsymbol{x}}}_\mathrm{x}, \underline{\boldsymbol{\theta}}) := \widehat{\underline{\boldsymbol{x}}}_\mathrm{x}^\top \underline{\boldsymbol{P}}_\mathrm{x}(\underline{\boldsymbol{\theta}})\widehat{\underline{\boldsymbol{x}}}_\mathrm{x}.$$

Although the right-hand side of (3.116) or (3.118) is locally Lipschitz continuous with bounded Lipschitz constant and bounded exogenous perturbation which implies a global solution of (3.116) or (3.118) on $\mathbb{R}_{\geq 0}$, it still might diverge as $t \to \infty$. The derivative of $\underline{V}_\mathrm{x}$ with respect to time along the solution of (3.116) or (3.118) is, for all $t \geq t_i$, given and upper bounded by

$$\begin{aligned}
\tfrac{\mathrm{d}}{\mathrm{d}t}\underline{V}_{\mathrm{x},x}(\widehat{\underline{\boldsymbol{x}}}_\mathrm{t}, \underline{\boldsymbol{\theta}}) \quad &= \quad \tfrac{\mathrm{d}}{\mathrm{d}t}\widehat{\underline{\boldsymbol{x}}}_\mathrm{x}^\top \underline{\boldsymbol{P}}_\mathrm{x}(\underline{\boldsymbol{\theta}})\widehat{\underline{\boldsymbol{x}}}_\mathrm{x} + \widehat{\underline{\boldsymbol{x}}}_\mathrm{x}^\top \underline{\boldsymbol{P}}_\mathrm{x}(\underline{\boldsymbol{\theta}})\tfrac{\mathrm{d}}{\mathrm{d}t}\widehat{\underline{\boldsymbol{x}}}_\mathrm{x} \\
&\overset{(3.116)}{=} \quad \left(\widehat{\underline{\boldsymbol{x}}}_\mathrm{x}^\top \widetilde{\underline{\boldsymbol{A}}}_\mathrm{x}^\top(\underline{\boldsymbol{\theta}}, \widehat{\underline{\boldsymbol{\theta}}}_\mathrm{x}) + \underline{\boldsymbol{l}}_\mathrm{x}^\top(\underline{\boldsymbol{\theta}})y\right)\underline{\boldsymbol{P}}_\mathrm{x}(\underline{\boldsymbol{\theta}})\widehat{\underline{\boldsymbol{x}}}_\mathrm{x} \\
&\qquad +\widehat{\underline{\boldsymbol{x}}}_\mathrm{x}^\top \underline{\boldsymbol{P}}_\mathrm{x}(\underline{\boldsymbol{\theta}})\left(\widetilde{\underline{\boldsymbol{A}}}_\mathrm{x}(\underline{\boldsymbol{\theta}}, \widehat{\underline{\boldsymbol{\theta}}}_\mathrm{x})\widehat{\underline{\boldsymbol{x}}}_\mathrm{x} + \underline{\boldsymbol{l}}_\mathrm{x}(\underline{\boldsymbol{\theta}})y\right) \\
&\overset{(3.106),(3.136)}{=} \quad -\widehat{\underline{\boldsymbol{x}}}_\mathrm{x}^\top \underline{\boldsymbol{Q}}_\mathrm{x}(\underline{\boldsymbol{\theta}})\widehat{\underline{\boldsymbol{x}}}_\mathrm{x} + 2\widehat{\underline{\boldsymbol{x}}}_\mathrm{x}^\top \underline{\boldsymbol{c}}_\mathrm{x}(\underline{\boldsymbol{\theta}})\underline{\boldsymbol{e}}_{\mathrm{t},\omega}^\top \underline{\boldsymbol{\Sigma}}_\mathrm{x}\widehat{\underline{\boldsymbol{x}}}_\mathrm{x} + 2y\underline{\boldsymbol{l}}_\mathrm{x}^\top(\underline{\boldsymbol{\theta}})\underline{\boldsymbol{P}}_\mathrm{x}(\underline{\boldsymbol{\theta}})\widehat{\underline{\boldsymbol{x}}}_\mathrm{x} \\
&\overset{(2.16)}{\leq} \quad -\|\widehat{\underline{\boldsymbol{x}}}_\mathrm{x}\|^2 \lambda_{\min}(\underline{\boldsymbol{Q}}_\mathrm{x}(\underline{\boldsymbol{\theta}})) + 2\|\widehat{\underline{\boldsymbol{x}}}_\mathrm{x}\|^2 \|\underline{\boldsymbol{c}}_\mathrm{x}(\underline{\boldsymbol{\theta}})\|\, \underline{c}_{\mathrm{x},e,\omega}\, \|\underline{\boldsymbol{\Sigma}}_\mathrm{x}\| \\
&\qquad +2\underbrace{\|\widehat{\underline{\boldsymbol{x}}}_\mathrm{x}\|}_{=:a}\underbrace{\|\underline{\boldsymbol{l}}_\mathrm{x}(\underline{\boldsymbol{\theta}})\|\,\|\underline{\boldsymbol{P}}_\mathrm{x}(\underline{\boldsymbol{\theta}})\|\,\|y\|_\infty}_{=:b} \\
&\overset{(2.15)}{\leq} \quad -\underbrace{\left(\lambda_{\min}(\underline{\boldsymbol{Q}}_\mathrm{x}(\underline{\boldsymbol{\theta}})) - \tfrac{1}{m} - 2\underline{c}_{\mathrm{x},e,\omega}\|\underline{\boldsymbol{c}}_\mathrm{x}(\underline{\boldsymbol{\theta}})\|\,\|\underline{\boldsymbol{\Sigma}}_\mathrm{x}\|\right)}_{(3.137)\colon (\cdot)\geq \underline{\epsilon}_{\mathrm{x},m}>0}\|\widehat{\underline{\boldsymbol{x}}}_\mathrm{x}\|^2 \\
&\qquad +\underbrace{m\|\underline{\boldsymbol{l}}_\mathrm{x}(\underline{\boldsymbol{\theta}})\|^2\,\|\underline{\boldsymbol{P}}_\mathrm{x}(\underline{\boldsymbol{\theta}})\|^2\,\|y\|_\infty^2}_{=:\underline{c}_{\mathrm{x},m}<\infty} \\
&\overset{(2.16)}{\leq} \quad -\tfrac{\underline{\epsilon}_{\mathrm{x},m}}{\lambda_{\max}(\underline{\boldsymbol{P}}_\mathrm{x}(\underline{\boldsymbol{\theta}}))}\underline{V}_{\mathrm{x},x}(\widehat{\underline{\boldsymbol{x}}}_\mathrm{x}, \underline{\boldsymbol{\theta}}) + \underline{c}_{\mathrm{x},m} \\
\overset{(2.17)}{\Longrightarrow} \underline{V}_{\mathrm{x},x}(\widehat{\underline{\boldsymbol{x}}}_\mathrm{x}, \underline{\boldsymbol{\theta}}) \quad &\leq \quad \underline{V}_{\mathrm{x},x}(\widehat{\underline{\boldsymbol{x}}}_{\mathrm{x},t_i}, \underline{\boldsymbol{\theta}}) + 2\underline{c}_{\mathrm{x},m}\tfrac{\lambda_{\max}(\underline{\boldsymbol{P}}_\mathrm{x}(\underline{\boldsymbol{\theta}}))}{\underline{\epsilon}_{\mathrm{x},m}}.
\end{aligned} \tag{3.138}$$

Thus, in view of (2.16) and (3.138) and with $\underline{\boldsymbol{c}}_\mathrm{x}$ as in (3.103) or (3.113), one can conclude that

$$\begin{aligned}
\forall\, t \in \mathbb{T}_i\colon\ \|\widehat{\underline{\boldsymbol{x}}}_\mathrm{x}\| &\overset{(2.16),(3.138)}{\leq} \sqrt{\tfrac{1}{\lambda_{\min}(\underline{\boldsymbol{P}}_\mathrm{x}(\underline{\boldsymbol{\theta}}))}\left(\underline{V}_{\mathrm{x},x}(\widehat{\underline{\boldsymbol{x}}}_{\mathrm{x},t_i}, \underline{\boldsymbol{\theta}}) + 2\underline{c}_{\mathrm{x},m}\tfrac{\lambda_{\max}(\underline{\boldsymbol{P}}_\mathrm{x}(\underline{\boldsymbol{\theta}}))}{\underline{\epsilon}_{\mathrm{x},m}}\right)} =: \underline{c}_\mathrm{x} < \infty \\
\text{and}\quad \left|\widehat{\underline{y}}_\mathrm{x}\right| &\overset{(3.116),(3.118)}{\leq} \|\underline{\boldsymbol{c}}_\mathrm{x}(\underline{\boldsymbol{\theta}})\|\,\|\widehat{\underline{\boldsymbol{x}}}_\mathrm{x}\| \leq \|\underline{\boldsymbol{c}}_\mathrm{x}(\underline{\boldsymbol{\theta}})\|\,\underline{c}_\mathrm{x} =: \widetilde{\underline{c}}_\mathrm{x} < \infty.
\end{aligned}$$

This proves the assertion. □

Theorem 3.4.8 (Boundedness and asymptotic decrease of the signal estimation error & the transformed angular frequency estimation error of the tFAO and tFAO$_\circ$ in transformed frame)**.** *Let* $\mathrm{x} \in \{\mathrm{t}, \mathrm{t}_\circ\}$ *and let* $v = 2n$ *if* $\mathrm{x} = \mathrm{t}$ *or* $v = 2n+1$ *if* $\mathrm{x} = \mathrm{t}_\circ$*. Consider any continuous and bounded input signal, i.e.* $y \in \mathcal{C}(\mathbb{R}_{\geq 0}; \mathbb{R}_{>0}) \cap \mathcal{L}^\infty(\mathbb{R}_{\geq 0}; \mathbb{R})$ *with bounded angular frequency, i.e.* $\underline{\boldsymbol{\theta}} \in \mathcal{L}^\infty(\mathbb{R}_{\geq 0}; \mathbb{R}^n)$ *and assume that* y *is fed to the parallelized tSOGIs in transformed frame* (3.116) *or the parallelized tSOGI$_\circ$s in transformed frame* (3.118)*, respectively, with* $\underline{\boldsymbol{A}}_\mathrm{x}$ *being a Hurwitz matrix. Let* $\underline{c}^\beta_{\mathrm{t},n}$ *be a real scalar. If the transformed angular frequency vector* $\widehat{\underline{\boldsymbol{\theta}}}_\mathrm{x}$ *is adapted by the update law*

$$\forall\, t \in \mathbb{T}_i\colon \quad \tfrac{\mathrm{d}}{\mathrm{d}t}\widehat{\underline{\boldsymbol{\theta}}}_\mathrm{x} = -\underline{e}_{\mathrm{x},y}\underline{\boldsymbol{\Gamma}}_\mathrm{x}(\underline{\boldsymbol{x}}_\mathrm{x}, \underline{\boldsymbol{\theta}})\underline{\boldsymbol{\Sigma}}_\mathrm{x}\widehat{\underline{\boldsymbol{x}}}_\mathrm{x}, \quad \widehat{\underline{\boldsymbol{\theta}}}_\mathrm{x}(t_i) = \widehat{\underline{\boldsymbol{\theta}}}_{\mathrm{x},t_i} \tag{3.139}$$

with a positive definite and symmetric matrix $\underline{\boldsymbol{\Gamma}}_\mathrm{x}$*, then*
(i) the signal estimation error vector $\underline{\boldsymbol{e}}_\mathrm{x}$ *as defined in* (3.130) *is bounded, i.e. there exists* $\underline{c}_{\mathrm{x},e} > 0$ *such that* $\|\underline{\boldsymbol{e}}_\mathrm{x}\| \leq \underline{c}_{\mathrm{x},e} < \infty$ *for all* $t \in \mathbb{T}_i$ *and, if* $n_\infty = n$ *for all* $t \in \mathbb{T}_i$*, it decreases asymptotically, i.e.* $\lim_{t\to\infty} \|\underline{\boldsymbol{e}}_\mathrm{x}\| \to 0$*;*
(ii) the transformed angular frequency error vector $\underline{\boldsymbol{e}}_{\mathrm{x},\omega}$ *is bounded, i.e. there exists* $\underline{c}_{\mathrm{x},e,\omega} > 0$ *such that* $\|\underline{\boldsymbol{e}}_{\mathrm{x},\omega}\| \leq \underline{c}_{\mathrm{x},e,\omega} < \infty$ *for all* $t \in \mathbb{T}_i$ *and, if* $n_\infty = n$ *for all* $t \in \mathbb{T}_i$*, it decreases asymptotically, i.e.* $\lim_{t\to\infty} \|\underline{\boldsymbol{e}}_{\mathrm{x},\omega}\| \to 0$*;*
(iii) the estimated transformed angular frequency vector $\widehat{\underline{\boldsymbol{\theta}}}_\mathrm{x}$ *is bounded, i.e. there exists* $\underline{c}_{\mathrm{x},\omega} > 0$ *such that* $\left\|\widehat{\underline{\boldsymbol{\theta}}}_\mathrm{x}\right\| \leq \underline{c}_{\mathrm{x},\omega} < \infty$ *for all* $t \in \mathbb{T}_i$*.*

Proof. The time derivative of the Lyapunov-like function

$$\underline{V}_\mathrm{x}(\underline{\boldsymbol{x}}_\mathrm{x}, \underline{\boldsymbol{\theta}}, \underline{\boldsymbol{e}}_\mathrm{x}, \underline{\boldsymbol{e}}_{\mathrm{x},\omega}) := \underbrace{\underline{\boldsymbol{e}}_\mathrm{x}^\top \underline{\boldsymbol{P}}_\mathrm{x}(\underline{\boldsymbol{\theta}})\underline{\boldsymbol{e}}_\mathrm{x}}_{=:\underline{V}_{\mathrm{x},x}(\underline{\boldsymbol{e}}_\mathrm{x}, \underline{\boldsymbol{\theta}})} + \underbrace{\underline{\boldsymbol{e}}_{\mathrm{x},\omega}^\top \underline{\boldsymbol{\Gamma}}_\mathrm{x}^{-1}(\underline{\boldsymbol{x}}_\mathrm{x}, \underline{\boldsymbol{\theta}})\underline{\boldsymbol{e}}_{\mathrm{x},\omega}}_{=:\underline{V}_{\mathrm{x},\omega}(\underline{\boldsymbol{x}}_\mathrm{x}, \underline{\boldsymbol{\theta}}, \underline{\boldsymbol{e}}_{\mathrm{x},\omega})}$$

(with $\underline{\boldsymbol{P}}_\mathrm{x}$ as used in the proof of Theorem 3.4.7 and $0 < \underline{\boldsymbol{\Gamma}}_\mathrm{x} = \underline{\boldsymbol{\Gamma}}_\mathrm{x}^\top \in \mathbb{R}^{n\times n}$), along the solution of (3.131) is given by

$$\begin{aligned}
\tfrac{\mathrm{d}}{\mathrm{d}t}\underline{V}_\mathrm{x}(\underline{\boldsymbol{x}}_\mathrm{x}, \underline{\boldsymbol{\theta}}, \underline{\boldsymbol{e}}_\mathrm{x}, \underline{\boldsymbol{e}}_{\mathrm{x},\omega}) \;&=\; \tfrac{\mathrm{d}}{\mathrm{d}t}\underline{\boldsymbol{e}}_\mathrm{x}^\top \underline{\boldsymbol{P}}_\mathrm{x}(\underline{\boldsymbol{\theta}})\underline{\boldsymbol{e}}_\mathrm{x} + \underline{\boldsymbol{e}}_\mathrm{x}^\top \underline{\boldsymbol{P}}_\mathrm{x}(\underline{\boldsymbol{\theta}})\tfrac{\mathrm{d}}{\mathrm{d}t}\underline{\boldsymbol{e}}_\mathrm{x} \\
&\quad + \tfrac{\mathrm{d}}{\mathrm{d}t}\underline{\boldsymbol{e}}_{\mathrm{x},\omega}^\top \underline{\boldsymbol{\Gamma}}_\mathrm{x}^{-1}(\underline{\boldsymbol{x}}_\mathrm{x}, \underline{\boldsymbol{\theta}})\underline{\boldsymbol{e}}_{\mathrm{x},\omega} + \underline{\boldsymbol{e}}_{\mathrm{x},\omega}^\top \underline{\boldsymbol{\Gamma}}_\mathrm{x}^{-1}(\underline{\boldsymbol{x}}_\mathrm{x}, \underline{\boldsymbol{\theta}})\tfrac{\mathrm{d}}{\mathrm{d}t}\underline{\boldsymbol{e}}_{\mathrm{x},\omega} \\
&\overset{(3.131)}{=} \underline{\boldsymbol{e}}_\mathrm{x}^\top \left(\underline{\boldsymbol{A}}_\mathrm{x}^\top(\underline{\boldsymbol{\theta}})\underline{\boldsymbol{P}}_\mathrm{x}(\underline{\boldsymbol{\theta}}) + \underline{\boldsymbol{P}}_\mathrm{x}(\underline{\boldsymbol{\theta}})\underline{\boldsymbol{A}}_\mathrm{x}(\underline{\boldsymbol{\theta}})\right)\underline{\boldsymbol{e}}_\mathrm{x} \\
&\quad -2\underline{\boldsymbol{e}}_\mathrm{x}^\top \underline{\boldsymbol{P}}_\mathrm{x}(\underline{\boldsymbol{\theta}})\underline{\boldsymbol{b}}_\mathrm{x}\underline{\boldsymbol{e}}_{\mathrm{x},\omega}^\top \underline{\boldsymbol{\Sigma}}_\mathrm{x}\widehat{\underline{\boldsymbol{x}}}_\mathrm{x} + 2\underline{\boldsymbol{e}}_{\mathrm{x},\omega}^\top \underline{\boldsymbol{\Gamma}}_\mathrm{x}^{-1}(\underline{\boldsymbol{x}}_\mathrm{x}, \underline{\boldsymbol{\theta}})\tfrac{\mathrm{d}}{\mathrm{d}t}\underline{\boldsymbol{e}}_{\mathrm{x},\omega} \\
&\overset{(3.131),(3.136)}{=} -\underline{\boldsymbol{e}}_\mathrm{x}^\top \underline{\boldsymbol{Q}}_\mathrm{x}(\underline{\boldsymbol{\theta}})\underline{\boldsymbol{e}}_\mathrm{x} - 2\underline{\boldsymbol{e}}_{\mathrm{x},\omega}^\top\left(\underline{e}_{\mathrm{x},y}\underline{\boldsymbol{\Sigma}}_\mathrm{x}\widehat{\underline{\boldsymbol{x}}}_\mathrm{x} - \underline{\boldsymbol{\Gamma}}_\mathrm{x}^{-1}(\underline{\boldsymbol{x}}_\mathrm{x}, \underline{\boldsymbol{\theta}})\tfrac{\mathrm{d}}{\mathrm{d}t}\underline{\boldsymbol{e}}_{\mathrm{x},\omega}\right).
\end{aligned} \tag{3.140}$$

Now, by choosing

$$\tfrac{\mathrm{d}}{\mathrm{d}t}\underline{\boldsymbol{e}}_{\mathrm{x},\omega} = \underline{e}_{\mathrm{x},y}\underline{\boldsymbol{\Gamma}}_\mathrm{x}(\underline{\boldsymbol{x}}_\mathrm{x}, \underline{\boldsymbol{\theta}})\underline{\boldsymbol{\Sigma}}_\mathrm{x}\widehat{\underline{\boldsymbol{x}}}_\mathrm{x} \tag{3.141}$$

it follows that

$$\begin{aligned}
\tfrac{\mathrm{d}}{\mathrm{d}t}\underline{V}_\mathrm{x}(\underline{\boldsymbol{x}}_\mathrm{x}, \underline{\boldsymbol{\theta}}, \underline{\boldsymbol{e}}_\mathrm{x}, \underline{\boldsymbol{e}}_{\mathrm{x},\omega}) \;&\overset{(3.140),(3.141)}{=}\; -\underline{\boldsymbol{e}}_\mathrm{x}^\top \underline{\boldsymbol{Q}}_\mathrm{x}(\underline{\boldsymbol{\theta}})\underline{\boldsymbol{e}}_\mathrm{x} \overset{(2.16)}{\leq} -\lambda_{\min}(\underline{\boldsymbol{Q}}_\mathrm{x}(\underline{\boldsymbol{\theta}}))\,\|\underline{\boldsymbol{e}}_\mathrm{x}\|^2 \\
&\overset{(2.16)}{\leq} -\underbrace{\frac{\lambda_{\min}(\underline{\boldsymbol{Q}}_\mathrm{x}(\underline{\boldsymbol{\theta}}))}{\lambda_{\max}(\underline{\boldsymbol{P}}_\mathrm{x}(\underline{\boldsymbol{\theta}}))}}_{=:\underline{\mu}_{\mathrm{x},\underline{V}}>0}\underline{V}_{\mathrm{x},x}(\underline{\boldsymbol{e}}_\mathrm{x}, \underline{\boldsymbol{\theta}}).
\end{aligned} \tag{3.142}$$

Note that these results are independent of $\underline{\boldsymbol{e}}_{\mathrm{x},\omega}$; hence, it might happen that $\|\underline{\boldsymbol{e}}_{\mathrm{x},\omega}\| \to \infty$ as

$t \to \infty$. In fact, the following holds

$$\forall t \in \mathbb{T}_i,\ \forall \underline{\boldsymbol{e}}_{\mathrm{x}} \in \mathbb{R}^v,\ \underline{\boldsymbol{e}}_{\mathrm{x},\omega} \in \mathbb{R}^n\colon\ \tfrac{\mathrm{d}}{\mathrm{d}t}\underline{V}_{\mathrm{x}}(\underline{\boldsymbol{x}}_{\mathrm{x}}, \underline{\boldsymbol{\theta}}, \underline{\boldsymbol{e}}_{\mathrm{x}}, \underline{\boldsymbol{e}}_{\mathrm{x},\omega}) \le 0$$
$$\text{and} \quad \forall t \in \mathbb{T}_i,\ \forall \underline{\boldsymbol{e}}_{\mathrm{x}} = \boldsymbol{0}_v,\ \underline{\boldsymbol{e}}_{\mathrm{x},\omega} \in \mathbb{R}^n\colon \quad \tfrac{\mathrm{d}}{\mathrm{d}t}\underline{V}_{\mathrm{x}}(\underline{\boldsymbol{x}}_{\mathrm{x}}, \underline{\boldsymbol{\theta}}, \underline{\boldsymbol{e}}_{\mathrm{x}}, \underline{\boldsymbol{e}}_{\mathrm{x},\omega}) = 0,$$

which allows to invoke LaSalle's invariance principle (see Fact 2.18). To verify its requirements, first observe that $(\underline{\boldsymbol{e}}_{\mathrm{x}}^\top, \underline{\boldsymbol{e}}_{\mathrm{x},\omega}^\top)^\top = (\boldsymbol{0}_v^\top, \boldsymbol{0}_n^\top)^\top$ is an equilibrium, i.e.

$$\tfrac{\mathrm{d}}{\mathrm{d}t}\underline{\boldsymbol{e}}_{\mathrm{x}}\Big|_{(\underline{\boldsymbol{e}}_{\mathrm{x}}^\top, \underline{\boldsymbol{e}}_{\mathrm{x},\omega}^\top)^\top = (\boldsymbol{0}_v^\top, \boldsymbol{0}_n^\top)^\top} = \boldsymbol{0}_v \quad \text{and} \quad \tfrac{\mathrm{d}}{\mathrm{d}t}\underline{\boldsymbol{e}}_{\mathrm{x},\omega}\Big|_{(\underline{\boldsymbol{e}}_{\mathrm{x}}^\top, \underline{\boldsymbol{e}}_{\mathrm{x},\omega}^\top)^\top = (\boldsymbol{0}_v^\top, \boldsymbol{0}_n^\top)^\top} = \boldsymbol{0}_n.$$

Second, the function $\underline{V}_{\mathrm{x}}$ is positive definite whereas its time derivative is negative semi-definite as shown above. The largest positive invariant subset of

$$\underline{S}_{\mathrm{x}} := \left\{ \begin{pmatrix} \underline{\boldsymbol{e}}_{\mathrm{x}} \\ \underline{\boldsymbol{e}}_{\mathrm{x},\omega} \end{pmatrix} \in \mathbb{R}^{v+n} \,\middle|\, \tfrac{\mathrm{d}}{\mathrm{d}t}\underline{V}_{\mathrm{x}}(\underline{\boldsymbol{x}}, \underline{\boldsymbol{e}}_{\mathrm{x}}, \underline{\boldsymbol{\theta}}, \underline{\boldsymbol{e}}_{\mathrm{x},\omega}) = 0 \right\} = \left\{ \begin{pmatrix} \boldsymbol{0}_v \\ \boldsymbol{\kappa}_{\mathrm{x}} \end{pmatrix} \,\middle|\, \boldsymbol{\kappa}_{\mathrm{x}} \in \mathbb{R}^n \right\}$$

is given by $\underline{M}_{\mathrm{x}} := \left\{ \begin{pmatrix} \boldsymbol{0}_v^\top & \boldsymbol{0}_n^\top \end{pmatrix}^\top \right\}$, since otherwise the following would hold:

$$\forall \left\{ \begin{pmatrix} \underline{\boldsymbol{e}}_{\mathrm{x}} \\ \underline{\boldsymbol{e}}_{\mathrm{x},\omega} \end{pmatrix} \right\} \in \underline{S}_{\mathrm{x}} \setminus \underline{M}_{\mathrm{x}}\colon \quad \tfrac{\mathrm{d}}{\mathrm{d}t}\underline{\boldsymbol{e}}_{\mathrm{x}} = \underline{\boldsymbol{A}}_{\mathrm{x}}(\underline{\boldsymbol{\theta}})\underline{\boldsymbol{e}}_{\mathrm{x}} - \underline{\boldsymbol{b}}_{\mathrm{x}}\,\underline{\boldsymbol{e}}_{\mathrm{x},\omega}^\top \underline{\boldsymbol{\Sigma}}_{\mathrm{x}}\,\underline{\widehat{\boldsymbol{x}}}_{\mathrm{x}} \neq \boldsymbol{0}_v$$

which violates the equilibrium condition. Hence, the error vector $(\underline{\boldsymbol{e}}_{\mathrm{x}}^\top, \underline{\boldsymbol{e}}_{\mathrm{x},\omega}^\top)^\top$ decreases global asymptotically and therefore, the estimation error vector and transformed angular frequency error vector are both bounded and converging asymptotically to zero, i.e.

$$\forall t \in \mathbb{T}_i\colon \quad \left. \begin{array}{rclcrcl} \left\|\underline{\boldsymbol{e}}_{\mathrm{x},\omega}\right\| \le \underline{c}_{\mathrm{x},e,\omega} & < & \infty, & \text{and} & \lim\limits_{t\to\infty} \left\|\underline{\boldsymbol{e}}_{\mathrm{x},\omega}\right\| & \to & 0, \\ \left\|\underline{\boldsymbol{e}}_{\mathrm{x}}\right\| \le \underline{c}_{\mathrm{x},e} & < & \infty & \text{and} & \lim\limits_{t\to\infty} \left\|\underline{\boldsymbol{e}}_{\mathrm{x}}\right\| & \to & 0. \end{array} \right\} \tag{3.143}$$

Note this asymptotic behavior only holds true if $n_\infty = n$. Otherwise, it converges asymptotically to some non-zero value, since the observers are not able to estimate the input signal completely. Moreover, in return, the boundedness and asymptotic decrease of the transformed angular frequency error implies a global boundedness of the angular frequency adaption. This becomes clear when taking into account

$$\tfrac{\mathrm{d}}{\mathrm{d}t}\underline{\boldsymbol{e}}_{\mathrm{x},\omega} \overset{(3.128)}{=} -\tfrac{\mathrm{d}}{\mathrm{d}t}\underline{\widehat{\boldsymbol{\theta}}}_{\mathrm{x}}. \tag{3.144}$$

Thus, it follows

$$\implies \tfrac{\mathrm{d}}{\mathrm{d}t}\underline{\widehat{\boldsymbol{\theta}}}_{\mathrm{x}} \overset{(3.141),(3.144)}{=} -\underline{e}_{\mathrm{x},y}\underline{\boldsymbol{\Gamma}}_{\mathrm{x}}(\underline{\boldsymbol{x}}_{\mathrm{x}}, \underline{\boldsymbol{\theta}})\underline{\boldsymbol{\Sigma}}_{\mathrm{x}}\,\underline{\widehat{\boldsymbol{x}}}_{\mathrm{x}}. \tag{3.145}$$

Finally, observe that

$$\forall t \in \mathbb{T}_i\colon \quad \left\|\underline{\widehat{\boldsymbol{\theta}}}_{\mathrm{x}}\right\| \overset{(3.128)}{=} \left\|\underline{\boldsymbol{\theta}} - \underline{\boldsymbol{e}}_{\mathrm{x},\omega}\right\| \le \underbrace{\left\|\underline{\boldsymbol{\theta}}\right\|}_{=: \underline{c}_\omega < \infty} + \left\|\underline{\boldsymbol{e}}_{\mathrm{x},\omega}\right\| \overset{(3.143)}{\le} \underline{c}_\omega + \underline{c}_{\mathrm{x},e,\omega} =: \underline{c}_{\mathrm{x},\omega} < \infty$$

which completes the proof. □

3.4.5.1 The tFLL in transformed frame and summary of the tFAO in transformed frame

As an outcome of Theorem 3.4.8, transformed angular frequency adaption is achieved by

$$\forall t \in \mathbb{T}_i: \quad \tfrac{\mathrm{d}}{\mathrm{d}t}\widehat{\underline{\boldsymbol{\theta}}}_{\mathrm{t}} = -\underline{e}_{\mathrm{t},y}\underline{\boldsymbol{\Gamma}}_{\mathrm{t}}(\underline{\boldsymbol{x}}, \underline{\boldsymbol{\theta}})\underline{\boldsymbol{\Sigma}}\widehat{\underline{\boldsymbol{x}}}_{\mathrm{t}}, \quad \widehat{\underline{\boldsymbol{\theta}}}_{\mathrm{t}}(t_i) = \widehat{\underline{\boldsymbol{\theta}}}_{\mathrm{t},t_i} \tag{3.146}$$

which is called the *transformation-based Frequency Locked Loop* (tFLL) in transformed frame. Its block diagram is illustrated in Figure 3.26.

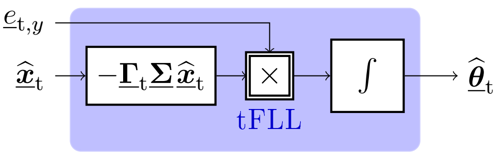

Figure 3.26: *Block diagram of the tFLL in transformed frame.*

Concluding, the overall system of parallelized tSOGIs in transformed frame and tFLL in transformed frame, called the *transformation-based Frequency Adaptive Observer* (tFAO) in transformed frame, is described by

$$\forall t \in \mathbb{T}_i: \quad \left.\begin{aligned} \tfrac{\mathrm{d}}{\mathrm{d}t}\widehat{\underline{\boldsymbol{x}}}_{\mathrm{t}} &= \widetilde{\underline{\boldsymbol{A}}}_{\mathrm{t}}(\underline{\boldsymbol{\theta}}, \widehat{\underline{\boldsymbol{\theta}}}_{\mathrm{t}})\widehat{\underline{\boldsymbol{x}}}_{\mathrm{t}} + \underline{\boldsymbol{l}}_{\mathrm{t}}(\underline{\boldsymbol{\theta}})y, & \widehat{\underline{\boldsymbol{x}}}_{\mathrm{t}}(t_i) &= \widehat{\underline{\boldsymbol{x}}}_{\mathrm{t},t_i} \\ \widetilde{\underline{\boldsymbol{A}}}_{\mathrm{t}}(\underline{\boldsymbol{\theta}}, \widehat{\underline{\boldsymbol{\theta}}}_{\mathrm{t}}) &= \begin{bmatrix} \boldsymbol{0}_{2n-1} & \boldsymbol{I}_{2n-1} \\ 0 & \boldsymbol{0}_{2n-1}^\top \end{bmatrix} - \underline{\boldsymbol{b}}\widehat{\underline{\boldsymbol{\theta}}}_{\mathrm{t}}^\top\underline{\boldsymbol{\Sigma}} - \underline{\boldsymbol{l}}_{\mathrm{t}}(\underline{\boldsymbol{\theta}})\underline{\boldsymbol{c}}_{\mathrm{t}}^\top(\underline{\boldsymbol{\theta}}) & & \\ \tfrac{\mathrm{d}}{\mathrm{d}t}\widehat{\underline{\boldsymbol{\theta}}}_{\mathrm{t}} &= \left(\underline{\boldsymbol{c}}_{\mathrm{t}}^\top(\underline{\boldsymbol{\theta}})\widehat{\underline{\boldsymbol{x}}}_{\mathrm{t}} - y\right)\underline{\boldsymbol{\Gamma}}_{\mathrm{t}}(\underline{\boldsymbol{x}}, \underline{\boldsymbol{\theta}})\underline{\boldsymbol{\Sigma}}\widehat{\underline{\boldsymbol{x}}}_{\mathrm{t}}, & \widehat{\underline{\boldsymbol{\theta}}}_{\mathrm{t}}(t_i) &= \widehat{\underline{\boldsymbol{\theta}}}_{\mathrm{t},t_i}. \end{aligned}\right\} \tag{3.147}$$

Its block diagram is depicted in Figure 3.27.

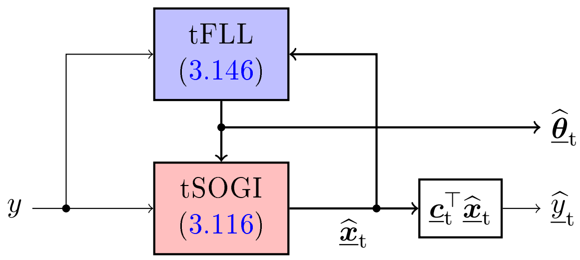

Figure 3.27: *Block diagram of the tFAO.*

3.4.5.2 The tFLL with offset in transformed frame and summary of the tFAO with offset in transformed frame

From Theorem 3.4.8, the transformed angular frequency update law is obtained as

$$\forall t \in \mathbb{T}_i: \quad \tfrac{\mathrm{d}}{\mathrm{d}t}\widehat{\underline{\boldsymbol{\theta}}}_{\mathrm{t}_\circ} = -\underline{e}_{\mathrm{t}_\circ,y}\underline{\boldsymbol{\Gamma}}_{\mathrm{t}_\circ}(\underline{\boldsymbol{x}}_\circ, \underline{\boldsymbol{\theta}})\underline{\boldsymbol{\Sigma}}_\circ\widehat{\underline{\boldsymbol{x}}}_{\mathrm{t}_\circ}, \quad \widehat{\underline{\boldsymbol{\theta}}}_{\mathrm{t}_\circ}(t_i) = \widehat{\underline{\boldsymbol{\theta}}}_{\mathrm{t}_\circ,t_i} \tag{3.148}$$

what is denoted as the *transformation-based Frequency Locked Loop with offset* ($\mathrm{tFLL}_\circ$) in transformed frame. Its block diagram is similar to the one illustrated in Figure 3.26. To conclude, the overall system is called the *transformation-based Frequency Adaptive Observer with offset*

($\mathrm{tFAO}_\circ$) in transformed frame. It is described by

$$\forall t \in \mathbb{T}_i: \quad \left.\begin{array}{rcll} \frac{\mathrm{d}}{\mathrm{d}t}\underline{\widehat{\boldsymbol{x}}}_{\mathrm{t}_\circ} & = & \underline{\widetilde{\boldsymbol{A}}}_{\mathrm{t}_\circ}(\underline{\boldsymbol{\theta}}, \underline{\widehat{\boldsymbol{\theta}}}_{\mathrm{t}_\circ})\underline{\widehat{\boldsymbol{x}}}_{\mathrm{t}_\circ} + \underline{\boldsymbol{l}}_{\mathrm{t}_\circ}(\underline{\boldsymbol{\theta}})y, & \underline{\widehat{\boldsymbol{x}}}_{\mathrm{t}_\circ}(t_i) = \underline{\widehat{\boldsymbol{x}}}_{\mathrm{t}_\circ,t_i} \\ \underline{\widetilde{\boldsymbol{A}}}_{\mathrm{t}_\circ}(\underline{\boldsymbol{\theta}}, \underline{\widehat{\boldsymbol{\theta}}}_{\mathrm{t}_\circ}) & = & \begin{bmatrix} \boldsymbol{0}_{2n} & \boldsymbol{I}_{2n} \\ 0 & \boldsymbol{0}_{2n}^\top \end{bmatrix} - \underline{\boldsymbol{b}}_\circ \underline{\widehat{\boldsymbol{\theta}}}_{\mathrm{t}_\circ}^\top \underline{\boldsymbol{\Sigma}}_\circ - \underline{\boldsymbol{l}}_{\mathrm{t}_\circ}(\underline{\boldsymbol{\theta}})\underline{\boldsymbol{c}}_{\mathrm{t}_\circ}^\top(\underline{\boldsymbol{\theta}}) & \\ \frac{\mathrm{d}}{\mathrm{d}t}\underline{\widehat{\boldsymbol{\theta}}}_{\mathrm{t}_\circ} & = & \left(\underline{\boldsymbol{c}}_{\mathrm{t}_\circ}^\top(\underline{\boldsymbol{\theta}})\underline{\widehat{\boldsymbol{x}}}_{\mathrm{t}_\circ} - y\right)\boldsymbol{\Gamma}_{\mathrm{t}_\circ}(\underline{\boldsymbol{x}}_\circ, \underline{\boldsymbol{\theta}})\underline{\boldsymbol{\Sigma}}_\circ \underline{\widehat{\boldsymbol{x}}}_{\mathrm{t}_\circ}, & \underline{\widehat{\boldsymbol{\theta}}}_{\mathrm{t}_\circ}(t_i) = \underline{\widehat{\boldsymbol{\theta}}}_{\mathrm{t}_\circ,t_i} \end{array}\right\} \tag{3.149}$$

and its block diagram is depicted in Figure 3.28.

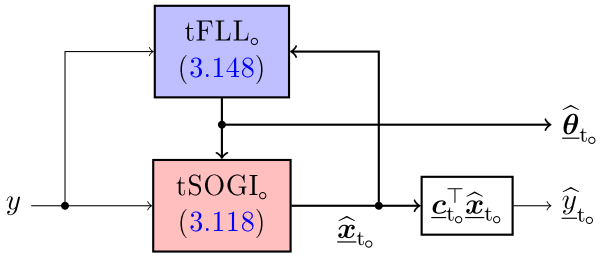

Figure 3.28: *Block diagram of the $\mathrm{tFAO}_\circ$ in transformed frame.*

Remark 3.4.9. *Let $\mathrm{x} \in \{\mathrm{t}, \mathrm{t}_\circ\}$. Note that the transformed angular frequency estimation vector $\underline{\widehat{\boldsymbol{\theta}}}_{\mathrm{x}}$ does not contain the unique frequencies $\widehat{\omega}_{\mathrm{x},i}, i \in \{1, \ldots, n\}$ but certain combinations of them as in* (3.104)*, i.e.*

$$\left.\begin{array}{rcl} \underline{\widehat{\theta}}_{\mathrm{x},1} & = & \sum_{j=1}^{n} \widehat{\omega}_{\mathrm{x},j}^2 \\ \underline{\widehat{\theta}}_{\mathrm{x},i} & = & \sum_{j_1 < j_i = 1}^{n} \prod_{k \in \{j_1, \ldots, j_i\}} \widehat{\omega}_{\mathrm{x},k}^2 \\ \underline{\widehat{\theta}}_{\mathrm{x},n} & = & \prod_{j=1}^{n} \widehat{\omega}_{\mathrm{x},j}^2. \end{array}\right\} \tag{3.150}$$

Inserting the $\underline{\widehat{\theta}}_{\mathrm{x},i}$ into each other yields

$$\forall i \in \{1, \ldots, n\}: \quad 0 = \widehat{\omega}_{\mathrm{x},i}^{2n} - \widehat{\omega}_{\mathrm{x},i}^{2n-2}\underline{\widehat{\theta}}_{\mathrm{x},1} + \widehat{\omega}_{\mathrm{x},i}^{2n-4}\underline{\widehat{\theta}}_{\mathrm{x},2} + \cdots + (-1)^n \underline{\widehat{\theta}}_{\mathrm{x},n} \tag{3.151}$$

where it should be noted that the $\widehat{\omega}_{\mathrm{x},i}$ are unknown, i.e. they can be treated as variables *whereas the $\underline{\widehat{\theta}}_{\mathrm{x},i}$ are known, i.e. they are treated as* coefficients*. Hence, the unique estimated angular frequencies can be calculated as the roots of the function*

$$\begin{array}{rcl} f(\kappa) & := & \kappa^{2n} + \overbrace{\begin{pmatrix} -\kappa^{2n-2} & \kappa^{2n-4} & \cdots & (-1)^{n+1}\kappa^2 & (-1)^n \end{pmatrix}}^{\in \mathbb{R}^n} \underline{\widehat{\boldsymbol{\theta}}}_{\mathrm{x}} \\ \Rightarrow \quad \{\kappa_0 |\, f(\kappa_0) = 0\} & = & \{\pm\widehat{\omega}_{\mathrm{x},1}, \ldots, \pm\widehat{\omega}_{\mathrm{x},n}\}; \end{array} \tag{3.152}$$

A proof for this assertion is provided in Appendix D. However, in view of the Theorem of Abel-Ruffini *shown in [583], the roots can only be calculated analytically for $n \leq 4$.*

Remark 3.4.10. *Let $\mathrm{x} \in \{\mathrm{t}, \mathrm{t}_\circ\}$. Post-processing the states collected in $\underline{\widehat{\boldsymbol{x}}}_{\mathrm{x}}$ – that is, back-transforming – into α, β frame is done straight forward according to* (3.97) *or* (3.107)*, respectively. In the inverse transformation matrix, the actual angular frequencies $\omega_i, i \in \{1, \ldots, n\}$ must be replaced by the estimated angular frequencies $\widehat{\omega}_{\mathrm{x},i}$. Then, the amplitudes $\underline{\widehat{a}}_{\mathrm{x},i}$ and phases $\underline{\widehat{\phi}}_{\mathrm{x},i}$ are calculated as shown in* (3.10).

Remark 3.4.11. *Since most likely, it holds that $n_\infty > n$ and $\widehat{\mathbb{H}}_n$ is not prescribed but estimated, the tFAO in transformed frame and the $\mathrm{tFAO}_\circ$ in transformed frame will detect the signal* *components with the most dominant amplitudes such that the estimation error is minimized.*

3.5 The transformation-based Frequency Adaptive Observer in α, β frame and the transformation-based Frequency Adaptive Observer with offset in α, β frame

In this section, the tFAO and tFAO$_\circ$ in transformed frame introduced in Section 3.4 are back-transformed into α, β frame. Although they do not require a prescribed set $\mathbb{H}_n$ but are capable of estimating all parameters of a fixed number of components with dominant amplitude of unknown signals, they have two significant numerical disadvantages:

1. The matrices $\underline{\boldsymbol{J}}_{\mathrm{x}}$ are bad conditioned due to the frequency vector $\underline{\boldsymbol{\theta}}$. For example, the transformed angular frequency vector follows from the angular frequency vector in α, β frame as

$$\begin{aligned} \boldsymbol{\omega} &= \begin{pmatrix} 2\pi 50 & 2\pi 100 & 2\pi 150 \end{pmatrix}^\top \\ \Longrightarrow \quad \underline{\boldsymbol{\theta}} &= \begin{pmatrix} (2\pi)^2 35 \cdot 10^3 & (2\pi)^4 306.25 \cdot 10^6 & (2\pi)^6 562.5 \cdot 10^9 \end{pmatrix}^\top . \end{aligned}$$

   Hence, the matrix

$$\underline{\boldsymbol{J}} = \begin{bmatrix} 0 & 1 & 0 & 0 & 0 & 0 \\ 0 & 0 & 1 & 0 & 0 & 0 \\ 0 & 0 & 0 & 1 & 0 & 0 \\ 0 & 0 & 0 & 0 & 1 & 0 \\ 0 & 0 & 0 & 0 & 0 & 1 \\ -\underline{\theta}_3 & 0 & -\underline{\theta}_2 & 0 & \underline{\theta}_1 & 0 \end{bmatrix}$$

   contains elements that vary by a factor of $(2\pi)^6 \cdot 562.5 \cdot 10^9 \approx 3.5 \cdot 10^{16}$. On the other hand, the matrix $\boldsymbol{J}$ or $\boldsymbol{J}_\circ$, respectively, is better conditioned since it varies by the factor of 3 in this example.

2. As already stated in Remark 3.4.9, the unique angular frequencies $\widehat{\omega}_{\mathrm{t},i}$ are not obtainable analytically for $n > 4$. In this case, numeric methods like the Newton-Raphson method must be applied which come with high computational burden. This might endanger real-time applicability.

Thus, the aim of the back-transformation is to maintain the advantages of the tFAO in transformed frame and the tFAO$_\circ$ in transformed frame such as the estimation of harmonic angular frequencies and to improve the numeric characteristics. This section is structured as follows:

Section 3.5.1 discusses the back-transformation of the tFLL in transformed frame (3.146) and tFLL$_\circ$ in transformed frame (3.148),

Section 3.5.2 shows the back-transformation of the tSOGI in transformed frame (3.116) and tSOGI$_\circ$ in transformed frame (3.118),

Section 3.5.3 discusses the gain selection for both systems and

Section 3.5.4 proves the stability for both methods.

3.5.1 back-transformation: The tFLL in α, β frame and the tFLL with offset in α, β frame

This section shows the back-transformation of the angular frequency adaption law. The transformed angular frequency vector $\underline{\widehat{\boldsymbol{\theta}}}_{\mathrm{t}}$ is back-transformed to a vector $\widehat{\boldsymbol{\omega}}_{\mathrm{t}}$ containing the single frequencies $\widehat{\omega}_{\mathrm{t},i}$ in Section 3.5.1.1. The same is done for offset in Section 3.5.1.2.

3.5.1.1 The tFLL in α, β frame

Recall the transformed angular frequency vector (3.105)

$$\underline{\widehat{\boldsymbol{\theta}}}_{\mathrm{t}} = \begin{pmatrix} \underline{\widehat{\theta}}_{\mathrm{t},1} & \cdots & \underline{\widehat{\theta}}_{\mathrm{t},n} \end{pmatrix}^{\top} = \begin{pmatrix} \sum_{j=1}^{n} \widehat{\omega}_{\mathrm{t},j}^{2} & \cdots & \prod_{j=1}^{n} \widehat{\omega}_{\mathrm{t},j}^{2} \end{pmatrix}^{\top}$$

and define the angular frequency vector in α, β coordinates,

$$\widehat{\boldsymbol{\omega}}_{\mathrm{t}} := \begin{pmatrix} \widehat{\omega}_{\mathrm{t},1} & \cdots & \widehat{\omega}_{\mathrm{t},n} \end{pmatrix}^{\top}.$$

Calculate the time derivatives of the elements of $\underline{\widehat{\boldsymbol{\theta}}}_{\mathrm{t}}$ as follows

$$\left.\begin{array}{lllll} \frac{\mathrm{d}}{\mathrm{d}t}\underline{\widehat{\theta}}_{\mathrm{t},1} & = & \frac{\mathrm{d}}{\mathrm{d}t}\sum_{j=1}^{n} \widehat{\omega}_{\mathrm{t},j}^{2} & = & 2\sum_{j=1}^{n} \widehat{\omega}_{\mathrm{t},j}\frac{\mathrm{d}}{\mathrm{d}t}\widehat{\omega}_{\mathrm{t},j} \\ \frac{\mathrm{d}}{\mathrm{d}t}\underline{\widehat{\theta}}_{\mathrm{t},i} & = & \frac{\mathrm{d}}{\mathrm{d}t}\sum_{j_1<j_i=1}^{n}\prod_{k\in j} \widehat{\omega}_{\mathrm{t},k}^{2} & = & 2\sum_{j_1<j_i=1}^{n}\sum_{k\in j} \widehat{\omega}_{\mathrm{t},k}\frac{\mathrm{d}}{\mathrm{d}t}\widehat{\omega}_{\mathrm{t},k}\prod_{l\in j\setminus k} \widehat{\omega}_{\mathrm{t},l}^{2} \\ \frac{\mathrm{d}}{\mathrm{d}t}\underline{\widehat{\theta}}_{\mathrm{t},n} & = & \frac{\mathrm{d}}{\mathrm{d}t}\prod_{j=1}^{n} \widehat{\omega}_{\mathrm{t},j}^{2} & = & 2\sum_{j=1}^{n} \widehat{\omega}_{\mathrm{t},j}\frac{\mathrm{d}}{\mathrm{d}t}\widehat{\omega}_{\mathrm{t},j}\prod_{\substack{k=1\\k\neq j}}^{n} \widehat{\omega}_{\mathrm{t},k}^{2}. \end{array}\right\} \tag{3.153}$$

From them, deduce the transformation matrix

$$\boldsymbol{\Omega}^{-1}(\widehat{\omega}_{\mathrm{t}}) := \begin{bmatrix} \varpi_{1,1}'(\widehat{\boldsymbol{\omega}}_{\mathrm{t}}) & \cdots & \varpi_{1,n}'(\widehat{\boldsymbol{\omega}}_{\mathrm{t}}) \\ \vdots & \ddots & \vdots \\ \varpi_{n,1}'(\widehat{\boldsymbol{\omega}}_{\mathrm{t}}) & \cdots & \varpi_{n,n}'(\widehat{\boldsymbol{\omega}}_{\mathrm{t}}) \end{bmatrix} \quad \text{with} \quad \varpi_{i,j}'(\widehat{\boldsymbol{\omega}}_{\mathrm{t}}) = 2\widehat{\omega}_{\mathrm{t},j}\sum_{k_1<k_{i-1}=1\setminus j}^{n}\prod_{l\in k}\widehat{\omega}_{\mathrm{t},l}^{2} \tag{3.154}$$

such that

$$\frac{\mathrm{d}}{\mathrm{d}t}\underline{\widehat{\boldsymbol{\theta}}}_{\mathrm{t}} = \boldsymbol{\Omega}^{-1}(\widehat{\boldsymbol{\omega}}_{\mathrm{t}})\frac{\mathrm{d}}{\mathrm{d}t}\widehat{\boldsymbol{\omega}}_{\mathrm{t}}. \tag{3.155}$$

The inverse of $\boldsymbol{\Omega}^{-1}$ is obtained as

$$\boldsymbol{\Omega}(\widehat{\boldsymbol{\omega}}_{\mathrm{t}}) = \begin{bmatrix} \varpi_{1,1}(\widehat{\boldsymbol{\omega}}_{\mathrm{t}}) & \cdots & \varpi_{1,n}(\widehat{\boldsymbol{\omega}}_{\mathrm{t}}) \\ \vdots & \ddots & \vdots \\ \varpi_{n,1}(\widehat{\boldsymbol{\omega}}_{\mathrm{t}}) & \cdots & \varpi_{n,n}(\widehat{\boldsymbol{\omega}}_{\mathrm{t}}) \end{bmatrix} \quad \text{with} \quad \varpi_{i,j}(\widehat{\boldsymbol{\omega}}_{\mathrm{t}}) = \frac{(-1)^{j+1}\widehat{\omega}_{\mathrm{t},i}^{2n-2j-1}}{2\prod_{\substack{k=1\\k\neq i}}^{n}(\widehat{\omega}_{\mathrm{t},i}^{2}-\widehat{\omega}_{\mathrm{t},k}^{2})} \tag{3.156}$$

since the product of the r-th row of $\boldsymbol{\Omega}$ and the c-th column of $\boldsymbol{\Omega}^{-1}$ yields

$$\frac{\widehat{\omega}_{\mathrm{t},r}^{2n-3}\widehat{\omega}_{\mathrm{t},c}}{\prod_{\substack{k=1\\k\neq r}}^{n}(\widehat{\omega}_{\mathrm{t},r}^{2}-\widehat{\omega}_{\mathrm{t},k}^{2})} - \frac{\widehat{\omega}_{\mathrm{t},r}^{2n-5}\widehat{\omega}_{\mathrm{t},c}\sum_{\substack{k=1\\k\neq c}}^{n}\widehat{\omega}_{\mathrm{t},k}^{2}}{\prod_{\substack{k=1\\k\neq r}}^{n}(\widehat{\omega}_{\mathrm{t},r}^{2}-\widehat{\omega}_{\mathrm{t},k}^{2})} + \cdots - \frac{(-1)^{n}\widehat{\omega}_{\mathrm{t},r}^{-1}\widehat{\omega}_{\mathrm{t},c}\prod_{\substack{k=1\\k\neq c}}^{n}\widehat{\omega}_{\mathrm{t},k}^{2}}{\prod_{\substack{k=1\\k\neq r}}^{n}(\widehat{\omega}_{\mathrm{t},r}^{2}-\widehat{\omega}_{\mathrm{t},k}^{2})}$$

$$= \left(\widehat{\omega}_{\mathrm{t},r}^{2n-2} - \widehat{\omega}_{\mathrm{t},r}^{2n-4} \sum_{\substack{k=1\\k\neq c}}^{n} \widehat{\omega}_{\mathrm{t},k}^{2} + \cdots - (-1)^n \prod_{\substack{k=1\\k\neq c}}^{n} \widehat{\omega}_{\mathrm{t},k}^{2} \right) \frac{\widehat{\omega}_{\mathrm{t},c}\widehat{\omega}_{\mathrm{t},r}^{-1}}{\prod\limits_{\substack{k=1\\k\neq r}}^{n} (\widehat{\omega}_{\mathrm{t},r}^{2} - \widehat{\omega}_{\mathrm{t},k}^{2})}$$

$$\overset{(2.18)}{=} \prod_{\substack{k=1\\k\neq c}}^{n} (\widehat{\omega}_{\mathrm{t},r}^{2} - \widehat{\omega}_{\mathrm{t},k}^{2}) \frac{\widehat{\omega}_{\mathrm{t},c}\widehat{\omega}_{\mathrm{t},r}^{-1}}{\prod\limits_{\substack{k=1\\k\neq r}}^{n} (\widehat{\omega}_{\mathrm{t},r}^{2} - \widehat{\omega}_{\mathrm{t},k}^{2})} = \begin{cases} 0, & c \neq r \\ 1, & c = r. \end{cases}$$

Now, by introducing the back-transformation for the tSOGI in transformed frame (what will be investigated in Section 3.5.2 in detail)

$$\widehat{\boldsymbol{x}}_{\mathrm{t}} := \widetilde{\boldsymbol{T}}_{\mathrm{t}}^{-1}(\boldsymbol{\omega}, \widehat{\boldsymbol{\omega}}_{\mathrm{t}}) \underline{\widehat{\boldsymbol{x}}}_{\mathrm{t}} \tag{3.157}$$

the differential equation for the angular frequency estimation can be finalized as

$$\begin{aligned} \forall t \in \mathbb{T}_i\colon \quad \tfrac{\mathrm{d}}{\mathrm{d}t}\widehat{\boldsymbol{\omega}}_{\mathrm{t}} &\overset{(3.146),(3.156)}{=} (\underline{\boldsymbol{c}}_{\mathrm{t}}^{\top}(\boldsymbol{\omega}) \underline{\widehat{\boldsymbol{x}}}_{\mathrm{t}} - y) \boldsymbol{\Omega}(\widehat{\boldsymbol{\omega}}_{\mathrm{t}}) \underline{\boldsymbol{\Gamma}}_{\mathrm{t}}(\boldsymbol{x}, \boldsymbol{\omega}) \underline{\boldsymbol{\Sigma}} \underline{\widehat{\boldsymbol{x}}}_{\mathrm{t}} \\ &\overset{(3.157)}{=} (\boldsymbol{c}^{\top} \widehat{\boldsymbol{x}}_{\mathrm{t}} - y) \underbrace{\boldsymbol{\Omega}(\widehat{\boldsymbol{\omega}}_{\mathrm{t}}) \underline{\boldsymbol{\Gamma}}_{\mathrm{t}}(\boldsymbol{x}, \boldsymbol{\omega}) \underline{\boldsymbol{\Sigma}} \widetilde{\boldsymbol{T}}_{\mathrm{t}}(\boldsymbol{\omega}, \widehat{\boldsymbol{\omega}}_{\mathrm{t}})}_{=: \widetilde{\boldsymbol{\Gamma}}_{\mathrm{t}}(\boldsymbol{x}, \boldsymbol{\omega}, \widehat{\boldsymbol{\omega}}_{\mathrm{t}}) \widetilde{\boldsymbol{\Sigma}}_{\mathrm{t}}(\boldsymbol{x}, \boldsymbol{\omega}, \widehat{\boldsymbol{\omega}}_{\mathrm{t}})} \widehat{\boldsymbol{x}}_{\mathrm{t}}, \quad \widehat{\boldsymbol{\omega}}_{\mathrm{t}}(t_i) = \widehat{\boldsymbol{\omega}}_{\mathrm{t},t_i}. \end{aligned} \tag{3.158}$$

It is called the *transformation-based Frequency Locked Loop* (tFLL) in α, β frame. Its block diagram is drawn in Figure 3.29.

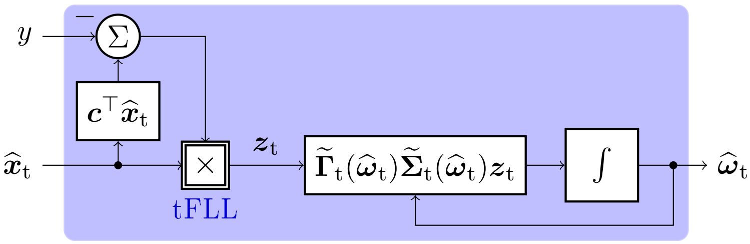

Figure 3.29: *Block diagram of the tFLL in α, β frame.*

3.5.1.2 The tFLL with offset in α, β frame

The *transformation-based Frequency Locked Loop with offset* ($\mathrm{tFLL}_{\circ}$) in α, β frame is obtained in an identical manner. It follows as

$$\forall t \in \mathbb{T}_i\colon \quad \tfrac{\mathrm{d}}{\mathrm{d}t}\widehat{\boldsymbol{\omega}}_{\mathrm{t}_\circ} = (\boldsymbol{c}_{\circ}^{\top} \widehat{\boldsymbol{x}}_{\mathrm{t}_\circ} - y) \underbrace{\boldsymbol{\Omega}(\widehat{\boldsymbol{\omega}}_{\mathrm{t}_\circ}) \underline{\boldsymbol{\Gamma}}_{\mathrm{t}_\circ}(\boldsymbol{x}_{\circ}, \boldsymbol{\omega}) \underline{\boldsymbol{\Sigma}}_{\circ} \widetilde{\boldsymbol{T}}_{\mathrm{t}_\circ}(\boldsymbol{\omega}, \widehat{\boldsymbol{\omega}}_{\mathrm{t}_\circ})}_{=: \widetilde{\boldsymbol{\Gamma}}_{\mathrm{t}_\circ}(\boldsymbol{x}_{\circ}, \boldsymbol{\omega}, \widehat{\boldsymbol{\omega}}_{\mathrm{t}_\circ}) \widetilde{\boldsymbol{\Sigma}}_{\mathrm{t}_\circ}(\boldsymbol{x}_{\circ}, \boldsymbol{\omega}, \widehat{\boldsymbol{\omega}}_{\mathrm{t}_\circ})} \widehat{\boldsymbol{x}}_{\mathrm{t}_\circ}, \quad \widehat{\boldsymbol{\omega}}_{\mathrm{t}_\circ}(t_i) = \widehat{\boldsymbol{\omega}}_{\mathrm{t}_\circ, t_i} \tag{3.159}$$

where its block diagram is similar to the one shown in Figure 3.29.

3.5.2 back-transformation: The parallelized tSOGIs in α, β frame and the parallelized tSOGIs with offset in α, β frame

This section describes the back-transformation of the parallelized tSOGIs in transformed frame and $\mathrm{tSOGI}_{\circ}$s in transformed frame from transformed coordinates to α, β coordinates. More precisely, the reverse procedure of what is shown in Sections 3.4.1.1 and 3.4.1.2 is applied to (3.116) in Section 3.5.2.1 and to (3.118) in Section 3.5.2.2.

3.5.2.1 The parallelized tSOGIs in α,β frame

According to (3.157), the back-transformation is achieved by

$$\begin{aligned}\tfrac{\mathrm{d}}{\mathrm{d}t}\widehat{\boldsymbol{x}}_{\mathrm{t}} &= \tfrac{\mathrm{d}}{\mathrm{d}t}\left[\widetilde{\boldsymbol{T}}_{\mathrm{t}}^{-1}(\boldsymbol{\omega},\widehat{\boldsymbol{\omega}}_{\mathrm{t}})\underline{\widehat{\boldsymbol{x}}}_{\mathrm{t}}\right] = \tfrac{\mathrm{d}}{\mathrm{d}t}\widetilde{\boldsymbol{T}}_{\mathrm{t}}^{-1}(\boldsymbol{\omega},\widehat{\boldsymbol{\omega}}_{\mathrm{t}})\widetilde{\boldsymbol{T}}_{\mathrm{t}}(\boldsymbol{\omega},\widehat{\boldsymbol{\omega}}_{\mathrm{t}})\widehat{\boldsymbol{x}}_{\mathrm{t}} + \widetilde{\boldsymbol{T}}_{\mathrm{t}}^{-1}(\boldsymbol{\omega},\widehat{\boldsymbol{\omega}}_{\mathrm{t}})\tfrac{\mathrm{d}}{\mathrm{d}t}\underline{\widehat{\boldsymbol{x}}}_{\mathrm{t}} \\ &\overset{(3.116)}{=} \left(\tfrac{\mathrm{d}}{\mathrm{d}t}\widetilde{\boldsymbol{T}}_{\mathrm{t}}^{-1}(\boldsymbol{\omega},\widehat{\boldsymbol{\omega}}_{\mathrm{t}}) + \widetilde{\boldsymbol{T}}_{\mathrm{t}}^{-1}(\boldsymbol{\omega},\widehat{\boldsymbol{\omega}}_{\mathrm{t}})\left(\underline{\boldsymbol{J}}(\widehat{\boldsymbol{\omega}}_{\mathrm{t}}) - \underline{\boldsymbol{l}}_{\mathrm{t}}(\boldsymbol{\omega})\underline{\boldsymbol{c}}_{\mathrm{t}}^{\top}(\boldsymbol{\omega})\right)\right)\widetilde{\boldsymbol{T}}_{\mathrm{t}}(\boldsymbol{\omega},\widehat{\boldsymbol{\omega}}_{\mathrm{t}})\widehat{\boldsymbol{x}}_{\mathrm{t}} + \widetilde{\boldsymbol{T}}_{\mathrm{t}}^{-1}(\boldsymbol{\omega},\widehat{\boldsymbol{\omega}}_{\mathrm{t}})\underline{\boldsymbol{l}}_{\mathrm{t}}(\boldsymbol{\omega})y\end{aligned} \tag{3.160}$$

with $\widehat{\boldsymbol{x}}_{\mathrm{t}}^{\top} := (\widehat{\boldsymbol{x}}_{\mathrm{t},1}^{\top}, \cdots, \widehat{\boldsymbol{x}}_{\mathrm{t},n}^{\top})$ and for all $i \in \{1,\ldots,n\}$ $\widehat{\boldsymbol{x}}_{\mathrm{t},i} := (\widehat{x}_{\mathrm{t},i}^{\alpha}, \widehat{x}_{\mathrm{t},i}^{\beta})^{\top}$. In (3.160), the transformation matrix $\boldsymbol{T}$, dependent on $\boldsymbol{\omega}$ and $\underline{\boldsymbol{c}}_{\mathrm{t}}(\boldsymbol{\omega})$, is substituted by $\widetilde{\boldsymbol{T}}_{\mathrm{t}}$ depending on $\widehat{\boldsymbol{\omega}}_{\mathrm{t}}$ and $\underline{\boldsymbol{c}}_{\mathrm{t}}(\boldsymbol{\omega})$. Next, the expressions in the α,β coordinates are introduced, which are

$$\left.\begin{array}{lrcl}
\text{(i)} & \boldsymbol{J}(\widehat{\boldsymbol{\omega}}_{\mathrm{t}}) & := & \widetilde{\boldsymbol{T}}_{\mathrm{t}}^{-1}(\boldsymbol{\omega},\widehat{\boldsymbol{\omega}}_{\mathrm{t}})\underline{\boldsymbol{J}}(\widehat{\boldsymbol{\omega}}_{\mathrm{t}})\widetilde{\boldsymbol{T}}_{\mathrm{t}}(\boldsymbol{\omega},\widehat{\boldsymbol{\omega}}_{\mathrm{t}}) = \underset{1,\ldots,n}{\mathrm{blkdiag}}(\widehat{\omega}_{\mathrm{t},i}\widetilde{\boldsymbol{J}}); \\
\text{(ii)} & \boldsymbol{c} & = & \widetilde{\boldsymbol{T}}_{\mathrm{t}}^{\top}(\boldsymbol{\omega},\widehat{\boldsymbol{\omega}}_{\mathrm{t}})\underline{\boldsymbol{c}}_{\mathrm{t}}(\boldsymbol{\omega}); \quad \text{and} \\
\text{(iii)} & \widetilde{\boldsymbol{l}}_{\mathrm{t}}(\boldsymbol{\omega},\widehat{\boldsymbol{\omega}}_{\mathrm{t}}) & := & \widetilde{\boldsymbol{T}}_{\mathrm{t}}^{-1}(\boldsymbol{\omega},\widehat{\boldsymbol{\omega}}_{\mathrm{t}})\underline{\boldsymbol{l}}_{\mathrm{t}}(\boldsymbol{\omega}) = \begin{pmatrix} \vdots \\ \dfrac{\sum_{j=1}^{n}(-1)^{j+n}\widehat{\omega}_{\mathrm{t},i}^{2j-2}\left(\frac{\underline{c}_{\mathrm{t},j}^{\alpha}(\boldsymbol{\omega})}{\underline{c}_{\mathrm{t},n}^{\beta}(\boldsymbol{\omega})}+\underline{c}_{\mathrm{t},j}^{\beta}(\boldsymbol{\omega})\right)}{\prod_{j=1, j\neq i}^{n}\left(\widehat{\omega}_{\mathrm{t},i}^{2}-\widehat{\omega}_{\mathrm{t},j}^{2}\right)} \\ \dfrac{\sum_{j=1}^{n}(-1)^{j+n}\widehat{\omega}_{\mathrm{t},i}^{2j-3}\left(\frac{\widehat{\omega}_{\mathrm{t},i}^{2}\underline{c}_{\mathrm{t},j}^{\beta}(\boldsymbol{\omega})}{\underline{c}_{\mathrm{t},n}^{\beta}(\boldsymbol{\omega})}-\underline{c}_{\mathrm{t},j}^{\alpha}(\boldsymbol{\omega})\right)}{\prod_{j=1, j\neq i}^{n}\left(\widehat{\omega}_{\mathrm{t},i}^{2}-\widehat{\omega}_{\mathrm{t},j}^{2}\right)} \\ \vdots \end{pmatrix}.
\end{array}\right\} \tag{3.161}$$

In view of the remaining term $\frac{\mathrm{d}}{\mathrm{d}t}\widetilde{\boldsymbol{T}}_{\mathrm{t}}^{-1}\widetilde{\boldsymbol{T}}_{\mathrm{t}}\widehat{\boldsymbol{x}}_{\mathrm{t}}$ in (3.161), the time derivative of $\widetilde{\boldsymbol{T}}_{\mathrm{t}}^{-1}$ is required. Thus, the time derivative of its sub matrix in the r-th row and c-th column is given by

$$\begin{aligned}
&\frac{\mathrm{d}}{\mathrm{d}t}\left[\frac{(-1)^{n+1}\sum_{j_1<j_{n-c}=1\backslash r}^{n}\prod_{k\in j}\widehat{\omega}_{\mathrm{t},k}^{2}}{\prod_{h=1, h\neq r}^{n}\left(\widehat{\omega}_{\mathrm{t},r}^{2}-\widehat{\omega}_{\mathrm{t},h}^{2}\right)}\widetilde{\boldsymbol{T}}_{\mathrm{t},r}^{-1}(\boldsymbol{\omega},\widehat{\boldsymbol{\omega}}_{\mathrm{t}})\right] \\
&= \frac{2(-1)^{n+1}\prod_{h=1, h\neq r}^{n}\left(\widehat{\omega}_{\mathrm{t},r}^{2}-\widehat{\omega}_{\mathrm{t},h}^{2}\right)\sum_{j_1<j_{n-c}=1\backslash r}^{n}\sum_{l\in j}\widehat{\omega}_{\mathrm{t},l}\frac{\mathrm{d}}{\mathrm{d}t}\widehat{\omega}_{\mathrm{t},l}\prod_{k\in j\backslash l}\widehat{\omega}_{\mathrm{t},k}^{2}}{\prod_{h=1, h\neq r}^{n}\left(\widehat{\omega}_{\mathrm{t},r}^{2}-\widehat{\omega}_{\mathrm{t},h}^{2}\right)^{2}}\widetilde{\boldsymbol{T}}_{\mathrm{t},r}^{-1}(\boldsymbol{\omega},\widehat{\boldsymbol{\omega}}_{\mathrm{t}}) \\
&- \frac{2(-1)^{n+1}\sum_{j_1<j_{n-c}=1\backslash r}^{n}\prod_{k\in j}\widehat{\omega}_{\mathrm{t},k}^{2}\sum_{l=1, l\neq r}^{n}\left(\widehat{\omega}_{\mathrm{t},r}\frac{\mathrm{d}}{\mathrm{d}t}\widehat{\omega}_{\mathrm{t},r}-\widehat{\omega}_{\mathrm{t},l}\frac{\mathrm{d}}{\mathrm{d}t}\widehat{\omega}_{\mathrm{t},l}\right)\prod_{h=1, h\neq l,r}^{n}\left(\widehat{\omega}_{\mathrm{t},r}^{2}-\widehat{\omega}_{\mathrm{t},h}^{2}\right)}{\prod_{h=1, h\neq r}^{n}\left(\widehat{\omega}_{\mathrm{t},r}^{2}-\widehat{\omega}_{\mathrm{t},h}^{2}\right)^{2}}\widetilde{\boldsymbol{T}}_{\mathrm{t},r}^{-1}(\boldsymbol{\omega},\widehat{\boldsymbol{\omega}}_{\mathrm{t}}) \\
&+ \frac{(-1)^{n+1}\sum_{j_1<j_{n-c}=1\backslash r}^{n}\prod_{k\in j}\widehat{\omega}_{\mathrm{t},k}^{2}}{\prod_{h=1, h\neq r}^{n}\left(\widehat{\omega}_{\mathrm{t},r}^{2}-\widehat{\omega}_{\mathrm{t},h}^{2}\right)}\frac{\mathrm{d}}{\mathrm{d}t}\widetilde{\boldsymbol{T}}_{\mathrm{t},r}^{-1}(\boldsymbol{\omega},\widehat{\boldsymbol{\omega}}_{\mathrm{t}})
\end{aligned}$$

$$= \frac{2(-1)^n \sum\limits_{j_1<j_{n-c}=1\backslash r}^{n} \prod\limits_{k\in j} \widehat{\omega}_{\mathrm{t},k}^2 \left(\sum\limits_{\substack{l=1\\l\neq r}}^{n} \frac{\widehat{\omega}_{\mathrm{t},r}\frac{\mathrm{d}}{\mathrm{d}t}\widehat{\omega}_{\mathrm{t},r}-\widehat{\omega}_{\mathrm{t},l}\frac{\mathrm{d}}{\mathrm{d}t}\widehat{\omega}_{\mathrm{t},l}}{\widehat{\omega}_{\mathrm{t},r}^2-\widehat{\omega}_{\mathrm{t},l}^2} - \sum\limits_{l\in j} \frac{\widehat{\omega}_{\mathrm{t},l}\frac{\mathrm{d}}{\mathrm{d}t}\widehat{\omega}_{\mathrm{t},l}}{\widehat{\omega}_{\mathrm{t},l}^2} \right)}{\prod\limits_{\substack{h=1\\h\neq r}}^{n}\left(\widehat{\omega}_{\mathrm{t},r}^2-\widehat{\omega}_{\mathrm{t},h}^2\right)} \widetilde{\boldsymbol{T}}_{\mathrm{t},r}^{-1}(\boldsymbol{\omega},\widehat{\boldsymbol{\omega}}_{\mathrm{t}})$$
$$+ \frac{(-1)^{n+1} \sum\limits_{j_1<j_{n-c}=1\backslash r}^{n} \prod\limits_{k\in j} \widehat{\omega}_{\mathrm{t},k}^2}{\prod\limits_{\substack{h=1\\h\neq r}}^{n}\left(\widehat{\omega}_{\mathrm{t},r}^2-\widehat{\omega}_{\mathrm{t},h}^2\right)} \frac{\mathrm{d}}{\mathrm{d}t}\widetilde{\boldsymbol{T}}_{\mathrm{t},r}^{-1}(\boldsymbol{\omega},\widehat{\boldsymbol{\omega}}_{\mathrm{t}}). \tag{3.162}$$

The time derivative of the transformation sub matrices is obtained as follows

$$\forall i \in \{1,\dots,n\}:$$
$$\frac{\mathrm{d}}{\mathrm{d}t}\widetilde{\boldsymbol{T}}_{\mathrm{t},i}^{-1}(\boldsymbol{\omega},\widehat{\boldsymbol{\omega}}_{\mathrm{t}}) = \frac{\mathrm{d}}{\mathrm{d}t}\widehat{\omega}_{\mathrm{t},i} \underbrace{\sum_{j=1}^{n}(-1)^j\widehat{\omega}_{\mathrm{t},i}^{2j-4}\begin{bmatrix} -(2j-2)\,\widehat{\omega}_{\mathrm{t},i}\underline{c}_{\mathrm{t},j}^{\alpha}(\boldsymbol{\omega}) & -(2j-2)\,\widehat{\omega}_{\mathrm{t},i}\underline{c}_{\mathrm{t},j}^{\beta}(\boldsymbol{\omega}) \\ -(2j-1)\,\widehat{\omega}_{\mathrm{t},i}^2\underline{c}_{\mathrm{t},j}^{\beta}(\boldsymbol{\omega}) & (2j-3)\,\underline{c}_{\mathrm{t},j}^{\alpha}(\boldsymbol{\omega}) \end{bmatrix}}_{=:\widetilde{\boldsymbol{S}}_{\mathrm{t},i}^{-1}(\boldsymbol{\omega},\widehat{\boldsymbol{\omega}}_{\mathrm{t}})}. \tag{3.163}$$

With (3.162), the matrix $\frac{\mathrm{d}}{\mathrm{d}t}\widetilde{\boldsymbol{T}}_{\mathrm{t}}^{-1}\widetilde{\boldsymbol{T}}_{\mathrm{t}}$ can be calculated, where only the sub matrix of the r-th row and c-th column is shown, as

$$\sum_{i=1}^{n}\frac{\mathrm{d}}{\mathrm{d}t}\left[\frac{(-1)^{n+1}\sum\limits_{j_1<j_{n-i}=1\backslash r}^{n}\prod\limits_{k\in j}\widehat{\omega}_{\mathrm{t},k}^2}{\prod\limits_{\substack{h=1\\h\neq r}}^{n}\left(\widehat{\omega}_{\mathrm{t},r}^2-\widehat{\omega}_{\mathrm{t},h}^2\right)}\widetilde{\boldsymbol{T}}_{\mathrm{t},r}^{-1}(\boldsymbol{\omega},\widehat{\boldsymbol{\omega}}_{\mathrm{t}})\right](-\widehat{\omega}_{\mathrm{t},c}^2)^{i-1}\widetilde{\boldsymbol{T}}_{\mathrm{t},c}(\boldsymbol{\omega},\widehat{\boldsymbol{\omega}}_{\mathrm{t}})$$
$$\overset{(3.162)}{=} \sum_{i=1}^{n}\frac{2(-1)^n\sum\limits_{j_1<j_{n-i}=1\backslash r}^{n}\prod\limits_{k\in j}\widehat{\omega}_{\mathrm{t},k}^2\sum\limits_{\substack{l=1\\l\neq r}}^{n}\frac{\widehat{\omega}_{\mathrm{t},r}\frac{\mathrm{d}}{\mathrm{d}t}\widehat{\omega}_{\mathrm{t},r}-\widehat{\omega}_{\mathrm{t},l}\frac{\mathrm{d}}{\mathrm{d}t}\widehat{\omega}_{\mathrm{t},l}}{\widehat{\omega}_{\mathrm{t},r}^2-\widehat{\omega}_{\mathrm{t},l}^2}(-\widehat{\omega}_{\mathrm{t},c}^2)^{i-1}}{\prod\limits_{\substack{h=1\\h\neq r}}^{n}\left(\widehat{\omega}_{\mathrm{t},r}^2-\widehat{\omega}_{\mathrm{t},h}^2\right)}\widetilde{\boldsymbol{T}}_{\mathrm{t},r}^{-1}(\boldsymbol{\omega},\widehat{\boldsymbol{\omega}}_{\mathrm{t}})\widetilde{\boldsymbol{T}}_{\mathrm{t},c}(\boldsymbol{\omega},\widehat{\boldsymbol{\omega}}_{\mathrm{t}})$$
$$-\sum_{i=1}^{n}\frac{2(-1)^n\sum\limits_{j_1<j_{n-i}=1\backslash r}^{n}\prod\limits_{k\in j}\widehat{\omega}_{\mathrm{t},k}^2\sum\limits_{l\in j}\frac{\widehat{\omega}_{\mathrm{t},l}\frac{\mathrm{d}}{\mathrm{d}t}\widehat{\omega}_{\mathrm{t},l}}{\widehat{\omega}_{\mathrm{t},l}^2}(-\widehat{\omega}_{\mathrm{t},c}^2)^{i-1}}{\prod\limits_{\substack{h=1\\h\neq r}}^{n}\left(\widehat{\omega}_{\mathrm{t},r}^2-\widehat{\omega}_{\mathrm{t},h}^2\right)}\widetilde{\boldsymbol{T}}_{\mathrm{t},r}^{-1}(\boldsymbol{\omega},\widehat{\boldsymbol{\omega}}_{\mathrm{t}})\widetilde{\boldsymbol{T}}_{\mathrm{t},c}(\boldsymbol{\omega},\widehat{\boldsymbol{\omega}}_{\mathrm{t}})$$
$$+\sum_{i=1}^{n}\frac{(-1)^{n+1}\sum\limits_{j_1<j_{n-i}=1\backslash r}^{n}\prod\limits_{k\in j}\widehat{\omega}_{\mathrm{t},k}^2(-\widehat{\omega}_{\mathrm{t},c}^2)^{i-1}}{\prod\limits_{\substack{h=1\\h\neq r}}^{n}\left(\widehat{\omega}_{\mathrm{t},r}^2-\widehat{\omega}_{\mathrm{t},h}^2\right)}\frac{\mathrm{d}}{\mathrm{d}t}\widetilde{\boldsymbol{T}}_{\mathrm{t},r}^{-1}(\boldsymbol{\omega},\widehat{\boldsymbol{\omega}}_{\mathrm{t}})\widetilde{\boldsymbol{T}}_{\mathrm{t},c}(\boldsymbol{\omega},\widehat{\boldsymbol{\omega}}_{\mathrm{t}})$$
$$\overset{(2.19),\,(2.20)}{=}\left(\sum_{\substack{j=1\\j\neq r}}^{n}\frac{\widehat{\omega}_{\mathrm{t},r}\frac{\mathrm{d}}{\mathrm{d}t}\widehat{\omega}_{\mathrm{t},r}-\widehat{\omega}_{\mathrm{t},j}\frac{\mathrm{d}}{\mathrm{d}t}\widehat{\omega}_{\mathrm{t},j}}{\widehat{\omega}_{\mathrm{t},r}^2-\widehat{\omega}_{\mathrm{t},j}^2}\prod_{\substack{k=1\\k\neq r}}^{n}\left(\widehat{\omega}_{\mathrm{t},k}^2-\widehat{\omega}_{\mathrm{t},c}^2\right)\right.$$
$$\left.-\sum_{\substack{j=1\\j\neq r}}^{n}\widehat{\omega}_{\mathrm{t},j}\frac{\mathrm{d}}{\mathrm{d}t}\widehat{\omega}_{\mathrm{t},j}\prod_{\substack{k=1\\k\neq r,j}}^{n}\left(\widehat{\omega}_{\mathrm{t},k}^2-\widehat{\omega}_{\mathrm{t},c}^2\right)\right)\frac{2(-1)^n}{\prod\limits_{\substack{h=1\\h\neq r}}^{n}\left(\widehat{\omega}_{\mathrm{t},r}^2-\widehat{\omega}_{\mathrm{t},h}^2\right)}\widetilde{\boldsymbol{T}}_{\mathrm{t},r}^{-1}(\boldsymbol{\omega},\widehat{\boldsymbol{\omega}}_{\mathrm{t}})\widetilde{\boldsymbol{T}}_{\mathrm{t},c}(\boldsymbol{\omega},\widehat{\boldsymbol{\omega}}_{\mathrm{t}})$$
$$+\frac{(-1)^{n+1}\prod\limits_{\substack{k=1\\k\neq r}}^{n}\left(\widehat{\omega}_{\mathrm{t},k}^2-\widehat{\omega}_{\mathrm{t},c}^2\right)}{\prod\limits_{\substack{k=1\\k\neq r}}^{n}\left(\widehat{\omega}_{\mathrm{t},r}^2-\widehat{\omega}_{\mathrm{t},k}^2\right)}\frac{\mathrm{d}}{\mathrm{d}t}\widetilde{\boldsymbol{T}}_{\mathrm{t},r}^{-1}(\boldsymbol{\omega},\widehat{\boldsymbol{\omega}}_{\mathrm{t}})\widetilde{\boldsymbol{T}}_{\mathrm{t},c}(\boldsymbol{\omega},\widehat{\boldsymbol{\omega}}_{\mathrm{t}})$$

$$
\begin{aligned}
&= \frac{2 \sum\limits_{\substack{j=1 \\ j\neq r}}^{n} \frac{\widehat{\omega}_{\mathrm{t},r} \frac{\mathrm{d}}{\mathrm{d}t}\widehat{\omega}_{\mathrm{t},r}\left(\widehat{\omega}_{\mathrm{t},j}^2-\widehat{\omega}_{\mathrm{t},c}^2\right)-\widehat{\omega}_{\mathrm{t},j}\frac{\mathrm{d}}{\mathrm{d}t}\widehat{\omega}_{\mathrm{t},j}\left(\widehat{\omega}_{\mathrm{t},r}^2-\widehat{\omega}_{\mathrm{t},c}^2\right)}{\widehat{\omega}_{\mathrm{t},r}^2-\widehat{\omega}_{\mathrm{t},j}^2} \prod\limits_{\substack{k=1 \\ k\neq r,j}}^{n}\left(\widehat{\omega}_{\mathrm{t},c}^2-\widehat{\omega}_{\mathrm{t},k}^2\right)}{\prod\limits_{\substack{k=1 \\ k\neq r}}^{n}\left(\widehat{\omega}_{\mathrm{t},r}^2-\widehat{\omega}_{\mathrm{t},k}^2\right)} \widetilde{\boldsymbol{T}}_{\mathrm{t},r}^{-1}(\boldsymbol{\omega},\widehat{\boldsymbol{\omega}}_{\mathrm{t}})\widetilde{\boldsymbol{T}}_{\mathrm{t},c}(\boldsymbol{\omega},\widehat{\boldsymbol{\omega}}_{\mathrm{t}}) \\
&+ \frac{\prod\limits_{\substack{k=1 \\ k\neq r}}^{n}\left(\widehat{\omega}_{\mathrm{t},c}^2-\widehat{\omega}_{\mathrm{t},k}^2\right)}{\prod\limits_{\substack{k=1 \\ k\neq r}}^{n}\left(\widehat{\omega}_{\mathrm{t},r}^2-\widehat{\omega}_{\mathrm{t},k}^2\right)} \frac{\mathrm{d}}{\mathrm{d}t}\widetilde{\boldsymbol{T}}_{\mathrm{t},r}^{-1}(\boldsymbol{\omega},\widehat{\boldsymbol{\omega}}_{\mathrm{t}})\widetilde{\boldsymbol{T}}_{\mathrm{t},c}(\boldsymbol{\omega},\widehat{\boldsymbol{\omega}}_{\mathrm{t}}) \\
&= \begin{cases} \frac{-2 \sum\limits_{\substack{j=1 \\ j\neq r}}^{n} \widehat{\omega}_{\mathrm{t},r}\frac{\mathrm{d}}{\mathrm{d}t}\widehat{\omega}_{\mathrm{t},r} \prod\limits_{\substack{k=1 \\ k\neq r,j}}^{n}\left(\widehat{\omega}_{\mathrm{t},c}^2-\widehat{\omega}_{\mathrm{t},k}^2\right)}{\prod\limits_{\substack{k=1 \\ k\neq r}}^{n}\left(\widehat{\omega}_{\mathrm{t},r}^2-\widehat{\omega}_{\mathrm{t},k}^2\right)} \boldsymbol{I}_2 + \frac{\mathrm{d}}{\mathrm{d}t}\widetilde{\boldsymbol{T}}_{\mathrm{t},r}^{-1}(\boldsymbol{\omega},\widehat{\boldsymbol{\omega}}_{\mathrm{t}})\widetilde{\boldsymbol{T}}_{\mathrm{t},c}(\boldsymbol{\omega},\widehat{\boldsymbol{\omega}}_{\mathrm{t}}), & r=c \\ \frac{-2\widehat{\omega}_{\mathrm{t},c}\frac{\mathrm{d}}{\mathrm{d}t}\widehat{\omega}_{\mathrm{t},c} \prod\limits_{\substack{k=1 \\ k\neq r,c}}^{n}\left(\widehat{\omega}_{\mathrm{t},c}^2-\widehat{\omega}_{\mathrm{t},k}^2\right)}{\prod\limits_{\substack{k=1 \\ k\neq r}}^{n}\left(\widehat{\omega}_{\mathrm{t},r}^2-\widehat{\omega}_{\mathrm{t},k}^2\right)} \widetilde{\boldsymbol{T}}_{\mathrm{t},r}^{-1}(\boldsymbol{\omega},\widehat{\boldsymbol{\omega}}_{\mathrm{t}})\widetilde{\boldsymbol{T}}_{\mathrm{t},c}(\boldsymbol{\omega},\widehat{\boldsymbol{\omega}}_{\mathrm{t}}), & r\neq c \end{cases} \quad (3.164) \\
&\overset{(3.163)}{=} \begin{cases} \frac{\mathrm{d}}{\mathrm{d}t}\widehat{\omega}_{\mathrm{t},r}\left(\frac{-2 \sum\limits_{\substack{j=1 \\ j\neq r}}^{n} \widehat{\omega}_{\mathrm{t},r} \prod\limits_{\substack{k=1 \\ k\neq r,j}}^{n}\left(\widehat{\omega}_{\mathrm{t},c}^2-\widehat{\omega}_{\mathrm{t},k}^2\right)}{\prod\limits_{\substack{k=1 \\ k\neq r}}^{n}\left(\widehat{\omega}_{\mathrm{t},r}^2-\widehat{\omega}_{\mathrm{t},k}^2\right)} \boldsymbol{I}_2 + \widetilde{\boldsymbol{S}}_{\mathrm{t},r}^{-1}(\boldsymbol{\omega},\widehat{\boldsymbol{\omega}}_{\mathrm{t}})\widetilde{\boldsymbol{T}}_{\mathrm{t},c}(\boldsymbol{\omega},\widehat{\boldsymbol{\omega}}_{\mathrm{t}})\right), & r=c \\ \frac{\mathrm{d}}{\mathrm{d}t}\widehat{\omega}_{\mathrm{t},c}\frac{-2\widehat{\omega}_{\mathrm{t},c} \prod\limits_{\substack{k=1 \\ k\neq r,c}}^{n}\left(\widehat{\omega}_{\mathrm{t},c}^2-\widehat{\omega}_{\mathrm{t},k}^2\right)}{\prod\limits_{\substack{k=1 \\ k\neq r}}^{n}\left(\widehat{\omega}_{\mathrm{t},r}^2-\widehat{\omega}_{\mathrm{t},k}^2\right)} \widetilde{\boldsymbol{T}}_{\mathrm{t},r}^{-1}(\boldsymbol{\omega},\widehat{\boldsymbol{\omega}}_{\mathrm{t}})\widetilde{\boldsymbol{T}}_{\mathrm{t},c}(\boldsymbol{\omega},\widehat{\boldsymbol{\omega}}_{\mathrm{t}}), & r\neq c \end{cases} \quad (3.165)
\end{aligned}
$$

Next, since the matrix $\frac{\mathrm{d}}{\mathrm{d}t}\widetilde{\boldsymbol{T}}_{\mathrm{t}}^{-1}\widetilde{\boldsymbol{T}}_{\mathrm{t}}$ is dependent on the time derivative of the estimated angular frequency vector $\widehat{\boldsymbol{\omega}}_{\mathrm{t}}$, the expression $\frac{\mathrm{d}}{\mathrm{d}t}\widetilde{\boldsymbol{T}}_{\mathrm{t}}^{-1}\widetilde{\boldsymbol{T}}_{\mathrm{t}}\widehat{\boldsymbol{x}}_{\mathrm{t}}$ must be rearranged such that

$$
\begin{aligned}
&\frac{\mathrm{d}}{\mathrm{d}t}\widetilde{\boldsymbol{T}}_{\mathrm{t}}^{-1}(\boldsymbol{\omega},\widehat{\boldsymbol{\omega}}_{\mathrm{t}})\widetilde{\boldsymbol{T}}_{\mathrm{t}}(\boldsymbol{\omega},\widehat{\boldsymbol{\omega}}_{\mathrm{t}})\widehat{\boldsymbol{x}}_{\mathrm{t}} = \widetilde{\boldsymbol{\Xi}}_{\mathrm{t}}(\widehat{\boldsymbol{x}}_{\mathrm{t}},\boldsymbol{\omega},\widehat{\boldsymbol{\omega}}_{\mathrm{t}})\frac{\mathrm{d}}{\mathrm{d}t}\widehat{\boldsymbol{\omega}}_{\mathrm{t}}, \\
&\widetilde{\boldsymbol{\Xi}}_{\mathrm{t}}(\widehat{\boldsymbol{x}}_{\mathrm{t}},\boldsymbol{\omega},\widehat{\boldsymbol{\omega}}_{\mathrm{t}}) := \begin{bmatrix} \boldsymbol{\xi}_{\mathrm{t},1,1}(\widehat{\boldsymbol{x}}_{\mathrm{t}},\boldsymbol{\omega},\widehat{\boldsymbol{\omega}}_{\mathrm{t}}) & \cdots & \boldsymbol{\xi}_{\mathrm{t},1,n}(\widehat{\boldsymbol{x}}_{\mathrm{t}},\boldsymbol{\omega},\widehat{\boldsymbol{\omega}}_{\mathrm{t}}) \\ \vdots & \ddots & \vdots \\ \boldsymbol{\xi}_{\mathrm{t},n,1}(\widehat{\boldsymbol{x}}_{\mathrm{t}},\boldsymbol{\omega},\widehat{\boldsymbol{\omega}}_{\mathrm{t}}) & \cdots & \boldsymbol{\xi}_{\mathrm{t},n,n}(\widehat{\boldsymbol{x}}_{\mathrm{t}},\boldsymbol{\omega},\widehat{\boldsymbol{\omega}}_{\mathrm{t}}) \end{bmatrix} \in \mathbb{R}^{2n\times n}. \quad (3.166)
\end{aligned}
$$

Therein, the sub vectors $\boldsymbol{\xi}_{\mathrm{t},r,c}$ are given as

$$
\boldsymbol{\xi}_{\mathrm{t},r,c}(\widehat{\boldsymbol{x}}_{\mathrm{t}},\boldsymbol{\omega},\widehat{\boldsymbol{\omega}}_{\mathrm{t}}) \overset{(3.165)}{=} \begin{cases} \left(\frac{-2 \sum\limits_{\substack{j=1 \\ j\neq r}}^{n} \widehat{\omega}_{\mathrm{t},r} \prod\limits_{\substack{k=1 \\ k\neq r,j}}^{n}\left(\widehat{\omega}_{\mathrm{t},c}^2-\widehat{\omega}_{\mathrm{t},k}^2\right)}{\prod\limits_{\substack{k=1 \\ k\neq r}}^{n}\left(\widehat{\omega}_{\mathrm{t},r}^2-\widehat{\omega}_{\mathrm{t},k}^2\right)} \boldsymbol{I}_2 + \widetilde{\boldsymbol{S}}_{\mathrm{t},r}^{-1}(\boldsymbol{\omega},\widehat{\boldsymbol{\omega}}_{\mathrm{t}})\overline{\boldsymbol{T}}_{\circ,c}(\boldsymbol{\omega},\widehat{\boldsymbol{\omega}}_{\mathrm{t}})\right)\widehat{\boldsymbol{x}}_{\mathrm{t},c}, & r=c \\ \frac{-2\widehat{\omega}_{\mathrm{t},c} \prod\limits_{\substack{k=1 \\ k\neq r,c}}^{n}\left(\widehat{\omega}_{\mathrm{t},c}^2-\widehat{\omega}_{\mathrm{t},k}^2\right)}{\prod\limits_{\substack{k=1 \\ k\neq r}}^{n}\left(\widehat{\omega}_{\mathrm{t},r}^2-\widehat{\omega}_{\mathrm{t},k}^2\right)} \overline{\boldsymbol{T}}_{\circ,r}^{-1}(\boldsymbol{\omega},\widehat{\boldsymbol{\omega}}_{\mathrm{t}})\overline{\boldsymbol{T}}_{\circ,c}(\boldsymbol{\omega},\widehat{\boldsymbol{\omega}}_{\mathrm{t}})\widehat{\boldsymbol{x}}_{\mathrm{t},c}, & r\neq c. \end{cases} \quad (3.167)
$$

Concluding, (3.160) can be rewritten as follows

$$
\forall\, t \in \mathbb{T}_i\colon \widehat{\boldsymbol{x}}_{\mathrm{t}}(t_i) \quad = \quad \widehat{\boldsymbol{x}}_{\mathrm{t},t_i},
$$

$$
\begin{aligned}
\tfrac{\mathrm{d}}{\mathrm{d}t}\widehat{\boldsymbol{x}}_{\mathrm{t}} &\overset{(3.160)}{=} \tfrac{\mathrm{d}}{\mathrm{d}t}\widetilde{\boldsymbol{T}}_{\mathrm{t}}^{-1}(\boldsymbol{\omega},\widehat{\boldsymbol{\omega}}_{\mathrm{t}})\widetilde{\boldsymbol{T}}_{\mathrm{t}}(\boldsymbol{\omega},\widehat{\boldsymbol{\omega}}_{\mathrm{t}})\widehat{\boldsymbol{x}}_{\mathrm{t}} + \widetilde{\boldsymbol{T}}_{\mathrm{t}}^{-1}(\boldsymbol{\omega},\widehat{\boldsymbol{\omega}}_{\mathrm{t}})\underline{\boldsymbol{J}}(\widehat{\boldsymbol{\omega}}_{\mathrm{t}})\widetilde{\boldsymbol{T}}_{\mathrm{t}}(\boldsymbol{\omega},\widehat{\boldsymbol{\omega}}_{\mathrm{t}})\widehat{\boldsymbol{x}}_{\mathrm{t}} \\
&\quad -\widetilde{\boldsymbol{T}}_{\mathrm{t}}^{-1}(\boldsymbol{\omega},\widehat{\boldsymbol{\omega}}_{\mathrm{t}})\underline{\boldsymbol{l}}_{\mathrm{t}}(\boldsymbol{\omega})\underline{\boldsymbol{c}}_{\mathrm{t}}^{\top}(\boldsymbol{\omega})\widetilde{\boldsymbol{T}}_{\mathrm{t}}(\boldsymbol{\omega},\widehat{\boldsymbol{\omega}}_{\mathrm{t}})\widehat{\boldsymbol{x}}_{\mathrm{t}} + \widetilde{\boldsymbol{T}}_{\mathrm{t}}^{-1}(\boldsymbol{\omega},\widehat{\boldsymbol{\omega}}_{\mathrm{t}})\underline{\boldsymbol{l}}_{\mathrm{t}}(\boldsymbol{\omega})y \\
&\overset{(3.166),\,(3.161)}{=} \widetilde{\boldsymbol{\Xi}}_{\mathrm{t}}(\widehat{\boldsymbol{x}}_{\mathrm{t}},\boldsymbol{\omega},\widehat{\boldsymbol{\omega}}_{\mathrm{t}})\tfrac{\mathrm{d}}{\mathrm{d}t}\widehat{\boldsymbol{\omega}}_{\mathrm{t}} \\
&\quad + \underbrace{\left(\boldsymbol{J}(\widehat{\boldsymbol{\omega}}_{\mathrm{t}}) - \widetilde{\boldsymbol{l}}_{\mathrm{t}}(\boldsymbol{\omega},\widehat{\boldsymbol{\omega}}_{\mathrm{t}})\boldsymbol{c}^{\top}(\boldsymbol{\omega})\right)}_{=:\,\widetilde{\boldsymbol{A}}_{\mathrm{t}}(\boldsymbol{\omega},\widehat{\boldsymbol{\omega}}_{\mathrm{t}})}\widehat{\boldsymbol{x}}_{\mathrm{t}} + \widetilde{\boldsymbol{l}}_{\mathrm{t}}(\boldsymbol{\omega},\widehat{\boldsymbol{\omega}}_{\mathrm{t}})y \\
&\overset{(3.158)}{=} \left(\widetilde{\boldsymbol{A}}_{\mathrm{t}}(\boldsymbol{\omega},\widehat{\boldsymbol{\omega}}_{\mathrm{t}}) + \widetilde{\boldsymbol{\Xi}}_{\mathrm{t}}(\widehat{\boldsymbol{x}}_{\mathrm{t}},\boldsymbol{\omega},\widehat{\boldsymbol{\omega}}_{\mathrm{t}})\widetilde{\boldsymbol{\Gamma}}_{\mathrm{t}}(\boldsymbol{x},\boldsymbol{\omega},\widehat{\boldsymbol{\omega}}_{\mathrm{t}})\widetilde{\boldsymbol{\Sigma}}_{\mathrm{t}}(\boldsymbol{x},\boldsymbol{\omega},\widehat{\boldsymbol{\omega}}_{\mathrm{t}})\widehat{\boldsymbol{x}}_{\mathrm{t}}\boldsymbol{c}^{\top}\right)\widehat{\boldsymbol{x}}_{\mathrm{t}} \\
&\quad + \left(\widetilde{\boldsymbol{l}}_{\mathrm{t}}(\boldsymbol{\omega},\widehat{\boldsymbol{\omega}}_{\mathrm{t}}) - \widetilde{\boldsymbol{\Xi}}_{\mathrm{t}}(\widehat{\boldsymbol{x}}_{\mathrm{t}},\boldsymbol{\omega},\widehat{\boldsymbol{\omega}}_{\mathrm{t}})\widetilde{\boldsymbol{\Gamma}}_{\mathrm{t}}(\boldsymbol{x},\boldsymbol{\omega},\widehat{\boldsymbol{\omega}}_{\mathrm{t}})\widetilde{\boldsymbol{\Sigma}}_{\mathrm{t}}(\boldsymbol{x},\boldsymbol{\omega},\widehat{\boldsymbol{\omega}}_{\mathrm{t}})\widehat{\boldsymbol{x}}_{\mathrm{t}}\right)y, \qquad (3.168) \\
\widehat{y}_{\mathrm{t}} &= \underline{\boldsymbol{c}}_{\mathrm{t}}^{\top}(\boldsymbol{\omega})\widetilde{\boldsymbol{T}}_{\mathrm{t}}(\boldsymbol{\omega},\widehat{\boldsymbol{\omega}}_{\mathrm{t}})\widehat{\boldsymbol{x}}_{\mathrm{t}} = \boldsymbol{c}^{\top}\widehat{\boldsymbol{x}}_{\mathrm{t}}.
\end{aligned}
$$

The so called parallelized *transformation-based Second Order Generalized Integrators* (tSOGI) in α,β frame and j-th tSOGI in α,β frame are illustrated in Figure 3.30.

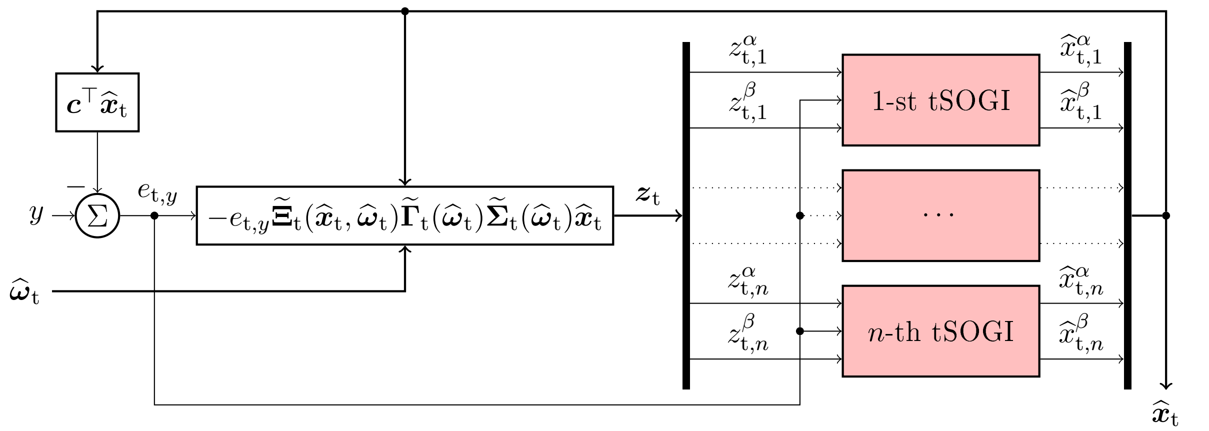

(a) *Block diagram of the parallelized tSOGIs in α,β frame.*

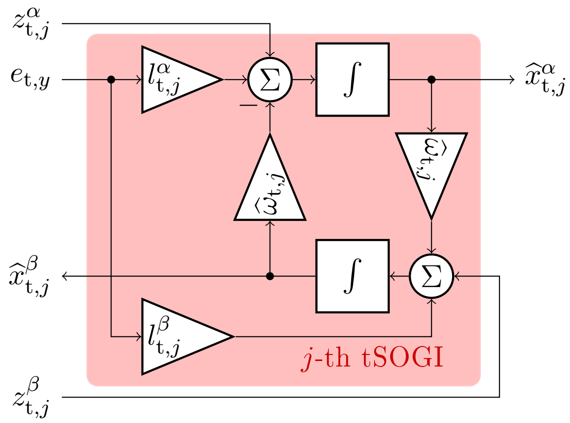

(b) *Construction of the j-th tSOGI in α,β frame.*

Figure 3.30: *(a): The parallelized structure of tSOGIs in α,β frame and (b): the j-th tSOGI in α,β frame for estimating amplitude and phase of the j-th component.*

3.5.2.2 The parallelized tSOGIs with offset in α, β frame

In view of (3.107), the back-transformation of the parallelized tSOGI$_\circ$s in transformed frame is given by

$$\begin{aligned}\tfrac{\mathrm{d}}{\mathrm{d}t}\widehat{\boldsymbol{x}}_{\mathrm{t}_\circ} = \tfrac{\mathrm{d}}{\mathrm{d}t}\left[\widetilde{\boldsymbol{T}}_{\mathrm{t}_\circ}^{-1}(\boldsymbol{\omega},\widehat{\boldsymbol{\omega}}_{\mathrm{t}_\circ})\widehat{\underline{\boldsymbol{x}}}_{\mathrm{t}_\circ}\right] &\overset{(3.118)}{=} \left(\tfrac{\mathrm{d}}{\mathrm{d}t}\widetilde{\boldsymbol{T}}_{\mathrm{t}_\circ}^{-1}(\boldsymbol{\omega},\widehat{\boldsymbol{\omega}}_{\mathrm{t}_\circ})\right.\\ &\left.+\widetilde{\boldsymbol{T}}_{\mathrm{t}_\circ}^{-1}(\boldsymbol{\omega},\widehat{\boldsymbol{\omega}}_{\mathrm{t}_\circ})\left(\underline{\boldsymbol{J}}_\circ(\widehat{\boldsymbol{\omega}}_{\mathrm{t}_\circ}) - \underline{\boldsymbol{l}}_{\mathrm{t}_\circ}(\boldsymbol{\omega})\underline{\boldsymbol{c}}_{\mathrm{t}_\circ}^\top(\boldsymbol{\omega})\right)\right)\widetilde{\boldsymbol{T}}_{\mathrm{t}_\circ}(\boldsymbol{\omega},\widehat{\boldsymbol{\omega}}_{\mathrm{t}_\circ})\widehat{\boldsymbol{x}}_{\mathrm{t}_\circ} + \widetilde{\boldsymbol{T}}_{\mathrm{t}_\circ}^{-1}(\boldsymbol{\omega},\widehat{\boldsymbol{\omega}}_{\mathrm{t}_\circ})\underline{\boldsymbol{l}}_{\mathrm{t}_\circ}(\boldsymbol{\omega})y \end{aligned} \tag{3.169}$$

with $\widehat{\boldsymbol{x}}_{\mathrm{t}_\circ}^\top := (\widehat{x}_{\mathrm{t}_\circ,0}, \widehat{\boldsymbol{x}}_{\mathrm{t}_\circ,1}, \cdots, \widehat{\boldsymbol{x}}_{\mathrm{t}_\circ,n})$ and $\widehat{\boldsymbol{x}}_{\mathrm{t}_\circ,i} := (\widehat{x}_{\mathrm{t}_\circ,i}^\alpha, \widehat{x}_{\mathrm{t}_\circ,i}^\beta)^\top$. Introduce

$$\left.\begin{array}{rrcl} \text{(i)} & \boldsymbol{J}_\circ(\widehat{\boldsymbol{\omega}}_{\mathrm{t}_\circ}) & := & \widetilde{\boldsymbol{T}}_{\mathrm{t}_\circ}^{-1}(\boldsymbol{\omega},\widehat{\boldsymbol{\omega}}_{\mathrm{t}_\circ})\underline{\boldsymbol{J}}_\circ(\widehat{\boldsymbol{\omega}}_{\mathrm{t}_\circ})\widetilde{\boldsymbol{T}}_{\mathrm{t}_\circ}(\boldsymbol{\omega},\widehat{\boldsymbol{\omega}}_{\mathrm{t}_\circ}) = \operatorname{blkdiag}\big(0, \boldsymbol{J}_\circ(\widehat{\boldsymbol{\omega}}_{\mathrm{t}_\circ})\big); \\ \text{(ii)} & \boldsymbol{c}_\circ & = & \widetilde{\boldsymbol{T}}_{\mathrm{t}_\circ}^\top(\boldsymbol{\omega},\widehat{\boldsymbol{\omega}}_{\mathrm{t}_\circ})\underline{\boldsymbol{c}}_{\mathrm{t}_\circ}(\boldsymbol{\omega}); \quad \text{and} \\ \text{(iii)} & \widetilde{\boldsymbol{l}}_{\mathrm{t}_\circ}(\boldsymbol{\omega},\widehat{\boldsymbol{\omega}}_{\mathrm{t}_\circ}) & := & \widetilde{\boldsymbol{T}}_{\mathrm{t}_\circ}^{-1}(\boldsymbol{\omega},\widehat{\boldsymbol{\omega}}_{\mathrm{t}_\circ})\underline{\boldsymbol{l}}_{\mathrm{t}_\circ}(\boldsymbol{\omega}) \\ & & = & \begin{pmatrix} \dfrac{\underline{c}_{\mathrm{t}_\circ,0}(\boldsymbol{\omega})}{\prod_{k=1}^n \widehat{\omega}_{\mathrm{t}_\circ,k}^2} \\ \vdots \\ \dfrac{(-1)^n\frac{\underline{c}_{\mathrm{t}_\circ,0}(\boldsymbol{\omega})}{\widehat{\omega}_{\mathrm{t}_\circ,i}^2} + \sum_{j=1}^n (-1)^{n+j}\widehat{\omega}_{\mathrm{t}_\circ,i}^{2j-2}\left(\frac{\underline{c}_{\mathrm{t}_\circ,j}^\alpha(\boldsymbol{\omega})}{\underline{c}_{\mathrm{t}_\circ,n}^\beta(\boldsymbol{\omega})} + \underline{c}_{\mathrm{t}_\circ,j}^\beta(\boldsymbol{\omega})\right)}{\prod_{\substack{k=1\\k\neq i}}^n\left(\widehat{\omega}_{\mathrm{t}_\circ,i}^2 - \widehat{\omega}_{\mathrm{t}_\circ,k}^2\right)} \\ \dfrac{\frac{(-1)^n\underline{c}_{\mathrm{t}_\circ,0}(\boldsymbol{\omega})}{\widehat{\omega}_{\mathrm{t}_\circ,i}\underline{c}_{\mathrm{t}_\circ,n}^\beta(\boldsymbol{\omega})} + \sum_{j=1}^n (-1)^{n+j}\widehat{\omega}_{\mathrm{t}_\circ,i}^{2j-3}\left(\frac{\widehat{\omega}_{\mathrm{t}_\circ,i}^2\underline{c}_{\mathrm{t}_\circ,j}^\beta(\boldsymbol{\omega})}{\underline{c}_{\mathrm{t}_\circ,n}^\beta(\boldsymbol{\omega})} - \underline{c}_{\mathrm{t}_\circ,j}^\alpha(\boldsymbol{\omega})\right)}{\prod_{\substack{k=1\\k\neq i}}^n\left(\widehat{\omega}_{\mathrm{t}_\circ,i}^2 - \widehat{\omega}_{\mathrm{t}_\circ,k}^2\right)} \\ \vdots \end{pmatrix}. \end{array}\right\} \tag{3.170}$$

Further, the time derivative of $\widetilde{\boldsymbol{T}}_{\mathrm{t}_\circ}^{-1}$ is required and given as

$$\tfrac{\mathrm{d}}{\mathrm{d}t}\widetilde{\boldsymbol{T}}_{\mathrm{t}_\circ}^{-1}(\boldsymbol{\omega},\widehat{\boldsymbol{\omega}}_{\mathrm{t}_\circ}) \overset{(3.109)}{=} \begin{bmatrix} 0 & -\underline{c}_{\mathrm{t}_\circ,0}(\boldsymbol{\omega})\boldsymbol{i}_{1,2n}^\top\tfrac{\mathrm{d}}{\mathrm{d}t}\left[\overline{\widetilde{\boldsymbol{T}}}_{\mathrm{t}_\circ}(\boldsymbol{\omega},\widehat{\boldsymbol{\omega}}_{\mathrm{t}_\circ})\boldsymbol{J}^{-1}(\widehat{\boldsymbol{\omega}}_{\mathrm{t}_\circ})\overline{\widetilde{\boldsymbol{T}}}_{\mathrm{t}_\circ}^{-1}(\boldsymbol{\omega},\widehat{\boldsymbol{\omega}}_{\mathrm{t}_\circ})\right] \\ \boldsymbol{0}_{2n} & \tfrac{\mathrm{d}}{\mathrm{d}t}\overline{\widetilde{\boldsymbol{T}}}_{\mathrm{t}_\circ}^{-1}(\boldsymbol{\omega},\widehat{\boldsymbol{\omega}}_{\mathrm{t}_\circ}) \end{bmatrix}. \tag{3.171}$$

The time derivative of $\overline{\widetilde{\boldsymbol{T}}}_{\mathrm{t}_\circ}^{-1}$ is obtained in the same manner as for the parallelized tSOGIs in α, β frame shown in (3.165) but with

$$\begin{aligned}\forall\, i \in \{1,\dots,n\}: \quad \tfrac{\mathrm{d}}{\mathrm{d}t}\overline{\widetilde{\boldsymbol{T}}}_{\mathrm{t}_\circ} i^{-1}(\boldsymbol{\omega},\widehat{\boldsymbol{\omega}}_{\mathrm{t}_\circ}) &= \tfrac{\mathrm{d}}{\mathrm{d}t}\widehat{\omega}_{\mathrm{t}_\circ,i}\left(\begin{bmatrix} 0 & \frac{2\underline{c}_{\mathrm{t}_\circ,0}(\boldsymbol{\omega})}{\widehat{\omega}_{\mathrm{t}_\circ,i}^3} \\ \frac{\underline{c}_{\mathrm{t}_\circ,0}(\boldsymbol{\omega})}{\widehat{\omega}_{\mathrm{t}_\circ,i}^2} & 0 \end{bmatrix}\right.\\ \left. - \sum_{j=1}^n(-1)^j\widehat{\omega}_{\mathrm{t}_\circ,i}^{2j-4}\begin{bmatrix} (2j-2)\,\widehat{\omega}_{\mathrm{t}_\circ,i}\underline{c}_{\mathrm{t}_\circ,j}^\alpha(\boldsymbol{\omega}) & (2j-2)\,\widehat{\omega}_{\mathrm{t}_\circ,i}\underline{c}_{\mathrm{t}_\circ,j}^\beta(\boldsymbol{\omega}) \\ (2j-1)\,\widehat{\omega}_{\mathrm{t}_\circ,i}^2\underline{c}_{\mathrm{t}_\circ,j}^\beta(\boldsymbol{\omega}) & -(2j-3)\,\underline{c}_{\mathrm{t}_\circ,j}^\alpha(\boldsymbol{\omega}) \end{bmatrix}\right) &=: \tfrac{\mathrm{d}}{\mathrm{d}t}\widehat{\omega}_{\mathrm{t}_\circ,i}\widetilde{\boldsymbol{S}}_{\mathrm{t}_\circ,i}^{-1}(\boldsymbol{\omega},\widehat{\boldsymbol{\omega}}_{\mathrm{t}_\circ}). \end{aligned} \tag{3.172}$$

Next, the calculation of the product

$$\tfrac{\mathrm{d}}{\mathrm{d}t}\widetilde{\boldsymbol{T}}_{\mathrm{t}_\circ}^{-1}(\boldsymbol{\omega},\widehat{\boldsymbol{\omega}}_{\mathrm{t}_\circ})\widetilde{\boldsymbol{T}}_{\mathrm{t}_\circ}(\boldsymbol{\omega},\widehat{\boldsymbol{\omega}}_{\mathrm{t}_\circ}) = \begin{bmatrix} 0 & -\underline{c}_{\mathrm{t}_\circ,0}(\boldsymbol{\omega})\boldsymbol{i}_{1,2n}^\top\tfrac{\mathrm{d}}{\mathrm{d}t}\left[\overline{\widetilde{\boldsymbol{T}}}_{\mathrm{t}_\circ}(\boldsymbol{\omega},\widehat{\boldsymbol{\omega}}_{\mathrm{t}_\circ})\boldsymbol{J}^{-1}(\widehat{\boldsymbol{\omega}}_{\mathrm{t}_\circ})\overline{\widetilde{\boldsymbol{T}}}_{\mathrm{t}_\circ}^{-1}(\boldsymbol{\omega},\widehat{\boldsymbol{\omega}}_{\mathrm{t}_\circ})\right]\overline{\widetilde{\boldsymbol{T}}}_{\mathrm{t}_\circ}(\boldsymbol{\omega},\widehat{\boldsymbol{\omega}}_{\mathrm{t}_\circ}) \\ \boldsymbol{0}_{2n} & \tfrac{\mathrm{d}}{\mathrm{d}t}\overline{\widetilde{\boldsymbol{T}}}_{\mathrm{t}_\circ}^{-1}(\boldsymbol{\omega},\widehat{\boldsymbol{\omega}}_{\mathrm{t}_\circ})\overline{\widetilde{\boldsymbol{T}}}_{\mathrm{t}_\circ}(\boldsymbol{\omega},\widehat{\boldsymbol{\omega}}_{\mathrm{t}_\circ}) \end{bmatrix}$$

is required wherein the south-eastern sub matrix $\frac{\mathrm{d}}{\mathrm{d}t}\widetilde{\widetilde{\boldsymbol{T}}}_{\mathrm{t}_\circ}^{-1}\widetilde{\widetilde{\boldsymbol{T}}}_{\mathrm{t}_\circ}$ is obtained in a similar manner as shown in (3.165). Hence, the vector $-\underline{c}_{\mathrm{t}_\circ,0}\boldsymbol{i}_{1,2n}^\top\frac{\mathrm{d}}{\mathrm{d}t}\left[\widetilde{\widetilde{\boldsymbol{T}}}_{\mathrm{t}_\circ}\boldsymbol{J}^{-1}\widetilde{\widetilde{\boldsymbol{T}}}_{\mathrm{t}_\circ}^{-1}\right]\widetilde{\widetilde{\boldsymbol{T}}}_{\mathrm{t}_\circ}$ is the only unknown expression. Its c-th sub vector follows as

$$
\begin{aligned}
&-\sum_{h=1}^{n}\underline{c}_{\mathrm{t}_\circ,0}(\boldsymbol{\omega})\boldsymbol{i}_{1,2}^\top\frac{\mathrm{d}}{\mathrm{d}t}\left[\sum_{i=1}^{n}\frac{(-1)^{n+1}\sum\limits_{j_1<j_{n-h}=1\setminus i}^{n}\prod\limits_{k\in j}\widehat{\omega}_{\mathrm{t}_\circ,k}^2\widetilde{\widetilde{\boldsymbol{T}}}_{\mathrm{t}_\circ,i}(\boldsymbol{\omega},\widehat{\boldsymbol{\omega}}_{\mathrm{t}_\circ})\widetilde{\boldsymbol{J}}^{-1}(\widehat{\boldsymbol{\omega}}_{\mathrm{t}_\circ})\widetilde{\widetilde{\boldsymbol{T}}}_{\mathrm{t}_\circ,i}^{-1}(\boldsymbol{\omega},\widehat{\boldsymbol{\omega}}_{\mathrm{t}_\circ})}{\widehat{\omega}_{\mathrm{t}_\circ,i}\prod\limits_{\substack{k=1\\k\neq i}}^{n}(\widehat{\omega}_{\mathrm{t}_\circ,i}^2-\widehat{\omega}_{\mathrm{t}_\circ,k}^2)}\right]\\
&\cdot(-\widehat{\omega}_{\mathrm{t}_\circ,c}^2)^{h-1}\widetilde{\widetilde{\boldsymbol{T}}}_{\mathrm{t}_\circ,c}(\boldsymbol{\omega},\widehat{\boldsymbol{\omega}}_{\mathrm{t}_\circ})\\
\overset{(3.3),(3.111)}{=}&\sum_{h=1}^{n}\underline{c}_{\mathrm{t}_\circ,0}(\boldsymbol{\omega})\frac{\mathrm{d}}{\mathrm{d}t}\left[\sum_{i=1}^{n}\frac{(-1)^{n+1}\sum\limits_{j_1<j_{n-h}=1\setminus i}^{n}\prod\limits_{k\in j}\widehat{\omega}_{\mathrm{t}_\circ,k}^2}{\widehat{\omega}_{\mathrm{t}_\circ,i}^2\prod\limits_{\substack{k=1\\k\neq i}}^{n}(\widehat{\omega}_{\mathrm{t}_\circ,i}^2-\widehat{\omega}_{\mathrm{t}_\circ,k}^2)}\boldsymbol{i}_{2,2}^\top\right](-\widehat{\omega}_{\mathrm{t}_\circ,c}^2)^{h-1}\widetilde{\widetilde{\boldsymbol{T}}}_{\mathrm{t}_\circ,c}(\boldsymbol{\omega},\widehat{\boldsymbol{\omega}}_{\mathrm{t}_\circ})\\
\overset{(3.162)}{=}&\sum_{h=1}^{n}\underline{c}_{\mathrm{t}_\circ,0}(\boldsymbol{\omega})\sum_{i=1}^{n}\frac{2(-1)^{n}\sum\limits_{j_1<j_{n-h}=1\setminus i}^{n}\prod\limits_{k\in j}\widehat{\omega}_{\mathrm{t}_\circ,k}^2\sum\limits_{\substack{l=1\\l\neq i}}^{n}\frac{\widehat{\omega}_{\mathrm{t}_\circ,i}\frac{\mathrm{d}}{\mathrm{d}t}\widehat{\omega}_{\mathrm{t}_\circ,i}-\widehat{\omega}_{\mathrm{t}_\circ,l}\frac{\mathrm{d}}{\mathrm{d}t}\widehat{\omega}_{\mathrm{t}_\circ,l}}{\widehat{\omega}_{\mathrm{t}_\circ,i}^2-\widehat{\omega}_{\mathrm{t}_\circ,l}^2}}{\widehat{\omega}_{\mathrm{t}_\circ,i}^2\prod\limits_{\substack{k=1\\k\neq i}}^{n}(\widehat{\omega}_{\mathrm{t}_\circ,i}^2-\widehat{\omega}_{\mathrm{t}_\circ,k}^2)}\boldsymbol{i}_{2,2}^\top(-\widehat{\omega}_{\mathrm{t}_\circ,c}^2)^{h-1}\widetilde{\widetilde{\boldsymbol{T}}}_{\mathrm{t}_\circ,c}(\boldsymbol{\omega},\widehat{\boldsymbol{\omega}}_{\mathrm{t}_\circ})\\
&-\sum_{h=1}^{n}\underline{c}_{\mathrm{t}_\circ,0}(\boldsymbol{\omega})\sum_{i=1}^{n}\frac{2(-1)^{n}\sum\limits_{j_1<j_{n-h}=1\setminus i}^{n}\prod\limits_{k\in j}\widehat{\omega}_{\mathrm{t}_\circ,k}^2\sum\limits_{j\in j}\frac{\frac{\mathrm{d}}{\mathrm{d}t}\widehat{\omega}_{\mathrm{t}_\circ,l}}{\widehat{\omega}_{\mathrm{t}_\circ,l}}}{\widehat{\omega}_{\mathrm{t}_\circ,i}^2\prod\limits_{\substack{k=1\\k\neq i}}^{n}(\widehat{\omega}_{\mathrm{t}_\circ,i}^2-\widehat{\omega}_{\mathrm{t}_\circ,k}^2)}\boldsymbol{i}_{2,2}^\top(-\widehat{\omega}_{\mathrm{t}_\circ,c}^2)^{h-1}\widetilde{\widetilde{\boldsymbol{T}}}_{\mathrm{t}_\circ,c}(\boldsymbol{\omega},\widehat{\boldsymbol{\omega}}_{\mathrm{t}_\circ})\\
&+\sum_{h=1}^{n}\underline{c}_{\mathrm{t}_\circ,0}(\boldsymbol{\omega})\sum_{i=1}^{n}\frac{2(-1)^{n}\frac{\mathrm{d}}{\mathrm{d}t}\widehat{\omega}_{\mathrm{t}_\circ,i}\sum\limits_{j_1<j_{n-h}=1\setminus i}^{n}\prod\limits_{k\in j}\widehat{\omega}_{\mathrm{t}_\circ,k}^2}{\widehat{\omega}_{\mathrm{t}_\circ,i}^3\prod\limits_{\substack{k=1\\k\neq i}}^{n}(\widehat{\omega}_{\mathrm{t}_\circ,i}^2-\widehat{\omega}_{\mathrm{t}_\circ,k}^2)}\boldsymbol{i}_{2,2}^\top(-\widehat{\omega}_{\mathrm{t}_\circ,c}^2)^{h-1}\widetilde{\widetilde{\boldsymbol{T}}}_{\mathrm{t}_\circ,c}(\boldsymbol{\omega},\widehat{\boldsymbol{\omega}}_{\mathrm{t}_\circ})\\
\overset{(2.19),(2.20)}{=}&\underline{c}_{\mathrm{t}_\circ,0}(\boldsymbol{\omega})\sum_{i=1}^{n}\frac{2(-1)^{n}\prod\limits_{\substack{h=1\\h\neq i}}^{n}(\widehat{\omega}_{\mathrm{t}_\circ,h}^2-\widehat{\omega}_{\mathrm{t}_\circ,c}^2)\sum\limits_{\substack{l=1\\l\neq i}}^{n}\frac{\widehat{\omega}_{\mathrm{t}_\circ,i}\frac{\mathrm{d}}{\mathrm{d}t}\widehat{\omega}_{\mathrm{t}_\circ,i}-\widehat{\omega}_{\mathrm{t}_\circ,l}\frac{\mathrm{d}}{\mathrm{d}t}\widehat{\omega}_{\mathrm{t}_\circ,l}}{\widehat{\omega}_{\mathrm{t}_\circ,i}^2-\widehat{\omega}_{\mathrm{t}_\circ,l}^2}}{\widehat{\omega}_{\mathrm{t}_\circ,i}^2\prod\limits_{\substack{k=1\\k\neq i}}^{n}(\widehat{\omega}_{\mathrm{t}_\circ,i}^2-\widehat{\omega}_{\mathrm{t}_\circ,k}^2)}\boldsymbol{i}_{2,2}^\top\widetilde{\widetilde{\boldsymbol{T}}}_{\mathrm{t}_\circ,c}(\boldsymbol{\omega},\widehat{\boldsymbol{\omega}}_{\mathrm{t}_\circ})\\
&-\underline{c}_{\mathrm{t}_\circ,0}(\boldsymbol{\omega})\sum_{i=1}^{n}\frac{2(-1)^{n}\sum\limits_{\substack{j=1\\j\neq i}}^{n}\widehat{\omega}_{\mathrm{t}_\circ,j}\frac{\mathrm{d}}{\mathrm{d}t}\widehat{\omega}_{\mathrm{t}_\circ,j}\prod\limits_{\substack{k=1\\k\neq i,j}}(\widehat{\omega}_{\mathrm{t}_\circ,k}^2-\widehat{\omega}_{\mathrm{t}_\circ,c}^2)}{\widehat{\omega}_{\mathrm{t}_\circ,i}^2\prod\limits_{\substack{k=1\\k\neq i}}^{n}(\widehat{\omega}_{\mathrm{t}_\circ,i}^2-\widehat{\omega}_{\mathrm{t}_\circ,k}^2)}\boldsymbol{i}_{2,2}^\top\widetilde{\widetilde{\boldsymbol{T}}}_{\mathrm{t}_\circ,c}(\boldsymbol{\omega},\widehat{\boldsymbol{\omega}}_{\mathrm{t}_\circ})\\
&+\underline{c}_{\mathrm{t}_\circ,0}(\boldsymbol{\omega})\sum_{i=1}^{n}\frac{2(-1)^{n}\frac{\mathrm{d}}{\mathrm{d}t}\widehat{\omega}_{\mathrm{t}_\circ,i}\prod\limits_{\substack{h=1\\h\neq i}}(\widehat{\omega}_{\mathrm{t}_\circ,h}^2-\widehat{\omega}_{\mathrm{t}_\circ,c}^2)}{\widehat{\omega}_{\mathrm{t}_\circ,i}^3\prod\limits_{\substack{k=1\\k\neq i}}^{n}(\widehat{\omega}_{\mathrm{t}_\circ,i}^2-\widehat{\omega}_{\mathrm{t}_\circ,k}^2)}\boldsymbol{i}_{2,2}^\top\widetilde{\widetilde{\boldsymbol{T}}}_{\mathrm{t}_\circ,c}(\boldsymbol{\omega},\widehat{\boldsymbol{\omega}}_{\mathrm{t}_\circ})\\
=&\underline{c}_{\mathrm{t}_\circ,0}(\boldsymbol{\omega})\frac{2(-1)^{n}\prod\limits_{\substack{h=1\\h\neq c}}^{n}(\widehat{\omega}_{\mathrm{t}_\circ,h}^2-\widehat{\omega}_{\mathrm{t}_\circ,c}^2)\sum\limits_{\substack{l=1\\l\neq c}}^{n}\frac{\widehat{\omega}_{\mathrm{t}_\circ,c}\frac{\mathrm{d}}{\mathrm{d}t}\widehat{\omega}_{\mathrm{t}_\circ,c}-\widehat{\omega}_{\mathrm{t}_\circ,l}\frac{\mathrm{d}}{\mathrm{d}t}\widehat{\omega}_{\mathrm{t}_\circ,l}}{\widehat{\omega}_{\mathrm{t}_\circ,c}^2-\widehat{\omega}_{\mathrm{t}_\circ,l}^2}}{\widehat{\omega}_{\mathrm{t}_\circ,c}^2\prod\limits_{\substack{k=1\\k\neq c}}^{n}(\widehat{\omega}_{\mathrm{t}_\circ,c}^2-\widehat{\omega}_{\mathrm{t}_\circ,k}^2)}\boldsymbol{i}_{2,2}^\top\widetilde{\widetilde{\boldsymbol{T}}}_{\mathrm{t}_\circ,c}(\boldsymbol{\omega},\widehat{\boldsymbol{\omega}}_{\mathrm{t}_\circ})\\
&-\underline{c}_{\mathrm{t}_\circ,0}(\boldsymbol{\omega})\frac{2(-1)^{n}\sum\limits_{\substack{j=1\\j\neq c}}^{n}\widehat{\omega}_{\mathrm{t}_\circ,j}\frac{\mathrm{d}}{\mathrm{d}t}\widehat{\omega}_{\mathrm{t}_\circ,j}\prod\limits_{\substack{k=1\\k\neq c,j}}(\widehat{\omega}_{\mathrm{t}_\circ,k}^2-\widehat{\omega}_{\mathrm{t}_\circ,c}^2)}{\widehat{\omega}_{\mathrm{t}_\circ,c}^2\prod\limits_{\substack{k=1\\k\neq c}}^{n}(\widehat{\omega}_{\mathrm{t}_\circ,c}^2-\widehat{\omega}_{\mathrm{t}_\circ,k}^2)}\boldsymbol{i}_{2,2}^\top\widetilde{\widetilde{\boldsymbol{T}}}_{\mathrm{t}_\circ,c}(\boldsymbol{\omega},\widehat{\boldsymbol{\omega}}_{\mathrm{t}_\circ})
\end{aligned}
$$

$$
\begin{aligned}
&-\underline{c}_{\mathrm{t_o},0}(\boldsymbol{\omega})\sum_{\substack{i=1\\i\neq c}}^{n}\frac{2(-1)^n\widehat{\omega}_{\mathrm{t_o},c}\frac{\mathrm{d}}{\mathrm{d}t}\widehat{\omega}_{\mathrm{t_o},c}\prod\limits_{\substack{k=1\\k\neq c,i}}(\widehat{\omega}^2_{\mathrm{t_o},k}-\widehat{\omega}^2_{\mathrm{t_o},c})}{\widehat{\omega}^2_{\mathrm{t_o},i}\prod\limits_{\substack{k=1\\k\neq i}}^{n}(\widehat{\omega}^2_{\mathrm{t_o},i}-\widehat{\omega}^2_{\mathrm{t_o},k})}\boldsymbol{i}_{2,2}^\top\widetilde{\overline{\boldsymbol{T}}}_{\mathrm{t_o},c}(\boldsymbol{\omega},\widehat{\boldsymbol{\omega}}_{\mathrm{t_o}})-\underline{c}_{\mathrm{t_o},0}(\boldsymbol{\omega})\frac{2\frac{\mathrm{d}}{\mathrm{d}t}\widehat{\omega}_{\mathrm{t_o},c}}{\widehat{\omega}^3_{\mathrm{t_o},c}}\boldsymbol{i}_{2,2}^\top\widetilde{\overline{\boldsymbol{T}}}_{\mathrm{t_o},c}(\boldsymbol{\omega},\widehat{\boldsymbol{\omega}}_{\mathrm{t_o}})\\
=&-\underline{c}_{\mathrm{t_o},0}(\boldsymbol{\omega})\frac{2(-1)^n\sum\limits_{\substack{l=1\\l\neq c}}^{n}\widehat{\omega}_{\mathrm{t_o},c}\frac{\mathrm{d}}{\mathrm{d}t}\widehat{\omega}_{\mathrm{t_o},c}\prod\limits_{\substack{k=1\\k\neq c,l}}(\widehat{\omega}^2_{\mathrm{t_o},k}-\widehat{\omega}^2_{\mathrm{t_o},c})}{\widehat{\omega}^2_{\mathrm{t_o},c}\prod\limits_{\substack{k=1\\k\neq c}}^{n}(\widehat{\omega}^2_{\mathrm{t_o},c}-\widehat{\omega}^2_{\mathrm{t_o},k})}\boldsymbol{i}_{2,2}^\top\widetilde{\overline{\boldsymbol{T}}}_{\mathrm{t_o},c}(\boldsymbol{\omega},\widehat{\boldsymbol{\omega}}_{\mathrm{t_o}})\\
&-\underline{c}_{\mathrm{t_o},0}(\boldsymbol{\omega})\sum_{\substack{i=1\\i\neq c}}^{n}\frac{2(-1)^n\widehat{\omega}_{\mathrm{t_o},c}\frac{\mathrm{d}}{\mathrm{d}t}\widehat{\omega}_{\mathrm{t_o},c}\prod\limits_{\substack{k=1\\k\neq c,i}}(\widehat{\omega}^2_{\mathrm{t_o},k}-\widehat{\omega}^2_{\mathrm{t_o},c})}{\widehat{\omega}^2_{\mathrm{t_o},i}\prod\limits_{\substack{k=1\\k\neq i}}^{n}(\widehat{\omega}^2_{\mathrm{t_o},i}-\widehat{\omega}^2_{\mathrm{t_o},k})}\boldsymbol{i}_{2,2}^\top\widetilde{\overline{\boldsymbol{T}}}_{\mathrm{t_o},c}(\boldsymbol{\omega},\widehat{\boldsymbol{\omega}}_{\mathrm{t_o}})-\underline{c}_{\mathrm{t_o},0}(\boldsymbol{\omega})\frac{2\frac{\mathrm{d}}{\mathrm{d}t}\widehat{\omega}_{\mathrm{t_o},c}}{\widehat{\omega}^3_{\mathrm{t_o},c}}\boldsymbol{i}_{2,2}^\top\widetilde{\overline{\boldsymbol{T}}}_{\mathrm{t_o},c}(\boldsymbol{\omega},\widehat{\boldsymbol{\omega}}_{\mathrm{t_o}})\\
=&\frac{2\underline{c}_{\mathrm{t_o},0}(\boldsymbol{\omega})\frac{\mathrm{d}}{\mathrm{d}t}\widehat{\omega}_{\mathrm{t_o},c}}{\widehat{\omega}_{\mathrm{t_o},c}}\left(\sum_{\substack{i=1\\i\neq c}}^{n}\left(\frac{1}{\widehat{\omega}^2_{\mathrm{t_o},i}-\widehat{\omega}^2_{\mathrm{t_o},c}}-\frac{\widehat{\omega}^2_{\mathrm{t_o},c}\prod\limits_{\substack{k=1\\k\neq c,i}}(\widehat{\omega}^2_{\mathrm{t_o},c}-\widehat{\omega}^2_{\mathrm{t_o},k})}{\widehat{\omega}^2_{\mathrm{t_o},i}\prod\limits_{\substack{k=1\\k\neq i}}^{n}(\widehat{\omega}^2_{\mathrm{t_o},i}-\widehat{\omega}^2_{\mathrm{t_o},k})}\right)-\frac{1}{\widehat{\omega}^2_{\mathrm{t_o},c}}\right)\boldsymbol{i}_{2,2}^\top\widetilde{\overline{\boldsymbol{T}}}_{\mathrm{t_o},c}(\boldsymbol{\omega},\widehat{\boldsymbol{\omega}}_{\mathrm{t_o}})\\
\overset{(2.22)}{=}&-2\underline{c}_{\mathrm{t_o},0}(\boldsymbol{\omega})\frac{\mathrm{d}}{\mathrm{d}t}\widehat{\omega}_{\mathrm{t_o},c}\frac{\prod\limits_{\substack{k=1\\k\neq c}}^{n}(\widehat{\omega}^2_{\mathrm{t_o},k}-\widehat{\omega}^2_{\mathrm{t_o},c})}{\widehat{\omega}_{\mathrm{t_o},c}\prod\limits_{k=1}^{n}\widehat{\omega}^2_{\mathrm{t_o},k}}\boldsymbol{i}_{2,2}^\top\widetilde{\overline{\boldsymbol{T}}}_{\mathrm{t_o},c}(\boldsymbol{\omega},\widehat{\boldsymbol{\omega}}_{\mathrm{t_o}}).
\end{aligned}
\tag{3.173}
$$

A rearrangement can be done as follows

$$
\begin{aligned}
&\tfrac{\mathrm{d}}{\mathrm{d}t}\widetilde{\boldsymbol{T}}^{-1}_{\mathrm{t_o}}(\boldsymbol{\omega},\widehat{\boldsymbol{\omega}}_{\mathrm{t_o}})\widetilde{\boldsymbol{T}}_{\mathrm{t_o}}(\boldsymbol{\omega},\widehat{\boldsymbol{\omega}}_{\mathrm{t_o}})\widehat{\boldsymbol{x}}_{\mathrm{t_o}}=\widetilde{\boldsymbol{\Xi}}_{\mathrm{t_o}}(\widehat{\boldsymbol{x}}_{\mathrm{t_o}},\boldsymbol{\omega},\widehat{\boldsymbol{\omega}}_{\mathrm{t_o}})\tfrac{\mathrm{d}}{\mathrm{d}t}\widehat{\boldsymbol{\omega}}_{\mathrm{t_o}},\\
&\widetilde{\boldsymbol{\Xi}}_{\mathrm{t_o}}(\widehat{\boldsymbol{x}}_{\mathrm{t_o}},\boldsymbol{\omega},\widehat{\boldsymbol{\omega}}_{\mathrm{t_o}}):=\begin{bmatrix}\xi_{\mathrm{t_o},1}(\widehat{\boldsymbol{x}}_{\mathrm{t_o}},\boldsymbol{\omega},\widehat{\boldsymbol{\omega}}_{\mathrm{t_o}}) & \cdots & \xi_{\mathrm{t_o},n}(\widehat{\boldsymbol{x}}_{\mathrm{t_o}},\boldsymbol{\omega},\widehat{\boldsymbol{\omega}}_{\mathrm{t_o}})\\ \boldsymbol{\xi}_{\mathrm{t_o},1,1}(\widehat{\boldsymbol{x}}_{\mathrm{t_o}},\boldsymbol{\omega},\widehat{\boldsymbol{\omega}}_{\mathrm{t_o}}) & \cdots & \boldsymbol{\xi}_{\mathrm{t_o},1,n}(\widehat{\boldsymbol{x}}_{\mathrm{t_o}},\boldsymbol{\omega},\widehat{\boldsymbol{\omega}}_{\mathrm{t_o}})\\ \vdots & \ddots & \vdots\\ \boldsymbol{\xi}_{\mathrm{t_o},n,1}(\widehat{\boldsymbol{x}}_{\mathrm{t_o}},\boldsymbol{\omega},\widehat{\boldsymbol{\omega}}_{\mathrm{t_o}}) & \cdots & \boldsymbol{\xi}_{\mathrm{t_o},n,n}(\widehat{\boldsymbol{x}}_{\mathrm{t_o}},\boldsymbol{\omega},\widehat{\boldsymbol{\omega}}_{\mathrm{t_o}})\end{bmatrix}\in\mathbb{R}^{2n+1\times n}
\end{aligned}
\tag{3.174}
$$

wherein the sub vectors $\boldsymbol{\xi}_{\mathrm{t_o},r,c}$ and scalars $\xi_{\mathrm{t_o},c}$ are given as

$$
\left.\begin{aligned}
&\boldsymbol{\xi}_{\mathrm{t_o},r,c}(\widehat{\boldsymbol{x}}_{\mathrm{t_o}},\boldsymbol{\omega},\widehat{\boldsymbol{\omega}}_{\mathrm{t_o}})\overset{(3.165)}{=}\begin{cases}\left.\begin{aligned}&\frac{-2\sum\limits_{\substack{j=1\\j\neq r}}^{n}\widehat{\omega}_{\mathrm{t_o},r}\prod\limits_{\substack{k=1\\k\neq r,j}}^{n}(\widehat{\omega}^2_{\mathrm{t_o},c}-\widehat{\omega}^2_{\mathrm{t_o},k})}{\prod\limits_{\substack{k=1\\k\neq r}}^{n}(\widehat{\omega}^2_{\mathrm{t_o},r}-\widehat{\omega}^2_{\mathrm{t_o},k})}\widehat{\boldsymbol{x}}_{\mathrm{t_o},c}\\&+\widetilde{\boldsymbol{S}}^{-1}_{\mathrm{t_o},r}(\boldsymbol{\omega},\widehat{\boldsymbol{\omega}}_{\mathrm{t_o}})\widetilde{\overline{\boldsymbol{T}}}_{\mathrm{t_o},c}(\boldsymbol{\omega},\widehat{\boldsymbol{\omega}}_{\mathrm{t_o}})\widehat{\boldsymbol{x}}_{\mathrm{t_o},c},\end{aligned}\right\} & r=c\\ \dfrac{-2\widehat{\omega}_{\mathrm{t_o},c}\prod\limits_{\substack{k=1\\k\neq r,c}}^{n}(\widehat{\omega}^2_{\mathrm{t_o},c}-\widehat{\omega}^2_{\mathrm{t_o},k})}{\prod\limits_{\substack{k=1\\k\neq r}}^{n}(\widehat{\omega}^2_{\mathrm{t_o},r}-\widehat{\omega}^2_{\mathrm{t_o},k})}\widetilde{\overline{\boldsymbol{T}}}^{-1}_{\mathrm{t_o},r}(\boldsymbol{\omega},\widehat{\boldsymbol{\omega}}_{\mathrm{t_o}})\widetilde{\overline{\boldsymbol{T}}}_{\mathrm{t_o},c}(\boldsymbol{\omega},\widehat{\boldsymbol{\omega}}_{\mathrm{t_o}})\widehat{\boldsymbol{x}}_{\mathrm{t_o},c}, & r\neq c\end{cases}\\
&\xi_{\mathrm{t_o},c}(\widehat{\boldsymbol{x}}_{\mathrm{t_o}},\boldsymbol{\omega},\widehat{\boldsymbol{\omega}}_{\mathrm{t_o}})\overset{(3.173)}{=}\left(0\quad-\frac{2\underline{c}_{\mathrm{t_o},0}(\boldsymbol{\omega})\prod\limits_{\substack{k=1\\k\neq c}}^{n}(\widehat{\omega}^2_{\mathrm{t_o},k}-\widehat{\omega}^2_{\mathrm{t_o},c})}{\widehat{\omega}_{\mathrm{t_o},c}\prod\limits_{k=1}^{n}\widehat{\omega}^2_{\mathrm{t_o},k}}\right)\widetilde{\overline{\boldsymbol{T}}}_{\mathrm{t_o},c}(\boldsymbol{\omega},\widehat{\boldsymbol{\omega}}_{\mathrm{t_o}})\widehat{\boldsymbol{x}}_{\mathrm{t_o},c}.
\end{aligned}\right\}
\tag{3.175}
$$

Hence, the dynamics of the parallelized tSOGI$_\mathrm{o}$s are described by

$$\forall\, t\in\mathbb{T}_i:\quad \widehat{\boldsymbol{x}}_{\mathrm{t_o}}(t_i)=\widehat{\boldsymbol{x}}_{\mathrm{t_o},t_i}$$

$$
\begin{aligned}
\frac{\mathrm{d}}{\mathrm{d}t}\widehat{\boldsymbol{x}}_{\mathrm{t}_\circ} &\overset{(3.159),\,(3.169)}{=} \Big(\underbrace{\big(\boldsymbol{J}_\circ(\widehat{\boldsymbol{\omega}}_{\mathrm{t}_\circ}) - \widetilde{\boldsymbol{l}}_{\mathrm{t}_\circ}(\boldsymbol{\omega},\widehat{\boldsymbol{\omega}}_{\mathrm{t}_\circ})\boldsymbol{c}_\circ^\top\big)}_{=:\,\widetilde{\boldsymbol{A}}_{\mathrm{t}_\circ}(\boldsymbol{\omega},\widehat{\boldsymbol{\omega}}_{\mathrm{t}_\circ})} + \widetilde{\boldsymbol{\Xi}}_{\mathrm{t}_\circ}(\widehat{\boldsymbol{x}}_{\mathrm{t}_\circ},\boldsymbol{\omega},\widehat{\boldsymbol{\omega}}_{\mathrm{t}_\circ})\widetilde{\boldsymbol{\Gamma}}_{\mathrm{t}_\circ}(\boldsymbol{x}_\circ,\boldsymbol{\omega},\widehat{\boldsymbol{\omega}}_{\mathrm{t}_\circ})\widetilde{\boldsymbol{\Sigma}}_{\mathrm{t}_\circ}(\boldsymbol{x}_\circ,\boldsymbol{\omega},\widehat{\boldsymbol{\omega}}_{\mathrm{t}_\circ})\widehat{\boldsymbol{x}}_{\mathrm{t}_\circ}\boldsymbol{c}_\circ^\top \Big)\widehat{\boldsymbol{x}}_{\mathrm{t}_\circ} \\
&\quad + \Big(\widetilde{\boldsymbol{l}}_{\mathrm{t}_\circ}(\boldsymbol{\omega},\widehat{\boldsymbol{\omega}}_{\mathrm{t}_\circ}) - \widetilde{\boldsymbol{\Xi}}_{\mathrm{t}_\circ}(\widehat{\boldsymbol{x}}_{\mathrm{t}_\circ},\boldsymbol{\omega},\widehat{\boldsymbol{\omega}}_{\mathrm{t}_\circ})\widetilde{\boldsymbol{\Gamma}}_{\mathrm{t}_\circ}(\boldsymbol{x}_\circ,\boldsymbol{\omega},\widehat{\boldsymbol{\omega}}_{\mathrm{t}_\circ})\widetilde{\boldsymbol{\Sigma}}_{\mathrm{t}_\circ}(\boldsymbol{x}_\circ,\boldsymbol{\omega},\widehat{\boldsymbol{\omega}}_{\mathrm{t}_\circ})\widehat{\boldsymbol{x}}_{\mathrm{t}_\circ}\Big)\, y, \qquad (3.176)\\
\widehat{y}_{\mathrm{t}_\circ} &= \boldsymbol{c}_\circ^\top \widehat{\boldsymbol{x}}_{\mathrm{t}_\circ}.
\end{aligned}
$$

Figure 3.31 shows the parallelized tSOGI$_\circ$s.

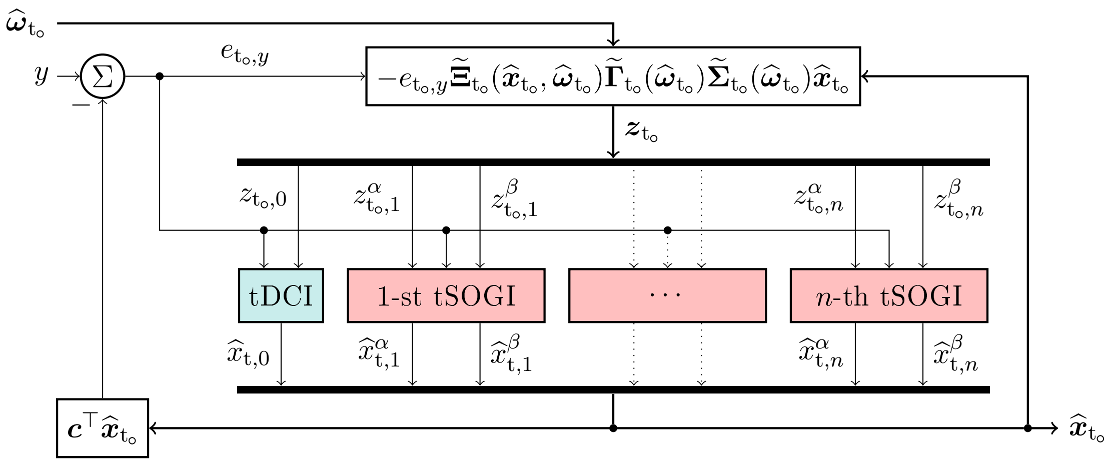

(a) *Block diagram of the parallelized tSOGI$_\circ$s in α,β frame.*

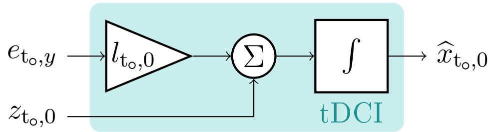

(b) *Construction of the tDCI in α,β frame.*

Figure 3.31: *(a): The parallelized structure of tSOGIs in α,β frame and (b): Offset estimation block in α,β frame.*

Remark 3.5.1. *Comparing the parallelized tSOGIs (or tSOGI$_\circ$s) in α,β frame to the parallelized mSOGIs (or mSOGI$_\circ$s), the parallelized tSOGIs (or parallelized tSOGI$_\circ$s) in α,β frame can be understood as generalizations of the parallelized mSOGIs (or mSOGI$_\circ$s) with state-dependent observer gain vector and a direct concatenation of SOGI- and FLL-dynamics.*
This becomes apparent if all (estimated) angular frequencies are constant: then it holds that $\frac{\mathrm{d}}{\mathrm{d}t}\widehat{\boldsymbol{\omega}}_{\mathrm{t}} = \frac{\mathrm{d}}{\mathrm{d}t}\widehat{\boldsymbol{\omega}}_{\mathrm{t}_\circ} = \boldsymbol{0}_n$ and the respective terms in (3.168) and (3.176) can be removed. As a result, the parallelized mSOGIs and parallelized tSOGIs in α,β frame (or mSOGI$_\circ$s and tSOGI$_\circ$s) are identical.

3.5.3 Gain selection for the parallelized tSOGIs in α,β frame and the parallelized tSOGIs with offset in α,β frame

Due to the equality of tFAO in transformed frame and tFAO in α,β frame or tFAO$_\circ$ in transformed frame and tFAO$_\circ$ in α,β frame, respectively, the parameter selection for the back-transformed systems can be inherited from Proposition 3.4.2.

Remark 3.5.2. *Let $\mathrm{x} \in \{\mathrm{t}, \mathrm{t}_\circ\}$ and let $v = 2n$ if $\mathrm{x} = \mathrm{t}$ or $v = 2n+1$ if $\mathrm{x} = \mathrm{t}_\circ$. The eigenvalues* *of the matrix $\widetilde{\boldsymbol{A}}_{\mathrm{x}}$ in α, β frame are identical to the ones of $\underline{\widetilde{\boldsymbol{A}}}_{\mathrm{x}}$ in transformed frame since*

$$\begin{aligned}\det\Big(s\boldsymbol{I}_v - \widetilde{\boldsymbol{A}}_{\mathrm{x}}(\boldsymbol{\omega}, \widehat{\boldsymbol{\omega}}_{\mathrm{x}})\Big) &= \det\Big(s\boldsymbol{T}_{\mathrm{x}}^{-1}(\boldsymbol{\omega}, \widehat{\boldsymbol{\omega}}_{\mathrm{x}})\boldsymbol{T}_{\mathrm{x}}(\boldsymbol{\omega}, \widehat{\boldsymbol{\omega}}_{\mathrm{x}}) - \boldsymbol{T}_{\mathrm{x}}^{-1}(\boldsymbol{\omega}, \widehat{\boldsymbol{\omega}}_{\mathrm{x}})\underline{\widetilde{\boldsymbol{A}}}_{\mathrm{x}}(\boldsymbol{\omega}, \widehat{\boldsymbol{\omega}}_{\mathrm{x}})\boldsymbol{T}_{\mathrm{x}}(\boldsymbol{\omega}, \widehat{\boldsymbol{\omega}}_{\mathrm{x}})\Big) \\ &= \det\big(\boldsymbol{T}_{\mathrm{x}}^{-1}(\boldsymbol{\omega}, \widehat{\boldsymbol{\omega}}_{\mathrm{x}})\big)\det\Big(s\boldsymbol{I}_v - \underline{\widetilde{\boldsymbol{A}}}_{\mathrm{x}}(\boldsymbol{\omega}, \widehat{\boldsymbol{\omega}}_{\mathrm{x}})\Big)\det(\boldsymbol{T}_{\mathrm{x}}(\boldsymbol{\omega}, \widehat{\boldsymbol{\omega}}_{\mathrm{x}})) = \det\Big(s\boldsymbol{I}_v - \underline{\widetilde{\boldsymbol{A}}}_{\mathrm{x}}(\boldsymbol{\omega}, \widehat{\boldsymbol{\omega}}_{\mathrm{x}})\Big).\end{aligned}$$

However, it should be noted that the overall system matrix

$$\boldsymbol{A}_{\mathrm{x,tot}}(\widehat{\boldsymbol{x}}_{\mathrm{x}}, \boldsymbol{\omega}, \widehat{\boldsymbol{\omega}}_{\mathrm{x}}) := \boldsymbol{J}_{\mathrm{x}}(\widehat{\boldsymbol{\omega}}_{\mathrm{x}}) - \Big(\widetilde{\boldsymbol{l}}_{\mathrm{x}}(\boldsymbol{\omega}, \widehat{\boldsymbol{\omega}}_{\mathrm{x}}) - \widetilde{\boldsymbol{\Xi}}_{\mathrm{x}}(\widehat{\boldsymbol{x}}_{\mathrm{x}}, \boldsymbol{\omega}, \widehat{\boldsymbol{\omega}}_{\mathrm{x}})\widetilde{\boldsymbol{\Gamma}}_{\mathrm{x}}(\boldsymbol{x}_{\mathrm{x}}, \boldsymbol{\omega}, \widehat{\boldsymbol{\omega}}_{\mathrm{x}})\widetilde{\boldsymbol{\Sigma}}_{\mathrm{x}}(\boldsymbol{x}_{\mathrm{x}}, \boldsymbol{\omega}, \widehat{\boldsymbol{\omega}}_{\mathrm{x}})\widehat{\boldsymbol{x}}_{\mathrm{x}}\Big)\boldsymbol{c}_{\mathrm{x}}^{\top}$$

has state-dependent eigenvalues. This has no impact on stability, as the following Section shows.

3.5.4 Stability proof and summary of the tFAO in α, β frame and the tFAO with offset in α, β frame

In this section, summaries of the presented systems are given. The parallelized tSOGIs in α, β frame together with the tFLL in α, β frame, called the *transformation-based Frequency Adaptive Observer* (tFAO) in α, β frame, is shown in Section 3.5.4.1. Afterwards, the parallelized tSOGI$_\circ$s in α, β frame with the tFLL$_\circ$ in α, β frame, denoted as the *transformation-based Frequency Adaptive Observer with offset* (tFAO$_\circ$) in α, β frame, is presented in Section 3.5.4.2. In these sections, the tFAO in α, β frame and tFAO$_\circ$ in α, β frame are evaluated using the test signals introduced in (3.12) and shown in Figure 3.2. Thereafter, their stability is proven.

3.5.4.1 Summary of the tFAO in α, β frame

The tFAO in α, β frame is described by the following set of differential equations:

$$\forall t \in \mathbb{T}_i: \quad \left.\begin{array}{rcll} \frac{\mathrm{d}}{\mathrm{d}t}\widehat{\boldsymbol{x}}_{\mathrm{t}} &=& (\boldsymbol{c}^{\top}\widehat{\boldsymbol{x}}_{\mathrm{t}} - y)\widetilde{\boldsymbol{\Xi}}_{\mathrm{t}}(\widehat{\boldsymbol{x}}_{\mathrm{t}}, \boldsymbol{\omega}, \widehat{\boldsymbol{\omega}}_{\mathrm{t}})\widetilde{\boldsymbol{\Gamma}}_{\mathrm{t}}(\boldsymbol{x}, \boldsymbol{\omega}, \widehat{\boldsymbol{\omega}}_{\mathrm{t}})\widetilde{\boldsymbol{\Sigma}}_{\mathrm{t}}(\boldsymbol{x}, \boldsymbol{\omega}, \widehat{\boldsymbol{\omega}}_{\mathrm{t}})\widehat{\boldsymbol{x}}_{\mathrm{t}} & \\ && + \Big(\boldsymbol{J}(\widehat{\boldsymbol{\omega}}_{\mathrm{t}}) - \widetilde{\boldsymbol{l}}_{\mathrm{t}}(\boldsymbol{\omega}, \widehat{\boldsymbol{\omega}}_{\mathrm{t}})\boldsymbol{c}^{\top}\Big)\widehat{\boldsymbol{x}}_{\mathrm{t}} + \widetilde{\boldsymbol{l}}_{\mathrm{t}}(\boldsymbol{\omega}, \widehat{\boldsymbol{\omega}}_{\mathrm{t}})y, & \widehat{\boldsymbol{x}}_{\mathrm{t}}(t_i) = \widehat{\boldsymbol{x}}_{\mathrm{t},t_i} \\ \frac{\mathrm{d}}{\mathrm{d}t}\widehat{\boldsymbol{\omega}}_{\mathrm{t}} &=& (\boldsymbol{c}^{\top}\widehat{\boldsymbol{x}}_{\mathrm{t}} - y)\widetilde{\boldsymbol{\Gamma}}_{\mathrm{t}}(\boldsymbol{x}, \boldsymbol{\omega}, \widehat{\boldsymbol{\omega}}_{\mathrm{t}})\widetilde{\boldsymbol{\Sigma}}_{\mathrm{t}}(\boldsymbol{x}, \boldsymbol{\omega}, \widehat{\boldsymbol{\omega}}_{\mathrm{t}})\widehat{\boldsymbol{x}}_{\mathrm{t}}, & \widehat{\boldsymbol{\omega}}_{\mathrm{t}}(t_i) = \widehat{\boldsymbol{\omega}}_{\mathrm{t},t_i} \\ \widehat{y}_{\mathrm{t}} &=& \boldsymbol{c}^{\top}\widehat{\boldsymbol{x}}_{\mathrm{t}}. & \end{array}\right\} \tag{3.177}$$

Its graphical representation is summarized in Figure 3.32.

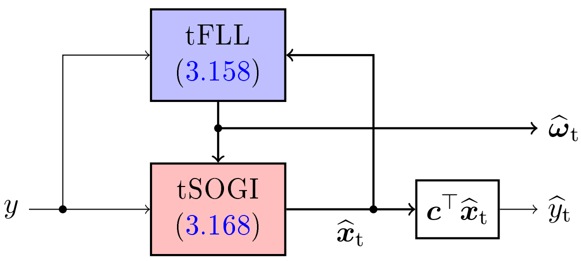

Figure 3.32: *Block diagram of the tFAO in α, β frame.*

Figure 3.33[19] shows the evaluation of the tFAO in α, β frame where all gains are chosen in the transformed frame and inherited by the α, β frame. The test signals from (3.12) are used. Recall that in the previous tests (shown in Figures 3.13, 3.22 and 3.24) only estimates for the fundamental angular frequency were provided by the respective models. Nevertheless, “estimates”

[19]Simulation parameters (in addition to Footnote 17) [in transformed frame]: $\underline{\boldsymbol{c}}_{\mathrm{t}} = (45703125 \cdot (2\pi)^4, 1453125 \cdot (2\pi)^3, 16875 \cdot (2\pi)^2, 75 \cdot 2\pi)^{\top}$, $\underline{\boldsymbol{\Gamma}}_{\mathrm{t}} = \begin{bmatrix} 10^{10} & 10^{10} \\ 10^{10} & 10^{19} \end{bmatrix}$.

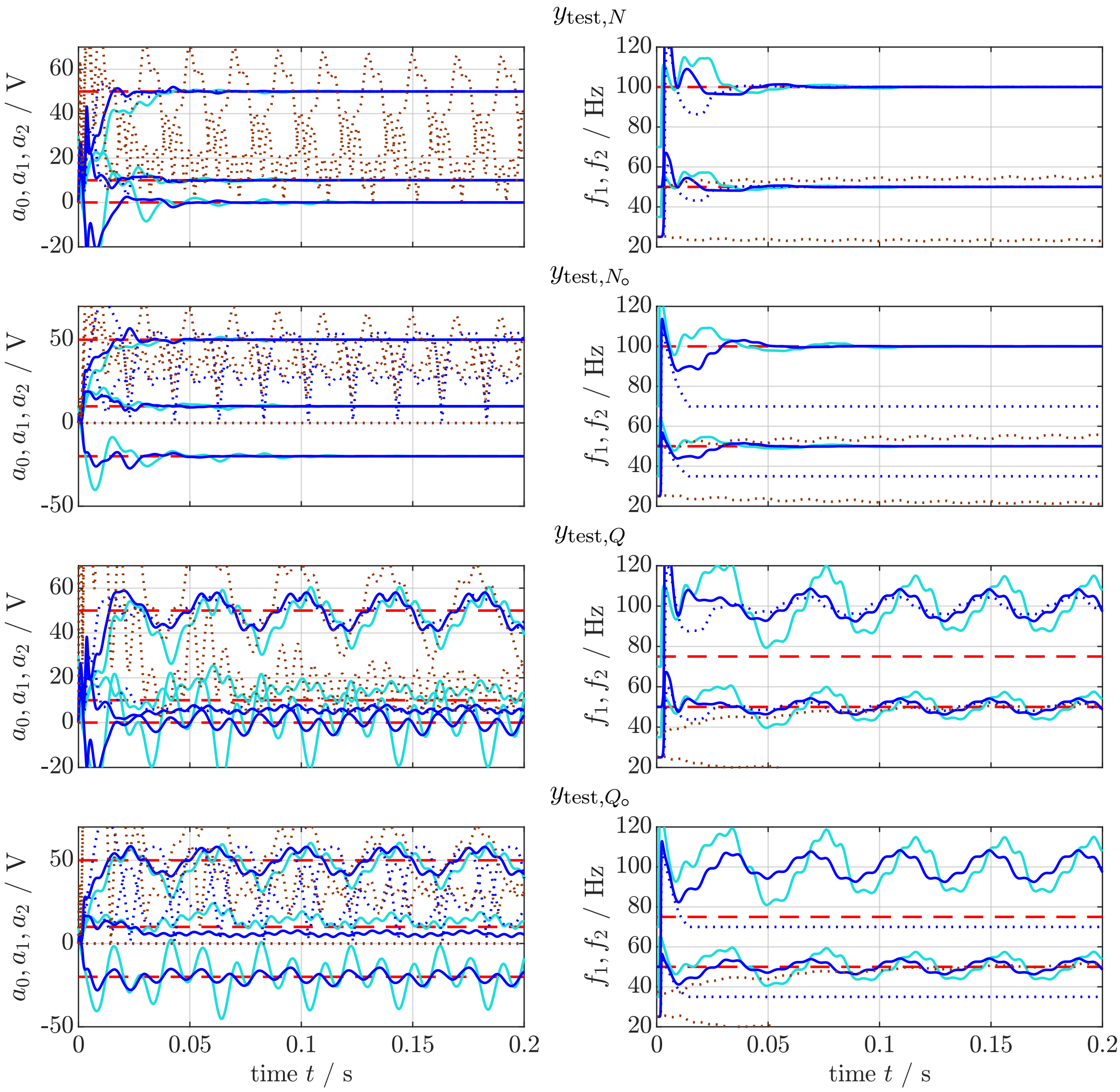

Figure 3.33: *Continuation of Figure 3.24. Offset, amplitudes and frequencies of the test signals estimated by the tFAO in α, β frame (·····).*

for the higher frequency components were shown as well. Considering the tFAO in α, β frame, it actually permits an additional angular frequency estimate. As can be seen in all the subplots, the estimation of the tFAO in α, β frame is very slow. However, a faster performance was not achieved since the model would diverge otherwise. The reasons for the possible divergence are twofold: (i) The gains for the tFAO in α, β frame are rather high (cf. Footnote 19) which might lead to numerical difficulties and (ii) the tFAO in α, β frame is only locally stable which will be shown in Theorem 3.5.3.

3.5.4.2 Summary of the tFAO with offset in α, β frame

The tFAO$_\circ$ in α, β frame is represented as

$\forall t \in \mathbb{T}_i:$

$$\left.\begin{aligned}
\tfrac{\mathrm{d}}{\mathrm{d}t}\widehat{\boldsymbol{x}}_{\mathrm{t}_\circ} &= (\boldsymbol{c}_\circ^\top \widehat{\boldsymbol{x}}_{\mathrm{t}_\circ} - y)\widetilde{\boldsymbol{\Xi}}_{\mathrm{t}_\circ}(\widehat{\boldsymbol{x}}_{\mathrm{t}_\circ}, \boldsymbol{\omega}\widehat{\boldsymbol{\omega}}_{\mathrm{t}_\circ})\widetilde{\boldsymbol{\Gamma}}_{\mathrm{t}_\circ}(\boldsymbol{x}_\circ, \boldsymbol{\omega}, \widehat{\boldsymbol{\omega}}_{\mathrm{t}_\circ})\widetilde{\boldsymbol{\Sigma}}_{\mathrm{t}_\circ}(\boldsymbol{x}_\circ, \boldsymbol{\omega}, \widehat{\boldsymbol{\omega}}_{\mathrm{t}_\circ})\widehat{\boldsymbol{x}}_{\mathrm{t}_\circ} \\
&\quad + \big(\boldsymbol{J}_\circ(\widehat{\boldsymbol{\omega}}_{\mathrm{t}_\circ}) - \widetilde{\boldsymbol{l}}_{\mathrm{t}_\circ}(\boldsymbol{\omega}, \widehat{\boldsymbol{\omega}}_{\mathrm{t}_\circ})\boldsymbol{c}_\circ^\top\big)\widehat{\boldsymbol{x}}_{\mathrm{t}_\circ} + \widetilde{\boldsymbol{l}}_{\mathrm{t}_\circ}(\boldsymbol{\omega}, \widehat{\boldsymbol{\omega}}_{\mathrm{t}_\circ})y, & \widehat{\boldsymbol{x}}_{\mathrm{t}_\circ}(t_i) &= \widehat{\boldsymbol{x}}_{\mathrm{t}_\circ, t_i} \\
\tfrac{\mathrm{d}}{\mathrm{d}t}\widehat{\boldsymbol{\omega}}_{\mathrm{t}_\circ} &= (\boldsymbol{c}_\circ^\top \widehat{\boldsymbol{x}}_{\mathrm{t}_\circ} - y)\widetilde{\boldsymbol{\Gamma}}_{\mathrm{t}_\circ}(\boldsymbol{x}_\circ, \boldsymbol{\omega}, \widehat{\boldsymbol{\omega}}_{\mathrm{t}_\circ})\widetilde{\boldsymbol{\Sigma}}_{\mathrm{t}_\circ}(\boldsymbol{x}_\circ, \boldsymbol{\omega}, \widehat{\boldsymbol{\omega}}_{\mathrm{t}_\circ})\widehat{\boldsymbol{x}}_{\mathrm{t}_\circ}, & \widehat{\boldsymbol{\omega}}_{\mathrm{t}_\circ}(t_i) &= \widehat{\boldsymbol{\omega}}_{\mathrm{t}_\circ, t_i} \\
\widehat{y}_{\mathrm{t}_\circ} &= \boldsymbol{c}_\circ^\top \widehat{\boldsymbol{x}}_{\mathrm{t}_\circ}
\end{aligned}\right\} \tag{3.178}$$

and illustrated in Figure 3.34.

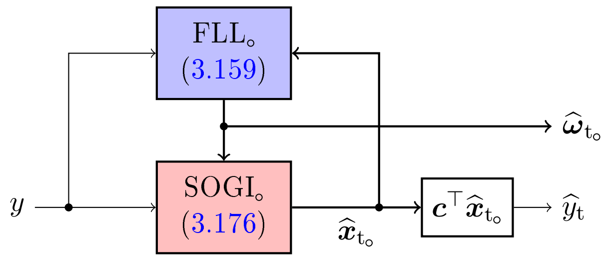

Figure 3.34: *Block diagram of the tFAO$_\circ$ in α, β frame.*

In Figure 3.35[20], the evaluation of the tFAO with offset in α, β frame is illustrated where the test signals from (3.12) are used.
Although the estimation performance of the tFAO$_\circ$ in α, β frame seems to be faster than for the tFAO in α, β frame with respect to angular frequency estimation, the performance is still limited and very slow.

Theorem 3.5.3 (Bounded-input bounded-state/bounded-output stability of the dynamics of the tFAO and tFAO$_\circ$ in α, β frame)**.** *Let $\mathrm{x} \in \{\mathrm{t}, \mathrm{t}_\circ\}$. Consider an essentially bounded input signal, i.e. $y \in \mathcal{L}^\infty(\mathbb{R}_{\geq 0}; \mathbb{R})$ and assume that (i) the matrix $\widetilde{\boldsymbol{A}}_{\mathrm{x}}$ as in (3.168) or (3.176), respectively, is a Hurwitz matrix, (ii) $\underline{c}^{\beta}_{\mathrm{x},n}$ is a real scalar, (iii) for all $i, j \in \{1, \ldots, n\}$ the elements $\widehat{\omega}_{\mathrm{x},i}$ of $\widehat{\boldsymbol{\omega}}_{\mathrm{x}}$ are non-zero and there does not exist $i \neq j$ such that $\widehat{\omega}_{\mathrm{t},i} = \widehat{\omega}_{\mathrm{t},j}$ and (iv) the matrix $\widetilde{\boldsymbol{T}}_{\mathrm{x}}$ is invertible. Then, the time-varying systems (3.158), (3.159), (3.176) and (3.168) are bounded-input bounded-state/bounded-output stable, i.e.*

$$\forall\, t \in \mathbb{T}_i\colon \quad \exists\, c_{\mathrm{x}},\, \widetilde{c}_{\mathrm{x}},\, c_{\mathrm{x},\omega} > 0\colon \quad \|\widehat{\boldsymbol{x}}_{\mathrm{x}}\| \leq c_{\mathrm{x}},\ \left|\widehat{y}_{\mathrm{x}}\right| \leq \widetilde{c}_{\mathrm{x}} \quad \textit{and} \quad \|\widehat{\boldsymbol{\omega}}_{\mathrm{x}}\| \leq c_{\mathrm{x},\omega}.$$

Proof. For the norm of the state vector in α, β frame it holds that

$$\|\widehat{\boldsymbol{x}}_{\mathrm{x}}\| = \left\|\widetilde{\boldsymbol{T}}_{\mathrm{x}}^{-1}(\boldsymbol{\omega}, \widehat{\boldsymbol{\omega}}_{\mathrm{x}})\underline{\widehat{\boldsymbol{x}}}_{\mathrm{x}}\right\| \leq \left\|\widetilde{\boldsymbol{T}}_{\mathrm{x}}^{-1}(\boldsymbol{\omega}, \widehat{\boldsymbol{\omega}}_{\mathrm{x}})\right\| \|\underline{\widehat{\boldsymbol{x}}}_{\mathrm{x}}\|. \tag{3.179}$$

First note that $\widetilde{\boldsymbol{T}}_{\mathrm{x}}$ must be invertible. Concerning the boundedness, $\underline{\widehat{\boldsymbol{x}}}_{\mathrm{x}}$ is bounded by $\|\underline{\widehat{\boldsymbol{x}}}_{\mathrm{x}}\| \leq \underline{c}_{\mathrm{x}}$ (cf. Theorem 3.4.7). Further, since $\|\underline{\boldsymbol{c}}_{\mathrm{x}}\| < \infty$ is bounded, the boundedness of $\widetilde{\boldsymbol{T}}_{\mathrm{x}}$ depends on the boundedness of the back-transformed angular frequency vector $\widehat{\boldsymbol{\omega}}_{\mathrm{x}}$. It might be unbounded which is contradicted in the following.
According to Theorem 3.4.8, the transformed angular frequency vector $\underline{\widehat{\boldsymbol{\theta}}}_{\mathrm{x}}$ is upper bounded by $\left\|\underline{\widehat{\boldsymbol{\theta}}}_{\mathrm{x}}\right\| \leq \underline{c}_{\mathrm{x},\omega} < \infty$. Consequently, this holds true for the vector's elements $\underline{\widehat{\theta}}_{\mathrm{t},i}, i \in \{1, \ldots, n\}$. Hence, in view of the first element of $\underline{\widehat{\boldsymbol{\theta}}}_{\mathrm{x}}$, the following holds

$$\underline{\widehat{\theta}}_{\mathrm{x},1} \stackrel{(3.153)}{=} \sum_{j=1}^{n} \widehat{\omega}_{\mathrm{x},j}^2 < \infty.$$

[20]Simulation parameters (in addition to Footnote 19) [in transformed frame]: $\underline{\boldsymbol{c}}_{\mathrm{t}_\circ} = (9521484375 \cdot (2\pi)^5, 267187500 \cdot (2\pi)^4, 3468750 \cdot (2\pi)^3, 22500 \cdot (2\pi)^2, 75 \cdot 2\pi)^\top$, $\underline{\boldsymbol{\Gamma}}_{\mathrm{t}} = \left[\begin{smallmatrix} 10^{11} & 10^{15} \\ 10^{15} & 10^{20} \end{smallmatrix}\right]$.

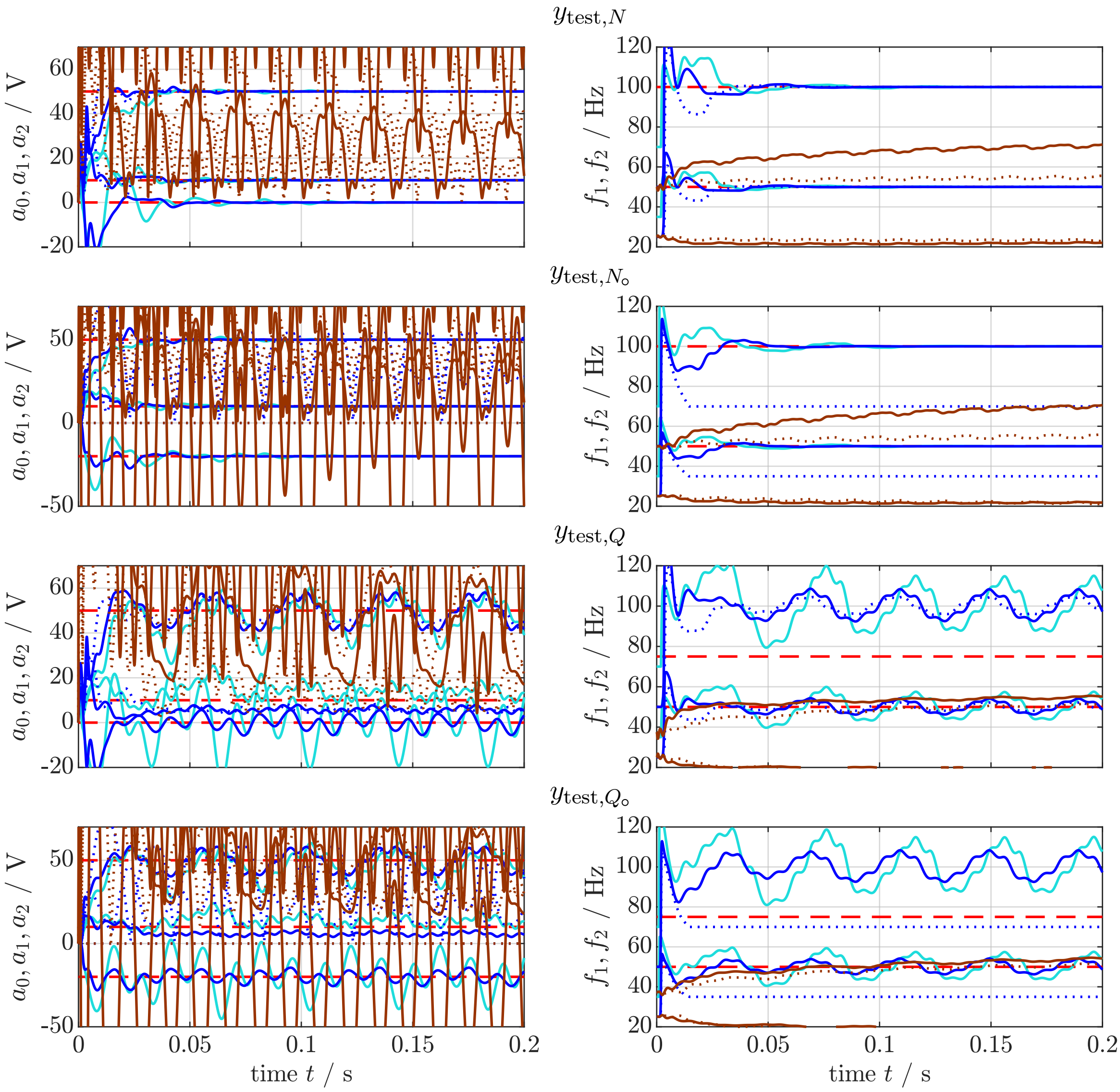

Figure 3.35: *Continuation of Figure 3.13. Offset, amplitudes and frequencies of the test signals estimated by the tFAO$_\circ$ (——).*

Since for all $j \in \{1, \ldots, n\}$ it is $\widehat{\omega}_{\mathrm{x},j} \in \mathbb{R}$, unbounded $\widehat{\omega}_{\mathrm{x},j}$ would result in unbounded $\widehat{\underline{\theta}}_{\mathrm{x},1}$. This contradicts the statement of Theorem 3.4.8 and, hence, all $\widehat{\omega}_{\mathrm{x},j}$ are bounded. Thus, the vector $\widehat{\boldsymbol{\omega}}_{\mathrm{x}}$ is bounded as well:

$$\forall\, t \in \mathbb{T}_i\colon \quad \exists\, c_{\mathrm{x},\omega} > 0\colon \quad \|\widehat{\boldsymbol{\omega}}_{\mathrm{x}}\| \leq c_{\mathrm{x},\omega} < \infty.$$

Thus, the matrix $\widetilde{\boldsymbol{T}}_{\mathrm{x}}$ is bounded by $c_{\mathrm{x},T} < \infty$ and it follows

$$\forall\, t \in \mathbb{T}_i\colon \quad \|\widehat{\boldsymbol{x}}_{\mathrm{x}}\| \overset{(3.179)}{\leq} c_{\mathrm{x},T}\,\underline{c}_{\mathrm{x}} =: c_{\mathrm{x}} < \infty$$
$$\text{and} \quad |\widehat{y}_{\mathrm{x}}| = \left|\boldsymbol{c}_{\mathrm{x}}^\top \widehat{\boldsymbol{x}}_{\mathrm{x}}\right| \leq \|\boldsymbol{c}_{\mathrm{x}}\|\, \|\widehat{\boldsymbol{x}}_{\mathrm{x}}\| \leq \|\boldsymbol{c}_{\mathrm{x}}\|\, c_{\mathrm{x}} =: \widetilde{c}_{\mathrm{x}} < \infty.$$

This completes the proof. □

Theorem 3.5.4 (Boundedness and asymptotic decrease of the signal estimation error of the tFAO and tFAO$_\circ$ in α, β frame)**.** *Let* $\mathrm{x} \in \{\mathrm{t}, \mathrm{t}_\circ\}$*. Consider any continuous and bounded input signal, i.e.* $y \in \mathcal{C}(\mathbb{R}_{\geq 0}; \mathbb{R}_{>0}) \cap \mathcal{L}^\infty(\mathbb{R}_{\geq 0}; \mathbb{R})$ *and assume that* y *is fed to the tFAO in* α, β *frame* (3.177) *or the tFAO$_\circ$ in* α, β *frame* (3.178)*, respectively, with* $\underline{\boldsymbol{A}}_\mathrm{x}$ *being a Hurwitz matrix. Let* $\underline{c}^\beta_{\mathrm{x},n}$ *be a real scalar. If the angular frequency vector* $\widehat{\boldsymbol{\omega}}_\mathrm{x}$ *is bounded away from the set of critical angular frequency vectors defined as*

$$\mathbb{W}_\mathrm{x} := \left\{ \boldsymbol{\kappa} \in \mathbb{R}^n \,|\, \forall i, j \in \{1, \ldots, n\}, i \neq j: \quad \boldsymbol{i}_{i,n}^\top \boldsymbol{\kappa} = 0 \vee (\boldsymbol{i}_{i,n} \pm \boldsymbol{i}_{j,n})^\top \boldsymbol{\kappa} = 0 \right\},$$

then
(i) the estimation error $\boldsymbol{e}_\mathrm{x} := \boldsymbol{x}_\mathrm{x} - \widehat{\boldsymbol{x}}_\mathrm{x}$ *is bounded, i.e. there exists* $c_{\mathrm{x},e} > 0$ *such that* $\|\boldsymbol{e}_\mathrm{x}\| \leq c_{\mathrm{x},e} < \infty$ *for all* $t \in \mathbb{T}_i$ *and, if* $n_\infty = n$ *for all* $t \in \mathbb{T}_i$*, it decreases asymptotically, i.e.* $\lim_{t\to\infty} \|\boldsymbol{e}_\mathrm{x}\| \to 0$*;*
(ii) the angular frequency error $\boldsymbol{e}_{\mathrm{x},\omega} := \boldsymbol{\omega} - \widehat{\boldsymbol{\omega}}_\mathrm{x}$ *is bounded, i.e. there exists* $c_{\mathrm{x},e,\omega} > 0$ *such that* $\|\boldsymbol{e}_{\mathrm{x},\omega}\| \leq c_{\mathrm{x},e,\omega} < \infty$ *for all* $t \in \mathbb{T}_i$ *and, if* $n_\infty = n$ *for all* $t \in \mathbb{T}_i$*, it decreases asymptotically, i.e.* $\lim_{t\to\infty} \|\boldsymbol{e}_{\mathrm{x},\omega}\| \to 0$.

Proof. The listed assertions are shown separately:
(i) In view of the result from Theorem 3.5.3, it follows

$$\forall t \in \mathbb{T}_i: \qquad \|\boldsymbol{e}_\mathrm{x}\| = \|\boldsymbol{x}_\mathrm{x} - \widehat{\boldsymbol{x}}_\mathrm{x}\| \leq \overbrace{\|\boldsymbol{x}_\mathrm{x}\|_\infty}^{=: c_x < \infty} + \|\widehat{\boldsymbol{x}}_\mathrm{x}\| \leq c_x + c_\mathrm{t} =: c_{\mathrm{x},e} < \infty$$

what shows boundedness of $\boldsymbol{e}_\mathrm{x}$. Note that, according to Theorem 3.5.3, this result only holds if $\widetilde{\boldsymbol{T}}_\mathrm{x}$ is invertible. Therefore, all forbidden angular frequency combinations which imply a non-invertibility of $\widetilde{\boldsymbol{T}}_\mathrm{x}$ are collected in the set $\mathbb{W}_\mathrm{x}$. Considering

$$\boldsymbol{c}_\mathrm{x}^\top \boldsymbol{e}_\mathrm{x} = \boldsymbol{c}_\mathrm{x}^\top (\boldsymbol{x}_\mathrm{x} - \widehat{\boldsymbol{x}}_\mathrm{x}) = \underline{\boldsymbol{c}}_\mathrm{x}^\top(\boldsymbol{\omega}) (\underline{\boldsymbol{x}}_\mathrm{x} - \widehat{\underline{\boldsymbol{x}}}_\mathrm{x}) = \underline{\boldsymbol{c}}_\mathrm{x}^\top(\boldsymbol{\omega}) \underline{\boldsymbol{e}}_\mathrm{x},$$

the asymptotic decrease of the signal estimation error is proven since according to Theorem 3.4.8, the signal estimation error $\underline{\boldsymbol{e}}_\mathrm{x}$ decreases asymptotically.
(ii) The norm of the frequency estimation error has the following bound:

$$\|\boldsymbol{e}_{\mathrm{x},\omega}\| = \|\boldsymbol{\omega} - \widehat{\boldsymbol{\omega}}_\mathrm{x}\| \leq \underbrace{\|\boldsymbol{\omega}\|_\infty}_{=: c_\omega < \infty} + \|\widehat{\boldsymbol{\omega}}_\mathrm{x}\| \leq c_\omega + c_{\mathrm{x},\omega} =: c_{\mathrm{x},e,\omega} < \infty$$

This shows boundedness of the angular frequency estimation error $\boldsymbol{e}_{\mathrm{x},\omega}$. Finally, since the estimation error $\boldsymbol{e}_\mathrm{x}$ decreases asymptotically, this holds true for the angular frequency error vector $\boldsymbol{e}_{\mathrm{x},\omega}$ as well. This completes the proof. □

Remark 3.5.5. *Let* $\mathrm{x} \in \{\mathrm{t}, \mathrm{t}_\circ\}$*. Let the initial angular frequency vector* $\widehat{\boldsymbol{\omega}}_\mathrm{x}(t_0)$ *be chosen as any vector ensuring the invertibility of* $\widetilde{\boldsymbol{T}}_\mathrm{x}$*. Furthermore, let the initial values of tFAO in* α, β *and transformed frame or tFAO$_\circ$ in* α, β *and transformed frame, respectively, be chosen equivalently (i.e.* $\widehat{\underline{\boldsymbol{x}}}_\mathrm{x}(t_0) = \widetilde{\boldsymbol{T}}_\mathrm{x}(\widehat{\boldsymbol{\omega}}_\mathrm{x}(t_0))\widehat{\boldsymbol{x}}_\mathrm{x}(t_0)$ *and* $\widehat{\boldsymbol{\omega}}_\mathrm{x}(t_0) = \boldsymbol{T}_{\mathrm{x},\omega}(\widehat{\boldsymbol{\omega}}_\mathrm{x}(t_0))\widehat{\underline{\boldsymbol{\theta}}}_\mathrm{x}(t_0)$ *with some angular frequency transformation matrix* $\boldsymbol{T}_{\mathrm{x},\omega}$*). Assuming that while estimation is running, it holds that* $\widehat{\boldsymbol{\omega}}_\mathrm{x} \notin \mathbb{W}_\mathrm{x}$ *without explicit restriction, the responses of tFAO or tFAO$_\circ$ in* α, β *and transformed frame, respectively, to any input signal* y *are identical in view of the estimation errors* $\underline{e}_{\mathrm{x},y}$ *and* $e_{\mathrm{x},y}$ *and estimated inputs* $\widehat{\underline{y}}_\mathrm{x}$ *and* $\widehat{y}_\mathrm{x}$*.*
For $\mathrm{x} = \mathrm{t}_\circ$*, an example is illustrated in Figure 3.36*[21]*.*

[21] Simulation parameters: $T_s = 100\,\mu\mathrm{s}$, $y = -0.5 + \cos(2\pi 50 t)$, Poles: $(\lambda_{\mathrm{t}_\circ,1}, \lambda_{\mathrm{t}_\circ,2}, \lambda_{\mathrm{t}_\circ,3}) = (-1.5, -1.5 + \jmath, -1.5 - \jmath)$, $\widetilde{\boldsymbol{\Gamma}}_{\mathrm{t}_\circ} = 10^9$, Solver: ode4. All initial values are 0 except for $\widehat{\omega}_{\mathrm{t},1}(0) = 2\pi 25$ and $\widehat{\underline{\theta}}_{\mathrm{t},1}(0) = (2\pi 25)^2$.

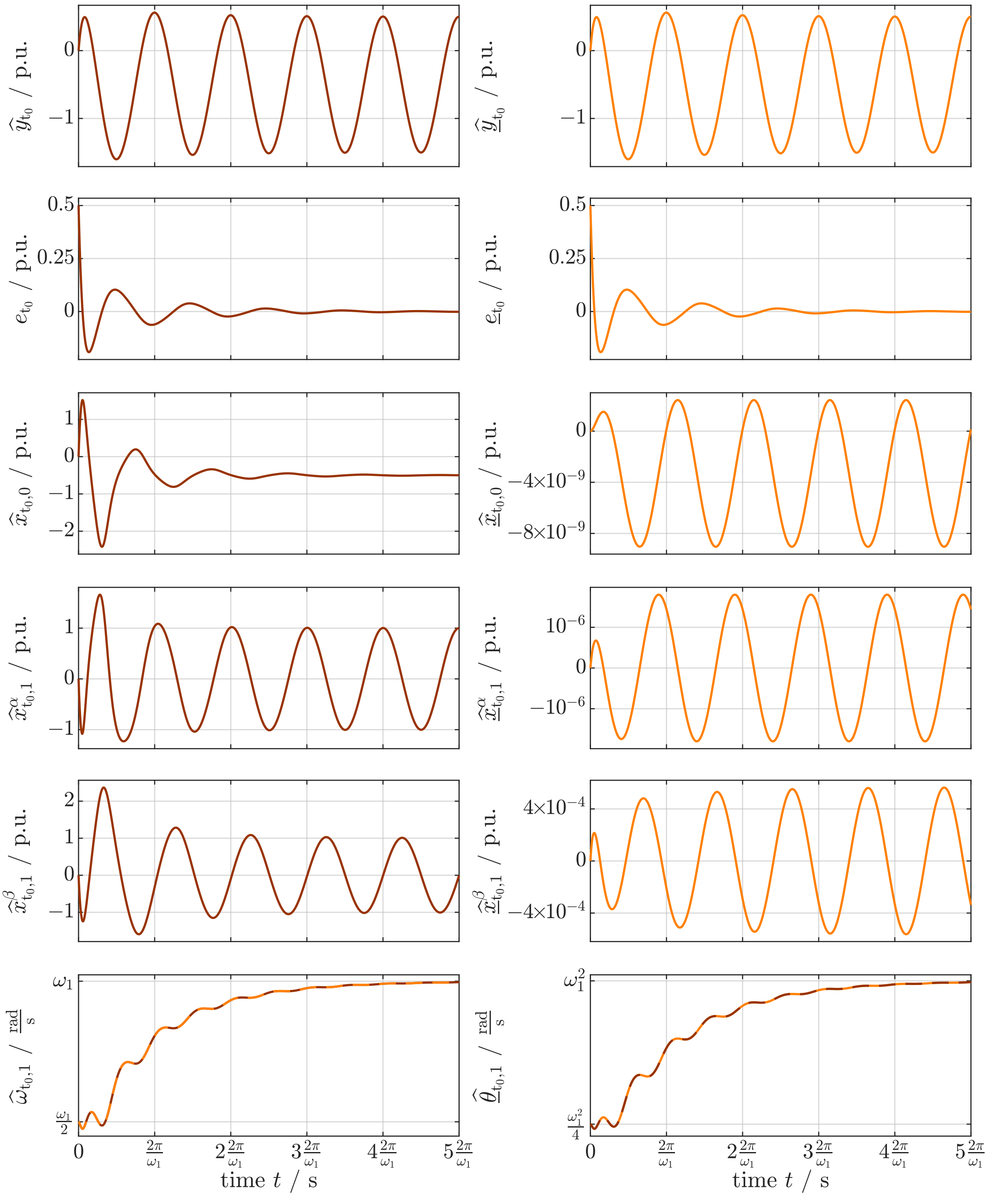

Figure 3.36: *Comparison between tFAO in α, β (—) and transformed (—) frame.*

Despite the differences in state estimates $\widehat{\underline{x}}_{t,0}$ & $\widehat{x}_{t,0}$, $\widehat{\underline{x}}^{\alpha}_{t,1}$ & $\widehat{x}^{\alpha}_{t,1}$ and $\widehat{\underline{x}}^{\beta}_{t,1}$ & $\widehat{x}^{\beta}_{t,1}$ for tFAO$_\circ$ in α, β frame (—) and tFAO$_\circ$ in transformed frame (—), their signal estimation errors $\underline{e}_{t,y}$ and $e_{t,y}$ and estimated inputs $\widehat{\underline{y}}_t$ and $\widehat{y}_t$ are identical. Note that this also holds true for the angular frequency estimates $\widehat{\underline{\theta}}_{t,1}$ and $\widehat{\omega}_{t,1}$. For a better comparability, the manually calculated (transformed) angular frequency values, obtained as $\widehat{\omega}_{t,1} = \sqrt{\widehat{\underline{\theta}}_{t,1}}$ (- - -) and $\widehat{\underline{\theta}}_{t,1} = \widehat{\omega}^2_{t,1}$ (- - -), are also drawn.

3.6 The exponential Frequency Adaptive Observer and the exponential Frequency Adaptive Observer with offset (an idea)

So far, no FAO was developed with the possibility to analyze a completely unknown signal **and** to perform this estimation in an acceptable time frame. The best options so far are:

(i) The mFAO (or mFAO$_\circ$) (cf. Section 3.3). They allow for an acceptable, but still limited estimation speed. However, they require knowledge on the harmonic orders $\mathbb{H}_\infty$;

(ii) The tFAO (or tFAO$_\circ$) in α, β frame (cf. Section 3.5). They do not require knowledge on the harmonic orders but, on the other hand, show an unacceptably slow performance and still have numerical problems.

The motivation for this section is to develop an idea of how to construct observers capable of unifying the advantages of mFAO and tFAO & mFAO$_\circ$ and tFAO$_\circ$ and to minimize numeric problems.
Unfortunately, the idea is unfinished. However, at the end a set of equations is obtained which remains to be solved in future approaches. This idea relies on some assumptions, which are justified in detail when made. This section is structured as follows:

Section 3.6.1 reintroduces signal generation and discusses observability;

Section 3.6.2 shows the actual progress in development of the exponential FAO and the exponential FAO with offset; and

Section 3.6.3 gives hints for future work and summarizes unsolved problems.

3.6.1 Generation of periodic signals and observability

According to Section 3.1, the generation of any periodic signal without offset is represented by

$$\forall\, t \in \mathbb{T}_i\colon\quad \left.\begin{array}{ll} \frac{\mathrm{d}}{\mathrm{d}t}\boldsymbol{x} = \boldsymbol{J}(\boldsymbol{\omega})\boldsymbol{x}, & \boldsymbol{x}(t_i) = \boldsymbol{x}_{t_i} \\ \frac{\mathrm{d}}{\mathrm{d}t}\boldsymbol{\omega} = \boldsymbol{0}_{n_\infty}, & \boldsymbol{\omega}(t_i) = \boldsymbol{\omega}_{t_i} \\ y_\sim = \boldsymbol{c}^\top \boldsymbol{x}. & \end{array}\right\} \tag{3.180}$$

Thus, the overall nonlinear system is described by

$$\forall\, t \in \mathbb{T}_i\colon\quad \left.\begin{array}{rcll} \frac{\mathrm{d}}{\mathrm{d}t} \overbrace{\begin{pmatrix}\boldsymbol{x}\\ \boldsymbol{\omega}\end{pmatrix}}^{:=\overline{\boldsymbol{x}}\in\mathbb{R}^{3n_\infty}} & \overset{(3.180)}{=} & \overbrace{\begin{bmatrix}\boldsymbol{J}(\boldsymbol{\omega}) & \boldsymbol{0}_{2n_\infty\times n_\infty}\\ \boldsymbol{0}_{n_\infty\times 2n_\infty} & \boldsymbol{0}_{n_\infty\times n_\infty}\end{bmatrix}}^{=:\boldsymbol{J}_{\mathrm{tot}}(\boldsymbol{\omega})\in\mathbb{R}^{3n_\infty\times 3n_\infty}} \overline{\boldsymbol{x}}, & \overline{\boldsymbol{x}}(t_i) = \overline{\boldsymbol{x}}_{t_i} \\ y_\sim & = & \underbrace{\begin{pmatrix}\boldsymbol{c}^\top & \boldsymbol{0}_{n_\infty}^\top\end{pmatrix}}_{=:\boldsymbol{c}_{\mathrm{tot}}^\top\in\mathbb{R}^{3n_\infty}} \overline{\boldsymbol{x}}. & \end{array}\right\} \tag{3.181}$$

If offset is additionally considered, the overall nonlinear system is obtained in a similar manner as

$$\forall\, t \in \mathbb{T}_i\colon\quad \left.\begin{array}{rcll} \frac{\mathrm{d}}{\mathrm{d}t} \overbrace{\begin{pmatrix}\boldsymbol{x}_\circ\\ \boldsymbol{\omega}\end{pmatrix}}^{:=\overline{\boldsymbol{x}}_\circ\in\mathbb{R}^{3n_\infty+1}} & \overset{(3.180)}{=} & \overbrace{\begin{bmatrix}\boldsymbol{J}_\circ(\boldsymbol{\omega}) & \boldsymbol{0}_{(2n_\infty+1)\times n_\infty}\\ \boldsymbol{0}_{n_\infty\times (2n_\infty+1)} & \boldsymbol{0}_{n_\infty\times n_\infty}\end{bmatrix}}^{=:\boldsymbol{J}_{\circ,\mathrm{tot}}(\boldsymbol{\omega})\in\mathbb{R}^{(3n_\infty+1)\times(3n_\infty+1)}} \overline{\boldsymbol{x}}_\circ, & \overline{\boldsymbol{x}}_\circ(t_i) = \overline{\boldsymbol{x}}_{\circ,t_i} \\ y & = & \underbrace{\begin{pmatrix}\boldsymbol{c}_\circ^\top & \boldsymbol{0}_{n_\infty}^\top\end{pmatrix}}_{=:\boldsymbol{c}_{\circ,\mathrm{tot}}^\top\in\mathbb{R}^{3n_\infty+1}} \overline{\boldsymbol{x}}. & \end{array}\right\} \tag{3.182}$$

To conclude this section, observability is investigated.

Proposition 3.6.1 (Observability of generation systems (3.181) and (3.182))**.** *Consider the dynamical systems* (3.181) *and* (3.182)*. Then, if and only if* $\omega_1 \neq 0$ *and* $\mathbb{H}_\infty \subseteq \mathbb{R} \setminus \{0\}$ *where for all* $\nu_i, \nu_j \in \mathbb{H}_\infty$*,* $i \neq j$*, it holds that* $|\nu_i| \neq |\nu_j|$*, these systems are observable.*

Proof. To prove the assertion, Fact 2.2 must be used. Writing out (2.2) in case of (3.181) yields

$$\begin{pmatrix} y \\ \frac{\mathrm{d}}{\mathrm{d}t} y \\ \vdots \\ \frac{\mathrm{d}^{3n_\infty-2}}{\mathrm{d}t^{3n_\infty-2}} y \\ \frac{\mathrm{d}^{3n_\infty-1}}{\mathrm{d}t^{3n_\infty-1}} y \end{pmatrix} \overset{(3.181)}{=} \begin{pmatrix} \boldsymbol{c}_{\mathrm{tot}}^\top \overline{\boldsymbol{x}} \\ \boldsymbol{c}_{\mathrm{tot}}^\top \begin{pmatrix} \boldsymbol{J}(\boldsymbol{\omega})\boldsymbol{x} \\ \boldsymbol{0}_{n_\infty} \end{pmatrix} \\ \vdots \\ \boldsymbol{c}_{\mathrm{tot}}^\top \begin{pmatrix} \boldsymbol{J}^{3n_\infty-2}(\boldsymbol{\omega})\boldsymbol{x} \\ \boldsymbol{0}_{n_\infty} \end{pmatrix} \\ \boldsymbol{c}_{\mathrm{tot}}^\top \begin{pmatrix} \boldsymbol{J}^{3n_\infty-1}(\boldsymbol{\omega})\boldsymbol{x} \\ \boldsymbol{0}_{n_\infty} \end{pmatrix} \end{pmatrix} = \begin{cases} \begin{pmatrix} \sum_{i=1}^{n_\infty} x_i^\alpha \\ -\sum_{i=1}^{n_\infty} \omega_i x_i^\beta \\ \vdots \\ (-1)^{\frac{n_\infty}{2}+1} \sum_{i=1}^{n_\infty} \omega_i^{3n_\infty-2} x_i^\alpha \\ (-1)^{\frac{n_\infty}{2}} \sum_{i=1}^{n_\infty} \omega_i^{3n_\infty-1} x_i^\beta \end{pmatrix}, & n_\infty \text{ even} \\ \begin{pmatrix} \sum_{i=1}^{n_\infty} x_i^\alpha \\ -\sum_{i=1}^{n_\infty} \omega_i x_i^\beta \\ \vdots \\ (-1)^{\frac{n_\infty+1}{2}} \sum_{i=1}^{n_\infty} \omega_i^{3n_\infty-2} x_i^\beta \\ (-1)^{\frac{n_\infty+1}{2}} \sum_{i=1}^{n_\infty} \omega_i^{3n_\infty-1} x_i^\alpha \end{pmatrix}, & n_\infty \text{ odd} \end{cases}. \tag{3.183}$$

In either case, the first $2n_\infty$ equations of (3.183) form a system of linear equations with observability matrix $\boldsymbol{O}$ as in (3.64). Since this matrix must be invertible, this implies that $\omega_1 \neq 0$ and $\mathbb{H}_\infty \subseteq \mathbb{R} \setminus \{0\}$ where for all $\nu_i, \nu_j \in \mathbb{H}_\infty$, $i \neq j$, it holds that $|\nu_i| \neq |\nu_j|$. More precisely, it holds that

$$\boldsymbol{x} = \boldsymbol{O}^{-1}(\boldsymbol{\omega}) \begin{pmatrix} y & \frac{\mathrm{d}}{\mathrm{d}t} y & \cdots & \frac{\mathrm{d}^{2n_\infty-2}}{\mathrm{d}t^{2n_\infty-2}} y & \frac{\mathrm{d}^{2n_\infty-1}}{\mathrm{d}t^{2n_\infty-1}} y \end{pmatrix}^\top \tag{3.184}$$

where the matrix $\boldsymbol{O}^{-1}$ follows as

$$\boldsymbol{O}^{-1}(\boldsymbol{\omega}) = (-1)^{n_\infty+1} \begin{bmatrix} \frac{\prod_{\substack{j=1 \\ j\neq 1}}^{n_\infty} \omega_j^2}{\prod_{\substack{j=1 \\ j\neq 1}}^{n_\infty} (\omega_1^2-\omega_j^2)} \boldsymbol{O}_1^{-1}(\omega_1) & \cdots & \frac{1}{\prod_{\substack{j=1 \\ j\neq 1}}^{n_\infty} (\omega_1^2-\omega_j^2)} \boldsymbol{O}_1^{-1}(\omega_1) \\ \vdots & \ddots & \vdots \\ \frac{\prod_{\substack{j=1 \\ j\neq n_\infty}}^{n_\infty} \omega_j^2}{\prod_{\substack{j=1 \\ j\neq n_\infty}}^{n_\infty} (\omega_{n_\infty}^2-\omega_j^2)} \boldsymbol{O}_{n_\infty}^{-1}(\omega_{n_\infty}) & \cdots & \frac{1}{\prod_{\substack{j=1 \\ j\neq n_\infty}}^{n_\infty} (\omega_{n_\infty}^2-\omega_j^2)} \boldsymbol{O}_{n_\infty}^{-1}(\omega_{n_\infty}) \end{bmatrix} \tag{3.185}$$

since for the product of the r-th row of (3.185) and the c-th column of (3.64) yields

$$(-1)^{n_\infty+1} \frac{\prod_{\substack{j=1 \\ j\neq r}}^{n_\infty} \omega_j^2}{\prod_{\substack{j=1 \\ j\neq r}}^{n_\infty} (\omega_r^2-\omega_j^2)} \boldsymbol{O}_r^{-1}(\omega_r)\boldsymbol{O}_c(\omega_c) + \cdots + (-1)^{n_\infty+1} \frac{1}{\prod_{\substack{j=1 \\ j\neq r}}^{n_\infty} (\omega_r^2-\omega_j^2)} \boldsymbol{O}_r^{-1}(\omega_r) \frac{(-\omega_c^2)^{n_\infty}}{-\omega_c^2} \boldsymbol{O}_c(\omega_c)$$

$$= \frac{(-1)^{n_\infty+1} \prod_{\substack{j=1 \\ j\neq r}}^{n_\infty} \omega_j^2 + \cdots + \omega_c^{2n_\infty-2}}{\prod_{\substack{j=1 \\ j\neq r}}^{n_\infty} (\omega_r^2-\omega_j^2)} \boldsymbol{O}_r^{-1}(\omega_r)\boldsymbol{O}_c(\omega_c) \overset{(2.18)}{=} \frac{\prod_{\substack{j=1 \\ j\neq r}}^{n_\infty} (\omega_c^2-\omega_j^2) \boldsymbol{O}_r^{-1}(\omega_r)\boldsymbol{O}_c(\omega_c)}{\prod_{\substack{j=1 \\ j\neq r}}^{n_\infty} (\omega_r^2-\omega_j^2)} = \begin{cases} \boldsymbol{0}_{2\times 2}, & c \neq r \\ \boldsymbol{I}_2, & c = r. \end{cases}$$

The last n equations of (3.183) are extracted as

$$\begin{pmatrix} \frac{\mathrm{d}^{2n_\infty}}{\mathrm{d}t^{2n_\infty}}y \\ \frac{\mathrm{d}^{2n_\infty+1}}{\mathrm{d}t^{2n_\infty+1}}y \\ \vdots \\ \frac{\mathrm{d}^{3n_\infty-2}}{\mathrm{d}t^{3n_\infty-2}}y \\ \frac{\mathrm{d}^{3n_\infty-1}}{\mathrm{d}t^{3n_\infty-1}}y \end{pmatrix} = \begin{cases} \begin{bmatrix} \omega_1^{2n_\infty} & 0 & \cdots & \omega_{n_\infty}^{2n_\infty} & 0 \\ \vdots & \vdots & \ddots & \vdots & \vdots \\ 0 & (-1)^{\frac{n_\infty}{2}}\omega_1^{3n_\infty-1} & \cdots & 0 & (-1)^{\frac{n_\infty}{2}}\omega_{n_\infty}^{3n_\infty-1} \end{bmatrix} \boldsymbol{x}, & n_\infty \text{ even} \\ \begin{bmatrix} -\omega_1^{2n_\infty} & 0 & \cdots & -\omega_{n_\infty}^{2n_\infty} & 0 \\ \vdots & \vdots & \ddots & \vdots & \vdots \\ (-1)^{\frac{n_\infty+1}{2}}\omega_1^{3n_\infty-1} & 0 & \cdots & (-1)^{\frac{n_\infty+1}{2}}\omega_{n_\infty}^{3n_\infty-1} & 0 \end{bmatrix} \boldsymbol{x}, & n_\infty \text{ odd.} \end{cases} \tag{3.186}$$

Inserting (3.184) with (3.185) into (3.186) yields the respective i-th equation as

$$0 = \frac{\mathrm{d}^{i-1}}{\mathrm{d}t^{i-1}}y \prod_{k=1}^{n_\infty}\omega_k^2 + \frac{\mathrm{d}^{2+i-1}}{\mathrm{d}t^{2+i-1}}y \sum_{k=1}^{n_\infty}\prod_{\substack{h=1\\h\neq k}}^{n_\infty}\omega_h^2 + \cdots + \frac{\mathrm{d}^{2n_\infty+i-3}}{\mathrm{d}t^{2n_\infty+i-3}}y \sum_{k=1}^{n_\infty}\omega_k^2 + \frac{\mathrm{d}^{2n_\infty+i-1}}{\mathrm{d}t^{2n_\infty+i-1}}y. \tag{3.187}$$

Using the short notation defined in (3.104), (3.187) can be reduced to

$$-\frac{\mathrm{d}^{2n_\infty+i-1}}{\mathrm{d}t^{2n_\infty+i-1}}y = \frac{\mathrm{d}^{2n_\infty+i-3}}{\mathrm{d}t^{2n_\infty+i-3}}y\underline{\theta}_1 + \cdots + \frac{\mathrm{d}^{2+i-1}}{\mathrm{d}t^{2+i-1}}y\underline{\theta}_{n_\infty-1} + \frac{\mathrm{d}^{i-1}}{\mathrm{d}t^{i-1}}y\underline{\theta}_{n_\infty}. \tag{3.188}$$

This consequently leads to the vector valued equation

$$-\underbrace{\begin{pmatrix} \frac{\mathrm{d}^{2n_\infty}}{\mathrm{d}t^{2n_\infty}}y \\ \vdots \\ \frac{\mathrm{d}^{3n_\infty-1}}{\mathrm{d}t^{3n_\infty-1}}y \end{pmatrix}}_{=:\,\boldsymbol{y}\,\in\mathbb{R}^{n_\infty}} = \underbrace{\begin{bmatrix} \frac{\mathrm{d}^{2n_\infty-2}}{\mathrm{d}t^{2n_\infty-2}}y & \cdots & y \\ \vdots & \ddots & \vdots \\ \frac{\mathrm{d}^{3n_\infty-3}}{\mathrm{d}t^{3n_\infty-3}}y & \cdots & \frac{\mathrm{d}^{n_\infty-1}}{\mathrm{d}t^{n_\infty-1}}y \end{bmatrix}}_{=:\,\boldsymbol{Y}\,\in\mathbb{R}^{n_\infty\times n_\infty}} \underline{\boldsymbol{\theta}} \quad \Rightarrow \quad \underline{\boldsymbol{\theta}} = -\boldsymbol{Y}^{-1}\boldsymbol{y}. \tag{3.189}$$

It must be noted that, although $\boldsymbol{Y}$ is not invertible for all times, the product $\boldsymbol{Y}^{-1}\boldsymbol{y}$ exists for all times. This becomes clear when taking into account that by inserting (3.2) and its time derivatives into (3.188), (3.188) holds independent of choices made for all $\omega_i, i \in \{1, \ldots, n_\infty\}$ and thus the solution (3.189) must exist. Now, as stated in Remark 3.4.9, the quadratic angular frequencies ω_i^2, $i \in \{1, \ldots, n_\infty\}$ are obtained as the solutions of (3.152),

$$0 = \kappa^{n_\infty} + \left(-\kappa^{n_\infty-1} \quad \cdots \quad (-1)^{n_\infty}\right)\underline{\boldsymbol{\theta}} \overset{(3.189)}{=} \kappa^{n_\infty} - \left(-\kappa^{n_\infty-1} \quad \cdots \quad (-1)^{n_\infty}\right)\boldsymbol{Y}^{-1}\boldsymbol{y}.$$

Finally, the quadratic angular frequencies ω_i^2 imply that there exist no unique solutions ω_i in $\mathbb{R}\setminus\{0\}$ which contradicts the requirement of Fact 2.2. However, one possible solution for each angular frequency was already discarded for the invertibility requirement of the matrix $\boldsymbol{O}$ and thus, the uniqueness is guaranteed.
In the case of (3.182), the procedure is carried out in a similar manner, which completes the proof. □

Remark 3.6.2. *Observability only implies the existence of (stable) observers but not the existence of exponentially stable observers. Note that an asymptotically stable observer was already constructed in Section 3.5.*

3.6.2 An idea for observer construction

Since observability was clarified in Section 3.6.1, a direct observer construction (unlike observer construction in transformed frame as in Section 3.4) for the nonlinear systems (3.181) and (3.182) is possible. The observer's parameters and states are subscribed by "e" for "exponential" or "$\mathrm{e}_\circ$" when including offset. In the following, the development is done independent of offset estimation, and thus the subscript $\mathrm{x} \in \{\mathrm{e}, \mathrm{e}_\circ\}$ is used, that comes with $v = 2n$ if $\mathrm{x} = \mathrm{e}$ or $v = 2n+1$ if $\mathrm{x} = \mathrm{e}_\circ$. A straight forward approach for observer construction is given by

$$\forall t \in \mathbb{T}_i\colon \quad \frac{\mathrm{d}}{\mathrm{d}t} \underbrace{\begin{pmatrix} \widehat{\boldsymbol{x}}_\mathrm{x} \\ \widehat{\boldsymbol{\omega}}_\mathrm{x} \end{pmatrix}}_{=:\, \widehat{\overline{\boldsymbol{x}}}_\mathrm{x} \in \mathbb{R}^{v+n}} = \left(\boldsymbol{J}_{\mathrm{x,tot}}(\widehat{\boldsymbol{\omega}}_\mathrm{x}) - \underbrace{\begin{pmatrix} \boldsymbol{l}_{\mathrm{x},x}(\widehat{\overline{\boldsymbol{x}}}_\mathrm{x}) \\ \boldsymbol{l}_{\mathrm{x},\omega}(\widehat{\overline{\boldsymbol{x}}}_\mathrm{x}) \end{pmatrix}}_{=:\, \boldsymbol{l}_\mathrm{x}(\widehat{\overline{\boldsymbol{x}}}_\mathrm{x}) \in \mathbb{R}^{v+n}} \boldsymbol{c}_{\mathrm{x,tot}}^\top \right) \widehat{\overline{\boldsymbol{x}}}_\mathrm{e} + \boldsymbol{l}_\mathrm{x}(\widehat{\overline{\boldsymbol{x}}}_\mathrm{x}) y, \quad \widehat{\overline{\boldsymbol{x}}}_\mathrm{x}(t_i) = \widehat{\overline{\boldsymbol{x}}}_{\mathrm{x},t_i}. \tag{3.190}$$

Assumption 3.6.3 (Dependency of $\boldsymbol{l}_\mathrm{x}$ from $\widehat{\overline{\boldsymbol{x}}}_\mathrm{x}$)**.** *Firstly, it is assumed that*

$$\boldsymbol{l}_{\mathrm{x},x}(\widehat{\overline{\boldsymbol{x}}}_\mathrm{x}) = \boldsymbol{l}_{\mathrm{x},x}(\widehat{\boldsymbol{\omega}}_\mathrm{x}) = \overline{\boldsymbol{l}}_{\mathrm{x},x} \boldsymbol{c}_{\mathrm{x},\omega}^\top \widehat{\boldsymbol{\omega}}_\mathrm{x} \tag{3.191}$$

with $\boldsymbol{c}_{\mathrm{x},\omega} \in \mathbb{R}^n$ *and* $\overline{\boldsymbol{l}}_{\mathrm{x},x} \in \mathbb{R}^v$ *being* constant *vectors.*
Secondly, w.l.o.g. it is assumed that

$$\boldsymbol{l}_{\mathrm{x},\omega}(\widehat{\overline{\boldsymbol{x}}}_\mathrm{x}) = \boldsymbol{L}_{\mathrm{x},\omega}(\widehat{\overline{\boldsymbol{x}}}_\mathrm{x}) \widehat{\boldsymbol{\omega}}_\mathrm{x}, \quad \boldsymbol{L}_{\mathrm{x},\omega} \in \mathbb{R}^{n \times n}. \tag{3.192}$$

Remark 3.6.4. *Without offset estimation, a more intuitive choice would be* $\boldsymbol{l}_{\mathrm{e},x}(\widehat{\overline{\boldsymbol{x}}}_\mathrm{e}) = \boldsymbol{l}_{\mathrm{e},x}(\widehat{\boldsymbol{\omega}}_\mathrm{e}) = \left(\mathrm{diag}(\widehat{\boldsymbol{\omega}}_\mathrm{e}) \otimes \boldsymbol{I}_2\right) \overline{\boldsymbol{l}}_{\mathrm{e},x} = (\widehat{\omega}_{\mathrm{e},1} l^\alpha_{\mathrm{e},x,1}, \widehat{\omega}_{\mathrm{e},1} l^\beta_{\mathrm{e},x,1}, \widehat{\omega}_{\mathrm{e},2} l^\alpha_{\mathrm{e},x,2}, \widehat{\omega}_{\mathrm{e},2} l^\beta_{\mathrm{e},x,2}, \cdots)^\top$. *However, when taking offset into account, this choice fails.*

Define

$$\boldsymbol{J}(\widehat{\boldsymbol{\omega}}_\mathrm{e}) \boldsymbol{x} = \underbrace{\begin{bmatrix} \widetilde{\boldsymbol{J}} \boldsymbol{x}_1 & \cdots & \boldsymbol{0}_2 \\ \vdots & \ddots & \vdots \\ \boldsymbol{0}_2 & \cdots & \widetilde{\boldsymbol{J}} \boldsymbol{x}_n \end{bmatrix}}_{=:\, \overline{\boldsymbol{J}}(\boldsymbol{x}) \in \mathbb{R}^{2n \times n}} \widehat{\boldsymbol{\omega}}_\mathrm{e}, \qquad \boldsymbol{J}_\circ(\widehat{\boldsymbol{\omega}}_{\mathrm{e}_\circ}) \boldsymbol{x}_\circ = \underbrace{\begin{bmatrix} 0 & \cdots & 0 \\ \widetilde{\boldsymbol{J}} \boldsymbol{x}_1 & \cdots & \boldsymbol{0}_2 \\ \vdots & \ddots & \vdots \\ \boldsymbol{0}_2 & \cdots & \widetilde{\boldsymbol{J}} \boldsymbol{x}_n \end{bmatrix}}_{=:\, \overline{\boldsymbol{J}}_\circ(\boldsymbol{x}) \in \mathbb{R}^{(2n+1) \times n}} \widehat{\boldsymbol{\omega}}_{\mathrm{e}_\circ}, \tag{3.193}$$

and

$$\overline{\boldsymbol{e}}_\mathrm{x} := \overline{\boldsymbol{x}}_\mathrm{x} - \widehat{\overline{\boldsymbol{x}}}_\mathrm{x} := \begin{pmatrix} \boldsymbol{e}_\mathrm{x} \\ \boldsymbol{e}_{\mathrm{x},\omega} \end{pmatrix} \in \mathbb{R}^{v+n}. \tag{3.194}$$

The differential equations for the signal estimation and angular frequency errors then can be written in various forms as follows

$$\left.\begin{aligned} \tfrac{\mathrm{d}}{\mathrm{d}t} \boldsymbol{e}_\mathrm{x} &= \overbrace{\left[\boldsymbol{J}_\mathrm{x}(\widehat{\boldsymbol{\omega}}_\mathrm{x}) - \overline{\boldsymbol{l}}_{\mathrm{x},x} \boldsymbol{c}_{\mathrm{x},\omega}^\top \widehat{\boldsymbol{\omega}}_\mathrm{x} \boldsymbol{c}_\mathrm{x}^\top \;\; \overline{\boldsymbol{J}}_\mathrm{x}(\boldsymbol{x}_\mathrm{x})\right]}^{=:\, \boldsymbol{A}_{\mathrm{x},x,1}(\boldsymbol{x}_\mathrm{x}, \widehat{\boldsymbol{\omega}}_\mathrm{x})} \overline{\boldsymbol{e}}_\mathrm{x} = \overbrace{\left[\boldsymbol{J}_\mathrm{x}(\boldsymbol{\omega}) - \overline{\boldsymbol{l}}_{\mathrm{x},x} \boldsymbol{c}_{\mathrm{x},\omega}^\top \widehat{\boldsymbol{\omega}}_\mathrm{x} \boldsymbol{c}_\mathrm{x}^\top \;\; \overline{\boldsymbol{J}}_\mathrm{x}(\widehat{\boldsymbol{x}}_\mathrm{x})\right]}^{=:\, \boldsymbol{A}_{\mathrm{x},x,2}(\boldsymbol{\omega}, \widehat{\overline{\boldsymbol{x}}}_\mathrm{x})} \overline{\boldsymbol{e}}_\mathrm{x} \\ &= \overbrace{\left[\boldsymbol{J}_\mathrm{x}(\widehat{\boldsymbol{\omega}}_\mathrm{x}) - \overline{\boldsymbol{l}}_{\mathrm{x},x} \boldsymbol{c}_{\mathrm{x},\omega}^\top \boldsymbol{\omega} \boldsymbol{c}_\mathrm{x}^\top \;\; \boldsymbol{c}_\mathrm{x}^\top \boldsymbol{e}_\mathrm{x} \overline{\boldsymbol{l}}_{\mathrm{x},x} \boldsymbol{c}_{\mathrm{x},\omega}^\top + \overline{\boldsymbol{J}}_\mathrm{x}(\boldsymbol{x}_\mathrm{x})\right]}^{=:\, \boldsymbol{A}_{\mathrm{x},x,3}(\overline{\boldsymbol{x}}_\mathrm{x}, \widehat{\overline{\boldsymbol{x}}}_\mathrm{x})} \overline{\boldsymbol{e}}_\mathrm{x} \\ \tfrac{\mathrm{d}}{\mathrm{d}t} \boldsymbol{e}_{\mathrm{x},\omega} &= \overbrace{\boldsymbol{L}_{\mathrm{x},\omega}(\widehat{\overline{\boldsymbol{x}}}_\mathrm{x}) \left[-\widehat{\boldsymbol{\omega}}_\mathrm{x} \boldsymbol{c}_\mathrm{x}^\top \;\; \boldsymbol{0}_{n \times n}\right]}^{=:\, \boldsymbol{A}_{\mathrm{x},\omega,1}(\widehat{\overline{\boldsymbol{x}}}_\mathrm{x})} \overline{\boldsymbol{e}}_\mathrm{x} = \overbrace{\boldsymbol{L}_{\mathrm{x},\omega}(\widehat{\overline{\boldsymbol{x}}}_\mathrm{x}) \left[-\boldsymbol{\omega} \boldsymbol{c}_\mathrm{x}^\top \;\; \boldsymbol{c}_\mathrm{x}^\top \boldsymbol{e}_\mathrm{x} \boldsymbol{I}_n\right]}^{=:\, \boldsymbol{A}_{\mathrm{x},\omega,2}(\overline{\boldsymbol{x}}_\mathrm{x}, \widehat{\overline{\boldsymbol{x}}}_\mathrm{x})} \overline{\boldsymbol{e}}_\mathrm{x}. \end{aligned}\right\} \tag{3.195}$$

To ease the following, the argument of all matrices is generalized as $(\overline{\boldsymbol{x}}_{\mathrm{x}}, \widehat{\overline{\boldsymbol{x}}}_{\mathrm{x}})$ and therefore dropped. Nevertheless, the argument is highlighted when necessary. Thus, the most general expression for the time derivative of the overall error $\overline{\boldsymbol{e}}_{\mathrm{x}}$ follows with weighting matrices

$$\boldsymbol{W}_{\mathrm{x},x,1}, \boldsymbol{W}_{\mathrm{x},x,2} \in \mathbb{R}^{v\times v} \quad \text{and} \quad \boldsymbol{W}_{\mathrm{x},\omega} \in \mathbb{R}^{n\times n}$$

as

$$\begin{aligned} \forall t \in \mathbb{T}_i\colon \quad \tfrac{\mathrm{d}}{\mathrm{d}t}\boldsymbol{e}_{\mathrm{x}} &= (\boldsymbol{W}_{\mathrm{x},x,1}\boldsymbol{A}_{\mathrm{x},x,1} + (\boldsymbol{I}_v - \boldsymbol{W}_{\mathrm{x},x,1})(\boldsymbol{W}_{\mathrm{x},x,2}\boldsymbol{A}_{\mathrm{x},x,2} \\ &\quad + (\boldsymbol{I}_v - \boldsymbol{W}_{\mathrm{x},x,2})\boldsymbol{A}_{\mathrm{x},x,3}))\overline{\boldsymbol{e}}_{\mathrm{x}} =: \boldsymbol{A}_{\mathrm{x},x}\overline{\boldsymbol{e}}_{\mathrm{x}} \\ \tfrac{\mathrm{d}}{\mathrm{d}t}\boldsymbol{e}_{\mathrm{x},\omega} &= (\boldsymbol{W}_{\mathrm{x},\omega}\boldsymbol{A}_{\mathrm{x},\omega,1} + (\boldsymbol{I}_n - \boldsymbol{W}_{\mathrm{x},\omega})\boldsymbol{A}_{\mathrm{x},\omega,2})\overline{\boldsymbol{e}}_{\mathrm{x}} =: \boldsymbol{A}_{\mathrm{x},\omega}\overline{\boldsymbol{e}}_{\mathrm{x}} \\ \Longrightarrow \quad \tfrac{\mathrm{d}}{\mathrm{d}t}\overline{\boldsymbol{e}}_{\mathrm{x}} &= \begin{bmatrix} \boldsymbol{A}_{\mathrm{x},x} \\ \boldsymbol{A}_{\mathrm{x},\omega} \end{bmatrix} \overline{\boldsymbol{e}}_{\mathrm{x}} =: \boldsymbol{A}_{\mathrm{x}}\overline{\boldsymbol{e}}_{\mathrm{x}}, \qquad \overline{\boldsymbol{e}}_{\mathrm{x}}(t_i) = \overline{\boldsymbol{e}}_{\mathrm{x},t_i} \qquad (3.196) \\ \overline{e}_{\mathrm{x},y} &= \boldsymbol{c}_{\mathrm{x,tot}}^\top \overline{\boldsymbol{e}}_{\mathrm{x}} = \boldsymbol{c}_{\mathrm{x}}^\top \boldsymbol{e}_{\mathrm{x}} = e_{\mathrm{x},y}. \qquad (3.197) \end{aligned}$$

Note that the overall error vector merges two vectors with different physical units. When considering a Lyapunov candidate, this fact implies state dependent matrices $\boldsymbol{P}_{\mathrm{x}}$ and $\boldsymbol{Q}_{\mathrm{x}}$ which consequently includes the time derivative of $\boldsymbol{P}_{\mathrm{x}}$. To avoid this issue and therefore ease the following calculations, introduce the invertible transformation matrix

$$\underline{\boldsymbol{e}}_{\mathrm{x}} := \begin{pmatrix} \underline{\boldsymbol{e}}_{\mathrm{x}} \\ \underline{\boldsymbol{e}}_{\mathrm{x},\omega} \end{pmatrix} := \overline{\boldsymbol{X}}_{\mathrm{x}}\overline{\boldsymbol{e}}_{\mathrm{x}}, \quad \underline{\boldsymbol{x}}_{\mathrm{x}} := \overline{\boldsymbol{X}}_{\mathrm{x}}\overline{\boldsymbol{x}}_{\mathrm{x}} \quad \text{and} \quad \widehat{\underline{\boldsymbol{x}}}_{\mathrm{x}} := \overline{\boldsymbol{X}}_{\mathrm{x}}\widehat{\overline{\boldsymbol{x}}}_{\mathrm{x}}. \qquad (3.198)$$

It is designed such that the vector $\underline{\boldsymbol{e}}_{\mathrm{x}}$ only has one physical unit. Now, consider the Lyapunov candidate

$$V_{\mathrm{x}}(\underline{\boldsymbol{e}}_{\mathrm{x}}) = \underline{\boldsymbol{e}}_{\mathrm{x}}^\top \underline{\boldsymbol{P}}_{\mathrm{x}}\underline{\boldsymbol{e}}_{\mathrm{x}}, \qquad \underline{\boldsymbol{P}}_{\mathrm{x}} = \underline{\boldsymbol{P}}_{\mathrm{x}}^\top > 0 \qquad (3.199)$$

and make the

Assumption 3.6.5 (Lyapunov and transformation matrix)**.** *Assume that the Lyapunov matrix $\underline{\boldsymbol{P}}_{\mathrm{x}}$ is constant. Defining the transformation matrix as*

$$\overline{\boldsymbol{X}}_{\mathrm{x}} := \begin{bmatrix} \boldsymbol{X}_{\mathrm{x}} & \boldsymbol{\Xi}_{\mathrm{x},\omega} \\ \boldsymbol{\Xi}_{\mathrm{x},x} & \boldsymbol{\Omega}_{\mathrm{x}} \end{bmatrix}, \quad \boldsymbol{X}_{\mathrm{x}} \in \mathbb{R}^{v\times v}, \quad \boldsymbol{\Omega}_{\mathrm{x}} \in \mathbb{R}^{n\times n}, \qquad (3.200)$$

it is assumed that $\boldsymbol{\Omega}_{\mathrm{x}}$ is invertible.

This assumption implies that the physical units of the block matrices of the transformation matrix must satisfy

$$\frac{\mathcal{U}(\boldsymbol{X}_{\mathrm{x}})}{\mathcal{U}(\boldsymbol{\Xi}_{\mathrm{x},\omega})} = \frac{\mathcal{U}(\omega)}{\mathcal{U}(y)}, \quad \frac{\mathcal{U}(\boldsymbol{X}_{\mathrm{x}})}{\mathcal{U}(\boldsymbol{\Xi}_{\mathrm{x},x})} = 1, \quad \text{and} \quad \frac{\mathcal{U}(\boldsymbol{X}_{\mathrm{x}})}{\mathcal{U}(\boldsymbol{\Omega}_{\mathrm{x}})} = \frac{\mathcal{U}(\omega)}{\mathcal{U}(y)}.$$

Calculate the time derivative of (3.199) as

$$\begin{aligned} \tfrac{\mathrm{d}}{\mathrm{d}t}V_{\mathrm{x}}(\underline{\boldsymbol{e}}_{\mathrm{x}}) &= \tfrac{\mathrm{d}}{\mathrm{d}t}\underline{\boldsymbol{e}}_{\mathrm{x}}^\top \underline{\boldsymbol{P}}_{\mathrm{x}}\underline{\boldsymbol{e}}_{\mathrm{x}} + \underline{\boldsymbol{e}}_{\mathrm{x}}^\top \underline{\boldsymbol{P}}_{\mathrm{x}}\tfrac{\mathrm{d}}{\mathrm{d}t}\underline{\boldsymbol{e}}_{\mathrm{x}} \\ &\overset{(3.196),(3.198)}{=} \underline{\boldsymbol{e}}_{\mathrm{x}}^\top \overline{\boldsymbol{X}}_{\mathrm{x}}^{-\top}\big(\tfrac{\mathrm{d}}{\mathrm{d}t}\overline{\boldsymbol{X}}_{\mathrm{x}}^\top + \boldsymbol{A}_{\mathrm{x}}^\top\overline{\boldsymbol{X}}_{\mathrm{x}}^\top\big)\underline{\boldsymbol{P}}_{\mathrm{x}}\underline{\boldsymbol{e}}_{\mathrm{x}} + \underline{\boldsymbol{e}}_{\mathrm{x}}^\top\underline{\boldsymbol{P}}_{\mathrm{x}}\big(\tfrac{\mathrm{d}}{\mathrm{d}t}\overline{\boldsymbol{X}}_{\mathrm{x}} + \overline{\boldsymbol{X}}_{\mathrm{x}}\boldsymbol{A}_{\mathrm{x}}\big)\overline{\boldsymbol{X}}_{\mathrm{x}}^{-1}\underline{\boldsymbol{e}}_{\mathrm{x}} \\ &=: -\underline{\boldsymbol{e}}_{\mathrm{x}}^\top \underline{\boldsymbol{Q}}_{\mathrm{x}}\underline{\boldsymbol{e}}_{\mathrm{x}}. \qquad (3.201) \end{aligned}$$

Thus, if and only if the matrix

$$\underline{\boldsymbol{A}}_{\mathrm{x}} := \big(\tfrac{\mathrm{d}}{\mathrm{d}t}\overline{\boldsymbol{X}}_{\mathrm{x}} + \overline{\boldsymbol{X}}_{\mathrm{x}}\boldsymbol{A}_{\mathrm{x}}\big)\overline{\boldsymbol{X}}_{\mathrm{x}}^{-1} \qquad (3.202)$$

is a Hurwitz matrix, the system (3.190) is stable.

Remark 3.6.6. *Unlike for linear time invariant systems like the mSOGI (with constant frequency) (3.66), the eigenvalues of $\underline{\boldsymbol{A}}_{\mathrm{x}}$ only give information on stability (shown in Section 3.6.3); they do* not *allow for a specification of the system dynamics, which is shown in the following. First, an additional requirement of $\underline{\boldsymbol{A}}_{\mathrm{x}}$ is formulated as*

$$\underline{\boldsymbol{A}}_{\mathrm{x}}(\overline{\boldsymbol{x}}_{\mathrm{x}}, \widehat{\overline{\boldsymbol{x}}}_{\mathrm{x}}) = \underline{\boldsymbol{V}}_{\mathrm{x}} \underline{\boldsymbol{D}}_{\mathrm{x}}(\overline{\boldsymbol{x}}_{\mathrm{x}}, \widehat{\overline{\boldsymbol{x}}}_{\mathrm{x}}) \underline{\boldsymbol{V}}_{\mathrm{x}}^{-1} \tag{3.203}$$

with constant $\underline{\boldsymbol{V}}_{\mathrm{x}}$. *If $\underline{\boldsymbol{A}}_{\mathrm{x}}$ can be decomposed into*

$$\underline{\boldsymbol{A}}_{\mathrm{x}} = \underline{\boldsymbol{B}}_{\mathrm{x}} + t \tfrac{\mathrm{d}}{\mathrm{d}t} \underline{\boldsymbol{B}}_{\mathrm{x}}, \tag{3.204}$$

then, by using Observation 2.19, the following holds:

$$\begin{aligned}
&\forall\, t \in \mathbb{T}_i\colon\ \tfrac{\mathrm{d}}{\mathrm{d}t} \underline{\overline{\boldsymbol{e}}}_{\mathrm{x}} = \underline{\boldsymbol{A}}_{\mathrm{x}} \underline{\overline{\boldsymbol{e}}}_{\mathrm{x}} \\
&\overset{(3.204)}{\Longrightarrow}\ \boldsymbol{0}_{v+n} = \mathrm{e}^{-\underline{\boldsymbol{B}}_{\mathrm{x}} t} \big(\underline{\boldsymbol{B}}_{\mathrm{x}} + t \tfrac{\mathrm{d}}{\mathrm{d}t} \underline{\boldsymbol{B}}_{\mathrm{x}}\big) \underline{\overline{\boldsymbol{e}}}_{\mathrm{x}} - \mathrm{e}^{-\underline{\boldsymbol{B}}_{\mathrm{x}} t} \tfrac{\mathrm{d}}{\mathrm{d}t} \underline{\overline{\boldsymbol{e}}}_{\mathrm{x}} \overset{(2.25)}{=} -\tfrac{\mathrm{d}}{\mathrm{d}t}\big(\mathrm{e}^{-\underline{\boldsymbol{B}}_{\mathrm{x}} t} \underline{\overline{\boldsymbol{e}}}_{\mathrm{x}}\big) \\
&\Longrightarrow \int_{t_i}^{t} \boldsymbol{0}_{v+n} \mathrm{d}\tau = -\int_{t_i}^{t} \tfrac{\mathrm{d}}{\mathrm{d}\tau}\big(\mathrm{e}^{-\underline{\boldsymbol{B}}_{\mathrm{x}} \tau} \underline{\overline{\boldsymbol{e}}}_{\mathrm{x}}\big) \mathrm{d}\tau = \mathrm{e}^{-\underline{\boldsymbol{B}}_{\mathrm{x}}(\overline{\boldsymbol{x}}_{\mathrm{x},t_i}, \widehat{\overline{\boldsymbol{x}}}_{\mathrm{x},t_i}) t_i} \underline{\overline{\boldsymbol{e}}}_{\mathrm{x},t_i} - \mathrm{e}^{-\underline{\boldsymbol{B}}_{\mathrm{x}}(\overline{\boldsymbol{x}}_{\mathrm{x}}, \widehat{\overline{\boldsymbol{x}}}_{\mathrm{x}}) t} \underline{\overline{\boldsymbol{e}}}_{\mathrm{x}} \\
&\quad \Longrightarrow \quad \underline{\overline{\boldsymbol{e}}}_{\mathrm{x}} = \mathrm{e}^{\underline{\boldsymbol{B}}_{\mathrm{x}}(\overline{\boldsymbol{x}}_{\mathrm{x}}, \widehat{\overline{\boldsymbol{x}}}_{\mathrm{x}}) t - \underline{\boldsymbol{B}}_{\mathrm{x}}(\overline{\boldsymbol{x}}_{\mathrm{x},t_i}, \widehat{\overline{\boldsymbol{x}}}_{\mathrm{x},t_i}) t_i} \underline{\overline{\boldsymbol{e}}}_{\mathrm{x},t_i}.
\end{aligned} \tag{3.205}$$

This expression does not allow insight into the system dynamics. So, neither $\underline{\boldsymbol{A}}_{\mathrm{x}}$ nor $\underline{\boldsymbol{B}}_{\mathrm{x}}$ can be manipulated such that certain *specifications (except stability) of (3.190) are met.*

Remark 3.6.7. *Since it is desirable to choose the eigenvalues of $\underline{\boldsymbol{A}}_{\mathrm{x}}$ as only being dependent on $\widehat{\boldsymbol{\omega}}_{\mathrm{x}}$, it is advised that*

$$\underline{\boldsymbol{A}}_{\mathrm{x}}(\overline{\boldsymbol{x}}_{\mathrm{x}}, \widehat{\overline{\boldsymbol{x}}}_{\mathrm{x}}) \overset{!}{=} \underline{\boldsymbol{A}}_{\mathrm{x}}(\widehat{\boldsymbol{\omega}}_{\mathrm{x}}) \qquad \Longrightarrow \qquad \underline{\boldsymbol{Q}}_{\mathrm{x}}(\overline{\boldsymbol{x}}_{\mathrm{x}}, \widehat{\overline{\boldsymbol{x}}}_{\mathrm{x}}) = \underline{\boldsymbol{Q}}_{\mathrm{x}}(\widehat{\boldsymbol{\omega}}_{\mathrm{x}}).$$

To meet the requirement of $\underline{\boldsymbol{A}}_{\mathrm{x}} := \begin{bmatrix} \underline{\boldsymbol{A}}_{\mathrm{x},x} & \underline{\boldsymbol{A}}_{\mathrm{x},\delta} \\ \underline{\boldsymbol{A}}_{\mathrm{x},\varepsilon} & \underline{\boldsymbol{A}}_{\mathrm{x},\omega} \end{bmatrix}$, its elements are investigated blockwise with

$$\underline{\boldsymbol{W}}_{\mathrm{x},x} := (\boldsymbol{I}_v - \boldsymbol{W}_{\mathrm{x},x,1})(\boldsymbol{I}_v - \boldsymbol{W}_{\mathrm{x},x,2}) \qquad \text{and} \qquad \underline{\boldsymbol{W}}_{\mathrm{x},J} := (\boldsymbol{I}_v - \boldsymbol{W}_{\mathrm{x},x,1}) \boldsymbol{W}_{\mathrm{x},x,2}$$

and by invoking (3.195), (3.196) and (3.200) as

$$\left.\begin{aligned}
\underline{\boldsymbol{A}}_{\mathrm{x},x}(\widehat{\boldsymbol{\omega}}_{\mathrm{x}}) &= \big(\underline{\boldsymbol{A}}_{\mathrm{x},1} - \underline{\boldsymbol{A}}_{\mathrm{x},2} \boldsymbol{\Xi}_{\mathrm{x},x}\big)\big(\boldsymbol{X}_{\mathrm{x}} - \boldsymbol{\Xi}_{\mathrm{x},\omega} \boldsymbol{\Omega}_{\mathrm{x}}^{-1} \boldsymbol{\Xi}_{\mathrm{x},x}\big)^{-1} \\
\underline{\boldsymbol{A}}_{\mathrm{x},\delta}(\widehat{\boldsymbol{\omega}}_{\mathrm{x}}) &= \underline{\boldsymbol{A}}_{\mathrm{x},2} - \big(\underline{\boldsymbol{A}}_{\mathrm{x},1} - \underline{\boldsymbol{A}}_{\mathrm{x},2} \boldsymbol{\Xi}_{\mathrm{x},x}\big)\big(\boldsymbol{X}_{\mathrm{x}} - \boldsymbol{\Xi}_{\mathrm{x},\omega} \boldsymbol{\Omega}_{\mathrm{x}}^{-1} \boldsymbol{\Xi}_{\mathrm{x},x}\big)^{-1} \boldsymbol{\Xi}_{\mathrm{x},\omega} \boldsymbol{\Omega}_{\mathrm{x}}^{-1} \\
\underline{\boldsymbol{A}}_{\mathrm{x},\varepsilon}(\widehat{\boldsymbol{\omega}}_{\mathrm{x}}) &= \big(\underline{\boldsymbol{A}}_{\mathrm{x},3} - \underline{\boldsymbol{A}}_{\mathrm{x},4} \boldsymbol{\Xi}_{\mathrm{x},x}\big)\big(\boldsymbol{X}_{\mathrm{x}} - \boldsymbol{\Xi}_{\mathrm{x},\omega} \boldsymbol{\Omega}_{\mathrm{x}}^{-1} \boldsymbol{\Xi}_{\mathrm{x},x}\big)^{-1} \\
\underline{\boldsymbol{A}}_{\mathrm{x},\omega}(\widehat{\boldsymbol{\omega}}_{\mathrm{x}}) &= \underline{\boldsymbol{A}}_{\mathrm{x},4} - \big(\underline{\boldsymbol{A}}_{\mathrm{x},3} - \underline{\boldsymbol{A}}_{\mathrm{x},4} \boldsymbol{\Xi}_{\mathrm{x},x}\big)\big(\boldsymbol{X}_{\mathrm{x}} - \boldsymbol{\Xi}_{\mathrm{x},\omega} \boldsymbol{\Omega}_{\mathrm{x}}^{-1} \boldsymbol{\Xi}_{\mathrm{x},x}\big)^{-1} \boldsymbol{\Xi}_{\mathrm{x},\omega} \boldsymbol{\Omega}_{\mathrm{x}}^{-1}.
\end{aligned}\right\} \tag{3.206}$$

Therein, the substitutes

$$\left.\begin{aligned}
\underline{\boldsymbol{A}}_{\mathrm{x},1} &:= \tfrac{\mathrm{d}}{\mathrm{d}t} \boldsymbol{X}_{\mathrm{x}} + \boldsymbol{X}_{\mathrm{x}} \underline{\boldsymbol{K}}_{\mathrm{x},1} - \boldsymbol{\Xi}_{\mathrm{x},\omega} \underline{\boldsymbol{K}}_{\mathrm{x},3} \\
\underline{\boldsymbol{A}}_{\mathrm{x},2} &:= \big(\tfrac{\mathrm{d}}{\mathrm{d}t} \boldsymbol{\Xi}_{\mathrm{x},\omega} + \boldsymbol{X}_{\mathrm{x}} \underline{\boldsymbol{K}}_{\mathrm{x},2} + \boldsymbol{\Xi}_{\mathrm{x},\omega} \underline{\boldsymbol{K}}_{\mathrm{x},4}\big) \boldsymbol{\Omega}_{\mathrm{x}}^{-1} \\
\underline{\boldsymbol{A}}_{\mathrm{x},3} &:= \tfrac{\mathrm{d}}{\mathrm{d}t} \boldsymbol{\Xi}_{\mathrm{x},x} + \boldsymbol{\Xi}_{\mathrm{x},x} \underline{\boldsymbol{K}}_{\mathrm{x},1} - \boldsymbol{\Omega}_{\mathrm{x}} \underline{\boldsymbol{K}}_{\mathrm{x},3} \\
\underline{\boldsymbol{A}}_{\mathrm{x},4} &:= \big(\tfrac{\mathrm{d}}{\mathrm{d}t} \boldsymbol{\Omega}_{\mathrm{x}} + \boldsymbol{\Xi}_{\mathrm{x},x} \underline{\boldsymbol{K}}_{\mathrm{x},2} + \boldsymbol{\Omega}_{\mathrm{x}} \underline{\boldsymbol{K}}_{\mathrm{x},4}\big) \boldsymbol{\Omega}_{\mathrm{x}}^{-1}
\end{aligned}\right\} \tag{3.207}$$

and

$$\left.\begin{aligned}
\underline{\boldsymbol{K}}_{\mathrm{x},1} &:= \boldsymbol{J}_{\mathrm{x}}(\widehat{\boldsymbol{\omega}}_{\mathrm{x}}) + \underline{\boldsymbol{W}}_{\mathrm{x},J}\boldsymbol{J}_{\mathrm{x}}(\boldsymbol{e}_{\mathrm{x},\omega}) - \underline{\boldsymbol{W}}_{\mathrm{x},x}\overline{\boldsymbol{l}}_{\mathrm{x},x}\boldsymbol{c}_{\mathrm{x},\omega}^{\top}\boldsymbol{e}_{\mathrm{x},\omega}\boldsymbol{c}_{\mathrm{x}}^{\top} - \overline{\boldsymbol{l}}_{\mathrm{x},x}\boldsymbol{c}_{\mathrm{x},\omega}^{\top}\widehat{\boldsymbol{\omega}}_{\mathrm{x}}\boldsymbol{c}_{\mathrm{x}}^{\top}\\
\underline{\boldsymbol{K}}_{\mathrm{x},2} &:= \overline{\boldsymbol{J}}_{\mathrm{x}}(\boldsymbol{x}_{\mathrm{x}}) - \underline{\boldsymbol{W}}_{\mathrm{x},J}\overline{\boldsymbol{J}}_{\mathrm{x}}(\boldsymbol{e}_{\mathrm{x}}) + e_{\mathrm{x},y}\underline{\boldsymbol{W}}_{\mathrm{x},x}\overline{\boldsymbol{l}}_{\mathrm{x},x}\boldsymbol{c}_{\mathrm{x},\omega}^{\top}\\
\underline{\boldsymbol{K}}_{\mathrm{x},3} &:= \boldsymbol{L}_{\mathrm{x},\omega}(\widehat{\overline{\boldsymbol{x}}}_{\mathrm{x}})\widehat{\boldsymbol{\omega}}_{\mathrm{x}}\boldsymbol{c}_{\mathrm{x}}^{\top} + (\boldsymbol{I}_n - \boldsymbol{W}_{\mathrm{x},\omega})\boldsymbol{L}_{\mathrm{x},\omega}(\widehat{\overline{\boldsymbol{x}}}_{\mathrm{x}})\boldsymbol{e}_{\mathrm{x},\omega}\boldsymbol{c}_{\mathrm{x}}^{\top}\\
\underline{\boldsymbol{K}}_{\mathrm{x},4} &:= e_{\mathrm{x},y}(\boldsymbol{I}_n - \boldsymbol{W}_{\mathrm{x},\omega})\boldsymbol{L}_{\mathrm{x},\omega}(\widehat{\overline{\boldsymbol{x}}}_{\mathrm{x}}).
\end{aligned}\right\} \tag{3.208}$$

are used.

3.6.3 Concluding remarks

In this section, some hints based on the calculations so far are given. Thereafter, all open tasks are summarized.
First note that, since $\underline{\boldsymbol{A}}_{\mathrm{x}}$ must be independent of $\boldsymbol{e}_{\mathrm{x}}$ and $\boldsymbol{e}_{\mathrm{x},\omega}$, the same must hold true for $\underline{\boldsymbol{A}}_{\mathrm{x},1},\dots,\underline{\boldsymbol{A}}_{\mathrm{x},4}$ since in view of (3.206), it holds exemplarily that

$$\begin{aligned}
\boldsymbol{0}_{v\times v} &= \big(\underline{\boldsymbol{A}}_{\mathrm{x},1}(\boldsymbol{e}_{\mathrm{x}}) - \underline{\boldsymbol{A}}_{\mathrm{x},2}(\boldsymbol{e}_{\mathrm{x}})\boldsymbol{\Xi}_{\mathrm{x},x}\big)\big(\boldsymbol{X}_{\mathrm{x}} - \boldsymbol{\Xi}_{\mathrm{x},\omega}\boldsymbol{\Omega}_{\mathrm{x}}^{-1}\boldsymbol{\Xi}_{\mathrm{x},x}\big)^{-1}\\
\boldsymbol{0}_{v\times n} &= \underline{\boldsymbol{A}}_{\mathrm{x},2}(\boldsymbol{e}_{\mathrm{x}}) - \big(\underline{\boldsymbol{A}}_{\mathrm{x},1}(\boldsymbol{e}_{\mathrm{x}}) - \underline{\boldsymbol{A}}_{\mathrm{x},2}(\boldsymbol{e}_{\mathrm{x}})\boldsymbol{\Xi}_{\mathrm{x},x}\big)\big(\boldsymbol{X}_{\mathrm{x}} - \boldsymbol{\Xi}_{\mathrm{x},\omega}\boldsymbol{\Omega}_{\mathrm{x}}^{-1}\boldsymbol{\Xi}_{\mathrm{x},x}\big)^{-1}\boldsymbol{\Xi}_{\mathrm{x},\omega}\boldsymbol{\Omega}_{\mathrm{x}}^{-1}\\
&\implies \quad \underline{\boldsymbol{A}}_{\mathrm{x},1}(\boldsymbol{e}_{\mathrm{x}}) = \boldsymbol{0}_{v\times v}, \qquad \underline{\boldsymbol{A}}_{\mathrm{x},2}(\boldsymbol{e}_{\mathrm{x}}) = \boldsymbol{0}_{v\times n}.
\end{aligned}$$

Second, the following assumption seems reasonable:

Assumption 3.6.8.

- *All weighting matrices* $\underline{\boldsymbol{W}}_{\mathrm{x},x}, \underline{\boldsymbol{W}}_{\mathrm{x},J}$ *and* $\boldsymbol{W}_{\mathrm{x},\omega}$ *are independent of* $\boldsymbol{e}_{\mathrm{x}}$ *and* $\boldsymbol{e}_{\mathrm{x},\omega}$*; and*
- *The matrix* $\overline{\boldsymbol{X}}_{\mathrm{x}}$ *is independent of* $\boldsymbol{e}_{\mathrm{x}}$ *and* $\boldsymbol{e}_{\mathrm{x},\omega}$.

What remains is to obtain a solution for $\overline{\boldsymbol{X}}_{\mathrm{x}}$ where the results shown in the previous Section 3.6.2 might help, and also the choice of $\underline{\boldsymbol{A}}_{\mathrm{x}}$ is a question to be answered. However, it is assumed that the matrices $\underline{\boldsymbol{A}}_{\mathrm{x}}$, $\overline{\boldsymbol{X}}_{\mathrm{x}}$, $\underline{\boldsymbol{W}}_{\mathrm{x},J}$, $\underline{\boldsymbol{W}}_{\mathrm{x},x}$ and $\boldsymbol{W}_{\mathrm{x},\omega}$ are unique (besides the tuning). Note that the matrices $\underline{\boldsymbol{W}}_{\mathrm{x},J}$, $\underline{\boldsymbol{W}}_{\mathrm{x},x}$ and $\boldsymbol{W}_{\mathrm{x},\omega}$ manipulate the matrix $\widetilde{\boldsymbol{J}}$ and the gains $\boldsymbol{l}_{\mathrm{x},x}$ and $\boldsymbol{L}_{\mathrm{x},\omega}$. This can be used to manipulate (3.208), which facilitates the existence of a solution.
Assuming a set of matrices $\underline{\boldsymbol{A}}_{\mathrm{x}}$, $\overline{\boldsymbol{X}}_{\mathrm{x}}$, $\underline{\boldsymbol{W}}_{\mathrm{x},J}$, $\underline{\boldsymbol{W}}_{\mathrm{x},x}$ and $\boldsymbol{W}_{\mathrm{x},\omega}$ satisfying the constraints is found, then the final steps are briefly drawn as
1. Pole placement:
A tuning rule must be derived, which outputs a tuning vector $\boldsymbol{l}_{\mathrm{x}}$ such that the matrix $\underline{\boldsymbol{A}}_{\mathrm{x}}$ has desired eigenvalues $\{\underline{\lambda}_{\mathrm{x},1},\dots,\underline{\lambda}_{\mathrm{x},v+n}\} \subset \mathbb{C}_{\mathrm{NHP}}$ and therefore is Hurwitz. As stated in Remark 3.6.6, these only give information on system stability but not on system dynamics. That is, their influence on system dynamics is not clear.
2. Proof of boundedness and decrease of $\underline{\overline{e}}_{\mathrm{x}}$:
If $\underline{\boldsymbol{A}}_{\mathrm{x}}$ is Hurwitz, it holds that

$$V_{\mathrm{x}}(\underline{\overline{e}}_{\mathrm{x}}) = \underline{\overline{e}}_{\mathrm{x}}^{\top}\underline{\boldsymbol{P}}_{\mathrm{x}}\underline{\overline{e}}_{\mathrm{x}} \;\Rightarrow\; \tfrac{\mathrm{d}}{\mathrm{d}t}V_{\mathrm{x}}(\underline{\overline{e}}_{\mathrm{x}}) = -\underline{\overline{e}}_{\mathrm{x}}^{\top}\underline{\boldsymbol{Q}}_{\mathrm{x}}(\widehat{\boldsymbol{\omega}}_{\mathrm{x}})\underline{\overline{e}}_{\mathrm{x}}.$$

Thus, it follows that

$$\forall t\in\mathbb{T}_i:\quad \tfrac{\mathrm{d}}{\mathrm{d}t}V_{\mathrm{x}}(\underline{\overline{e}}_{\mathrm{x}}) \overset{(2.16)}{\leq} -\lambda_{\min}(\underline{\boldsymbol{Q}}_{\mathrm{x}}(\widehat{\boldsymbol{\omega}}_{\mathrm{x}}))\,\|\underline{\overline{e}}_{\mathrm{x}}\|^2$$

$$\stackrel{(2.16)}{\leq} -\underbrace{\frac{\lambda_{\min}(\underline{\boldsymbol{Q}}_{\mathrm{x}}(\widehat{\boldsymbol{\omega}}_{\mathrm{x}}))}{\lambda_{\max}(\underline{\boldsymbol{P}}_{\mathrm{x}})}}_{=:\,\mu_{\mathrm{x},V}(\widehat{\boldsymbol{\omega}}_{\mathrm{x}})>0} V_{\mathrm{x}}(\underline{\overline{\boldsymbol{e}}}_{\mathrm{x}}) \quad \stackrel{(2.17)}{\Longrightarrow} \quad V_{\mathrm{x}}(\underline{\overline{\boldsymbol{e}}}_{\mathrm{x}}) \leq V_{\mathrm{x}}(\underline{\overline{\boldsymbol{e}}}_{\mathrm{x},t_i})\mathrm{e}^{-\int_{t_i}^{t}\mu_{\mathrm{x},V}(\widehat{\boldsymbol{\omega}}_{\mathrm{x}})\mathrm{d}\tau}$$

and therefore

$$\forall\, t \in \mathbb{T}_i: \qquad \|\underline{\overline{\boldsymbol{e}}}_{\mathrm{x}}\|^2 \stackrel{(2.16)}{\leq} \frac{V_{\mathrm{x}}(\underline{\overline{\boldsymbol{e}}}_{\mathrm{x},t_i})\mathrm{e}^{-\int_{t_i}^{t}\mu_{\mathrm{x},V}(\widehat{\boldsymbol{\omega}}_{\mathrm{x}})\mathrm{d}\tau}}{\lambda_{\min}(\underline{\boldsymbol{P}}_{\mathrm{x}})} \stackrel{(2.16)}{\leq} \underbrace{\frac{\lambda_{\max}(\underline{\boldsymbol{P}}_{\mathrm{x}})}{\lambda_{\min}(\underline{\boldsymbol{P}}_{\mathrm{x}})}}_{=:\,c_{\mathrm{x},V}^2>0} \left\|\underline{\overline{\boldsymbol{e}}}_{\mathrm{x},t_i}\right\|^2 \mathrm{e}^{-\int_{t_i}^{t}\mu_{\mathrm{x},V}(\widehat{\boldsymbol{\omega}}_{\mathrm{x}})\mathrm{d}\tau}.$$

Since $\mu_{\mathrm{x},V} > 0$ for all $t \in \mathbb{T}_i$, $\int_{t_i}^{t} \mu_{\mathrm{x},V}\mathrm{d}\tau$ is a strictly monotonically increasing function. Thus, it holds that

$$\forall\, t \in \mathbb{T}_i: \qquad \|\underline{\overline{\boldsymbol{e}}}_{\mathrm{x}}\| < \infty \quad \text{and} \quad \lim_{t\to\infty} \|\underline{\overline{\boldsymbol{e}}}_{\mathrm{x}}\| \to 0.$$

Remark 3.6.9. *Note that this does* not *prove stability of the overall error $\overline{\boldsymbol{e}}_{\mathrm{x}}$ in α, β frame. To be able to show this, more information on the transformation matrix is necessary. Hereby, several methods are possible. It can be shown that*

(i) the spectral norm of $\overline{\boldsymbol{X}}_{\mathrm{x}}^{-1}$ is bounded, wich implies that $\|\overline{\boldsymbol{e}}_{\mathrm{x}}\| \stackrel{(3.198)}{\leq} \left\|\overline{\boldsymbol{X}}_{\mathrm{x}}^{-1}\right\| \|\underline{\overline{\boldsymbol{e}}}_{\mathrm{x}}\| < \infty$;

(ii) every element of $\overline{\boldsymbol{e}}_{\mathrm{x}}$ must be bounded, since every element of $\|\underline{\overline{\boldsymbol{e}}}_{\mathrm{x}}\| \stackrel{(3.198)}{=} \left\|\overline{\boldsymbol{X}}_{\mathrm{x}}\overline{\boldsymbol{e}}_{\mathrm{x}}\right\|$ is bounded (as it was used in Theorem 3.5.3).

If boundedness of $\overline{\boldsymbol{e}}_{\mathrm{x}}$ can be shown, this implies boundedness of $\widehat{\overline{\boldsymbol{x}}}_{\mathrm{x}}$ since

$$\|\overline{\boldsymbol{x}}\|_{\infty} < \infty, \quad \|\overline{\boldsymbol{e}}_{\mathrm{x}}\| < \infty \quad \Longrightarrow \quad \left\|\widehat{\overline{\boldsymbol{x}}}_{\mathrm{x}}\right\| \stackrel{(3.194)}{=} \|\overline{\boldsymbol{x}} - \overline{\boldsymbol{e}}_{\mathrm{x}}\| \leq \|\overline{\boldsymbol{x}}\|_{\infty} + \|\overline{\boldsymbol{e}}_{\mathrm{x}}\| < \infty.$$

Chapter 4

Experimental validation

Now, the theoretical results shown in Chapter 3 are investigated in terms of experimental validation. Additionally, comparisons to existing methods taken from literature are shown. Therefore, firstly the chosen systems from literature are shown in Section 4.1. Afterwards, in Section 4.2, the signals to be investigated are defined. In Section 4.3, these signals are used for validation and comparison purposes of proposed systems and literature.

4.1 Reference systems

As reference systems, a set of systems has been selected with the aim of covering a wide variety of functionalities. However, these are chosen with the restriction of time-continuous implementation and estimation in the α, β-frame. Angular frequency estimation and offset estimation/detection is optional. The selected systems are shown in the following, where

Section 4.1.1 shows the Multi-Magnitude Integrator Quadrature Signal Generator,

Section 4.1.2 shows the Multiple Second Order Generalized Integrators Frequency Locked Loop and

Section 4.1.3 shows the Multi Adapted Frequency Locked Loop.

4.1.1 The Multi-Magnitude Integrator Quadrature Signal Generator

The first system selected is taken from [494]. It is called the *Multi Magnitude Integrator Quadrature Signal Generator* (MMI-QSG). It is designed to extract the harmonic components x_i^α, x_i^β; estimation of frequency or offset is not its purpose. The MMI-QSG's dynamics, marked by the subscript "mmi", are described by the set of differential equations[1]

$$\forall\, t \in \mathbb{T}_i\colon \quad \left.\begin{aligned} \tfrac{\mathrm{d}}{\mathrm{d}t}\widehat{\boldsymbol{x}}_{\mathrm{mmi}} &= \left(\boldsymbol{J}_{\mathrm{mmi}} - \boldsymbol{l}_{\mathrm{mmi}}\boldsymbol{c}_{\mathrm{mmi}}^\top\right)\widehat{\boldsymbol{x}}_{\mathrm{mmi}} + \boldsymbol{l}_{\mathrm{mmi}} y, \quad \widehat{\boldsymbol{x}}_{\mathrm{mmi}}(t_i) = \widehat{\boldsymbol{x}}_{\mathrm{mmi},t_i} \\ \widehat{y}_{\mathrm{mmi}} &= \boldsymbol{c}_{\mathrm{mmi}}^\top \widehat{\boldsymbol{x}}_{\mathrm{mmi}}. \end{aligned}\right\} \tag{4.1}$$

The system vectors and matrix are specified as

$$\boldsymbol{J}_{\mathrm{mmi}} = \underset{1,\ldots,n}{\mathrm{blkdiag}}\left(\begin{bmatrix} 0 & -\omega_i^2 & 2l_{\mathrm{mmi}} \\ 1 & 0 & 0 \\ 0 & 0 & 0 \end{bmatrix}\right) \in \mathbb{R}^{3n\times 3n},$$

[1] The system equations are obtained from Figure 3 inside [494]. Since it only shows the MMI-QSG for $n = 4$, it is generically parallelized here.

$$\begin{aligned}
&\boldsymbol{l}_{\mathrm{mmi}} = (2l_{\mathrm{mmi}},\, 0,\, \tfrac{l_{\mathrm{mmi}}}{2},\, \cdots,\, 2l_{\mathrm{mmi}},\, 0,\, \tfrac{l_{\mathrm{mmi}}}{2})^\top \in \mathbb{R}^{3n},\\
&\boldsymbol{c}_{\mathrm{mmi}} = (1,\, 0,\, 0,\, \cdots,\, 1,\, 0,\, 0)^\top \in \mathbb{R}^{3n},\\
\text{and}\quad &\widehat{\boldsymbol{x}}_{\mathrm{mmi}} = (\widehat{x}^{\alpha}_{\mathrm{mmi},1},\, \widehat{x}^{\beta}_{\mathrm{mmi},1},\, \widehat{x}^{\gamma}_{\mathrm{mmi},1},\, \cdots,\, \widehat{x}^{\alpha}_{\mathrm{mmi},n},\, \widehat{x}^{\beta}_{\mathrm{mmi},n},\, \widehat{x}^{\gamma}_{\mathrm{mmi},n})^\top \in \mathbb{R}^{3n}.
\end{aligned}$$

The block diagram of the MMI-QSG is illustrated in Figure 4.1.

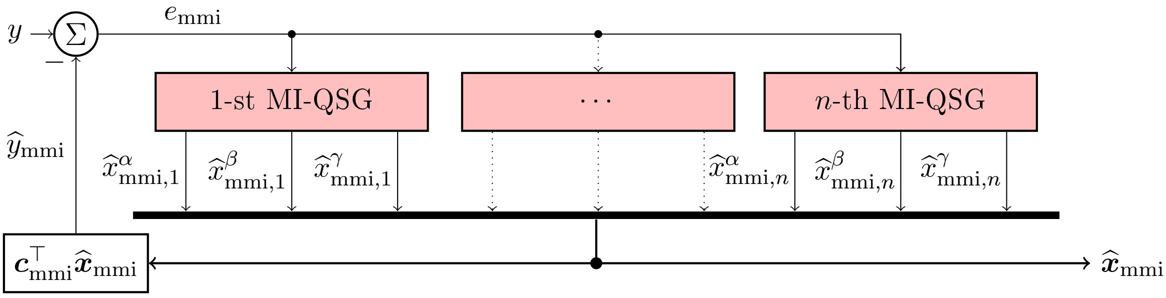

(a) *Block diagram of the MMI-QSG structure.*

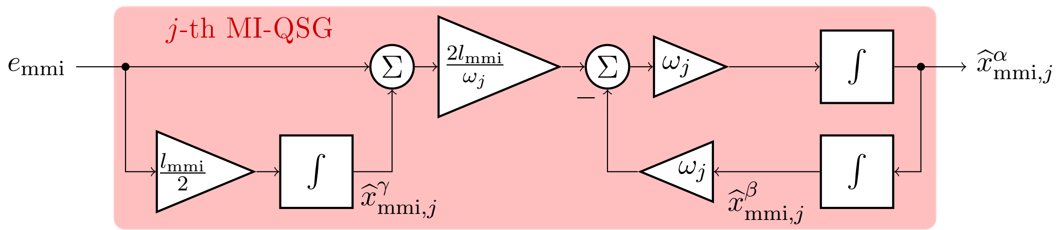

(b) *Construction of the j-th MI-QSG.*

Figure 4.1: *(a): The parallelized structure of MI-QSGs and (b): the j-th MI-QSG for amplitude and phase estimation of the j-th component.*

4.1.2 The Multiple Second-Order Generalized Integrators-Frequency Locked Loop

The next reference considered is selected from [492]. In the paper, it is denoted as the *Multiple Second-Order Generalized Integrators-Frequency Locked Loop* (MSOGI-FLL). Its purpose is to estimate the harmonic components x_i^α, x_i^β and the fundamental angular frequency ω_1; offset estimation is not considered. Here, it is indicated by the subscript “msf”. It is a parallelization of sSOGIs; the used SOGI structure is similar to the right block diagram shown in Figure 3.4. Additionally, it comes with an sFLL with Gain Normalization as in (3.51). Although in [492], a lower amplitude limitation $\varepsilon_{\mathrm{msf}} > 0$ was not used inside the FLL, it is included here. The overall system dynamics are described by

$$\forall t \in \mathbb{T}_i:\quad \left.\begin{aligned}
\tfrac{\mathrm{d}}{\mathrm{d}t}\widehat{\boldsymbol{x}}_{\mathrm{msf}} &= \left(\boldsymbol{J}_{\mathrm{msf}} - \boldsymbol{l}_{\mathrm{msf}}\boldsymbol{c}^\top_{\mathrm{msf}}\right)\widehat{\boldsymbol{x}}_{\mathrm{msf}} + \boldsymbol{l}_{\mathrm{msf}}y, && \widehat{\boldsymbol{x}}_{\mathrm{msf}}(t_i) = \widehat{\boldsymbol{x}}_{\mathrm{msf},t_i}\\
\widehat{y}_{\mathrm{msf}} &= \boldsymbol{c}^\top_{\mathrm{msf}}\widehat{\boldsymbol{x}}_{\mathrm{msf}}\\
e_{\mathrm{msf}} &= y - \boldsymbol{c}^\top_{\mathrm{msf}}\widehat{\boldsymbol{x}}_{\mathrm{msf}}\\
\tfrac{\mathrm{d}}{\mathrm{d}t}\widehat{\omega}_{\mathrm{msf}} &= \frac{-l_{\mathrm{msf}}\Gamma_{\mathrm{msf}}\widehat{\omega}_{\mathrm{msf}}e_{\mathrm{msf}}\widehat{x}^{\beta}_{\mathrm{msf},\nu_1}}{\max\left(\left\|(\widehat{x}^{\alpha}_{\mathrm{msf},\nu_1}, \widehat{x}^{\beta}_{\mathrm{msf},\nu_1})\right\|^2, \varepsilon_{\mathrm{msf}}\right)}, && \widehat{\omega}_{\mathrm{msf}}(t_i) = \widehat{\omega}_{\mathrm{msf},t_i}.
\end{aligned}\right\} \tag{4.2}$$

The matrices and vectors are given as follows

$$\boldsymbol{J}_{\mathrm{msf}} = \operatorname*{blkdiag}_{1,\ldots,n}\left(\begin{bmatrix} 0 & -\nu_i^2\widehat{\omega}^2_{\mathrm{msf}} \\ 1 & 0 \end{bmatrix}\right) \in \mathbb{R}^{2n\times 2n},$$

$$\begin{aligned} \boldsymbol{l}_{\text{msf}} &= \widehat{\omega}_{\text{msf}}(l_{\text{msf}},\, 0,\, \cdots,\, l_{\text{msf}},\, 0)^\top \in \mathbb{R}^{2n}, \\ \boldsymbol{c}_{\text{msf}} &= (1,\, 0,\, \cdots,\, 1,\, 0)^\top \in \mathbb{R}^{2n}, \\ \text{and} \quad \widehat{\boldsymbol{x}}_{\text{msf}} &= (\widehat{x}^{\alpha}_{\text{msf},1},\, \widehat{x}^{\beta}_{\text{msf},1},\, \cdots,\, \widehat{x}^{\alpha}_{\text{msf},n},\, \widehat{x}^{\beta}_{\text{msf},n}) \in \mathbb{R}^2. \end{aligned}$$

4.1.3 The multi-Adapted Frequency Locked Loop

The last reference system chosen is taken from [545]. It is called the *multi-Adapted Frequency Locked Loop* (mAFLL) and subscripted by "maf". It is designed to estimate all harmonic components x_i^α, x_i^β and all angular frequencies ω_i. Its mathematical representation is given as

$$\forall\, t \in \mathbb{T}_i: \quad \left.\begin{aligned} \tfrac{\mathrm{d}}{\mathrm{d}t}\widehat{\boldsymbol{x}}_{\text{maf}} &= \left(\boldsymbol{J}_{\text{maf}} - \boldsymbol{l}_{\text{maf}}\boldsymbol{c}_{\text{maf}}^\top\right)\widehat{\boldsymbol{x}}_{\text{maf}} + \boldsymbol{l}_{\text{maf}}y, \qquad \widehat{\boldsymbol{x}}_{\text{maf}}(t_i) = \widehat{\boldsymbol{x}}_{\text{maf},t_i} \\ \widehat{y}_{\text{maf}} &= \boldsymbol{c}_{\text{maf}}^\top\widehat{\boldsymbol{x}}_{\text{maf}} \\ e_{\text{maf}} &= y - \boldsymbol{c}_{\text{maf}}^\top\widehat{\boldsymbol{x}}_{\text{maf}} \\ \tfrac{\mathrm{d}}{\mathrm{d}t}\widehat{\boldsymbol{\omega}}_{\text{maf}} &= \left(\boldsymbol{L}_{\text{maf}}e_{\text{maf}} - \widehat{\boldsymbol{X}}_{\text{maf}}\right)\boldsymbol{\Gamma}_{\text{maf}}\boldsymbol{\Sigma}_{\text{maf}}\widehat{\boldsymbol{x}}_{\text{maf}}, \quad \widehat{\boldsymbol{\omega}}_{\text{maf}}(t_i) = \widehat{\boldsymbol{\omega}}_{\text{maf},t_i}. \end{aligned}\right\} \tag{4.3}$$

The system matrices and vectors are obtained from [545] generically as

$$\begin{aligned} \boldsymbol{J}_{\text{maf}} &= \underset{i\in\{1,\dots,n\}}{\text{blkdiag}}\left(\widehat{\omega}_{\text{maf},i}\begin{bmatrix} 0 & -1 & 0 \\ 1 & 0 & 0 \\ 0 & 0 & -l_{\text{maf},i} \end{bmatrix}\right) \in \mathbb{R}^{3n\times 3n}, \\ \boldsymbol{L}_{\text{maf}} &= \underset{i\in\{1,\dots,n\}}{\text{diag}}\left(l_{\text{maf},i}\right) \in \mathbb{R}^{n\times n}, \quad \boldsymbol{\Sigma}_{\text{maf}} = \underset{i\in\{1,\dots,n\}}{\text{blkdiag}}\left(\begin{pmatrix} 0 & -1 & l_{\text{maf},i}\end{pmatrix}\right) \in \mathbb{R}^{n\times 3n}, \\ \widehat{\boldsymbol{X}}_{\text{maf}} &= \underset{i\in\{1,\dots,n\}}{\text{diag}}\left(\widehat{x}^{\gamma}_{\text{maf},i}\right) \in \mathbb{R}^{n\times n}, \quad \boldsymbol{\Gamma}_{\text{maf}} = \underset{i\in\{1,\dots,n\}}{\text{diag}}\left(\widehat{\omega}_{\text{maf},i}\Gamma_{\text{maf},i}\right) \in \mathbb{R}^{n\times n}, \\ \boldsymbol{l}_{\text{maf}} &= (\widehat{\omega}_{\text{maf},1}l^2_{\text{maf},1},\, 0,\, \widehat{\omega}_{\text{maf},1}l^2_{\text{maf},1},\, \cdots,\, \widehat{\omega}_{\text{maf},n}l^2_{\text{maf},n},\, 0,\, \widehat{\omega}_{\text{maf},n}l^2_{\text{maf},n})^\top \in \mathbb{R}^{3n}, \\ \boldsymbol{c}_{\text{maf}} &= (\tfrac{1}{l_{\text{maf},1}},\, 0,\, 0,\, \cdots,\, \tfrac{1}{l_{\text{maf},n}},\, 0,\, 0)^\top \in \mathbb{R}^{3n}, \\ \widehat{\boldsymbol{x}}_{\text{maf}} &= (\widehat{x}^{\alpha}_{\text{maf},1},\, \widehat{x}^{\beta}_{\text{maf},1},\, \widehat{x}^{\gamma}_{\text{maf},1},\, \cdots,\, \widehat{x}^{\alpha}_{\text{maf},n},\, \widehat{x}^{\beta}_{\text{maf},n},\, \widehat{x}^{\gamma}_{\text{maf},n})^\top \in \mathbb{R}^{3n}, \\ \widehat{\boldsymbol{\omega}}_{\text{maf}} &= (\widehat{\omega}_{\text{maf},1},\, \cdots,\, \widehat{\omega}_{\text{maf},n})^\top \in \mathbb{R}^{n}. \end{aligned}$$

However, in [545], they only described their implementation for $n \in \{1, 3\}$ with varying sets of parameters and initial values for each of their investigated four examples. A generic tuning rule or an allowed set of initial values guaranteeing convergence of the mAFLL was not given. Hence, the sets of parameters and initial values showing convergence in the paper are adapted to the examples considered in this thesis. A block diagram of the mAFLL is presented in Figure 4.2.

4.2 Reference signals and scenarios

This section introduces the reference signals used for evaluation and defines eight scenarios. The evaluation is shown in the next Section 4.3.
The scenarios explained in the following list:

Scenario (S1) considers an input signal consisting of only a fundamental wave *without* offset and with a *known* fundamental angular frequency. The FAOs, MMI-QSG, MSOGI-FLL and mAFLL are designed to estimate *one* component wherein angular frequency adaption is implemented but *turned off*. The time frame is $\mathbb{T} = [0\,\text{s}, 0.1\,\text{s}, 0.2\,\text{s}, 0.3\,\text{s}, 0.4\,\text{s}]$. The input signal is designed as follows: At $t = 0.1\,\text{s}$, the amplitude jumps, at $t = 0.2\,\text{s}$, the phase angle jumps and at $t = 0.3\,\text{s}$, the amplitude and phase angle jump. The respective values for

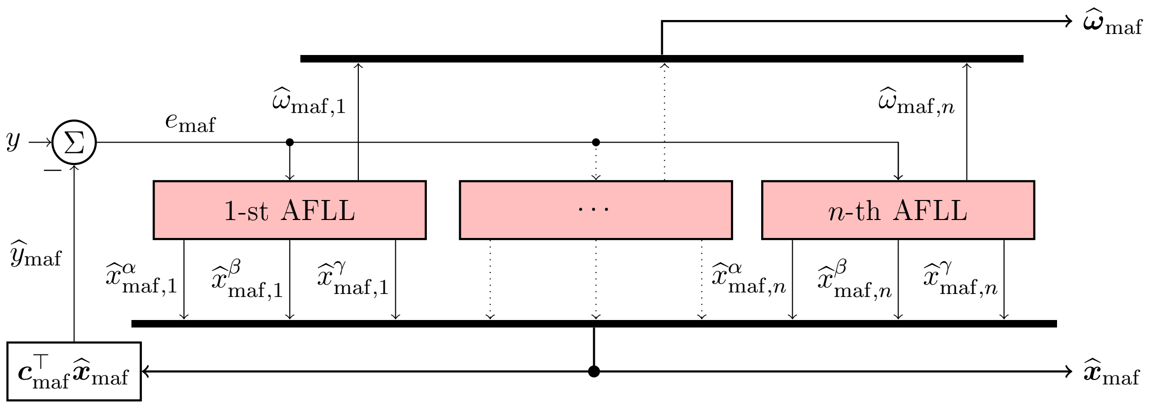

(a) *Block diagram of the mAFLL structure.*

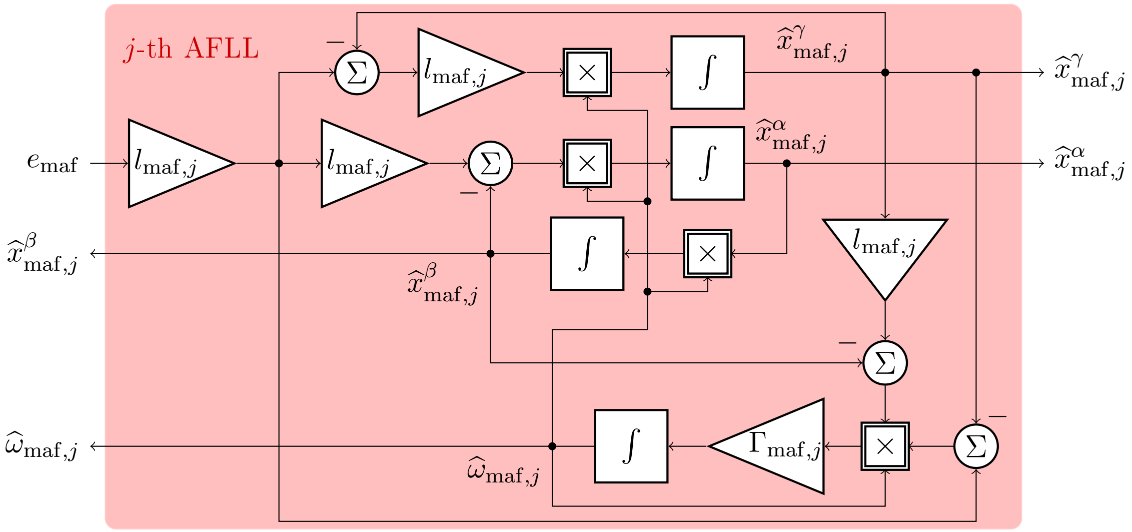

(b) *Construction of the j-th AFLL.*

Figure 4.2: *(a): The parallelized structure of AFLLs and (b): the j-th AFLL for amplitude, phase and frequency estimation of the j-th component.*

amplitude, phase angle, offset, and fundamental angular frequency are collected in Table 4.1. The input signal is plotted in Figure 4.3.

Scenario (S2) considers an input signal consisting of only a fundamental wave *without* offset and with an *unknown* fundamental angular frequency. The FAOs, MMI-QSG, MSOGI-FLL and mAFLL are designed to estimate *one* component wherein angular frequency adaption is *turned on*. The time frame is $\mathbb{T} = [0\,\mathrm{s}, 0.2\,\mathrm{s}, 0.4\,\mathrm{s}, 0.6\,\mathrm{s}, 0.8\,\mathrm{s}]$. The input signal is designed as follows: At $t = 0.2\,\mathrm{s}$, the angular frequency jumps, at $t = 0.4\,\mathrm{s}$, the amplitude and phase angle jump and at $t = 0.6\,\mathrm{s}$, the amplitude, phase angle and angular frequency jump. The respective values for amplitude, phase angle, offset, and fundamental angular frequency are collected in Table 4.2. The input signal is plotted in Figure 4.5.

Scenario (S3) considers an input signal consisting of only a fundamental wave *with* offset and with a *known* fundamental angular frequency. The FAOs, MMI-QSG, MSOGI-FLL and mAFLL are designed to estimate *one* component wherein angular frequency adaption is implemented but *turned off*. The time frame is $\mathbb{T} = [0\,\mathrm{s}, 0.1\,\mathrm{s}, 0.2\,\mathrm{s}, 0.3\,\mathrm{s}, 0.4\,\mathrm{s}]$. The input signal is designed as follows: At $t = 0.1\,\mathrm{s}$, the amplitude and offset jump, at $t = 0.2\,\mathrm{s}$, the phase angle jumps and at $t = 0.3\,\mathrm{s}$, the amplitude, phase angle and offset jump. The respective values for amplitude, phase angle, offset, and fundamental angular frequency are collected in Table 4.3. The input signal is plotted in Figure 4.7.

Scenario (S4) considers an input signal consisting of only a fundamental wave *with* offset and with an *unknown* fundamental angular frequency. The FAOs, MMI-QSG, MSOGI-FLL and mAFLL are designed to estimate *one* component wherein angular frequency adaption is *turned on*. The time frame is $\mathbb{T} = [0\,\mathrm{s}, 0.2\,\mathrm{s}, 0.4\,\mathrm{s}, 0.6\,\mathrm{s}, 0.8\,\mathrm{s}]$. The input signal is designed as follows: At $t = 0.2\,\mathrm{s}$, the fundamental angular frequency jumps, at $t = 0.4\,\mathrm{s}$, the amplitude and offset jump and at $t = 0.6\,\mathrm{s}$, the amplitude, offset and fundamental angular frequency jump. The respective values for amplitude, phase angle, offset, and fundamental angular frequency are collected in Table 4.4. The input signal is plotted in Figure 4.9.

Scenario (S5) considers an input signal consisting of a fundamental wave plus nine harmonic waves *without* offset, with a *known* fundamental angular frequency and *known* harmonic orders. The esFAO, mFAO$_{\circ}$, MMI-QSG and MSOGI-FLL are designed to estimate *ten* components wherein angular frequency adaption is implemented but *turned off*. The time frame is $\mathbb{T} = [0\,\mathrm{s}, 0.1\,\mathrm{s}, 0.2\,\mathrm{s}, 0.3\,\mathrm{s}, 0.4\,\mathrm{s}]$. The input signal is designed as follows: At $t = 0.1\,\mathrm{s}$, all amplitudes jump, at $t = 0.2\,\mathrm{s}$, all phase angles jump and at $t = 0.3\,\mathrm{s}$, all amplitude and phase angles jump. The respective values for amplitudes, phase angles, offset, fundamental angular frequency, and harmonic orders are collected in Table 4.1. The input signal is plotted in Figure 4.4.

Scenario (S6) considers an input signal consisting of a fundamental wave plus nine harmonic waves *without* offset, with an *unknown* fundamental angular frequency and *known* harmonic orders. The esFAO, mFAO$_{\circ}$, MMI-QSG and MSOGI-FLL are designed to estimate *ten* components wherein angular frequency adaption is *turned on*. The time frame is $\mathbb{T} = [0\,\mathrm{s}, 0.2\,\mathrm{s}, 0.4\,\mathrm{s}, 0.6\,\mathrm{s}, 0.8\,\mathrm{s}]$. The input signal is designed as follows: At $t = 0.2\,\mathrm{s}$, the fundamental angular frequency jumps, at $t = 0.4\,\mathrm{s}$, all amplitudes and phase angles jump and at $t = 0.6\,\mathrm{s}$, all amplitudes, phase angles and the fundamental angular frequency jump. The respective values for amplitudes, phase angles, offset, fundamental angular frequency, and harmonic orders are collected in Table 4.2. The input signal is plotted in Figure 4.6.

Scenario (S7) considers an input signal consisting of a fundamental wave plus nine harmonic waves *with* offset, with a *known* fundamental angular frequency and *known* harmonic orders. The esFAO, mFAO$_{\circ}$, MMI-QSG and MSOGI-FLL are designed to estimate *ten* components wherein angular frequency adaption is implemented but *turned off*. The time frame is $\mathbb{T} = [0\,\mathrm{s}, 0.1\,\mathrm{s}, 0.2\,\mathrm{s}, 0.3\,\mathrm{s}, 0.4\,\mathrm{s}]$. The input signal is designed as follows: At $t = 0.1\,\mathrm{s}$, all amplitudes and the offset jump, at $t = 0.2\,\mathrm{s}$, all phase angles jump and at $t = 0.3\,\mathrm{s}$, all amplitudes, phase angles and the offset jump. The respective values for amplitudes, phase angles, offset, fundamental angular frequency, and harmonic orders are collected in Table 4.3. The input signal is plotted in Figure 4.8.

Scenario (S8) considers an input signal consisting of a fundamental wave plus nine harmonic waves *with* offset, with an *unknown* fundamental angular frequency and *known* harmonic orders. The esFAO, mFAO$_{\circ}$, MMI-QSG and MSOGI-FLL are designed to estimate *ten* components wherein angular frequency adaption is *turned on*. The time frame is $\mathbb{T} = [0\,\mathrm{s}, 0.2\,\mathrm{s}, 0.4\,\mathrm{s}, 0.6\,\mathrm{s}, 0.8\,\mathrm{s}]$. The input signal is designed as follows: At $t = 0.2\,\mathrm{s}$, the fundamental angular frequency jumps, at $t = 0.4\,\mathrm{s}$, all amplitudes and the offset jump and at $t = 0.6\,\mathrm{s}$, all amplitudes, the offset and fundamental angular frequency jump. The respective values for amplitudes, phase angles, offset, fundamental angular frequency, and harmonic orders are collected in Table 4.4. The input signal is plotted in Figure 4.10.

i	1	2	3	4	5	6	7	8	9	10
$0\,\mathrm{s} \leq t < 0.1\,\mathrm{s}$										
Harmonic orders ν_i	1	2	3	4	5	6	7	8	9	10
Amplitudes a_i/V	200	35	70	45	35	30	30	20	25	20
Phase angles ϕ_i	0	$\frac{\pi}{4}$	$\frac{10\pi}{7}$	$\frac{\pi}{5}$	$\frac{3\pi}{2}$	$\frac{3\pi}{4}$	0	π	$\frac{\pi}{2}$	0
Offset a_0/V	0									
Fundamental frequency f_1/Hz	50									
$0.1\,\mathrm{s} \leq t < 0.2\,\mathrm{s}$										
Harmonic orders ν_i	1	2	3	4	5	6	7	8	9	10
Amplitudes a_i/V	100	17.5	35	22.5	17.5	15	15	10	12.5	10
Phase angles ϕ_i	0	$\frac{\pi}{4}$	$\frac{10\pi}{7}$	$\frac{\pi}{5}$	$\frac{3\pi}{2}$	$\frac{3\pi}{4}$	0	π	$\frac{\pi}{2}$	0
Offset a_0/V	0									
Fundamental frequency f_1/Hz	50									
$0.2\,\mathrm{s} \leq t < 0.3\,\mathrm{s}$										
Harmonic orders ν_i	1	2	3	4	5	6	7	8	9	10
Amplitudes a_i/V	100	17.5	35	22.5	17.5	15	15	10	12.5	10
Phase angles ϕ_i	$\frac{\pi}{2}$	$\frac{3\pi}{4}$	$\frac{27\pi}{14}$	$\frac{7\pi}{10}$	0	$\frac{5\pi}{4}$	$\frac{\pi}{2}$	$\frac{3\pi}{2}$	π	$\frac{\pi}{2}$
Offset a_0/V	0									
Fundamental frequency f_1/Hz	50									
$0.3\,\mathrm{s} \leq t \leq 0.4\,\mathrm{s}$										
Harmonic orders ν_i	1	2	3	4	5	6	7	8	9	10
Amplitudes a_i/V	200	35	70	45	35	30	30	20	25	20
Phase angles ϕ_i	0	$\frac{\pi}{4}$	$\frac{10\pi}{7}$	$\frac{\pi}{5}$	$\frac{3\pi}{2}$	$\frac{3\pi}{4}$	0	π	$\frac{\pi}{2}$	0
Offset a_0/V	0									
Fundamental frequency f_1/Hz	50									

Table 4.1: *Signal parameters for scenarios (S1) and (S5).*

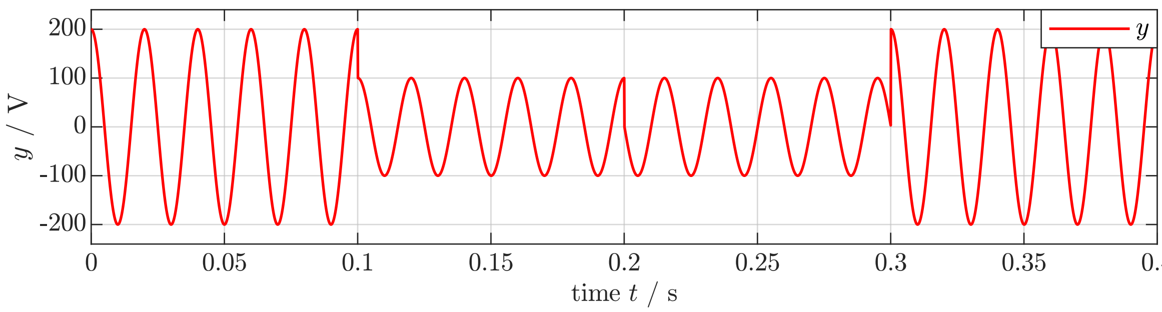

Figure 4.3: *Input signal y for scenario (S1).*

The system parameters for all systems involved in the experiments (esFAO, mFAO, mFAO$_\circ$, MMI-QSG, MSOGI-FLL, mAFLL) are shown in Tables 4.5 and 4.6.

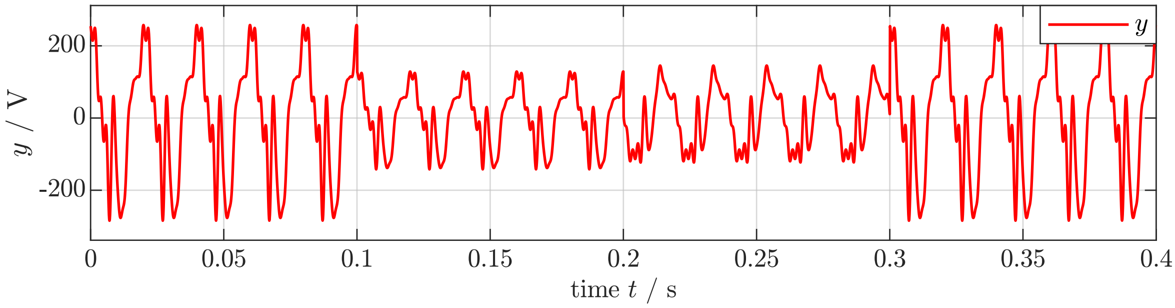

Figure 4.4: *Input signal y for scenario (S5).*

i	1	2	3	4	5	6	7	8	9	10
$0\,\mathrm{s} \le t < 0.2\,\mathrm{s}$										
Harmonic orders ν_i	1	2	3	4	5	6	7	8	9	10
Amplitudes a_i/V	200	35	70	45	35	30	30	20	25	20
Phase angles ϕ_i	0	$\frac{\pi}{4}$	$\frac{10\pi}{7}$	$\frac{\pi}{5}$	$\frac{3\pi}{2}$	$\frac{3\pi}{4}$	0	π	$\frac{\pi}{2}$	0
Offset a_0/V	0									
Fundamental frequency f_1/Hz	50									
$0.2\,\mathrm{s} \le t < 0.4\,\mathrm{s}$										
Harmonic orders ν_i	1	2	3	4	5	6	7	8	9	10
Amplitudes a_i/V	200	35	70	45	35	30	30	20	25	20
Phase angles ϕ_i	0	$\frac{\pi}{4}$	$\frac{10\pi}{7}$	$\frac{\pi}{5}$	$\frac{3\pi}{2}$	$\frac{3\pi}{4}$	0	π	$\frac{\pi}{2}$	0
Offset a_0/V	0									
Fundamental frequency f_1/Hz	62.5									
$0.4\,\mathrm{s} \le t < 0.6\,\mathrm{s}$										
Harmonic orders ν_i	1	2	3	4	5	6	7	8	9	10
Amplitudes a_i/V	400	70	140	90	70	60	60	40	50	40
Phase angles ϕ_i	$\frac{15\pi}{8}$	$\frac{\pi}{8}$	$\frac{73\pi}{56}$	$\frac{3\pi}{40}$	$\frac{11\pi}{8}$	$\frac{5\pi}{8}$	$\frac{15\pi}{8}$	$\frac{7\pi}{8}$	$\frac{3\pi}{8}$	$\frac{15\pi}{8}$
Offset a_0/V	0									
Fundamental frequency f_1/Hz	62.5									
$0.6\,\mathrm{s} \le t \le 0.8\,\mathrm{s}$										
Harmonic orders ν_i	1	2	3	4	5	6	7	8	9	10
Amplitudes a_i/V	200	35	70	45	35	30	30	20	25	20
Phase angles ϕ_i	0	$\frac{\pi}{4}$	$\frac{10\pi}{7}$	$\frac{\pi}{5}$	$\frac{3\pi}{2}$	$\frac{3\pi}{4}$	0	π	$\frac{\pi}{2}$	0
Offset a_0/V	0									
Fundamental frequency f_1/Hz	40									

Table 4.2: *Signal parameters for scenarios (S2) and (S6).*

4.3 Experiments

In this section, the methods proposed and taken from literature are compared to each other. But first, the experimental setup is described in Section 4.3.1. Input signals with only fundamental waves (Scenarios (S1) – (S4)) are discussed in Section 4.3.2 and in Section 4.3.3, input signals with ten components (Scenarios (S5) – (S8)) are shown.

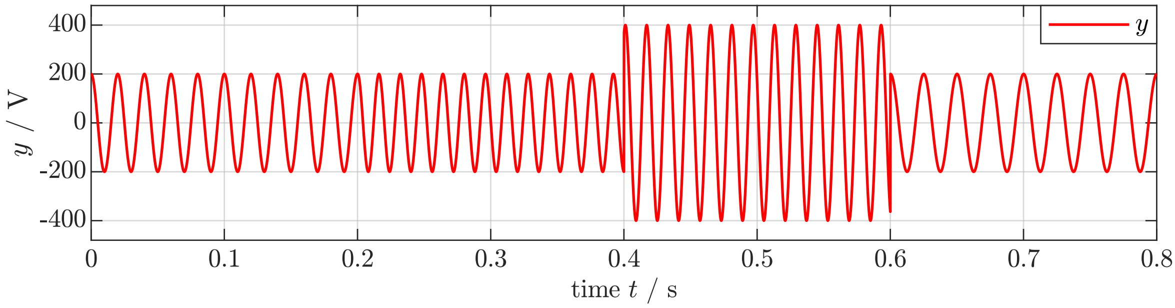

Figure 4.5: *Input signal y for scenario (S2).*

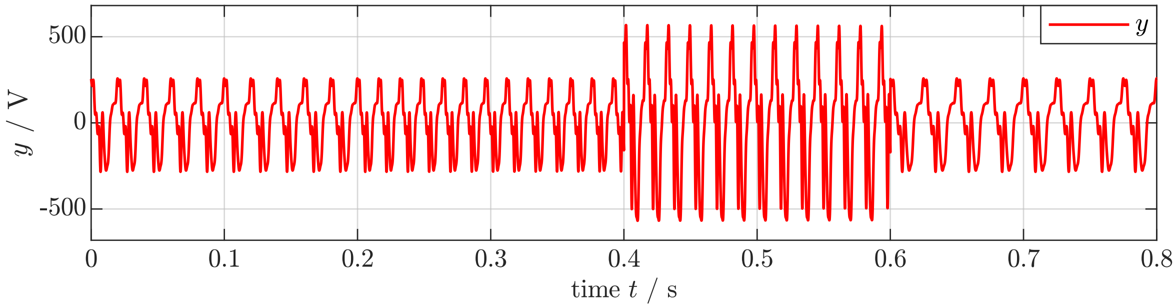

Figure 4.6: *Input signal y for scenario (S6).*

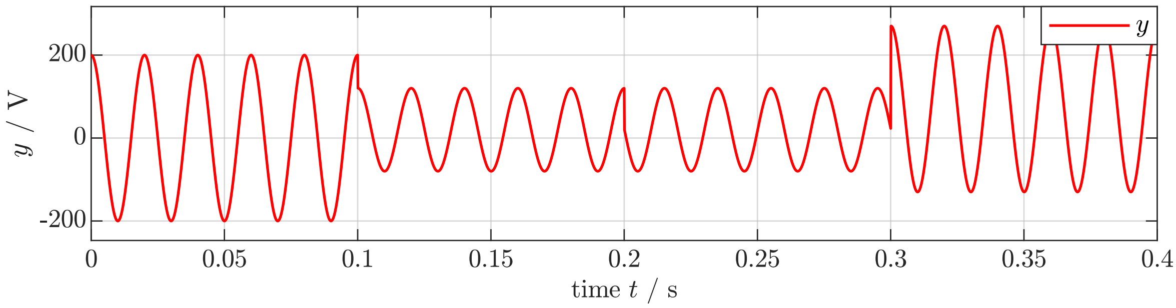

Figure 4.7: *Input signal y for scenario (S3).*

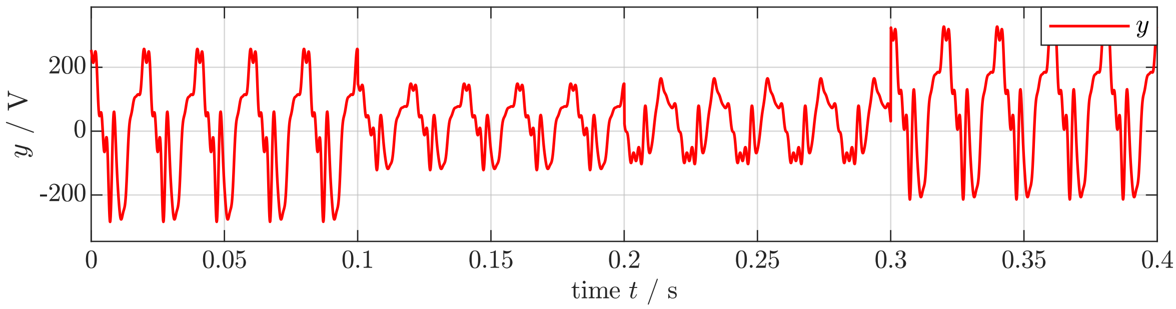

Figure 4.8: *Input signal y for scenario (S7).*

4.3.1 Experimental setup

The measurements are obtained from the experimental setup described in the following:

i	1	2	3	4	5	6	7	8	9	10
$0\,\mathrm{s} \leq t < 0.1\,\mathrm{s}$										
Harmonic orders ν_i	1	2	3	4	5	6	7	8	9	10
Amplitudes a_i/V	200	35	70	45	35	30	30	20	25	20
Phase angles ϕ_i	0	$\frac{\pi}{4}$	$\frac{10\pi}{7}$	$\frac{\pi}{5}$	$\frac{3\pi}{2}$	$\frac{3\pi}{4}$	0	π	$\frac{\pi}{2}$	0
Offset a_0/V					0					
Fundamental frequency f_1/Hz					50					
$0.1\,\mathrm{s} \leq t < 0.2\,\mathrm{s}$										
Harmonic orders ν_i	1	2	3	4	5	6	7	8	9	10
Amplitudes a_i/V	100	17.5	35	22.5	17.5	15	15	10	12.5	10
Phase angles ϕ_i	0	$\frac{\pi}{4}$	$\frac{10\pi}{7}$	$\frac{\pi}{5}$	$\frac{3\pi}{2}$	$\frac{3\pi}{4}$	0	π	$\frac{\pi}{2}$	0
Offset a_0/V					20					
Fundamental frequency f_1/Hz					50					
$0.2\,\mathrm{s} \leq t < 0.3\,\mathrm{s}$										
Harmonic orders ν_i	1	2	3	4	5	6	7	8	9	10
Amplitudes a_i/V	100	17.5	35	22.5	17.5	15	15	10	12.5	10
Phase angles ϕ_i	$\frac{\pi}{2}$	$\frac{3\pi}{4}$	$\frac{27\pi}{14}$	$\frac{7\pi}{10}$	0	$\frac{5\pi}{4}$	$\frac{\pi}{2}$	$\frac{3\pi}{2}$	π	$\frac{\pi}{2}$
Offset a_0/V					20					
Fundamental frequency f_1/Hz					50					
$0.3\,\mathrm{s} \leq t \leq 0.4\,\mathrm{s}$										
Harmonic orders ν_i	1	2	3	4	5	6	7	8	9	10
Amplitudes a_i/V	200	35	70	45	35	30	30	20	25	20
Phase angles ϕ_i	0	$\frac{\pi}{4}$	$\frac{10\pi}{7}$	$\frac{\pi}{5}$	$\frac{3\pi}{2}$	$\frac{3\pi}{4}$	0	π	$\frac{\pi}{2}$	0
Offset a_0/V					70					
Fundamental frequency f_1/Hz					50					

Table 4.3: *Signal parameters for scenarios (S3) and (S7).*

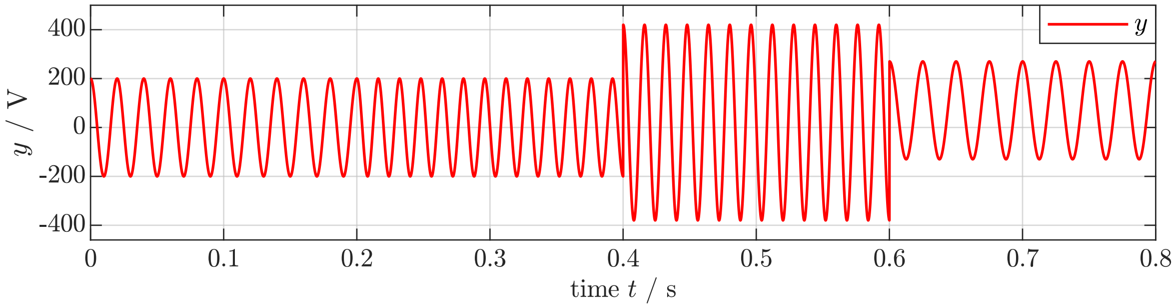

Figure 4.9: *Input signal y for scenario (S4).*

- All models for signal generation or decomposition are built in Matlab/Simulink R2018b on the host computer;
- Two models per measurement (one for generation and one for decomposition) are downloaded via LAN to the dPSACE Processor Board DS1007;
- The generated signal is D/A-converted by the dSPACE I/O card DS2103;

i	1	2	3	4	5	6	7	8	9	10
$0\,\mathrm{s} \leq t < 0.2\,\mathrm{s}$										
Harmonic orders ν_i	1	2	3	4	5	6	7	8	9	10
Amplitudes a_i/V	200	35	70	45	35	30	30	20	25	20
Phase angles ϕ_i	0	$\frac{\pi}{4}$	$\frac{10\pi}{7}$	$\frac{\pi}{5}$	$\frac{3\pi}{2}$	$\frac{3\pi}{4}$	0	π	$\frac{\pi}{2}$	0
Offset a_0/V	0									
Fundamental frequency f_1/Hz	50									
$0.2\,\mathrm{s} \leq t < 0.4\,\mathrm{s}$										
Harmonic orders ν_i	1	2	3	4	5	6	7	8	9	10
Amplitudes a_i/V	200	35	70	45	35	30	30	20	25	20
Phase angles ϕ_i	0	$\frac{\pi}{4}$	$\frac{10\pi}{7}$	$\frac{\pi}{5}$	$\frac{3\pi}{2}$	$\frac{3\pi}{4}$	0	π	$\frac{\pi}{2}$	0
Offset a_0/V	0									
Fundamental frequency f_1/Hz	62.5									
$0.4\,\mathrm{s} \leq t < 0.6\,\mathrm{s}$										
Harmonic orders ν_i	1	2	3	4	5	6	7	8	9	10
Amplitudes a_i/V	400	70	140	90	70	60	60	40	50	40
Phase angles ϕ_i	$\frac{\pi}{2}$	$\frac{3\pi}{4}$	$\frac{27\pi}{14}$	$\frac{7\pi}{10}$	0	$\frac{5\pi}{4}$	$\frac{\pi}{2}$	$\frac{3\pi}{2}$	π	$\frac{\pi}{2}$
Offset a_0/V	20									
Fundamental frequency f_1/Hz	50									
$0.6\,\mathrm{s} \leq t \leq 0.8\,\mathrm{s}$										
Harmonic orders ν_i	1	2	3	4	5	6	7	8	9	10
Amplitudes a_i/V	200	35	70	45	35	30	30	20	25	20
Phase angles ϕ_i	0	$\frac{\pi}{4}$	$\frac{10\pi}{7}$	$\frac{\pi}{5}$	$\frac{3\pi}{2}$	$\frac{3\pi}{4}$	0	π	$\frac{\pi}{2}$	0
Offset a_0/V	70									
Fundamental frequency f_1/Hz	40									

Table 4.4: *Signal parameters for scenarios (S4) and (S8).*

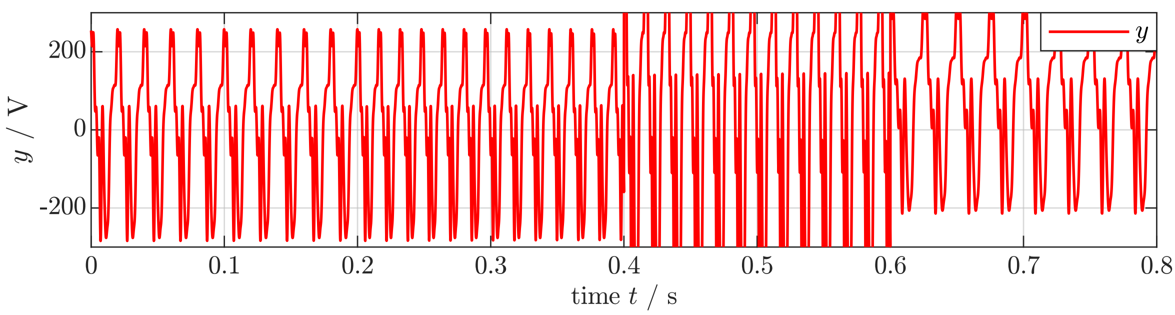

Figure 4.10: *Input signal y for scenario (S8).*

- The generated signal is transmitted from the dSPACE system to the amplifier via a BNC cable with a length of 10 m;
- The generated signal is amplified by a Spitzenberger Spies PAS 5000 four quadrant amplifier;
- The amplified signal is measured by a LEM CV 3 – 1000 voltage sensor;

$\mathrm{x} \in \{\mathrm{es}, \mathrm{m}, \mathrm{m}_\circ\}$	esFAO		mFAO	mFAO$_\circ$	
n	1	10	1	1	10
SOGIs					
$\boldsymbol{l}_\mathrm{x}$	(3.27)	(3.27)	(3.78)	(3.78)	(3.78)
`resolution`	10^{-3}	10^{-3}	✗	✗	✗
Poles ($\nu \in \{(0), \pm 1, \ldots, \pm n\}$)	✗	✗	$-\frac{3}{2}+\nu$	$-\frac{3}{2}+\nu$	$-\frac{3}{2}+\nu$
Initial values	$\mathbf{0}_2$	$\mathbf{0}_{20}$	$\mathbf{0}_2$	$\mathbf{0}_3$	$\mathbf{0}_{21}$
LPF					
ω_lpf	✗	✗	$2\pi 100$	$2\pi 100$	$2\pi 100$
Initial values	✗	✗	$\mathbf{0}_3$	$\mathbf{0}_3$	$\mathbf{0}_3$
HPF					
ω_hpf	$2\pi 500$	$2\pi 500$	✗	✗	✗
Initial value	0	0	✗	✗	✗
FLL					
Γ_x	0.1	0.1	0.35	0.2	0.2
$\boldsymbol{\sigma}_{\mathrm{x},1}$	$\widetilde{\boldsymbol{J}}\boldsymbol{l}_\mathrm{es}$	$\widetilde{\boldsymbol{J}}\boldsymbol{l}_\mathrm{es}$	$\widetilde{\boldsymbol{J}}\boldsymbol{l}_\mathrm{m}$	$\widetilde{\boldsymbol{J}}\boldsymbol{l}_{\mathrm{m}_\circ}$	$\widetilde{\boldsymbol{J}}\boldsymbol{l}_{\mathrm{m}_\circ}$
ε_x	10^{-5}	10^{-5}	10^{-5}	10^{-5}	10^{-5}
$\frac{\underline{z}_\mathrm{x}}{2\pi}, \frac{\overline{z}_\mathrm{x}}{2\pi}$	✗	✗	$-10^5, 10^5$	$-10^5, 10^5$	$-10^5, 10^5$
$\frac{\underline{\omega}_\mathrm{x}}{2\pi}, \frac{\overline{\omega}_\mathrm{x}}{2\pi}$	35, 65	35, 65	35, 65	35, 65	35, 65
Initial value	$2\pi 25$	$2\pi 25$	$2\pi 25$	$2\pi 25$	$2\pi 25$

Table 4.5: *System parameters for the esFAO, mFAO and mFAO with offset.*

$\mathrm{x} \in \{\mathrm{mmi}, \mathrm{msf}, \mathrm{maf}\}$	MMI-QSG		MSOGI-FLL		mAFLL
n	1	10	1	10	1
“SOGI”					
l_x	100	100	$\sqrt{2}$	$\sqrt{2}$	2
Initial values	$\mathbf{0}_3$	$\mathbf{0}_{30}$	$\mathbf{0}_2$	$\mathbf{0}_{20}$	$\mathbf{0}_3$
“FLL”					
Γ_x	✗	✗	50	50	0.02
ε_x	✗	✗	10^{-5}	10^{-5}	✗
Initial value	✗	✗	$2\pi 25$	$2\pi 25$	$2\pi 25$

Table 4.6: *System parameters for the MMI-QSG, MSOGI-FLL and mAFLL.*

- The measured signal is transmitted from the voltage sensor to the dSPACE system via a BNC cable with a length of 10 m;
- The measured signal is A/D-converted by the dSPACE A/D card DS2004;
- The measured signal is decomposed in real time by the downloaded model for signal decomposition and recorded on the host computer.

The experimental setup is illustrated in Figure 4.11.

Remark 4.3.1. *Due to the length of the BNC cables, any constant is damped out and, hence, forbids transmission of offset. This problem is solved by splitting the generation signal into an*

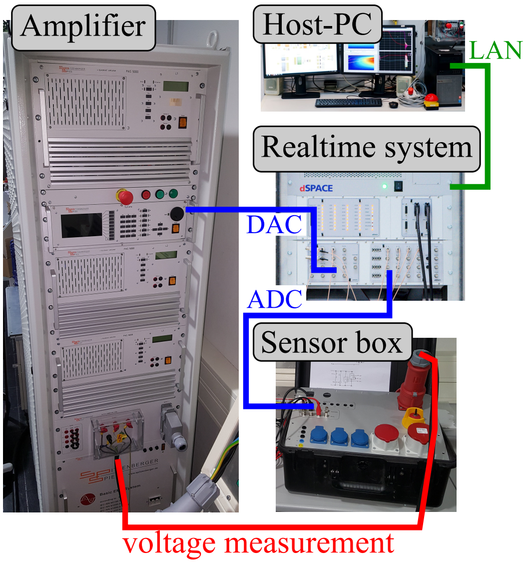

Figure 4.11: *The experimental setup used for the measurements.*

AC signal including the fundamental and all harmonic waves and a DC signal including only the offset:

$$y_{\mathrm{gen}}(t) = \underbrace{a_0}_{=:\,y_{\mathrm{DC,gen}}} + \underbrace{\sum_{j=1}^{n} a_j \cos(\phi_j(t))}_{=:\,y_{\mathrm{AC,gen}}(t)} .$$

The AC signal is transmitted directly using one cable. Instead of the DC signal two pure sinusoids are transmitted using two cables. The sinusoids have a phase angle lag of $\frac{\pi}{2}$ with respect to each other and their amplitudes are set as the value of the DC signal:

$$y_{\mathrm{DC,gen,sin}}(t) := a_0 \sin(\omega_{\mathrm{DC}} t)\,, \qquad y_{\mathrm{DC,gen,cos}}(t) := a_0 \cos(\omega_{\mathrm{DC}} t)\,.$$

The sinusoid's angular frequency is chosen as $\omega_{\mathrm{DC}} = 2\pi 100\,\frac{\mathrm{rad}}{\mathrm{s}}$. Clearly, all AC signals are damped as well. But, contrary to a constant value, the damping is negligible. By measuring these three signals as described above, the original signal can be reconstructed by

$$y_{\mathrm{meas}}(t) = y_{\mathrm{AC,meas}}(t) + \mathrm{sgn}(y_{\mathrm{DC,gen}})\sqrt{y^2_{\mathrm{DC,meas,sin}}(t) + y^2_{\mathrm{DC,meas,cos}}(t)}.$$

Remark 4.3.2. *Due to the sampling, there is a time lag of one sampling period between generation and measurement. Hence, all signals based on the measured signals are shifted backwards by one sample to match the generation signal.*

Remark 4.3.3. *For all scenarios (S1) – (S8), the offset, direct, quadrature and frequency errors are shown. However, for the calculation of the error metrics $\mathcal{M}_{\mathrm{IAE}}$ and $\mathcal{M}_{\mathrm{ITAE}}$, only the overall estimation error e_y is taken into account since the others are not measurable.*

4.3.2 Experimental results for Scenarios (S1) – (S4)

The first scenario (S1) compares the methods MMI-QSG, MSOGI-FLL, mAFLL, esFAO, mFAO, and mFAO$_\circ$ in Figure 4.12. A fundamental wave without offset and with a known angular frequency is used as a reference. Thus, angular frequency adaption is turned off (but still implemented with correct initial angular frequency). The parameters for the input signal are shown in Table 4.1 (where the column $i = 1$ is used) and the parameters for the methods are shown in Tables 4.5 — 4.6.

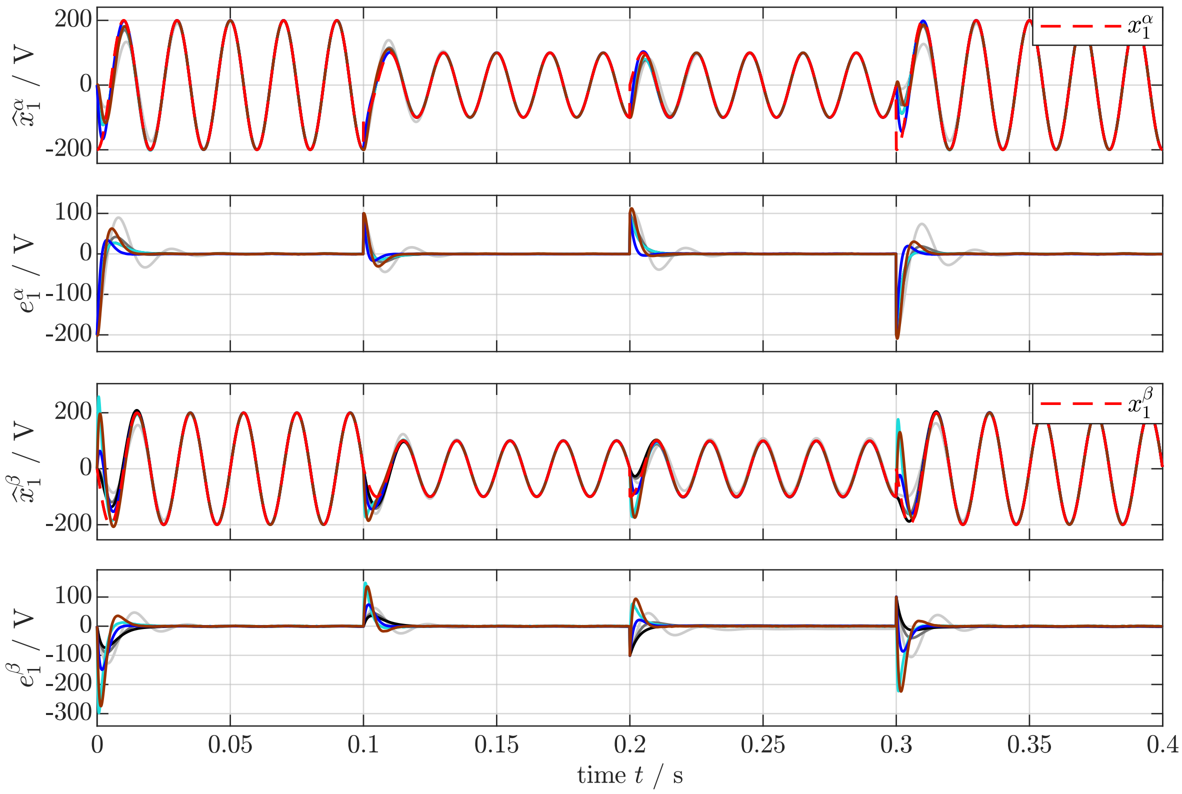

Figure 4.12: *Measurement results for scenario (S1). Used methods: MMI-QSG (—), MSOGI-FLL (—), mAFLL (—), esFAO (—), mFAO (—) and mFAO with offset (—). Shown are the estimated states* $\widehat{x}_1^\alpha, \widehat{x}_1^\beta$ *and their estimation errors* $e_1^\alpha := x_1^\alpha - \widehat{x}_1^\alpha, e_1^\beta := x_1^\beta - \widehat{x}_1^\beta$.

Figure 4.12 illustrates the experimental result for scenario (S1). The first subplot shows the direct reference signal x_1^α and their estimates $\widehat{x}_1^\alpha$ (MMI-QSG: —, MSOGI-FLL: —, mAFLL: —, esFAO: —, mFAO: —, mFAO$_\circ$: —) and the second shows the respective errors $e_1^\alpha := x_1^\alpha - \widehat{x}_1^\alpha$. The third and fourth subplot show the quadrature reference signal x_1^β, its estimates $\widehat{x}_1^\beta$ and the errors $e_1^\beta := x_1^\beta - \widehat{x}_1^\beta$. All methods decompose the reference precisely. The fastest estimation is achieved by the mFAO and mFAO$_\circ$ within 10 ms followed by the esFAO being slightly slower. Although the MSOGI-FLL and mAFLL estimate the direct component almost as fast as the esFAO, they are slower in quadrature estimation (about 20 ms). The slowest method is the MMI-QSG, which takes about 40 ms for correct estimation. In view of overshooting, the MSOGI-FLL and mAFLL are best, followed by mFAO, MMI-QSG, esFAO and mFAO$_\circ$ showing the highest overshoot. The error metrics $\mathcal{M}_{\text{IAE}}$ and $\mathcal{M}_{\text{ITAE}}$ for the used methods, which are calculated from the overall estimation error e_y, are listed in Table 4.7.

Method	MMI-QSG	MSOGI-FLL	mAFLL	esFAO	mFAO	mFAO$_\circ$
$\mathcal{M}_{\text{IAE}}$ / Vs	4.521	2.389	1.919	**0.940**	1.462	1.387
$\mathcal{M}_{\text{ITAE}}$ / Vs^2	0.070	0.044	0.041	0.039	**0.038**	0.039

Table 4.7: *IAE and ITAE for the different methods used in scenario (S1).*

In view of the metrics shown in Table 4.7, the esFAO performs best; it is only slightly outperformed by the mFAO in view of the $\mathcal{M}_{\mathrm{ITAE}}$.
Scenario (S2) compares the methods MMI-QSG, MSOGI-FLL, mAFLL, esFAO, mFAO, and mFAO$_\circ$ in Figure 4.13. The reference signal is a fundamental wave without offset and with an unknown angular frequency. Thus, angular frequency adaption is turned on. The parameters for the input signal are shown in Table 4.2 (where the column $i = 1$ is used) and the parameters for the methods are shown in Tables 4.5 — 4.6.

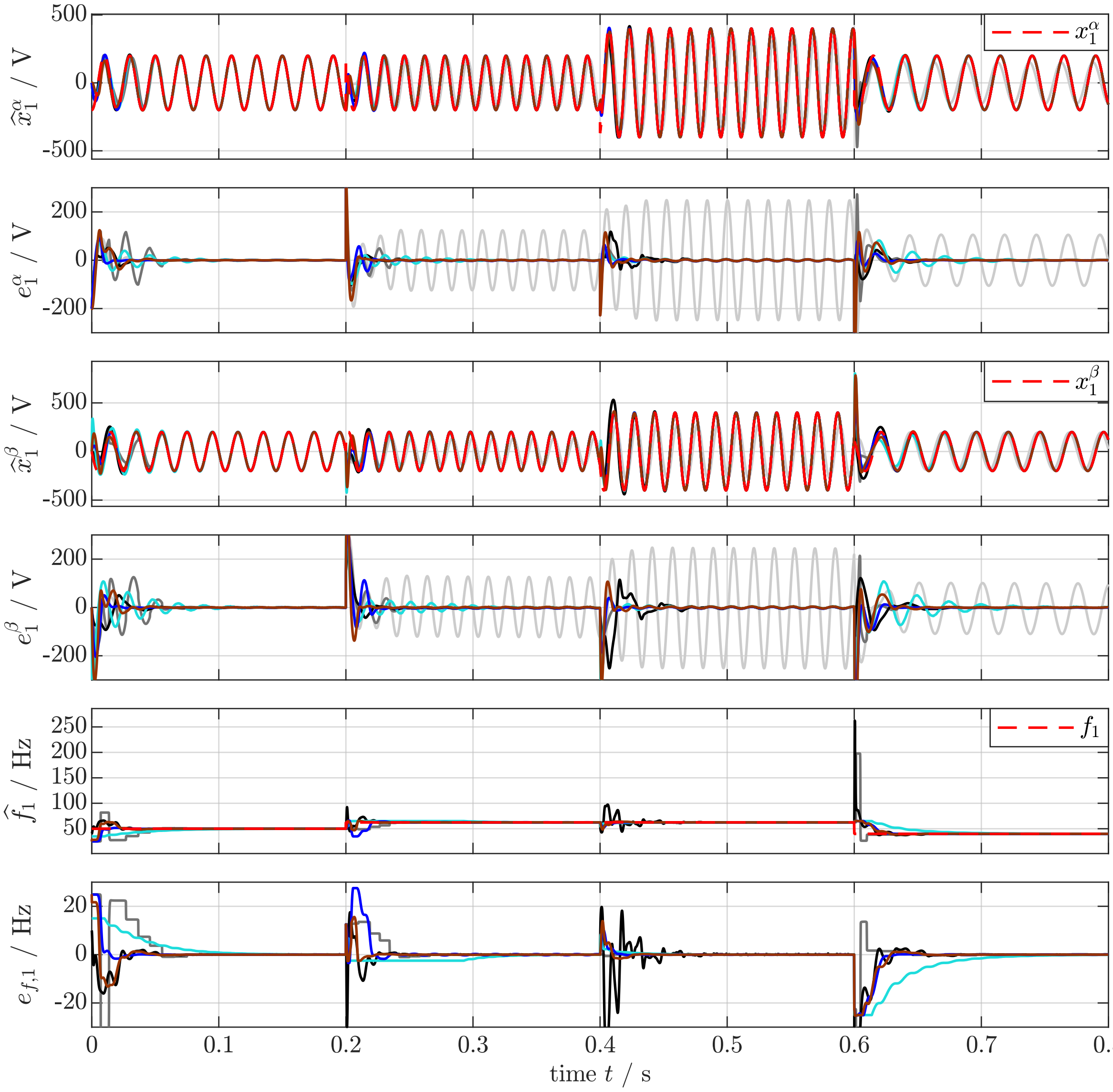

Figure 4.13: *Measurement results for scenario (S2). Used methods: MMI-QSG (—), MSOGI-FLL (—), mAFLL (—), esFAO (—), mFAO (—) and mFAO with offset (—). Shown are the estimated states $\widehat{x}_1^\alpha, \widehat{x}_1^\beta$, their estimation errors e_1^α, e_1^β, the estimated fundamental frequency $\widehat{f}_1 := \frac{\widehat{\omega}_1}{2\pi}$ and its estimation error $e_{f,1} := f_1 - \widehat{f}_1$.*

In Figure 4.13, the experimental results for scenario (S2) are depicted. The first and second subplots show the direct reference signal x_1^α, their estimates $\widehat{x}_1^\alpha$ (MMI-QSG: —, MSOGI-FLL: —, mAFLL: —, esFAO: —, mFAO: —, mFAO$_\circ$: —) and the respective errors e_1^α. In the third and fourth subplot, the same signals for the quadrature component are shown. The last two subplots show the fundamental frequency f_1, its estimate $\widehat{f}_1$ and the respective estimation error $e_{f,1} := f_1 - \widehat{f}_1$. Therein, no plot for the MMI-QSG is shown because no signals exist for this model. Except for the MMI-QSG, which comes without frequency adaption, all methods are able to decompose the reference. The fastest estimation is achieved by the mFAO and mFAO$_\circ$ within 30 ms. The esFAO, MSOGI-FLL and mAFLL still are able to estimate the input signal in the observed time frames but take significantly more time to reach quasi-steady state. In the time frame with correct reference angular frequency for the MMI-QSG, it estimates the signal components correctly. However, a wrong reference angular frequency causes the MMI-QSG estimates to deliver wrong results. Due to the OS of the esFLL and the AWU in the mFLL and mFLL$_\circ$, overshooting is prevented in the frequency adaption. In contrast, MSOGI-FLL and mAFLL show high overshooting. The overshooting characteristics of the SOGIs (or equivalent structures in the MMI-QSG and mAFLL) are as described in scenario (S1). The error metrics calculated for this scenario from the overall estimation error e_y are listed in Table 4.8.

Method	MMI-QSG	MSOGI-FLL	mAFLL	esFAO	mFAO	mFAO$_\circ$
$\mathcal{M}_{\text{IAE}}$ / Vs	62.956	8.958	6.360	**3.242**	4.988	4.202
$\mathcal{M}_{\text{ITAE}}$ / Vs^2	6.149	0.350	0.299	0.268	0.267	**0.261**

Table 4.8: *IAE and ITAE for the different methods used in scenario (S2).*

The metrics shown in Table 4.7 indicate that the esFAO performs best when taking the $\mathcal{M}_{\text{IAE}}$ value. In view of the $\mathcal{M}_{\text{ITAE}}$ value, the mFAO$_\circ$ is the best choice.
In scenario (S3), the methods MMI-QSG, MSOGI-FLL, mAFLL, esFAO, mFAO, and mFAO$_\circ$ are compared in Figure 4.14. The reference signal is a fundamental wave with offset and with a known angular frequency. Thus, angular frequency adaption is turned off. The parameters for the input signal are shown in Table 4.3 (where the column $i = 1$ is used) and the parameters for the methods are shown in Tables 4.5 — 4.6.
Figure 4.14 shows the experimental results for this scenario. Therein, the first two subplots show the offset x_0, its estimates $\widehat{x}_0$ and the respective estimation errors $e_0 := x_0 - \widehat{x}_0$. However, only the results from the methods capable of estimating/detecting offset (esFAO, mFAO$_\circ$) are drawn. The last four subplots show the direct and quadrature reference signals x_1^α, x_1^β, their estimates $\widehat{x}_1^\alpha, \widehat{x}_1^\beta$ and estimation errors e_1^α, e_1^β (MMI-QSG: —, MSOGI-FLL: —, mAFLL: —, esFAO: —, mFAO: —, mFAO$_\circ$: —). Fastest correct estimation is achieved by the mFAO$_\circ$ within 10 ms, which is closely followed by the esFAO. Although the MMI-QSG, MSOGI-FLL and mAFLL are not capable of estimating offset, this has no impact on the estimation of x_1^α, unlike the mFAO showing a biased estimation. Considering the quadrature estimation, all methods except for esFAO and FAO$_\circ$ fail to give correct estimations. More precisely, MSOGI-FLL, mAFLL and mFAO show a biased quadrature estimate whereas the MMI-QSG even diverges linearly. The overshooting behavior, only described for the esFAO and the mFAO$_\circ$, is almost identical, which can also be seen in the error metrics shown in Table 4.9.

Method	MMI-QSG	MSOGI-FLL	mAFLL	esFAO	mFAO	mFAO$_\circ$
$\mathcal{M}_{\text{IAE}}$ / Vs	12.466	11.924	11.585	**0.950**	4.178	1.380
$\mathcal{M}_{\text{ITAE}}$ / Vs^2	0.526	0.561	0.562	**0.039**	0.184	0.039

Table 4.9: *IAE and ITAE for the different methods used in scenario (S3).*

From Table 4.9, it can be deduced that the esFAO shows the best performance for scenario (S3).
Scenario (S4) compares the methods MMI-QSG, MSOGI-FLL, mAFLL, esFAO, mFAO, and mFAO$_\circ$ in Figure 4.14. A fundamental wave with offset and with an unknown angular frequency

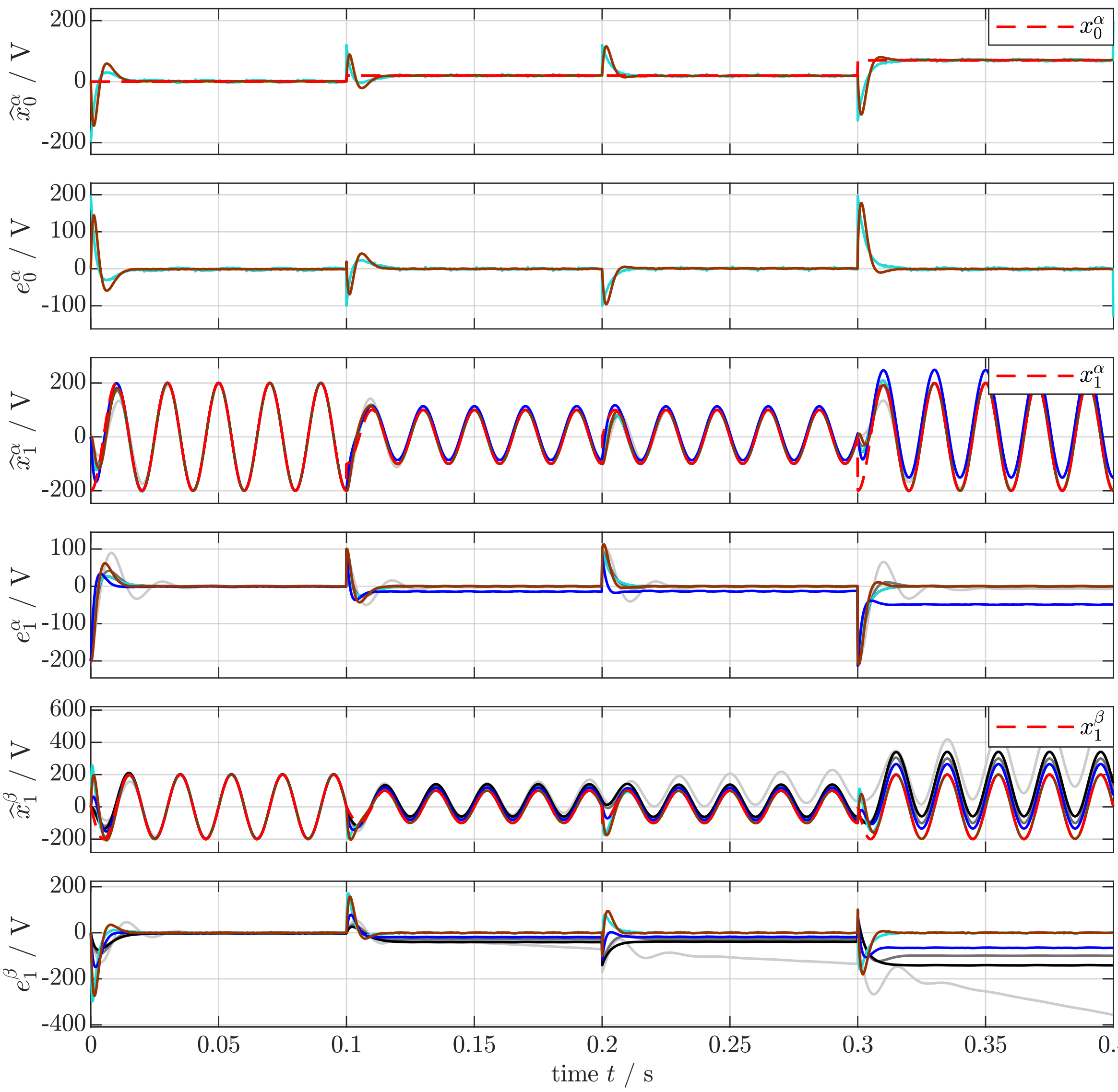

Figure 4.14: *Measurement results for scenario (S3). Used methods: MMI-QSG (—), MSOGI-FLL (—), mAFLL (—), esFAO (—), mFAO (—) and mFAO with offset (—). Shown are the estimated states* $\widehat{x}_1^\alpha, \widehat{x}_1^\beta$ *and their estimation errors* e_1^α, e_1^β.

is used as a reference. Thus, angular frequency adaption is turned on. The parameters for the input signal are shown in Table 4.4 (where the column $i = 1$ is used) and the parameters for the methods are shown in Tables 4.5 — 4.6.

Figure 4.15 shows the experimental results for scenario (S4). The subplots depict the reference offset x_0, its estimates $\widehat{x}_0$ and the respective errors e_0 (for the esFAO and the mFAO$_\circ$), the direct and quadrature signals x_1^α, x_1^β, their estimates $\widehat{x}_1^\alpha, \widehat{x}_1^\beta$ and estimation errors e_1^α, e_1^β, and reference frequency f_1, its estimates $\widehat{f}_1$ and estimation errors $e_{f,1}$ (MMI-QSG: —, MSOGI-FLL: —, mAFLL: —, esFAO: —, mFAO: —, mFAO$_\circ$: —). Similar to scenario (S3), only the esFAO and mFAO$_\circ$ are able to decompose the input signal appropriately. The MMI-QSG again fails when offset is present or when its angular frequency is wrong. Due to activated frequency adaption, the esFAO now takes significantly more time to settle ($\geq$ 100 ms). The mFAO$_\circ$ achieves correct estimation in maximal 50 ms. The esFAO shows less overshooting than the mFAO$_\circ$. In

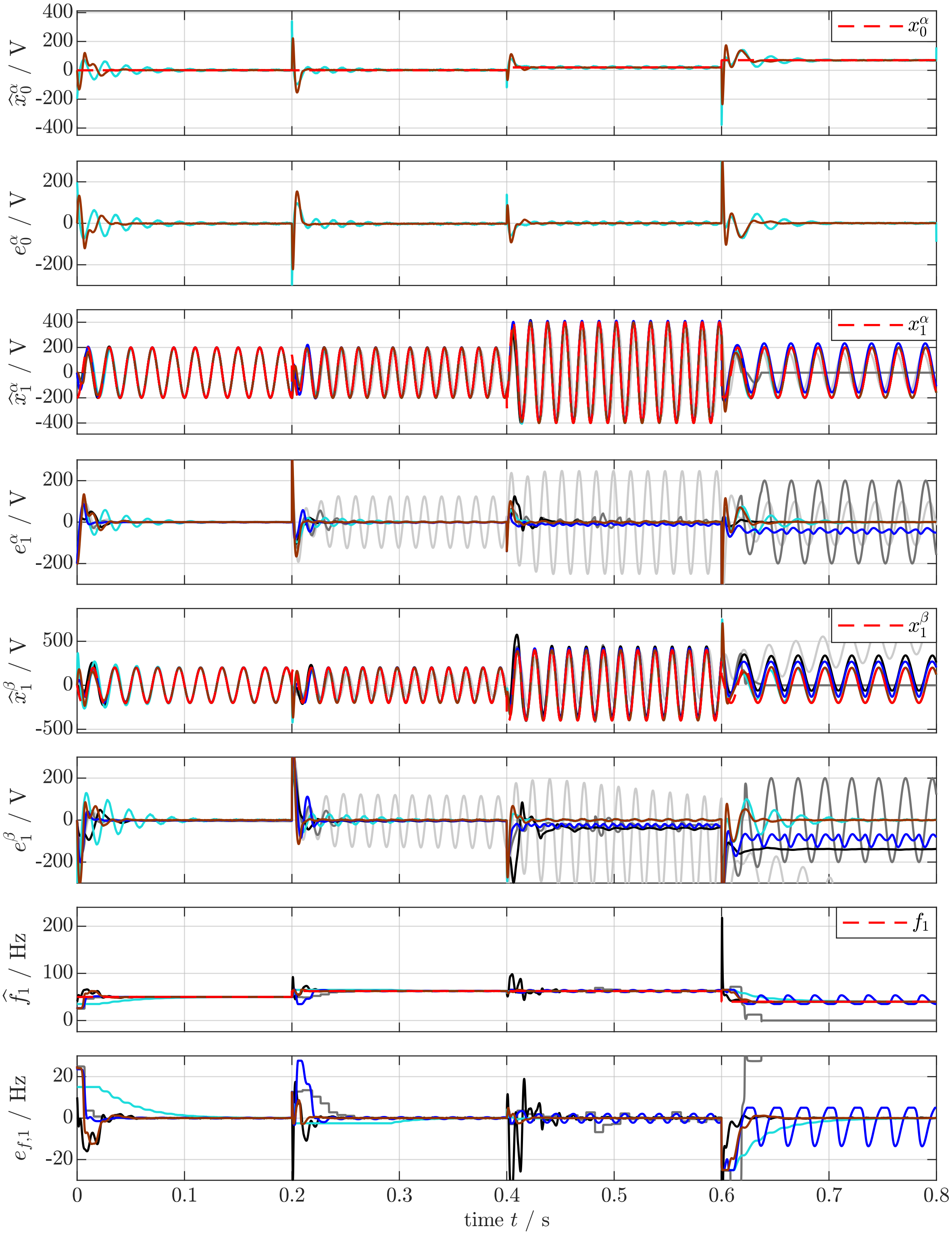

Figure 4.15: *Measurement results for scenario (S4). Used methods: MMI-QSG (—), MSOGI-FLL (—), mAFLL (—), esFAO (—), mFAO (—) and mFAO with offset (—). Shown are the estimated states* $\widehat{x}_1^\alpha, \widehat{x}_1^\beta$*, their estimation errors* e_1^α, e_1^β*, the estimated fundamental frequency* $\widehat{f}_1$ *and its estimation error* $e_{f,1}$.

view of frequency adaption of the other methods, the mFAO and MSOGI-FLL show an oscillation due to offset, whereas the offset does not affect the functionality of frequency adaption of the mAFLL. In the last time frame ($0.6\,\mathrm{s} \le t \le 0.8\,\mathrm{s}$) the MSOGI-FLL locks at $\widehat{f}_1 = 0\,\mathrm{Hz}$ and thus sets all estimated signals to zero. The error metrics for this scenario, calculated from the overall estimation error e_y, are listed in Table 4.10.

Method	MSOGI-FLL	mAFLL	esFAO	mFAO	mFAO$_\circ$
$\mathcal{M}_{\mathrm{IAE}}$ / Vs	34.246	21.386	**3.184**	10.249	4.005
$\mathcal{M}_{\mathrm{ITAE}}$ / Vs^2	3.235	1.925	0.265	0.846	**0.257**

Table 4.10: *IAE and ITAE for the different methods used in scenario (S4).*

From Table 4.10, it can be seen that the esFAO is best when referring to the $\mathcal{M}_{\mathrm{IAE}}$ value and the mFAO$_\circ$ is best when referring to the $\mathcal{M}_{\mathrm{ITAE}}$ value, closely followed by the esFAO.
As a conclusion from scenarios (S1) — (S4), only the esFAO and the mFAO$_\circ$ are capable of decomposing a signal consisting of a fundamental wave and offset with an unknown angular frequency, which is also indicated by the error metrics $\mathcal{M}_{\mathrm{IAE}}$ and $\mathcal{M}_{\mathrm{ITAE}}$. These show that the mFAO$_\circ$ is the better choice, if the frequency is to be estimated, whereas the esFAO is preferred when not. However, it should be kept in mind that these values do not take frequency errors into account, which emphasizes the proposed choice since the mFAO$_\circ$ is significantly faster than the esFAO in adapting an unknown angular frequency. On the other hand, the esFAO shows lesser overshooting. In total, both methods outperform the ones taken from literature and the mFAO. Since the mFAO is not capable of decomposing a signal comprising offset, it is neglected in the following scenarios. Moreover, since no generic tuning rule was given for the mAFLL in [545], it is also discarded.

4.3.3 Experimental results for Scenarios (S5) – (S8)

The fifth scenario (S5) compares the methods MMI-QSG, MSOGI-FLL, esFAO, and mFAO$_\circ$ in Figure 4.16. A signal composed of a fundamental wave and nine harmonics without offset and with a known angular frequency is used as a reference. Thus, angular frequency adaption is turned off. The parameters for the input signal are shown in Table 4.1 and the parameters for the methods are shown in Tables 4.5 — 4.6.
Figure 4.16 depicts the actual input signal y, its quadrature signal q and their estimates $\widehat{y}, \widehat{q}$ (MMI-QSG: —, MSOGI-FLL: —, esFAO: —, mFAO$_\circ$: —). All methods are able to estimate the input signal satisfyingly, what can be seen in the error plots. In view of estimation speed, the mFAO$_\circ$ performs best and needs about 20 ms, followed by the esFAO, MSOGI-FLL and MMI-QSG. The MMI-QSG and the MSOGI-FLL show the highest overshooting, whereas the esFAO shows the lowest. In the quadrature error plot, time frame $0.2\,\mathrm{s} \le t < 0.6\,\mathrm{s}$, the MMI-QSG shows very little convergence and cannot settle down within the time frame.
To give deeper insight into the single states, its estimates and errors, Figures 4.17 and 4.18 compare the estimated states $\widehat{x}_1^\alpha, \widehat{x}_1^\beta$ – $\widehat{x}_{10}^\alpha, \widehat{x}_{10}^\beta$ to the references x_1^α, x_1^β – $x_{10}^\alpha, x_{10}^\beta$ and show the respective estimation errors e_1^α, e_1^β – $e_{10}^\alpha, e_{10}^\beta$.
In Figures 4.17 and 4.18, all estimates of the direct and quadrature components $\widehat{x}_1^\alpha$, $\widehat{x}_1^\beta$ – $\widehat{x}_{10}^\alpha$, $\widehat{x}_{10}^\beta$ and their respective errors e_1^α, e_1^β – e_{10}^α, e_{10}^β are plotted. All methods are capable of decomposing the input signal into its harmonic components. However, the higher the harmonic number is, the noisier the respective signal is. It can be seen that the mFAO$_\circ$ is the fastest method in each component and estimates all components uniformly in about 20 ms. For the other methods, estimation of components with higher order takes longer. For example, considering the performance of the MSOGI-FLL, estimation of the fundamental signals $\widehat{x}_1^\alpha$, $\widehat{x}_1^\beta$ takes about 60 ms and

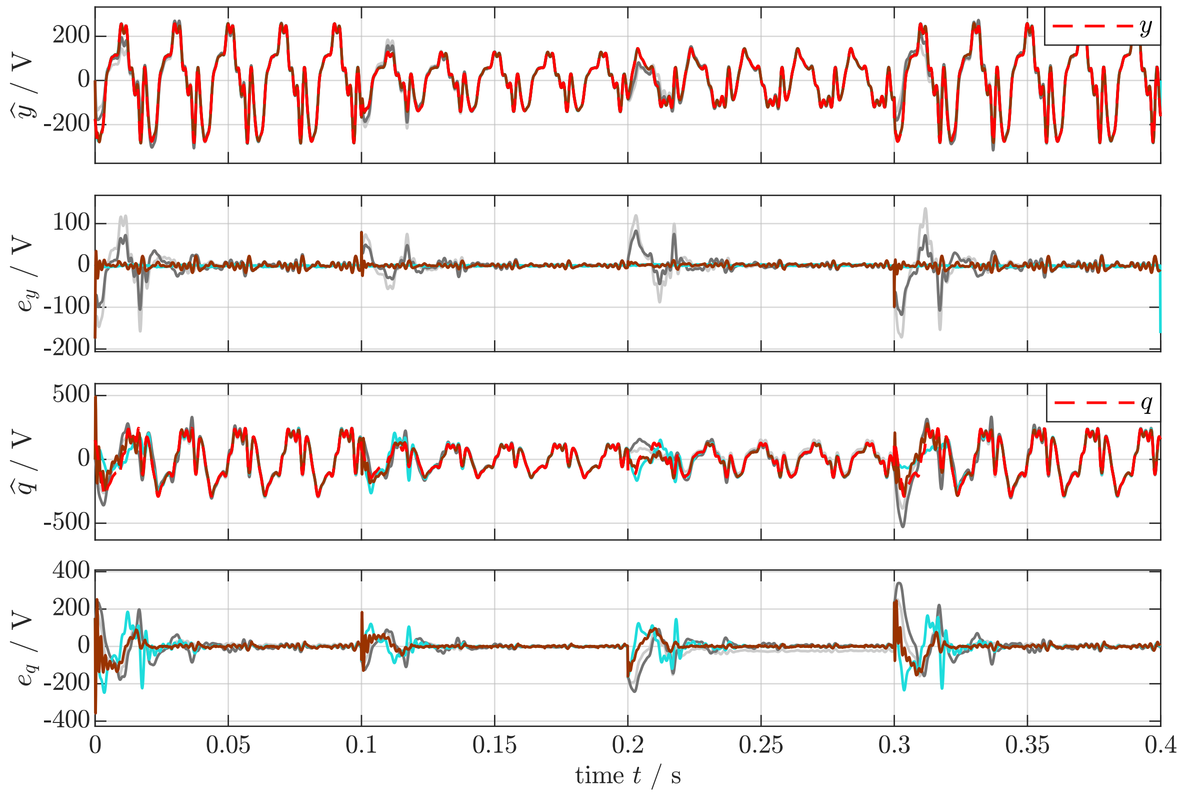

Figure 4.16: *Measurement results for scenario (S5). Used methods: MMI-QSG (—), MSOGI-FLL (—), esFAO (—) and mFAO with offset (—). Shown are the estimated direct and quadrature inputs $\widehat{y}, \widehat{q}$ and their estimation errors e_y, e_q.*

approximately 100 ms for $\widehat{x}_{10}^{\alpha}$, $\widehat{x}_{10}^{\beta}$.
To give a more objective comparison, Table 4.11 lists $\mathcal{M}_{\text{IAE}}$ and $\mathcal{M}_{\text{ITAE}}$ of the investigated methods for scenario (S5).

Method	MMI-QSG	MSOGI-FLL	esFAO	mFAO$_\circ$
$\mathcal{M}_{\text{IAE}}$ / Vs	6.027	4.936	2.576	**1.827**
$\mathcal{M}_{\text{ITAE}}$ / Vs^2	0.131	0.138	0.098	**0.092**

Table 4.11: *IAE and ITAE for the different methods used in scenario (S5).*

From Table 4.11, it can be deduce that the mFAO$_\circ$ outruns the other methods. But, in case of the $\mathcal{M}_{\text{ITAE}}$, the esFAO is very close to the mFAO$_\circ$, which indicates that the mFAO$_\circ$ comes with higher overshooting than the esFAO.
In scenario (S6), the methods MMI-QSG, MSOGI-FLL, esFAO, and mFAO$_\circ$ are compared in Figure 4.19. A signal composed of a fundamental wave and nine harmonics without offset and with an unknown angular frequency is used as a reference. Thus, angular frequency adaption is turned on. The parameters for the input signal are shown in Table 4.2 and the parameters for the methods are shown in Tables 4.5 — 4.6.
In Figure 4.19, the input signal y, its fictive quadrature signal q and their estimates $\widehat{y}, \widehat{q}$ (MMI-QSG: —, MSOGI-FLL: —, esFAO: —, mFAO$_\circ$: —) are shown. Since the MMI-QSG has no frequency adaption, it fails to decompose the input signal appropriately if the actual frequency f does not match the MMI-QSG's reference frequency. The MSOGI-FLL also cannot

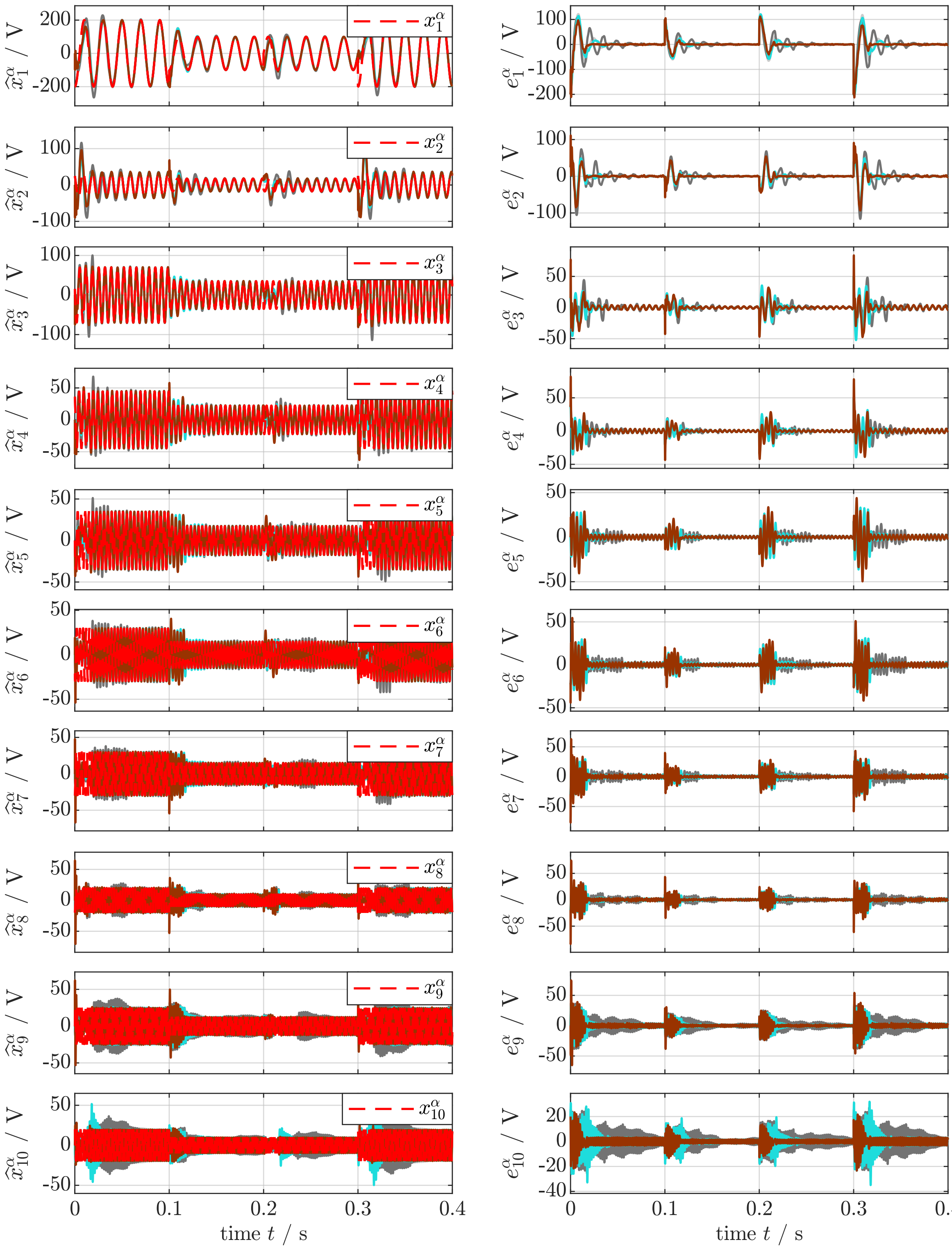

(a)

(b)

Figure 4.17: *Measurement results for scenario (S5). Used methods: MMI-QSG (—), MSOGI-FLL (—), esFAO (—) and mFAO with offset (—). Shown are the estimated states* $\widehat{x}_1^\alpha$ – $\widehat{x}_{10}^\alpha$ *in subfigure (a) and the estimation errors* e_1^α – e_{10}^α *in subfigure (b).*

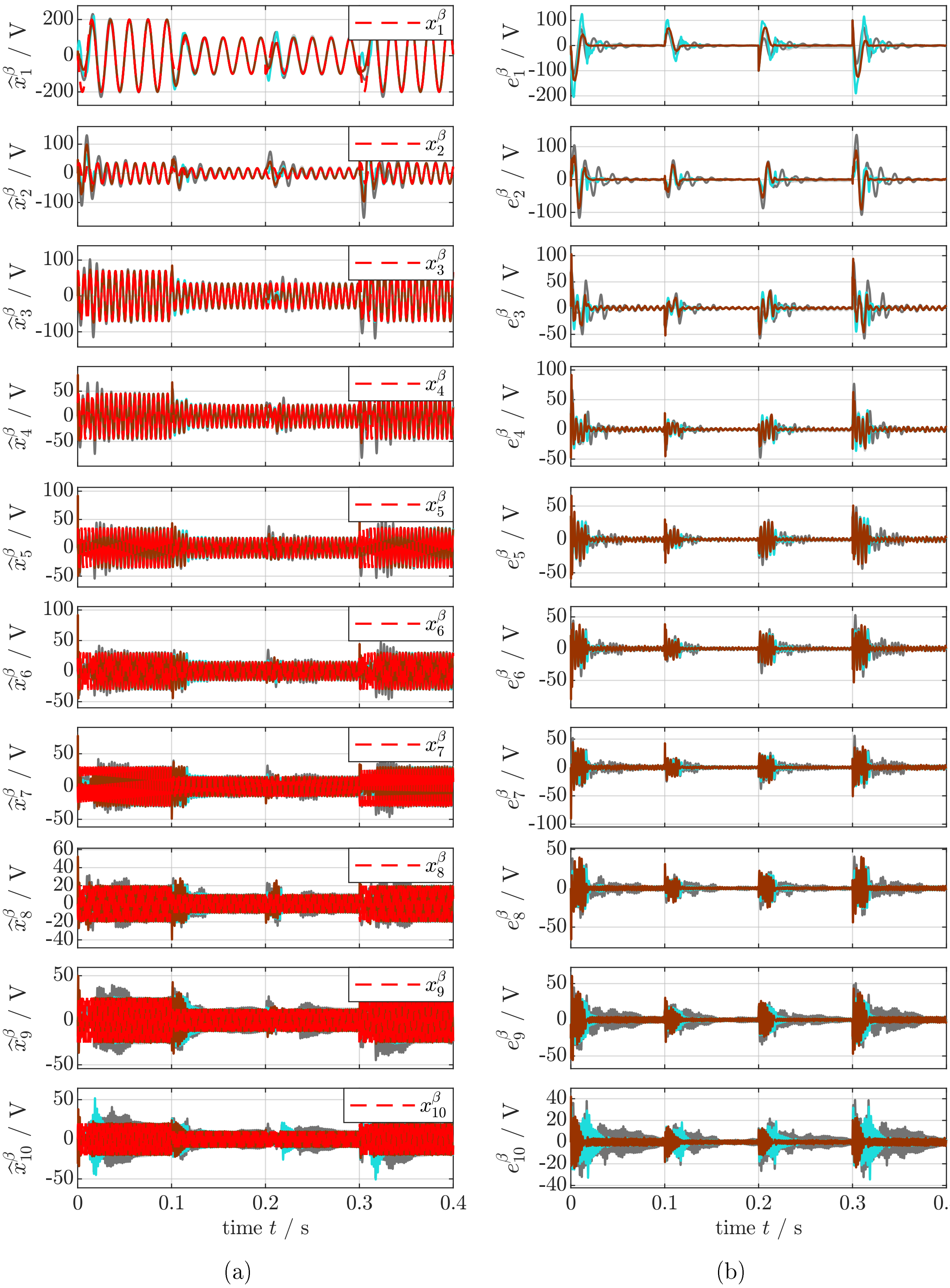

Figure 4.18: *Measurement results for scenario (S5). Used methods: MMI-QSG (—), MSOGI-FLL (—), esFAO (—) and mFAO with offset (—). Shown are the estimated states* $\widehat{x}_1^\beta$ – $\widehat{x}_{10}^\beta$ *in subfigure (a) and the estimation errors* e_1^β – e_{10}^β *in subfigure (b).*

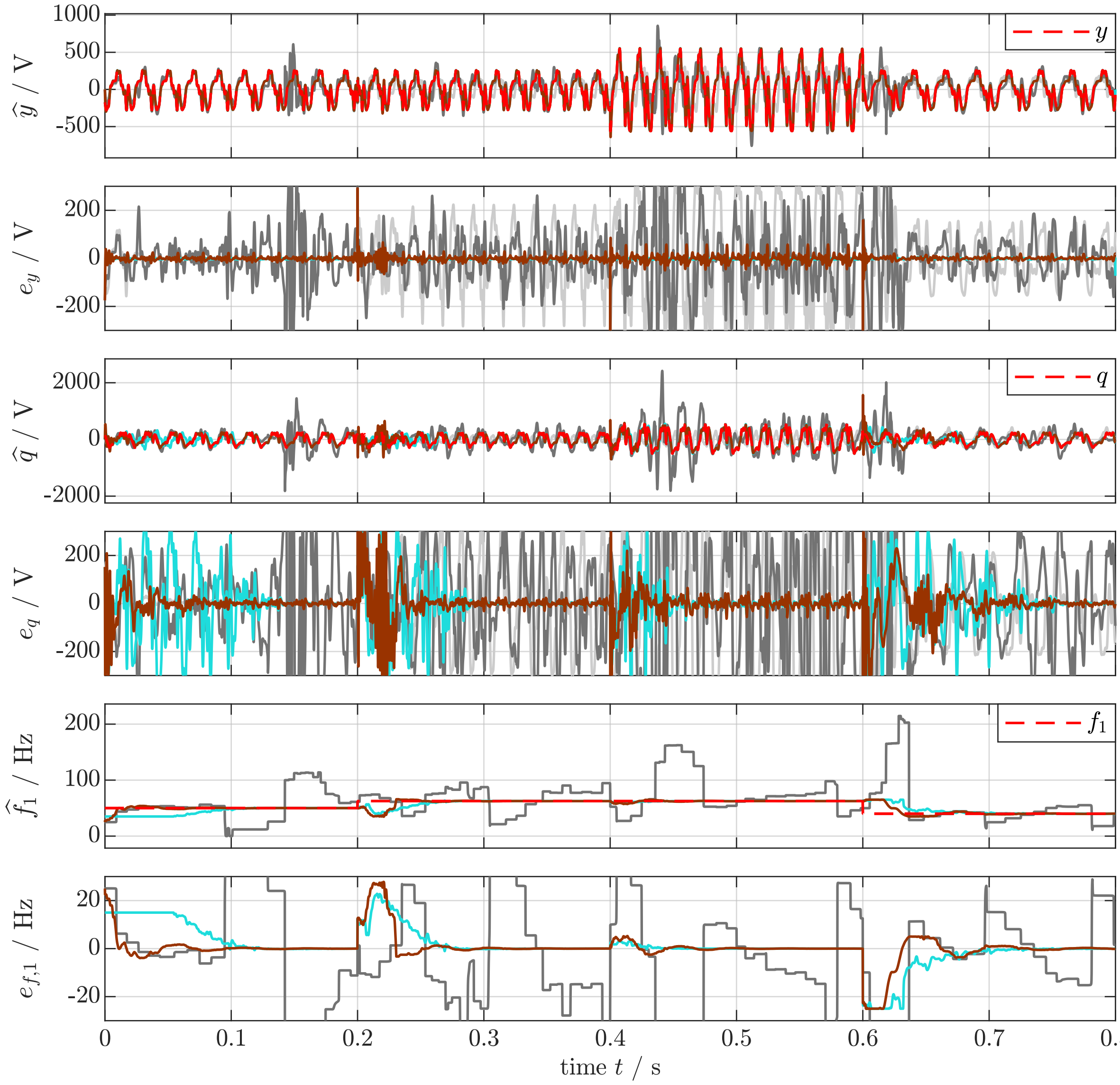

Figure 4.19: *Measurement results for scenario (S6). Used methods: MMI-QSG (—), MSOGI-FLL (—), esFAO (—) and mFAO with offset (—). Shown are the estimated direct and quadrature input* $\widehat{y}, \widehat{q}$*, their estimation errors* e_y, e_q*, the estimated fundamental frequency* $\widehat{f}_1$ *and its estimation errors* $e_{f,1}$*.*

decompose the input signal since its frequency shows a semi-stable behavior. For the esFAO and the mFAO$_\circ$, the output saturation or anti windup, respectively, come to action at $t \geq 0.6$ s and thus facilitate convergence of the frequency estimation such that the correct estimate is obtained in about 100 ms. Instead of stopping integration as the anti windup does in the mFAO$_\circ$, the output saturation simply limits the angular frequency output of the esFAO, which could explain the longer duration until these limits are left. Nevertheless, input estimation is achieved very quickly by the mFAO$_\circ$ as well as by the esFAO. In quadrature signal estimation, both the mFAO$_\circ$ and the esFAO take longer to settle down, whereas the esFAO is significantly slower.
In the following Figures 4.20 and 4.21, the estimated states $\widehat{x}_1^\alpha, \widehat{x}_1^\beta - \widehat{x}_{10}^\alpha, \widehat{x}_{10}^\beta$ and the reference signals $x_1^\alpha, x_1^\beta - x_{10}^\alpha, x_{10}^\beta$ are compared. Additionally, the respective estimation errors $e_1^\alpha, e_1^\beta - e_{10}^\alpha, e_{10}^\beta$ are plotted.

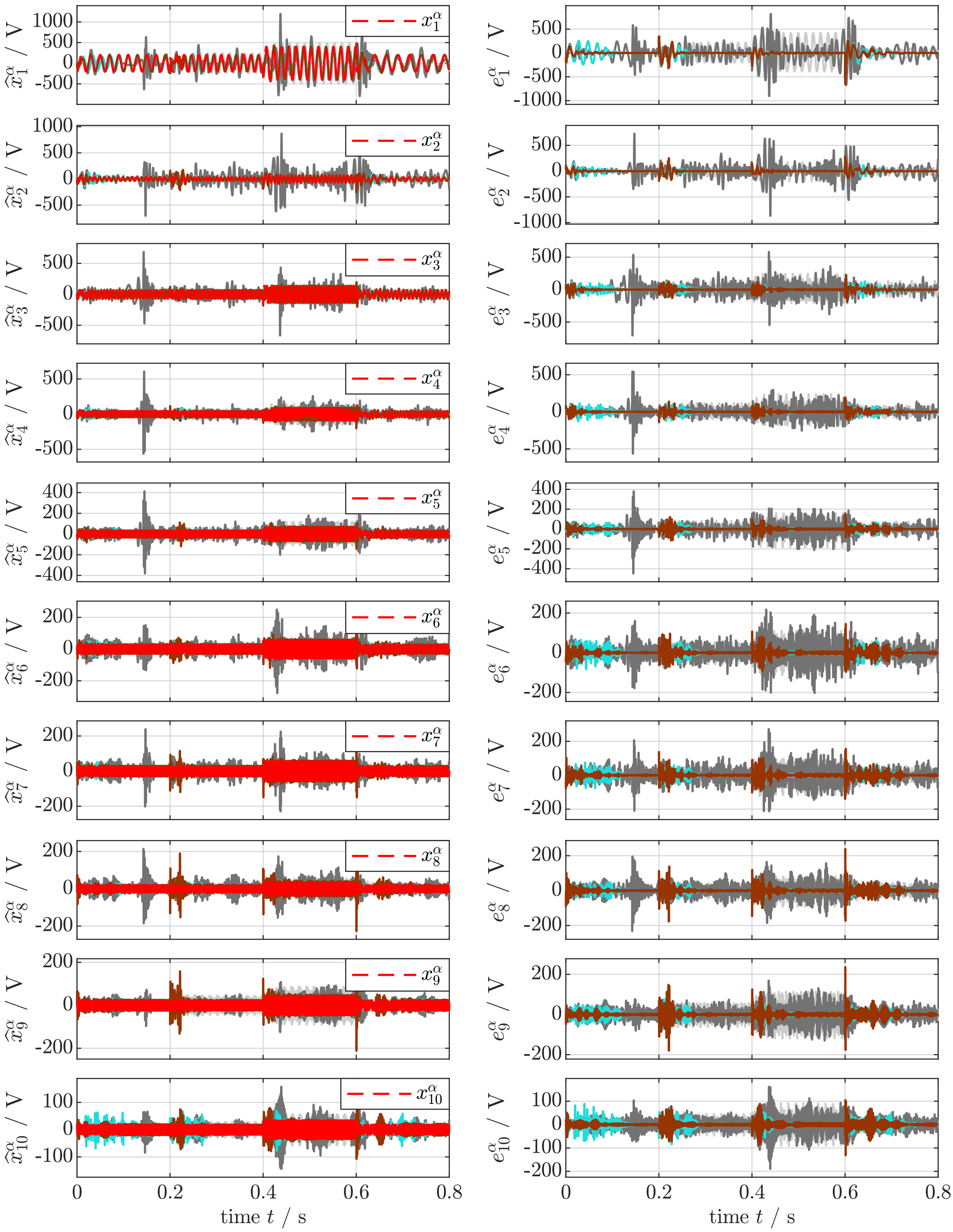

(a) (b)

Figure 4.20: *Measurement results for scenario (S6). Used methods: MMI-QSG (—), MSOGI-FLL (—), esFAO (—) and mFAO with offset (—). Shown are the estimated states* $\widehat{x}_1^\alpha$ – $\widehat{x}_{10}^\alpha$ *in subfigure (a) and the estimation errors* e_1^α – e_{10}^α *in subfigure (b).*

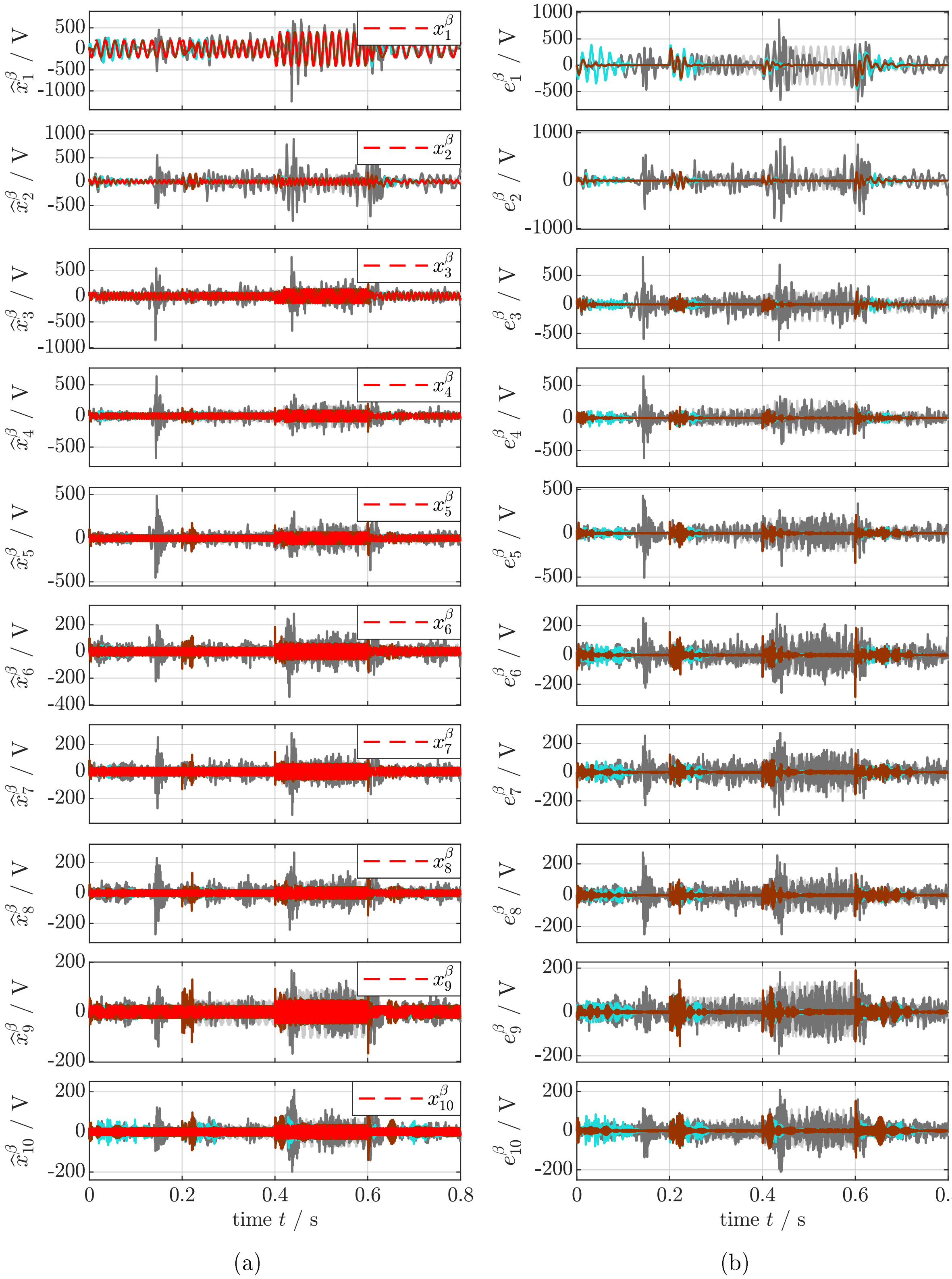

Figure 4.21: *Measurement results for scenario (S6). Used methods: MMI-QSG (—), MSOGI-FLL (—), esFAO (—) and mFAO with offset (—). Shown are the estimated states* $\widehat{x}_1^\beta$ – $\widehat{x}_{10}^\beta$ *in subfigure (a) and the estimation errors* e_1^β – e_{10}^β *in subfigure (b).*

As can be seen in the Figures 4.20 and 4.21, the esFAO and mFAO$_\circ$ are able to decompose the input signal into its components, whereas the MMI-QSG and the MSOGI-FLL fail. In contrast to 4.19, the estimation of direct components $\widehat{x}_1^\alpha$, – $\widehat{x}_{10}^\alpha$ takes as much time as estimation of quadrature components $\widehat{x}_1^\beta$ – $\widehat{x}_{10}^\beta$.
The $\mathcal{M}_{\text{IAE}}$ and $\mathcal{M}_{\text{ITAE}}$ for scenario (S6) are shown in Table 4.12.

Method	MMI-QSG	MSOGI-FLL	esFAO	mFAO$_\circ$
$\mathcal{M}_{\text{IAE}}$ / Vs	87.453	67.323	13.080	**7.050**
$\mathcal{M}_{\text{ITAE}}$ / Vs^2	8.603	6.553	0.928	**0.659**

Table 4.12: *IAE and ITAE for the different methods used in scenario (S6).*

These values indicate that the mFAO$_\circ$ comes with higher overshooting and the esFAO takes longer to settle down. Since the MMI-QSG and the MSOGI-FLL fail to converge, their metrics are very high.
Scenario (S7) compares the methods MMI-QSG, MSOGI-FLL, esFAO, and mFAO$_\circ$ in Figure 4.22. A signal composed of a fundamental wave and nine harmonics with offset and with a known angular frequency is used as a reference. Thus, angular frequency adaption is turned off. The parameters for the input signal are shown in Table 4.3 and the parameters for the methods are shown in Tables 4.5 — 4.6.

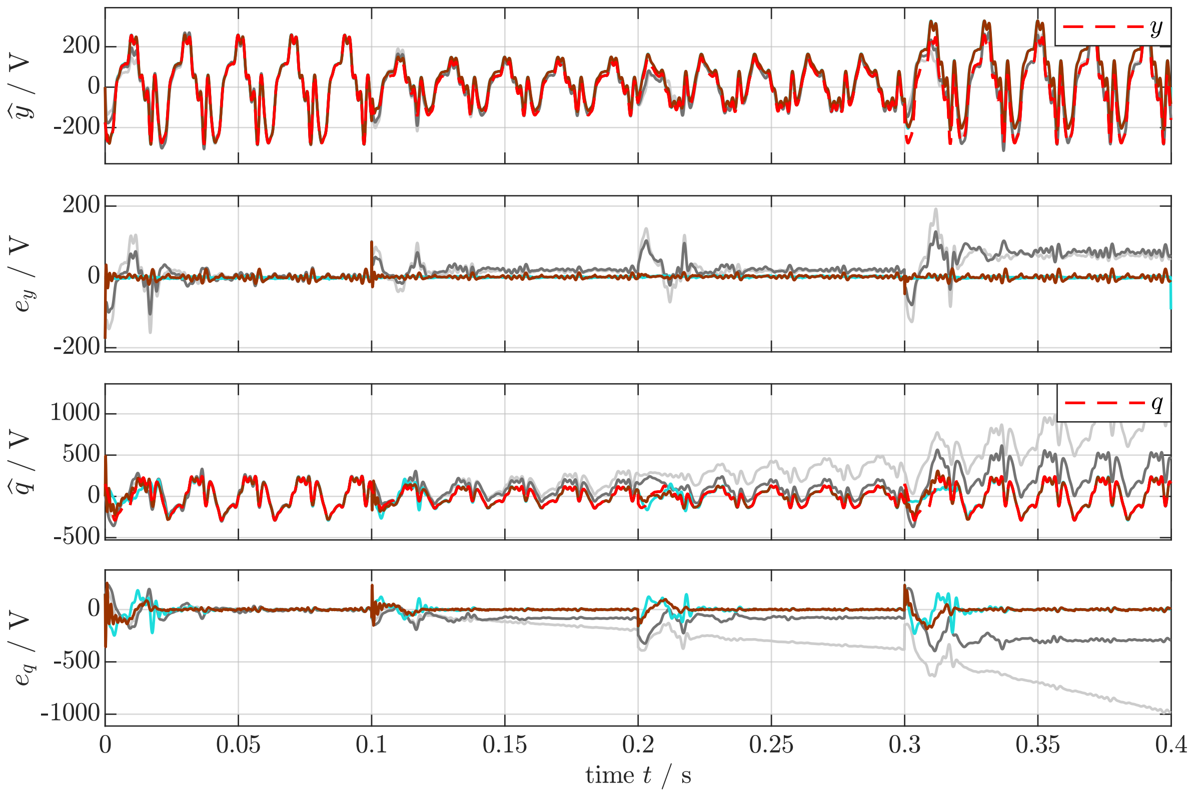

Figure 4.22: *Measurement results for scenario (S7). Used methods: MMI-QSG (—), MSOGI-FLL (—), esFAO (—) and mFAO with offset (—). Shown are the estimated direct and quadrature inputs $\widehat{y}, \widehat{q}$ and their estimation errors e_y, e_q.*

Figure 4.22 depicts the direct and quadrature input y, q, their estimates $\widehat{y}, \widehat{q}$, the respective errors e_y, e_q and the fundamental frequency f_1 as well as its estimates $\widehat{f}_1$ and errors $e_{f,1}$ (MMI-QSG:

—, MSOGI-FLL: —, esFAO: —, mFAO$_\circ$: —). As in scenario (S3), the MMI-QSG diverges in the presence of offset in its quadrature estimation, which can be seen in the third and fourth subplot. Moreover, its direct signal estimation error e_y shown in the second subplot converges to some wrong result. The MSOGI-FLL also shows an incorrect estimation in the case of offset but, contrary to the MMI-QSG, converges in both the direct and quadrature estimates. Only the esFAO and the mFAO$_\circ$ can accurately estimate direct and quadrature input. The mFAO$_\circ$ achieves correct estimation in about 20 ms, whereas the esFAO takes about 30 ms.
Figures 4.23 and 4.24 show the decomposition of the direct and quadrature input signals into its components.
In Figure 4.24, it can be seen that every quadrature signal diverges in the MMI-QSG. Concerning the MSOGI-FLL, every quadrature component is biased. In view of the direct signal components, the MMI-QSG, the MSOGI-FLL, the esFAO, and the mFAO$_0$ estimate these components correctly. Comparing the esFAO and the mFAO$_0$, the mFAO$_0$ shows a faster estimation speed in every component of the direct and quadrature signals. This can be seen especially in the fundamental and the tenth component.
A qualitative comparison is shown in Table 4.13.

Method	MMI-QSG	MSOGI-FLL	esFAO	mFAO$_\circ$
$\mathcal{M}_{\text{IAE}}$ / Vs	12.878	12.698	2.571	**1.827**
$\mathcal{M}_{\text{ITAE}}$ / Vs^2	0.529	0.593	0.097	**0.092**

Table 4.13: *IAE and ITAE for the different methods used in scenario (S7).*

In view of $\mathcal{M}_{\text{ITAE}}$, Table 4.13 also indicates that the overall performances of the esFAO and the mFAO$_\circ$ are comparable whereby the mFAO$_0$ shows a slightly better value. When taking the $\mathcal{M}_{\text{IAE}}$ value into account, it becomes clear that the mFAO$_\circ$ performs better. This also indicates that the esFAO has higher overshooting.
Scenario (S8) compares the methods MMI-QSG, MSOGI-FLL, esFAO, and mFAO$_\circ$ in Figure 4.25. A signal composed of a fundamental wave and nine harmonics with offset and with an unknown angular frequency is used as a reference. Thus, angular frequency adaption is turned on. The parameters for the input signal are shown in Table 4.4 and the parameters for the methods are shown in Tables 4.5 — 4.6.
Figure 4.25 shows the direct and quadrature input signal y, q, their estimates $\widehat{y}, \widehat{q}$, estimation errors e_y, e_q, fundamental frequency f_1, its estimates $\widehat{f}_1$ and estimation errors $e_{f,1}$ (MMI-QSG: —, MSOGI-FLL: —, esFAO: —, mFAO$_\circ$: —). As in scenario (S6) & (S7), the MMI-QSG oscillates and diverges. In view of the MSOGI-FLL, frequency estimation diverges and even leads to instability resulting in an abortion of estimation due to a missing frequency limitation, where this guarantees stability of the esFAO and the mFAO$_\circ$. Hereby, the mFAO$_\circ$ takes about 50 ms and the esFAO 130 ms, whereas in scenario (S6) the overall estimation error e_y settles down very quickly in contrast to the overall quadrature error e_q.
Figures 4.26 and 4.27 illustrate the decomposed direct and quadrature components.
From Figures 4.26 and 4.27 it becomes apparent that the esFAO and the mFAO$_\circ$ are able to estimate the fundamental and all harmonic components. As in scenario (S6), the component errors of direct and quadrature signals decrease in a similar way contrary to Figure 4.25. It remains to state that the mFAO$_\circ$ decreases faster in every component than the esFAO.
To conclude this scenario, Table 4.14 shows the $\mathcal{M}_{\text{IAE}}$ and $\mathcal{M}_{\text{ITAE}}$ values.
Clearly, the mFAO$_\circ$ outruns the other methods where for the MSOGI-FLL no value can be calculated due to abortion of estimation.
As a conclusion for the scenarios (S1) – (S8), the mFAO$_\circ$ is the best choice to decompose an input signal into its components. However, if only a fundamental wave with known angular frequency

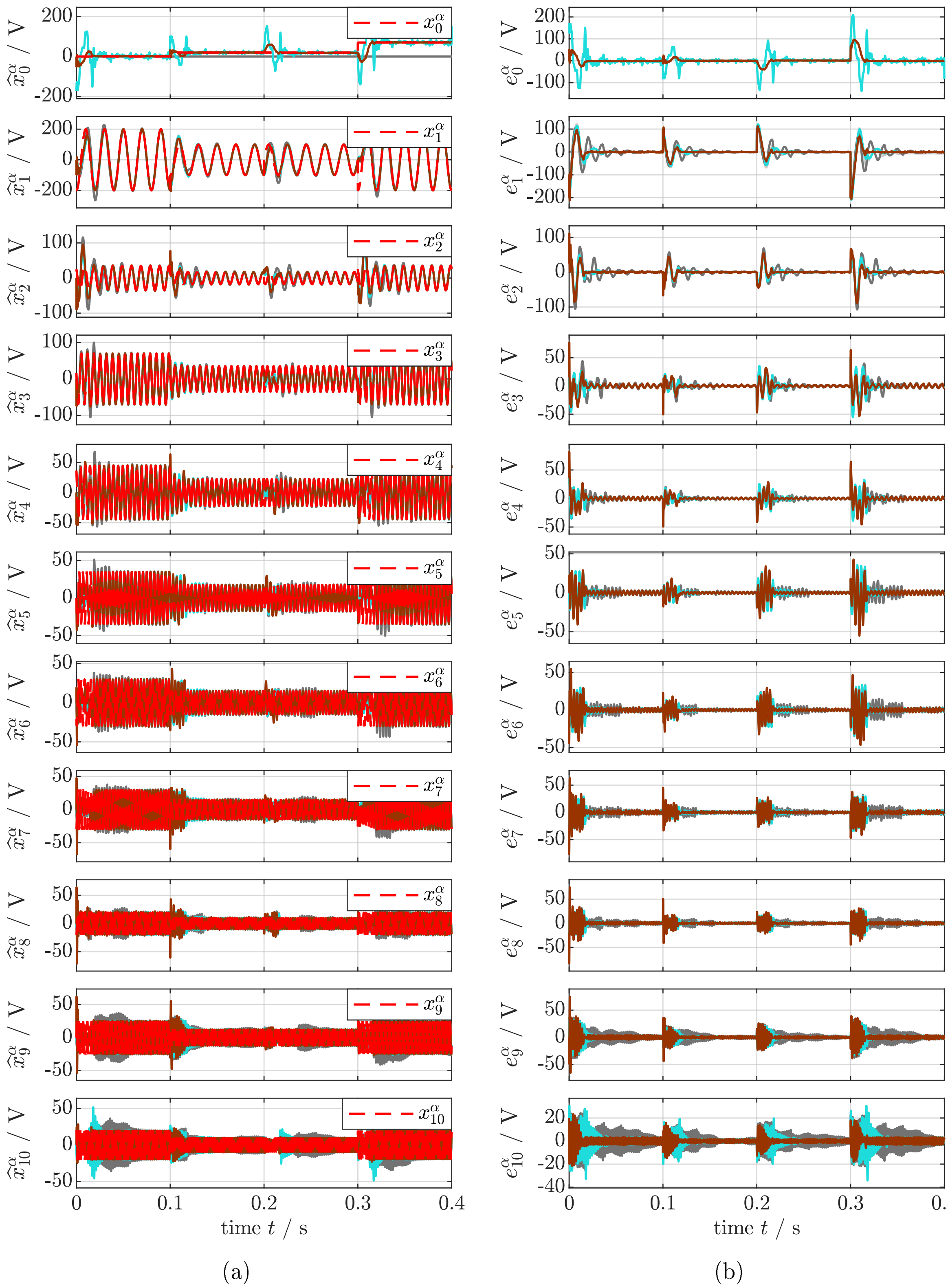

Figure 4.23: *Measurement results for scenario (S7). Used methods: MMI-QSG (—), MSOGI-FLL (—), esFAO (—) and mFAO with offset (—). Shown are the estimated states* $\widehat{x}_1^\alpha$ – $\widehat{x}_{10}^\alpha$ *in subfigure (a) and the estimation errors* e_1^α – e_{10}^α *in subfigure (b).*

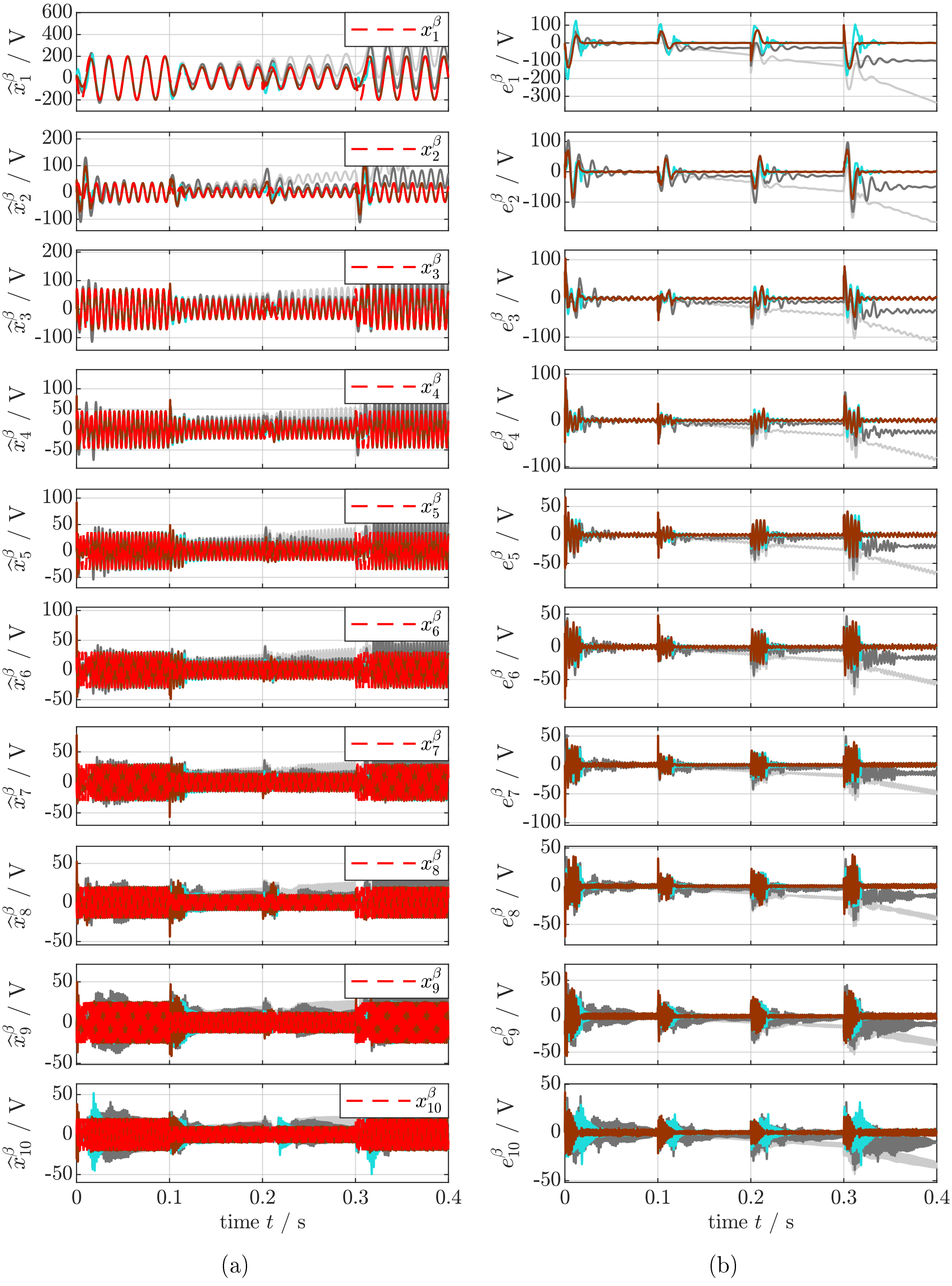

Figure 4.24: *Measurement results for scenario (S7). Used methods: MMI-QSG (—), MSOGI-FLL (—), esFAO (—) and mFAO with offset (—). Shown are the estimated states* $\widehat{x}_1^\beta$ – $\widehat{x}_{10}^\beta$ *in subfigure (a) and the estimation errors* e_1^β – e_{10}^β *in subfigure (b).*

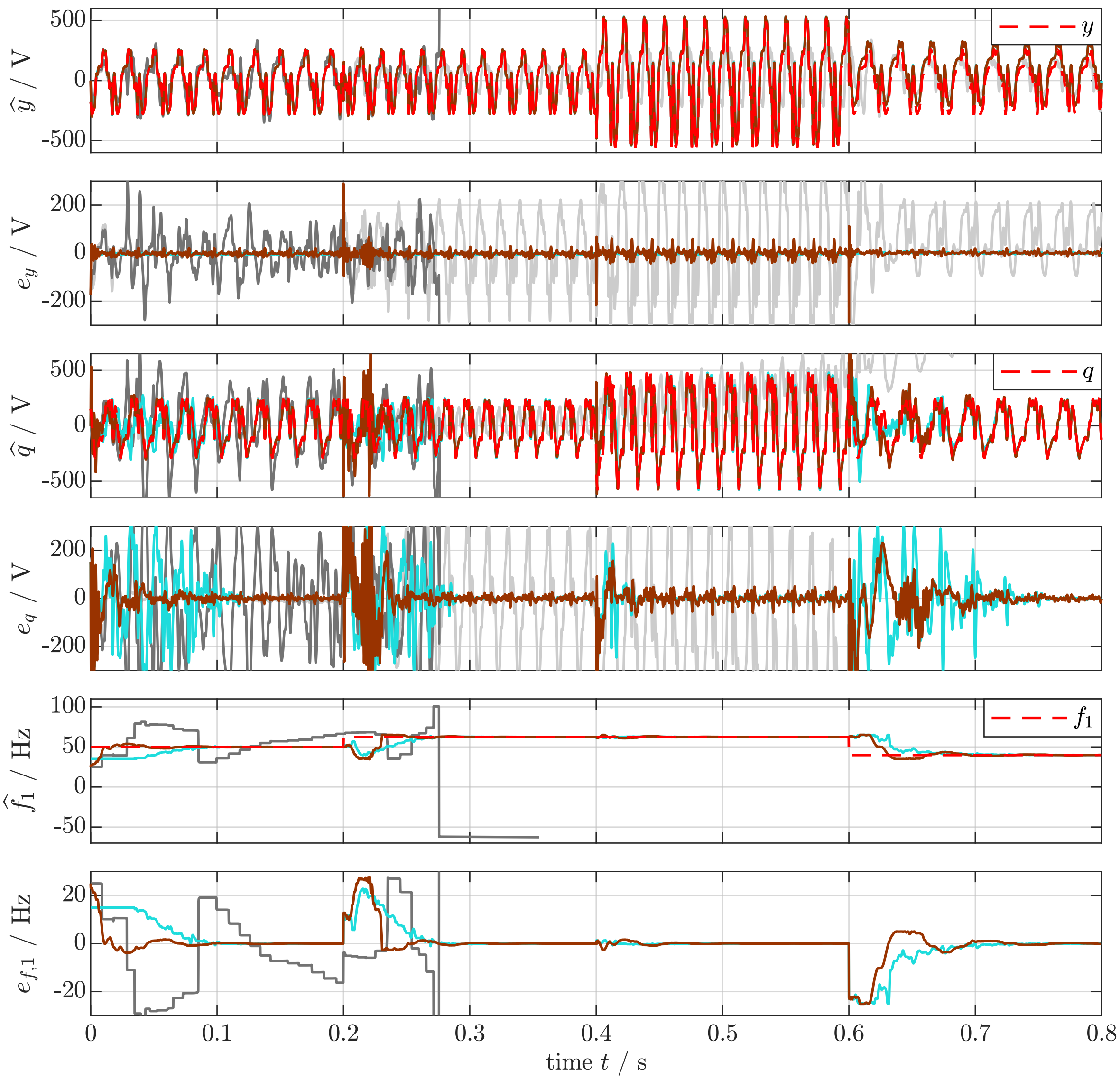

Figure 4.25: *Measurement results for scenario (S8). Used methods: MMI-QSG (—), MSOGI-FLL (—), esFAO (—) and mFAO with offset (—). Shown are the estimated direct and quadrature inputs $\widehat{y}, \widehat{q}$, their estimation errors e_y, e_q, the estimated fundamental frequency $\widehat{f}_1$ and its estimation errors $e_{f,1}$.*

Method	MMI-QSG	MSOGI-FLL	esFAO	mFAO$_\circ$
$\mathcal{M}_{\text{IAE}}$ / Vs	86.949	✗	11.843	**6.950**
$\mathcal{M}_{\text{ITAE}}$ / Vs^2	8.535	✗	0.851	**0.652**

Table 4.14: *IAE and ITAE for the different methods used in scenario (S8).*

has to be analyzed, the esFAO is more promising.

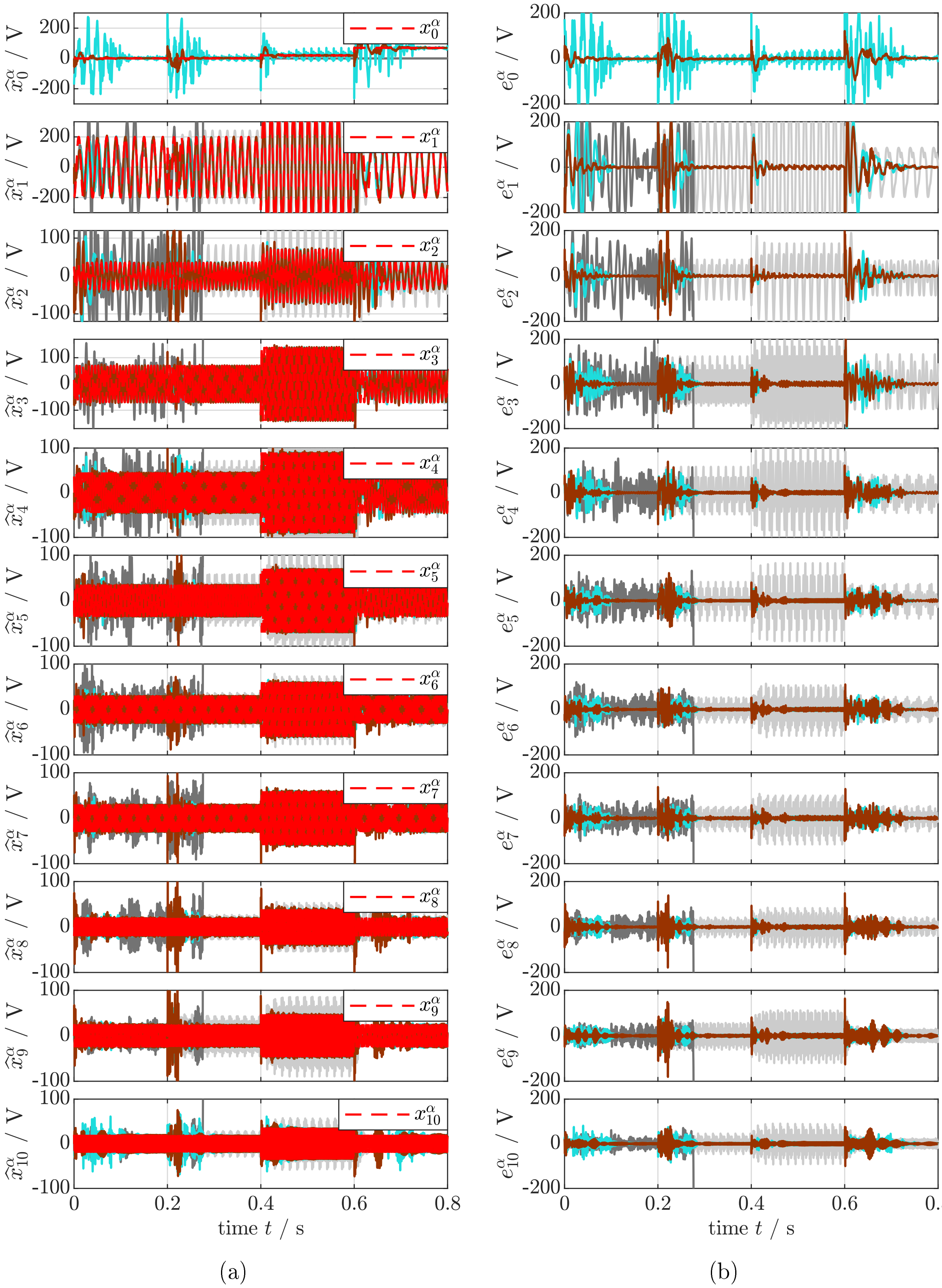

Figure 4.26: *Measurement results for scenario (S8). Used methods: MMI-QSG (—), MSOGI-FLL (—), esFAO (—) and mFAO with offset (—). Shown are the estimated states* $\widehat{x}_1^\alpha$ – $\widehat{x}_{10}^\alpha$ *in subfigure (a) and the estimation errors* e_1^α – e_{10}^α *in subfigure (b).*

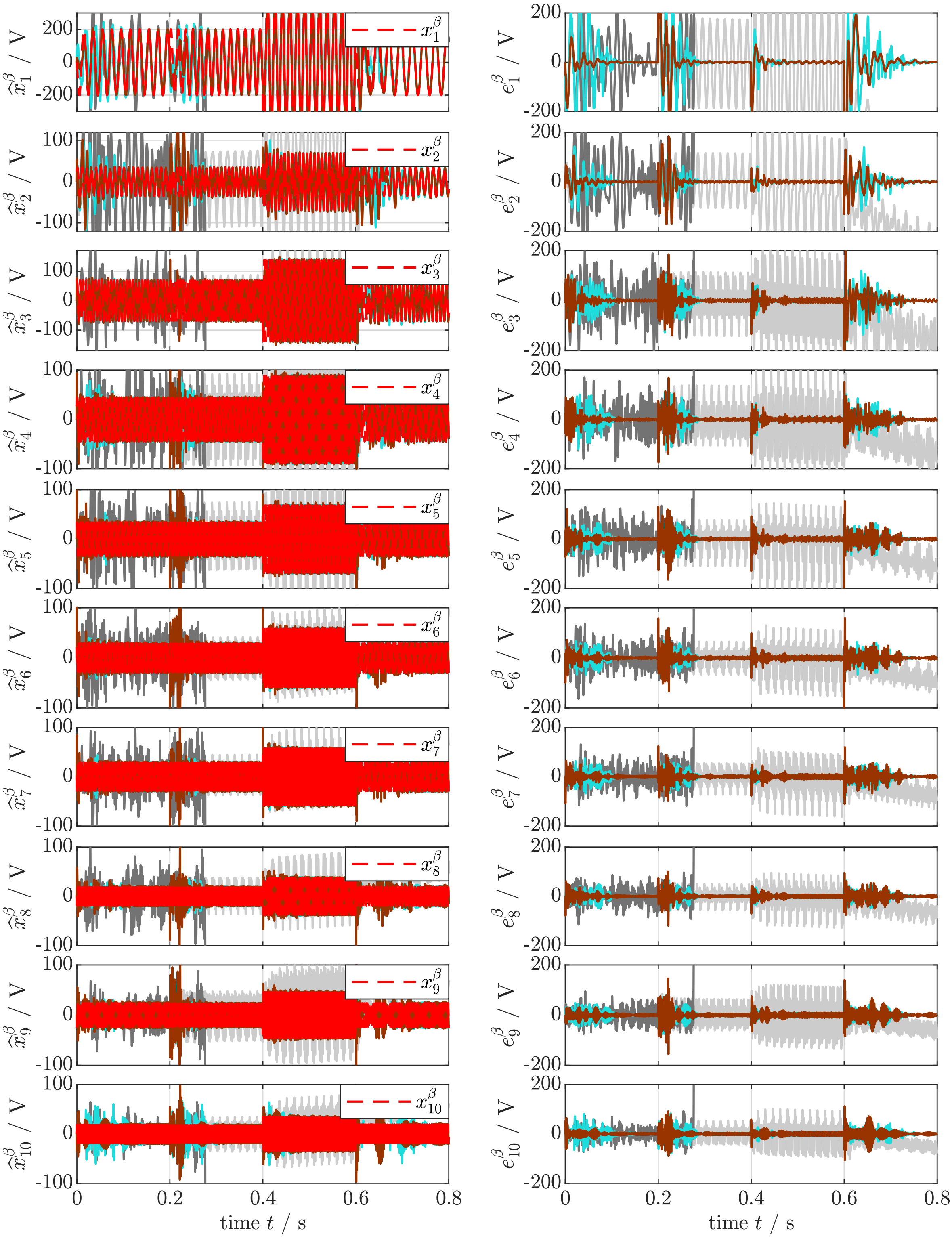

(a)

(b)

Figure 4.27: *Measurement results for scenario (S8). Used methods: MMI-QSG (—), MSOGI-FLL (—), esFAO (—) and mFAO with offset (—). Shown are the estimated states* $\widehat{x}_1^\beta$ – $\widehat{x}_{10}^\beta$ *in subfigure (a) and the estimation errors* e_1^β – e_{10}^β *in subfigure (b).*

Chapter 5

Conclusion and Outlook

In this thesis, five different observers to decompose a periodic signal into its fundamental parameters, namely esFAO, mFAO, mFAO$_\circ$, tFAO and tFAO$_\circ$, were developed. The esFAO is capable of detecting offset, estimating a predefined number of harmonic components and fundamental angular frequency. Thereafter, the mFAO was designed to accelerate the estimation process. It comes without offset estimation, which was covered by the mFAO$_\circ$. To also be capable of estimating multiple angular frequencies and harmonic components, the tFAO was constructed, which was extended to the tFAO$_\circ$ to cover offset estimation. Besides these properties, Table 5.1 summarizes the unique theoretical characteristics of each observer. These characteristics are based on the investigations from Section 3.

	Tuning	Stability	Decrease	Frequency
esFAO without FLL	limited	global	exponential	none
esFAO with FLL	limited	local	exponential	only fundamental
mFAO without FLL	unlimited	global	exponential	none
mFAO with FLL	limited	local	exponential	only fundamental
mFAO$_\circ$ without FLL	unlimited	global	exponential	none
mFAO$_\circ$ with FLL	limited	local	exponential	only fundamental
tFAO (transformed)	unlimited	global	asymptotic	all (transformed)
tFAO$_\circ$ (transformed)	unlimited	global	asymptotic	all (transformed)
tFAO (α, β)	unlimited	local	asymptotic	all (α, β)
tFAO$_\circ$ (α, β)	unlimited	local	asymptotic	all (α, β)

Table 5.1: *Theoretical characteristics of esFAO, mFAO, mFAO$_\circ$, tFAO in transformed frame, tFAO$_\circ$ in transformed frame, tFAO in α, β frame and tFAO$_\circ$ in α, β frame.*

In Section 4, these observers were tested in an experimental setup and compared to existing observers from literature. Due to the asymptotic decrease characteristic of tFAO and tFAO$_\circ$, which was already visualized in Figures 3.33 and 3.35, it was not included in the tests. The result of these tests, deduced from the error metrics, is the following:

(i) The esFAO is the best choice when estimating a signal that only has a fundamental component and whose angular frequency is known;

(ii) For signals comprising more harmonics and/or with unknown angular frequency but known harmonic orders, the mFAO$_\circ$ is advised.

For signals that are composed of more harmonics with unknown angular frequencies and unknown harmonic orders, so far the best choice is the tFAO$_\circ$ in α, β frame. Unfortunately, it requires

an unrealistic large time frame, making real-time decomposition impossible. In order to find a solution for this issue, an idea for exponential frequency adaptive observers (eFAO and eFAO$_\circ$) was discussed. Since it is not finished yet, the remaining tasks as well as a few ideas for future investigations are collected in the following.
For the eFAO, open tasks are (i) to find a set of matrices $\underline{\boldsymbol{A}}_\mathrm{e}$, $\overline{\boldsymbol{X}}_\mathrm{e}$, $\underline{\boldsymbol{W}}_{\mathrm{e},J}$, $\underline{\boldsymbol{W}}_{\mathrm{e},x}$ and $\boldsymbol{W}_{\mathrm{e},\omega}$ and (ii) to derive an algorithm for the assignment of eigenvalues to $\underline{\boldsymbol{A}}_\mathrm{e}$. Other tasks are to obtain insight into the system dynamics and to prove stability. The same tasks must be accomplished for the eFAO$_\circ$.
More generally, discretization of all observers was not considered in this thesis, so it is a topic to be dealt with in future works. Nevertheless, some effort was already put into this field in [557–569].
As a last idea, the development of a damped Second Order Generalized Integrator is proposed. Its benefits are the manipulation of amplitude and phase responses of the observer, which means that the observer can be designed to be less sensitive to noise in a certain frequency spectrum. Hereby, to the best knowledge of the author, the structure depicted in Figure 5.1 has not been published yet.

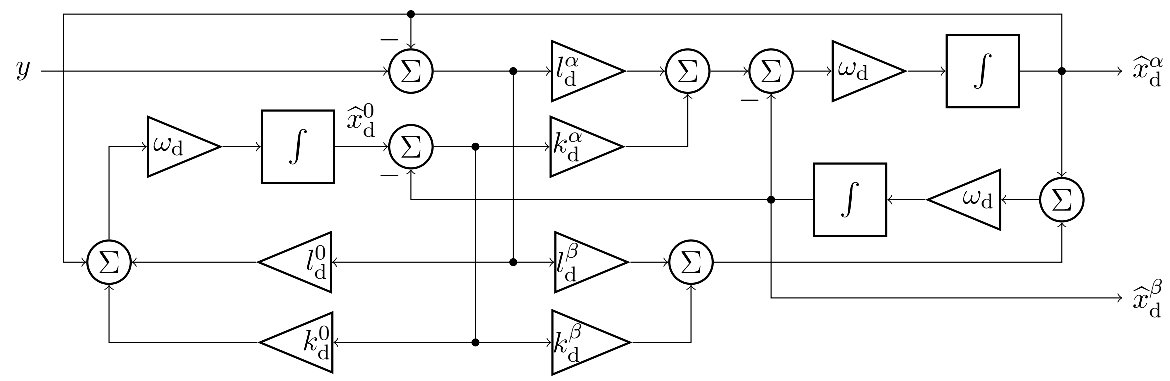

Figure 5.1: *Block diagram of the dSOGI^1.*

This structure, called the *damped Second Order Generalized Integrator of first order* (dSOGI^1) can be understood as an advanced mSOGI (but *not* mFAO) as reported in Section 3.3.2.1 in this thesis. Clearly, this system has more gains than states and, hence, has additional degrees of freedom compared to e.g. the mSOGI. These degrees of freedom can possibly be used for different purposes, which must be investigated in the future. For now conceivable purposes are (i) output noise reduction and (ii) speeding the frequency adaption. As a short motivation, the possibility to reduce output noise is validated in Figure 5.2[1]. In it, the amplitude responses A_d^0, A_d^α and A_d^β of the signals $\widehat{x}_\mathrm{d}^0$, $\widehat{x}_\mathrm{d}^\alpha$ and $\widehat{x}_\mathrm{d}^\beta$, respectively, are compared to the ones from the mSOGI (see Section 3.3.2.1).
The first subplot of Figure 5.2 shows the amplitude response of the signal $\widehat{x}_\mathrm{d}^0$, which only exists for the dSOGI^1. The second and third subplots show the responses of the direct signal $\widehat{x}^\alpha$ and quadrature signal $\widehat{x}^\beta$, respectively. It can be seen that the dSOGI^1 shows a better filtering capability than the mSOGI, especially for higher frequencies. For frequencies lower than the resonance frequency (located at $f = 50\,\mathrm{Hz}$), the quadrature signal $\widehat{x}^\beta$ shows a less effective filtering capability than the mSOGI. In view of the direct signal $\widehat{x}^\alpha$, the dSOGI^1 shows a lower filtering capability only in a very short frequency frame above the resonance frequency.
In conclusion, Figure 5.2 motivates that further efforts should be put into researching dSOGI^1.

[1]Simulation parameters: $\begin{pmatrix} l^0 & l^\alpha & l^\beta \end{pmatrix} = \begin{pmatrix} \frac{19}{14} & 0 & \frac{1}{7} \end{pmatrix}$, $\begin{pmatrix} k^0 & k^\alpha & k^\beta \end{pmatrix} = \begin{pmatrix} -10 & 10 & -4 \end{pmatrix}$, $\boldsymbol{l}_\mathrm{m} = \begin{pmatrix} 4 & -4 \end{pmatrix}^\top$, $\widehat{\omega} = \widehat{\omega}_{\mathrm{m},1} = 2\pi 50\,\frac{\mathrm{rad}}{\mathrm{s}}$.

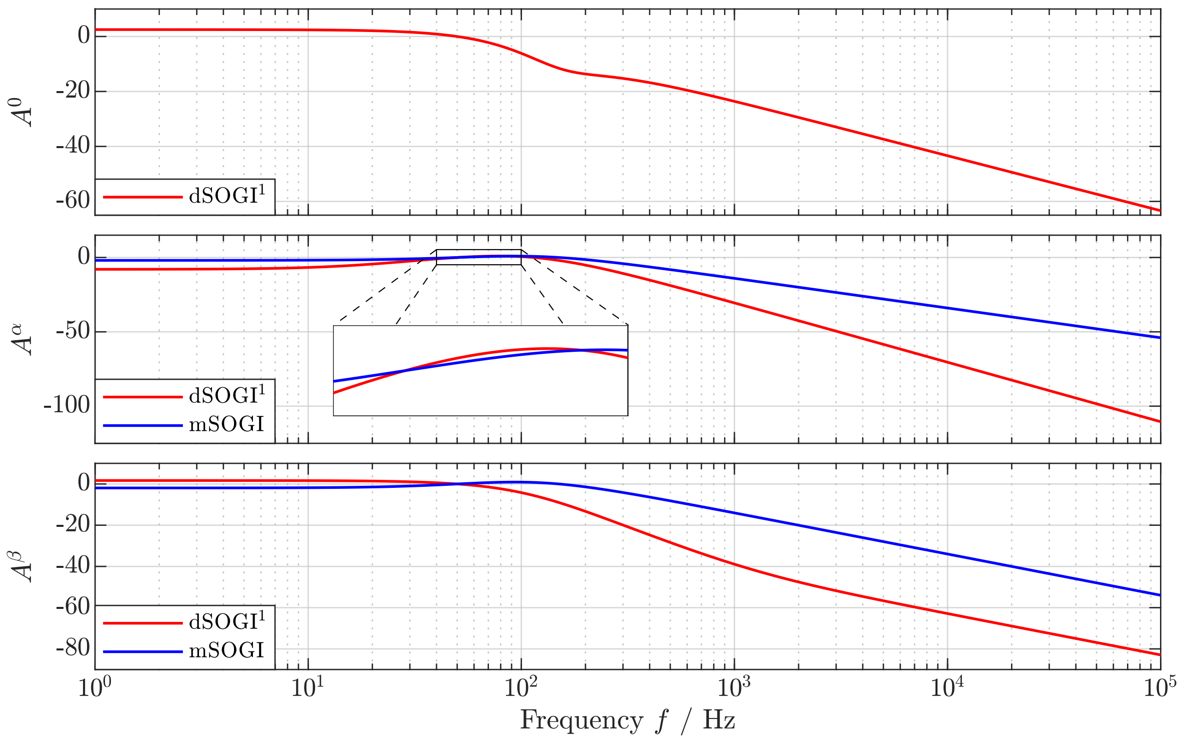

Figure 5.2: *Comparison of the amplitude responses of dSOGI^1 (—) and mSOGI (—).*

In this context, the following ideas are developed:

(a) A *Second Order Generalized Integrator of* m-*th order* (dSOGI^m) for more advanced noise reduction, which uses a cascade of m "pre-integrators" instead of only one as in Figure 5.1;

(b) Parallelized *Second Order Generalized Integrator of first order* (pdSOGI^1) comprising n parallel SOGIs;

(c) A *Second Order Generalized Integrator of first order* with offset (dSOGI$^1_\circ$) including an offset estimation capability;

(d) And a combination of (a) - (c).

Appendix A

Derivation of transfer functions, amplitude and phase responses of a SOGI

In this appendix, the general transfer functions and their amplitude and phase responses of a SOGI are derived. But first, the relation between the amplitude and phase response and the respective transfer function is shown. Consider a transfer function $\mathcal{F}(s) := \frac{n(s)}{d(s)}$. Inserting $s := \jmath\omega$ yields

$$\begin{aligned}\mathcal{F}(\jmath\omega) = \frac{n(\jmath\omega)}{d(\jmath\omega)} &= \frac{\Re(n(\jmath\omega))+\jmath\Im(n(\jmath\omega))}{\Re(d(\jmath\omega))+\jmath\Im(d(\jmath\omega))} = \frac{(\Re(n(\jmath\omega))+\jmath\Im(n(\jmath\omega)))(\Re(d(\jmath\omega))-\jmath\Im(d(\jmath\omega)))}{(\Re(d(\jmath\omega))+\jmath\Im(d(\jmath\omega)))(\Re(d(\jmath\omega))-\jmath\Im(d(\jmath\omega)))} \\ &= \underbrace{\frac{\Re(d(\jmath\omega))\Re(n(\jmath\omega))+\Im(d(\jmath\omega))\Im(n(\jmath\omega))}{\Re(d(\jmath\omega))^2+\Im(d(\jmath\omega))^2}}_{=:\,\Re(\mathcal{F}(\jmath\omega))} + \jmath \underbrace{\frac{\Re(d(\jmath\omega))\Im(n(\jmath\omega))-\Re(n(\jmath\omega))\Im(d(\jmath\omega))}{\Re(d(\jmath\omega))^2+\Im(d(\jmath\omega))^2}}_{=:\,\Im(\mathcal{F}(\jmath\omega))}.\end{aligned} \tag{A.1}$$

The amplitude and phase responses are obtained as

$$A_{\mathcal{F}}(\omega) = \sqrt{\Re\left(\mathcal{F}(\jmath\omega)\right)^2 + \Im\left(\mathcal{F}(\jmath\omega)\right)^2} \overset{(A.1)}{=} \sqrt{\frac{\Re(n(\jmath\omega))^2+\Im(n(\jmath\omega))^2}{\Re(d(\jmath\omega))^2+\Im(d(\jmath\omega))^2}} \tag{A.2}$$

$$\Phi_{\mathcal{F}}(\omega) = \operatorname{arctan2}\left(\frac{\Im(\mathcal{F}(\jmath\omega))}{\Re(\mathcal{F}(\jmath\omega))}\right) \overset{(A.1)}{=} \operatorname{arctan2}\left(\frac{\Re(d(\jmath\omega))\Im(n(\jmath\omega))-\Re(n(\jmath\omega))\Im(d(\jmath\omega))}{\Re(d(\jmath\omega))\Re(n(\jmath\omega))+\Im(d(\jmath\omega))\Im(n(\jmath\omega))}\right). \tag{A.3}$$

Now, consider the signal estimation error e_y, the direct signals $\widehat{x}_{\nu_i}^{\alpha}$ and the quadrature signals $\widehat{x}_{\nu_i}^{\beta}$ given as

$$\left.\begin{aligned} e_y(s) &= y(s) - \sum_{j=1}^{n} \widehat{x}_j^{\alpha}(s) \\ \widehat{x}_i^{\alpha}(s) &= \frac{\widehat{\omega}_1}{s}\left(l_i^{\alpha} e_y(s) - \nu_i \widehat{x}_i^{\beta}(s)\right) \\ \widehat{x}_i^{\beta}(s) &= \frac{\widehat{\omega}_1}{s}\left(l_i^{\beta} e_y(s) + \nu_i \widehat{x}_i^{\alpha}(s)\right). \end{aligned}\right\} \tag{A.4}$$

Inserting $\widehat{x}_i^{\beta}$ into $\widehat{x}_i^{\alpha}$ yields

$$\begin{aligned} \widehat{x}_i^{\alpha}(s) &\overset{(A.4)}{=} \frac{\widehat{\omega}_1}{s}\left(l_i^{\alpha} e_y(s) - \frac{\nu_i\widehat{\omega}_1}{s}\left(l_i^{\beta} e_y(s) + \nu_i \widehat{x}_i^{\alpha}(s)\right)\right) \\ \Rightarrow\ \widehat{x}_i^{\alpha}(s) &= \frac{\frac{\widehat{\omega}_1}{s}\left(l_i^{\alpha} e_y(s) - \frac{\nu_i\widehat{\omega}_1}{s} l_i^{\beta} e_y(s)\right)}{1+\frac{\nu_i^2\widehat{\omega}_1^2}{s^2}} = \frac{\widehat{\omega}_1 l_i^{\alpha} s - \nu_i \widehat{\omega}_1^2 l_i^{\beta}}{s^2+\nu_i^2\widehat{\omega}_1^2} e_y(s). \end{aligned} \tag{A.5}$$

By inserting (A.5) into e_y in (A.4), the transfer function for the signal estimation error is obtained:

$$e_y(s) \overset{(A.4),(A.5)}{=} y(s) - \sum_{j=1}^{n} \frac{\widehat{\omega}_1 l_j^\alpha s - \nu_j \widehat{\omega}_1^2 l_j^\beta}{s^2+\nu_j^2\widehat{\omega}_1^2} e_y(s)$$

$$\Rightarrow \mathcal{E}_y(s) := \frac{e_y(s)}{y(s)} = \frac{\prod_{k=1}^{n}\left(s^2+\nu_k^2\widehat{\omega}_1^2\right)}{\prod_{k=1}^{n}\left(s^2+\nu_k^2\widehat{\omega}_1^2\right)+\sum_{j=1}^{n}\left(\widehat{\omega}_1 l_j^\alpha s-\nu_j\widehat{\omega}_1^2 l_j^\beta\right)\prod_{\substack{k=1\\k\neq j}}^{n}\left(s^2+\nu_k^2\widehat{\omega}_1^2\right)}. \quad (A.6)$$

In a similar way, the transfer functions for the direct and quadrature signals are obtained as

$$\mathcal{X}_i^\alpha(s) := \frac{\widehat{x}_i^\alpha(s)}{y(s)} \overset{(A.5),(A.6)}{=} \frac{\widehat{\omega}_1\left(l_i^\alpha s-\nu_i\widehat{\omega}_1 l_i^\beta\right)\prod_{\substack{k=1\\k\neq i}}^{n}\left(s^2+\nu_k^2\widehat{\omega}_1^2\right)}{\prod_{k=1}^{n}\left(s^2+\nu_k^2\widehat{\omega}_1^2\right)+\sum_{j=1}^{n}\left(\widehat{\omega}_1 l_j^\alpha s-\nu_j\widehat{\omega}_1^2 l_j^\beta\right)\prod_{\substack{k=1\\k\neq j}}^{n}\left(s^2+\nu_k^2\widehat{\omega}_1^2\right)} \quad (A.7)$$

$$\text{and} \quad \mathcal{X}_i^\beta(s) := \frac{\widehat{x}_i^\beta(s)}{y(s)} \overset{(A.4),(A.5),(A.6)}{=} \frac{\widehat{\omega}_1\left(l_i^\beta s+\nu_i\widehat{\omega}_1 l_i^\alpha\right)\prod_{\substack{k=1\\k\neq i}}^{n}\left(s^2+\nu_k^2\widehat{\omega}_1^2\right)}{\prod_{k=1}^{n}\left(s^2+\nu_k^2\widehat{\omega}_1^2\right)+\sum_{j=1}^{n}\left(\widehat{\omega}_1 l_j^\alpha s-\nu_j\widehat{\omega}_1^2 l_j^\beta\right)\prod_{\substack{k=1\\k\neq j}}^{n}\left(s^2+\nu_k^2\widehat{\omega}_1^2\right)}. \quad (A.8)$$

The transfer functions include the characteristic polynomial of a SOGI's system matrix in their denominators, which can be read off as follows:

$$\chi(s) = \prod_{k=1}^{n}\left(s^2+\nu_k^2\widehat{\omega}_1^2\right) + \sum_{j=1}^{n}\left(\widehat{\omega}_1 l_j^\alpha s - \nu_j\widehat{\omega}_1^2 l_j^\beta\right)\prod_{\substack{k=1\\k\neq j}}^{n}\left(s^2+\nu_k^2\widehat{\omega}_1^2\right). \quad (A.9)$$

Finally, by introducing the abbreviations

$$\rho := \prod_{k=1}^{n}\left(\nu_k^2\widehat{\omega}_1^2-\omega^2\right) - \sum_{j=1}^{n}\nu_j\widehat{\omega}_1^2 l_j^\beta \prod_{\substack{k=1\\k\neq j}}^{n}\left(\nu_k^2\widehat{\omega}_1^2-\omega^2\right) \quad (A.10)$$

$$\upsilon := \sum_{j=1}^{n}\widehat{\omega}_1\omega l_j^\alpha \prod_{\substack{k=1\\k\neq j}}^{n}\left(\nu_k^2\widehat{\omega}_1^2-\omega^2\right) \quad (A.11)$$

the amplitude responses are obtained according to (A.2) as follows

$$A_{\mathcal{E}_y}(\omega) \overset{(A.2),(A.6)}{=} \frac{\prod_{k=1}^{n}\left(\nu_k^2\widehat{\omega}_1^2-\omega^2\right)}{\sqrt{\rho^2+\upsilon^2}} \quad (A.12)$$

$$A_{\mathcal{X}_{\nu_i}^\alpha}(\omega) \overset{(A.2),(A.7)}{=} \frac{\widehat{\omega}_1\prod_{\substack{k=1\\k\neq i}}^{n}\left(\nu_k^2\widehat{\omega}_1^2-\omega^2\right)\sqrt{\nu_i^2\widehat{\omega}_1^2(l_i^\beta)^2+\omega^2(l_i^\alpha)^2}}{\sqrt{\rho^2+\upsilon^2}} \quad (A.13)$$

$$A_{\mathcal{X}_{\nu_i}^\beta}(\omega) \overset{(A.2),(A.8)}{=} \frac{\widehat{\omega}_1\prod_{\substack{k=1\\k\neq i}}^{n}\left(\nu_k^2\widehat{\omega}_1^2-\omega^2\right)\sqrt{\nu_i^2\widehat{\omega}_1^2(l_i^\alpha)^2+\omega^2(l_i^\beta)^2}}{\sqrt{\rho^2+\upsilon^2}}. \quad (A.14)$$

Using (A.3), the phase responses follow as

$$\Phi_{\mathcal{E}_y}(\omega) \overset{(A.3),(A.6)}{=} \operatorname{arctan2}\left(\frac{-\upsilon}{\rho}\right) \tag{A.15}$$

$$\Phi_{\mathcal{X}^{\alpha}_{\nu_i}}(\omega) \overset{(A.3),(A.7)}{=} \operatorname{arctan2}\left(\frac{\omega l_i^{\alpha}\rho+\nu_i\widehat{\omega}_1 l_i^{\beta}\upsilon}{\omega l_i^{\alpha}\upsilon-\nu_i\widehat{\omega}_1 l_i^{\beta}\rho}\right) \tag{A.16}$$

$$\Phi_{\mathcal{X}^{\beta}_{\nu_i}}(\omega) \overset{(A.3),(A.8)}{=} \operatorname{arctan2}\left(\frac{\omega l_i^{\beta}\rho-\nu_i\widehat{\omega}_1 l_i^{\alpha}\upsilon}{\omega l_i^{\beta}\upsilon+\nu_i\widehat{\omega}_1 l_i^{\alpha}\rho}\right). \tag{A.17}$$

If the SOGI is extended to estimate offset, the transfer functions, abbreviations and responses follow in a similar way as

$$\chi_{\circ}(s) = (s+\widehat{\omega}_{\circ,1}l_{\circ,0})\prod_{k=1}^{n}\left(s^2+\nu_k^2\widehat{\omega}_{\circ,1}^2\right) + s\sum_{j=1}^{n}\left(\widehat{\omega}_{\circ,1}l_{\circ,j}^{\alpha}s-\nu_j\widehat{\omega}_{\circ,1}^2 l_{\circ,j}^{\beta}\right)\prod_{\substack{k=1\\k\neq j}}^{n}\left(s^2+\nu_k^2\widehat{\omega}_{\circ,1}^2\right) \tag{A.18}$$

$$\rho_{\circ} = \omega\prod_{k=1}^{n}\left(\nu_k^2\widehat{\omega}_{\circ,1}^2-\omega^2\right) - \omega\sum_{j=1}^{n}\nu_j\widehat{\omega}_{\circ,1}^2 l_{\circ,j}^{\beta}\prod_{\substack{k=1\\k\neq j}}^{n}\left(\nu_k^2\widehat{\omega}_{\circ,1}^2-\omega^2\right) \tag{A.19}$$

$$\upsilon_{\circ} = \omega^2\sum_{j=1}^{n}\widehat{\omega}_{\circ,1}l_{\circ,j}^{\alpha}\prod_{\substack{k=1\\k\neq j}}^{n}\left(\nu_k^2\widehat{\omega}_{\circ,1}^2-\omega^2\right) - \widehat{\omega}_{\circ,1}l_{\circ,0}\prod_{k=1}^{n}\left(\nu_k^2\widehat{\omega}_{\circ,1}^2-\omega^2\right) \tag{A.20}$$

$$A_{\mathcal{E}_{\circ,y}}(\omega) = \frac{\omega\prod_{k=1}^{n}\left(\nu_k^2\widehat{\omega}_{\circ,1}^2-\omega^2\right)}{\sqrt{\upsilon_{\circ}^2+\rho_{\circ}^2}} \tag{A.21}$$

$$A_{\mathcal{X}_{\circ,0}}(\omega) = \frac{\widehat{\omega}_{\circ,1}l_{\circ,0}\prod_{k=1}^{n}\left(\nu_k^2\widehat{\omega}_{\circ,1}^2-\omega^2\right)}{\sqrt{\upsilon_{\circ}^2+\rho_{\circ}^2}} \tag{A.22}$$

$$A_{\mathcal{X}^{\alpha}_{\circ,\nu_i}}(\omega) = \frac{\omega\widehat{\omega}_{\circ,1}\prod_{\substack{k=1\\k\neq i}}^{n}\left(\nu_k^2\widehat{\omega}_{\circ,1}^2-\omega^2\right)\sqrt{\omega^2(l_{\circ,i}^{\alpha})^2+\nu_i^2\widehat{\omega}_{\circ,1}^2(l_{\circ,i}^{\beta})^2}}{\sqrt{\upsilon_{\circ}^2+\rho_{\circ}^2}} \tag{A.23}$$

$$A_{\mathcal{X}^{\beta}_{\circ,\nu_i}}(\omega) = \frac{\omega\widehat{\omega}_{\circ,1}\prod_{\substack{k=1\\k\neq i}}^{n}\left(\nu_k^2\widehat{\omega}_{\circ,1}^2-\omega^2\right)\sqrt{\nu_i^2\widehat{\omega}_{\circ,1}^2(l_{\circ,i}^{\alpha})^2+\omega^2(l_{\circ,i}^{\beta})^2}}{\sqrt{\upsilon_{\circ}^2+\rho_{\circ}^2}} \tag{A.24}$$

$$\Phi_{\mathcal{E}_{\circ,y}}(\omega) = \operatorname{arctan2}\left(\frac{-\upsilon_{\circ}}{\rho_{\circ}}\right) \tag{A.25}$$

$$\Phi_{\mathcal{X}_{\circ,0}}(\omega) = \operatorname{arctan2}\left(\frac{-\rho_{\circ}}{-\upsilon_{\circ}}\right) \tag{A.26}$$

$$\Phi_{\mathcal{X}^{\alpha}_{\circ,\nu_i}}(\omega) = \operatorname{arctan2}\left(\frac{\nu_i\widehat{\omega}_{\circ,1}l_{\circ,i}^{\beta}\upsilon_{\circ}+\omega l_{\circ,i}^{\alpha}\rho_{\circ}}{\omega l_{\circ,i}^{\alpha}\upsilon_{\circ}-\nu_i\widehat{\omega}_{\circ,1}l_{\circ,i}^{\beta}\rho_{\circ}}\right) \tag{A.27}$$

$$\Phi_{\mathcal{X}^{\beta}_{\circ,\nu_i}}(\omega) = \operatorname{arctan2}\left(\frac{\omega l_{\circ,i}^{\beta}\rho_{\circ}-\nu_i\widehat{\omega}_{\circ,1}l_{\circ,i}^{\alpha}\upsilon_{\circ}}{\nu_i\widehat{\omega}_{\circ,1}l_{\circ,i}^{\alpha}\rho_{\circ}+\omega l_{\circ,i}^{\beta}\upsilon_{\circ}}\right). \tag{A.28}$$

Appendix B

Matlab code for finding the optimal gain vector for system (3.19)

This section shows the MATLAB-code for minimizing the dominant eigenvalue of $\boldsymbol{A}_{\mathrm{es}}$ as in (3.19). The choices for the system order `n`, the initial gain vector `lvec_init`, the resolution `resolution` and the expected harmonic set `nu_expected` are exemplarily and should be adapted to the system of interest.

```
function lvec = iterative_optimal_gains
%% Define parameters

% system order
n = 10;

% starting values
lvec_init = zeros(2*n,1);

% resolution
resolution = 1e-3;
step_vector = zeros(2*n,1);
step_vector(1) = resolution;

% to prevent numerical issues (should be much smaller than the resolution)
numerical_value = 0.5*resolution;

% calculate required system matrices and vectors
J = zeros(2*n);
cy = zeros(2*n,1);

nu_expected = (1:n)';

for z = 1:2*n
    for y = 1:2*n
        if mod(z,2) ~= 0 && y == (z+1)
            J(z,y) = - nu_expected(y/2);
        elseif mod(z,2) == 0 && y == (z-1)
            J(z,y) = nu_expected(z/2);
        end
```

```
    end
    if mod(z,2) ~= 0
        cy(z) = 1;
    end
end

% number of directions
possible_directions = 1;
for i = 2:n
    possible_directions = 2*possible_directions + 1;
end

% initialize vectors and cells
eigenvalues_cell = cell(possible_directions,1);
lvec_cell = cell(possible_directions,1);
lvec_optimal = lvec_init;
for row = 1:2*n
    if mod(row,2) == 0
        lvec_optimal(row) = 0;
    end
end

%% Find minimum
% initialize eigenvalues
eigenvalues_optimal = eig(J-lvec_optimal*cy');

% breaking condition initialization
looping = true;

while looping
    % breaking condition for each loop
    count = 0;
    % build new gain vectors and compute respective eigenvalues
    for i = 1:possible_directions
        if i == 1
            lvec_cell{i} = lvec_optimal + step_vector;
        else
            lvec_cell{i} = lvec_cell{i-1} + step_vector;
        end
        for row = 1:n
            if (lvec_cell{i}(2*row-1) - lvec_optimal(2*row-1)) > (resolution + numerical_value)
                lvec_cell{i}(2*row-1) = lvec_cell{i}(2*row-1) - 2*resolution;
                lvec_cell{i}(2*row+1) = lvec_cell{i}(2*row+1) + resolution;
            end
        end
        eigenvalues_cell{i} = eig(J-lvec_cell{i}*cy');
    end
    % compare eigenvalues
    for i = 1:possible_directions
        if max(real(eigenvalues_cell{i})) <= max(real(eigenvalues_optimal))
```

```
            count = count + 1;
            lvec_optimal = lvec_cell{i};
            eigenvalues_optimal = eigenvalues_cell{i};
        end
    end
    % breaking condition test
    if count == 0
        looping = false;
    end
end

end
```

Appendix C

Low Pass Filter and Amplitude Phase Correction

This section describes the impact of *Low Pass Filter*s (LPF) to any type of SOGI outputting harmonic components (i.e. all but the tSOGI in transformed frame, see Section 3.4). Moreover, the correction of this effect is proposed. Such an LPF with state space representation

$$\begin{aligned} \forall\, t \in \mathbb{T}_i\colon \quad & \tfrac{\mathrm{d}}{\mathrm{d}t} x_{\mathrm{lpf}} = -\omega_{\mathrm{lpf}} x_{\mathrm{lpf}} + \omega_{\mathrm{lpf}} y, \quad x_{\mathrm{lpf}}(0) = x_{\mathrm{lpf},t_i} \\ & y_{\mathrm{lpf}} = x_{\mathrm{lpf}}, \end{aligned} \tag{C.1}$$

transfer function

$$\mathcal{X}^p_{\mathrm{lpf}}(s) := \tfrac{x_{\mathrm{lpf}}(s)}{y(s)} = \tfrac{\omega_{\mathrm{lpf}}}{s+\omega_{\mathrm{lpf}}} \tag{C.2}$$

and amplitude and phase responses

$$A^p_{\mathcal{X}_{\mathrm{lpf}}}(\omega) = \tfrac{\omega_{\mathrm{lpf}}}{\sqrt{(\omega_{\mathrm{lpf}})^2+(\omega)^2}}, \qquad \Phi(\omega)^p_{\mathcal{X}_{\mathrm{lpf}}} = \operatorname{arctan2}\Big(\tfrac{-\omega}{\omega_{\mathrm{lpf}}}\Big) \tag{C.3}$$

is drawn in Figure C.1. Clearly, the cut-off frequency ω_{lpf} must be positive in view of stability.

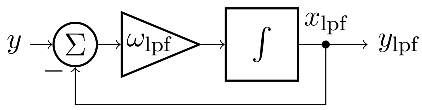

Figure C.1: *A Low Pass Filter.*

By feeding the LPF's output signal y_{lpf} to a SOGI system, this signal comes with damping and shifting with respect to the actual signal y according to (C.3). Consequently, the SOGIs estimate these modified signals, so that these have to be corrected again. This is achieved by an APC for an LPF, which is stated in the following proposition.

Proposition C.1 (Amplitude Phase Correction for LPF)**.** *Let* $\omega_{\mathrm{lpf}}, \omega_\nu > 0$, $y := a\cos(\omega_\nu t + \phi)$ *and* $y_{\mathrm{lpf}} := aA^p_{\mathcal{X}_{\mathrm{lpf}}}(\omega_\nu)\cos(\omega_\nu t + \phi + \Phi^p_{\mathcal{X}_{\mathrm{lpf}}}(\omega_\nu))$ *with* $A^p_{\mathcal{X}_{\mathrm{lpf}}}$ *and* $\Phi^p_{\mathcal{X}_{\mathrm{lpf}}}$ *as in* (C.3)*. Moreover, let* q *and* q_{lpf} *be signals having identical amplitude and a phase lag of* $-\frac{\pi}{2}$ *with respect to* y *and* y_{lpf}*, respectively. Then, there exists a transformation matrix* $\boldsymbol{C}_{\mathrm{lpf},\nu} \in \mathbb{R}^{2\times 2}$ *such that the amplitude- and phase-corrected signals* $\widetilde{y}_{\mathrm{lpf}}$ *and* $\widetilde{q}_{\mathrm{lpf}}$ *have identical phase and amplitude as the input signals, i.e.* $y = \widetilde{y}_{\mathrm{lpf}}$ *and* $q = \widetilde{q}_{\mathrm{lpf}}$ *for all* $t \in \mathbb{T}$*. The correction matrix is given by*

$$\boldsymbol{C}_{\mathrm{lpf},\nu} := \begin{bmatrix} 1 & -\frac{\omega_\nu}{\omega_{\mathrm{lpf}}} \\ \frac{\omega_\nu}{\omega_{\mathrm{lpf}}} & 1 \end{bmatrix}. \tag{C.4}$$

Proof. Define

$$\begin{pmatrix} \widetilde{y}_{\mathrm{lpf}} \\ \widetilde{q}_{\mathrm{lpf}} \end{pmatrix} := \boldsymbol{C}_{\mathrm{lpf},\nu} \begin{pmatrix} y_{\mathrm{lpf}} \\ q_{\mathrm{lpf}} \end{pmatrix}, \qquad \boldsymbol{C}_{\mathrm{lpf},\nu} := \begin{bmatrix} c_{\mathrm{lpf},1,\nu} & -c_{\mathrm{lpf},2,\nu} \\ c_{\mathrm{lpf},2,\nu} & c_{\mathrm{lpf},1,\nu} \end{bmatrix} \tag{C.5}$$

and observe that

$$\begin{pmatrix} \widetilde{y}_{\mathrm{lpf}} \\ \widetilde{q}_{\mathrm{lpf}} \end{pmatrix} = \begin{bmatrix} c_{\mathrm{lpf},1,\nu} & -c_{\mathrm{lpf},2,\nu} \\ c_{\mathrm{lpf},2,\nu} & c_{\mathrm{lpf},1,\nu} \end{bmatrix} \begin{pmatrix} y_{\mathrm{lpf}} \\ q_{\mathrm{lpf}} \end{pmatrix} = \underbrace{\begin{bmatrix} y_{\mathrm{lpf}} & -q_{\mathrm{lpf}} \\ q_{\mathrm{lpf}} & y_{\mathrm{lpf}} \end{bmatrix}}_{=: \boldsymbol{S}_{\mathrm{lpf},\nu}} \begin{pmatrix} c_{\mathrm{lpf},1,\nu} \\ c_{\mathrm{lpf},2,\nu} \end{pmatrix}. \tag{C.6}$$

Note that the matrix $\boldsymbol{S}_{\mathrm{lpf},\nu}$ is invertible (except for $(y_{\mathrm{lpf}},\, q_{\mathrm{lpf}})^\top = \boldsymbol{0}_2^\top$) with inverse

$$\begin{aligned} \boldsymbol{S}_{\mathrm{lpf},\nu}^{-1} &= \tfrac{1}{(y_{\mathrm{lpf}})^2+(q_{\mathrm{lpf}})^2} \begin{bmatrix} y_{\mathrm{lpf}} & q_{\mathrm{lpf}} \\ -q_{\mathrm{lpf}} & y_{\mathrm{lpf}} \end{bmatrix} \\ &\overset{\mathrm{def.}}{=} \tfrac{1}{a A^p_{\mathcal{X}_{\mathrm{lpf}}}(\omega_\nu)} \begin{bmatrix} \cos\Big(\omega_\nu t + \phi + \Phi^p_{\mathcal{X}_{\mathrm{lpf}}}(\omega_\nu)\Big) & \sin\Big(\omega_\nu t + \phi + \Phi^p_{\mathcal{X}_{\mathrm{lpf}}}(\omega_\nu)\Big) \\ -\sin\Big(\omega_\nu t + \phi + \Phi^p_{\mathcal{X}_{\mathrm{lpf}}}(\omega_\nu)\Big) & \cos\Big(\omega_\nu t + \phi + \Phi^p_{\mathcal{X}_{\mathrm{lpf}}}(\omega_\nu)\Big) \end{bmatrix}. \end{aligned} \tag{C.7}$$

This allows the unique solution of the following identity for $c_{\mathrm{lpf},1,\nu}$ and $c_{\mathrm{lpf},2,\nu}$:

$$\begin{pmatrix} c_{\mathrm{lpf},1,\nu} \\ c_{\mathrm{lpf},2,\nu} \end{pmatrix} = \boldsymbol{S}_{\mathrm{lpf},\nu}^{-1} \begin{pmatrix} \widetilde{y}_{\mathrm{lpf}} \\ \widetilde{q}_{\mathrm{lpf}} \end{pmatrix} \overset{!}{=} \boldsymbol{S}_{\mathrm{lpf},\nu}^{-1} \begin{pmatrix} y \\ q \end{pmatrix} \overset{(2.3),(C.7)}{=} \frac{1}{A^p_{\mathcal{X}_{\mathrm{lpf}}}(\omega_\nu)} \begin{pmatrix} \cos\big(\Phi^p_{\mathcal{X}_{\mathrm{lpf}}}(\omega_\nu)\big) \\ -\sin\big(\Phi^p_{\mathcal{X}_{\mathrm{lpf}}}(\omega_\nu)\big) \end{pmatrix} \overset{(C.3)}{=} \begin{pmatrix} 1 \\ \frac{\omega_\nu}{\omega_{\mathrm{lpf}}} \end{pmatrix}. \tag{C.8}$$

Inserting (C.8) into (C.5) yields the matrix as in (C.4). This completes the proof. □

Appendix D

Proof for Assertion (3.151) (Frequency polynomial)

Proposition D.1. *Let $n \in \mathbb{N}$, $\kappa_i \in \mathbb{C}$, $i \in \{1, \ldots, n\}$ and*

$$\left.\begin{array}{rcl} \upsilon_1 & = & \sum\limits_{k=1}^{n} \kappa_k \\ \upsilon_i & = & \sum\limits_{k_1,\ldots,k_i=1}^{n} \prod\limits_{j \in k} \kappa_j \\ \upsilon_n & = & \prod\limits_{k=1}^{n} \kappa_k . \end{array}\right\} \tag{D.1}$$

Then, the κ_i are obtained as the roots of the function

$$f(x) := x^n - x^{n-1}\upsilon_1 + \cdots + (-1)^{n-1} x \upsilon_{n-1} + (-1)^n \upsilon_n \tag{D.2}$$

i.e.

$$x_0 \in \{x \mid f(x) = 0\} = \{\kappa_1, \ldots, \kappa_n\} . \tag{D.3}$$

Proof. The function f is rewritten as

$$\begin{aligned} f(x) &\overset{(D.2)}{=} x^n - x^{n-1}\upsilon_1 + \cdots + (-1)^{n-1} x \upsilon_{n-1} + (-1)^n \upsilon_n \\ &\overset{(D.1)}{=} x^n - x^{n-1} \sum_{k=1}^{n} \kappa_k + \cdots + (-1)^{n-1} x \sum_{k=1}^{n} \prod_{\substack{j=1 \\ j \neq k}}^{n} \kappa_j + (-1)^n \prod_{k=1}^{n} \kappa_k \\ &\overset{(2.18)}{=} \prod_{k=1}^{n} (x - \kappa_k). \end{aligned} \tag{D.4}$$

The roots of f are determined as shown in (D.3). This completes the proof. □

Bibliography

[1] M. Bormann, *Experimentalphysik: Mechanik der Massenpunkte und des starren Körpers*. Experimentalphysik, Brockmeyer, 1978.

[2] M. Mohri, "Edit-distance of weighted automata: General definitions and algorithms," *International Journal of Foundations of Computer Science*, vol. 14, no. 06, pp. 957–982, 2003.

[3] A. Keller, *Breitbandkabel und Zugangsnetze*. Springer-Verlag Berlin Heidelberg, 2 ed., 2011.

[4] C. L. Fortescue, "Method of symmetrical co-ordinates applied to the solution of polyphase networks," *Proceedings of the American Institute of Electrical Engineers*, vol. 37, pp. 629–716, June 1918.

[5] M. Koch and T. Prevost, "Analysis of dielectric response measurements for condition assessment of oil-paper transformer insulation," *IEEE Transactions on Dielectrics and Electrical Insulation*, vol. 19, no. 6, pp. 1908–1915, 2012.

[6] M. Koch and M. Kruger, "A fast and reliable dielectric diagnostic method to determine moisture in power transformers," in *2008 International Conference on Condition Monitoring and Diagnosis*, pp. 467–470, 2008.

[7] K. R. Patil and H. H. Patel, "Modified dual second-order generalised integrator fll for synchronization of a distributed generator to a weak grid," in *2016 IEEE 16th International Conference on Environment and Electrical Engineering (EEEIC)*, pp. 1–5, June 2016.

[8] C. Van Loan, *Computational frameworks for the fast Fourier transform*. SIAM, 1992.

[9] H. K. Yada and M. S. R. Murthy, "A new topology and control strategy for extraction of reference current using single phase SOGI-PLL for three-phase four-wire shunt active power filter," in *2014 IEEE International Conference on Power Electronics, Drives and Energy Systems (PEDES)*, pp. 1–6, 2014.

[10] A. Kulkarni and V. John, "A novel design method for SOGI-PLL for minimum settling time and low unit vector distortion," in *IECON 2013 - 39th Annual Conference of the IEEE Industrial Electronics Society*, pp. 274–279, Nov 2013.

[11] Ke Chen, Wu Ai, Bing Chen, and Yi Liu, "A simulation study on tracking and restructuring AC signals based on enhanced SOGI-PLL," in *2016 IEEE Power and Energy Conference at Illinois (PECI)*, pp. 1–5, 2016.

[12] H. K. Yada and M. S. R. Murthy, "An improved control algorithm for DSTATCOM based on single-phase SOGI-PLL under varying load conditions and adverse grid conditions," in *2016 IEEE International Conference on Power Electronics, Drives and Energy Systems (PEDES)*, pp. 1–6, Dec 2016.

[13] V. Blahnik, T. Kosan, and J. Talla, "Control of single-phase AC/DC converter based on SOGI-PLL voltage synchronization," in *Proceedings of the 16th International Conference on Mechatronics - Mechatronika 2014*, pp. 652–655, 2014.

[14] U. Mumtahina, S. Alakahoon, and P. Wolfs, "A comparative study of phase locked loops for microgrid and storage converter applications," in *2021 IEEE PES Innovative Smart Grid Technologies - Asia (ISGT Asia)*, pp. 1–5, 2021.

[15] A. Ortiz, M. Aredes, L. G. B. Rolim, E. Bueno, and P. Rodriguez, "A new current control for the statcom based on secondary order generalized integrators," in *2008 IEEE Power Electronics Specialists Conference*, pp. 1378–1383, 2008.

[16] C. Jain and B. Singh, "An offset reduction second order generalized integrator based control algorithm for single-phase s-dstatcom," in *2015 39th National Systems Conference (NSC)*, pp. 1–6, Dec 2015.

[17] H. A. Pereira, M. R. Haddioui, L. O. M. de Oliveira, L. Mathe, M. Bongiorno, and R. Teodorescu, "Circulating current suppression strategies for d-statcom based on modular multilevel converters," in *2015 IEEE 13th Brazilian Power Electronics Conference and 1st Southern Power Electronics Conference (COBEP/SPEC)*, pp. 1–6, 2015.

[18] B. K. Verma, S. Devassy, S. K. Ram, A. Abhishek, and A. K. Dhakar, "Performance evaluation of pv integrated dstatcom based on complex variable filter," in *2018 4th International Conference on Electrical Energy Systems (ICEES)*, pp. 94–99, 2018.

[19] H. K. Yada and M. S. R. Murthy, "Reference current extraction for three-phase four-wire h-bridge DSTATCOM using SOGI-PLL algorithm," in *2014 Annual IEEE India Conference (INDICON)*, pp. 1–6, 2014.

[20] P. Chittora, A. Singh, and M. Singh, "Simple and efficient control of DSTATCOM in three-phase four-wire polluted grid system using MCCF-SOGI based controller," *IET Generation, Transmission Distribution*, vol. 12, no. 5, pp. 1213–1222, 2018.

[21] A. Dash, D. P. Bagarty, P. K. Hota, R. K. Behera, U. R. Muduli, and K. Al Hosani, "Dc-offset compensation for three-phase grid-tied spv-dstatcom under partial shading condition with improved pr controller," *IEEE Access*, vol. 9, pp. 132215–132224, 2021.

[22] G. S. Chawda, O. P. Mahela, B. Khan, H. H. Alhelou, E. Heydarian-Forushani, and A. S. Al-Sumaiti, "Performance evaluation of second order generalized integrator-quadrature algorithm for dstatcom in non-ideal grid," in *IECON 2020 The 46th Annual Conference of the IEEE Industrial Electronics Society*, pp. 2551–2556, 2020.

[23] B. B. Rath, M. K. Panda, B. Jha, A. Dash, S. Prakash, R. K. Behera, K. Al Hosani, S. Tegala, and U. R. Muduli, "Photovoltaic partial shading performance evaluation with a dstatcom controller," *IEEE Access*, vol. 10, pp. 69041–69052, 2022.

[24] M. Kale, F. Akar, and M. Karabacak, "A SOGI based band stop filter approach for a single-phase shunt active power filter," in *2018 2nd International Symposium on Multidisciplinary Studies and Innovative Technologies (ISMSIT)*, pp. 1–4, 2018.

[25] W. Li, B. Rahmani, and G. Liu, "A wavelet-based shunt active power filter to integrate a photovoltaic system to power grid," in *2016 Sixth International Conference on Instrumentation Measurement, Computer, Communication and Control (IMCCC)*, pp. 482–485, 2016.

[26] I. K. Otchere, D. O. Ampofo, and E. A. Frimpong, "A 2nd order lpf wavelet based control scheme for shunt active power filter," in *2017 IEEE PES PowerAfrica*, pp. 444–448, 2017.

[27] F. M. Serra, D. G. Forchetti, and C. H. De Angelo, "Comparison of positive sequence detectors for shunt active filter control," in *2010 9th IEEE/IAS International Conference on Industry Applications - INDUSCON 2010*, pp. 1–6, 2010.

[28] S. Karbasforooshan and M. Monfared, "An improved reference current generation and digital deadbeat controller for single-phase shunt active power filters," *IEEE Transactions on Power Delivery*, pp. 1–1, 2020.

[29] B. Kaka and A. Maji, "Performance evaluation of shunt active power filter (sapf) connected to three phase four wire distribution networks," in *2016 IEEE International Telecommunications Energy Conference (INTELEC)*, pp. 1–9, 2016.

[30] K. R. Patil and H. H. Patel, "Performance of shunt active power filter with DSOGI-FLL under distorted grid voltage," in *2017 Second International Conference on Electrical, Computer and Communication Technologies (ICECCT)*, pp. 1–6, 2017.

[31] S. Golestan, M. Monfared, and J. M. Guerrero, "Second order generalized integrator based reference current generation method for single-phase shunt active power filters under adverse grid conditions," in *4th Annual International Power Electronics, Drive Systems and Technologies Conference*, pp. 510–517, 2013.

[32] M. Farhadi-Kangarlu and Y. Neyshabouri, "Shunt active power filter based on cross-switched multilevel inverter," in *2020 28th Iranian Conference on Electrical Engineering (ICEE)*, pp. 1–6, 2020.

[33] J. Pei, X. Pei, Y. Zhang, and Y. Yao, "The stability improvement strategy of shunt active power filter based on sogi feedforward," in *2021 IEEE 2nd China International Youth Conference on Electrical Engineering (CIYCEE)*, pp. 1–6, 2021.

[34] N. Daou and F. Khatounian, "A combined phase locked loop technique for grid synchronization of power converters under highly distorted grid conditions," in *2016 IEEE International Multidisciplinary Conference on Engineering Technology (IMCET)*, pp. 108–114, Nov 2016.

[35] N. Lokesh and M. K. Mishra, "A comparative performance study of advanced plls for grid synchronization," in *2020 IEEE International Conference on Power Electronics, Smart Grid and Renewable Energy (PESGRE2020)*, pp. 1–6, 2020.

[36] S. S. Rauth, M. Kumar, and K. Srinivas, "A proportional resonant power controller and a combined amplitude adaptive notch filter with pll for better power control and synchronization of single phase on grid solar photovoltaic system," in *2018 International Conference on Smart Systems and Inventive Technology (ICSSIT)*, pp. 378–384, 2018.

[37] Yulin Yang, Guihua Liu, Hongpeng Liu, and Wei Wang, "A single-phase grid synchronization method based on frequency locked loop for pv grid-connected inverter under weak grid," in *Proceeding of the 11th World Congress on Intelligent Control and Automation*, pp. 5453–5456, 2014.

[38] A. Sahoo, K. Mahmud, M. Ciobotaru, and J. Ravishankar, "Adaptive grid synchronization technique for single-phase inverters in ac microgrid," in *2019 IEEE Energy Conversion Congress and Exposition (ECCE)*, pp. 4441–4446, 2019.

[39] P. Rodriguez, A. Luna, M. Ciobotaru, R. Teodorescu, and F. Blaabjerg, "Advanced grid synchronization system for power converters under unbalanced and distorted operating conditions," in *IECON 2006 - 32nd Annual Conference on IEEE Industrial Electronics*, pp. 5173–5178, 2006.

[40] Y. Song, P. Davari, and F. Blaabjerg, "Analysis of multi-drive system performance under unbalanced grid using different grid synchronization solutions," in *2018 20th European Conference on Power Electronics and Applications (EPE'18 ECCE Europe)*, pp. P.1–P.9, 2018.

[41] Y. Yang, L. Hadjidemetriou, F. Blaabjerg, and E. Kyriakides, "Benchmarking of phase locked loop based synchronization techniques for grid-connected inverter systems," in *2015 9th International Conference on Power Electronics and ECCE Asia (ICPE-ECCE Asia)*, pp. 2167–2174, 2015.

[42] Z. Zhang, Y. Yang, F. Blaabjerg, and R. Ma, "Challenges to grid synchronization of single-phase grid-connected inverters in zero-voltage ride-through operation," in *2016 IEEE 2nd Annual Southern Power Electronics Conference (SPEC)*, pp. 1–6, 2016.

[43] H. Yi, X. Wang, F. Blaabjerg, and F. Zhuo, "Comparative analysis about dynamic performances of grid synchronization schemes," in *2017 IEEE Energy Conversion Congress and Exposition (ECCE)*, pp. 5726–5730, 2017.

[44] T. Ngo and T. Vu, "Comparative study of the second-order and third-order systems for the synchronization system under distorted grid conditions," in *2019 IEEE Power Energy Society General Meeting (PESGM)*, pp. 1–5, 2019.

[45] Mingzhi Gao, Baohong Li, Min Chen, Wei Yao, and Zhaoming Qian, "Analysis and implementation of a pll structure for single-phase grid-connected inverter system," in *2009 IEEE 6th International Power Electronics and Motion Control Conference*, pp. 716–719, 2009.

[46] I. Bourguiba, A. Houari, H. Belloumi, and F. Kourda, "Control of single-phase grid connected photovoltaic inverter," in *2016 4th International Conference on Control Engineering Information Technology (CEIT)*, pp. 1–6, 2016.

[47] Seema and B. Singh, "Control of variable speed wecs-pv-bes based microgrid with grid synchronization," in *2019 IEEE International Conference on Environment and Electrical Engineering and 2019 IEEE Industrial and Commercial Power Systems Europe (EEEIC / I CPS Europe)*, pp. 1–6, 2019.

[48] X. Li, H. Zhang, and R. Balog, "Control strategy for seamless transfer between island and grid-connected operation for a dual-mode photovoltaic inverter," in *2015 IEEE Energy Conversion Congress and Exposition (ECCE)*, pp. 5983–5990, 2015.

[49] A. Singhal and A. singh, "Design and performance analysis of synchronization techniques under non-ideal conditions," in *2019 International Conference on Power Electronics, Control and Automation (ICPECA)*, pp. 1–6, 2019.

[50] Tuan Ngo, Quan Nguyen, and S. Santoso, "Detecting positive-sequence component in active power filter under distorted grid voltage," in *2015 IEEE Power Energy Society General Meeting*, pp. 1–5, 2015.

[51] B. Sen, D. Sharma, and B. C. Babu, "DSRF and SOGI based PLL-two viable scheme for grid synchronization of DG systems during grid abnormalities," in *2012 Students Conference on Engineering and Systems*, pp. 1–6, 2012.

[52] J. C. Alfonso-Gil, J. J. Vague-Cardona, S. Orts-Grau, F. J. Gimeno-Sales, and S. Segui-Chilet, "Enhanced grid fundamental positive-sequence digital synchronization structure," *IEEE Transactions on Power Delivery*, vol. 28, no. 1, pp. 226–234, 2013.

[53] J. A. Suul, A. Luna, P. Rodriguez, and T. Undeland, "Frequency-adaptive virtual flux estimation for grid synchronization under unbalanced conditions," in *IECON 2010 - 36th Annual Conference on IEEE Industrial Electronics Society*, pp. 486–492, 2010.

[54] T. Ngo, T. Vu, and S. Biriciki, "Generalized configurations for the synchronization system based on transfer function approach," in *2018 IEEE Power Energy Society General Meeting (PESGM)*, pp. 1–5, 2018.

[55] Y. Li, J. Li, Y. Lei, and W. Sun, "Grid synchronization technology for distributed power generation system," in *2014 IEEE Conference and Expo Transportation Electrification Asia-Pacific (ITEC Asia-Pacific)*, pp. 1–6, 2014.

[56] B. Trento, L. M. Tolbert, and D. Costinett, "Grid synchronization using fixed filtering with magnitude and phase compensation," in *2014 IEEE Energy Conversion Congress and Exposition (ECCE)*, pp. 2641–2647, 2014.

[57] A. Luna, J. Rocabert, J. I. Candela, J. R. Hermoso, R. Teodorescu, F. Blaabjerg, and P. Rodríguez, "Grid voltage synchronization for distributed generation systems under grid fault conditions," *IEEE Transactions on Industry Applications*, vol. 51, no. 4, pp. 3414–3425, 2015.

[58] H. Yi, X. Wang, F. Blaabjerg, and F. Zhuo, "Impedance analysis of SOGI-FLL-based grid synchronization," *IEEE Transactions on Power Electronics*, vol. 32, pp. 7409–7413, Oct 2017.

[59] K. Mozdzynski, M. Malinowski, and S. Stynski, "Modified voltage oriented control resistant to grid voltage disturbances," in *2017 IEEE Southern Power Electronics Conference (SPEC)*, pp. 1–6, 2017.

[60] A. Nagliero, R. A. Mastromauro, M. Liserre, and A. Dell'Aquila, "Monitoring and synchronization techniques for single-phase pv systems," in *SPEEDAM 2010*, pp. 1404–1409, 2010.

[61] M. Ciobotaru, R. Teodorescu, and V. G. Agelidis, "Offset rejection for pll based synchronization in grid-connected converters," in *2008 Twenty-Third Annual IEEE Applied Power Electronics Conference and Exposition*, pp. 1611–1617, 2008.

[62] N. Ikken, A. Bouknadel, A. Haddou, N. Tariba, H. El omari, and H. El omari, "Pll synchronization method based on second-order generalized integrator for single phase grid connected inverters systems during grid abnormalities," in *2019 International Conference on Wireless Technologies, Embedded and Intelligent Systems (WITS)*, pp. 1–5, 2019.

[63] G. I. Orfanoudakis, S. M. Sharkh, and M. A. Yuratich, "Positive-sequence flux estimator based on second-order generalized integrators for grid synchronization and motor control under imbalanced conditions," in *2019 21st European Conference on Power Electronics and Applications (EPE '19 ECCE Europe)*, pp. P.1–P.10, 2019.

[64] C. Blanco, D. Reigosa, F. Briz, and J. M. Guerrero, "Quadrature signal generator based on all-pass filter for single-phase synchronization," in *2014 IEEE Energy Conversion Congress and Exposition (ECCE)*, pp. 2655–2662, 2014.

[65] G. Zhu, Q. Yuan, and X. Yang, "Research and analysis of SOGI-QSG integral saturation in the application of grid synchronization," in *2019 IEEE International Conference on Mechatronics and Automation (ICMA)*, pp. 1167–1171, 2019.

[66] H. Zhang, C. Dai, and S. Wu, "Research on single-phase pll for the synchronization of thyristor controlled series capacitor," in *2012 Asia-Pacific Power and Energy Engineering Conference*, pp. 1–5, 2012.

[67] F. Ben Youssef and L. Sbita, "Sensorless control strategy for three-phase grid side converter," in *2017 International Conference on Green Energy Conversion Systems (GECS)*, pp. 1–6, 2017.

[68] V. Blahnik and J. Talla, "Single-phase synchronization for traction active rectifier," in *2016 International Conference on Applied Electronics (AE)*, pp. 23–26, 2016.

[69] F. Ben Youssef and L. Sbita, "Sliding mode control strategy for grid connected pv system," in *2017 International Conference on Green Energy Conversion Systems (GECS)*, pp. 1–7, 2017.

[70] D. G. Patino, E. G. G. Erira, E. E. Rosero, and J. R. Fuelagan, "SOGI-FLL for synchronization and fault detection in an inverter connected to the grid," in *2015 IEEE PES Innovative Smart Grid Technologies Latin America (ISGT LATAM)*, pp. 833–838, 2015.

[71] C. Tarasantisuk, S. Kumsup, W. Piyarat, and K. Witheepanich, "Stationary frame current regulation using proportional resonant controller for single phase grid connected inverter," in *2016 13th International Conference on Electrical Engineering/Electronics, Computer, Telecommunications and Information Technology (ECTI-CON)*, pp. 1–5, 2016.

[72] Y. Yang and F. Blaabjerg, "Synchronization in single-phase grid-connected photovoltaic systems under grid faults," in *2012 3rd IEEE International Symposium on Power Electronics for Distributed Generation Systems (PEDG)*, pp. 476–482, 2012.

[73] T. Komrska, D. Janík, and Z. Peroutka, "Synchronization of grid-connected converters for single-phase systems," in *2013 15th European Conference on Power Electronics and Applications (EPE)*, pp. 1–8, 2013.

[74] M. Sibanyoni and S. P. Daniel Chowdhury, "Synchronization strategy for single phase inverters for feeding renewable energy in south african national grid," in *2017 52nd International Universities Power Engineering Conference (UPEC)*, pp. 1–4, 2017.

[75] X. Li and G. Chen, "Synchronization strategy for virtual synchronous generator based energy storage system," in *IECON 2019 - 45th Annual Conference of the IEEE Industrial Electronics Society*, vol. 1, pp. 2512–2517, 2019.

[76] J. A. Suul, A. Luna, P. Rodriguez, and T. Undeland, "Voltage-sensor-less synchronization to unbalanced grids by frequency-adaptive virtual flux estimation," *IEEE Transactions on Industrial Electronics*, vol. 59, no. 7, pp. 2910–2923, 2012.

[77] F. B. Youssef, A. B. Youssef, and L. Sbita, "Real time implementation of sv - hcc of grid side converter for pv application," in *2018 15th International Multi-Conference on Systems, Signals Devices (SSD)*, pp. 750–755, 2018.

[78] D. X. Llano and R. A. McMahon, “Single phase grid integration of permanent magnet generators associated with a wind turbine emulator test-rig,” in *IECON 2014 - 40th Annual Conference of the IEEE Industrial Electronics Society*, pp. 2246–2252, 2014.

[79] R. Pandey, T. N. Gupta, and M. S. Rawat, “A sogi-aqsg-based control technique for improving power quality in unusual grid conditions,” in *2022 2nd International Conference on Emerging Frontiers in Electrical and Electronic Technologies (ICEFEET)*, pp. 1–6, 2022.

[80] M. P. Thakre, N. P. Matale, and P. S. Borse, “A survey based on pll and its synchronization techniques for interconnected system,” in *2021 International Conference on Artificial Intelligence and Smart Systems (ICAIS)*, pp. 1011–1016, 2021.

[81] K. S. Mumbere, Y. Sasaki, N. Yorino, Y. Zoka, A. Bedawy, and Y. Tanioka, “An interconnected prosumer energy management system model for improved outage resilience,” in *2022 IEEE PES/IAS PowerAfrica*, pp. 1–5, 2022.

[82] Z. Zhang, L. Yang, X. Zhao, X. Wang, and C. Zhang, “Analysis and suppression of bifurcation behaviors for a new electric energy router based on series-parallel architecture,” in *2022 IEEE International Power Electronics and Application Conference and Exposition (PEAC)*, pp. 1223–1228, 2022.

[83] S. Roy, F. Chishti, B. Singh, and B. Panigrahi, “Asz-3lad control for single-stage solar pv-battery based microgrid with enhanced sogi-fll synchronization,” in *2022 IEEE IAS Global Conference on Emerging Technologies (GlobConET)*, pp. 300–305, 2022.

[84] M. M. de Carvalho, I. V. de Bessa, R. L. P. Medeiros, L. E. S. e Silva, F. A. C. A. Junior, and V. F. L. Junior, “Comparative study of control methodologies and pll topologies to enhance the performance of the synchronization of grid-tied pv system,” in *2021 14th IEEE International Conference on Industry Applications (INDUSCON)*, pp. 218–225, 2021.

[85] P. K. Pardhi and S. K. Sharma, “Design and control of isolated boost converter in photovoltaic supply system integrated with grid,” in *2020 IEEE International Conference on Computing, Power and Communication Technologies (GUCON)*, pp. 540–545, 2020.

[86] K. Dimitriadou, A. Boubaris, N. Rigogiannis, and N. Papanikolaou, “Digital implementation of p-q control in grid-tied inverters for educational purposes,” in *2022 22nd International Symposium on Electrical Apparatus and Technologies (SIELA)*, pp. 1–4, 2022.

[87] N. Z. Kashani, M. A. Parazdeh, M. Eldoromi, A. A. M. Birjandi, and P. Amiri, “Grid synchronization of bidirectional electric vehicle chargers using second order generalized integrator based phase lock loop,” in *2021 12th Power Electronics, Drive Systems, and Technologies Conference (PEDSTC)*, pp. 1–5, 2021.

[88] S. B. Qaiser Naqvi and B. Singh, “Improved sogi based control for a weak grid coupled pv-battery system with controlled power injection,” in *2021 IEEE 6th International Conference on Computing, Communication and Automation (ICCCA)*, pp. 783–788, 2021.

[89] H. Ding, Z. Wang, L. Fan, and Z. Miao, “Modeling and control of grid-following single-phase voltage-sourced converter,” in *2020 52nd North American Power Symposium (NAPS)*, pp. 1–6, 2021.

[90] A. Sharma, K. J. Veeramraju, and J. W. Kimball, “Power flow control of a single-stage ac-ac solid-state transformer for ac distribution system,” in *2022 IEEE Power and Energy Conference at Illinois (PECI)*, pp. 1–6, 2022.

[91] S. D. Meinggariyad, M. Facta, and I. Setiawan, "Rate of change of frequency estimation based on sogi-pll for islanding detection," in *2022 9th International Conference on Information Technology, Computer, and Electrical Engineering (ICITACEE)*, pp. 189–194, 2022.

[92] F. Chishti, B. Singh, A. Chandra, and K. Al-Haddad, "Resilient synchronization control of distributed generation based reconfigurable microgrid," in *IECON 2021 - 47th Annual Conference of the IEEE Industrial Electronics Society*, pp. 1–6, 2021.

[93] A. Kumar, V. Narayanan, and B. Singh, "Robust control for rooftop solar pv-bes microgrid and its seamless grid synchronization," in *2022 IEEE Global Conference on Computing, Power and Communication Technologies (GlobConPT)*, pp. 1–6, 2022.

[94] V. Yadav, Seema, B. Singh, and A. Verma, "Seamless control of renewable energy system with grid connected and islanded modes," in *2020 IEEE 17th India Council International Conference (INDICON)*, pp. 1–6, 2020.

[95] M. F. Uddin, U. Asif, F. Mukhtar, and O. Imtiaz, "Single-phase transformer-less dynamic power flow control of transmission network using cascaded converter based sssc," in *2022 Global Energy Conference (GEC)*, pp. 32–37, 2022.

[96] F. Mulolani, "Virtual-flux based active power filter for power quality improvement," in *2020 IEEE PES/IAS PowerAfrica*, pp. 1–5, 2020.

[97] J. Li, Z. Zhang, C. Zhang, H. Bai, and Z. Yan, "A new method of high frequency link matrix inverter in parallel," in *2016 Sixth International Conference on Instrumentation Measurement, Computer, Communication and Control (IMCCC)*, pp. 350–355, 2016.

[98] H. Li, Y. Han, P. Yang, J. Xiong, C. Wang, and J. M. Guerrero, "A proportional harmonic power sharing scheme for hierarchical controlled microgrids considering unequal feeder impedances and nonlinear loads," in *2017 IEEE Energy Conversion Congress and Exposition (ECCE)*, pp. 3722–3727, 2017.

[99] N. D. Dao, D. Lee, and S. Lee, "A simple and robust sensorless control based on stator current vector for pmsg wind power systems," *IEEE Access*, vol. 7, pp. 8070–8080, 2019.

[100] A. Verma, B. Singh, A. Chandra, and K. Al Haddad, "An implementation of solar pv array based multifunctional ev charger," *IEEE Transactions on Industry Applications*, pp. 1–1, 2020.

[101] Y. Liu, W. Xu, T. Long, and F. Blaabjerg, "An improved rotor speed observer for standalone brushless doubly-fed induction generator under unbalanced and nonlinear loads," *IEEE Transactions on Power Electronics*, vol. 35, no. 1, pp. 775–788, 2020.

[102] S. Murshid and B. Singh, "An improved smo for position sensorless operation of pmsm driven solar water pumping system," in *2020 IEEE International Conference on Power Electronics, Smart Grid and Renewable Energy (PESGRE2020)*, pp. 1–5, 2020.

[103] R. R. Ahrabi and A. Ajami, "Controlling of a three phase vienna rectifier under utility side distortion based on sliding mode controller," in *The 6th Power Electronics, Drive Systems Technologies Conference (PEDSTC2015)*, pp. 334–339, 2015.

[104] L. S. Xavier, A. F. Cupertino, V. F. Mendes, and H. A. Pereira, "Detection method for multi-harmonic current compensation applied in three-phase photovoltaic inverters," in *2016 12th IEEE International Conference on Industry Applications (INDUSCON)*, pp. 1–8, 2016.

[105] G. Zhang, G. Wang, and D. Xu, "Dual SOGI-network based current ripple and position error fluctuation elimination for PMSM sensorless drives," in *PCIM Asia 2018; International Exhibition and Conference for Power Electronics, Intelligent Motion, Renewable Energy and Energy Management*, pp. 1–5, 2018.

[106] Bing Liu, Bo Zhou, and Tianheng Ni, "Enhanced position observer with a selective harmonic error eliminator and an error feed-forward compensator for sensor-less surface-mounted permanent magnet synchronous motor drives," in *2017 IEEE 3rd International Future Energy Electronics Conference and ECCE Asia (IFEEC 2017 - ECCE Asia)*, pp. 1210–1214, 2017.

[107] J. Xu, Q. Qian, S. Xie, and B. Zhang, "Grid-voltage feedforward based control for grid-connected lcl-filtered inverter with high robustness and low grid current distortion in weak grid," in *2016 IEEE Applied Power Electronics Conference and Exposition (APEC)*, pp. 1919–1925, 2016.

[108] X. Song, B. Han, S. Zheng, and J. Fang, "High-precision sensorless drive for high-speed bldc motors based on the virtual third harmonic back-emf," *IEEE Transactions on Power Electronics*, vol. 33, no. 2, pp. 1528–1540, 2018.

[109] B. Singh, S. S. Murthy, R. S. Reddy, and P. Arora, "Implementation of modified current synchronous detection method for voltage control of self-excited induction generator," *IET Power Electronics*, vol. 8, no. 7, pp. 1146–1155, 2015.

[110] S. Ouchen, H. Steinhart, and D. Lebsanft, "Low voltage ride through control for grid-connected inverter under balanced and unbalanced voltage drops," in *2019 IEEE 6th International Conference on Energy Smart Systems (ESS)*, pp. 47–51, 2019.

[111] B. Wang, X. Zhang, Y. Yu, J. Zhang, and D. Xu, "Maximum torque analysis and extension in six-step mode-combined field-weakening control for induction motor drives," *IEEE Transactions on Industrial Electronics*, vol. 66, no. 12, pp. 9129–9138, 2019.

[112] M. Hasan, B. Singh, and S. Devassy, "Modified control technique for series and shunt converters of upqc to enhance power quality," in *2020 IEEE 9th Power India International Conference (PIICON)*, pp. 1–6, 2020.

[113] M. Fallah, M. Imani, H. M. Kojabadi, M. Abarzadeh, M. T. Bina, and L. Chang, "Novel structure for unbalance, reactive power and harmonic compensation based on VFF-RLS and SOGI-FLL in three phase four wire power system," in *2015 IEEE Energy Conversion Congress and Exposition (ECCE)*, pp. 6254–6260, 2015.

[114] B. Misra and B. Nayak, "Performance analysis of adaptive filters based on robust second order generalized integrator under adverse grid condition," in *2018 International Conference on Recent Innovations in Electrical, Electronics Communication Engineering (ICRIEECE)*, pp. 2677–2681, 2018.

[115] L. Goebel, S. Raab, M. Landauer, and A. Ackva, "Resonant switching and power control of dc-dc-converters with a variable transmission path," in *2018 20th European Conference on Power Electronics and Applications (EPE'18 ECCE Europe)*, pp. P.1–P.9, 2018.

[116] S. Pradhan, B. Singh, and B. K. Panigrahi, "A digital disturbance estimator (dde) for multiobjective grid connected solar pv based distributed generating system," *IEEE Transactions on Industry Applications*, vol. 54, no. 5, pp. 5318–5330, 2018.

[117] S. Murshid and B. Singh, "A multiobjective gi-based control for effective operation of pv pumping system under abnormal grid conditions," *IEEE Transactions on Industrial Informatics*, vol. 16, no. 11, pp. 6880–6891, 2020.

[118] M. Zarkab, B. Singh, and B. K. Panigrahi, "A multiport ev-fleet charging station based on modular multilevel converter," in *2021 IEEE 12th Energy Conversion Congress and Exposition - Asia (ECCE-Asia)*, pp. 1765–1770, 2021.

[119] B. Li, M. Zeng, Z. Hou, L. Ding, and Q. He, "A selective order voltage ripple suppression control strategy for dc-dc converter," in *2021 IEEE Vehicle Power and Propulsion Conference (VPPC)*, pp. 1–4, 2021.

[120] S. Mohamadian, H. Pairo, and A. Ghasemian, "A straightforward quadrature signal generator for single-phase sogi-pll with low susceptibility to grid harmonics," *IEEE Transactions on Industrial Electronics*, vol. 69, no. 7, pp. 6997–7007, 2022.

[121] J. Y. Su, J. Liu, and J. Liu, "Accurate power loop design of a single-phase grid-forming power converter via linearization of sogi-based power calculation," in *IECON 2022 - 48th Annual Conference of the IEEE Industrial Electronics Society*, pp. 1–6, 2022.

[122] E. Avdiaj, J. A. Suul, S. D'Arco, and L. Piegari, "Adaptive filtering for energy control of a modular multilevel converter operated as a virtual synchronous machine under unbalanced conditions," in *2022 IEEE 16th International Conference on Compatibility, Power Electronics, and Power Engineering (CPE-POWERENG)*, pp. 1–8, 2022.

[123] L. Ding, D. Zhou, C. Gong, and Y. W. Li, "Discrete-time adaptive smo based sensorless fixed-switching-frequency mpc of three-level npc-fed pmsm drives," in *2022 25th International Conference on Electrical Machines and Systems (ICEMS)*, pp. 1–6, 2022.

[124] C. Jones, A. Sahoo, J. Ravishankar, I. Nikolakakos, and T. Ghaoud, "Grid fault resilient hybrid grid synchronization for single-phase solar inverter," in *2022 IEEE 31st International Symposium on Industrial Electronics (ISIE)*, pp. 436–441, 2022.

[125] M. Guo, Z. Wu, and H. Qin, "Harmonics reduction for resolver-to-digital conversion via second-order generalized integrator with frequency-locked loop," *IEEE Sensors Journal*, vol. 21, no. 6, pp. 8209–8217, 2021.

[126] Q. Lu, T. Zhang, and L. Mo, "Improved rotor position observer for sensorless controlled stator permanent magnet motor based on second order generalized integrator," in *2020 IEEE International Conference on Applied Superconductivity and Electromagnetic Devices (ASEMD)*, pp. 1–2, 2020.

[127] R. Huang, M. Zhang, Z. Li, C. Hou, M. Zhu, and M. Guo, "Influence of sogi bandwidth on stability of single phase inverter in weak grid," in *IECON 2020 The 46th Annual Conference of the IEEE Industrial Electronics Society*, pp. 3779–3784, 2020.

[128] L. Gou, C. Wang, X. You, M. Zhou, and S. Dong, "Ipmsm sensorless control for zero- and low-speed regions under low switching frequency condition based on fundamental model," *IEEE Transactions on Transportation Electrification*, vol. 8, no. 1, pp. 1182–1193, 2022.

[129] J. Xu, H. Qian, Q. Qian, and S. Xie, "Modeling, stability, and design of the single-phase sogi-based phase-locked loop considering the frequency feedback loop effect," *IEEE Transactions on Power Electronics*, vol. 38, no. 1, pp. 987–1002, 2023.

[130] K. H. Krishna, I. Prudhviraj, J. Prabhavathi, M. Kartheek, and K. S. Gopi, "Performance investigation of multifunctional hybrid wind-solar pv-bes-degs based microgrid system with eaf and sogi based control," in *2021 Innovations in Power and Advanced Computing Technologies (i-PACT)*, pp. 1–8, 2021.

[131] A. T. Nguyen and D.-C. Lee, "Sensorless control of dfig wind turbine systems based on sogi and rotor position correction," *IEEE Transactions on Power Electronics*, vol. 36, no. 5, pp. 5486–5495, 2021.

[132] K. V and B. Singh, "Sensorless control of induction motor using mstogi based super twisting sliding mode flux observer for electric vehicle," in *2022 IEEE Global Conference on Computing, Power and Communication Technologies (GlobConPT)*, pp. 1–6, 2022.

[133] H. Cheng, S. Sun, X. Zhou, D. Shao, S. Mi, and Y. Hu, "Sensorless dpcc of pmlsm using sogi-pll-based high-order smo with cogging force feedforward compensation," *IEEE Transactions on Transportation Electrification*, vol. 8, no. 1, pp. 1094–1104, 2022.

[134] S. Sun, H. Cheng, W. Wang, H. Liu, S. Mi, and X. Zhou, "Sensorless dpcc of pmlsm using sogi-pll based high-order smo with cogging force feedforward compensation," in *2021 13th International Symposium on Linear Drives for Industry Applications (LDIA)*, pp. 1–7, 2021.

[135] G. Modi and B. Singh, "Sogi-$\alpha\beta$cdsc quasi type-l pll control for seamless transition between grid connected and autonomous operating modes of microgrid," in *2022 IEEE Global Conference on Computing, Power and Communication Technologies (GlobConPT)*, pp. 1–6, 2022.

[136] M. Kashif, S. Murshid, and B. Singh, "Solar pv array fed self-sensing control of pmsm drive with robust adaptive hybrid sogi based flux observer for water pumping," *IEEE Transactions on Industrial Electronics*, vol. 68, no. 8, pp. 6962–6972, 2021.

[137] S. Jin, S. Song, W. Jin, and W. Jiang, "Speed sensorless control for novel dual-stator low-speed high-torque synchronous motor with hybrid rotor," in *2020 23rd International Conference on Electrical Machines and Systems (ICEMS)*, pp. 1123–1127, 2020.

[138] S. K. Sahoo and B. Singh, "Voltage regulation of weak grid-tied dfig based wecs using ϵ-vpnmn control," in *2022 IEEE IAS Global Conference on Emerging Technologies (GlobConET)*, pp. 441–446, 2022.

[139] Z. Feng, G. Zhang, S. Wang, G. Wang, and D. Xu, "Voltage-current hybrid model based extended flux observer with multiple sogis for sensorless ipmsm drives," in *IECON 2021 - 47th Annual Conference of the IEEE Industrial Electronics Society*, pp. 1–6, 2021.

[140] A. Ammar, A. Kheldoun, B. Metidji, M. Benakcha, and T. Ameid, "Efficient model predictive control for induction machine with sogi-fll based flux estimator," in *2022 19th International Multi-Conference on Systems, Signals and Devices (SSD)*, pp. 1664–1669, 2022.

[141] L. F. Monteiro, C. Freitas, M. Tcheou, and D. Lessa, "Improvements on e-pll to mitigate transient low-frequency oscillations," *IEEE Latin America Transactions*, vol. 20, no. 10, pp. 2244–2253, 2022.

[142] Y. G. Kang and D. Diaz Reigosa, "Improving harmonic rejection capability of osg based on n-th order bandpass filter for single-phase system," *IEEE Access*, vol. 9, pp. 81728–81739, 2021.

[143] K. Tiwari and B. Singh, "Integration of php-spv-bes based renewable energy sources with dual mode operation," in *2021 IEEE 2nd International Conference on Smart Technologies for Power, Energy and Control (STPEC)*, pp. 1–6, 2021.

[144] C. Zhang, S. Føyen, J. A. Suul, and M. Molinas, "Modeling and analysis of sogi-pll/fll-based synchronization units: Stability impacts of different frequency-feedback paths," *IEEE Transactions on Energy Conversion*, vol. 36, no. 3, pp. 2047–2058, 2021.

[145] S. tripathi and R. Batra, "Operation and control of single phase front end converter," in *2020 First IEEE International Conference on Measurement, Instrumentation, Control and Automation (ICMICA)*, pp. 1–6, 2020.

[146] R. Mastromauro, L. Bongini, and F. A. Gervasio, "Performance comparison of cascade control systems for single-phase grid-forming converters with lcl filter," in *2021 IEEE 15th International Conference on Compatibility, Power Electronics and Power Engineering (CPE-POWERENG)*, pp. 1–6, 2021.

[147] M. Shahab and S. Wang, "Seamless transition strategy for micro-grid inverter based on improved droop control strategy," in *2021 4th International Conference on Energy, Electrical and Power Engineering (CEEPE)*, pp. 782–787, 2021.

[148] S. Roy, F. Chishti, B. Singh, and B. Panigrahi, "Synchronization and power quality improvement of 2spv-bes based microgrid," in *2022 IEEE 2nd International Conference on Sustainable Energy and Future Electric Transportation (SeFeT)*, pp. 1–6, 2022.

[149] Z. Jiang, Q. Teng, and X. Zheng, "Voltage sliding mode control of autonomous single phase microgrid based on second order generalized integral algorithm," in *2020 Chinese Automation Congress (CAC)*, pp. 5245–5250, 2020.

[150] R. Xu, T. Lan, H. Yin, X. Wu, and Y. Lan, "A novel three-phase phase-locked loop based on DSOGI and adaptive observer algorithm," in *2019 4th IEEE Workshop on the Electronic Grid (eGRID)*, pp. 1–5, 2019.

[151] N. F. Roslan, J. A. Suul, A. Luna, I. Candela, and P. Rodriguez, "A simulation study of proportional resonant controller based on the implementation of frequency-adaptive virtual flux estimation with the lcl filter," in *IECON 2015 - 41st Annual Conference of the IEEE Industrial Electronics Society*, pp. 001934–001941, 2015.

[152] P. Wang, W. Cao, K. Liu, and J. Zhao, "An unbalanced component detection method and compensation strategy based on second-order generalized integrator (SOGI)," in *2019 IEEE Power and Energy Conference at Illinois (PECI)*, pp. 1–6, 2019.

[153] S. Devassy and B. Singh, "Discrete SOGI based control of solar photovoltaic integrated unified power quality conditioner," in *2016 National Power Systems Conference (NPSC)*, pp. 1–6, 2016.

[154] M. Jamarani, A. Abrishamifar, M. Pichan, and M. Fazeli, "Evaluation of different positive sequence detection structures applied to grid-connected systems," in *The 5th Annual International Power Electronics, Drive Systems and Technologies Conference (PEDSTC 2014)*, pp. 126–130, 2014.

[155] M. R. Curti, F. M. Serra, D. G. Forchetti, and C. H. De Angelo, "Experimental implementation of psds," in *2012 10th IEEE/IAS International Conference on Industry Applications*, pp. 1–6, 2012.

[156] A. Bolzoni and R. Perini, "Experimental validation of a novel angular estimator for synthetic inertia support under disturbed network conditions," in *2019 21st European Conference on Power Electronics and Applications (EPE '19 ECCE Europe)*, pp. P.1–P.10, 2019.

[157] J. Restrepo, J. Viola, F. Quizhpi, and A. Ginart, "Fast detection of sequence components using savitzky-golay filters," in *IECON 2014 - 40th Annual Conference of the IEEE Industrial Electronics Society*, pp. 4453–4457, 2014.

[158] A. Kanaan, F. Sebaaly, and H. Y. Kanaan, "Fcs-mpc with pnsc reference generation method for a 3l-npc inverter under grid faults," in *2017 11th IEEE International Conference on Compatibility, Power Electronics and Power Engineering (CPE-POWERENG)*, pp. 223–228, 2017.

[159] L. Liu, D. Xie, D. Zhao, Y. Jia, Y. Yu, Q. Fan, Y. Shen, and W. Qi, "Harmonic current detection and reactive power compensation method for photovoltaic system based on fbd method," in *2019 IEEE 3rd Conference on Energy Internet and Energy System Integration (EI2)*, pp. 1970–1975, 2019.

[160] L. Wang, T. Qiao, B. Zhao, and X. Zeng, "Modeling and parameter identification of grid-connected pv system during asymmetrical grid faults," in *2019 IEEE 3rd Conference on Energy Internet and Energy System Integration (EI2)*, pp. 2086–2090, 2019.

[161] A. Kanaan, F. Sebaaly, and H. Y. Kanaan, "Mpc based on balanced positive-sequence extraction strategy for grid-tied converter control," in *2017 IEEE 26th International Symposium on Industrial Electronics (ISIE)*, pp. 1685–1691, 2017.

[162] S. K. Chaudhary, R. Teodorescu, P. Rodriguez, P. C. Kjaer, and A. M. Gole, "Negative sequence current control in wind power plants with vsc-hvdc connection," *IEEE Transactions on Sustainable Energy*, vol. 3, no. 3, pp. 535–544, 2012.

[163] W. Ma, S. Ouyang, Q. Ke, and S. Ma, "Research on control strategy for pv inverter under unbalanced power grid," in *2017 2nd International Conference on Power and Renewable Energy (ICPRE)*, pp. 1036–1040, 2017.

[164] H. Khan, B. G. Fernandes, and A. Kulkarni, "Simultaneous unbalance and harmonic compensation from ress with neutral wire connected to a lv distribution grid," in *2018 20th European Conference on Power Electronics and Applications (EPE'18 ECCE Europe)*, pp. P.1–P.10, 2018.

[165] B. Hoepfner and R. Vick, "Symmetrical components detection with FFDSOGI-PLL under distorted grid conditions," in *2019 International Conference on Smart Energy Systems and Technologies (SEST)*, pp. 1–6, 2019.

[166] C. Qiming, T. Fengren, G. Jie, Z. Yu, and Y. Deqing, "The separation of positive and negative sequence component based on SOGI and cascade DSC and its application at unbalanced PWM rectifier," in *2017 29th Chinese Control And Decision Conference (CCDC)*, pp. 5804–5808, May 2017.

[167] B. Mondal and B. A. Karuppaswamy, "A new approach to fourth-order quadrature signal generation for a fast and noise-free pll output under non-ideal grid voltage conditions," *IEEE Access*, vol. 10, pp. 38472–38482, 2022.

[168] M. Golla, S. Thangavel, S. P. Simon, and N. P. Padhy, "A novel control scheme using uapf in an integrated pv grid-tied system," *IEEE Transactions on Power Delivery*, vol. 38, no. 1, pp. 133–145, 2023.

[169] B. Mondal and A. K. B, "An analytical approach to parameter selection for sogi-based fourth-order quadrature signal generators," in *2021 IEEE 12th Energy Conversion Congress and Exposition - Asia (ECCE-Asia)*, pp. 2363–2368, 2021.

[170] C. Xu, S. Hou, and J. Chen, "An improved high bandwidth dsogi-pll and its optimized digital implementation," in *2022 IEEE International Power Electronics and Application Conference and Exposition (PEAC)*, pp. 1063–1068, 2022.

[171] G. I. Orfanoudakis, S. M. Sharkh, and M. A. Yuratich, "Combined positive-sequence flux estimation and current balancing for sensorless motor control under imbalanced conditions," *IEEE Transactions on Industry Applications*, vol. 57, no. 5, pp. 5099–5107, 2021.

[172] S. Ghosh and S. Chattopadhyay, "Correction of line-voltage unbalance by the decentralized inverters in an islanded microgrid," in *2020 IEEE Applied Power Electronics Conference and Exposition (APEC)*, pp. 622–628, 2020.

[173] G. I. Orfanoudakis, M. A. Yuratich, and S. M. Sharkh, "Current balancing of scalar-controlled induction motors with imbalanced cables," in *2022 14th Seminar on Power Electronics and Control (SEPOC)*, pp. 1–6, 2022.

[174] S. Jiang, R. S. Munoz-Aguilar, and I. Colak, "Frequency locked loop with frozen mechanism," in *2021 23rd European Conference on Power Electronics and Applications (EPE'21 ECCE Europe)*, pp. P.1–P.8, 2021.

[175] H. Zhang, G. Liu, X. Zhou, and S. Zheng, "High-precision sensorless optimal commutation deviation correction strategy of bldc motor with asymmetric back emf," *IEEE Transactions on Industrial Informatics*, vol. 17, no. 8, pp. 5250–5259, 2021.

[176] H. Wu, X. Wang, K. Wang, G. Li, B. Zhang, and Y. Lu, "Passivity-based harmonic stability analysis of voltage source converters considering the impact of sequence decomposition algorithms," in *2020 IEEE 9th International Power Electronics and Motion Control Conference (IPEMC2020-ECCE Asia)*, pp. 1930–1934, 2020.

[177] G. Modi and B. Singh, "Power quality improvements in spv system operating with weak ac network," in *2020 IEEE Industry Applications Society Annual Meeting*, pp. 1–6, 2020.

[178] J. Dragoun and J. Talla, "Real-time algorithm for the transformation of multiple harmonic unbalanced voltages into symmetrical components," in *2022 20th International Conference on Mechatronics - Mechatronika (ME)*, pp. 1–4, 2022.

[179] X. Dong, R. Zhao, Y. Wang, and H. Xu, "Real-time power angle measurement based on second-order generalized integrator with frequency-locked loop," in *2021 IEEE 4th International Electrical and Energy Conference (CIEEC)*, pp. 1–6, 2021.

[180] W. Medhat and M. A. Azzouz, "Triple current control of four-wire inverter-interfaced dgs for correct fault type identification," *IEEE Transactions on Smart Grid*, vol. 13, no. 5, pp. 3607–3618, 2022.

[181] R. J. Ferreira, R. E. Araújo, and J. A. P. Lopes, "A comparative analysis and implementation of various pll techniques applied to single-phase grids," in *Proceedings of the 2011 3rd International Youth Conference on Energetics (IYCE)*, pp. 1–8, July 2011.

[182] S. Golestan, S. Y. Mousazadeh, J. M. Guerrero, and J. C. Vasquez, "A critical examination of frequency-fixed second-order generalized integrator-based phase-locked loops," *IEEE Transactions on Power Electronics*, vol. 32, pp. 6666–6672, Sept 2017.

[183] F. Xiao, L. Dong, L. Li, and X. Liao, "A frequency-fixed SOGI-based PLL for single-phase grid-connected converters," *IEEE Transactions on Power Electronics*, vol. 32, pp. 1713–1719, March 2017.

[184] M. Z. Hasan, I. F. Shiam, T. T. Nova, and M. S. Reza, "A modified pll based on second order generalized integrator for single-phase voltage system," in *2019 International Conference on Electrical, Computer and Communication Engineering (ECCE)*, pp. 1–6, 2019.

[185] M. Rasheduzzaman, S. Khorbotly, and J. W. Kimball, "A modified srf-pll for phase and frequency measurement of single-phase systems," in *2016 IEEE Energy Conversion Congress and Exposition (ECCE)*, pp. 1–7, 2016.

[186] Z. Guo, Q. Zhang, C. Zhang, J. Pang, and Z. Yan, "A new method of double fundamental frequency phase-locked loop based on two integrators," in *2016 Sixth International Conference on Instrumentation Measurement, Computer, Communication and Control (IMCCC)*, pp. 659–664, 2016.

[187] M. Ciobotaru, R. Teodorescu, and F. Blaabjerg, "A new single-phase pll structure based on second order generalized integrator," in *2006 37th IEEE Power Electronics Specialists Conference*, pp. 1–6, 2006.

[188] L. S. Xavier, A. F. Cupertino, V. F. Mendes, and H. A. Pereira, "A novel adaptive current harmonic control strategy applied in multifunctional single-phase solar inverters," in *2015 IEEE 13th Brazilian Power Electronics Conference and 1st Southern Power Electronics Conference (COBEP/SPEC)*, pp. 1–6, 2015.

[189] Y. Xu, Y. Chen, W. Wu, Z. Xie, L. Xie, J. Liu, and S. Peng, "A simplified wide-bandwidth generalized impedance model for single-phase grid-connected inverter in polar coordinate system," in *2019 IEEE PES Asia-Pacific Power and Energy Engineering Conference (APPEEC)*, pp. 1–5, 2019.

[190] C. Dang and X. Zhao, "A spll technique under unbalanced and seriously distorted grid voltage conditions," in *The 26th Chinese Control and Decision Conference (2014 CCDC)*, pp. 4523–4528, 2014.

[191] A. Bamigbade, V. Khadkikar, and M. Al Hosani, "A type-3 pll for single-phase applications," *IEEE Transactions on Industry Applications*, pp. 1–1, 2020.

[192] M. Ciobotaru, V. G. Agelidis, R. Teodorescu, and F. Blaabjerg, “Accurate and less-disturbing active antiislanding method based on pll for grid-connected converters,” *IEEE Transactions on Power Electronics*, vol. 25, no. 6, pp. 1576–1584, 2010.

[193] M. Ciobotaru, V. Agelidis, and R. Teodorescu, “Accurate and less-disturbing active anti-islanding method based on pll for grid-connected pv inverters,” in *2008 IEEE Power Electronics Specialists Conference*, pp. 4569–4576, 2008.

[194] S. Golestan, J. M. Guerrero, A. Abusorrah, M. M. Al-Hindawi, and Y. Al-Turki, “An adaptive quadrature signal generation-based single-phase phase-locked loop for grid-connected applications,” *IEEE Transactions on Industrial Electronics*, vol. 64, no. 4, pp. 2848–2854, 2017.

[195] C. Zhang, X. Wang, and F. Blaabjerg, “Analysis of phase-locked loop influence on the stability of single-phase grid-connected inverter,” in *2015 IEEE 6th International Symposium on Power Electronics for Distributed Generation Systems (PEDG)*, pp. 1–8, 2015.

[196] C. Hou, M. Zhu, Y. Chen, and X. Cai, “Analysis of prefilter phase-locked loop under inter-harmonics perturbation,” in *8th Renewable Power Generation Conference (RPG 2019)*, pp. 1–6, 2019.

[197] A. Nicastri and A. Nagliero, “Comparison and evaluation of the pll techniques for the design of the grid-connected inverter systems,” in *2010 IEEE International Symposium on Industrial Electronics*, pp. 3865–3870, 2010.

[198] M. M. de Carvalho, R. L. P. Medeiros, I. V. Bessa, F. A. C. Junior, K. E. Lucas, and D. A. Vaca, “Comparison of the pll control techniques applied in photovoltaic system,” in *2019 IEEE 15th Brazilian Power Electronics Conference and 5th IEEE Southern Power Electronics Conference (COBEP/SPEC)*, pp. 1–6, 2019.

[199] A. Verma and B. Singh, “Control of vehicle-to-home operation of electric vehicle with seamless transition capabilities,” in *2018 IEEMA Engineer Infinite Conference (eTechNxT)*, pp. 1–6, 2018.

[200] A. A. Nazib, D. G. Holmes, and B. P. McGrath, “Decoupled DSOGI-PLL for improved three phase grid synchronisation,” in *2018 International Power Electronics Conference (IPEC-Niigata 2018 -ECCE Asia)*, pp. 3670–3677, 2018.

[201] A. Kulkarni and V. John, “Design of a fast response time single-phase pll with dc offset rejection capability,” in *2016 IEEE Applied Power Electronics Conference and Exposition (APEC)*, pp. 2200–2206, 2016.

[202] K. Zeb, Saif-ul-Islam, W. Uddin, I. Khan, M. Ishfaq, Z. Ullah, T. D. C. Busarello, and H. J. Kim, “Design of adaptive sliding mode controller for single-phase grid-tied pv system,” in *2019 15th International Conference on Emerging Technologies (ICET)*, pp. 1–6, 2019.

[203] T. D. C. Busarello, K. Zeb, A. Péres, V. S. R. V. Oruganti, and M. G. Simões, “Designing a second order generalized integrator digital phase locked loop based on a frequency response approach,” in *2019 IEEE PES Innovative Smart Grid Technologies Conference - Latin America (ISGT Latin America)*, pp. 1–6, 2019.

[204] J. C. Astrada, G. G. Oggier, and G. O. García, “Discrete time control of single phase inverters for ups applications through a synchronous reference frame,” in *2018 IEEE Biennial Congress of Argentina (ARGENCON)*, pp. 1–8, 2018.

[205] S. Golestan, M. Monfared, F. D. Freijedo, and J. M. Guerrero, “Dynamics assessment of advanced single-phase pll structures,” *IEEE Transactions on Industrial Electronics*, vol. 60, no. 6, pp. 2167–2177, 2013.

[206] S. Foyen, C. Zhang, O. Fosso, and M. Molinas, “Frequency domain modelling for assessment of hilbert and SOGI based single-phase synchronisation,” in *IECON 2019 - 45th Annual Conference of the IEEE Industrial Electronics Society*, vol. 1, pp. 1780–1785, 2019.

[207] O. M. Arafa, “High performance single-phase pll with sliding fourier transform as a phase detector,” in *2019 6th International Conference on Advanced Control Circuits and Systems (ACCS) 2019 5th International Conference on New Paradigms in Electronics information Technology (PEIT)*, pp. 65–70, 2019.

[208] Y. Liao, Z. Liu, H. Zhang, and B. Wen, “Low-frequency stability analysis of single-phase system with dq-frame impedance approach - part i: Impedance modeling and verification,” *IEEE Transactions on Industry Applications*, vol. 54, no. 5, pp. 4999–5011, 2018.

[209] L. Zhao, X. Liu, K. Wang, M. Han, Y. Yao, and D. Xu, “Model-based disturbance rejection for current control of bidirectional single-phase ac/dc converters used in household energy router,” in *2019 22nd International Conference on Electrical Machines and Systems (ICEMS)*, pp. 1–6, 2019.

[210] A. K. George and P. Sumathi, “Mono-component am-fm signal decomposition using srf-pll,” in *2014 International Conference on Communication and Signal Processing*, pp. 298–302, 2014.

[211] N. Abbassi and S. Reichert, “Novel control structure for grid connected and islanding inverters,” in *7th IET International Conference on Power Electronics, Machines and Drives (PEMD 2014)*, pp. 1–5, 2014.

[212] D. Janík, J. Talla, T. Komrska, and Z. Peroutka, “Optimalization of SOGI PLL for single-phase converter control systems: Second order generalized integrator (SOGI),” in *2013 International Conference on Applied Electronics*, pp. 1–4, Sept 2013.

[213] H. K. Yada and M. S. R. Murthy, “Phase locked loop techniques for power quality improvement in polluted grids,” in *2016 IEEE 1st International Conference on Power Electronics, Intelligent Control and Energy Systems (ICPEICES)*, pp. 1–6, 2016.

[214] S. Gao and M. Barnes, “Phase-locked loop for ac systems: Analyses and comparisons,” in *6th IET International Conference on Power Electronics, Machines and Drives (PEMD 2012)*, pp. 1–6, 2012.

[215] C. Y. Wu, Y. J. Chen, and J. W. Cao, “Power pulsation decoupling and power control of a single-phase voltage source inverter in a renewable energy conversion system,” in *2018 IEEE International Conference on Applied System Invention (ICASI)*, pp. 1199–1202, 2018.

[216] M. Karimi Ghartemani, S. A. Khajehoddin, P. K. Jain, and A. Bakhshai, “Problems of startup and phase jumps in pll systems,” *IEEE Transactions on Power Electronics*, vol. 27, no. 4, pp. 1830–1838, 2012.

[217] L. Zhang, X. Lin, J. Zhang, and Y. Hou, “Research on grid-connected control of doubly-fed wind power generation,” in *2017 9th International Conference on Modelling, Identification and Control (ICMIC)*, pp. 406–411, 2017.

[218] D. Xie, D. Zhang, and P. Gao, "Research on phase-locked loop control and its application," in *2016 IEEE Information Technology, Networking, Electronic and Automation Control Conference*, pp. 818–821, 2016.

[219] J. Zhang and A. Zurfi, "Single-phase smart load controller with a battery storage," in *IECON 2018 - 44th Annual Conference of the IEEE Industrial Electronics Society*, pp. 271–275, 2018.

[220] S. Shah, P. Koralewicz, V. Gevorgian, and L. Parsa, "Small-signal modeling and design of phase-locked loops using harmonic signal-flow graphs," *IEEE Transactions on Energy Conversion*, vol. 35, no. 2, pp. 600–610, 2020.

[221] S. Shah and L. Parsa, "Small-signal modeling of single-phase plls using harmonic signal-flow graphs," in *2017 IEEE Energy Conversion Congress and Exposition (ECCE)*, pp. 4989–4995, 2017.

[222] Q. Hui, Y. Teng, L. Yang, M. Zong, X. Yu, D. Si, X. Yu, and W. Zhang, "Study of low voltage distortion control strategy for pv system," in *2016 International Conference on Smart City and Systems Engineering (ICSCSE)*, pp. 449–452, 2016.

[223] K. Colombage, J. Wang, T. Edo, and B. Sen, "Suppression of harmonic distortions in second order generalised integrator based plls for grid connected converters," in *8th IET International Conference on Power Electronics, Machines and Drives (PEMD 2016)*, pp. 1–6, 2016.

[224] C. Zhang, X. Wang, F. Blaabjerg, W. Wang, and C. Liu, "The influence of phase-locked loop on the stability of single-phase grid-connected inverter," in *2015 IEEE Energy Conversion Congress and Exposition (ECCE)*, pp. 4737–4744, 2015.

[225] S. Gerngross and C. P. Dick, "Turnkey solution for single-phase grid-connected dc/ac converter controls," in *PCIM Europe 2014; International Exhibition and Conference for Power Electronics, Intelligent Motion, Renewable Energy and Energy Management*, pp. 1–8, 2014.

[226] P. Lamo, A. Pigazo, and F. J. Azcondo, "Two-sample pll with harmonic filtering capability applicable to single-phase grid-connected converters," *IEEE Journal of Emerging and Selected Topics in Power Electronics*, pp. 1–1, 2020.

[227] S. Prakash and S. Mishra, "A three-sample-based pll-less hysteresis current control and stability analysis of a single-phase active distribution system," *IEEE Transactions on Industrial Electronics*, vol. 68, no. 8, pp. 7045–7060, 2021.

[228] Y. Zhenyu and Q. Qiang, "A virtual-rectifier ac/ac converter-based dynamic voltage restorer," in *2022 IEEE 5th International Electrical and Energy Conference (CIEEC)*, pp. 2824–2829, 2022.

[229] S. Wang, Z. Yuan, J. Ma, T. Liu, Z. Wu, and R. Wang, "Accurate ltp model and stability analysis of the second-order generalized integrator-based single-phase phase-locked loop," *IEEE Transactions on Industrial Electronics*, vol. 69, no. 6, pp. 6225–6235, 2022.

[230] S. Kalkoul, H. Benalla, K. Nabti, and A. Reama, "Comparison among single-phase plls based on sogi," in *2020 6th International Conference on Electric Power and Energy Conversion Systems (EPECS)*, pp. 118–122, 2020.

[231] Y. Lv, Z. Peng, and Y. Wang, "Design of a novel 2.5kw energy storage bidirectional power conversion system," in *2021 IEEE 12th Energy Conversion Congress and Exposition - Asia (ECCE-Asia)*, pp. 2022–2027, 2021.

[232] S. Gautam, W. Xiao, D. D.-C. Lu, H. Ahmed, and J. M. Guerrero, "Development of frequency-fixed all-pass filter-based single-phase phase-locked loop," *IEEE Journal of Emerging and Selected Topics in Power Electronics*, vol. 10, no. 1, pp. 506–517, 2022.

[233] R. Mittal, L. Fan, and Z. Miao, "Harmonic state-space model of second-order generalized integrator phase-locked loop," in *2021 IEEE Power and Energy Society General Meeting (PESGM)*, pp. 1–5, 2021.

[234] D. Kalke and G. Gurrala, "Iec/ieee 60255-118-1-2018 compliance testing of srf, sogi and park plls for synchrophasors," in *2022 International Conference on Electrical, Computer and Energy Technologies (ICECET)*, pp. 1–6, 2022.

[235] Y. Zhou, T. Zang, B. Zhou, H. Hu, S. Chen, and H. Luo, "Impacts of dynamic frequency feedback loop in sogi-pll on low-frequency oscillation in an electric railway system," *IEEE Transactions on Transportation Electrification*, pp. 1–1, 2023.

[236] C. Cheng, S. Xie, Q. Qian, J. Xu, and X. Zhang, "Nonlinear modeling and global stability condition of single-phase grid-tied inverter considering srf-pll and duty-cycle saturation," *IEEE Transactions on Industrial Electronics*, vol. 69, no. 7, pp. 6973–6983, 2022.

[237] J. Xu, H. Qian, Y. Hu, S. Bian, and S. Xie, "Overview of sogi-based single-phase phase-locked loops for grid synchronization under complex grid conditions," *IEEE Access*, vol. 9, pp. 39275–39291, 2021.

[238] F. Hassan, A. Kumar, and A. Pati, "Recent advances in phase locked loops for grid connected systems: A review," in *2022 IEEE Delhi Section Conference (DELCON)*, pp. 1–6, 2022.

[239] A. Bamigbade, B. S. Umesh, V. Khadkikar, M. S. E. Moursi, H. H. Zeineldin, and M. A. Hosani, "Reduced-order generalized integrator-based phase-locked loop: Performance improvement for grid synchronization of single-phase inverters," *IEEE Transactions on Power Delivery*, vol. 37, no. 5, pp. 4382–4393, 2022.

[240] L. Bin, "Research on leakage current suppression mechanism and control strategy of single-phase heric inverter," in *2021 IEEE 1st International Power Electronics and Application Symposium (PEAS)*, pp. 1–4, 2021.

[241] J. Choi, "Robust position-sensorless algorithm for dc motor using ripple current and model-based method," in *2021 IEEE 12th Energy Conversion Congress and Exposition - Asia (ECCE-Asia)*, pp. 2104–2109, 2021.

[242] X. Zhang, L. Gong, B. Wang, and J. Si, "The optimal design of the second-order generalized integrator phase-locked loop under power voltage distortion conditions," in *2021 IEEE 5th Conference on Energy Internet and Energy System Integration (EI2)*, pp. 2942–2947, 2021.

[243] A. Eltarouty, M. Aboudan, S. Biricik, H. Ahmed, and M. Benbouzid, "Unbalance and disturbance rejection based phase locked loop for grid synchronization," in *IECON 2020 The 46th Annual Conference of the IEEE Industrial Electronics Society*, pp. 4967–4972, 2020.

[244] G. Fedele, "A fractional-order repetitive controller for periodic disturbance rejection," *IEEE Transactions on Automatic Control*, vol. 63, no. 5, pp. 1426–1433, 2018.

[245] J. Matas, H. Martin, J. de la Hoz, A. Abusorrah, Y. Al-Turki, and H. Alshaeikh, "A new THD measurement method with small computational burden using a SOGI-FLL grid monitoring system," *IEEE Transactions on Power Electronics*, vol. 35, no. 6, pp. 5797–5811, 2020.

[246] R. Zhao, Z. Xin, P. C. Loh, and F. Blaabjerg, "A novel flux estimator based on multiple second-order generalized integrators and frequency-locked loop for induction motor drives," *IEEE Transactions on Power Electronics*, vol. 32, no. 8, pp. 6286–6296, 2017.

[247] G. Han, J. Zhang, and X. Cai, "A novel hybrid spll for polluted grid environment," in *2014 International Power Electronics and Application Conference and Exposition*, pp. 520–526, 2014.

[248] C. Jain and B. Singh, "A SOGI-FLL based control algorithm for single phase grid interfaced multifunctional SPV under non ideal distribution system," in *2014 Annual IEEE India Conference (INDICON)*, pp. 1–6, 2014.

[249] I. Ralev, A. Klein-Hessling, B. Pariti, and R. W. D. Doncker, "Adopting a SOGI filter for flux-linkage based rotor position sensing of switched reluctance machines," in *2017 IEEE International Electric Machines and Drives Conference (IEMDC)*, pp. 1–7, May 2017.

[250] J. Kang, S. Hyun, S. Hong, and C. Won, "Advanced control method of 3-phase AC/DC PWM converter for DC distribution using the SOGI-FLL," in *2016 IEEE 8th International Power Electronics and Motion Control Conference (IPEMC-ECCE Asia)*, pp. 2120–2124, 2016.

[251] N. Babu P., R. B. Peesapati, and G. Panda, "An adaptive current control technique in grid-tied pv system with active power filter for power quality improvement," in *TENCON 2019 - 2019 IEEE Region 10 Conference (TENCON)*, pp. 187–191, 2019.

[252] Z. Xin, R. Zhao, F. Blaabjerg, L. Zhang, and P. C. Loh, "An improved flux observer for field-oriented control of induction motors based on dual second-order generalized integrator frequency-locked loop," *IEEE Journal of Emerging and Selected Topics in Power Electronics*, vol. 5, no. 1, pp. 513–525, 2017.

[253] A. Kherbachi, A. Bendib, K. Kara, and A. Chouder, "ARM based implementation of sogi-fll method for power calculation in single-phase power system," in *2017 5th International Conference on Electrical Engineering - Boumerdes (ICEE-B)*, pp. 1–6, 2017.

[254] A. Silani, M. Mojiri, and J. Askari, "Cancellation of uncertain frequency disturbance acting on unknown time-delay plants," in *2016 24th Iranian Conference on Electrical Engineering (ICEE)*, pp. 865–869, 2016.

[255] L. Huang, H. Zhu, and Y. Hua, "Composite control of speed sensorless for bearingless permanent magnet synchronous motor," in *2018 IEEE Student Conference on Electric Machines and Systems*, pp. 1–5, 2018.

[256] J. Zhang, H. Wang, M. Zhu, and X. Cai, "Control implementation of the full-scale wind power converter without grid voltage sensors," in *2014 International Power Electronics Conference (IPEC-Hiroshima 2014 - ECCE ASIA)*, pp. 1753–1760, 2014.

[257] W. Chen and M. Wang, "Design of dynamic voltage restorer and active power filter for wind power systems subject to unbalanced and harmonic distorted grid," in *2016 IEEE Applied Power Electronics Conference and Exposition (APEC)*, pp. 3471–3475, 2016.

[258] M. S. Reza, M. Ciobotaru, and V. G. Agelidis, "Frequency adaptive linear kalman filter for fast and accurate estimation of grid voltage parameters," in *2012 IEEE International Conference on Power System Technology (POWERCON)*, pp. 1–6, 2012.

[259] M. S. Reza, M. Ciobotaru, and V. G. Agelidis, "Grid voltage offset and harmonics rejection using second order generalized integrator and kalman filter technique," in *Proceedings of The 7th International Power Electronics and Motion Control Conference*, vol. 1, pp. 104–111, 2012.

[260] D. G. Patino, E. G. Erira, J. R. Fuelagän, and E. E. Rosero, "Implementation a HERIC inverter prototype connected to the grid controlled by SOGI-FLL," in *2015 IEEE Workshop on Power Electronics and Power Quality Applications (PEPQA)*, pp. 1–6, 2015.

[261] Y. Jiang, W. Xu, and C. Mu, "Improved soifo-based rotor flux observer for pmsm sensorless control," in *IECON 2017 - 43rd Annual Conference of the IEEE Industrial Electronics Society*, pp. 8219–8224, 2017.

[262] Z. Jianya, L. Wenqi, G. Xiaowei, Y. Yanhong, L. Hu, and Y. Zhiyuan, "Motor speed estimation method based on second order generalized integrator-frequency locked loop," in *2015 34th Chinese Control Conference (CCC)*, pp. 4367–4372, 2015.

[263] P. Shah, I. Hussain, B. Singh, A. Chandra, and K. Al-Haddad, "Optimal control scheme for single stage grid interfaced secs for power quality improvement," in *2017 IEEE Industry Applications Society Annual Meeting*, pp. 1–8, 2017.

[264] R. Sharma, Seema, and B. Singh, "Power quality improvement in SyRG-PV-BES based standalone microgrid using SOGI-WIF control algorithm," in *2018 IEEE 8th Power India International Conference (PIICON)*, pp. 1–6, 2018.

[265] R. W. C. G. R. Wijshoff, M. Mischi, and R. M. Aarts, "Reduction of periodic motion artifacts in photoplethysmography," *IEEE Transactions on Biomedical Engineering*, vol. 64, no. 1, pp. 196–207, 2017.

[266] W. Cao, D. Fan, K. Liu, J. Zhao, L. ruan, and X. Wu, "Resonance detection strategy for multiple grid-connected inverters-based system using cascaded second-order generalized integrator," in *2018 International Power Electronics Conference (IPEC-Niigata 2018 -ECCE Asia)*, pp. 3010–3014, 2018.

[267] A. T. Nguyen and D. Lee, "Sensorless control scheme of DFIG wind energy conversion systems based on SOGIs and FLL," in *2019 IEEE 10th International Symposium on Power Electronics for Distributed Generation Systems (PEDG)*, pp. 466–472, 2019.

[268] N. D. Dao, D. Lee, and D. Lim, "Sensorless speed control of diesel-generator systems based on multiple SOGI-FLLs," in *2018 International Power Electronics Conference (IPEC-Niigata 2018 -ECCE Asia)*, pp. 1212–1216, 2018.

[269] K. Mozdzynski, "Simple digital integration algorithm with saturation and drift elimination based second-order generalized integrator," in *2015 9th International Conference on Compatibility and Power Electronics (CPE)*, pp. 312–316, 2015.

[270] Q. Zhong and P. Nguyen, "Sinusoid-locked loops based on the principles of synchronous machines," in *2012 24th Chinese Control and Decision Conference (CCDC)*, pp. 1518–1523, 2012.

[271] A. Bendib, A. Chouder, K. Kara, A. Kherbachi, and S. Barkat, "SOGI-FLL based optimal current control scheme for single-phase grid-connected photovoltaic VSIs with LCL filter," in *2018 International Conference on Electrical Sciences and Technologies in Maghreb (CISTEM)*, pp. 1–6, 2018.

[272] H. Wang, Y. Yang, Y. Zuo, S. Li, X. Hu, and X. Ge, "A speed estimation scheme based on an improved sogi-fll for speed-sensorless control of induction motor drives," in *IECON 2020 The 46th Annual Conference of the IEEE Industrial Electronics Society*, pp. 852–857, 2020.

[273] I. Bennia, A. Harrag, and Y. Daili, "Adaptive resonant controller based sogi-fll for three-phase voltage source inverters," in *2022 19th International Multi-Conference on Systems, Signals and Devices (SSD)*, pp. 756–762, 2022.

[274] A. T. Nguyen and D.-C. Lee, "Advanced grid voltage synchronization method under abnormal grid conditions," in *2021 International Symposium on Electrical and Electronics Engineering (ISEE)*, pp. 209–213, 2021.

[275] M. Satyanarayana and A. V. Ravi Teja, "An adaptive digital frequency locked loop with quarter cycle update for distorted single phase grid," in *2022 IEEE 2nd International Conference on Sustainable Energy and Future Electric Transportation (SeFeT)*, pp. 1–6, 2022.

[276] R. Sharma, S. Seema, and B. Singh, "Improved adaptive filter fll control algorithm for enhancing performance of islanded microgrid supplying dynamic loads," in *2020 IEEE Energy Conversion Congress and Exposition (ECCE)*, pp. 3880–3887, 2020.

[277] A. T. Nguyen, V. N. Nguyen, and D.-C. Lee, "Sensorless control of pmsg wind power systems based on rogi-fll," in *2022 International Power Electronics Conference (IPEC-Himeji 2022- ECCE Asia)*, pp. 1213–1218, 2022.

[278] Q. Huang and K. Rajashekara, "A unified selective harmonic compensation strategy using dg-interfacing inverter in both grid-connected and islanded microgrid," in *2017 IEEE Energy Conversion Congress and Exposition (ECCE)*, pp. 1588–1593, 2017.

[279] C. Xiao, X. Pei, Y. Liu, Y. Lu, C. Wang, and F. Xu, "Adaptive harmonic current compensation method with SAPF based on SOGI," in *2018 IEEE International Power Electronics and Application Conference and Exposition (PEAC)*, pp. 1–6, 2018.

[280] Y. Zhu, T. Wang, L. Xiong, P. Yang, and Z. Xu, "An enhanced power sharing strategy for droop controlled microgrids based on consensus algorithm," in *IECON 2017 - 43rd Annual Conference of the IEEE Industrial Electronics Society*, pp. 7724–7730, 2017.

[281] F. Jiang, K. Yang, S. Sun, Y. Xu, and A. Liu, "Back-emf based sensorless control of pmsm with an improved pll for eliminating the position estimation fluctuation," in *2019 22nd International Conference on Electrical Machines and Systems (ICEMS)*, pp. 1–4, 2019.

[282] Phuong Le Minh, Hoa Pham Thi Xuan, Duy Hoang Vo Duc, and Huy Nguyen Minh, "Control of power inverter in islanded microgrids based on online line impedance estimation," in *2017 International Conference on System Science and Engineering (ICSSE)*, pp. 180–185, 2017.

[283] Y. Zheng, J. Long, and H. Yang, "Electric spring control based on intelligent controller and cascade second-order generalized integrator phase locked loop," in *2019 IEEE Innovative Smart Grid Technologies - Asia (ISGT Asia)*, pp. 2105–2110, 2019.

[284] G. Wang, L. Ding, Z. Li, J. Xu, G. Zhang, H. Zhan, R. Ni, and D. Xu, "Enhanced position observer using second-order generalized integrator for sensorless interior permanent magnet synchronous motor drives," *IEEE Transactions on Energy Conversion*, vol. 29, no. 2, pp. 486–495, 2014.

[285] M. J. Diaz, E. Bueno, R. Mateos, F. J. Rodriguez, and E. Monmasson, "Fpga implementation of harmonic detector based on second order generalized integrators," in *2008 34th Annual Conference of IEEE Industrial Electronics*, pp. 2453–2458, 2008.

[286] B. Singh, K. Mathuria, I. Hussain, and S. Kumar, "Implementation of demodulation-SOGI control algorithm for improving the power quality," in *IECON 2017 - 43rd Annual Conference of the IEEE Industrial Electronics Society*, pp. 2540–2545, 2017.

[287] M. Malekpour, B. T. Phung, and E. Ambikairajah, "Modelling and diagnostic of incipient stator inter-turn short circuit fault in induction motors," in *2018 Condition Monitoring and Diagnosis (CMD)*, pp. 1–6, 2018.

[288] H. K. Yada and M. S. R. Murthy, "Operation and control of single-phase DVR based on SOGI-PLL," in *2016 IEEE International Conference on Power Electronics, Drives and Energy Systems (PEDES)*, pp. 1–5, 2016.

[289] H. K. Yada and M. S. R. Murthy, "Operation and control of single-phase UPQC based on SOGI-PLL," in *2016 7th India International Conference on Power Electronics (IICPE)*, pp. 1–6, 2016.

[290] K. Mathuria, I. Hussain, and B. Singh, "Robust control algorithm of grid interfaced solar pv system," in *2017 6th International Conference on Computer Applications In Electrical Engineering-Recent Advances (CERA)*, pp. 270–275, 2017.

[291] S. Biricik, H. Komurcugil, and M. Basu, "Sliding mode control strategy for three-phase dvr employing twelve-switch voltage source converter," in *IECON 2015 - 41st Annual Conference of the IEEE Industrial Electronics Society*, pp. 000921–000926, 2015.

[292] M. S. Reza, M. Ciobotaru, and V. G. Agelidis, "Tracking of time-varying grid voltage using dft based second order generalized integrator technique," in *2012 IEEE International Conference on Power System Technology (POWERCON)*, pp. 1–6, 2012.

[293] Q. Zhang, H. Guo, Y. Liu, C. Guo, F. Zhang, Z. Zhang, and G. Li, "A novel error-injected solution for compensation of current measurement errors in pmsm drive," *IEEE Transactions on Industrial Electronics*, vol. 70, no. 5, pp. 4608–4619, 2023.

[294] R. Sharma and B. Singh, "A resilient fll control for solar-hydro generation based utility interactive microgrid with enhanced power quality," *IEEE Transactions on Industry Applications*, vol. 57, no. 6, pp. 5716–5725, 2021.

[295] A. Mukherjee and C. S., "Cascaded sogi-fll based reference current extraction method for active power filter in more electric aircraft," in *2020 IEEE 17th India Council International Conference (INDICON)*, pp. 1–5, 2020.

[296] Y. P. Y. Deng, J. Liu, M. O. Faruque, and S. Pamidi, "Delay analysis and compensation for digital msogi-qsg implementation in back-to-back interfacing converter between micro-grid and utility grid for harmonic extraction," in *2022 IEEE Industrial Electronics and Applications Conference (IEACon)*, pp. 163–168, 2022.

[297] V. Rai, P. Saraf, and V. S. S. P. K. Hari, "Design and control of bidirectional dc- dc converter for active power decoupling," in *2021 IEEE Texas Power and Energy Conference (TPEC)*, pp. 1–6, 2021.

[298] S. Djabali, A. Ammar, and A. Kheldoun, "Enhanced sensorless predictive direct power control for pwm rectifier with constant switching frequency under grid disturbances," in *2021 9th International Conference on Systems and Control (ICSC)*, pp. 411–416, 2021.

[299] B. Tian, M. Molinas, Q. An, B. Zhou, and J. Wei, "Freewheeling current-based sensorless field-oriented control of five-phase permanent magnet synchronous motors under insulated gate bipolar transistor failures of a single phase," *IEEE Transactions on Industrial Electronics*, vol. 69, no. 1, pp. 213–224, 2022.

[300] S. Hou, C. Chen, and Y. Chu, "Grid-voltage-sensorless method based continuous sliding mode control of three-phase active power filter," in *2020 Chinese Control And Decision Conference (CCDC)*, pp. 2805–2809, 2020.

[301] Z. Yan, S. Wang, and S. Muyeen, "Harmonic current detection method of double frequency phase lock based on cascade sogi," in *2021 31st Australasian Universities Power Engineering Conference (AUPEC)*, pp. 1–6, 2021.

[302] S. Golestan, J. M. Guerrero, J. C. Vasquez, A. M. Abusorrah, and Y. Al-Turki, "Harmonic linearization and investigation of three-phase parallel-structured signal decomposition algorithms in grid-connected applications," *IEEE Transactions on Power Electronics*, vol. 36, no. 4, pp. 4198–4213, 2021.

[303] H. Wang, P. Chen, Y. Cao, Z. Chen, Y. Zheng, and Y. Zhou, "High-order sogi-based observation technology of leakage electrical impedance," in *2021 IEEE/IAS Industrial and Commercial Power System Asia (I and CPS Asia)*, pp. 1053–1058, 2021.

[304] G. Modi and B. Singh, "Improved cascaded sogi control for islanding-synchronization in photovoltaic system," *IEEE Transactions on Industry Applications*, vol. 58, no. 6, pp. 6909–6919, 2022.

[305] Y. Zhang and R. Zhao, "On-line detection of transformer excitation parameters based on fundamental wave extraction," in *2020 IEEE 1st China International Youth Conference on Electrical Engineering (CIYCEE)*, pp. 1–5, 2020.

[306] X. Wang, "Optimization strategy of dsogi-pll precision under harmonic interference conditions," in *2020 IEEE Sustainable Power and Energy Conference (iSPEC)*, pp. 852–857, 2020.

[307] J. Shen, J. Zhou, and J. Liu, "Sensorless control of permanent magnet synchronous motors based on high frequency square wave injection," in *2022 International Conference on Manufacturing, Industrial Automation and Electronics (ICMIAE)*, pp. 106–110, 2022.

[308] I. Pavlic, L. Pravica, M. Kutija, I. Erceg, and J. Matusko, "Sliding mode observers combined with locked loop techniques for sensorless vector controlled synchronous reluctance machines," in *2021 IEEE 19th International Power Electronics and Motion Control Conference (PEMC)*, pp. 594–601, 2021.

[309] S. Roy, S. Das, B. Singh, and B. Panigrahi, "Zero-tracking sogi enabled synchronization and control of dfig-bes based ac microgrid," in *2022 IEEE Global Conference on Computing, Power and Communication Technologies (GlobConPT)*, pp. 1–6, 2022.

[310] S. Sen, S. P. Singh, and S. G. Choudhuri, "A communicationless control of single phase two winding seig by vsi battery based system," in *2019 IEEE Region 10 Symposium (TENSYMP)*, pp. 196–201, 2019.

[311] N. F. Roslan, J. A. Suul, J. Rocabert, and P. Rodriguez, "A comparative study of methods for estimating virtual flux at the point of common coupling in grid-connected voltage source converters with lcl filter," *IEEE Transactions on Industry Applications*, vol. 53, no. 6, pp. 5795–5809, 2017.

[312] L. Goebel, S. Raab, and A. Ackva, "A fpga-based algorithm for soft switched dc-dc converters with a variable transmission path," in *PCIM Europe 2018; International Exhibition and Conference for Power Electronics, Intelligent Motion, Renewable Energy and Energy Management*, pp. 1–6, 2018.

[313] R. Emamalipour and J. Lam, "A new ac/dc half-bridge/string-inverter hybrid-structured isolated bi-directional converter," in *2019 IEEE Energy Conversion Congress and Exposition (ECCE)*, pp. 2713–2718, 2019.

[314] J. Castello, J. M. Espi, and R. Garcia-Gil, "A new generalized robust predictive current control for grid-connected inverters compensates anti-aliasing filters delay," *IEEE Transactions on Industrial Electronics*, vol. 63, no. 7, pp. 4485–4494, 2016.

[315] R. Zhao, Z. Xin, P. C. Loh, and F. Blaabjerg, "A novel flux estimator based on SOGI with FLL for induction machine drives," in *2016 IEEE Applied Power Electronics Conference and Exposition (APEC)*, pp. 1995–2002, 2016.

[316] F. Zhang, S. Dong, J. Wang, Z. He, and Q. Zhang, "A novel signal processing method of sliding mode observer for position sensorless pmsm drives," in *2019 14th IEEE Conference on Industrial Electronics and Applications (ICIEA)*, pp. 2479–2484, 2019.

[317] S. Beheshtaein, M. Savaghebi, J. M. Guerrero, R. Cuzner, and J. C. Vasquez, "A secondary-control based fault current limiter for four-wire three phase inverter-interfaced dgs," in *IECON 2017 - 43rd Annual Conference of the IEEE Industrial Electronics Society*, pp. 2363–2368, 2017.

[318] S. Prakash and S. Misra, "A three sample based pll-less hysteresis current control and stability analysis of a single phase active distribution system," *IEEE Transactions on Industrial Electronics*, pp. 1–1, 2020.

[319] C. Wu, H. Nian, B. Pang, and P. Cheng, "Adaptive repetitive control of dfig-dc system considering stator frequency variation," *IEEE Transactions on Power Electronics*, vol. 34, no. 4, pp. 3302–3312, 2019.

[320] Q. Huang and K. Rajashekara, "An inverter-current-feedback based reactive power sharing method for parallel inverters in microgrid," in *2016 IEEE Energy Conversion Congress and Exposition (ECCE)*, pp. 1–7, 2016.

[321] C. M. Nirmal Mukundan, P. Jayaprakash, U. Subramaniam, and D. J. Almakhles, "Binary hybrid multilevel inverter-based grid integrated solar energy conversion system with damped SOGI control," *IEEE Access*, vol. 8, pp. 37214–37228, 2020.

[322] J. J. Cabezas, R. González-Medina, E. Figueres, and G. Garcerá, "Comparison and combination of digital controls for single-phase boost pfc converters in avionic power systems," in *2017 IEEE 26th International Symposium on Industrial Electronics (ISIE)*, pp. 645–650, 2017.

[323] A. Tejero Revelles and H. Steinhart, "Comparison of current control structures for three-phase four-wire systems in natural frame," in *PCIM Europe 2019; International Exhibition and Conference for Power Electronics, Intelligent Motion, Renewable Energy and Energy Management*, pp. 1–7, 2019.

[324] V. R. Chowdhury, S. Mukherjee, P. Shamsi, and M. Ferdowsi, "Control of a three phase inverter mimicking synchronous machine with fault ridethrough capability," in *2017 Ninth Annual IEEE Green Technologies Conference (GreenTech)*, pp. 1–6, 2017.

[325] S. Devassy and B. Singh, "Control of solar photovoltaic integrated upqc operating in polluted utility conditions," *IET Power Electronics*, vol. 10, no. 12, pp. 1413–1421, 2017.

[326] M. G. Jahromi, G. Mirzaeva, and S. D. Mitchell, "Control strategy for a high power dc transformer with soft switching scheme for mining applications," in *2016 IEEE Industry Applications Society Annual Meeting*, pp. 1–8, 2016.

[327] Q. Wang, W. Zuo, M. Cheng, F. Deng, and G. Buja, "Decoupled power control with indepth analysis of single-phase electric springs," *IEEE Access*, vol. 8, pp. 21866–21874, 2020.

[328] R. C. de Barros, W. V. Ribeiro, G. L. E. Mata, L. S. Xavier, A. F. Cupertino, and H. A. Pereira, "Design of a current harmonic detector method applied in photovoltaic inverters with ancillary service capability," in *2017 IEEE 8th International Symposium on Power Electronics for Distributed Generation Systems (PEDG)*, pp. 1–7, 2017.

[329] L. Li, H. Nian, and P. Cheng, "Direct power control for voltage source inverter without phase-locked loop under harmonically distorted voltage conditions," in *2016 19th International Conference on Electrical Machines and Systems (ICEMS)*, pp. 1–6, 2016.

[330] I. Jayathilaka, L. Lakpriya, D. De Alwis, G. Jayakody, K. T. M. U. Hemapala, J. P. Karunadasa, and H. Lakshika, "Dq transform based current controller for single-phase grid connected inverter," in *2018 2nd International Conference On Electrical Engineering (EECon)*, pp. 32–37, 2018.

[331] Z. Xin, R. Zhao, X. Wang, P. C. Loh, and F. Blaabjerg, "Four new applications of second-order generalized integrator quadrature signal generator," in *2016 IEEE Applied Power Electronics Conference and Exposition (APEC)*, pp. 2207–2214, 2016.

[332] U. Kundu and P. Sensarma, "Gain-relationship-based automatic resonant frequency tracking in parallel *llc* converter," *IEEE Transactions on Industrial Electronics*, vol. 63, no. 2, pp. 874–883, 2016.

[333] M. Jang, M. Ciobotaru, and V. G. Agelidis, "Grid-connected fuel cell system based on a boost-inverter with a battery back-up unit," in *8th International Conference on Power Electronics - ECCE Asia*, pp. 1637–1644, 2011.

[334] H. Xiang-Hui and H. Cen-Cen, "Harmonic suppression for low speed sensorless control of spmsm based on high voltage frequency pulsating signal injection," in *2019 IEEE 3rd Information Technology, Networking, Electronic and Automation Control Conference (ITNEC)*, pp. 686–690, 2019.

[335] Seema and B. Singh, "Improved damped quadrature SOGI control algorithm for solar PV-hydro battery based microgrid," in *2018 8th IEEE India International Conference on Power Electronics (IICPE)*, pp. 1–6, 2018.

[336] H. K. Yada, A. S. Kumar, and K. Prakash, "Improved dual-SOGI control for three-phase unified power quality conditioner under distorted grid and load conditions," in *TENCON 2017 - 2017 IEEE Region 10 Conference*, pp. 2536–2541, 2017.

[337] W. Chen, W. Cao, K. Liu, and J. Zhao, "Improved single-loop voltage control with stability enhancement using second order generalized integrator (SOGI)," in *2019 9th International Conference on Power and Energy Systems (ICPES)*, pp. 1–6, 2019.

[338] P. M. de Almeida, P. G. Barbosa, J. L. Duarte, and P. F. Ribeiro, "Improvement of dc and ac side performance of renewable source inverters under fault conditions," in *2015 IEEE Eindhoven PowerTech*, pp. 1–5, 2015.

[339] B. Trento, B. Wang, K. Sun, and L. M. Tolbert, "Integration of phase-locked loop based real-time oscillation tracking in grid synchronized systems," in *2014 IEEE PES General Meeting | Conference Exposition*, pp. 1–5, 2014.

[340] S. Pranith, S. Kumar, B. Singh, and T. S. Bhatti, "MAF-SOGI-PLL based single-phase multimode PV-battery system with improved power quality," in *2018 8th IEEE India International Conference on Power Electronics (IICPE)*, pp. 1–6, 2018.

[341] X. Wu, C. Xiong, F. Diao, and Y. Zhang, "Modularized model predictive control scheme with capacitor voltage balance control for single-phase cascaded h-bridge rectifier," in *2018 IEEE Energy Conversion Congress and Exposition (ECCE)*, pp. 4021–4023, 2018.

[342] H. Z. Butt, M. Awon, and H. A. Khalid, "Performance analysis of a continuous and discretized second order generalized integrator based phase lock loop for single phase grid connected pv systems," in *2018 International Conference on Power Generation Systems and Renewable Energy Technologies (PGSRET)*, pp. 1–6, 2018.

[343] C. Xie, X. Zhao, K. Ki, D. Liu, J. M. Guerrero, and J. C. Vasquez, "Phase compensated reduced order generalized integrators for grid-tied vscs with harmonics compensation capability," *IEEE Transactions on Industry Applications*, vol. 54, no. 3, pp. 2568–2578, 2018.

[344] L. Kong, Z. Shi, G. Cai, C. Liu, and C. Xiong, "Phase-locked strategy of photovoltaic connected to distribution network with high proportion electric arc furnace," *IEEE Access*, vol. 8, pp. 86012–86023, 2020.

[345] M. G. Jahromi, G. Mirzaeva, and S. D. Mitchell, "Practical design and validation of an lcl dc-dc converter," in *2016 IEEE 2nd Annual Southern Power Electronics Conference (SPEC)*, pp. 1–6, 2016.

[346] Q. Liu, H. Bai, F. Luo, and Z. Fu, "Research on harmonic suppression method based on drooping control strategy," in *2018 10th International Conference on Intelligent Human-Machine Systems and Cybernetics (IHMSC)*, vol. 02, pp. 77–80, 2018.

[347] G. Wrona and K. Malon, "Sensorless operation of an active front end converter with lcl filter," in *2014 IEEE 23rd International Symposium on Industrial Electronics (ISIE)*, pp. 2697–2702, 2014.

[348] D. Pavkovic, P. Kristovic, M. Hrgetic, A. Komljenovic, and V. Uzarevic, "Single phase ac inverter current pr control with auxiliary pi controller for dc current suppression," in *IEEE EUROCON 2017 -17th International Conference on Smart Technologies*, pp. 324–329, 2017.

[349] Z. Zeng, R. Zhao, H. Yang, C. Cheng, and Shengqing Tang, "Single-phase virtual synchronous generator for distributed energy sources," in *2013 International Conference on Electrical Machines and Systems (ICEMS)*, pp. 190–195, 2013.

[350] A. Uphues, K. Nötzold, R. Wegener, and S. Soter, "SOGI based grid fault detection for feeding asymmetrical reactive currents to fulfill LVRT requirements," in *2013 Africon*, pp. 1–5, 2013.

[351] L. Zhai, Z. Yang, W. Zhang, J. Wang, X. Liang, and Y. Zhu, "Speed sensorless control of axial field flux-switching permanent magnet machine based on improved adaptive sliding mode observer," in *2019 22nd International Conference on Electrical Machines and Systems (ICEMS)*, pp. 1–5, 2019.

[352] Guihua Liu, Yulin Yang, Pangbao Wang, Wei Wang, and Dianguo Xu, "Stability control method based on virtual inductance of grid-connected pv inverter under weak grid," in *IECON 2013 - 39th Annual Conference of the IEEE Industrial Electronics Society*, pp. 1867–1872, 2013.

[353] M. Malekpour, B. T. Phung, and E. Ambikairajah, "Stator current envelope extraction for analysis of broken rotor bar in induction motors," in *2017 IEEE 11th International Symposium on Diagnostics for Electrical Machines, Power Electronics and Drives (SDEMPED)*, pp. 240–246, 2017.

[354] Y. Liu, Y. Xie, F. Zhang, and J. Hu, "Two-step model predictive power control for a single-phase npc inverter with fixed switching frequency and optimal switching sequences," in *2020 Asia Energy and Electrical Engineering Symposium (AEEES)*, pp. 401–408, 2020.

[355] J. Matas, M. Castilla, L. G. d. Vicuña, J. Miret, and J. C. Vasquez, "Virtual impedance loop for droop-controlled single-phase parallel inverters using a second-order general-integrator scheme," *IEEE Transactions on Power Electronics*, vol. 25, no. 12, pp. 2993–3002, 2010.

[356] V. P. Chandran, S. Murshid, and B. Singh, "Voltage and frequency controller with power quality improvement for pmsg based pico-hydro system," in *2018 IEEE International Conference on Power Electronics, Drives and Energy Systems (PEDES)*, pp. 1–6, 2018.

[357] Q. Lu, Y. Zuo, T. Zhang, and L. Mo, "Zero-sequence current suppression for open-winding permanent magnet brushless motor driving system based on second order generalized integrator," *IEEE Access*, vol. 8, pp. 37465–37473, 2020.

[358] Jian Yang, Ying Chen, Mi Dong, and Hua Han, "A harmonic and reactive power sharing control strategy for islanded microgrids," in *2015 Chinese Automation Congress (CAC)*, pp. 1422–1427, 2015.

[359] P. Martín, E. Bueno, F. J. Rodríguez, and V. Sáez, "A methodology for optimizing the fpga implementation of industrial control systems," in *2009 35th Annual Conference of IEEE Industrial Electronics*, pp. 2811–2816, 2009.

[360] S. Murshid and B. Singh, "A multi-objective gi based control for effective operation of pv pumping system under abnormal grid conditions," *IEEE Transactions on Industrial Informatics*, pp. 1–1, 2019.

[361] R. Teodorescu, F. Blaabjerg, U. Borup, and M. Liserre, "A new control structure for grid-connected lcl pv inverters with zero steady-state error and selective harmonic compensation," in *Nineteenth Annual IEEE Applied Power Electronics Conference and Exposition, 2004. APEC '04.*, vol. 1, pp. 580–586 Vol.1, 2004.

[362] Y. Liu, W. Xu, T. Long, and F. Blaabjerg, "A new rotor speed observer for stand-alone brushless doubly-fed induction generators," in *2017 IEEE Energy Conversion Congress and Exposition (ECCE)*, pp. 5086–5092, 2017.

[363] J. Moriano, V. Bermejo, E. Bueno, M. Rizo, and A. Rodriguez, "A novel approach to the grid inductance estimation based on second order generalized integrators," in *2017 IEEE Energy Conversion Congress and Exposition (ECCE)*, pp. 1794–1801, 2017.

[364] J. Lu, Y. Wen, Yingchao Zhang, and W. Wen, "A novel power calculation method based on second order general integrator," in *2016 IEEE 8th International Power Electronics and Motion Control Conference (IPEMC-ECCE Asia)*, pp. 1975–1979, 2016.

[365] Y. Chen, J. Zhao, K. Qu, and F. Li, "A pq control strategy for voltage-controlled inverters applied in low-voltage power system," in *2014 International Power Electronics and Application Conference and Exposition*, pp. 843–846, 2014.

[366] C. Jain and B. Singh, "A SOGI-Q based control algorithm for multifunctional grid connected SECS," in *2014 IEEE 6th India International Conference on Power Electronics (IICPE)*, pp. 1–6, 2014.

[367] M. Malekpour, B. T. Phung, and E. Ambikairajah, "An envelope-based method with second order generalized integrator adaptive notch filter for diagnosis of rotor bar breakage at very low slips," in *2017 IEEE 11th International Symposium on Diagnostics for Electrical Machines, Power Electronics and Drives (SDEMPED)*, pp. 1–7, 2017.

[368] Y. Su, S. Liu, X. Zhao, and X. Chen, "An improved power control with virtual impedance based on a second-order general-integrator," in *2015 34th Chinese Control Conference (CCC)*, pp. 9037–9042, 2015.

[369] H. K. Yada and A. S. Kumar, "An SO-SOGI based control for a three-phase DVR under distorted grid conditions including DC offset," in *TENCON 2017 - 2017 IEEE Region 10 Conference*, pp. 3000–3005, 2017.

[370] Y. Han, M. Luo, X. Zhao, J. M. Guerrero, and L. Xu, "Comparative performance evaluation of orthogonal-signal-generators-based single-phase pll algorithm - a survey," *IEEE Transactions on Power Electronics*, vol. 31, no. 5, pp. 3932–3944, 2016.

[371] T. Ngo, K. Min, and T. Vu, "Comparative study of fault detection methods based on time domain rms calculation," in *2019 IEEE Power Energy Society General Meeting (PESGM)*, pp. 1–5, 2019.

[372] E. S. Kim, U. S. Seong, J. S. Lee, and S. H. Hwang, "Compensation of dead time effects in grid-tied single-phase inverter using SOGI," in *2017 IEEE Applied Power Electronics Conference and Exposition (APEC)*, pp. 2633–2637, March 2017.

[373] M. E. T. Souza, . C. Resende, F. C. Melo, G. B. de Lima, and L. C. G. de Freitas, "Computational implementation and comparative analysis of phase-locked loop (pll) methods under different power quality disturbances," in *2019 IEEE PES Innovative Smart Grid Technologies Conference - Latin America (ISGT Latin America)*, pp. 1–6, 2019.

[374] P. Mlodzikowski, A. Milczarek, S. Stynski, M. Malinowski, and S. Kouro, "Control of simplified multilevel ac-dc-ac converter for small power generation systems," in *IECON 2013 - 39th Annual Conference of the IEEE Industrial Electronics Society*, pp. 5951–5956, 2013.

[375] B. Singh, S. Kumar, and C. Jain, "Damped-SOGI-based control algorithm for solar PV power generating system," *IEEE Transactions on Industry Applications*, vol. 53, pp. 1780–1788, May 2017.

[376] H. Saxena, A. Singh, and J. N. Rai, "Design and analysis of cascaded generalized integrators for mitigation of power quality problems," in *2019 International Symposium on Advanced Electrical and Communication Technologies (ISAECT)*, pp. 1–6, 2019.

[377] F. Zhang, J. Hui, and L. Wu, "Design of single phase photovoltaic grid-connected inverter based on dsp arm," in *2014 International Power Electronics and Application Conference and Exposition*, pp. 1339–1344, 2014.

[378] M. Rizo, A. Rodríguez, F. J. Rodríguez, E. Bueno, and M. Liserre, "Different approaches of stationary reference frames saturators," in *IECON 2012 - 38th Annual Conference on IEEE Industrial Electronics Society*, pp. 2245–2250, 2012.

[379] T. Q. Tho, T. V. Anh, and L. M. Phuong, "Estimation of voltage parameters for grid-connected inverters," in *2015 International Conference on Advanced Technologies for Communications (ATC)*, pp. 610–615, 2015.

[380] E. Habboub, J. Sawma, N. Daou, and F. Khatounian, "Experimental validation of a combined multi-variable filter - dual second order generalized integrator phase-locked loop technique," in *2018 IEEE International Multidisciplinary Conference on Engineering Technology (IMCET)*, pp. 1–6, 2018.

[381] V. Sáez, A. Rodríguez, M. Rizo, E. Bueno, . Hernández, and F. J. Rodríguez, "Fixed point implementation of iir filters using delta operator applied to distributed power generation systems," in *IECON 2010 - 36th Annual Conference on IEEE Industrial Electronics Society*, pp. 1709–1714, 2010.

[382] M. S. Reza, M. Ciobotaru, and V. G. Agelidis, "Frequency adaptive instantaneous power quality analysis using frequency locked loop based kalman filter technique," in *2012 3rd IEEE International Symposium on Power Electronics for Distributed Generation Systems (PEDG)*, pp. 767–774, 2012.

[383] Z. Xin, X. Wang, P. C. Loh, and F. Blaabjerg, "Grid-current-feedback control for lcl-filtered grid converters with enhanced stability," *IEEE Transactions on Power Electronics*, vol. 32, no. 4, pp. 3216–3228, 2017.

[384] B. Özmen and S. Biricik, "Harmonic current detection based on the dual-tree complex wavelet transform," in *2019 2nd International Conference on Smart Grid and Renewable Energy (SGRE)*, pp. 1–5, 2019.

[385] P. Cossutta, S. Raffo, A. Cao, F. Ditaranto, M. P. Aguirre, and M. I. Valla, “High speed single phase SOGI-PLL with high resolution implementation on an FPGA,” in *2015 IEEE 24th International Symposium on Industrial Electronics (ISIE)*, pp. 1004–1009, June 2015.

[386] A. K. Giri, S. R. Arya, and R. Maurya, “Hybrid order generalized integrator based control for vsc to improve the pmsg operation in isolated mode,” in *2020 First International Conference on Power, Control and Computing Technologies (ICPC2T)*, pp. 373–378, 2020.

[387] W. Xu, Y. Jiang, C. Mu, and F. Blaabjerg, “Improved nonlinear flux observer-based second-order soifo for pmsm sensorless control,” *IEEE Transactions on Power Electronics*, vol. 34, no. 1, pp. 565–579, 2019.

[388] T. Chen, S. Huang, X. Wu, and T. Wu, “Improved-reduced order generalized integrator based sliding-mode observer for interior permanent magnet synchronous motor sensorless control,” in *2019 22nd International Conference on Electrical Machines and Systems (ICEMS)*, pp. 1–6, 2019.

[389] G. Bergna, J. A. Suul, A. Garcés, E. Berne, P. Egrot, A. Arzandé, J. Vannier, and M. Molinas, “Improving the dynamics of lagrange-based mmc controllers by means of adaptive filters for single-phase voltage, power and energy estimation,” in *IECON 2013 - 39th Annual Conference of the IEEE Industrial Electronics Society*, pp. 6239–6244, 2013.

[390] C. Ke, A. Wu, C. Bing, and L. Yi, “Measuring and reconstruction algorithm based on improved second-order generalised integrator configured as a quadrature signal generator and phase locked loop for the three-phase ac signals of independent power generation systems,” *IET Power Electronics*, vol. 9, no. 11, pp. 2155–2161, 2016.

[391] Y. Zhang, J. Jiao, J. Liu, H. Yang, Q. Wan, and W. Xu, “Model predictive control of pwm rectifier under unbalanced and distorted network without ac voltage sensor,” in *2019 IEEE Energy Conversion Congress and Exposition (ECCE)*, pp. 5584–5589, 2019.

[392] I. Roasto, T. Jalakas, and O. Husev, “Modeling of grid-connected quasi-z-source series resonant topology based microinverter,” in *2016 10th International Conference on Compatibility, Power Electronics and Power Engineering (CPE-POWERENG)*, pp. 192–195, 2016.

[393] M. Malekpour, A. Pouramin, A. Malekpour, T. Phung, and E. Ambikairajah, “Monitoring and measurement of high-frequency oscillatory transient recovery voltage of circuit breakers,” *IET Science, Measurement Technology*, vol. 12, no. 6, pp. 764–769, 2018.

[394] M. Ghadiri-Modarres, M. Mojiri, and M. Karimi-Ghartemani, “New adaptive algorithm for delay estimation of sinusoidal signals with unknown frequency,” *IEEE Transactions on Instrumentation and Measurement*, vol. 64, no. 9, pp. 2360–2366, 2015.

[395] M. Kabalan and P. Singh, “Optimizing a virtual impedance droop controller for parallel inverters,” in *2015 IEEE Power Energy Society General Meeting*, pp. 1–5, 2015.

[396] M. Fallah, H. M. Kojabadi, H. J. Kaleybar, J. Modarresi, and Liuchen Chang, “Performance enhancement of active power filter in the presence of low order harmonics and distorted voltage,” in *2016 IEEE 8th International Power Electronics and Motion Control Conference (IPEMC-ECCE Asia)*, pp. 2577–2581, 2016.

[397] P. Tan, H. He, and X. Gao, "Phase compensation, ZVS operation of wireless power transfer system based on SOGI-PLL," in *2016 IEEE Applied Power Electronics Conference and Exposition (APEC)*, pp. 3185–3188, 2016.

[398] B. Liu, B. Zhou, and T. Ni, "Principle and stability analysis of an improved self-sensing control strategy for surface-mounted pmsm drives using second-order generalized integrators," *IEEE Transactions on Energy Conversion*, vol. 33, no. 1, pp. 126–136, 2018.

[399] Y. Si, Y. Liu, C. Liu, Z. Zhang, and Q. Lei, "Reactive power injection and SOGI based active anti-islanding protection method," in *2019 IEEE Energy Conversion Congress and Exposition (ECCE)*, pp. 2637–2642, 2019.

[400] C. Xie, K. Li, X. Zhao, J. C. Vasquez, and J. M. Guerrero, "Reduced order generalized integrators with phase compensation for three-phase active power filter," in *2017 IEEE Applied Power Electronics Conference and Exposition (APEC)*, pp. 2759–2766, 2017.

[401] D. Song, J. Ma, Y. Ma, H. Lin, and S. Liu, "Research on the switching arc loss of on-load tap changer," *IEEE Access*, vol. 7, pp. 180793–180803, 2019.

[402] Seema and B. Singh, "Robust control for islanded and seamless mode switching of wind-pv-grid tied generation system," in *2019 IEEE Energy Conversion Congress and Exposition (ECCE)*, pp. 1012–1019, 2019.

[403] G. Lo Calzo, M. Lega, A. Lidozzi, L. Solero, and F. Crescimbini, "Single-phase three-level transformer-less inverter for residential distributed generation," in *2012 IEEE International Energy Conference and Exhibition (ENERGYCON)*, pp. 7–12, 2012.

[404] D. Sun and X. Wang, "Sliding-mode DPC using SOGI for DFIG under unbalanced grid condition," *Electronics Letters*, vol. 53, no. 10, pp. 674–676, 2017.

[405] Z. Xin, X. Wang, P. C. Loh, and F. Blaabjerg, "SOGI-based capacitor voltage feedback active damping in LCL-filtered grid converters," in *2015 IEEE 6th International Symposium on Power Electronics for Distributed Generation Systems (PEDG)*, pp. 1–6, 2015.

[406] C. Jain and B. Singh, "Solar energy used for grid connection: A detailed assessment including frequency response and algorithm comparisons for an energy conversion system," *IEEE Industry Applications Magazine*, vol. 23, no. 2, pp. 37–50, 2017.

[407] M. Xie, C. Zhu, Y. Yang, and H. Wen, "Srf-pll with in-loop differentiator decouple filter for unbalanced three-phase systems," in *2017 IEEE Applied Power Electronics Conference and Exposition (APEC)*, pp. 1314–1318, 2017.

[408] Z. Li, M. Zhu, C. Hou, and X. Cai, "The influence of phase-locked loop on the impedance of single phase voltage source converter," in *8th Renewable Power Generation Conference (RPG 2019)*, pp. 1–7, 2019.

[409] G. Xu, L. Zhu, and Z. Pan, "Virtual synchronous control using SOGI for standalone DFIG-based wind turbines with unbalanced and nonlinear loads," in *2018 21st International Conference on Electrical Machines and Systems (ICEMS)*, pp. 1133–1138, 2018.

[410] Y. K. Tao, Q. H. Wu, W. H. Tang, and L. Wang, "Voltage sensorless predictive direct power control for renewable energy integration under grid fault conditions," in *2015 IEEE Innovative Smart Grid Technologies - Asia (ISGT ASIA)*, pp. 1–5, 2015.

[411] J. Wei, H. Xue, B. Zhou, Z. Zhang, and T. Yang, “Rotor position estimation method for brushless synchronous machine based on second-order generated integrator in the starting mode,” *IEEE Transactions on Industrial Electronics*, vol. 67, no. 7, pp. 6135–6146, 2020.

[412] B. N. de Andrade, L. H. S. Silva, A. J. Sguarezi Filho, and F. F. Costa, “Enhanced SOGI-PLL by moving-average filter and one-cycle fourier algorithm,” in *2017 IEEE 6th International Conference on Renewable Energy Research and Applications (ICRERA)*, pp. 1019–1023, 2017.

[413] C. A. Busada, S. Gomez Jorge, A. E. Leon, and J. A. Solsona, “Current controller based on reduced order generalized integrators for distributed generation systems,” *IEEE Transactions on Industrial Electronics*, vol. 59, no. 7, pp. 2898–2909, 2012.

[414] P. Lamo, F. J. Azcondo, and A. Pigazo, “1phi sogi phase locked loop with secondary control path in grid-connected power converters,” in *2020 IEEE Applied Power Electronics Conference and Exposition (APEC)*, pp. 2979–2983, 2020.

[415] S. Mondal, P. K. Gayen, and D. N. Gaonkar, “A hybrid islanding detection method based on lissajous pattern having robust performance under various power quality scenarios,” *IEEE Systems Journal*, pp. 1–11, 2022.

[416] S. Gautam, W. Hassan, A. Bhatta, D. D.-C. Lu, and W. Xiao, “A comprehensive study of orthogonal signal generation schemes for single phase systems,” in *2021 1st International Conference on Power Electronics and Energy (ICPEE)*, pp. 1–8, 2021.

[417] A. Mishra, B. Dash, A. K. Naik, and R. Sharma, “A cascaded generalized integrator based algorithm for grid intefaced pv system,” in *2022 2nd Odisha International Conference on Electrical Power Engineering, Communication and Computing Technology (ODICON)*, pp. 1–5, 2022.

[418] L. Qu and J. Teng, “A linear active disturbance rejection control based sensor lesscontrol for ipmsms considering harmonic current suppression,” in *2022 IEEE Applied Power Electronics Conference and Exposition (APEC)*, pp. 687–692, 2022.

[419] R. Sharma and B. Singh, “A multifunctional solar pv-syrg based hydr generation utility interactive microgrid,” in *2020 IEEE 5th International Conference on Computing Communication and Automation (ICCCA)*, pp. 623–628, 2020.

[420] Z. Xu, X. Ren, Z. Zheng, Z. Zhang, Q. Chen, and Z. Hao, “A quadrature signal-based control strategy for vienna rectifier under unbalanced aircraft grids,” *IEEE Journal of Emerging and Selected Topics in Power Electronics*, vol. 10, no. 5, pp. 5280–5289, 2022.

[421] H. K. Yada, B. A. Kumar, and V. P. Muddineni, “A second order-second order generalized integrator for three - phase single - stage multifunctional grid-connected spv system,” in *2020 International Conference on Smart Technologies in Computing, Electrical and Electronics (ICSTCEE)*, pp. 554–559, 2020.

[422] S. Chaurasiya and B. Singh, “A single-phase low cost, compact/high power density portable ev charger for high voltage ev battery packs with weak/strong grid operation capability,” in *2022 IEEE Global Conference on Computing, Power and Communication Technologies (GlobConPT)*, pp. 1–6, 2022.

[423] S. Prakash, J. K. Singh, R. K. Behera, and A. Mondal, "A type-3 modified sogi-pll with grid disturbance rejection capability for single-phase grid-tied converters," *IEEE Transactions on Industry Applications*, vol. 57, no. 4, pp. 4242–4252, 2021.

[424] A. Verma and B. Singh, "Aff-sogi-drc control of renewable energy based grid interactive charging station for ev with power quality improvement," *IEEE Transactions on Industry Applications*, vol. 57, no. 1, pp. 588–597, 2021.

[425] V. Saxena, N. Kumar, B. Singh, and B. K. Panigrahi, "An enhanced multilayer gi based control for grid integrated solar pv system," in *2020 IEEE International Conference on Power Electronics, Drives and Energy Systems (PEDES)*, pp. 1–6, 2020.

[426] R. Shi, G. Wang, L. Zhang, Y. Yu, Y. Zhang, and X. Zhang, "An enhanced virtual inertia control strategy based on an improved sogi-fll scheme for energy storage converters," in *2021 IEEE 4th International Electrical and Energy Conference (CIEEC)*, pp. 1–6, 2021.

[427] A. Singhal, H. M. Suryawanshi, K. R. S, P. P. Nachankar, D. Govind, and C. L. Narayana, "An improved dual fixed frequency sogi-pll for three-phase grid-connected converter under unbalanced condition," in *2022 IEEE IAS Global Conference on Emerging Technologies (GlobConET)*, pp. 687–691, 2022.

[428] Y. Lin, Y. Liu, W. Xu, M. G. Hussien, and E. M. Rashad, "An improved speed observer based on super-twisting algorithm for standalone brushless doubly-fed induction generator-dc system," in *2022 25th International Conference on Electrical Machines and Systems (ICEMS)*, pp. 1–6, 2022.

[429] C. M. Nirmal Mukundan, P. Jayaprakash, U. Subramaniam, and D. J. Almakhles, "Binary hybrid multilevel inverter-based grid integrated solar energy conversion system with damped sogi control," *IEEE Access*, vol. 8, pp. 37214–37228, 2020.

[430] L. Q. Huy, N. Duc Hung, T. P. Hoa, and N. Dinh Tuyen, "Control and monitor of single-stage single-phase t-type grid-connected inverter based on iot," in *2021 International Conference on System Science and Engineering (ICSSE)*, pp. 231–236, 2021.

[431] G. Modi and B. Singh, "Control of low voltage grid-tied solar pv system," in *2021 International Conference on Sustainable Energy and Future Electric Transportation (SEFET)*, pp. 1–6, 2021.

[432] T. N. Gupta, B. Singh, A. Chandra, and K. Al-Haddad, "Control of single-phase solar pv-bes microgrid," in *IECON 2020 The 46th Annual Conference of the IEEE Industrial Electronics Society*, pp. 3660–3665, 2020.

[433] F. Chishti and B. Singh, "Dual mode control of ac microgrid to facilitate seamless transition between operating modes," in *2020 International Conference on Power, Instrumentation, Control and Computing (PICC)*, pp. 1–6, 2020.

[434] M. M. Amin, F. F. M. El-Sousy, and O. A. Mohammed, "Encoderless control of pma-synrg based-stator current vector for renewable energy systems," in *2021 IEEE Industry Applications Society Annual Meeting (IAS)*, pp. 1–8, 2021.

[435] M. M. Amin, A. S. Soliman, F. F. M. El-Sousy, and O. A. Mohammed, "Encoderless control of pma-synrg based-stator current vector for wind generation systems," *IEEE Transactions on Industry Applications*, pp. 1–13, 2023.

[436] S. Mittal, A. Singh, and P. Chittora, "Ev control in g2v and v2g modes using sogi controller," in *2022 IEEE 3rd Global Conference for Advancement in Technology (GCAT)*, pp. 1–6, 2022.

[437] W.-q. Cai, M.-f. Guo, Z.-y. Zheng, and H. Wang, "Flexible arc suppression method based on sogi-fll-pci controller and fault status identification for distribution networks," in *2021 11th International Conference on Power and Energy Systems (ICPES)*, pp. 359–364, 2021.

[438] J. Wei, J. Wang, Z. Zhang, H. Lu, and B. Zhou, "Frequency-insensitive rotor position estimation method for three-stage synchronous machine based on indirect high-frequency signal injection," *IEEE Transactions on Transportation Electrification*, vol. 8, no. 2, pp. 1785–1793, 2022.

[439] A. K. Mishra and B. Singh, "Grid-integrated srm-driven solar water pump with power flow management," *IEEE Journal of Emerging and Selected Topics in Power Electronics*, vol. 9, no. 3, pp. 2723–2734, 2021.

[440] H. Bai, B. Yu, W. Ouyang, X. Yan, and J. Zhu, "Hf-based sensorless control of a ftpmm in ship shaftless rim-driven thruster system," *IEEE Transactions on Intelligent Transportation Systems*, vol. 23, no. 9, pp. 16867–16877, 2022.

[441] K. Tiwari, S. Seema, and B. Singh, "Hybrid generation based utility grid connected microgrid using sogi-pll-wtpf control technique," in *2021 IEEE Industry Applications Society Annual Meeting (IAS)*, pp. 1–6, 2021.

[442] Y. Xu, C. Lin, J. Xing, Q. Zeng, and J. Sun, "I-f starting rapid and smooth transition method of full-speed sensorless control for low current harmonic ultra-high-speed pmsm," in *2022 IEEE Applied Power Electronics Conference and Exposition (APEC)*, pp. 1820–1826, 2022.

[443] K. Kumari and A. K. Jain, "Iir digital filter based discrete sogi controller and discrete dsogi pll for grid integrated solar photovoltaic system," in *2022 IEEE IAS Global Conference on Emerging Technologies (GlobConET)*, pp. 310–315, 2022.

[444] S. Murshid, B. Singh, H. B. Gooi, and Y. S. Eddy Foo, "Implementation of frequency adaptive damped sogi based control for power quality improvement in wind-solar-bes based ac microgrids," in *2021 IEEE Power and Energy Society General Meeting (PESGM)*, pp. 1–5, 2021.

[445] G. B. N. S. Lala, L. S. Rao, P. B. Shankar, K. N. V. Sravani, and J. Lokesh, "Improved power quality sogi based grid integrated pv system under abnormal conditions by using interweaved gi," in *2022 International Conference on Intelligent Controller and Computing for Smart Power (ICICCSP)*, pp. 1–6, 2022.

[446] S. DJABALI, M. A. H. ALI, and A. AMMAR, "Improved virtual flux-direct power control for pwm rectifier based on second-order generalized integrators," in *2020 International Conference on Electrical Engineering (ICEE)*, pp. 1–6, 2020.

[447] K. Tiwari and B. Singh, "Multiple converter based ac microgrid for pev and local loads," in *2022 IEEE Global Conference on Computing, Power and Communication Technologies (GlobConPT)*, pp. 1–6, 2022.

[448] Q. Zeng, C. Lin, J. Xing, X. Jiang, and Y. Xu, "Nonlinear flux observer based on extended flux model for sensorless control of ipmsm in electric vehicles," in *2021 24th International Conference on Electrical Machines and Systems (ICEMS)*, pp. 1–5, 2021.

[449] K. Ravali and N. Yadaiah, "Performance analysis of anfis-pso based grid integration using improved sogi-fll algorithm under fluctuating solar irradiance," in *2021 International Conference on Smart Generation Computing, Communication and Networking (SMART GENCON)*, pp. 1–8, 2021.

[450] V. Narayanan and B. Singh, "Performance of a multifunctional battery integrated solar pv based microgrid under abnormal grid conditions with seamless mode transfer capability," in *2021 IEEE 8th Uttar Pradesh Section International Conference on Electrical, Electronics and Computer Engineering (UPCON)*, pp. 1–6, 2021.

[451] Chuncheng-Han, Zhenyu-Shi, Huan-He, Junde-Liu, and Yang-Cao, "Research on control strategy of photovoltaic grid connected converter under voltage distortion," in *2020 15th IEEE Conference on Industrial Electronics and Applications (ICIEA)*, pp. 715–721, 2020.

[452] J. Shi, J. Yang, L. Wen, J. Shen, G. Che, and S. Li, "Research on filter enhanced phase locked loop based on multiple second order generalized integrator," in *2022 International Conference on Wireless Communications, Electrical Engineering and Automation (WCEEA)*, pp. 267–274, 2022.

[453] Y. Hu, J. Xu, H. Qian, S. Bian, and S. Xie, "Robustness and harmonics suppression of grid-connected inverters with different grid voltage feedforward compensations in weak grid," in *2020 IEEE 29th International Symposium on Industrial Electronics (ISIE)*, pp. 779–784, 2020.

[454] D. Kong, W. Li, J. Han, C. Deng, M. Yan, and L. Zhou, "Sensorless control of permanent magnet synchronous linear motor based on improved second-order generalized integrators," in *2022 5th Asia Conference on Energy and Electrical Engineering (ACEEE)*, pp. 90–96, 2022.

[455] A. T. Nguyen and D.-C. Lee, "Sensorless control of variable-speed scig wind energy conversion systems based on rotor flux estimation using rogi-fll," *IEEE Journal of Emerging and Selected Topics in Power Electronics*, vol. 10, no. 6, pp. 7786–7796, 2022.

[456] B. Mohammed, G. Ismail, and B. Riad, "Sensorless scalar control based on sogi-fll for an induction motor u sed in electric vehicle," in *2022 19th International Multi-Conference on Systems, Signals and Devices (SSD)*, pp. 2121–2126, 2022.

[457] K. Wang, P. Yan, C. Lin, and X. Ge, "Stability enhancement strategy based on an improved osg method for high-speed train-network system," in *2021 IEEE 12th Energy Conversion Congress and Exposition - Asia (ECCE-Asia)*, pp. 2274–2279, 2021.

[458] P. Cui, Y. Li, J. Li, L. Du, and Y. Wu, "Synchronous vibration force suppression of magnetically suspended cmg based on modified double sogi-fll," *IEEE Transactions on Industrial Electronics*, pp. 1–10, 2022.

[459] W. Shi, J. Yu, and Y. Guo, "Unified viewpoint of soft startup and rate limiter for sogi-fll," *IEEE Transactions on Power Electronics*, vol. 37, no. 11, pp. 12949–12954, 2022.

[460] X. Song, Z. Qin, W. Li, W. Cao, S. Hu, W. Li, and B. Shi, “Virtual inertia control for renewable energy integration based on the improved sogi-fll,” in *2022 IEEE/IAS Industrial and Commercial Power System Asia (I and CPS Asia)*, pp. 1447–1452, 2022.

[461] M. Zarei, M. Karimadini, M. Nadjafi, and A. Salami, “A novel method for estimation of the fundamental parameters of distorted single phase signals,” in *2015 30th International Power System Conference (PSC)*, pp. 271–276, Nov 2015.

[462] G. Fedele, A. Ferrise, and D. Frascino, “A practical approach to the time-derivative estimation problem based on PI-SOGI filters bank,” in *18th Mediterranean Conference on Control and Automation, MED'10*, pp. 1417–1422, 2010.

[463] H. Saxena, A. Singh, and J. N. Rai, “Design and testing of frequency adaptive zero- crossing detector as a synchronizing technique,” in *2020 IEEE 9th Power India International Conference (PIICON)*, pp. 1–6, 2020.

[464] L. Hadjidemetriou, E. Kyriakides, Y. Yang, and F. Blaabjerg, “A synchronization method for single-phase grid-tied inverters,” *IEEE Transactions on Power Electronics*, vol. 31, no. 3, pp. 2139–2149, 2016.

[465] H. Ahmed, S. Amamra, and I. Salgado, “Fast estimation of phase and frequency for single-phase grid signal,” *IEEE Transactions on Industrial Electronics*, vol. 66, no. 8, pp. 6408–6411, 2019.

[466] Q. Guan, Y. Zhang, Y. Kang, and J. M. Guerrero, “Single-phase phase-locked loop based on derivative elements,” *IEEE Transactions on Power Electronics*, vol. 32, no. 6, pp. 4411–4420, 2017.

[467] C. Lee, T. Chun, and H. Lee, “A second-order generalized differentiator method for eliminating dc component in the three-phase pll for grid-connected inverters,” in *2017 20th International Conference on Electrical Machines and Systems (ICEMS)*, pp. 1–5, 2017.

[468] F. Xiao, L. Dong, L. Li, and X. Liao, “A frequency-fixed sogi-based pll for single-phase grid-connected converters,” *IEEE Transactions on Power Electronics*, vol. 32, no. 3, pp. 1713–1719, 2017.

[469] M. A. Akhtar and S. Saha, “An adaptive frequency-fixed second-order generalized integrator-quadrature signal generator using fractional-order conformal mapping based approach,” *IEEE Transactions on Power Electronics*, vol. 35, no. 6, pp. 5548–5552, 2020.

[470] A. Bamigbade, V. Khadkikar, H. H. Zeineldin, M. S. E. Moursi, and M. A. Hosani, “A novel power-based orthogonal signal generator for single-phase systems,” *IEEE Transactions on Power Delivery*, vol. 36, no. 1, pp. 469–472, 2021.

[471] K. Dash, M. R. Mishra, and S. Mishra, “Adaptive sogi gain based control of single phase inverter under distorted grid condition,” in *2020 3rd International Conference on Energy, Power and Environment: Towards Clean Energy Technologies*, pp. 1–6, 2021.

[472] P. Rodríguez, A. Luna, R. S. Muñoz-Aguilar, I. Etxeberria-Otadui, R. Teodorescu, and F. Blaabjerg, “A stationary reference frame grid synchronization system for three-phase grid-connected power converters under adverse grid conditions,” *IEEE Transactions on Power Electronics*, vol. 27, no. 1, pp. 99–112, 2012.

[473] P. Rodríguez, R. Teodorescu, I. Candela, A. V. Timbus, M. Liserre, and F. Blaabjerg, "New positive-sequence voltage detector for grid synchronization of power converters under faulty grid conditions," in *2006 37th IEEE Power Electronics Specialists Conference*, pp. 1–7, 2006.

[474] Z. Zeng, J. Yang, S. Chen, and J. Huang, "Reduced order generalized integrators based selective harmonic compensation current controller for shunt active power filters," in *2014 IEEE Energy Conversion Congress and Exposition (ECCE)*, pp. 1650–1655, 2014.

[475] S. Taghizadeh, M. J. Hossain, and J. Lu, "Enhanced orthogonal signal generator for a single-phase grid-connected converter," *IET Power Electronics*, vol. 11, no. 15, pp. 2563–2572, 2018.

[476] S. Golestan, J. M. Guerrero, J. C. Vasquez, A. M. Abusorrah, and Y. Al-Turki, "Modeling, tuning, and performance comparison of second-order-generalized-integrator-based FLLs," *IEEE Transactions on Power Electronics*, vol. 33, pp. 10229–10239, Dec 2018.

[477] J. Matas, M. Castilla, J. Miret, L. García de Vicuña, and R. Guzman, "An adaptive prefiltering method to improve the speed/accuracy tradeoff of voltage sequence detection methods under adverse grid conditions," *IEEE Transactions on Industrial Electronics*, vol. 61, no. 5, pp. 2139–2151, 2014.

[478] Z. Xin, X. Wang, Z. Qin, M. Lu, P. C. Loh, and F. Blaabjerg, "An improved second-order generalized integrator based quadrature signal generator," *IEEE Transactions on Power Electronics*, vol. 31, no. 12, pp. 8068–8073, 2016.

[479] Z. Xin, R. Zhao, P. Mattavelli, P. C. Loh, and F. Blaabjerg, "Re-investigation of generalized integrator based filters from a first-order-system perspective," *IEEE Access*, vol. 4, pp. 7131–7144, 2016.

[480] Z. Xin, Z. Qin, M. Lu, P. C. Loh, and F. Blaabjerg, "A new second-order generalized integrator based quadrature signal generator with enhanced performance," in *2016 IEEE Energy Conversion Congress and Exposition (ECCE)*, pp. 1–7, Sept 2016.

[481] S. Prakash, J. K. Singh, R. K. Behera, and A. Mondal, "Comprehensive analysis of SOGI-PLL based algorithms for single-phase system," in *2019 National Power Electronics Conference (NPEC)*, pp. 1–6, 2019.

[482] C. Zhang, X. Zhao, X. Wang, X. Chai, Z. Zhang, and X. Guo, "A grid synchronization pll method based on mixed second- and third-order generalized integrator for dc offset elimination and frequency adaptability," *IEEE Journal of Emerging and Selected Topics in Power Electronics*, vol. 6, no. 3, pp. 1517–1526, 2018.

[483] G. Fedele, A. Ferrise, and P. Muraca, "An adaptive quasi-notch filter for a biased sinusoidal signal estimation," in *2011 9th IEEE International Conference on Control and Automation (ICCA)*, pp. 1060–1065, 2011.

[484] K.-H. Nguyen, A. A. Nazeri, X. Yu, and P. Zacharias, "A novel modified-togi based pll for the three-phase unbalanced and distorted grid conditions," in *2022 24th European Conference on Power Electronics and Applications (EPE'22 ECCE Europe)*, pp. 1–10, 2022.

[485] B. Liu, M. An, H. Wang, Y. Chen, Z. Zhang, C. Xu, S. Song, and Z. Lv, "A simple approach to reject dc offset for single-phase synchronous reference frame pll in grid-tied converters," *IEEE Access*, vol. 8, pp. 112297–112308, 2020.

[486] N. Hui, D. Wang, and Y. Li, "A novel hybrid filter-based pll to eliminate effect of input harmonics and dc offset," *IEEE Access*, vol. 6, pp. 19762–19773, 2018.

[487] A. Bamigbade and V. Khadkikar, "Benchmarking of different orthogonal signal generator configurations for sogi pll applications," in *2021 IEEE Industry Applications Society Annual Meeting (IAS)*, pp. 1–6, 2021.

[488] B. Misra and B. Nayak, "Second order generalized integrator based synchronization technique for polluted grid conditions," in *2017 2nd International Conference for Convergence in Technology (I2CT)*, pp. 1080–1084, 2017.

[489] S. Golestan, J. M. Guerrero, J. C. Vasquez, A. M. Abusorrah, and Y. Al-Turki, "Standard sogi-fll and its close variants: Precise modeling in ltp framework and determining stability region/robustness metrics," *IEEE Transactions on Power Electronics*, vol. 36, no. 1, pp. 409–422, 2021.

[490] F. Muzi and M. Barbati, "A real-time harmonic monitoring aimed at improving smart grid power quality," in *2011 IEEE International Conference on Smart Measurements of Future Grids (SMFG) Proceedings*, pp. 95–100, Nov 2011.

[491] P. Rodriguez, A. Luna, I. Candela, R. Teodorescu, and F. Blaabjerg, "Grid synchronization of power converters using multiple second order generalized integrators," in *2008 34th Annual Conference of IEEE Industrial Electronics*, pp. 755–760, 2008.

[492] P. Rodríguez, A. Luna, I. Candela, R. Mujal, R. Teodorescu, and F. Blaabjerg, "Multiresonant frequency-locked loop for grid synchronization of power converters under distorted grid conditions," *IEEE Transactions on Industrial Electronics*, vol. 58, pp. 127–138, Jan 2011.

[493] C. Xie, K. Li, J. Zou, K. Zhou, and J. M. Guerrero, "Multiple second-order generalized integrators based comb filter for fast selective harmonic extraction," in *2019 IEEE Applied Power Electronics Conference and Exposition (APEC)*, pp. 2427–2432, 2019.

[494] Y. Singh, B. Singh, and S. Mishra, "Real time implementation of solar pv energy system under weak grid conditions," in *2018 8th IEEE India International Conference on Power Electronics (IICPE)*, pp. 1–6, 2018.

[495] P. Rodriguez, A. Luna, I. Etxeberria, J. R. Hermoso, and R. Teodorescu, "Multiple second order generalized integrators for harmonic synchronization of power converters," in *2009 IEEE Energy Conversion Congress and Exposition*, pp. 2239–2246, 2009.

[496] F. Antunes, L. S. Xavier, A. F. Cupertino, L. B. Felix, and H. A. Pereira, "Comparison of harmonic detection methods applied in a photovoltaic inverter during harmonic current compensation," in *2017 Brazilian Power Electronics Conference (COBEP)*, pp. 1–6, 2017.

[497] M. Mojiri, M. Karimi-Ghartemani, and A. Bakhshai, "Time-domain signal analysis using adaptive notch filter," *IEEE Transactions on Signal Processing*, vol. 55, no. 1, pp. 85–93, 2007.

[498] G. Fedele, A. Ferrise, and D. Frascino, "Structural properties of the SOGI system for parameters estimation of a biased sinusoid," in *2010 9th International Conference on Environment and Electrical Engineering*, pp. 438–441, May 2010.

[499] G. Fedele and A. Ferrise, "Non adaptive second-order generalized integrator for identification of a biased sinusoidal signal," *IEEE Transactions on Automatic Control*, vol. 57, no. 7, pp. 1838–1842, 2012.

[500] Z. Yan, H. He, J. Li, M. Su, and C. Zhang, "Double fundamental frequency PLL with second order generalized integrator under unbalanced grid voltages," in *2014 International Power Electronics and Application Conference and Exposition*, pp. 108–113, Nov 2014.

[501] M. Mansouri, M. Mojiri, M. A. Ghadiri-Modarres, and M. Karimi-Ghartemani, "Estimation of electromechanical oscillations from phasor measurements using second-order generalized integrator," *IEEE Transactions on Instrumentation and Measurement*, vol. 64, no. 4, pp. 943–950, 2015.

[502] M. R. Krstić, S. Lubura, S. Lale, M. Šoja, M. Ikić, and D. Milovanović, "Analysis of discretization methods applied on DC-SOGI block as part of SRF-PLL structure," in *2016 International Symposium on Industrial Electronics (INDEL)*, pp. 1–5, Nov 2016.

[503] J. Li, J. Zhao, J. Wu, and P. Xu, "Improved dual second-order generalized integrator pll for grid synchronization under non-ideal grid voltages including dc offset," in *2014 IEEE Energy Conversion Congress and Exposition (ECCE)*, pp. 136–141, 2014.

[504] V. Narayanan and B. Singh, "Seamless mode control of microgrid for optimal coordination of conventional and renewable energy resources," in *2021 IEEE 6th International Conference on Computing, Communication and Automation (ICCCA)*, pp. 755–761, 2021.

[505] A. Bamigbade and V. Khadkikar, "Extended state-based osg configurations for sogi pll with an enhanced disturbance rejection capability," *IEEE Transactions on Industry Applications*, vol. 58, no. 6, pp. 7792–7804, 2022.

[506] M. Karimi-Ghartemani, S. A. Khajehoddin, P. K. Jain, A. Bakhshai, and M. Mojiri, "Addressing DC component in PLL and notch filter algorithms," *IEEE Transactions on Power Electronics*, vol. 27, pp. 78–86, Jan 2012.

[507] M. Xie, H. Wen, C. Zhu, and Y. Yang, "DC offset rejection improvement in single-phase SOGI-PLL algorithms: Methods review and experimental evaluation," *IEEE Access*, vol. 5, pp. 12810–12819, 2017.

[508] G. Pin, B. Chen, G. Fedele, and T. Parisini, "Globally-stable tracking and estimation for single-phase electrical signals with dc-offset rejection," in *IECON 2019 - 45th Annual Conference of the IEEE Industrial Electronics Society*, vol. 1, pp. 4663–4668, 2019.

[509] B. Liu, M. An, H. Wang, Y. Chen, Z. Zhang, C. Xu, S. Song, and Z. Lv, "A simple approach to reject dc offset for single-phase synchronous reference frame pll in grid-tied converters," *IEEE Access*, vol. 8, pp. 112297–112308, 2020.

[510] T. Ngo, Q. Nguyen, and S. Santoso, "Improving performance of single-phase SOGI-FLL under DC-offset voltage condition," in *IECON 2014 - 40th Annual Conference of the IEEE Industrial Electronics Society*, pp. 1537–1541, Oct 2014.

[511] K. De Brabandere, T. Loix, K. Engelen, B. Bolsens, J. Van den Keybus, J. Driesen, and R. Belmans, "Design and operation of a phase-locked loop with kalman estimator-based filter for single-phase applications," in *IECON 2006 - 32nd Annual Conference on IEEE Industrial Electronics*, pp. 525–530, 2006.

[512] F. Ul-Nazir, N. Kumar, B. C. Pal, B. Singh, and B. K. Panigrahi, "Enhanced SOGI controller for weak grid integrated solar PV system," *IEEE Transactions on Energy Conversion*, pp. 1–1, 2020.

[513] Z. Xin, C. Yoon, R. Zhao, P. C. Loh, and F. Blaabjerg, "Realization of quadrature signal generator using accurate magnitude integrator," in *2016 IEEE Energy Conversion Congress and Exposition (ECCE)*, pp. 1–8, 2016.

[514] N. Kumar, I. Hussain, B. Singh, and B. K. Panigrahi, "Implementation of multilayer fifth-order generalized integrator-based adaptive control for grid-tied solar pv energy conversion system," *IEEE Transactions on Industrial Informatics*, vol. 14, no. 7, pp. 2857–2868, 2018.

[515] R. Teodorescu, M. Liserre, and P. Rodriguez, *Grid Converters for Photovoltaic and Wind Power Systems*. Chichester, United Kingdom: John Wiley & Sons, Ltd., 2011.

[516] J. Matas, H. Martin, J. de la Hoz, A. Abusorrah, Y. A. Al-Turki, and M. Al-Hindawi, "A family of gradient descent grid frequency estimators for the SOGI filter," *IEEE Transactions on Power Electronics*, vol. PP, no. 99, pp. 1–1, 2017.

[517] X. He, H. Geng, and G. Yang, "Reinvestigation of single-phase FLLs," *IEEE Access*, vol. 7, pp. 13178–13188, 2019.

[518] S. Golestan, J. M. Guerrero, F. Musavi, and J. Vasquez, "Single-phase frequency-locked loops: A comprehensive review," *IEEE Transactions on Power Electronics*, pp. 1–1, 2019.

[519] S. Golestan, J. M. Guerrero, J. C. Vasquez, A. M. Abusorrah, and Y. Al-Turki, "Single-phase flls based on linear kalman filter, limit-cycle oscillator, and complex bandpass filter: Analysis and comparison with a standard fll in grid applications," *IEEE Transactions on Power Electronics*, vol. 34, no. 12, pp. 11774–11790, 2019.

[520] A. Bamigbade and V. Khadkikar, "Frequency estimators for sogi fll: Modeling, design, and equivalence for fll advancements," *IEEE Transactions on Instrumentation and Measurement*, vol. 71, pp. 1–12, 2022.

[521] Z. Luo, M. Kaye, C. Diduch, and L. Chang, "Frequency measurement using a frequency locked loop," in *2011 IEEE Energy Conversion Congress and Exposition*, pp. 917–921, Sept 2011.

[522] J. S. Park, D. C. Lee, and T. L. Van, "Advanced single-phase SOGI-FLL using self-tuning gain based on fuzzy logic," in *2013 IEEE ECCE Asia Downunder*, pp. 1282–1288, June 2013.

[523] S. K. Panda and T. K. Dash, "An improved method of frequency detection for grid synchronization of DG systems during grid abnormalities," in *2014 International Conference on Circuits, Power and Computing Technologies [ICCPCT-2014]*, pp. 153–157, March 2014.

[524] A. E. Karkevandi and M. J. Daryani, "Frequency estimation with antiwindup to improve SOGI filter transient response to voltage sags," in *2018 6th International Istanbul Smart Grids and Cities Congress and Fair (ICSG)*, pp. 188–192, April 2018.

[525] S. Lyu, L. Zheng, and J. Song, "A second-order generalized integrator frequency locked loop with damping ratio adaptation," *IEEE Transactions on Power Electronics*, vol. 37, no. 3, pp. 2694–2704, 2022.

[526] M. Satyanarayana and A. V. R. Teja, "A digital frequency locked loop with minimum computation overhead for heavily distorted single-phase grid systems," *IEEE Transactions on Instrumentation and Measurement*, vol. 71, pp. 1–13, 2022.

[527] P. Sun, X. Liu, L. Zhao, M. Han, Y. Yao, and D. Xu, "Robust frequency lock loop based power control and harmonic compensation method for bidirectional ac/dc converter," in *2020 IEEE 4th Conference on Energy Internet and Energy System Integration (EI2)*, pp. 601–606, 2020.

[528] G. Fedele, A. Ferrise, and C. Picardi, "Periodic signal frequency tracking via a shifted second-order generalized integrator," in *2013 Africon*, pp. 1–5, 2013.

[529] S. Golestan, J. M. Guerrero, J. C. Vasquez, A. M. Abusorrah, and Y. Al-Turki, "A study on three-phase flls," *IEEE Transactions on Power Electronics*, vol. 34, no. 1, pp. 213–224, 2019.

[530] S. Golestan, J. M. Guerrero, and J. C. Vasquez, "High-order frequency-locked loops: A critical analysis," *IEEE Transactions on Power Electronics*, vol. 32, no. 5, pp. 3285–3291, 2017.

[531] S. Golestan, J. M. Guerrero, and J. C. Vasquez, "Modeling and stability assessment of single-phase grid synchronization techniques: Linear time-periodic versus linear time-invariant frameworks," *IEEE Transactions on Power Electronics*, vol. 34, no. 1, pp. 20–27, 2019.

[532] S. Golestan, J. Guerrero, J. Vasquez, A. M. Abusorrah, and Y. A. Al-Turki, "Standard SOGI-FLL and its close variants: Precise LTP modeling and determining stability region/robustness metrics," *IEEE Transactions on Power Electronics*, pp. 1–1, 2020.

[533] S. Golestan, J. M. Guerrero, J. C. Vasquez, A. M. Abusorrah, and Y. Al-Turki, "Linear time-periodic modeling, examination, and performance enhancement of grid synchronization systems with dc component rejection/estimation capability," *IEEE Transactions on Power Electronics*, vol. 36, no. 4, pp. 4237–4253, 2021.

[534] S. Golestan, J. M. Guerrero, A. M. Abusorrah, J. C. Vasquez, and Y. Al-Turki, "Ltp modeling and stability assessment of multiple second-order generalized integrator-based signal processing/synchronization algorithms and their close variants," *IEEE Transactions on Power Electronics*, vol. 37, no. 5, pp. 5062–5077, 2022.

[535] M. S. Reza, M. Ciobotaru, and V. G. Agelidis, "Robust technique for accurate estimation of single-phase grid voltage fundamental frequency and amplitude," *IET Generation, Transmission Distribution*, vol. 9, no. 2, pp. 183–192, 2015.

[536] J. Fang, S. Yang, Z. Xie, and L. Wang, "Enhanced frequency-locked loop based on a third-order generalized integrator," in *2021 IEEE 12th International Symposium on Power Electronics for Distributed Generation Systems (PEDG)*, pp. 1–8, 2021.

[537] R. Xu, H. Yin, T. Lan, X. Wu, and Y. Lan, "A novel phase-locked loop under grid fault condition," in *2019 4th IEEE Workshop on the Electronic Grid (eGRID)*, pp. 1–5, 2019.

[538] A. Bamigbade, V. Khadkikar, H. Zeineldin, M. El Moursi, and M. Al Hosani, "A novel power-based orthogonal signal generator for single-phase systems," *IEEE Transactions on Power Delivery*, pp. 1–1, 2020.

[539] M. S. Reza, M. Ciobotaru, and V. G. Agelidis, “Accurate estimation of single-phase grid voltage parameters under distorted conditions,” *IEEE Transactions on Power Delivery*, vol. 29, pp. 1138–1146, June 2014.

[540] L. Coluccio, A. Eisinberg, G. Fedele, C. Picardi, and D. Sgro, “Modulating functions method plus SOGI scheme for signal tracking,” in *2008 IEEE International Symposium on Industrial Electronics*, pp. 854–859, 2008.

[541] A. Sahoo, K. Mahmud, and J. Ravishankar, “An enhanced frequency-adaptive single-phase grid synchronization technique,” *IEEE Transactions on Instrumentation and Measurement*, vol. 70, pp. 1–11, 2021.

[542] A. Pigazo, F. J. Azcondo, C. Brañas, and P. Lamo, “Frequency estimation in dsogi cells by means of the teager energy operator,” in *2022 IEEE 23rd Workshop on Control and Modeling for Power Electronics (COMPEL)*, pp. 1–5, 2022.

[543] A. Sahoo, J. Ravishankar, and C. Jones, “Phase-locked loop independent second-order generalized integrator for single-phase grid synchronization,” *IEEE Transactions on Instrumentation and Measurement*, vol. 70, pp. 1–9, 2021.

[544] H. Yang, K. Dai, B. Yang, H. Luo, K. He, and Z. Xu, “Unknown resonance frequency detection by particle swarm optimization for active damper,” in *2022 IEEE 3rd China International Youth Conference on Electrical Engineering (CIYCEE)*, pp. 1–7, 2022.

[545] G. Fedele and A. Ferrise, “A frequency-locked-loop filter for biased multi-sinusoidal estimation,” *IEEE Transactions on Signal Processing*, vol. 62, no. 5, pp. 1125–1134, 2014.

[546] L. Pan, Z. Li, J. Zhang, and Y. Pang, “Frequency-locked loop based on active noise cancellation syncretized two first-order low pass filters,” *IEEE Access*, vol. 10, pp. 7277–7288, 2022.

[547] Z. Dai, W. Lin, H. Lin, and C. Qian, “Estimation of single-phase grid voltage parameters: An adaptive observer-based approach,” in *2016 12th World Congress on Intelligent Control and Automation (WCICA)*, pp. 2009–2014, 2016.

[548] Z. Dai, W. Lin, and H. Lin, “Estimation of single-phase grid voltage parameters with zero steady-state error,” *IEEE Transactions on Power Electronics*, vol. 31, pp. 3867–3879, May 2016.

[549] Z. Dai and W. Lin, “Adaptive estimation of three-phase grid voltage parameters under unbalanced faults and harmonic disturbances,” *IEEE Transactions on Power Electronics*, vol. 32, no. 7, pp. 5613–5627, 2017.

[550] H. Ahmed, M. Ahsan, M. Benbouzid, A. Albarbar, M. Shahjalal, and S. Biricik, “Coordinate transformation-free observer-based adaptive estimation of distorted single-phase grid voltage signal,” *IEEE Access*, vol. 8, pp. 74280–74290, 2020.

[551] M. Hou, “Parameter identification of sinusoids,” *IEEE Transactions on Automatic Control*, vol. 57, no. 2, pp. 467–472, 2012.

[552] A. Bonaventura, L. Coluccio, and G. Fedele, “Frequency estimation of multi-sinusoidal signal by multiple integrals,” in *2007 IEEE International Symposium on Signal Processing and Information Technology*, pp. 564–569, 2007.

[553] G. Fedele, A. Ferrise, and G. D'Aquila, "A global frequency estimator based on a frequency-locked-loop filter," in *2016 American Control Conference (ACC)*, pp. 7001–7006, 2016.

[554] B. Chen, G. Pin, W. M. Ng, C. K. Lee, S. Y. R. Hui, and T. Parisini, "An adaptive observer-based switched methodology for the identification of a perturbed sinusoidal signal: Theory and experiments," *IEEE Transactions on Signal Processing*, vol. 62, no. 24, pp. 6355–6365, 2014.

[555] G. Fedele and A. Ferrise, "Biased sinusoidal disturbance rejection with plant uncertainty via an adaptive third-order generalized integrator," in *2012 20th Mediterranean Conference on Control Automation (MED)*, pp. 253–258, 2012.

[556] G. Fedele and A. Ferrise, "Biased sinusoidal disturbance compensation with unknown frequency," *IEEE Transactions on Automatic Control*, vol. 58, no. 12, pp. 3207–3212, 2013.

[557] B. P. McGrath and D. G. Holmes, "Accurate state space realisations of resonant filters for high performance inverter control applications," in *2016 IEEE 2nd Annual Southern Power Electronics Conference (SPEC)*, pp. 1–6, 2016.

[558] C. Yang, J. Wang, X. You, C. Wang, and M. Zhou, "Comparison of discretization methods on the second-order generalized integrator frequency-locked loop," in *2018 IEEE Energy Conversion Congress and Exposition (ECCE)*, pp. 3095–3102, 2018.

[559] F. Tedesco, A. Casavola, and G. Fedele, "Discrete-time frequency-locked-loop filters for exact asymptotic rejection of sinusoidal disturbances," in *2014 American Control Conference*, pp. 2285–2290, 2014.

[560] F. Tedesco, A. Casavola, and G. Fedele, "Discrete-time frequency-locked-loop filters for parameters estimation of sinusoidal signals," in *52nd IEEE Conference on Decision and Control*, pp. 4399–4404, 2013.

[561] F. J. Rodriguez, E. Bueno, M. Aredes, L. G. B. Rolim, F. A. S. Neves, and M. C. Cavalcanti, "Discrete-time implementation of second order generalized integrators for grid converters," in *2008 34th Annual Conference of IEEE Industrial Electronics*, pp. 176–181, 2008.

[562] F. Tedesco, A. Casavola, and G. Fedele, "Unbiased estimation of sinusoidal signal parameters via discrete-time frequency-locked-loop filters," *IEEE Transactions on Automatic Control*, vol. 62, no. 3, pp. 1484–1490, 2017.

[563] J. Yu, W. Shi, J. Li, L. Deng, and M. Pei, "A discrete-time non-adaptive sogi-based frequency-locked loop," *IEEE Transactions on Power Systems*, vol. 35, no. 6, pp. 4912–4915, 2020.

[564] R. Zhao, S. Wu, C. Wang, H. Xu, X. Jiang, and Y. Wang, "A novel discretization method for multiple second-order generalized integrators," *IEEE Transactions on Power Electronics*, vol. 36, no. 10, pp. 10998–11002, 2021.

[565] Y. Wu, Q. Hu, X. Quan, H. Ding, K. Hou, and Y. Jiang, "A state space discrete-time realization of the three-phase generalized second-order integrator frequency locked loop," in *2021 IEEE Sustainable Power and Energy Conference (iSPEC)*, pp. 804–809, 2021.

[566] S. Wu, C. Wang, and R. Zhao, "An improved integrator discretization method for multiple second-order generalized integrators," in *2021 IEEE 4th International Electrical and Energy Conference (CIEEC)*, pp. 1–6, 2021.

[567] H. Zheng, Z. Liu, R. An, J. Liu, K. Feng, and Y. Tu, "Discrete multiple second-order generalized integrator with low-pass filters and frequency-locked loop for dc rejection," *IEEE Transactions on Power Electronics*, vol. 37, no. 10, pp. 11814–11827, 2022.

[568] A. T. Nguyen and D. D. Nguyen, "Implementation of discretization methods for second-order generalized integrator in grid voltage estimation systems," in *2022 11th International Conference on Control, Automation and Information Sciences (ICCAIS)*, pp. 124–129, 2022.

[569] H. Zheng, Z. Liu, K. Feng, J. Liu, and H. Zhang, "Ltp modeling and harmonic analysis of discrete universal sogi-fll," in *2022 IEEE Energy Conversion Congress and Exposition (ECCE)*, pp. 1–7, 2022.

[570] C. M. Hackl and M. Landerer, "A unified method for online detection of phase variables and symmetrical components of unbalanced three-phase systems with harmonic distortion," *Energies*, vol. 12, no. 17, 2019.

[571] C. M. Hackl and M. Landerer, "Modified second-order generalized integrators with modified frequency locked loop for fast harmonics estimation of distorted single-phase signals," *arXiv e-prints*, p. arXiv:1902.04653, Feb 2019.

[572] C. Hackl and M. Landerer, "A unified method for generic signal parameter estimation of arbitrarily distorted single-phase grids with dc-offset," *IEEE Open Journal of the Industrial Electronics Society*, vol. 1, pp. 235–246, 2020.

[573] J. Adamy, *Nichtlineare Systeme und Regelungen.* Springer Vieweg, Berlin, Heidelberg, 2 ed.

[574] T. Kailath, *Linear systems.* Upper Saddle River, New Jersey: Prentice Hall International Inc., 1980.

[575] L. Råde, B. Westergren, and P. Vachenauer, *Springers mathematische Formeln: Taschenbuch für Ingenieure, Naturwissenschaftler, Informatiker, Wirtschaftswissenschaftler.* Springer-Verlag, 3. ed., 2000.

[576] D. S. Bernstein, *Matrix Mathematics — Theory, Facts, and Formulas with Application to Linear System Theory.* Princeton and Oxford: Princeton University Press, 2nd ed., 2009.

[577] D. Hinrichsen and A. Pritchard, *Mathematical Systems Theory I — Modelling, State Space Analysis, Stability and Robustness.* No. 48 in Texts in Applied Mathematics, Berlin: Springer-Verlag, 2005.

[578] D. Bainov and P. Simeonov, *Integral Inequalities and Applications.* Mathematics and its Applications, Springer Netherlands, 2013.

[579] P. Ioannou and J. Sun, *Robust Adaptive Control.* Upper Saddle River, New Jersey: Prentice Hall International Inc., 1996. (out of print in 2003, electronic copy at: `http://www-rcf.usc.edu/~ioannou/Robust_Adaptive_Control.htm`).

[580] J. Salle and S. Lefschetz, *Stability by Liapunov's Direct Method with Applications by Joseph L Salle and Solomon Lefschetz.* ISSN, Elsevier Science, 2012.

[581] M. Abramowitz and I. A. Stegun, eds., *Handbook of Mathematical Functions with Formulas, Graphs, and Mathematical Tables.* Applied Mathematics Series, National Bureau of Standards, tenth printing, december 1972 ed., 1964.

[582] G. Ludyk, *Theoretische Regelungstechnik 1*. Springer-Verlag, 1995.

[583] J. Bewersdorff, *Algebra für Einsteiger Von der Gleichungsauflösung zur Galois-Theorie*. 2019.